Simplified models for turbulent diffusion: Theory, numerical modelling, and physical phenomena

Andrew J. Majda*, Peter R. Kramer

New York University, Courant Institute, 251 Mercer Street, New York, NY 10012, USA

Contents

---

* Corresponding author. Tel.: (212) 998-3324; fax: (212) 995-4121; e-mail: jonjon@cims.nyu.edu.

Abstract

Several simple mathematical models for the turbulent diffusion of a passive scalar field are developed here with an emphasis on the symbiotic interaction between rigorous mathematical theory (including exact solutions), physical intuition, and numerical simulations. The homogenization theory for periodic velocity fields and random velocity fields with short-range correlations is presented and utilized to examine subtle ways in which the flow geometry can influence the large-scale effective scalar diffusivity. Various forms of anomalous diffusion are then illustrated in some exactly solvable random velocity field models with long-range correlations similar to those present in fully developed turbulence. Here both random shear layer models with special geometry but general correlation structure as well as isotropic rapidly decorrelating models are emphasized. Some of the issues studied in detail in these models are superdiffusive and subdiffusive transport, pair dispersion, fractal dimensions of scalar interfaces, spectral scaling regimes, small-scale and large-scale scalar intermittency, and qualitative behavior over finite time intervals. Finally, it is demonstrated how exactly solvable models can be applied to test and design numerical simulation strategies and theoretical closure approximations for turbulent diffusion. © 1999 Elsevier Science B.V. All rights reserved.

1. Introduction

In this review, we consider the problem of describing and understanding the transport of some physical entity, such as heat or particulate matter, which is immersed in a fluid flow. Most of our attention will be on situations in which the fluid is undergoing some disordered or turbulent motion. If the transported quantity does not significantly influence the fluid motion, it is said to be passive, and its concentration density is termed a *passive scalar* field. Weak heat fluctuations in a fluid, dyes utilized in visualizing turbulent flow patterns, and chemical pollutants dispersing in the environment may all be reasonably modelled as passive scalar systems in which the immersed quantity is transported in two ways: ordinary molecular diffusion and passive advection by its fluid environment. The general problem of describing turbulent diffusion of a passive quantity may be stated mathematically as follows:

Let $v(x, t)$ be the velocity field of the fluid prescribed as a function of spatial coordinates x and time t, which we will always take to be incompressible ($\nabla \cdot v(x, t) = 0$). Also let $f(x, t)$ be a prescribed pumping (source and sink) field, and $T_0(x)$ be the passive scalar field prescribed at some initial time $t = 0$. Each may have a mixture of deterministic and random components, the latter modelling noisy fluctuations. In addition, molecular diffusion may be relevant, and is represented by a diffusivity coefficient κ. The passive scalar field then evolves according to the *advection–diffusion equation*

$$\partial T(x, t)/\partial t + v(x, t) \cdot \nabla T(x, t) = \kappa \Delta T(x, t) + f(x, t) ,$$

$$T(x, t = 0) = T_0(x) . \tag{1}$$

The central aim is to describe some desired statistics of the passive scalar field $T(x, t)$ at times $t > 0$. For example, a typical goal is to obtain effective equations of motion for the mean passive scalar density, denoted $\langle T(x, t) \rangle$.

While the PDE in Eq. (1) is linear, the relation between the passive scalar field $T(x, t)$ and the velocity field $v(x, t)$ is nonlinear. The influence of the statistics of the random velocity field on the passive scalar field is subtle and very difficult to analyze in general. For example, a closed equation for $\langle T(x, t) \rangle$ typically cannot be obtained by simply averaging the equation in Eq. (1), because $\langle v(x, t) \cdot \nabla T(x, t) \rangle$ cannot be simply related to an explicit functional of $\langle T(x, t) \rangle$ in general. This is a manifestation of the "turbulence moment closure problem" [227].

In applications such as the predicting of temperature profiles in high Reynolds number turbulence [196,227,247,248], the tracking of pollutants in the atmosphere [78], and the estimating of the transport of groundwater through a heterogeneous porous medium [79], the problem is further complicated by the presence of a wide range of excited space and time scales in the velocity field, extending all the way up to the scale of observational interest. It is precisely for these kinds of problems, however, that a simplified effective description of the evolution of statistical quantities such as the mean passive scalar density $\langle T(x, t) \rangle$ is extremely desirable, because the range of active scales of velocity fields which can be resolved is strongly limited even on supercomputers [154].

For some purposes, one may be interested in following the progress of a specially marked particle as it is carried by a flow. Often this particle is light and small enough so that its presence

only negligibly disrupts the existing flow pattern, and we will generally refer to such a particle as a (passive) *tracer*, reflecting the terminology of experimental science in which fluid motion is visualized through the motion of injected, passively advected particles (often optically active dyes) [227]. The problem of describing the statistical transport of tracers may be formulated as follows:

Let $v(x, t)$ be a prescribed, incompressible velocity field of the fluid, with possibly both a mean component and a random component with prescribed statistics modelling turbulent or other disordered fluctuations. We seek to describe some desired statistics of the trajectory $X(t)$ of a tracer particle released initially from some point x_0 and subsequently transported jointly by the flow $v(x, t)$ and molecular diffusivity κ. The equation of motion for the trajectory is a (vector-valued) stochastic differential equation [112,257]

$$dX(t) = v(X(t), t)\, dt + \sqrt{2\kappa}\, dW(t) , \qquad (2a)$$

$$X(t = 0) = x_0 . \qquad (2b)$$

The second term in Eq. (2a) is a random increment due to Brownian motion [112,257]. Basic statistical functions of interest are the mean trajectory, $\langle X(t) \rangle$, and the mean-square displacement of a tracer from its initial location, $\langle |X(t) - x_0|^2 \rangle$.

It is often of interest to track multiple particles simultaneously; these will each individually obey the trajectory equations in Eqs. (2a) and (2b) with the same realization of the velocity field v but independent Brownian motions. The advection–diffusion PDE in Eq. (1) and the tracer trajectory equations in Eqs. (2a) and (2b) are related to each other by the theory of Ito diffusion processes [107,257], which is just a generalization of the method of characteristics [150] to handle second-order derivatives via a random noise term in the characteristic equations. We will work with both of these equations in this review.

In principle, the turbulent velocity field $v(x, t)$ which advects the passive scalar field should be a solution to the Navier–Stokes equations

$$\partial v(x, t)/\partial t + v(x, t) \cdot \nabla v(x, t) = -\nabla p(x, t) + \nu \Delta v(x, t) + F(x, t) ,$$

$$\nabla \cdot v(x, t) = 0 , \qquad (3)$$

where p is the pressure field, ν is viscosity, and $F(x, t)$ is some external stirring which maintains the fluid in a turbulent state. But the analytical representation of such solutions corresponding to complex, especially turbulent flows, are typically unwieldy or unknown.

We shall therefore instead utilize simplified velocity field models which exhibit some empirical features of turbulent or other flows, though these models may not be actual solutions to the Navier–Stokes equations. Incompressibility $\nabla \cdot v(x, t) = 0$ is however, enforced in all of our velocity field models. Our primary aim in working with simplified models is to obtain mathematically explicit and unambiguous results which can be used as a sound basis for the scientific investigation of more complex turbulent diffusion problems arising in applications for which no analytical solution is available. We therefore emphasize the aspects of the model results which illustrate general physical mechanisms and themes which can be expected to be manifest in wide classes of turbulent flows. We will also show how simplified models can be used to strengthen and refine the

arsenal of numerical methods designed for quantitative physical exploration in natural and practical applications. First of all, simplified models offer themselves as a pool of test problems to assess the variety of numerical simulations schemes proposed for turbulent diffusion [109,180,190,219,291,335]. Moreover, we shall explicitly describe in Section 6 how mathematical (harmonic) analysis of simplified models can be used as a basis to design new numerical simulation algorithms with superior performance [82,84–86]. Accurate and reliable numerical simulations in turn enrich various mathematical asymptotic theories by furnishing explicit data concerning the quality of the asymptotic approximation and the significance of corrections at finite values of the small or large parameter, and can reveal new physical phenomena in strongly nonlinear situations unamenable to a purely theoretical treatment. Physical intuition, for its part, suggests fruitful mathematical model problems for investigation, guides their analyses, and informs the development of numerical strategies. We will repeatedly appeal to this symbiotic interaction between simplified mathematical models, asymptotic theory, physical understanding, and numerical simulation.

Though we do not dwell on this aspect in this review, we wish to mention the more distant goal of using simplified velocity field models in turbulent diffusion to gain some understanding in the theoretical analysis and practical treatment of the Navier–Stokes equations in Eq. (3) in situations where strong driving gives rise to complicated turbulent motion [196,227]. The advection–diffusion equation in Eq. (1) has some essential features in common with the Navier–Stokes equations: they are both transport equations in which the advection term gives rise to a nonlinearity of the *statistics* of the solution. At the same time, the advection–diffusion equation is more managable since it is a scalar, linear PDE without an auxiliary constraint analogous to incompressibility. The advection–diffusion equation, in conjunction with a velocity field model with turbulent characteristics, therefore serves as a simplified prototype problem for developing theories for turbulence itself.

Our study of passive scalar advection–diffusion begins in Section 2 with velocity fields which have either a periodic cell structure or random fluctuations with only mild short-range spatial correlations. We explain the general homogenization theory [12,32,148] which describes the behavior of the passive scalar field at large scales and long times in these flows via an enhanced "homogenized" diffusivity matrix. Through mathematical theory, exact results from simplified models, and numerical simulations, we examine how the homogenized diffusion coefficient depends on the flow structure, and investigate how well the observation of the passive scalar system at large but finite space–time scales agrees with the homogenized description. In Section 3, we use simple random shear flow models [10,14] with a flexible statistical spatio-temporal structure to demonstrate explicitly a number of anomalies of turbulent diffusion when the velocity field has sufficiently strong long-range correlations. These simple shear flow models are also used to explore turbulent diffusion in situations where the velocity field has a wide inertial range of spatio-temporal scales excited in a statistically self-similar manner, as in a high Reynolds number turbulent flow. We also describe some universal small-scale features of the passive scalar field which may be derived in an exact and rigorous fashion in such flows. Other aspects of small-scale passive scalar fluctuations are similarly addressed in Section 4 using a complementary velocity field model [152,179] with a statistically isotropic geometry but very rapid decorrelations in time. In Section 5, we present a special family of exactly solvable shear flow models [207,233] which explicitly demonstrates the phenomenon of large-scale intermittency in the statistics of the passive scalar field, by which we mean the occurrence of a broader-than-Gaussian distribution for the value of the passive scalar

field $T(\boldsymbol{x}, t)$ recorded at a single location in a turbulent flow [155,127,146,147,191]. Next, in Section 6, we focus on the challenge of developing efficient and accurate numerical "Monte Carlo" methods for simulating the motion of tracers in turbulent flows. Using the simple shear models from Section 3 and other mathematical analysis [83,87,140], we illustrate explicitly some subtle and significant pitfalls of some conventional numerical approaches. We then discuss the theoretical basis and demonstrate the exceptional practical performance of a recent wavelet-based Monte Carlo algorithm [82,84–86] which is designed to handle an extremely wide inertial range of self-similar scales in the velocity field. We conclude in Section 7 with a brief discussion of the application of exactly solvable models to assess approximate closure theories [177,182,196,200,227,285,286,344] which have been formulated to describe the evolution of the mean passive scalar density in a high Reynolds number turbulent flow [13,17].

Detailed introductions to all these topics are presented at the beginning of the respective sections.

2. Enhanced diffusion with periodic or short-range correlated velocity fields

In the introduction, we mentioned the moment closure problem for obtaining statistics of the passive scalar field immersed in a turbulent fluid. To make this issue concrete, consider the challenge of deriving an equation for the mean passive scalar density $\langle T(\boldsymbol{x}, t) \rangle$ advected by a velocity field which is a superposition of a mean flow pattern $\boldsymbol{V}(\boldsymbol{x}, t)$ and random, turbulent fluctuations $\boldsymbol{v}(\boldsymbol{x}, t)$ with mean zero. Angle brackets will denote an ensemble average of the included quantity over the statistics of the random velocity field. Since the advection–diffusion equation is linear, one might naturally seek an equation for the mean passive scalar density by simply averaging it:

$$\partial \langle T(\boldsymbol{x}, t) \rangle / \partial t + \boldsymbol{V}(\boldsymbol{x}, t) \cdot \nabla \langle T(\boldsymbol{x}, t) \rangle + \langle \boldsymbol{v}(\boldsymbol{x}, t) \cdot \nabla T(\boldsymbol{x}, t) \rangle = \kappa \Delta \langle T(\boldsymbol{x}, t) \rangle + \langle f(\boldsymbol{x}, t) \rangle ,$$

$$\langle T(\boldsymbol{x}, t = 0) \rangle = \langle T_0(\boldsymbol{x}) \rangle . \tag{4}$$

Eq. (4) is not a closed equation for $\langle T(\boldsymbol{x}, t) \rangle$ because the average of the advective term, $\langle \boldsymbol{v} \cdot \nabla T \rangle$, cannot generally be simply related to a functional of $\langle T(\boldsymbol{x}, t) \rangle$.

An early idea for circumventing this obstacle was to represent the effect of the random advection by a diffusion term:

$$\langle \boldsymbol{v}(\boldsymbol{x}, t) \cdot \nabla T(\boldsymbol{x}, t) \rangle = - \nabla \cdot (\bar{\mathcal{K}}_T \cdot \nabla T(\boldsymbol{x}, t)) , \tag{5}$$

where $\bar{\mathcal{K}}_T$ is some constant "eddy diffusivity" matrix (usually a scalar multiple of the identity matrix $\mathscr{I}$) which is to be estimated in some manner, such as mixing-length theory ([320], Section 2.4). From assumption (5) follows a simple effective advection–diffusion equation for the mean passive scalar density

$$\partial \langle T(\boldsymbol{x}, t) \rangle / \partial t + \boldsymbol{V}(\boldsymbol{x}, t) \cdot \nabla \langle T(\boldsymbol{x}, t) \rangle = \nabla \cdot ((\kappa \mathscr{I} + \bar{\mathcal{K}}_T) \cdot \nabla \langle T(\boldsymbol{x}, t) \rangle) + \langle f(\boldsymbol{x}, t) \rangle ,$$

$$\langle T(\boldsymbol{x}, t = 0) \rangle = \langle T_0(\boldsymbol{x}) \rangle ,$$

where the diffusivity matrix $(\kappa \mathcal{I} + \bar{\mathcal{K}}_T)$ is (presumably) enhanced over its bare molecular value by the turbulent eddy diffusivity $\bar{\mathcal{K}}_T$ coming from the fluctuations of the velocity. The closure hypothesis (5) is the "Reynolds analogy" of a suggestion first made by Prandtl in the context of the Navier–Stokes equations (see [227], Section 13.1). It may be viewed as an extension of kinetic theory, where microscopic particle motion produces ordinary diffusive effects on the macroscale. There are, however, some serious deficiencies of the Prandtl eddy diffusivity hypothesis, both in terms of theoretical justification and of practical application to general turbulent flows (see [227], Section 13.1; [320], Ch. 2). First of all, kinetic theory requires a strong separation between the microscale and macroscale, but the turbulent fluctuations typically extend up to the scale at which the mean passive scalar density is varying. Moreover, the recipes for computing the eddy diffusivity $\bar{\mathcal{K}}_T$ are rather vague, and are generally only defined up to some unknown numerical constant "of order unity". More sophisticated schemes for computing eddy viscosities based on renormalization group ideas have been proposed in more recent years [243,300,344], but these involve other ad hoc assumptions of questionable validity.

In Section 2, we will discuss some contexts in which rigorous sense can be made of the eddy diffusivity hypothesis (5), and an exact formula provided for the enhanced diffusivity. All involve the fundamental assumption that, in some sense, the fluctuations of the velocity field occur on a much smaller scales than those of the mean passive scalar field. These rigorous theories therefore are not applicable to strongly turbulent flows, but they provide a solid, instructive, and relatively simple framework for examining a number of subtle aspects of passive scalar advection–diffusion in unambiguous detail. Moreover, they can be useful in practice for certain types of laboratory or natural flows at moderate or low Reynolds numbers [301,302].

Overview of Section 2: We begin in Section 2.1 with a study of advection–diffusion by velocity fields that are deterministic and *periodic* in space and time. Generally, we will be considering passive scalar fields which are varying on scales much larger than those of the periodic velocity field in which they are immersed. Though the velocity field is deterministic, one may formally view the periodic fluctuations as an extremely simplified model for small-scale turbulent fluctuations. Averaging over the fluctuations may be represented by spatial averaging over a period cell. After a convenient nondimensionalization in Section 2.1.1, we formulate in Sections 2.1.2 and 2.1.3 the *homogenization theory* [32,149] which provides an asymptotically exact representation of the effects of the small-scale periodic velocity field on the large-scale passive scalar field in terms of a homogenized, effective diffusivity matrix $\mathcal{K}^*$ which is enhanced above bare molecular diffusion. Various alternative ways of computing this effective diffusivity matrix are presented in Section 2.1.4. We remark that, in contrast to usual eddy diffusivity models, the enhanced diffusivity in the rigorous homogenization theory has a highly nontrivial dependence on molecular diffusivity. We will express this dependence in terms of the Péclet number, which is a measure of the strength of advection by the velocity field relative to diffusion by molecular processes (see Section 2.1.1). The physically important limit of high Péclet number will be of central interest throughout Section 2.

In Section 2.2, we apply the homogenization theory to evaluate the tracer transport in a variety of periodic flows. We demonstrate the symbiotic interplay between the rigorous asymptotic theories and numerical computations in these investigations, and how they can reveal some important and subtle physical transport mechanisms. We first examine periodic shear flows with various types of cross sweeps (Sections 2.2.1 and 2.2.2), where exact analytical formulas can be derived. Next we turn to flows with a cellular structure and their perturbations (Section 2.2.3), and

the subtle effects which the addition of a mean sweep can produce (Section 2.2.4). We discuss how other types of periodic flows can be profitably examined through the joint use of analytical and numerical means in Section 2.2.5.

An important practical issue is the accuracy with which the effective diffusivity from homogenization theory describes the evolution of the passive scalar field at finite times. We examine this question in Section 2.3 by computing the mean-square displacement of a tracer over a finite interval of time. For shear flows with cross sweeps, an exact analytical expression can be obtained (Section 2.3.1). The finite time behavior of tracers in more general periodic flows may be estimated numerically through Monte Carlo simulations (Section 2.3.2). In all examples considered, the rate of change of the mean-square tracer displacement is well described by (twice) the homogenized diffusivity after a transient time interval which is not longer than the time it would take molecular diffusion to spread over a few spatial period cells [230,231].

In Section 2.4, we begin our discussion of advection–diffusion by homogenous random velocity fields. We identify two different large-scale, long-time asymptotic limits in which a closed effective diffusion equation can be derived for the mean passive scalar density $\langle T(\boldsymbol{x},t) \rangle$. First is the "Kubo theory" [160,188,313], where the time scale of the velocity field varies much more rapidly than that of the passive scalar field, but the length scales of the two fields are comparable (Section 2.4.1). The "Kubo diffusivity" appearing in the effective equation is simply related to the correlation function of the velocity field. Next we concentrate on steady random velocity fields which have only short-range spatial correlations, so that there can be a meaningfully strong separation of scales between the passive scalar field and the velocity field. A homogenization theorem applies in such cases [12,98,256], and rigorously describes the effect of the small-scale random velocity field on the large-scale mean passive scalar field through a homogenized, effective diffusivity matrix (Section 2.4.2). Homogenization for the steady periodic flow fields described in the earlier Sections 2.1, 2.2 and 2.3 is a special case of this more general theory for random fields. We present various formulas for the homogenized diffusivity in Section 2.4.3, and discuss its parametric behavior in some example random vortex flows in Section 2.4.4.

We emphasize again that high Reynolds number turbulent flows have strong long-range correlations which do not fall under the purview of the homogenization theory discussed in Section 2. The ramifications of these long-range correlations will be one of the main foci in the remaining sections of this review.

2.1. Homogenization theory for spatio-temporal periodic flows

Here we present the rigorous homogenization theory which provides a formula for the effective diffusion of a passive scalar field at large scales and long times due to the combined effects of molecular diffusion and advection by a *periodic* velocity field. We first prepare for our discussion with some definitions and a useful nondimensionalization in Section 2.1.1. Next, in Section 2.1.2, we state the formula prescribed by homogenization theory for the effective diffusivity of the passive scalar field on large scales and long times, and show formally how to derive it through a multiple scale asymptotic analysis [32,205]. We indicate in Section 2.1.3 how to generalize the homogenization theory to include large-scale mean flows superposed upon the periodic flow structure [38,230]. In Section 2.1.4, we describe some alternative formulas for the effective diffusivity, involving Stieltjes measures [9,12,20] and variational principles [12,97]. These representations can

be exploited to bound and estimate the effective diffusivity in various examples and classes of periodic flows [40,97,210], as we shall illustrate in Section 2.2.

2.1.1. Nondimensionalization

We begin our discussion of convection-enhanced diffusivity with smooth periodic velocity fields $v(x, t)$ defined on $\mathbb{R}^d$ which have temporal period t_v, and a common spatial period L_v along each of the coordinate axes:

$$v(x, t + t_v) = v(x, t) \,,$$

$$v(x + L_v \hat{e}_j, t) = v(x, t) \,,$$

where $\{\hat{e}_j\}_{j=1}^d$ denotes a unit vector in the jth coordinate direction. More general periodic velocity fields can be treated similarly; the resulting formulas would simply have some additional notational complexity. We also demand for the moment that the velocity field have "mean zero", in that its average over space and time vanishes:

$$L_v^{-d} t_v^{-1} \int_0^{t_v} \int_{[0,L_v]^d} v(x, t) \, dx \, dt = 0 \,.$$

In Section 2.1.3, we will extend our discussion to include the possibility of a large-scale mean flow superposed upon the periodic velocity field just described.

It will be useful to nondimensionalize space and time so that the dependence of the effective diffusivity on the various physical parameters of the problem can be most concisely described. The spatial period L_v provides a natural reference length unit. To illuminate the extent to which the periodic velocity field enhances the diffusivity of the passive scalar field above the bare molecular value κ, we choose as a basic time unit the cell-diffusion time $t_\kappa = L_v^2/\kappa$, which describes the time scale over which a finely concentrated spot of the passive scalar field will spread over a spatial period cell. This will render the molecular diffusivity to be exactly 1 in nondimensional units.

The velocity field is naturally nondimensionalized as follows:

$$v(x, t) = v_0 v^\circ(x/L_v, t/t_v) \,,$$

where v° is a nondimensional function with period 1 in time and in each spatial coordinate direction, and v_0 is some constant with dimension of velocity which measures the magnitude of the velocity field. The precise definition of v_0 is not important; it may be chosen as the maximum of $|v(x, t)|$ over a space–time period for example.

The initial passive scalar density $T_0(x)$ will be assumed to be characterized by some total "mass"

$$M_0 = \int_{\mathbb{R}^d} T_0(x) \, dx$$

and length scale L_T:

$$T_0(x) = \frac{M_0}{L_T^d} T_0^\circ(x/L_T) \,.$$

We choose M_0 as a reference unit for the dimension characterizing the passive scalar quantity (which may, for example, be heat or mass of some contaminant), and we nondimensionalize accordingly the passive scalar density at all times:

$$T(\mathbf{x},t) = \frac{M_0}{L_v^d} T^\circ(\mathbf{x}/L_v, t/t_v) .$$

Passing now to nondimensional units $\mathbf{x}^\circ = \mathbf{x}/L_v$, $t^\circ = t/t_v$, in the advection–diffusion equation, and subsequently dropping the superscripts $^\circ$ on all nondimensional functions, we obtain the following advection–diffusion equation:

$$\frac{\partial T(\mathbf{x},t)}{\partial t} + \frac{v_0 L_v}{\kappa} \mathbf{v}(\mathbf{x}, t(L_v^2/\kappa t_v)) \cdot \nabla T(\mathbf{x},t) = \Delta T(\mathbf{x},t) ,$$

$$T(\mathbf{x},t=0) = (L_v/L_T)^d T_0(\mathbf{x}(L_v/L_T)) . \tag{6}$$

We now identify several key nondimensional parameters which appear in this equation. The first is the *Péclet number*

$$\mathrm{Pe} \equiv v_0 L_v/\kappa , \tag{7}$$

which formally describes the ratio between the magnitudes of the advection and diffusion terms [325]. It plays a role for the passive scalar advection–diffusion equation similar to the Reynolds number for the Navier–Stokes equations. Next, we have the parameter

$$\tau_v = \kappa t_v/L_v^2 ,$$

which is the ratio of the temporal period of the velocity field to the cell-diffusion time. Thirdly, we have the ratio of the length scale of the velocity field to the length scale of the initial data, which we simply denote

$$\delta \equiv L_v/L_T . \tag{8}$$

Rewriting Eq. (6) in terms of these newly defined nondimensional parameters, we obtain the final nondimensionalized form of the advection–diffusion equation which we will use throughout Section 2:

$$\partial T(\mathbf{x},t)/\partial t + \mathrm{Pe}\, \mathbf{v}(\mathbf{x}, t/\tau_v) \cdot \nabla T(\mathbf{x},t) = \Delta T(\mathbf{x},t) ,$$

$$T(\mathbf{x},t=0) = \delta^d T_0(\delta \mathbf{x}) . \tag{9}$$

Notice especially how the Péclet number describes, formally, the extent to which the advection–diffusion equation differs from a pure diffusion equation.

We note that the nondimensional velocity field $\mathbf{v}(\mathbf{x}, t/\tau_v)$ has period 1 in each spatial coordinate direction and temporal period τ_v. It will be convenient in what follows to define a concise notation for averaging a function g over a spatio-temporal period:

$$\langle g \rangle_p \equiv \tau_v^{-1} \int_0^{\tau_v} \int_{[0,1]^d} g(\mathbf{x},t)\, \mathrm{d}\mathbf{x}\, \mathrm{d}t .$$

2.1.2. Homogenization theory for periodic flows with zero mean

We now seek to describe the evolution of the passive scalar field on length scales and time scales large compared to those of the periodic velocity field. It is natural in this regard to take the initial length scale ratio δ between the velocity and passive scalar length scales to be very small. From experience with kinetic theory in which microscopic collision processes give rise to ordinary diffusive transport on macroscales, we can expect that the joint action of the mean zero velocity field and molecular diffusion will give rise to a net diffusion on the large scales. We therefore rescale time with space according to the standard diffusive relation $x \to \delta x$, $t \to \delta^2 t$, and the passive scalar density according to

$$T^{(\delta)}(x, t) \equiv \delta^{-d} T(\delta x, \delta^2 t) . \tag{10}$$

The amplitude rescaling preserves the total mass of the passive scalar quantity. We note that the choice of diffusive rescaling is appropriate here only because of the strong separation of scales between the velocity field and the passive scalar field; when this scale separation fails to hold, other "anomalous" space–time scaling laws may be required (see Section 3.4).

The rescaled form of the advection–diffusion equation (9) reads

$$\partial T^{(\delta)}(x, t)/\partial t + \delta^{-1} \mathrm{Pe}\, v\left(\frac{x}{\delta}, \frac{t}{\delta^2 \tau_v}\right) \cdot \nabla T^{(\delta)}(x, t) = \Delta T^{(\delta)}(x, t) ,$$

$$T^{(\delta)}(x, t = 0) = T_0(x) . \tag{11}$$

On these large space–time scales ($\delta \ll 1$), the advection by the velocity field has a large magnitude ($O(\delta^{-1})$) and is rapidly oscillating in space and/or time. Because the velocity field has mean zero, the strong and rapidly fluctuating advection term has a finite diffusive influence on $T^{(\delta)}(x, t)$ in the $\delta \to 0$ limit, i.e. on large scales and long times. This is the content of the homogenization theory for advection–diffusion in a periodic flow, which we now state [205].

2.1.2.1. Homogenized effective diffusion equation for periodic velocity fields.
In the long time, large-scale limit, the rescaled passive scalar field converges to a finite limit

$$\lim_{\delta \to 0} T^{(\delta)}(x, t) = \bar{T}(x, t) , \tag{12}$$

which satisfies an effective diffusion equation

$$\partial \bar{T}(x, t)/\partial t = \nabla \cdot (\mathscr{K}^* \nabla \bar{T}(x, t)) , \tag{13a}$$

$$\bar{T}(x, t = 0) = T_0(x) , \tag{13b}$$

with constant, positive definite, symmetric *effective diffusivity* matrix $\mathscr{K}^*$. This effective diffusivity matrix can be expressed as

$$\mathscr{K}^* = \mathscr{I} + \bar{\mathscr{K}} ,$$

where $\mathscr{I}$ is the identity matrix (representing the nondimensionalized molecular diffusion) and $\bar{\mathscr{K}}$ is a nonnegative-definite *enhanced diffusivity* matrix which represents the additional diffusivity due to

the periodic flow. The enhanced diffusivity matrix $\bar{\mathscr{K}}$ can be computed as follows. Let $\boldsymbol{\chi}(\boldsymbol{x}, t)$ be the (unique) mean zero, periodic solution to the following auxiliary parabolic *cell problem* (in the unscaled nondimensional space–time coordinates):

$$\partial\boldsymbol{\chi}(\boldsymbol{x}, t)/\partial t + \mathrm{Pe}\,\boldsymbol{v}(\boldsymbol{x}, t/\tau_v)\cdot\nabla\boldsymbol{\chi}(\boldsymbol{x}, t) - \varDelta\boldsymbol{\chi}(\boldsymbol{x}, t) = -\mathrm{Pe}\,\boldsymbol{v}(\boldsymbol{x}, t/\tau_v)\ . \tag{14}$$

Then the components of the enhanced diffusivity matrix may be expressed as

$$\bar{\mathscr{K}}_{ij} = \langle\nabla\chi_i\cdot\nabla\chi_j\rangle_p\ . \tag{15}$$

For the special case of a *steady*, periodic velocity field, the cell problem (14) becomes elliptic, again with a unique mean zero, periodic solution:

$$\varDelta\boldsymbol{\chi}(\boldsymbol{x}) - \mathrm{Pe}\,\boldsymbol{v}(\boldsymbol{x})\cdot\nabla\chi_j(\boldsymbol{x}) = \mathrm{Pe}\,\boldsymbol{v}(\boldsymbol{x})\ . \tag{16}$$

The convergence (12) of the passive scalar field rescaled on large scales and long times to the solution of the effective diffusion equation (13) can be rigorously established in the following sense:

$$\lim_{\delta\to 0}\ \sup_{0\le t\le t_0}\ \sup_{\boldsymbol{x}\in\mathbb{R}^d}|T^{(\delta)}(\boldsymbol{x}, t) - \bar{T}(\boldsymbol{x}, t)| = 0$$

for every finite $t_0 > 0$, provided that T_0 and $\boldsymbol{v}$ obey some mild smoothness and boundedness conditions [205]. We will sketch the derivation of the above results in a moment, but first we make a few remarks on the nature of the equation and the effective diffusivity matrix.

The effective large-scale, long-time equation (13) is often called a "homogenized" equation because the effects of the advection by the relatively small-scale (heterogeneous) velocity field fluctuations (along with molecular diffusion) have been replaced by an overall effective diffusivity matrix $\mathscr{K}^*$ which is a constant "bulk" property of the fluid medium. Note that this homogenized diffusivity need not simply be a scalar multiple of the identity; anisotropies in the periodic flow can definitely influence the large scales. The homogenization procedure was first developed for problems such as heat conduction in a medium with periodic, fine-scale spatial fluctuations in conductivity (see for example [32]), and was adapted to advection–diffusion problems in [229,263].

We emphasize that the effective diffusivity is truly enhanced over the (nondimensionalized) bare molecular diffusion because $\bar{\mathscr{K}}$ is evidently a nonnegative-definite, symmetric matrix. The enhanced diffusivity matrix $\bar{\mathscr{K}}$ is always nontrivial when the flow has nonvanishing spatial gradients, and it depends, in our nondimensional units, on both the Péclet number and the temporal period τ_v. Of particular interest is its behavior at large Péclet number, and we develop some precise results along these lines in Paragraph 2.1.4.1 and in Section 2.2.

We finally remark that the homogenized effective equation (13a) also describes the long-time asymptotic evolution of the passive scalar density evolving from small-scale or even concentrated initial data [149]. The point is that even a delta-concentrated source will, on time scales $\mathrm{O}(\delta^{-2})$, spread over a large spatial scale $\mathrm{O}(\delta^{-1})$ due to molecular diffusion. Since the probability distribution function (PDF) of the position $\boldsymbol{X}(t)$ of a single tracer initially located at $\boldsymbol{x}_0$ obeys the advection–diffusion equation with initial data $T_0(\boldsymbol{x}) = \delta(\boldsymbol{x} - \boldsymbol{x}_0)$, it follows that the PDF for the tracer's location becomes Gaussian in the long-time limit, with mean $\boldsymbol{x}_0$ and covariance matrix growing at an enhanced diffusive rate:

$$\lim_{t\to\infty}\langle(\boldsymbol{X}(t) - \boldsymbol{x}_0)\otimes(\boldsymbol{X}(t) - \boldsymbol{x}_0)\rangle \sim 2\mathscr{K}^*t\ .$$

Note in particular that the asymptotic behavior of the tracer is independent of its initial position; the reason is that molecular diffusion will in time smear out the memory of the initial position.

We next sketch, following [32,149,205,263], how the homogenized effective equation for the rescaled passive scalar density $T^{(\delta)}(x,t)$ arises from a multiple scale asymptotic analysis. Subsequently, we will offer some physical interpretations for the homogenization formulas (14) and (15) for the effective diffusivity matrix.

2.1.2.2. Derivation of homogenized equation. We seek an asymptotic approximation to $T^{(\delta)}(x,t)$ of the following form in the $\delta \to 0$ limit:

$$T^{(\delta)}(x,t) = T_{\text{app},0}\left(x,\frac{x}{\delta},t,\frac{t}{\delta^2}\right) + \delta T_{\text{app},1}\left(x,\frac{x}{\delta},t,\frac{t}{\delta^2}\right) + \delta^2 T_{\text{app},2}\left(x,\frac{x}{\delta},t,\frac{t}{\delta^2}\right) + \cdots .\tag{17}$$

In accordance with the usual prescription for multiple scale analysis [158], we have explicitly accounted for the fact that the terms in the asymptotic expansion may suffer rapid oscillations in the $\delta \to 0$ limit due to the rapid oscillations in the coefficient of the advection term in the rescaled advection–diffusion equation (11). We label the arguments corresponding to the rapid oscillations as $\xi = x/\delta$ and $\tau = t/\delta^2$. In the functions appearing in the multiple scale asymptotic expansion (17), the variables (x, ξ, t, τ) may be treated as varying independently of one another, provided we replace space and time derivatives as follows:

$$\frac{\partial}{\partial t} \to \frac{\partial}{\partial t} + \delta^{-2}\frac{\partial}{\partial \tau} ,$$

$$\nabla \to \nabla_x + \delta^{-1}\nabla_\xi .$$

Substituting now Eq. (17) into the rescaled advection–diffusion equation (11), and separately equating terms of the three leading orders results in the following PDEs:

$$O(\delta^{-2})\colon Q^{(\text{per})} T_{\text{app},0} = 0 ,\tag{18a}$$

$$O(\delta^{-1})\colon Q^{(\text{per})} T_{\text{app},1} = -\,\text{Pe}\,v \cdot \nabla_x T_{\text{app},0} + 2\nabla_x \cdot \nabla_\xi T_{\text{app},0} ,\tag{18b}$$

$$O(\delta^0)\colon Q^{(\text{per})} T_{\text{app},2} = -\frac{\partial T_{\text{app},0}}{\partial t} - \text{Pe}\,v \cdot \nabla_x T_{\text{app},1} + 2\nabla_x \cdot \nabla_\xi T_{\text{app},1} + \Delta_x T_{\text{app},0} ,\tag{18c}$$

where the differential operator $Q^{(\text{per})}$ is defined:

$$Q^{(\text{per})} \equiv \partial/\partial\tau + \text{Pe}\,v(\xi, \tau/\tau_v) \cdot \nabla_\xi - \Delta_\xi .$$

Note that it involves only the variables ξ and τ, and that we may view $Q^{(\text{per})}$ as operating on functions with spatial period 1 in ξ and temporal period τ_v in τ. From the uniform parabolicity of this operator and the incompressibility of the velocity field, it follows from classical linear PDE theory ([105], Ch. 7) that we have the following *solvability condition* for $Q^{(\text{per})}$:

Given any smooth space–time periodic function $f(\xi, \tau)$, the equation

$$Q^{(\text{per})} g(\xi, \tau) = f(\xi, \tau)\tag{19}$$

has a smooth periodic solution $g(\xi, \tau)$ if and only if $f(\xi, \tau)$ has mean zero. This solution is moreover unique up to an arbitrary additive constant.

It follows in particular that the only functions of ξ and τ annihilated by $Q^{(\mathrm{per})}$ are constants, so Eq. (18a) implies that $T_{\mathrm{app},0}$ in fact only depends on the large-scale variables x and t:

$$T_{\mathrm{app},0}(x, \xi, t, \tau) = \bar{T}(x, t) \ . \tag{20}$$

Eq. (18b) therefore satisfies the solvability condition, since the right-hand side may be written as

$$- v(\xi, \tau) \cdot \nabla_x \bar{T}(x, t) \ ,$$

and v has mean zero. We can consequently express $T_{\mathrm{app},1}$ as

$$T_{\mathrm{app},1}(x, \xi, t, \tau) = \chi(\xi, \tau) \cdot \nabla_x \bar{T}(x, t) + C \ , \tag{21}$$

where C is some constant and $\chi(\xi, \tau)$ is the unique, periodic, mean zero solution to

$$Q^{(\mathrm{per})} \chi(\xi, \tau) = - \mathrm{Pe}\, v(\xi, \tau) \ . \tag{22}$$

Next, applying the solvability condition to Eq. (18c), we find that a necessary condition for the solution $T_{\mathrm{app},2}(x, \xi, t, \tau)$ to exist is that

$$\left\langle - \frac{\partial T_{\mathrm{app},0}}{\partial t} - \mathrm{Pe}\, v \cdot \nabla_x T_{\mathrm{app},1} + 2\nabla_\xi \cdot \nabla_x T_{\mathrm{app},1} + \varDelta_x T_{\mathrm{app},0} \right\rangle_{\mathrm{p}} = 0 \ . \tag{23}$$

The third term, which is the average of a divergence with respect to the variable ξ, vanishes by the divergence theorem. Substituting Eqs. (20) and (21) into this solvability relation, we have

$$- \frac{\partial \bar{T}(x, t)}{\partial t} - \mathrm{Pe} \sum_{i,j=1}^{d} \langle \chi_i(\xi, \tau) v_j(\xi, \tau) \rangle_{\mathrm{p}} \frac{\partial^2 \bar{T}(x, t)}{\partial x_i \partial x_j} + \varDelta_x \bar{T}(x, t) = 0 \ .$$

Symmetrizing the coefficient of the Hessian of $\bar{T}$ in the second term, we can rewrite this as

$$\partial \bar{T}(x, t)/\partial t = \nabla \cdot (\mathcal{K}^* \nabla \bar{T}(x, t)) \ , \tag{24}$$

where the effective diffusivity matrix is expressed

$$\mathcal{K}^* = \mathcal{I} + \bar{\mathcal{K}} \ , \tag{25}$$

$$\bar{\mathcal{K}}_{ij} = - \tfrac{1}{2}\mathrm{Pe}(\langle \chi_i(\xi, \tau) v_j(\xi, \tau) \rangle_{\mathrm{p}} + \langle \chi_j(\xi, \tau) v_i(\xi, \tau) \rangle_{\mathrm{p}}).$$

This is the content of the homogenization theorem, except that the formula for the enhanced diffusivity $\bar{\mathcal{K}}$ must still be massaged a bit more to bring it in the form stated in Eq. (15). Note that the effective diffusion equation for $\bar{T}(x, t)$ arises from a solvability condition for a higher-order $(\mathrm{O}(\delta^2))$, rapidly fluctuating term; this reflects the fact that the effective diffusivity is determined by how the small-scale passive scalar fluctuations equilibrate under the influence of the small-scale periodic variations in the velocity field (see below).

To show that Eq. (25) is equivalent to Eq. (15), use Eq. (22) to express v_j in terms of χ_j:

$$-\tfrac{1}{2}\text{Pe}\langle\chi_i v_j + \chi_j v_i\rangle_{\text{p}} = \tfrac{1}{2}\langle\chi_i Q^{(\text{per})}\chi_j + \chi_j Q^{(\text{per})}\chi_i\rangle_{\text{p}} = \tfrac{1}{2}\langle Q^{(\text{per})}(\chi_i\chi_j) + 2\nabla_\xi\chi_j\cdot\nabla_\xi\chi_i\rangle$$

$$= \langle\nabla_\xi\chi_i\cdot\nabla_\xi\chi_j\rangle\ .$$

The first term in the average in the penultimate equality vanishes because $\langle Q^{(\text{per})}g\rangle = 0$ for any function g (see the discussion near Eq. (19)).

The derivation we have presented shows that, at least formally, there exist functions $T_{\text{app},1}$ and $T_{\text{app},2}$ so that

$$\left(\frac{\partial}{\partial t} + \delta^{-1}v\left(\frac{x}{\delta},\frac{t}{\delta^2}\right) - \Delta\right)[T^{(\delta)}(x,t) - T^{(\delta)}_{\text{app}}(x,t)] = \text{O}(\delta)\ ,$$

where

$$T^{(\delta)}_{\text{app}}(x,t) \equiv \bar{T}(x,t) + \delta T_{\text{app},1}\left(x,\frac{x}{\delta},t,\frac{t}{\delta^2}\right) + \delta^2 T_{\text{app},2}\left(x,\frac{x}{\delta},t,\frac{t}{\delta^2}\right)$$

and $\bar{T}(x,t)$ solves Eq. (24). Using energy estimates and the maximum principle, it can be rigorously shown from this development that $T_{\text{app},1}$ and $T_{\text{app},2}$ are bounded and $\lim_{\delta\to 0}|T^{(\delta)}(x,t) - T^{(\delta)}_{\text{app}}(x,t)| = 0$, with both the boundedness and convergence uniform over all of space and over finite time intervals [149,205]. It follows from this that the $T^{(\delta)}(x,t)$ converges to $\bar{T}(x,t)$ in maximum norm as $\delta\to 0$. The gradient of $T^{(\delta)}(x,t)$, however, does not converge (strongly) to the gradient of $\bar{T}(x,t)$ because of rapid oscillations [264]; note from Eq. (21) that $\delta\nabla T_{\text{app},1}$ does not vanish in the $\delta\to 0$ limit.

2.1.2.3. Physical meaning of homogenization formulas and relation to eddy diffusivity modelling. We pause to remark upon the physical meaning of the cell problem (14) and the formula (15) for the homogenized diffusivity matrix which arose rather mechanically through self-consistent solvability conditions in the asymptotic expansion just presented. Note first that the passive scalar field will evolve much more rapidly on the small scales than the large, so the small-scale fluctuations of the passive scalar field will quickly reach a quasi-equilibrium state which depends on the local large-scale behavior of the passive scalar field. (This quasi-equilibrium state will be periodic in time, rather than steady, when the velocity field has periodic temporal fluctuations.) According to Eq. (21), the quasi-equilibrium behavior of the small-scale fluctuations is determined to leading order by the local gradient $\nabla T(x,t)$ of the large-scale variations of the passive scalar field. This is formally obvious from the advection–diffusion Eq. (11) rescaled to large space and time scales. From Eqs. (21) and (22), we see that $\chi_j(x,t)$ is exactly the response of the small-scale passive scalar fluctuations to a large-scale gradient of $T(x,t)$ directed along $\hat{e}_j$. Further discussion of this point may be found in [97,264].

We now show how the effective diffusivity formula (15) can be understood from a direct consideration of the advection–diffusion equation along with the multiple scale representation of the passive scalar field. When we view the passive scalar field on large scales, we are effectively taking a coarse-grained average over small scales. As the small-scale fluctuations are periodic, this coarse-graining is equivalent to (local) averaging over a spatio-temporal period cell. The

coarse-grained and rescaled advection–diffusion equation therefore reads

$$\frac{\partial \langle T^{(\delta)}(\boldsymbol{x}, t)\rangle_{\mathrm{p}}}{\partial t} + \delta^{-1}\mathrm{Pe}\left\langle \boldsymbol{v}\left(\frac{\boldsymbol{x}}{\delta}, \frac{t}{\delta^2 \tau_v}\right) \cdot \nabla T^{(\delta)}(\boldsymbol{x}, t)\right\rangle_{\mathrm{p}} = \varDelta \langle T^{(\delta)}(\boldsymbol{x}, t)\rangle_{\mathrm{p}} \,,$$

$$\langle T^{(\delta)}(\boldsymbol{x}, t = 0)\rangle_{\mathrm{p}} = T_0(\boldsymbol{x}) \,. \tag{26}$$

According to both formal intuition and the multiple scale analysis, the coarse-grained passive scalar field $\langle T^{(\delta)}(\boldsymbol{x}, t)\rangle_{\mathrm{p}}$ is, in the limit of strong scale separation ($\delta \to 0$), well approximated by a function $\bar{T}(\boldsymbol{x}, t)$ varying only on the large scales and independent of δ. The main challenge is to represent the coarse-grained average of the advective term in terms of $\bar{T}(\boldsymbol{x}, t)$. This differs from the simple factorization into averages over $\boldsymbol{v}$ and $T^{(\delta)}$ because of the coupling between the small-scale fluctuations of the velocity field and the small-scale fluctuations they induce in the passive scalar field. Though the small-scale fluctuations of the passive scalar field are O(δ) weak in amplitude relative to the main large-scale variation, they are relevant in determining the large-scale transport because they are integrated over large space and time scales.

We mentioned at the beginning of Section 2 an ad hoc approach to estimate the coarse-grained advective term as an eddy diffusivity. For the present case in which the velocity field has periodic spatio-temporal variations on scales strongly separated from those characterizing the leading-order passive scalar field, the closure hypothesis (5) is in fact precise and may be constructed from the multiple scale representation of the passive scalar field which was obtained in the derivation of the homogenization theorem:

$$T^{(\delta)}(\boldsymbol{x}, t) = \bar{T}(\boldsymbol{x}, t) + \delta T_{\mathrm{app}, 1}\left(\boldsymbol{x}, \frac{\boldsymbol{x}}{\delta}, t, \frac{t}{\delta^2}\right) + \mathrm{O}(\delta^2) \,,$$

$$T_{\mathrm{app}, 1}(\boldsymbol{x}, \boldsymbol{\xi}, t, \tau) = \boldsymbol{\chi}(\boldsymbol{\xi}, \tau) \cdot \nabla_x \bar{T}(\boldsymbol{x}, t) + C \,. \tag{27}$$

Using the incompressibility of the velocity field to re-express the average of the advective term in Eq. (26), and substituting the asymptotic expansion (27) into it, we obtain

$$\delta^{-1}\mathrm{Pe}\left\langle \boldsymbol{v}\left(\frac{\boldsymbol{x}}{\delta}, \frac{t}{\delta^2 \tau_v}\right) \cdot \nabla T^{(\delta)}(\boldsymbol{x}, t)\right\rangle_{\mathrm{p}} = \delta^{-1}\mathrm{Pe} \, \nabla \cdot \left\langle \boldsymbol{v}\left(\frac{\boldsymbol{x}}{\delta}, \frac{t}{\delta^2 \tau_v}\right) T^{(\delta)}(\boldsymbol{x}, t)\right\rangle_{\mathrm{p}}$$

$$= \delta^{-1}\mathrm{Pe} \, \nabla \cdot \left\langle \boldsymbol{v}\left(\frac{\boldsymbol{x}}{\delta}, \frac{t}{\delta^2 \tau_v}\right) \bar{T}(\boldsymbol{x}, t)\right\rangle_{\mathrm{p}} + \mathrm{Pe} \, \nabla \cdot \left\langle \boldsymbol{v}\left(\frac{\boldsymbol{x}}{\delta}, \frac{t}{\delta^2 \tau_v}\right) T_{\mathrm{app}, 1}\left(\boldsymbol{x}, \frac{\boldsymbol{x}}{\delta}, t, \frac{t}{\delta^2}\right)\right\rangle_{\mathrm{p}} + \mathrm{O}(\delta) \,. \tag{28}$$

The remainder term is indeed O(δ), not withstanding the divergence acting on the expectation $\langle \cdot \rangle_{\mathrm{p}}$, because the averaging over the period cell removes the rapid oscillations. The first term appearing after the last equality in Eq. (28) vanishes because $\boldsymbol{v}$ is the only rapidly oscillating factor in the argument, and has zero average over the period cell. Therefore, we are left with an expression which takes the form of an enhanced diffusion term involving the coupling of the small-scale fluctuations of the velocity field with the small-amplitude, small-scale fluctuations induced in the passive scalar field

$$\delta^{-1}\mathrm{Pe}\left\langle \boldsymbol{v}\left(\frac{\boldsymbol{x}}{\delta}, \frac{t}{\delta^2 \tau_v}\right) \cdot \nabla T^{(\delta)}(\boldsymbol{x}, t)\right\rangle_{\mathrm{p}} = \mathrm{Pe} \, \nabla \cdot \left\langle \boldsymbol{v}\left(\frac{\boldsymbol{x}}{\delta}, \frac{t}{\delta^2 \tau_v}\right) T_{\mathrm{app}, 1}\left(\boldsymbol{x}, \frac{\boldsymbol{x}}{\delta}, t, \frac{t}{\delta^2}\right)\right\rangle_{\mathrm{p}}$$

$$= \mathrm{Pe} \sum_{i=1}^{d} \frac{\partial}{\partial x_i}\left(\langle v_i \chi_j\rangle_{\mathrm{p}} \frac{\partial \bar{T}(\boldsymbol{x}, t)}{\partial x_j}\right) = -\mathrm{Pe} \sum_{i=1}^{d} \mathscr{K}_{ij} \frac{\partial^2 \bar{T}(\boldsymbol{x}, t)}{\partial x_i \partial x_j} \,,$$

with the enhanced diffusivity

$$\bar{\mathcal{K}}_{ij} = -\tfrac{1}{2}(\langle v_i \chi_j \rangle_{\mathrm{p}} + \langle v_j \chi_i \rangle_{\mathrm{p}}) \ .$$

This agrees with expression (25), which was subsequently shown to be equivalent to formula (15).

2.1.3. Generalization of homogenization theory to include large-scale flows

We now show how the homogenization for periodic flows described above can be extended to allow for the presence of certain kinds of large-scale mean flow components in the velocity field. We treat in turn the cases of a steady periodic flow with a constant mean drift, and then a superposition of a weak, large-scale mean flow with small-scale, periodic spatio-temporal fluctuations.

2.1.3.1. Constant mean flow. In several applications, fluid is driven along a specific direction by a large-scale pressure gradient, and the resulting flow pattern consists of some mean constant motion and fluctuations induced either by flow instability or by variations in the properties of the medium through which the fluid is drawn [223]. A simple but instructive idealization of such flows is a superposition of a constant, uniform velocity V with a mean zero, steady periodic flow $v(x)$ representing the fluctuations. This can serve as a prototype model for hydrological flows through porous media [130]. We will often refer to a spatially constant mean flow such as V as a *mean sweep*. Now we show how the homogenization theory can be generalized to incorporate the mean sweep V.

The nondimensionalized form of the advection–diffusion equation (9) is modified to

$$\partial T(x,t)/\partial t + \mathrm{Pe}(V + v(x))\cdot\nabla T(x,t) = \Delta T(x,t) \ ,$$
$$T(x,t = 0) = \delta^d T_0(\delta x) \ . \tag{29}$$

An immediate large-scale, long-time rescaling (10) of this equation would produce a term $\delta^{-1}\mathrm{Pe}V\cdot\nabla T^{(\delta)}(x,t)$. This term is singular in the $\delta \to 0$ limit, and would create difficulties at the $O(\delta^{-1})$ level in the multiple scale analysis of Paragraph 2.1.2.2 because V does not have zero average over a period cell.

A preliminary Galilean transformation to a frame comoving with the mean flow,

$$\tilde{T}(x,t) \equiv T(x + Vt)$$

however, averts this obstacle. The advection–diffusion equation for $\tilde{T}(x,t)$ reads

$$\partial \tilde{T}(x,t)/\partial t + \mathrm{Pe}\,v(x - Vt)\cdot\nabla\tilde{T}(x,t) = \Delta\tilde{T}(x,t) \ ,$$
$$\tilde{T}(x,t = 0) = \delta^d T_0(\delta x) \ .$$

Now, if each component of V is an integer multiple of a common real number λ, then $v(x - Vt)$ would be mean zero with spatial period 1 in each coordinate direction and temporal period λ^{-1}. The homogenization theory of Section 2.1.2 can then be directly applied, yielding the following statement.

Homogenized effective diffusion equation for steady, periodic velocity fields with constant mean flow: The large-scale, long-time limit of the passive scalar field,

$$\bar{T}(x,t) \equiv \lim_{\delta \to 0} T^{(\delta)}(x,t), \qquad T^{(\delta)}(x,t) \equiv \delta^{-d}\tilde{T}(\delta x, \delta^2 t) \ ,$$

obeys an effective diffusion equation

$$\partial \bar{T}(\boldsymbol{x}, t)/\partial t = \nabla \cdot (\mathcal{K}^* \nabla \bar{T}(\boldsymbol{x}, t)) , \tag{30}$$

$$\bar{T}(\boldsymbol{x}, t = 0) = T_0(\boldsymbol{x}) . \tag{31}$$

The effective diffusivity matrix $\mathcal{K}^*$ in this equation can be expressed as

$$\mathcal{K}^* = \mathcal{I} + \bar{\mathcal{K}}$$

with the enhanced diffusivity $\bar{\mathcal{K}}$ given by

$$\bar{\mathcal{K}}_{ij} = \langle \nabla \chi_i \cdot \nabla \chi_j \rangle_{\mathrm{p}} , \tag{32}$$

where $\boldsymbol{\chi}(\boldsymbol{x})$ is the (unique) mean zero, periodic solution to the following parabolic cell problem:

$$\frac{\partial \boldsymbol{\chi}(\boldsymbol{x}, t)}{\partial t} + \mathrm{Pe}\, \boldsymbol{v}(\boldsymbol{x} - \boldsymbol{V}t) \cdot \nabla \boldsymbol{\chi}(\boldsymbol{x}, t) - \Delta \boldsymbol{\chi}(\boldsymbol{x}, t) = -\mathrm{Pe}\, \boldsymbol{v}(\boldsymbol{x} - \boldsymbol{V}t) .$$

It is helpful to note that the period cell average in Eq. (32) is unchanged if $\boldsymbol{\chi}(\boldsymbol{x}, t)$ is replaced by $\boldsymbol{\chi}(\boldsymbol{x} - \boldsymbol{V}t, t)$, so the cell problem can be replaced by the purely spatial, elliptic PDE [210,230]:

$$\mathrm{Pe}(\boldsymbol{V} + \boldsymbol{v}(\boldsymbol{x})) \cdot \nabla \boldsymbol{\chi}(\boldsymbol{x}) - \Delta \boldsymbol{\chi}(\boldsymbol{x}) = -\mathrm{Pe}\, \boldsymbol{v}(\boldsymbol{x}) . \tag{33}$$

When the components of $\boldsymbol{V}$ cannot be expressed as integer multiples of a common real number, then the velocity field $\boldsymbol{v}(\boldsymbol{x} + \boldsymbol{V}t)$ is *quasiperiodic* rather than periodic. It can still be argued through more sophisticated means [38], however, that the homogenization formulas presented above carry over for general $\boldsymbol{V}$ without change.

2.1.3.2. Weak large-scale mean flow. It would be very interesting to describe the large-scale, long-time evolution of the passive scalar field in the more general situation in which the mean flow varies on large spatial and slow time scales. Such a velocity field could be a heuristically useful (but greatly simplified) idealization of an inhomogenous turbulent flow in which some mean large-scale flow profile is disturbed by turbulent fluctuations represented as small-scale periodic fluctuations. Unfortunately, there does not appear to be a homogenization theory which generally describes the net large-scale transport properties arising from the interaction between the large-scale mean flow, the periodic fluctuations, and molecular diffusion. The goals of such a program, however, can be concretely illustrated by consideration of large-scale mean flows which are *weak* in a sense which we now describe.

For simplicity, we shall assume that the length scale of the large-scale velocity field coincides with that of the initial passive scalar field $L_V = L_T$ and that the time scale of the large-scale velocity field is given by $\delta^{-2} L_v^2/\kappa$, which is $O(\delta^{-2})$ slow relative to the natural molecular diffusion time scale. We do *not* assume that the large-scale velocity field is periodic. As important special cases, we allow the large-scale velocity field to be steady and/or spatially uniform. The large-scale mean flow will further be assumed weak in that its amplitude is $O(\delta)$ relative to the amplitude of the small-scale periodic velocity field. In units nondimensionalized according to the prescription in Section 2.1.1, the total velocity field (mean flow with periodic fluctuations) has the form

$$\mathrm{Pe}[\delta \boldsymbol{V}(\delta \boldsymbol{x}, \delta^2 t/\tau_v) + \boldsymbol{v}(\boldsymbol{x}, t/\tau_v)] .$$

The advection–diffusion equation for the passive scalar field $T^{(\delta)}(\mathbf{x}, t)$ (10) rescaled to large scales and long times then becomes (cf. (11))

$$\frac{\partial T^{(\delta)}(\mathbf{x}, t)}{\partial t} + \mathrm{Pe}\left[\mathbf{V}(\mathbf{x}, t/\tau_v) + \delta^{-1}\mathbf{v}\left(\frac{\mathbf{x}}{\delta}, \frac{t}{\delta^2\tau_v}\right)\right] \cdot \nabla T^{(\delta)}(\mathbf{x}, t) = \varDelta T^{(\delta)}(\mathbf{x}, t) ,$$

$$T^{(\delta)}(\mathbf{x}, t = 0) = T_0(\mathbf{x}) .$$

Because the mean flow was assumed to be $O(\delta)$ weak, it produces a regular, order unity advection term in the rescaled coordinates. The multiple scale analysis of Paragraph 2.1.2.2 can now be directly generalized to include the effects of the weak mean flow, which only modifies the $O(\delta^0)$ equation in Eq. (18c). If $\mathbf{V}(\mathbf{x}, t/\tau_v)$ is smooth and bounded, the homogenization theorem for purely periodic velocity fields can be rigorously extended [209] to state that in the present case, $T^{(\delta)}(\mathbf{x}, t)$ converges as $\delta \to 0$ to a nontrivial limit $\bar{T}(\mathbf{x}, t)$ which satisfies the following large-scale, effective "homogenized" advection–diffusion equation:

$$\partial \bar{T}(\mathbf{x}, t)/\partial t + \mathbf{V}(\mathbf{x}, t/\tau_v) \cdot \nabla \bar{T}(\mathbf{x}, t) = \nabla \cdot (\mathscr{K}^* \nabla \bar{T}(\mathbf{x}, t)) , \tag{34}$$

$$\bar{T}(\mathbf{x}, t = 0) = T_0(\mathbf{x}) . \tag{35}$$

The homogenized diffusivity $\mathscr{K}^*$ is determined through the same formula and cell problem (14) as in the case of no mean flow. In other words, $\mathscr{K}^*$ is completely independent of $\mathbf{V}(\mathbf{x}, t/\tau_v)$.

The homogenized equation (35) is a rigorous realization of the goal of large-scale modelling of passive scalar transport by a velocity field with a macroscopic mean flow component and small-scale fluctuations. The small-scale periodic fluctuations affect the large-scale passive scalar dynamics purely through an enhancement of diffusivity, while the mean flow appears straightfor-wardly in the advection term. We stress that this simple picture relies crucially on the assumptions that the mean flow is weak and that there is a strong separation between the scales of the fluctuating and mean components of the velocity field. Neither of these assumptions is generally valid in realistic turbulent flows, and the effective description of the large-scale passive scalar dynamics can be expected to be considerably more complicated [182,286]. Moreover, homogeniz-ation theory is only valid on sufficiently large $(O(\delta^{-2}))$ time scales; we explore the practical relevance of this condition in Section 2.3. Nonetheless, since no precise theories analogous to homogenization theory have yet been developed for realistic turbulent flows, there is much we can learn about passive scalar transport by careful study of small-scale periodic velocity fields, for which we can obtain certain results rigorously.

McLaughlin and Forest [232] have recently investigated the effects of another kind of large-scale variation on the transport of a passive scalar field in a periodic velocity field. In this work, the velocity field is chosen as a large-scale, compressible modulation of a periodic, incompressible, small-scale flow. The weak compressibility of the flow models the response to a large-scale stratification of the density of the fluid (as in the atmosphere) through the anelastic equations. A homogenized equation for the evolution of the passive scalar field on large scales and long times is derived through a modification of the multiple scale analysis described in Paragraph 2.1.2.2. This homogenized equation has variable coefficients reflecting the large-scale variation in the fluid density, and its solutions can exhibit focusing and the formation of nontrivial spatial structures. Several numerical simulations in [232] compare the evolution of these solutions to those of the

standard diffusion equations resulting from the homogenization of purely incompressible, periodic velocity fields.

We proceed next to develop some tools for characterizing the effective diffusivity arising from homogenization theory, which we will apply in Section 2.2 to several instructive classes of flows. We will in particular underscore the subtle influence which a constant mean flow can have on the effective passive scalar diffusivity [210]. Some aspects of passive scalar transport at finite (non-asymptotic) time scales will be illustrated explicitly in Section 2.3.

2.1.4. Alternative representations and bounds for effective diffusivity

Homogenization theory rigorously reduces the description of the large-scale, long-time dynamics of the passive scalar field to the determination of a constant effective diffusivity matrix $\mathscr{K}^*$, which however still requires the solution of a nontrivial cell problem (14). This cell problem can be solved explicitly for some special flows (see Sections 2.2.1 and 2.2.2), but must in general be treated by some approximate analytical or numerical methods. We present here some alternative analytical representations of the effective diffusivity which are useful for obtaining rigorous, computable estimates, particularly concerning its asymptotic dependence on large Péclet number. We will discuss the numerical solution of cell problems for some specific flows in Sections 2.2.3, 2.2.4 and 2.2.5.

2.1.4.1. Stieltjes integral representation.

One way to attempt to analyze the cell problem in general is to treat Pe as a small parameter, and to construct a perturbative solution for $\chi(x, t)$ as an ascending power series in Pe [181,224]. This is not difficult to construct, since the zeroth-order equation is just the ordinary heat equation in periodic geometry. The drawback to this approach is that the resulting series has a very limited radius of convergence [9,12,181], making this approach limited for typical applications in which the Péclet number is substantial or very large. Some formal diagramatic resummation techniques have been proposed in the context of turbulence and field theory to attempt to extract meaningful information from a formal power series at parameter values (i.e. high Péclet number) where they diverge [181]. The validity of these methods is open to question, however, since they typically neglect a wide class of terms in the power series, without clean justification. Fortunately, an exact and rigorous diagrammatic resummation is possible for the homogenized effective diffusivity matrix $\mathscr{K}^*$ of a periodic velocity field, and gives rise to a *Stieltjes measure representation* which is valid for arbitrary Péclet number [9,11,12]. Here we will formally sketch a more direct way [9,12,39,210] of achieving the Stieltjes measure representation formula, focusing on the case of a *steady* periodic velocity field with a constant (possibly zero) mean sweep V.

The cell problem for each component $\chi_j(x)$ in this case may be expressed as follows (cf. Eq. (33)):

$$\Delta \chi_j(x) - \mathrm{Pe}(V + v(x)) \cdot \nabla \chi_j(x) = \mathrm{Pe}\, v_j(x) \ .$$

This equation can be rewritten as an abstract integral equation for $\nabla \chi_j(x)$ by application of the operator $\nabla \Delta^{-1}$ to both sides. We then obtain

$$(\mathscr{I} - \mathrm{Pe}\, \mathscr{A}^V) \cdot \nabla \chi_j = \mathrm{Pe}\, \mathscr{A} \hat{e}_j \ , \tag{36}$$

with $\mathscr{I}$ the identity matrix. The other operators are defined on the Hilbert space $L^2(\mathbb{T}^d)$ of periodic, square-integrable functions as follows:

$$\mathscr{A}\boldsymbol{g} = \nabla\Delta^{-1}(\boldsymbol{v}(\boldsymbol{x})\cdot\boldsymbol{g}) \,, \tag{37a}$$

$$\mathscr{A}^V\boldsymbol{g} = \nabla\Delta^{-1}((\boldsymbol{V} + \boldsymbol{v}(\boldsymbol{x}))\cdot\boldsymbol{g}) \,. \tag{37b}$$

A key property of these operators, which follows from incompressibility of the velocity field, is that they are *compact* [281] and *skew symmetric* when restricted to the subspace $L^2_{\bar{\mathrm{V}}}(\mathbb{T}^d)$ of square-integrable (generalized) *gradients* of periodic functions

$$L^2_{\bar{\mathrm{V}}}(\mathbb{T}^d) = \{\boldsymbol{g} = \nabla f \colon \langle|f|^2\rangle_{\mathrm{p}} + \langle|\boldsymbol{g}|^2\rangle_{\mathrm{p}} < \infty\} \,. \tag{38}$$

These properties are more apparent when the operators are reformulated in terms of the stream function (or stream matrix), see [12]. The spectral theory of compact, skew-symmetric operators [281] guarantees the existence of an orthonormal basis of functions in $L^2_{\bar{\mathrm{V}}}(\mathbb{T}^d)$ which are eigenfunctions of $\mathscr{A}^V$ with purely imaginary eigenvalues. Moreover, the eigenvalues and eigenfunctions come in complex conjugate pairs, with the magnitude of the eigenvalues clustering asymptotically near zero. We may therefore index the eigenvalues by $\{\pm i\mu^{(n)}\}_{n=1}^{\infty}$ where $\mu^{(n)}$ is a real, positive sequence decreasing toward zero; there may also possibly be a zero eigenvalue of $\mathscr{A}^V$.

The cell problem (36) may now be solved by expanding $\nabla\chi_j(\boldsymbol{x})$ and $\mathscr{A}\hat{e}_j$ (which is in $L^2_{\bar{\mathrm{V}}}(\mathbb{T}^d)$) in terms of the eigenfunctions of the operator $\mathscr{A}^V$. Substituting the result into the effective diffusivity formula (32), we thereby achieve the *Stieltjes Integral Representation Formula* for the enhanced diffusivity along any given direction $\hat{e}$ in a steady periodic velocity field with a possible constant mean sweep:

$$\hat{e}\cdot\bar{\mathscr{K}}\cdot\hat{e} = \mathrm{Pe}^2\|\boldsymbol{v}\cdot\hat{e}\|^2_{-1}\left[a^{(0)} + 2\sum_{n=1}^{\infty}\frac{a^{(n)}}{1 + \mathrm{Pe}^2(\mu^{(n)})^2}\right]. \tag{39}$$

The parts of this formula which remain to be explained are:

- An order unity prefactor measuring the magnitude of the nondimensionalized velocity field in a certain (Sobolev) norm ([105], Ch. 6),

$$\|\boldsymbol{v}\cdot\hat{e}\|^2_{-1} \equiv \langle|\mathscr{A}\hat{e}|^2\rangle_{\mathrm{p}} = \sum_{\boldsymbol{k}\in\mathbb{Z}^d}\frac{|\hat{\boldsymbol{v}}_{\boldsymbol{k}}\cdot\hat{e}|^2}{4\pi^2|\boldsymbol{k}|^2} \,, \tag{40}$$

where $\hat{\boldsymbol{v}}_{\boldsymbol{k}}$ are the Fourier coefficients of $\boldsymbol{v}(\boldsymbol{x})$.
- The mean square $a^{(0)} = \langle|g^{(0)}|^2\rangle_{\mathrm{p}}$ of the projection $g^{(0)}$ of the normalized function $\mathscr{A}\hat{e}/\langle|\mathscr{A}\hat{e}|^2\rangle_{\mathrm{p}}^{1/2}$ onto the null space of $\mathscr{A}^V$ in $L^2_{\bar{\mathrm{V}}}(\mathbb{T}^d)$.
- The mean square $a^{(n)} = \langle|g^{(n)}|^2\rangle_{\mathrm{p}}$ of the projection $g^{(n)}$ of the normalized function $\mathscr{A}\hat{e}/\langle|\mathscr{A}\hat{e}|^2\rangle_{\mathrm{p}}^{1/2}$ onto the eigenspace of $\mathscr{A}^V$ in $L^2_{\bar{\mathrm{V}}}(\mathbb{T}^d)$ corresponding to eigenvalue $i\mu^{(n)}$ (or equivalently to $-i\mu^{(n)}$).

The normalization by the factor $\langle|\mathscr{A}\hat{e}^2\rangle_{\mathrm{p}}$ implies that

$$\sum_{n=-\infty}^{\infty}a^{(n)} = a^{(0)} + 2\sum_{n=1}^{\infty}a^{(n)} = 1 \,,$$

so the $\{a^{(n)}\}$ may be interpreted as the weights of a normalized discrete measure,

$$\mathrm{d}\rho_{v,V} = \left[a^{(0)}\delta(\mu) + \sum_{n=1}^{\infty} a^{(n)}(\delta(\mu - \mu^{(n)}) + \delta(\mu + \mu^{(n)})) \right]\mathrm{d}\mu \ .$$

The summation appearing in Eq. (39) therefore has the form of a Stieltjes integral against this discrete measure:

$$\hat{e}\cdot\bar{\mathscr{K}}\cdot\hat{e} = \mathrm{Pe}^2\|\boldsymbol{v}\cdot\hat{e}\|^2_{-1}\int_{-\infty}^{\infty}\frac{\mathrm{d}\rho_{v,V}}{1 + \mathrm{Pe}^2\mu^2} \ . \tag{41}$$

The Stieltjes integral representation for the effective diffusivity in a periodic velocity field was derived by Avellaneda and the first author [9,12] and in a slightly different form by Bhattacharya et al. [39]. Similar, but more notationally complex, formulas for off-diagonal elements of $\bar{\mathscr{K}}$ may be found in [39]. A similar Stieltjes integral representation was derived by Avellaneda and Vergassola [20] for spatio-temporal periodic velocity fields with no mean sweep. The only difference is that the definition (37b) of the operator $\mathscr{A}^V$ is to be replaced by

$$\mathscr{A}^V\boldsymbol{g} = \nabla\varDelta^{-1}(\boldsymbol{v}(\boldsymbol{x}, t/\tau_v)\cdot\boldsymbol{g}) + (\partial/\partial t)\varDelta^{-1}\boldsymbol{g} \ , \tag{42}$$

which is still real, compact and skew-symmetric on the subspace of square-integrable gradients of spatio-temporal periodic functions, $L^2_{\bar{\nabla}}(\mathbb{T}^d \times [0, \tau_v])$.

Note that the formal expansion of the summands in Eq. (39) in powers of Pe will recover a formal power series which converges only for $|\mathrm{Pe}| < (\mu^{(1)})^{-1}$ [9,12]. The Stieltjes integral representation may be interpreted as a rigorous resummation of this series which is valid for all Pe; this is demonstrated explicitly in [11]. The Stieltjes integral is admittedly too difficult to evaluate directly in general because the full spectral information of the operator $\mathscr{A}^V$ is required. Nonetheless, as we shall now describe, much practically useful information can be deduced from the Stieltjes integral representation.

Rigorous bounds through Padé approximants: The Stieltjes integral representation (41) first of all permits the construction of rigorous upper and lower bounds on the effective diffusivity for *all Péclet number*. By noting that $\mathrm{d}\rho_{v,V}$ is a nonnegative measure with total integral equal to unity, we can immediately deduce the following elementary lower and upper bounds on the effective diffusivity [12]:

$$1 \le \hat{e}\cdot\mathscr{K}^*\cdot\hat{e} \le 1 + \mathrm{Pe}^2\|\boldsymbol{v}\cdot\hat{e}\|^2_{-1} \ . \tag{43}$$

The Stieltjes integral representation also makes it possible to construct sharper bounds on the effective diffusivity using information from a finite number of terms in a *small Péclet number* expansion, which can be determined by a straightforward formal perturbation procedure [12,181]. Suppose one has obtained in this way a small Péclet number asymptotic expansion of $\hat{e}\cdot\mathscr{K}^*\cdot\hat{e}$:

$$\hat{e}\cdot\mathscr{K}^*\cdot\hat{e} = 1 + \sum_{m=1}^{M} \mathrm{Pe}^{2m}b_{2m} + \mathrm{O}(\mathrm{Pe}^{2m+2}) \ , \tag{44}$$

where b_{2m} are some constants involving explicit integrals which can be evaluated or at least estimated numerically [12,40]. Comparing with a formal small Péclet number expansion of the Stieltjes integral representation (41), we find that each b_{2m} is proportional to the moment of order $2(m-1)$ of the measure $d\rho_{v,V}$. The knowledge of these moments implies rigorous restrictions for the values which $\hat{e} \cdot \mathcal{K}^* \cdot \hat{e}$, given by the Stieltjes integral representation (41), may attain for arbitrary values of Péclet number. More precisely, it has been shown [12,337] that $\hat{e} \cdot \mathcal{K}^* \cdot \hat{e}$ is rigorously bounded above and below, for all Péclet number, by certain Padé approximants, which are rational functions of Pe explicitly constructed from the coefficients of the perturbation series (44) (see for example [30]). Padé approximants were applied to construct rigorous bounds for the effective diffusivity in certain periodic flows in [40]; some of this work will be briefly discussed in Section 2.2.5. The Padé approximant bounds may also be used to rigorously extrapolate the value of $\mathcal{K}^*$ over a range of Pe, given its measured value at a finite set of Pe, and to check the validity of Monte Carlo simulations for the effective diffusivity [12,40].

Maximal and minimal enhanced diffusivity: While the Padé approximants can produce sharp estimates of the effective diffusivity for small and moderate values of the Péclet number, they eventually deteriorate at sufficiently large Pe [40]. One finds only that the effective diffusivity in the asymptotic regime of large Péclet number must exceed some constant independent of Pe, but cannot grow more quickly than Pe^2, which is indicated already by the simplest bounds (43). The high Péclet number asymptotics of the effective diffusivity are however of considerable practical interest, since the Péclet number can be quite large in a number of natural and experimental situations.

One important question is how rapidly the effective diffusivity grows with Péclet number. Following the work of McLaughlin and the first author in [210], we classify two extreme situations. We say that flows produce

- *maximally enhanced diffusion* in a certain direction $\hat{e}$ when the diffusivity along this direction grows quadratically with Pe as Pe $\to \infty$. This is the most rapid growth possible, according to Eq. (43).
- *minimally enhanced diffusion* in the direction $\hat{e}$ if the effective diffusivity remains uniformly bounded in this direction for arbitrarily large Pe.

Explicit shear flow examples will be presented in Section 2.2.1 which demonstrate the realizability of both of these extreme behaviors. Other large Pe number behavior can be realized by various flows (see Section 2.2.3); the classes of flow which are maximally or minimally diffusive in a given direction are not exhaustive.

The Stieltjes integral representation provides some simple general criteria for determining whether a given flow will be maximally or minimally diffusive in a given direction $\hat{e}$. It is evident from Eq. (39) that maximally enhanced diffusion is equivalent to $a^{(0)} \neq 0$. This is rigorously verified in [39,210], where it is moreover demonstrated that maximal diffusivity along $\hat{e}$ is equivalent to the existence of a complex periodic function $h(x)$ which is constant along streamlines,

$$(V + v(x)) \cdot \nabla h(x) = 0 , \tag{45}$$

has a nontrivial projection against $v(x) \cdot \hat{e}$,

$$\langle hv \cdot \hat{e} \rangle_p \neq 0 ,$$

and is sufficiently smooth that it belongs to the Sobolev space $H^1(\mathbb{T}^d)$ of complex periodic, square-integrable functions with square-integrable (generalized) derivatives ([105], Ch. 6).

These conditions for maximal diffusivity along a direction $\hat{e}$ have been interpreted in a rigorous, geometric manner by Mezić et al. [239] as indicating a lack of ergodicity of $\boldsymbol{v} \cdot \hat{e}$; that is, the average value of $\boldsymbol{v} \cdot \hat{e}$ along streamlines is not everywhere zero. The reason why this situation gives rise to maximally enhanced diffusion is that, in the absence of molecular diffusion, particles on streamlines with a nonzero average value of $\boldsymbol{v} \cdot \hat{e}$ would proceed in the direction $\hat{e}$ at a ballistic rate (distance linearly proportional to time) [168]. Such streamlines are often manifested as open channels [210], as we shall see concretely in Section 2.2. Molecular diffusion acts as an impediment to the rapid transport along these open channels by knocking tracers into other streamline channels with average values of $\boldsymbol{v} \cdot \hat{e}$ with the opposite sign. (Such compensatory channels must exist since $\boldsymbol{v} \cdot \hat{e}$ has mean zero). The net result at long time is a diffusive motion along $\hat{e}$ (on top of any constant mean drift $\boldsymbol{V} \cdot \hat{e}$), with the effective diffusivity constant growing rapidly with Péclet number, since a high Péclet number permits particles to travel a long way along open channels before getting knocked away from them by molecular diffusion.

If $a^{(0)} = 0$, then the Stieltjes integral representation (39) implies that the tracer diffusion is not maximally diffusive, but does not necessarily imply that the tracer motion is minimally diffusive. Even though the contribution from each term in the sum from $n = 1$ to ∞ individually approaches a finite constant in the Pe $\to \infty$ limit, the full sum can still diverge in the Pe $\to \infty$ limit depending on how rapidly the eigenvalues $\mu^{(n)}$ approach zero. More information is needed to determine whether a flow produces minimally enhanced diffusion or not. One sufficient condition for minimally enhanced diffusion along a direction $\hat{e}$ established in [39,210] is the existence of a periodic function $\boldsymbol{g} \in H^1(\mathbb{T}^d)$ which satisfies the equation

$$(\boldsymbol{V} + \boldsymbol{v}(\boldsymbol{x})) \cdot \nabla g(\boldsymbol{x}) = - v(\boldsymbol{x}) \ . \tag{46}$$

Whereas maximally enhanced diffusion along a direction $\hat{e}$ is associated with open channels, minimally enhanced diffusion along $\hat{e}$ appears to be related to the presence of a layer of streamlines which block flow along the $\hat{e}$ direction [210], as we shall illustrate in Sections 2.2.3 and 2.2.4. The effective diffusivity along blocked directions $\hat{e}$ remains bounded in proportion to the molecular diffusivity, regardless of how large Pe becomes, because the transport rate is always limited by the need for the tracer to cross the layer of blocked streamlines, which only molecular diffusion can accomplish. Indeed, in the limit of no molecular diffusivity, the motion of the tracer along a blocked direction $\hat{e}$ would remain forever trapped.

We caution the reader that our care in stating the function spaces to which solutions of Eqs. (45) and (46) is quite essential. If one were to naively treat these equations in the same way as finite-dimensional linear algebra problems, one would wrongly conclude that any flow produces either maximally or minimally enhanced diffusion. Such a supposition is falsified by the example of steady cellular flows which are neither maximally nor minimally diffusive, as we shall discuss in Section 2.2.3. In particular, even though the nice streamline structure of this flow (Fig. 2) permits a formal construction of a function h constant along streamlines and thereby satisfying Eq. (45), it turns out that any such function is not smooth enough at the corners of the period cell to be in $H^1(\mathbb{T}^d)$. Therefore, the condition for maximally enhanced diffusion is *not* satisfied by the steady cellular flow, but one could be misled if the smoothness considerations are not taken into account.

The above rigorous criteria for maximal and minimal diffusivity have been gainfully applied by McLaughlin and the first author [210] to categorize the effects of a nonzero constant mean flow on effective transport, and we shall describe some of these results in Section 2.2.4. Some other applications of the critera for maximal and minimal diffusivity to some special classes of flows, particularly involving special kinds of streamline blocking, may be found in [39].

2.1.4.2. Variational principles. Another useful representation of the homogenized diffusivity is through a variational principle. Avellaneda and the first author [12] introduced the first such variational principle for steady, periodic velocity fields $v(x)$ with no mean sweep:

For all vectors $\hat{e} \in \mathbb{R}^d$, the effective diffusivity along direction $\hat{e}$ may be expressed as the following minimization problem:

$$\hat{e} \cdot \mathcal{K}^* \cdot \hat{e} = \min_{g : g - \hat{e} \in L^2_{\mathrm{v}}(\mathbb{T}^d)} \langle |g|^2 + \mathrm{Pe}^2 g \cdot \mathcal{K} \cdot g \rangle_{\mathrm{p}} , \qquad (47)$$

where the nonnegative, self-adjoint operator $\mathcal{K}$ is defined

$$\mathcal{K} = (\mathscr{A})^{\dagger} \mathscr{A}$$

and $L^2_{\mathrm{v}}(\mathbb{T}^d)$ is the Hilbert space of square-integrable gradients defined in (38).

This variational principle allows us to generate rigorous upper bounds on the effective diffusivity by substituting arbitrary functions g with $g - \hat{e} \in L^2_{\mathrm{v}}(\mathbb{T}^d)$ into the functional on the right-hand side of Eq. (47). Note that the functional to be minimized involves the *nonlocal* operator $\mathcal{K}$. Fortunately, in certain cases, the calculation can be greatly simplified by a suitable choice of trial fields g.

A related dual (nonlocal) maximal variational principle was later derived by Fannjiang and Papanicolaou [97]. By carefully using the minimal and maximal variational principles in tandem, the effective diffusivity can be estimated in a fairly sharp manner for certain tractable classes of flows. These authors also formulate some *local* minimax variational principles as well as variational principles for the effective diffusivity of time-dependent periodic velocity fields.

We mention in passing that another, philosophically different, variational approach to deriving rigorous upper bounds for the effective diffusivity of a passive scalar field over finite regions has been developed by Krommes and coworkers [161,187]. Also, a rigorous bound on the effective diffusivity depending on the maximum of the stream function (or stream matrix) has been obtained by Tatarinova et al. [314] for arbitrary velocity fields which are confined to finite regions. This result is a different weaker interpretation of the upper bound in Eq. (43).

2.2. Effective diffusivity in various periodic flow geometries

We now demonstrate the utility of the rigorous formulas for the effective diffusivity of a tracer over long times by applying them to a various specific classes of periodic flows. Explicit formulas for the effective diffusivity can be derived for shear flows with spatially uniform cross sweeps, as we will show in Sections 2.2.1 and 2.2.2; in other cases one can turn to a numerical solution of the cell problem [40,165,210]. We will for the most part, however, be concerned with the asymptotic behavior of the effective diffusivity in the case of large Péclet number Pe, which arises in many

practical situations. We will show in the rest of Section 2.2 how the variational and the Stieltjes measure representation for the effective diffusivity can be utilized to rigorously determine its exact scaling behavior with respect to large Pe, even when the cell problem (14) cannot be analytically solved. By such means, we shall study in Section 2.2.3 the tracer transport in a special one-parameter family of two-dimensional, steady, periodic flows which interpolate between a cellular flow and a shear flow, and we shall describe in Section 2.2.4 the subtle effects which arise upon the addition of a constant mean sweep V. The effective diffusivity scales as $\|\mathscr{K}^*\| \sim \mathrm{Pe}^{1/2}$ in the pure cellular flow [67], but the presence of a mean sweep can produce either maximally enhanced diffusion ($\hat{e} \cdot \mathscr{K}^* \cdot \hat{e} \sim \mathrm{Pe}^2$) along most directions $\hat{e}$ or minimally enhanced diffusion in all directions ($\|\mathscr{K}^*\| \sim \mathrm{Pe}^0$), depending on such sensitive criteria as whether the components of V are rationally related, whether V is transverse to a mean shear flow pattern, and whether the total flow has stagnation points [210]. Numerical evaluations of the effective diffusivity [210] confirm these mathematically derived asymptotics, and reveal a variety of interesting crossover behavior at large but finite Péclet number which demonstrate the practical relevance of the criteria for maximally and minimally enhanced diffusion just listed. The numerical and mathematical analysis of the long-time effective diffusivity of a tracer in some other periodic flows using the formulas from Section 2.1.4 will be discussed briefly in Section 2.2.5. We stress that the results to be presented throughout Section 2.2 all deal with the asymptotic long-time behavior of the passive scalar field. Some issues concerning the observation of the tracer motion and passive scalar field evolution at finite times will be discussed in Section 2.3.

We shall endeavor throughout Section 2.2 to supplement the rigorous homogenization theory results with intuitive physical explanations for the large Péclet number behavior of the effective diffusivity through consideration of the streamline geometry. A common qualitative theme which will emerge is that, in steady flows at large Péclet number, open channels are associated with greatly enhanced diffusion and blocked streamlines with only moderately enhanced diffusion. This notion will become clearer through discussion and pictures of streamlines for the specific examples we shall discuss. Another way of intuitively understanding the behavior of the effective diffusivity is through an informal consideration of Taylor's formula [317] for the mean-square tracer displacement in terms of the correlation function of the tracer (Lagrangian) velocity. We will emphasize the geometric perspective here, and elaborate upon the heuristic use of Taylor's formula in Section 3, where we examine tracer diffusion in *random* shear flows.

2.2.1. Periodic shear flows with constant (or zero) cross sweep

Shear flows are a very useful class of examples for the examination and illustration of general theories for turbulent diffusion, as we shall see now and in much greater depth in a random context in Section 3. They arise naturally in various physical applications, and they are quite tractable analytically due to their simple structure. A two-dimensional spatio-temporal shear velocity field aligned along the y-axis has the general form

$$\boldsymbol{v}(\boldsymbol{x}, t) = \boldsymbol{v}(x, y, t) = \begin{bmatrix} 0 \\ v(x, t) \end{bmatrix}.$$

In particular, it is completely described by a scalar function $v(x, t)$ which depends on only one spatial variable x in addition to time for nonsteady flows. In this sense, shear flows play the role of

a one-dimensional model for incompressible flows. This feature often permits explicit solution and analysis for various passive scalar and tracer statistics with quite general $v(x,t)$, as we shall show at greater length in Sections 2.3.1 and 3 (see also other mathematical developments for shear flows in [10,206]). A particularly useful extension of the shear flow model which preserves much of its exact solvability is the inclusion of a purely time-dependent cross sweep $w(t)$:

$$\boldsymbol{v}(\boldsymbol{x},t) = \boldsymbol{v}(x,y,t) = \begin{bmatrix} w(t) \\ v(x,t) \end{bmatrix} . \tag{48}$$

One could also allow a purely time-dependent sweeping component along the shear flow, but this is less interesting because the resulting tracer motion would simply be the sum of its motion due to Eq. (48) and due to this additional shear-parallel sweep. On the other hand, a cross sweep $w(t)$, as appears in Eq. (48), interacts nonlinearly with the shear flow convection by dragging the tracer across its spatial variations.

   In our present discussion, we will be able to write down explicit formulas for the effective diffusivity of a tracer in a periodic, mean zero, spatio-temporal shear flow $v(x,t)$ with periodic, constant, or vanishing cross sweep $w(t)$, and thereby identify the influence of the various para-meters. We will moreover be able to explicitly relate these formulas to their abstract Stieltjes measure representation. To fix the main ideas, we concentrate in Section 2.2.1 on the case of constant or zero cross sweep. We treat in turn a steady periodic shear flow with no cross sweep ($v = v(x)$, $w(t) = 0$), a steady periodic shear flow with a nonzero constant cross sweep ($v = v(x)$, $w(t) = \bar{w} \neq 0$), a spatio-temporal periodic shear flow with no cross sweep ($v = v(x,t)$, $w(t) = 0$), and a spatio-temporal periodic shear flow with nonzero constant cross sweep ($v = v(x,t)$, $w(t) = \bar{w} \neq 0$). The interesting features created by a periodically fluctuating $w(t)$ will be elaborated upon in Section 2.2.2.

2.2.1.1. Steady shear flow with no cross sweep. A steady, mean zero, periodic shear flow (48) with $v = v(x)$ and $w(t) = 0$ has been used as a simple model for flow in a stratified porous medium [130]. The cell problem (16) reads

$$
\begin{aligned}
&- \Delta\chi_x(x,y) + \mathrm{Pe}\, v(x)\frac{\partial\chi_x(x,y)}{\partial y} = 0 \ , \\[2mm]
&- \Delta\chi_y(x,y) + \mathrm{Pe}\, v(x)\frac{\partial\chi_y(x,y)}{\partial y} = - \mathrm{Pe}\, v(x) \ .
\end{aligned}
\tag{49}
$$

Clearly $\chi_x(x,y) = 0$, and we can seek a solution for $\chi_y(x,y)$ which is independent of y in terms of a Fourier series expansion:

$$v(x) = \sum_{k \neq 0} \hat{v}_k \mathrm{e}^{2\pi \mathrm{i} k x} \ ,$$

$$\chi_y(x) = - \mathrm{Pe} \sum_{k \neq 0} \frac{\hat{v}_k}{4\pi^2 k^2} \mathrm{e}^{2\pi \mathrm{i} k x} \ .$$

Substituting the functions χ_x and χ_y into Eq. (15), we find the following expression for the effective diffusivity matrix:

$$\mathscr{K}^* = \begin{bmatrix} 1 & 0 \\ 0 & 1 + \bar{K}_{yy} \end{bmatrix}.$$ (50)

It differs from the molecular diffusivity matrix only through the enhancement

$$\bar{K}_{yy} = \bar{K}_{yy}^{(0)} = \mathrm{Pe}^2 \sum_{k \neq 0} \frac{|\hat{v}_k|^2}{4\pi^2 k^2} = \mathrm{Pe}^2 \sum_{k=1}^{\infty} \frac{|\hat{v}_k|^2}{2\pi^2 k^2}$$ (51)

along the shearing direction. This formula was first derived by Zeldovich [348] through a direct computation, and later by Gupta and Bhattacharya [130] through the homogenization approach put forth here. We see explicitly that diffusion is maximally enhanced along all directions $\hat{e}$ which are not transverse to the shear flow.

This can be easily understood from the streamline structure, which in this case corresponds to straight lines parallel to the y-axis. In the absence of molecular diffusion, tracers would move along the streamlines at a ballistic rate (meaning that the distance travelled grows linearly in time). The addition of molecular diffusion knocks the tracer off of its original streamline and eventually onto streamlines with velocity in the opposite direction, destroying the ballistic motion and producing a diffusive transport behavior instead. Since molecular diffusion is therefore an impediment to transport in a steady shear flow with no cross sweep, the effective diffusivity grows very rapidly as Pe (which is inversely proportional to the molecular diffusivity) becomes large.

Another physical interpretation for the effective diffusivity formula (51) can be found in Section 3.2.1 in the context of a steady *random* shear flow, for which a closely related formula applies when the the statistical correlations are sufficiently short-ranged.

2.2.1.2. Steady shear flow with constant cross sweep. We now add a constant cross sweep $w(t) = \bar{w} \neq 0$ to the shear flow. In the context of porous media, this cross sweep can model a mean flow through a stratified aquifer due to gravity (where x is taken as the vertical direction) [130,223]. The cell problem (49) is then altered only by the addition of the term $\bar{w}(\partial \chi_{x,y}(x,y)/\partial x)$ on the left-hand side of each equation. The solution method proceeds as before, yielding the effective diffusivity matrix (50) with enhanced diffusivity along the shear now given by [130]

$$\bar{K}_{yy} = \bar{K}_{yy}^{(w)} = 2\mathrm{Pe}^2 \sum_{k=1}^{\infty} \frac{|\hat{v}_k|^2}{4\pi^2 k^2 + \mathrm{Pe}^2 \bar{w}^2}.$$ (52)

The cross sweep $\bar{w}$ causes $\bar{K}_{yy}^{(\bar{w})}$ to remain uniformly bounded in Pe, corresponding to minimally enhanced diffusion.

The reason for this drastic change from maximally enhanced diffusion is that the cross sweep blocks streamlines along the shearing direction [210]; see Fig. 1. Without molecular diffusion, the tracers would simply be swept along the x direction at a constant rate and oscillate within a bounded interval along the y direction. Molecular diffusion is thus necessary for effective transport along the shearing direction, as is generally the case for situations of minimally enhanced
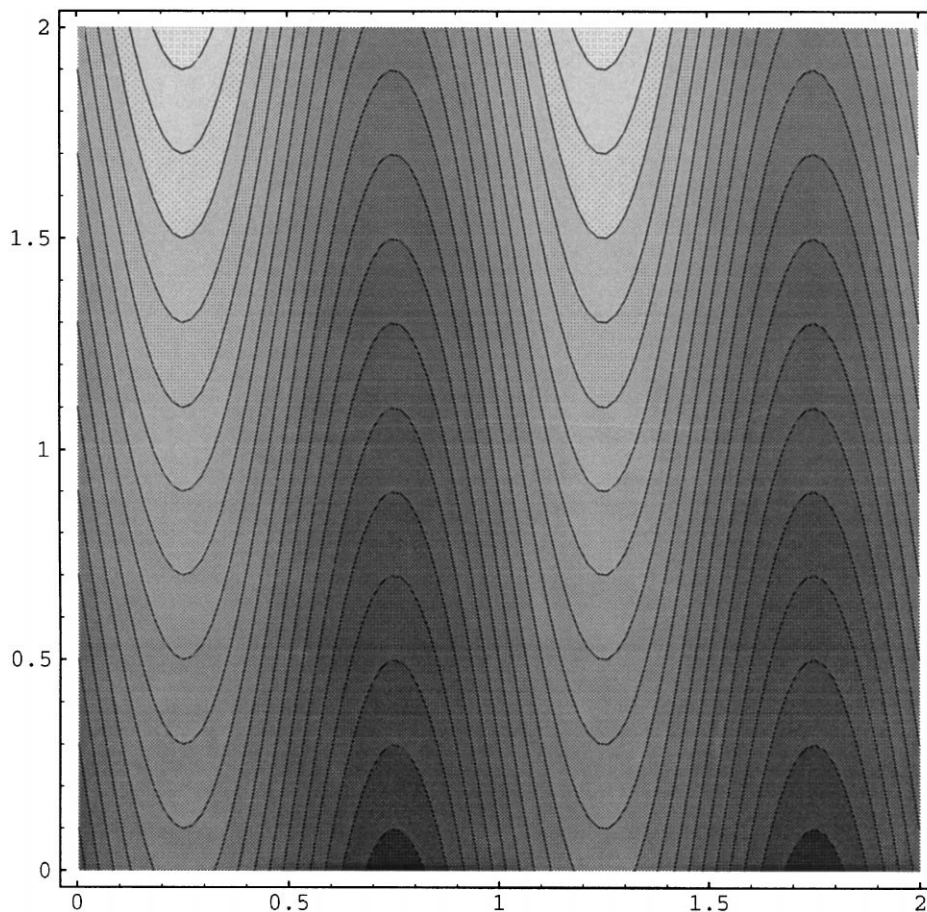
Fig. 1. Streamlines for $v(x) = \sin 2\pi x$ and $w(t) = \bar{w} = 1$ (from [210]).

diffusion. The molecular diffusion along the y direction of course induces a standard tracer diffusion along the y direction, but the enhancement $\bar{K}_{yy}^{(\bar{w})}$ due to the convection comes only from its interaction with the x component of the molecular diffusion. Indeed, the net tracer displacement along the shear over any time interval $1/\bar{w}$ would be exactly zero without molecular diffusion, but becomes a nonzero random number when molecular diffusion is active. Part of this randomness comes directly from the molecular diffusion along the y direction. The more interesting component of the random displacement along the shear results from the randomness induced by the molecular diffusion in the cross-shear tracer motion, which breaks up the exact periodicity of its motion along the shear. It is these extra random displacements which produces the shear-assisted diffusion enhancement $\bar{K}_{yy}^{(\bar{w})}$. A similar formula for the enhanced diffusivity applies for the case of a random steady shear flow with sufficiently short-ranged correlations and a constant cross sweep; see Paragraph 3.2.5.2. Another perspective on the qualitative dependence of $\bar{K}_{yy}^{(\bar{w})}$ with respect to the various parameters is provided there.

We pause to remark that Eq. (52) provides a concrete example of the Stieltjes measure representation for the effective diffusivity. This is better seen by rewriting Eq. (52) slightly:

$$\bar{K}_{yy} = \bar{K}_{yy}^{(\bar{w})} = \text{Pe}^2 \sum_{k \neq 0} \frac{|\hat{v}_k/(2\pi k)|^2}{1 + \text{Pe}^2(\bar{w}/(2\pi k))^2} \ . \tag{53}$$

The eigenvalues $\pm \mathrm{i}\{\mu^{(n)}\}_{n=1}^{\infty}$ and eigenfunctions $\{\boldsymbol{\phi}^{(n)}, \overline{\boldsymbol{\phi}^{(n)}}\}_{n=1}^{\infty}$ of the operator $\mathscr{A}^V$ (Eq. (37b)), after some rearranging, can be shown to be determined by the equations

$$\boldsymbol{\phi}^{(n)} = \nabla \psi^{(n)} \ ,$$

$$\bar{w} \frac{\partial \psi^{(n)}(x, y)}{\partial x} + v(x) \frac{\partial \psi^{(n)}(x, y)}{\partial y} = \mathrm{i}\mu^{(n)} \varDelta \psi^{(n)}(x, y) \ ,$$

where $\psi^{(n)} \in H^1(\mathbb{T}^2)$. It is readily seen that a subset of eigenvalues and eigenfunctions is given by

$$\mu^{(n_k)} = \bar{w}/2\pi k, \qquad \psi^{(n_k)}(x, y) = \mathrm{e}^{-2\pi\mathrm{i}kx} \ .$$

The square of these eigenvalues appear in the denominator of Eq. (53), and the square modulus of the projection of $\mathscr{A}\hat{y} = \nabla \varDelta^{-1} v(x)$ against these eigenfunctions appears in the numerator. By factoring out $\|\mathscr{A}\hat{y}\|^2$, we obtain exactly the Stieltjes measure formula (39) for the enhanced diffusivity along the shear direction $\hat{y}$. Of course, we have not found *all* the eigenfunctions and eigenvalues of $\mathscr{A}^V$, but since $\mathscr{A}\hat{y}$ depends only on x and the eigenfunctions we have found provide a complete (Fourier) basis for such functions in the Hilbert space $L_V^2(\mathbb{T}^d)$ with mean zero, the projection of $\mathscr{A}\hat{y}$ against the remaining eigenfunctions of $\mathscr{A}^V$ must be zero.

As can be seen, it is more cumbersome in the present case to use the Stieltjes measure formula to obtain explicit formulas than it is to solve to cell problem. The Stieltjes measure formula, however, becomes extremely useful in analyzing the high Péclet number behavior of tracer transport in situations where explicit solutions are not available, as we shall show in Section 2.2.4.

2.2.1.3. Spatio-temporal periodic shear flow with no cross sweep. We now briefly consider how the tracer transport is influenced by temporal oscillations in a periodic shear flow $v = v(x, t)$, first with no cross sweep $w(t) = \bar{w} = 0$. The cell problem (49) now becomes parabolic with the addition of the term $\partial \chi_{x,y}(x, y, t)/\partial t$ on the left-hand sides, but can still be solved in terms of the space–time Fourier series of the shear velocity field:

$$v(x, t) = \sum_{(k,m) \neq (0,0)} \hat{v}_{k,m} \mathrm{e}^{2\pi\mathrm{i}(kx + mt/\tau_v)} \ . \tag{54}$$

Again, the effective diffusivity matrix assumes the form (50), with the enhanced diffusivity along the shear given by

$$\bar{K}_{yy} = \bar{K}_{yy}^{(t)} = \text{Pe}^2 \sum_{(k,m) \neq (0,0)} \frac{k^2 |\hat{v}_{k,m}|^2}{4\pi^2 k^4 + m^2 \tau_v^{-2}} \ . \tag{55}$$

This formula was first computed by direct calculation (with no appeal to homogenization theory) by Zeldovich [348].

We note that, as for the steady shear flow, each Fourier mode of the shear contributes additively to the effective diffusivity, and therefore we may discuss them on an individual basis. The spatio-temporal Fourier modes with $m = 0$ are steady, and their presence produces maximally enhanced diffusion for the reasons presented in our discussion of the steady shear flow. The diffusivity contributed by the temporally oscillating Fourier components ($m \neq 0$), is depleted however, particularly when the (nondimensional) temporal period τ_v is small. The inefficiency of transport by the temporally oscillating shear modes relative to the steady shear modes is related to the fact that, in the absence of molecular diffusion, the temporally oscillating Fourier shear modes induce bounded tracer oscillations rather than a unidirectional ballistic drift. Molecular diffusion is therefore necessary for effective tracer transport, and interacts with the periodically oscillating shear flow to produce enhanced diffusivity along the shear by the same type of phase-randomizing mechanism as we discussed above for the case of a constant cross sweep in a steady shear flow.

2.2.1.4. Spatio-temporal periodic shear flow with constant cross sweep. The inclusion of a constant cross sweep $w(t) = \bar{w} \neq 0$ in a spatio-temporal shear flow $v(x, t)$ is straightforward, either by direct calculation (as in [348] or in Section 3) or by homogenization. The enhanced diffusivity along the shear has the form

$$\bar{K}_{yy} = \bar{K}_{yy}^{(w,t)} = \text{Pe}^2 \sum_{(k,m) \neq (0,0)} \frac{k^2 |\hat{v}_{k,m}|^2}{4\pi^2 k^4 + (\text{Pe}\,\bar{w}k + m\tau_v^{-1})^2} \,.$$

The new phenomenon here is the possibility of resonances between the cross sweep and the temporal oscillations of the flow. When $\text{Pe}\,\bar{w}k + m\tau_v^{-1}$ is near zero, the contribution from the temporally oscillating mode $\hat{v}_{k,m}$ (with $m \neq 0$) can be boosted far above what it would be without the mean sweep.

2.2.2. Steady periodic shear flow with periodic cross sweep

We now consider how tracer transport is influenced when a cross sweep $w(t/\tau_v)$ acting across the shear flow (see Eq. (48)) has periodic variations in time (with period τ_v). We focus the case of a steady periodic shear flow $v = v(x)$ in which the main features are all manifest.

The cell problem involved in the homogenization theory can be solved exactly in a manner similar to that described in Section 2.2.1, but as the computations are a bit lengthier, we defer their presentation until after we discuss the results. The effective diffusivity matrix will in general have the form (50), with diffusivity enhanced along the shear above its bare molecular value (1) by an amount $\bar{K}_{yy}$. There is no enhanced diffusivity across the shear; the cross-shear motion is simply a sum of a drift due to the mean of $\bar{w} = \langle w(t/\tau_v) \rangle$, a periodic motion due to the periodic temporal variations of $w(t/\tau_v)$, and a Brownian motion due to molecular diffusion. There is no interaction between these cross-shear advection and diffusion processes because they are all independent of spatial location.

We saw in Section 2.2.1 that the enhanced diffusivity along the shear is maximal ($\lim_{\text{Pe} \to \infty} \bar{K}_{yy} \sim \text{Pe}^2$) when the cross sweep vanishes ($w(t/\tau_v) \equiv 0$) and the flow streamlines are unbounded along the y direction, and that the enhanced diffusivity is minimal ($\lim_{\text{Pe} \to \infty} \bar{K}_{yy} \sim \text{Pe}^0$) when a nonzero, constant cross sweep $w(t/\tau_v) = \bar{w} \neq 0$ is active which blocks streamlines along the y direction.

In our current study, where $w(t/\tau_v)$ is periodic, we can expect the shear-enhanced diffusivity to behave in a way intermediate to the $w \equiv 0$ and $w \equiv \bar{w} \neq 0$ cases. If we take instantaneous snapshots of the streamlines of the flow, then, we will see that they are almost always blocked along the y direction. But as $w(t/\tau_v)$ oscillates, there may be times when it passes through zero. Near these times, the amplitude of the streamline oscillations in the y direction will grow unboundedly until the instant t_* at which $w(t/\tau_v) = 0$, when the streamlines will form parallel lines along the y direction. Thus, the flow will sometimes act on the tracer like a shear flow blocked by a cross sweep (where enhanced diffusivity is bounded in Péclet number), and other times like a shear flow without cross sweep (where enhanced diffusivity grows quadratically with Péclet number).

The rigorous homogenization theory bears out this intuition. Let us assume that $w(t/\tau_v)$ vanishes at most to finite order at a finite number of times in each period. Then the enhancement of the diffusivity along the shear flow has the high Péclet number asymptotics

$$\lim_{\mathrm{Pe} \to \infty} \bar{K}_{yy} \sim C_{\bar{K}}(\mathrm{Pe}, \tau_v)\mathrm{Pe}^{2N/(N+1)} \,, \tag{56}$$

where N is the order of the highest zero of $w(t)$, and $C_{\bar{K}}(\mathrm{Pe}, \tau_v)$ is a positive function bounded strictly away from zero and infinity *when the temporal oscillation period τ_v is held fixed*. The order n of a zero t_* of $w(t/\tau_v)$ is defined to be the unique positive integer n for which

$$w(t_*/\tau_v) = w'(t_*/\tau_v) = \cdots = w^{(n-1)}(t_*/\tau_v) = 0 \,,$$

$$w^{(n)}(t_*/\tau_v) \neq 0 \,,$$

where $w^{(j)}$ denotes the jth derivative of w. If the cross sweep never vanishes, then one should take $N = 0$.

We see that indeed the enhanced diffusivity is some sort of compromise between the Pe^2 scaling associated to the zero cross sweep case and the Pe^0 scaling associated to a constant cross sweep. Note that the asymptotic scaling exponent $\alpha = 2N/(N+1)$ of $\bar{K}_{yy}$ as function of Péclet number increases from 0 to 2 as the maximal order of vanishing, N, increases. This can be understood by noting that a function with a high-order zero at t_* is flatter and "stays closer to zero" in the vicinity t_* than a function with a simple zero would. Thus, a higher-order zero of $w(t)$ should permit the shear flow to contribute more strongly toward tracer diffusion because the cross sweep is more nearly vanishing over a broader time interval. We can formally think of the case of an identically vanishing cross sweep $w(t/\tau_v) = 0$ as an $N \to \infty$ limit.

Note that the scaling exponent is set only by the behavior of $w(t)$ near times (if any) at which it vanishes. This is in accordance with the intuition that, at high Péclet number, diffusivity along a shear is much more effective when there is no cross sweep, so most of the transport will occur in narrow time intervals about those moments at which $w(t/\tau_v)$ vanishes and the streamline blocking is released. These time intervals of efficient diffusion are responsible for the main contribution to the effective diffusivity $\bar{K}_{yy}$. We remark that this relation relies crucially on the fact that the occasions of rapid transport occur periodically without fail. There is an important distinction here from the case of an isotropic material with random, inhomogenous diffusivity in which the regions of low diffusivity percolate. In this case, the passive scalar entity will get "trapped" for long times by the regions of slow motion, and the effective long-time diffusivity is likely to feel a strong effect from the presence of regions of ineffective transport. There is no such feedback in the present situation.

2.2.2.1. Computation of effective diffusivity. We now indicate how homogenization theory produces the results described above. The parabolic cell problem reads

$$\frac{\partial \chi_x(x,y,t)}{\partial t} + \mathrm{Pe}\, w(t/\tau_v)\frac{\partial \chi_x(x,y,t)}{\partial x} + \mathrm{Pe}\, v(x)\frac{\partial \chi_x(x,y,t)}{\partial y} - \varDelta \chi_x(x,y,t) = -\mathrm{Pe}\, w_f(t/\tau_v)\,, \quad (57a)$$

$$\frac{\partial \chi_y(x,y,t)}{\partial t} + \mathrm{Pe}\, w(t/\tau_v)\frac{\partial \chi_y(x,y,t)}{\partial x} + \mathrm{Pe}\, v(x)\frac{\partial \chi_y(x,y,t)}{\partial y} - \varDelta \chi_y(x,y,t) = -\mathrm{Pe}\, v(x)\,, \quad (57b)$$

where $w_f(t/\tau_v) = w(t/\tau_v) - \bar{w}$ is the periodically fluctuating part of the cross sweep. Since the right-hand side of Eq. (57a) is purely time-dependent, we can readily find a mean zero periodic solution for χ_x:

$$\chi_x = \chi_x(t) = -\mathrm{Pe} \int_0^t w_f(s/\tau_v)\,\mathrm{d}s\,. \quad (58)$$

The solution of Eq. (57b) requires a little more work, but is still straightforward. As the inhomogeneity depends only on x and t, we are led to seek a solution $\chi_y = \chi_y(x,t)$. Taking a partial Fourier transform with respect to x,

$$\chi_y(x,t) = \sum_{k=-\infty}^{\infty} \hat{\chi}_{y,k}(t)\mathrm{e}^{2\pi \mathrm{i} k x}\,,$$

$$v(x,t) = \sum_{k=-\infty}^{\infty} \hat{v}_k(t)\mathrm{e}^{2\pi \mathrm{i} k x}\,,$$

we reduce this part of the cell problem to a system of decoupled ODEs:

$$\frac{\mathrm{d}\hat{\chi}_{y,k}(t)}{\mathrm{d}t} + 2\pi \mathrm{i}\mathrm{Pe}\, k w(t/\tau_v)\hat{\chi}_{y,k}(t) + 4\pi^2 k^2 \hat{\chi}_{y,k}(t) = -\mathrm{Pe}\, \hat{v}_k(t)\,.$$

These linear ODEs may be solved directly to produce the following time-periodic solutions:

$$\hat{\chi}_{y,k}(t) = -\mathrm{Pe} \int_{-\infty}^t \hat{v}_k(t')\,\mathrm{e}^{-2\pi \mathrm{i}\mathrm{Pe} k \int_{t'}^t w(s/\tau_v)\,\mathrm{d}s}\mathrm{e}^{-4\pi^2 k^2(t-t')}\,\mathrm{d}t' \quad \text{for } k \neq 0\,, \quad (59a)$$

$$\hat{\chi}_{y,0}(t) = -\mathrm{Pe} \int_0^t \hat{v}_0(t')\,\mathrm{d}t'\,. \quad (59b)$$

We used the usual trick that the periodic solution of a periodically forced, dissipative equation may be represented by using Duhamel's formula with the initial data formally taken at $t = -\infty$ (so that all nonperiodic transients have died out by any finite time). Substituting the solutions (58) and (59) of the cell problem into formula (15) for effective diffusivity, we find an enhancement only for the component $K_{yy}^* = 1 + \bar{K}_{yy}$, which may be expressed as

$$\bar{K}_{yy} = \bar{K}_{yy}^{(w)} = 8\pi^2 \sum_{k=1}^{\infty} k^2 \tau_v^{-1} \int_0^{\tau_v} |\hat{\chi}_{y,k}(t')|^2\,\mathrm{d}t'\,. \quad (60)$$

In the high Péclet number limit, the integrand in Eq. (59a) becomes a rapidly oscillating function of time. The asymptotic behavior of the integral may be rigorously evaluated through the method of stationary phase (see [250] or [312]). The dominant contribution to the integral comes from the vicinity of those points at which the phase $\mathrm{Pe} \int_t^t w(s/\tau_v) \, ds$ has zero derivative, and these points are precisely the zeroes of $w(t)$. The contribution to $\hat{\chi}_{y,k}(t)$ from integration near a nth-order zero t_* of $w(t/\tau_v)$ is given by [250]

$$- 2\mathrm{Pe}^{n/(n+1)} \tau_v^{n/(n+1)} \left(\frac{(n+1)!}{2\pi} \right)^{1/(n+1)} \frac{\Gamma(1/(n+1))}{n+1} k^{-1/(n+1)}$$

$$\times \frac{s_n \hat{v}_k(t_*)}{|w^{(n)}(t_*)|^{1/(n+1)}} \, e^{2\pi i \mathrm{Pe} \, k \int_{t_*}^t w(s/\tau_v) \, ds} e^{-4\pi^2 k^2 (t - t_*)} \tag{61}$$

where

$$s_n = \begin{cases} e^{i\pi/2(n+1)} \mathrm{sgn} \, w^{(n)}(t_*) & \text{for } n \geq 1 \text{ and odd}, \\ \cos\dfrac{\pi}{2(n+1)} & \text{for } n \geq 2 \text{ and even}. \end{cases}$$

Note that the magnitude of this contribution is an increasing function of the order n of the zero. The high Péclet number asymptotics of $\hat{\chi}_{y,k}$ are obtained by summing the contributions 61 from each zero t_* of $w(s/\tau_v)$ on the interval $(-\infty, t]$, and the high Péclet number asymptotics (56) of $\bar{K}_{yy}^{(w)}$ then follow from Eq. (60).

The effective diffusivity can be computed in a similar manner when the shear velocity field has temporal fluctuations in time. We do not provide details; it suffices to say that the high Péclet number asymptotics can be understood by putting together the principles which we described separately above for the case of a spatio-temporal periodic shear flow with constant cross sweep and for a steady shear flow with periodic cross sweep.

2.2.3. Steady cellular and related flows

A natural periodic flow which has received much attention is the steady two-dimensional cellular flow, which is defined through a stream function $\psi(x, y)$ as follows:

$$\boldsymbol{v}(x, y) = \begin{bmatrix} \dfrac{\partial \psi(x,y)}{\partial y} \\ -\dfrac{\partial \psi(x,y)}{\partial x} \end{bmatrix}, \tag{62a}$$

$$\psi(x, y) = \psi_{\mathrm{cell}}(x, y) = \sin(2\pi x) \sin(2\pi y). \tag{62b}$$

The streamlines of this flow are plotted in Fig. 2. No exact solution is known to the homogenization cell problem (16). A number of authors [260,287,294,303], starting with Childress [67], have instead endeavored to compute the effective diffusivity of the passive scalar field by various matched asymptotic expansion techniques applied directly to the advection–diffusion equation. The homogenized cell problem is not used in these works. The basic idea is that at high Péclet number, the tracer is rapidly transported across any given cell, but is then trapped to remain in that cell for a while until molecular diffusion allows it to leak across the boundary to an adjacent cell.
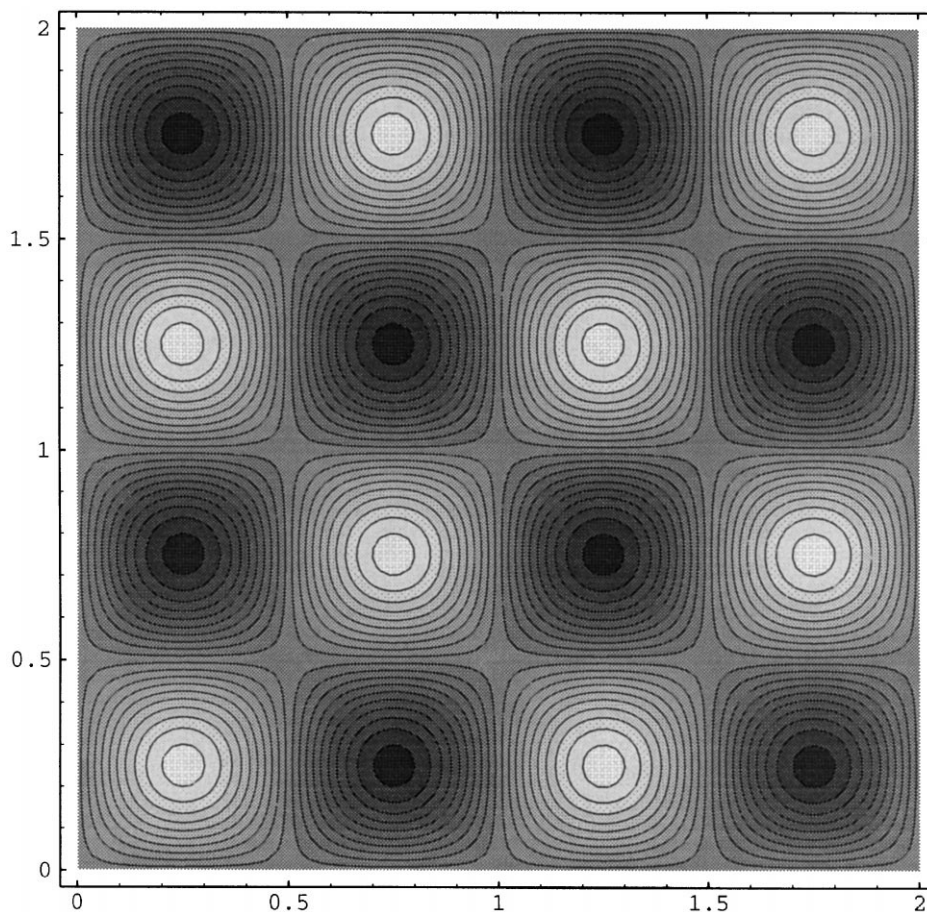
Fig. 2. Contour plot of stream function $\psi_{\text{cell}}(x, y)$ (62) of cellular flow (from [210]).

The communication of the passive scalar field between cells is the rate-limiting process determining the effective diffusivity, and this flux is determined by the sharp gradient of the passive scalar field formed in a thin layer (with width $\sim \text{Pe}^{-1/2}$) near the separatrices between the cells. The common conclusion of all the matched asymptotic expansions [67,260,287,294,303] is that, in the limit of large Péclet number, the effective diffusivity matrix is isotropic with diagonal entries scaling as $\text{Pe}^{1/2}$, though there is some slight disagreement as to the precise value of the prefactor of the scaling law [260,287,294,303]. The predicted asymptotic $\text{Pe}^{1/2}$ scaling of the effective diffusivity was later rigorously confirmed by Fannjiang and Papanicoloau [97,99] through the use of variational principles within the framework of homogenization theory (see Paragraph 2.1.4.2).

This implies in particular that steady cellular flows are neither maximally diffusive nor minimally diffusive. The reason they are not maximally diffusive is quite apparent; there are no open channels, and molecular diffusion is crucially relevant for the tracer to hop from one cell to the next. But the

streamline barrier between the cells is not of the same blocking character as in Fig. 1 for a shear flow with a transverse cross sweep. Only a single streamline separates the two cells in a cellular flow, and the tracer must only move an infinitesimal amount across it before it can be carried a great distance by the convection of the neighboring cell. By contrast, a tracer moving infinitesimal amounts across the streamlines in Fig. 1 gets no help from the flow itself in making further headway. This helps explain why the effective diffusion in the cellular flow is more than minimally enhanced. But molecular diffusion is clearly still a facilitator, rather than a disruptor, of transport in a steady cellular flow, and this is reflected in the fact that the *dimensionalized* effective diffusivity is directly proportional to the square root of the molecular diffusion coefficient.

McCarty and Hortshemke [226] investigated the effective diffusivity of the passive scalar field in the cellular flow (62) at finite Péclet numbers to ascertain the range of validity of the asymptotic $Pe^{1/2}$ scaling law and the corrections thereto. These authors computed the homogenized effective diffusivity through a finite mode Fourier truncation of the cell problem (16). They find that the $Pe^{1/2}$ scaling is well satisfied for $Pe > 500$, with a leading order correction of magnitude $O(Pe^{1/3})$, in accordance with an earlier theoretical estimate [287]. Similar conclusions were reached by Biferale et al. [40] through other numerical approximations for the homogenized diffusivity; we discuss these further in Section 2.2.5 below. Tracer transport in the steady cellular flow (62) at finite Péclet number was numerically studied in a quite different way by Rosenbluth et al. [287] and Biferale et al. [40] using direct Monte Carlo simulations; see Paragraph 2.3.2.1 below.

Solomon and Gollub [302] experimentally measured the transport rates of dyes and latex spheres in a laboratory Rayleigh–Bénard steady convection cell with a flow pattern similar to Eqs. (62a) and (62b). They found effective diffusivities in general accord with the high Péclet number theoretical predictions for $10^3 \lesssim Pe \lesssim 10^7$.

In addition to the studies of the steady cellular flow (62), there are also a number of theoretical and numerical investigations of various periodic modifications of it which elucidate other types of transport mechanisms. We discuss briefly three such lines of inquiry.

2.2.3.1. Childress–Soward flows. A useful one-parameter family of steady two-dimensional flows which interpolate between a shear flow and a cellular flow were introduced and analyzed by Childress and Soward [68]. The stream functions $\psi_{CS}^{(\varepsilon)}(x, y)$ of this "Childress–Soward" family of flows is defined as

$$\psi_{CS}^{(\varepsilon)}(x, y) = \sin(2\pi x)\sin(2\pi y) + \varepsilon\cos(2\pi x)\cos(2\pi y) , \tag{63}$$

with the parameter ε chosen from the range $0 \leq \varepsilon \leq 1$. For $\varepsilon = 0$, we recover the steady cellular flow (62), while for $\varepsilon = 1$, the Childress–Soward flow is a shear flow directed parallel to the vector $(1,1)^\dagger$. For $0 < \varepsilon < 1$, the flow takes the form of a mixture of "cat's eye" vortices and open channels parallel to $(1,1)^\dagger$ on the whole (Fig. 3). As ε increases, the width of the channels increase at the expense of the cat's eyes. Inspection of the streamline structure of the Childress–Soward flows with $0 < \varepsilon < 1$ suggests that tracer motion should be easy along open channels in the $(1,1)^\dagger$ direction, but must work against streamline blocking in the $(1, -1)^\dagger$ direction. Based upon our discussion in Paragraph 2.1.4.1, we may therefore expect that diffusion is maximally enhanced along any direction with a nonzero component along the open channels, but only minimally enhanced in the
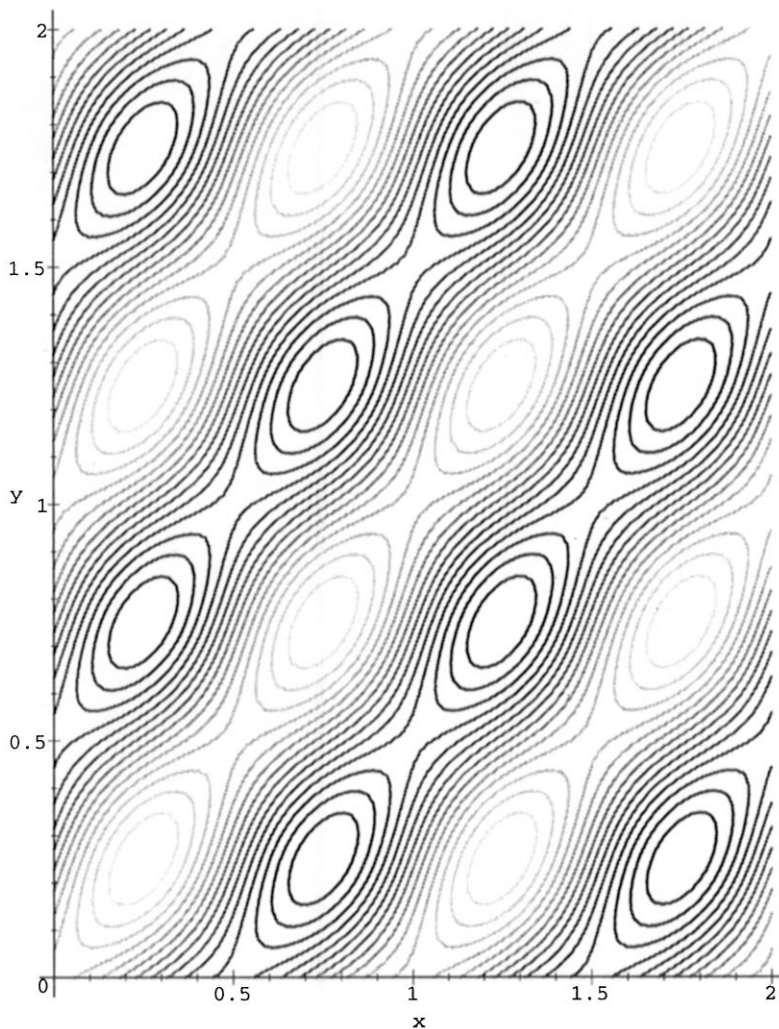
Fig. 3. Contour plot of stream function $\psi_{\text{CS}}^{(\varepsilon)}(x, y)$ of Childress–Soward flow (63) with $\varepsilon = 0.5$ (from [231]).

orthogonal, blocked direction. We may therefore hypothesize for $0 < \varepsilon < 1$ the high Péclet number scalings

$$\lim_{\text{Pe} \to \infty} \hat{e} \cdot \bar{\mathcal{K}} \cdot \hat{e} \sim \text{O}(\text{Pe}^2) \quad \text{for } \hat{e} \neq (1/\sqrt{2}) \begin{bmatrix} 1 \\ -1 \end{bmatrix},$$

$$\lim_{\text{Pe} \to \infty} \hat{e} \cdot \bar{\mathcal{K}} \cdot \hat{e} \sim \text{O}(1) \quad \text{for } \hat{e} = (1/\sqrt{2}) \begin{bmatrix} 1 \\ -1 \end{bmatrix}. \tag{64}$$

An elaborate boundary layer analysis by Childress and Soward [68] produces the same predictions with specific values for the scaling prefactors, and Fannjiang and Papanicoloau [97] recover the general scaling relations (64) through variational methods.
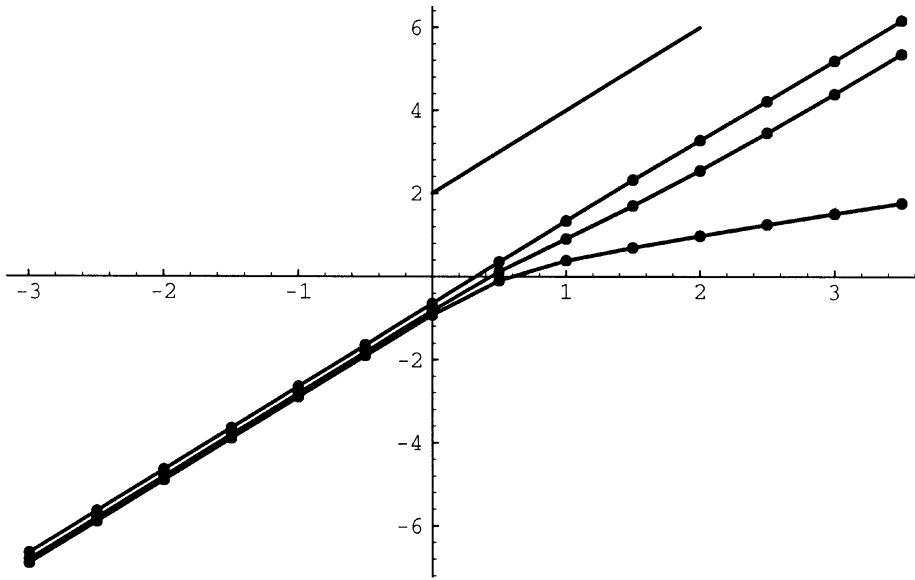
Fig. 4. Log–log plot of enhanced diffusion coefficient $\bar{K}_{xx}$ versus Pe for Childress–Soward flows (63) (from [210]). Upper curve: $\varepsilon = 0.9$, middle curve: $\varepsilon = 0.5$, lower curve: $\varepsilon = 0$. Also shown is a line with slope 2 for reference.

Numerical computation [210] of the homogenized effective diffusivity matrix confirm the maximally enhanced diffusion along the x direction when $0 < \varepsilon < 1$. The effective diffusivity for Childress–Soward flows with $\varepsilon = 0$, 0.2, and 0.5 are plotted in Fig. 4; the contrast of the maximally enhanced diffusion ($\bar{K}_{xx} \sim O(Pe^2)$) for $\varepsilon \neq 0$ with the $\bar{K}_{xx} \sim O(Pe^{1/2})$ scaling for the cellular flow $\varepsilon = 0$ is evident.

Crisanti et al. [77] investigated a family of flows with the same essential features of the Childress–Soward flows (63), and predicted the same kind of high Péclet number behavior of the effective diffusivity through intuitive scaling arguments. These predictions were supported by Monte Carlo numerical simulations [77].

We will use the Childress–Soward flows in Section 2.2.4 to illustrate some of the dramatic effects which the addition of a constant mean sweep to a periodic velocity field can cause.

2.2.3.2. Checkerboard flows. Fannjiang and Papanicoloau [97] considered a "checkerboard flow" variation of the steady cellular flow (62) in which the flow is active only in every other cell, so that transport is dominated by passage through the corners of diagonally adjacent cells. Through the use of variational principles, they rigorously show that the effective diffusivity can have a high Péclet number asymptotic form $\lim_{Pe \to \infty} \|\bar{\mathcal{K}}\| \sim O(Pe^{\alpha})$, with any $\frac{1}{2} \leq \alpha \leq 1$, by further modifying the checkerboard flow so that the corners are suitably widened.

2.2.3.3. Temporally fluctuating cellular flows. A few interesting studies of the effective diffusivity have been undertaken concerning cellular flows with periodic temporal fluctuations. Knobloch and Merryfield [165] numerically investigated the effective diffusion of a passive scalar field in a standing wave obtained by multiplying the cellular flow (62) by a periodic time factor $\cos \omega t$. The

effective diffusivity was found to decrease as a function of the temporal frequency ω. This phenomenon was also manifested in the analytical formula (55) for the effective diffusivity in a shear flow with periodic temporal variations, and is due to the diminishing persistence of tracer motion as the temporal oscillations become more rapid. Knobloch and Merryfield [165] also examined the effective diffusivity in a travelling wave with stream function

$$\psi_{\mathrm{TW}}(x, y, t) = \sin(2\pi(x - Ut))\sin(2\pi y) \;,$$

where U is the phase speed. Note that the velocity field averaged over a temporal period still vanishes everywhere. Through some numerical experiments, it was found in [165] that tracer transport is faster in a travelling wave than in a standing wave. This was attributed to the action of the Stokes drift of the travelling wave, and to the trapping and dragging of particles within the cores of the moving cells. Note, however, that there is no long-term net drift of the tracer along any direction [165].

Another interesting question is how tracer transport is modified when a periodic time-dependent perturbation is added to the steady cellular flow (62). Solomon and Gollub [301] measured how the effective diffusivity of the dyes and latex spheres in their laboratory convection cells changes when the Rayleigh number is increased to a point at which the steady cellular flow becomes unstable via a Hopf bifurcation to a temporally periodic oscillation. They found the effective diffusivity to be enhanced by several orders of magnitude over that for a steady cellular flow, and attributed this increase to the chaotic transport of tracers across the cellular boundaries due to the temporal fluctuations. Such a conclusion was supported by various numerical computations of the homogenized diffusivity in a simple model by Biferale et al. [40]. They found that the (dimensionalized) effective diffusivity is independent of molecular diffusion at large Péclet number, consistent with the notion that chaotic advection is the dominant transport mechanism.

2.2.4. Effects of constant mean sweep on transport in steady periodic flow

We next consider the dramatic and subtle effects which a constant mean flow can have on the effective diffusivity of a periodic flow, with particular attention to the special class of Childress–Soward flows (63) discussed in Paragraph 2.2.3.1. Our discussion draws primarily from the results and ideas in the original study by McLaughlin and the first author [210]. We first formulate some general mathematically rigorous criteria to decide when the addition of a mean flow to a two-dimensional, steady, periodic flow will give rise to maximal or minimal diffusivity. Roughly speaking for the moment, a mean flow V with rationally related components will "generically" give rise to maximally enhanced diffusion along all directions other than those perpendicular to V, whereas a mean flow with components forming an irrational ratio will create minimally enhanced diffusion along all directions $\hat{e}$ if there are no stagnation points in the flow [210]. Through numerical evaluation of the effective diffusivity, we next demonstrate that this sensitive dependence of the large Péclet number asymptotics of the effective diffusivity on the ratio of the components of the mean flow and other features manifests itself clearly at accessibly large but finite Péclet numbers. The numerical experiments moreover reveal some striking crossover phenomena for the behavior of the effective diffusivity as a function of Pe which reflect the competing influences of various flow qualities suggested by the mathematical asymptotic theory [210]. All these phenomena indicate subtle, complex, and mathematically rigorous behavior for eddy diffusivity modelling in such flow fields.

2.2.4.1. Conditions for maximal or minimal enhanced diffusion in presence of constant mean sweep. In Paragraph 2.1.4.1, we stated general conditions for maximally enhanced and minimally enhanced diffusion which can be deduced from the Stieltjes integral representation of the effective diffusivity [39]. In [210], some rigorous corollaries of these conditions were derived which provide some further general insights into how the large Péclet number behavior of the effective diffusivity of a two dimensional, steady, periodic flow

$$\boldsymbol{v}(\boldsymbol{x}) = \boldsymbol{v}(x, y) = \begin{bmatrix} v_x(x, y) \\ v_y(x, y) \end{bmatrix}$$

is affected by the presence of a constant mean flow (sweep)

$$V = \begin{bmatrix} V_x \\ V_y \end{bmatrix} .$$

These results were later rederived in slightly different form in [97], using variational principles mentioned in Paragraph 2.1.4.2.

We consider separately the cases where the ratio of the components of the mean sweep V_x/V_y (or its inverse) is rational and irrational.

Effect of a mean sweep with rationally related coefficients. If the constant mean flow has rationally related components, then the effective diffusivity is maximally enhanced in all directions $\hat{e}$ with $V \cdot \hat{e} \neq 0$, provided that there exists a real number λ and a positive integer p so that:

- λV_x and λV_y are each integers, and
- $\int_{\mathbb{T}^2} e^{-2\pi i \lambda (V_y x - V_x y)} \psi^p(x, y) \, dx \, dy \neq 0$, $\qquad (65)$

where $\psi(x, y)$ is the stream function corresponding to the velocity field, i.e. $v_x = \partial \psi / \partial y$ and $v_y = - \partial \psi / \partial x$ [210].

The effective diffusion is always minimally enhanced in the direction $\hat{e}$ perpendicular to the mean flow V when it has rationally related components [97].

The technical condition (65) is clearly satisfied by "most" flows, with the significant exception of shear flows aligned perpendicularly to V. In the generic case, therefore, a mean sweep with rationally related coefficients will induce maximally enhanced diffusion in all directions other than the one perpendicular to itself, along which diffusion will instead be minimally enhanced. Shear flows directed perpendicularly to the mean sweep fail to adhere to this paradigm quite simply because they have no velocity component parallel to the mean sweep, and therefore cannot induce any additional diffusion in this direction. We will return below to discuss crossover effects in the effective diffusivity produced by flows which are small perturbations of shear flows.

It is shown in [210] that the condition (65) is satisfied for the family of Childress–Soward flows (63) described in Paragraph 2.2.3.1, provided that $0 \leq \varepsilon < 1$. Recall that for $\varepsilon = 1$, the Childress–Soward flow degenerates to a shear flow; the effect of the addition of a constant mean sweep for this case was discussed in Paragraph 2.2.1.2. We now discuss the effects of the addition of a mean sweep with rationally related components to Childress–Soward flows in the parameter range $0 \leq \varepsilon < 1$, for which the theorem stated above can be applied.

The special value $\varepsilon = 0$ corresponds to a cellular flow which gave rise to an effective diffusivity scaling at large Péclet number as $\mathrm{Pe}^{1/2}$ in all directions, when no mean flow is present. The addition of a mean sweep with rationally related coefficients however dramatically changes the large Péclet number asymptotics: the effective diffusivity is now maximal, scaling as Pe^2, in all directions $\hat{e}$ other than the one perpendicular to V, along which it is bounded in Pe. The intuitive reason for this change is that the mean flow has opened up channels which facilitate transport parallel to itself, but which block transport in the perpendicular direction [304]. The rational relation between the components of the mean sweep V is, however, critical to this conclusion, as we shall explain below when we consider mean sweeps V with irrationally related components.

For $0 < \varepsilon < 1$, the Childress–Soward flow without a mean sweep has a mixture of open channels and cats-eye trapping regions, and asymptotic analysis indicates maximally enhanced diffusion along all directions except orthogonally to the channel direction, along which the diffusion is minimally enhanced. The addition of a mean sweep maintains the generally maximally diffusive character of the flow, but shifts the direction of minimal diffusivity to be orthogonal to the mean sweep V, rather than orthogonal to the direction of the original channels (in the absence of the mean sweep). The change in the streamline structure for various Childress–Soward flows under the addition of a mean sweep is graphically illustrated in [210].

Effect of a mean sweep with irrationally related coefficients. By contrast to the generally maximally enhanced diffusion promoted by the presence of a mean sweep with rationally related components, we have the following result for the case of a mean sweep with irrationally related components [210]:

If the ratio V_x/V_y (or its inverse) is irrational, and the total flow has no stagnation points (that is, $|V + v(x, y)|$ vanishes nowhere), then no direction $\hat{e}$ is maximally diffusive. Moreover, if the irrational ratio V_x/V_y (or its inverse) can be normally approximated by rationals, then the effective diffusion is only minimally enhanced in all directions.

The proof of this statement is given in [210], and relies on Kolmogorov's theorem for dynamical systems on the torus which permits a convenient global change of coordinates ([297], Ch. 11). The number theoretic property of an irrational number being "normally approximated" by rationals is discussed in ([297], p. 95). It suffices for our present purposes merely to mention that the set of irrational numbers having this property has full Lebesgue measure, i.e. almost every irrational number has the normal approximation property.

It is readily checked that the above statement can be applied to Childress–Soward flows, provided that the mean sweep with irrationally related components is strong enough to preclude stagnation points. We therefore have for these flows (and in fact, quite generically) a very sensitive dependence of the effective diffusivity on the ratio of the components of the mean sweep. A rational

ratio implies maximally enhanced diffusion in almost all directions, whereas an irrational ratio usually implies minimally enhanced diffusion in all directions (provided there are no stagnation points). In particular, while the effective diffusivity for the cellular flow described in Section 2.2.3 scales at high Péclet number as $Pe^{1/2}$, the addition of a mean flow with rationally related coefficients will further enhance diffusion with Pe^2 scaling in almost all directions, whereas the addition of a sufficiently strong mean flow with irrationally related coefficients will usually interfere with the enhanced transport mechanism of the cellular flow, and limit the effective diffusivity to a finite constant no matter how large Pe becomes.

Similar results were obtained by Koch et al. [168] and Mauri [224] in asymptotic computations for the special case of a flow drawn by a large-scale pressure gradient through a periodic array of small spheres, and by Soward and Childress [304] for the case of a *weak* mean sweep past a steady cellular flow (62). Golden, Goldstein, and Lebowitz [125] found an analogous phenomenon in the diffusion of a particle through a oscillatory potential with two characteristic wavelengths; the effective diffusivity takes different values depending on whether the ratio of the wavelengths is rational or irrational.

An intuitive reason to understand why a mean sweep with rational ratios generally produces much more effective transport than mean sweeps with irrational ratios is that the former can set up resonant open channels of finite width extending forever periodically in a given direction. The addition of a mean flow with irrationally related components, by contrast, gives rise to an aperiodic total stream function with fine structures which will not support these clean open channels [304]. This explains, in a heuristic way, why one should not generally expect maximally enhanced diffusion when the mean sweep has irrationally related components, but falls short of explaining why the diffusion should be so inhibited as to be only minimally enhanced. Some mechanism other than streamline blocking must be playing an active role in this regard. It may possibly be related to a dense sampling of the period cell by every streamline which leads to a rapid averaging over the mean zero velocity field [168]. It would be interesting to concretely identify and clarify the relevant mechanism producing minimally enhanced diffusion in this situation.

2.2.4.2. Numerical evaluations of effective diffusivity at large but finite Péclet number. The mathematical theorems presented above concerning the addition of a mean sweep to a periodic flow describe the asymptotic scaling of the effective diffusivity in the limit of large Péclet number. They neither provide a numerical value for the prefactor in the scaling law, nor do they designate how large the Péclet number must actually be for these asymptotic scalings to be observed. Such questions generally require specific computation through either numerical solution of the cell problem (33) or Monte Carlo simulations of the tracer motion (see Section 2.3.2). We describe here some numerical computations of the enhanced diffusivity for certain Childress–Soward flows with mean sweep which are suggested by the asymptotic mathematical theory to display potentially interesting "crossover" behavior at finite Péclet number. These computations, reported in [210], solve the cell problem (33) using a finite Fourier mode truncation scheme similar to the one used in [226].

Perturbed shear flow with transverse cross sweep: We recall that the rigorous mathematical theory proceeding from the Stieltjes integral representation stated that the addition of a mean flow with rationally related components to a Childress–Soward flow (63) with $0 \le \varepsilon < 1$ produces maximally enhanced diffusion in all directions with $\hat{e} \cdot V \neq 0$. On the other hand for $\varepsilon = 1$, the

Childress–Soward flow reduces to a shear flow parallel to the vector $(1, 1)^\dagger$, and we know from Paragraph 2.2.1.2 that the addition of a mean sweep in any other direction will produce minimally enhanced diffusion in all directions. Therefore, in particular, the addition of a mean flow parallel to $(-1, 1)^\dagger$ will produce maximally enhanced diffusion for Childress–Soward flows with $0 \leq \varepsilon < 1$, but only minimally enhanced diffusion for the limiting shear flow case $\varepsilon = 1$. This motivates a study of how the enhanced diffusivity varies at finite Péclet number when ε is slightly below 1.

We therefore choose a Childress–Soward flow with $\varepsilon = 0.9$, which, in the absence of any mean flow, has the structure of a perturbed shear flow, with long and narrow cat's eyes interspersed between wide channels (see Fig. 5). For comparison and contrast, we present in Fig. 6 the numerical computations for the enhanced diffusivity along the x direction, $\bar{K}_{xx}$, which results when the mean flow $V = (2, 2)^\dagger$ or $V = (-2, 2)^\dagger$ is added. In both situations, the asymptotic theory predicts maximally enhanced diffusion ($\lim_{Pe \to \infty} \bar{K}_{xx} \sim O(Pe^2)$), and this is confirmed by the numerical computations, but a substantial difference between the two cases is manifest at finite Péclet number.
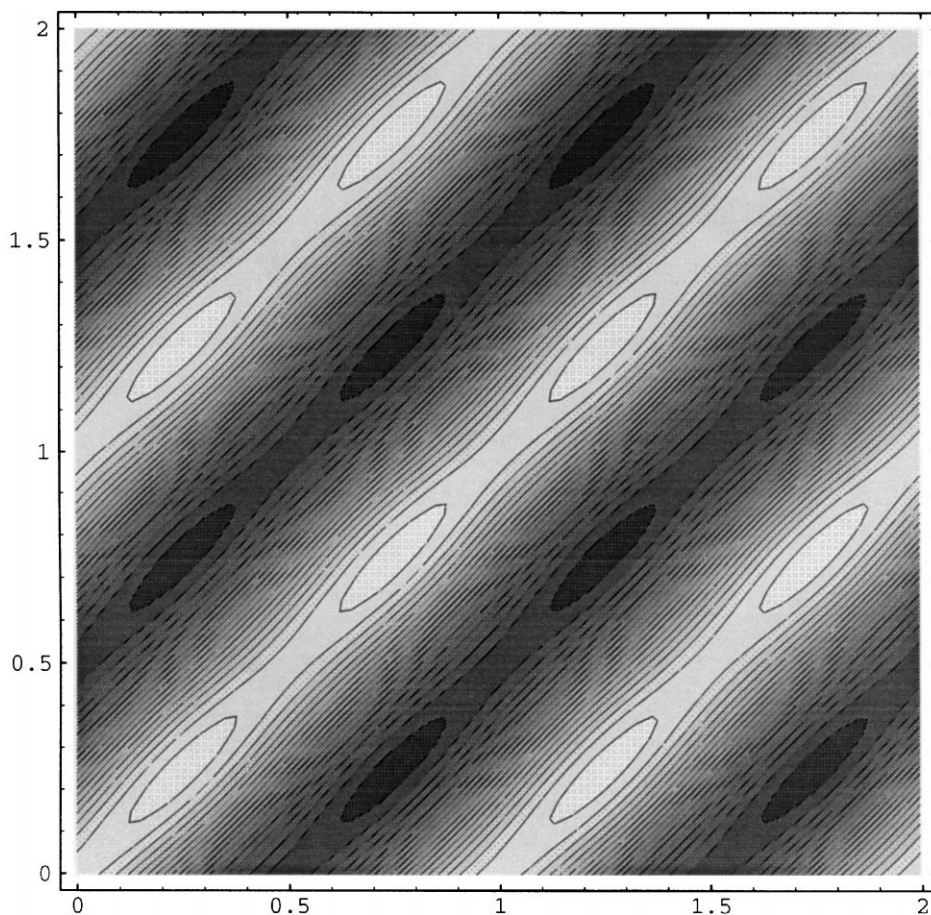

Fig. 5. Contour plot of stream function $\psi_{CS}^{(\varepsilon)}(x, y)$ of Childress–Soward flow (63) with $\varepsilon = 0.9$ (from [210]).
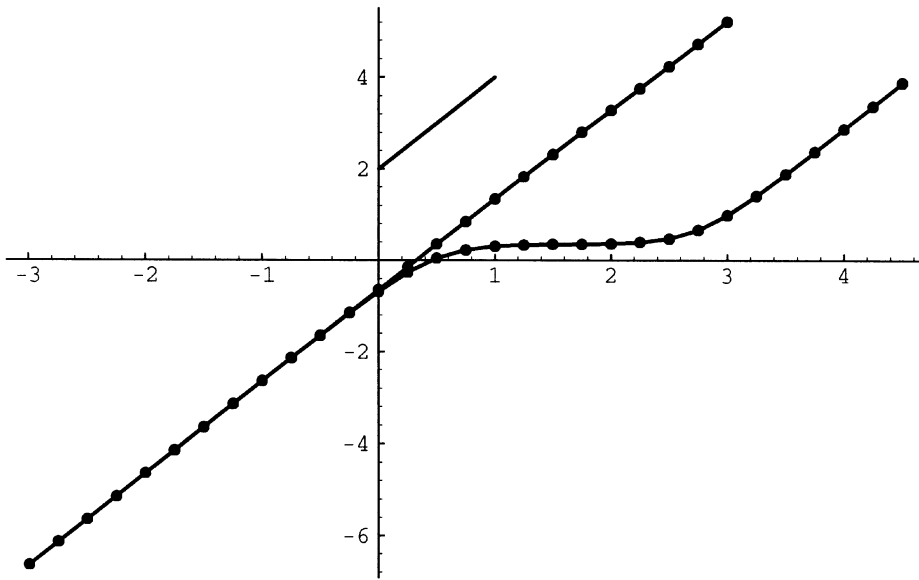
Fig. 6. Log–log plot of enhanced diffusion coefficient $\bar{K}_{xx}$ versus Pe for Childress–Soward flow (63) with $\varepsilon = 0.9$ (from [210]). Upper curve: mean flow $V = (2, 2)^{\dagger}$, lower curve: $V = (-2, 2)^{\dagger}$. Also shown is a line with slope 2 for reference.

In the case $V = (2, 2)^{\dagger}$, the mean flow is aligned parallel to the overall shearing direction, and has almost no effect on the enhanced diffusivity of the flow. (Compare with the effective diffusivity computed for this flow in the absence of any mean flow in Fig. 4.) The second case, in which the mean sweep is directed orthogonally to the shearing direction, exhibits instead two distinct scaling crossovers in the plot of $\ln \bar{K}_{xx}$ vs. $\ln$ Pe. For small Pe, the curve has slope 2, a general consequence of the Stieltjes integral representation (39) for arbitrary periodic flows [12]. As Pe increases through the range 10 to 10^3, the enhanced diffusivity temporarily plateaus to a constant level, then finally turns back to a quadratic rate of growth. The intermediate regime of constancy of $\bar{K}_{xx}$ is clearly attributable to the presence of the mean sweep transverse to the shearing direction. In fact, one may infer that for Pe $\lesssim 10^3$, the tracer diffusion behaves in the same way as if the velocity field were a superposition of a shear flow ($\varepsilon = 1$) with a transverse cross sweep. The enhanced diffusivity temporarily saturates at a finite level in accordance with the minimal enhancement of diffusion in such a flow. The reason why the perturbation to the shear flow (i.e. the difference of ε from 1) may not yet be noticable is that the finiteness of the Péclet number implies a sufficient amount of molecular diffusion which could blur out the sensitivity of the tracer to the rather small-amplitude deviations to the shear flow. For Pe $\gtrsim 10^3$, the departure of $v(x)$ from a parallel shear flow begins to be felt, and the enhanced diffusivity correspondingly turns over to a maximally diffusive character. The association of the intermediate plateau regime $10 \lesssim$ Pe $\lesssim 10^3$ with a regime in which the shear flow plus transverse sweep dominates the effects of the $\varepsilon \neq 1$ perturbations is also borne out by a computation of the eigenvectors of the enhanced diffusivity matrix [210]. Based on this numerical evidence and the rigorous asymptotic theory, we can conjecture that as $\varepsilon \nearrow 1$, the intermediate plateau regime in the plot of $\ln \bar{K}_{xx}$ vs. $\ln$ Pe extends ever further to the right, pushing the transition to the ultimate $\bar{K}_{xx} \sim O(\text{Pe}^2)$ growth stage to ever higher Péclet number.

The present study of the effective diffusivity in a perturbed shear flow with transverse cross sweep exemplifies the symbiotic interaction between mathematical theory, physical intuition, and numerical computations. The mathematical theory furnished some general asymptotic statements, which left open some details concerning the behavior of the effective diffusivity at finite Péclet number, but brought out some of the essential physical features of the flow which determine how effectively diffusion is enhanced. These considerations suggested some illustrative problems and questions to address numerically, and we thereby uncovered some interesting finite Péclet number crossover behavior which is beyond the reach of the asymptotic theory. On the other hand, the asymptotic theory plays a crucial role in checking the inferences we make from numerical simulations. If we had only computed the enhanced diffusivity up to Pe = 100, we would have missed the second transition in the curve in Fig. 6 corresponding to $V = (-2, 2)^\dagger$. The empirical evidence alone might misleadingly suggest that the enhanced diffusivity had reached a permanent finite limit, but the rigorous asymptotic theory would inform us that this could not possibly be the case, and that we would find another transition if we pushed our computations to higher Péclet number.

Contrast between mean sweeps with rational and irrational ratio of components: One particularly intriguing conclusion from the rigorous asymptotic theory is that the effective diffusivity can display diametrically opposite behavior, i.e. minimally or maximally enhanced diffusion in most directions, depending on whether a mean flow with rationally or irrationally related components is superposed. This is, taken at face value, a statement applicable only at enormously large Péclet number, since it is clear the effective diffusivity at any finite but large Péclet number cannot be much affected by an infinitesimal shift of the mean flow between rational and irrational ratios. Nonetheless, we understood above that this asymptotic statement had some apparent physical content, in that mean sweeps with rationally related components can be expected to open more efficient channels of rapid transport than mean flows with irrationally related components. Clearly, the practical issue suggested by both the asymptotic theory and this physical intuition is whether there can be a strong difference at finite Péclet number between the effective diffusivities when the ratio of the components of a mean flow pointing in a general direction is well approximated or is not well approximated by a *low-order* rational number (one with small integers in the numerator and denominator) [304].

This question was strikingly answered in the affirmative by [210] using a Childress–Soward flow (63) with $\varepsilon = 0.9$, and comparing the effects of two different mean sweeps, both generally transverse to the overall shearing direction. The first mean sweep is defined $V = (7.1, -7.1)^\dagger$, which clearly has a low order rational ratio (-1) of components. The tracer transport in this case is guaranteed by the rigorous asymptotic theory to be maximally diffusive at large Péclet numbers, and the numerical simulation results presented as the upper curve in Fig. 7 confirm this behavior. The enhanced diffusivity in this case exhibits a crossover at intermediate Péclet numbers $1 \lesssim \text{Pe} \lesssim 10$ in just the same way as the same Childress–Soward flow with rationally related mean sweep $V = (-2, 2)^\dagger$ which we discussed following Fig. 6. The reason for this crossover is that the perturbations to the shear flow play a subdominant role to the gross shear plus cross sweep structure until Péclet number is sufficiently large.

The enhanced diffusivity was next computed for a mean sweep $V = (7.14142, 7.1)^\dagger$, which has the same general direction as the first mean sweep, but is clearly not well approximated by any low-order rational. We therefore expect the enhanced diffusivity to behave for accessibly large
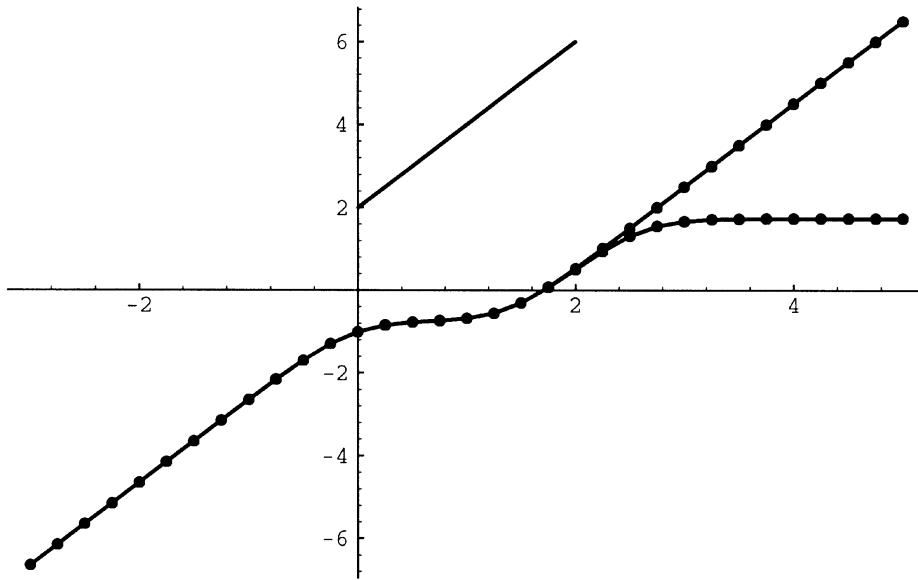
Fig. 7. Log–log plot of enhanced diffusion coefficient $\bar{K}_{xx}$ versus Pe for Childress–Soward flow (63) with $\varepsilon = 0.9$ (from [210]). Upper curve: mean flow $V = (7.1, -7.1)^{\dagger}$, lower curve: $V = (7.14142, -7.1)^{\dagger}$. Also shown is a line with slope 2 for reference.

values of Pe as if the mean flow had irrationally related components. Since the flow is readily shown to have no stagnation points, the mathematical theory predicts that the diffusivity should be only minimally enhanced for $V = (7.14142, 7.1)^{\dagger}$, in stark contrast to the maximally enhanced diffusion for $V = (7.1, 7.1)^{\dagger}$. This distinction is clearly manifested by the numerical computations in Fig. 7 at finite but large values of the Péclet number. The enhanced diffusivity behave identically for the two mean flows up to Pe $\sim 10^3$, at which point the flow with irrationally related mean sweep exhibits a second crossover to a minimally diffusive regime in which the enhanced diffusivity remains constant at least up to Pe $\sim 10^5$. This crossover may clearly be interpreted as a fairly sudden onset of sensitivity of the tracer transport to the fine structure of the flow created by the departure of the mean sweep $V = (7.14142, 7.1)^{\dagger}$ from a low-order rational. For smaller values of Péclet number, the molecular diffusion is sufficiently strong to coarse-grain the discrepancy between the two mean sweeps, but at larger values of Péclet number, the differences in the streamline structure are acutely felt by the tracer [304]. Similar crossover behavior is also exhibited in approximate analytical formulas for the enhanced diffusivity in flow drawn past a cubic array of small spheres [168].

Role of stagnation points: Recall that the theorem guaranteeing that mean flows with irrationally related components produce minimally enhanced diffusion required the absence of stagnation points of the total flow. This condition was needed in the proof of [210] to employ a theorem of Kolmogorov to effect a helpful change of coordinates. To examine whether this condition might be truly necessary or is just an artifact of the method of proof, those authors conducted some numerical studies of the effective diffusivity of a tracer in a flow with an irrationally related mean

sweep and stagnation points. They found that the presence of stagnation points did affect the large Péclet number behavior of the tracer transport so that it no longer had a minimally diffusive character [210]. Some discussion on the role of stagnation points in tracer transport also may be found in [97].

General implications: The examples presented above alert us to be cautious in inferring asymptotic scaling behavior of the effective diffusivity from computations at finite Péclet number because multiple crossovers can and do occur. They also explicitly demonstrate how the effective diffusivity can truly be exquisitively sensitive to fine details of the flow, particularly at high Péclet number. For instance, the two mean sweeps just considered differ by less than one percent, yet the enhanced diffusivity which results differs by orders of magnitude for moderately large values of Pe (see Fig. 7). We will see in Paragraph 2.3.2.1 that these differences are moreover manifested on practical, finite time scales [231]. These examples raise important concerns for the modelling of the effective diffusivity of a flow by nonrigorous, approximate, or *ad hoc* arguments, and provide simple, natural, and instructive test problems which can help determine whether these approximate theories are rich enough to capture the substantial variations in effective diffusivity produced by subtle changes in the flow.

2.2.5. Other spatio-temporal periodic flows

We have focused our above discussion of homogenized diffusivity to flows of shear and cellular type, but quite general periodic flows can be studied through a concerted use of numerical methods with the mathematical tools described in Paragraph 2.1.4.1. Such an approach is exemplified in the work of Biferale et al. [40], in which they compute the effective diffusivity of tracers in various interesting kinds of flows through three different numerical approaches. One is the numerical solution of the cell problem (14) through a conjugate gradient algorithm (rather than through the finite mode Fourier truncation method adopted in [210,226]. The second is through the construction of suitable Padé approximants from the numerical computation of a finite number of terms of a low Péclet number expansion of the effective diffusivity. As described in [9,12] and Paragraph 2.1.4.1, these Padé approximants can be used to bound the effective diffusivity rigorously and tightly over finite ranges of Péclet number, provided the coefficients of the low Péclet number expansion are computed with sufficient precision [40]. Finally, the effective diffusivity is computed through direct Monte Carlo simulations of the motion of a large number of tracers, which we will discuss at further length in Section 2.3.2.

For all flows considered, the effective diffusivities computed by the various methods agreed well over several decades of Péclet number. The computation by Padé approximants has some peculiar advantages and disadvantages. On the one hand, only a finite number of quantities must be computed to obtain rigorous bounds for *all* Péclet number, whereas the other approaches can compute the effective diffusivity for only one Péclet number at a time. Unfortunately, it is difficult to obtain good numerical precision with Padé approximants at high Péclet number [40], and this practically restricts the method to moderate and low Péclet number ($\mathrm{Pe} \lesssim O(10^2)$). The numerical solution of the homogenization cell problem (14) was found to be the most efficient means of computing the effective diffusivity at large Péclet number. One important consequence of the good agreement between this computation and those of the Monte Carlo simulations is that the asymptotic predictions of homogenization theory are realized on practical, finite time scales. We return to this point in Section 2.3.

Besides the steady cellular flow and its time-dependent perturbation mentioned in Section 2.2.3, Biferale et al. [40] considered a quite different, steady, three-dimensional "ABC flow":

$$\boldsymbol{v}(\boldsymbol{x}) = \boldsymbol{v}_{\text{ABC}}(x, y, z) = \begin{bmatrix} v_x(y, z) \\ v_y(x, z) \\ v_z(x, y) \end{bmatrix} ,$$

$$v_x(y, z) = \sin z + \cos y ,$$

$$v_y(x, z) = \sin x + \cos z ,$$

$$v_z(x, y) = \sin y + \cos x .$$

This ABC flow is an exact steady solution of Euler's equations. The streamlines form regular open tubes surrounded by chaotic regions. The transport is expected to be dominated by the open tubes, producing maximally enhanced diffusion, and this is verified numerically [40].

2.3. Tracer transport in periodic flows at finite times

The homogenization theory presented in Sections 2.1 and 2.2 for the effective diffusion of a passive scalar field by a periodic velocity field is an asymptotic theory guaranteed to be valid only at sufficiently large space and long time scales. In practical applications, it is important to know the time scale on which this asymptotic effective diffusive behavior is attained and the nature of the corrections to the diffusive behavior over finite intervals of time. We now address these questions by computing the statistical behavior of a single tracer in several classes of periodic flows at finite times.

First, we return to the periodic shear flows with constant or zero cross sweep, which we introduced in Section 2.2.1. Due to the special geometry of these flows, the equations of motion for tracers can be exactly integrated, and exact formulas for the moments of the tracer displacement can be derived for arbitrary time. From these, we can directly read off the rate of relaxation to the homogenized, long-time diffusive behavior as well as the character of the finite-time corrections. We will find that the homogenized description is accurate after a fixed time of order unity (nondimensionalized with respect to molecular diffusion scales as in Section 2.1.1), irrespective of Péclet number [230].

For general periodic flows, the tracer equations are too difficult to integrate exactly. The passive scalar evolution over pre-homogenized time scales for some special flows other than shear flows have been addressed through various *approximate* analytical techniques. As examples, we refer the reader in this regard to the finite time analysis by Young et al. [346] (and also [47]) for a high Péclet number steady cellular flow, and to Camassa and Wiggins' [52] treatment of tracer advection in a temporally oscillating cell flow by dynamical systems techniques which neglect molecular diffusion. Methods such as these rely upon a sufficiently simple geometry of the streamlines, as well as other asymptotic or ad hoc assumptions.

An alternative and effective way to study the motion of a tracer with quantitative accuracy over finite time intervals in a general periodic flow with complex geometry is by careful *Monte Carlo* numerical simulations. A Monte Carlo simulation is simply an integration of the particle trajectory

equations for a large number of particles undergoing independent random molecular diffusion in addition to advection by the flow. Averages computed from this finite sample are then used to estimate statistics of the full ensemble, such as the mean-square tracer displacmeent. We report on several Monte Carlo simulations [40,231] which show very good quantitative agreement with the predictions of homogenization theory after an initial transient stage extending at most over a (nondimensionalized) time interval of order unity. In particular, the subtle crossover behaviors predicted by homogenization theory for the class of Childress–Soward flows with a mean sweep in Section 2.2.4 are explicitly manifested over finite time intervals. This underscores the care which is required in formulating effective diffusivity models for practical applications, even in the relatively simple case of a periodic velocity field varying on spatial scales well separated from the macroscale. On the positive side, the good agreement between homogenization theory and the Monte Carlo simulations indicate that the effective diffusivity of tracers in a periodic flow on practical time scales can be computed through the numerical solution of a single cell problem (such as Eq. (33)), rather than through the generally more expensive simulation of the motion of a large number of tracers [40].

2.3.1. Periodic sinusoidal shear flow

We mentioned in Section 2.2.1 that many nontrivial aspects of passive scalar transport can be illuminated through explicit formulas within the class of shear flows. Here, we present exact formulas for the evolution *at all times* of the first and second spatial moments of a passive scalar field immersed in a steady, periodic shear flow with constant (possibly zero) cross sweep,

$$\boldsymbol{v}(\boldsymbol{x}) = \boldsymbol{v}(x, y) = \begin{bmatrix} \bar{w} \\ v(x) \end{bmatrix}.$$

These formulas for the behavior of the passive scalar field momentsat finite times will be compared to the predictions of homogenization theory worked out in Section 2.2.1.

We shall adopt a tracer-centered perspective to complement the field-centered perspective emphasized so far in Section 2. These are related in that the probability distribution function (PDF) for a single tracer in an incompressible velocity field obeys the advection–diffusion equation with initial data delta-concentrated at the initial tracer location; see the discussion in Section 1. The location $(X(t), Y(t))$ at time t of a single tracer (2) originating from (x_0, y_0) in the presence of a periodic shear flow with constant cross sweep obeys the following nondimensionalized stochastic equations of motion:

$$dX(t) = \mathrm{Pe}\,\bar{w}\,dt + \sqrt{2}\,dW_x(t), \quad X(t = 0) = x_0 \,, \tag{66}$$

$$dY(t) = \mathrm{Pe}\,v(X(t))\,dt + \sqrt{2}\,dW_y(t), \quad Y(t = 0) = y_0 \,.$$

The random increments $dW_x(t)$ and $dW_y(t)$ are differentials of independent Brownian motions [112,257] arising from molecular diffusion. Brownian motion has the following formal properties (for $W(t) = W_x(t)$ or $W(t) = W_y(t)$):

- $W(t)$ is a continuous random function.
- $W(t) - W(s)$ is a Gaussian random variable with mean zero and variance $|t - s|$.
- Increments of $W(t)$ over disjoint time intervals are independent of one another.
- $W(t = 0) = 0$.

Due to the spatially decoupled dynamics induced by a shear flow, the stochastic trajectory equations (66) can be integrated successively by quadrature:

$$X(t) = x_0 + \text{Pe}\,\bar{w}t + \sqrt{2}W_x(t) \,, \tag{67a}$$

$$Y(t) = y_0 + \text{Pe}\int_0^t v(X(s))\,\mathrm{d}s + \sqrt{2}W_y(t) \,. \tag{67b}$$

Note that the tracer position is random due to the Brownian motions arising from molecular diffusion.

Two statistics of fundamental interest are the mean displacement of the tracer,

$$\mu_X(t|x_0, y_0) \equiv \langle X(t) - x_0\rangle_W \,,$$
$$\mu_Y(t|x_0, y_0) \equiv \langle Y(t) - y_0\rangle_W \,, \tag{68}$$

and the variance of its location,

$$\sigma_X^2(t|x_0,y_0) \equiv \langle (X(t) - \mu_X(t))^2\rangle_W \,,$$
$$\sigma_Y^2(t|x_0,y_0) \equiv \langle (Y(t) - \mu_Y(t))^2\rangle_W \,. \tag{69}$$

The brackets $\langle\,\cdot\,\rangle_W$ denote an averaging over the Brownian motion statistics. Because the PDF of the tracer displacement is identical to the solution of the advection–diffusion equation with initial data

$$T_0(x, y) = \delta(x - x_0)\delta(y - y_0) \,,$$

the spatial moments of the passive scalar field evolving from such initial data are directly related to the tracer statistics (68) and (69) as follows:

$$\int_{-\infty}^{\infty}\int_{-\infty}^{\infty} (x - x_0)T(x, y)\,\mathrm{d}x\,\mathrm{d}y = \mu_X(t|x_0, y_0) \,,$$

$$\int_{-\infty}^{\infty}\int_{-\infty}^{\infty} (y - y_0)T(x, y)\,\mathrm{d}x\,\mathrm{d}y = \mu_Y(t|x_0, y_0) \,,$$

$$\int_{-\infty}^{\infty}\int_{-\infty}^{\infty} (x - x_0)^2 T(x, y)\,\mathrm{d}x\,\mathrm{d}y = \langle (X(t) - x_0)^2\rangle = \sigma_X^2(t|x_0, y_0) + (\mu_X(t|x_0, y_0))^2 \,, \tag{70}$$

$$\int_{-\infty}^{\infty}\int_{-\infty}^{\infty} (y - y_0)^2 T(x, y)\,\mathrm{d}x\,\mathrm{d}y = \langle (Y(t) - y_0)^2\rangle = \sigma_Y^2(t|x_0, y_0) + (\mu_Y(t|x_0, y_0))^2 \,.$$

In particular, $\mu_X(t|x_0, y_0)$ is the mean displacement of the center of mass and $\sigma_X^2(t|x_0, y_0)$ is the mean-square radius of a cloud of passive scalar particles initially released at (x_0, y_0).

The tracer motion across the shear flow is very simple to describe: $X(t)$ is a Gaussian random variable with mean

$$\mu_X(t|x_0, y_0) = x_0 + \text{Pe}\,\bar{w}t$$

and variance

$$\sigma_X^2(t|x_0, y_0) = 2t \ ,$$

as may be checked from the fundamental properties of the Brownian motion $W_x(t)$.

The statistics of tracer motion along the shear direction is naturally much richer. The main features for a periodic shear flow can be illustrated in the simple context of a single-mode sinusoidal shear flow:

$$v(x) = \sin 2\pi x \ .$$

The shear-parallel tracer displacement in a more general periodic shear velocity field can be computed in a similar manner by decomposing the shear flow into a sum of Fourier modes, see [230].

2.3.1.1. Mean tracer displacement along sinusoidal shear. For the single-mode case under current consideration, the mean displacement of the tracer along the shear is given by

$$\mu_Y(t|x_0, y_0) = \mathrm{Pe} \int_0^t \langle \sin(2\pi X(s)) \rangle_W \, \mathrm{d}s + \langle W_y(t) \rangle_W$$

$$= \mathrm{Pe} \int_0^t \langle \sin(2\pi(x_0 + \bar{w}s + \sqrt{2}W_x(s))) \rangle_W \, \mathrm{d}s \ . \tag{71}$$

The expectation in the integrand may be computed by expressing it as a complex exponential:

$$\langle \sin(2\pi(x_0 + \bar{w}s + \sqrt{2}W_x(s))) \rangle_W = \Im \langle \exp(2\pi i(x_0 + \bar{w}s + \sqrt{2}W_x(s))) \rangle_W \ , \tag{72}$$

where $\Im$ denotes the imaginary part of the subsequent expression. The right-hand side now involves the expectation of the exponential of a Gaussian random variable $2\pi i Z$, which can be explicitly computed according to the following general formula [257]:

$$\langle \mathrm{e}^{2\pi i Z} \rangle = \mathrm{e}^{2\pi i \langle Z \rangle} \mathrm{e}^{-2\pi^2 \langle (Z - \langle Z \rangle)^2 \rangle} \quad \text{for Gaussian } Z \ . \tag{73}$$

Evaluating Eq. (72) in this way, using the fact that $W_x(s)$ is a Gaussian random variable with mean zero and variance s, substituting the result into Eq. (71), integrating the resulting complex exponential, and taking the imaginary part of the resulting expression, we achieve the following exact formula for the mean displacement of the tracer along the shear:

$$\mu_Y(t|x_0, y_0) = \mathrm{Pe}^2 \frac{\bar{w}[\cos(2\pi x_0) - \mathrm{e}^{-4\pi^2 t} \cos(2\pi(x_0 + \mathrm{Pe}\,\bar{w}t))]}{2\pi(4\pi^2 + \mathrm{Pe}^2 \bar{w}^2)}$$

$$+ \mathrm{Pe} \frac{[\sin(2\pi x_0) - \mathrm{e}^{-4\pi^2 t} \sin(2\pi(x_0 + \mathrm{Pe}\,\bar{w}t))]}{4\pi^2 + \mathrm{Pe}^2 \bar{w}^2} \ . \tag{74}$$

The mean displacement is essentially characterized by exponentially decaying sinusoidal fluctuations. Clearly, the oscillations are induced by the sweeping of the tracer across the sinusoidal shear flow. Indeed, in the presence of a cross sweep $\bar{w} \neq 0$ and in the absence of molecular diffusion, tracers would simply follow the deterministic streamlines

$$y = y_0 + \frac{1}{2\pi\bar{w}}(\cos(2\pi x_0) - \cos(2\pi x))$$

and forever oscillate in a regular manner. Molecular diffusion breaks up the phase coherent motion of the tracer by pushing it randomly across different streamlines, and thereby causes the periodic component of the tracer's motion to decay exponentially. If we view $\mu_Y(t|x_0, y_0)$ as the mean center of mass (along the y direction) of a cloud initially released from (x_0, y_0), then we can say that molecular diffusion causes the cloud to spread out and eventually sample many period cells. The cloud's center of mass motion along the shear will therefore decay to zero by the law of large numbers, since the mean velocity along the shear is zero. Similar considerations apply when $\bar{w} = 0$, except that the coherent motion in the absence of molecular diffusion would be ballistic motion along straight streamlines aligned parallel to the y direction.

We note that in the long-time limit, the mean tracer displacement along the shear settles down to a constant:

$$\lim_{t \to \infty} \mu_Y(t|x_0, y_0) = \frac{2\pi \, \mathrm{Pe} \sin(2\pi x_0) + \mathrm{Pe}^2 \, \bar{w} \cos(2\pi x_0)}{2\pi(4\pi^2 + \mathrm{Pe}^2 \bar{w}^2)} \,.$$

This is consistent with the above reasoning that the mean tracer velocity along the shear should eventually vanish due to the averaging effects of molecular diffusion. The finite net displacement is determined by the accumulated transient momentum from early times where the tracer motion is still largely coherent. Indeed, the long-time net displacement is manifestly sensitive to the initial location x_0 of the tracer.

2.3.1.2. Variance of tracer displacement along shear. An exact formula can also be derived for

$$\sigma_Y^2(t|x_0, y_0) \equiv \langle (Y(t) - \langle Y(t) \rangle_W)^2 \rangle_W = \langle (Y(t) - y_0)^2 \rangle_W - (\langle Y(t) \rangle_W - y_0)^2 \,,$$

the variance of the tracer displacement along the shearing direction. The second term in the rightmost expression is just the square of $\mu_Y(t|x_0, y_0)$, which was evaluated above (see Eq. (74)). The first term may be evaluated similarly, starting from Eq. (67b) and using the standard properties of the independent Brownian motions $W_x(t)$ and $W_y(t)$:

$$\langle (Y(t) - y_0)^2 \rangle_W = 2t + \mathrm{Pe}^2 \int_0^t \int_0^t \langle \sin(2\pi X(s)) \sin(2\pi X(s')) \rangle_W \, \mathrm{d}s \, \mathrm{d}s'$$

$$= 2t + \frac{1}{2}\mathrm{Pe}^2 \int_0^t \int_0^t \langle \cos(2\pi(X(s) - X(s'))) - \cos(2\pi(X(s) + X(s'))) \rangle \, \mathrm{d}s \, \mathrm{d}s'$$

$$= 2t + \frac{1}{2}\mathrm{Pe}^2 \int_0^t \int_0^t \langle \cos(2\pi(\bar{w}(s - s') + W_x(s) - W_x(s'))$$

$$- \cos(2\pi(2x_0 + \bar{w}(s + s') + W_x(s) + W_x(s'))) \rangle_W \, \mathrm{d}s \, \mathrm{d}s'.$$

The integrand in the last expression is now in the form of a difference of the real parts of complex exponentials of Gaussian random variables, and may be evaluated using Eq. (73). The resulting integrand is again a complex exponential, which may be integrated over time in a straightforward albeit tedious manner. We finally find that the variance of the tracer displacement along the shear

may be expressed as follows:

$$\sigma_Y^2(t) = 2(1 + \bar{K}_{yy})t + \mathrm{Pe}^2 B_1(\mathrm{Pe}\,\bar{w})(1 - e^{-4\pi^2 t}\cos(2\pi\mathrm{Pe}\,\bar{w}t))$$

$$+ \mathrm{Pe}^2 B_2(\mathrm{Pe}\,\bar{w})e^{-4\pi^2 t}\sin(2\pi\mathrm{Pe}\,\bar{w}t)$$

$$+ \mathrm{Pe}^2 B_3(\mathrm{Pe}\,\bar{w})e^{-4\pi^2 t}[\cos(4\pi x_0) - \cos(2\pi(2x_0 + \mathrm{Pe}\,\bar{w}t))]$$

$$+ \mathrm{Pe}^2 B_4(\mathrm{Pe}\,\bar{w})e^{-4\pi^2 t}[\sin(4\pi x_0) - \sin(2\pi(2x_0 + \mathrm{Pe}\,\bar{w}t))]$$

$$+ \mathrm{Pe}^2 B_5(\mathrm{Pe}\,\bar{w})e^{-16\pi^2 t}[\cos(4\pi x_0) - \cos(4\pi(x_0 + \mathrm{Pe}\,\bar{w}t))]$$

$$+ \mathrm{Pe}^2 B_6(\mathrm{Pe}\,\bar{w})e^{-16\pi^2 t}[\sin(4\pi x_0) - \sin(4\pi(x_0 + \mathrm{Pe}\,\bar{w}t))]$$

$$+ \mathrm{Pe}^2 B_7(\mathrm{Pe}\,\bar{w})[\sin(2\pi x_0) - e^{-4\pi^2 t}\sin(2\pi(x_0 + \mathrm{Pe}\,\bar{w}t))]^2$$

$$+ \mathrm{Pe}^2 B_8(\mathrm{Pe}\,\bar{w})[\cos(2\pi x_0) - e^{-4\pi^2 t}\cos(2\pi(x_0 + \mathrm{Pe}\,\bar{w}t))]^2 , \tag{75}$$

where

$$\bar{K}_{yy} = \frac{\mathrm{Pe}^2}{2(4\pi^2 k^2 + \mathrm{Pe}^2\bar{w}^2)} \tag{76}$$

is the enhanced diffusivity predicted by homogenization theory (cf. (52)) and each B_j satisfies $B_j(z) \le C_j/(1 + z^2)$ for some numerical constant C_j independent of Péclet number. Precise formulas for these constants may be found in [231]. We note that the variance of the tracer displacement consists of a sum of a linear, diffusive growth, a constant, and some decaying, oscillating terms. Their presence may be explained in a similar way to analogous terms in the mean tracer displacement. Another method of derivation of the mean-square displacement of a tracer in a shear flow with cross sweep and some numerical plots of its behavior may be found in [131].

2.3.1.3. Relaxation to asymptotic homogenization regime. Homogenization theory predicts that at sufficiently long times, the PDF for the tracer displacement along the shear direction y will obey an effective diffusion equation with effective diffusivity $1 + \bar{K}_{yy}$ given by Eq. (76). In conjunction with Eq. (70), this implies that the mean of the tracer displacement along the shear, $\mu_Y(t|x_0, y_0)$ should settle down to a constant (since there is no advective term in the homogenized diffusion equation), and that its variance $\sigma_Y^2(t|x_0, y_0)$ should grow at an asymptotically linear rate

$$\lim_{t \to \infty} \sigma_Y^2(t|x_0, y_0) \sim 2(1 + \bar{K}_{yy})t .$$

The exact finite-time calculations (74) and (75) are in agreement with these homogenization asymptotic predictions. The tracer displacement departs at finite times from the effective diffusion description through some constant terms and transient, exponentially decaying, oscillatory terms. These finite-time corrections to the homogenized behavior do depend sensitively on initial data, in contrast to the effective diffusivity $\bar{K}_{yy}$.

An important question for applications is how much time must pass before the tracer displacement is accurately described by the homogenized diffusion equation. It is readily seen from

Eqs. (74) and (75) that for a steady, periodic shear flow with constant or zero cross sweep, the mean and variance of the tracer displacement relax to their homogenized limits on an order unity time scale which is independent of Pe. Recalling our reference units for nondimensionalization (Section 2.1.1), we conclude that for a periodic shear flow with constant or zero cross sweep, the homogenization theory becomes valid on a time scale comparable to that over which molecular diffusion, acting alone, would cause an initially concentrated cloud of tracers to disperse over several period cells. That this should be the governing time scale for the validity of the homogenized equations may be understood from the fact that homogenization theory appeals to an averaging over the periodic fluctuations of the velocity field. Without molecular diffusion, tracers would forever move along neatly ordered, periodic streamlines. One must therefore wait for molecular diffusion to buffet the tracer across all the streamlines in a period cell before the tracer has effectively sampled the velocity field over several period cells. We shall discuss in Paragraph 2.3.2.1 some types of periodic velocity fields for which homogenization is achieved on faster time scales.

2.3.2. Monte Carlo simulations over finite times

We now discuss the statistical behavior of tracers over finite-time intervals in more general flows. The general stochastic equations of motion for a tracer are, in nondimensionalized units (see Eqs. (2a) and (2b)):

$$dX(t) = \text{Pe}(V + v(X(t), t))\, dt + \sqrt{2}\, dW(t)\;, \tag{77a}$$

$$X(t = 0) = x_0\;, \tag{77b}$$

where $W(t)$ is a vector-valued random process with each component an independent Brownian motion. We showed in Section 2.3.1 how to integrate these equations in an exact closed form for the case in which $v(x, t)$ is a shear flow, but this is not generally possible. Instead, Eq. (77a) can be quantitatively studied over finite-time intervals through *Monte Carlo* numerical simulations. By this we simply mean a numerical discretization of these equations of motion, along with an artificial random number generator to simulate the discretized influence of the random Brownian motion term $\sqrt{2}\, dW(t)$ in (77a). In this way, one can numerically integrate the equations of motion (77a) and (77b) to produce a simulation of a single random realization of a tracer trajectory. To compute statistical quantities associated with the tracer motion, one simply performs a large number N of simulations of the tracer trajectory $\{X^{(j)}(t)\}_{j=1}^{N}$, using *independent* simulations of the Brownian motion for each case, and then averages over the sample. For example, one can numerically simulate the evolution of the mean-square displacement $\sigma_X^2(t) \equiv \langle |X(t) - x_0|^2 \rangle$ over a finite-time interval by computing the average

$$\sigma_{X,\text{app}}^2(t) \equiv \frac{1}{N} \sum_{j=1}^{N} |X^{(j)}(t) - x_0|^2$$

over the squared-displacements of the N independent runs.

The two numerical concerns in Monte Carlo simulations are the accurate discretization of the equations of motion (77a), (77b) and the choice of a sufficiently large sample size N to obtain accurate statistics reflecting the influence of the Brownian motion. Standard generalizations of the Euler and Runge–Kutta schemes for the stochastic equations (77a) may be found in [163]; one

must take care that a sufficiently small step size is chosen [231]. The random number generator must also be of sufficient quality to avoid spurious artifacts in the simulation of the Brownian motion [230]. Other substantial numerical challenges must be faced when conducting Monte Carlo simulations of the advection–diffusion of a tracer by a random velocity field with long-range correlations; we address this problem at length in Section 6.

2.3.2.1. Realization of homogenized behavior at finite time. Monte Carlo simulations have been utilized by McLaughlin [231] and Biferale et al. [40] to examine the extent to which the effective diffusion behavior predicted by homogenization theory describes the evolution of the mean square tracer displacement over finite time intervals in some interesting classes of flows. In both of these works, it was found that, after some transient period, the homogenized diffusivity does accurately describe (half) the rate of growth of the mean-square tracer displacement computed from the Monte Carlo simulations.

In particular, McLaughlin [231] showed in this way that the strong sensitivity of the effective diffusivity to the rationality or irrationality of the ratio of the components of a mean sweep across a two-dimensional steady periodic flow (see Section 2.2.4) is a relevant effect at finite times. He considered a Childress–Soward flow (63) with $\varepsilon = 0.5$, with two alternative mean sweeps, $V = (-15,15)$ and $V = (-15.5,15)$. The former clearly has a lower order rational ratio of coefficients than the latter, so greater enhanced diffusion is expected for the former in almost all directions. In Fig. 8, the enhanced diffusivity (along the x direction) computed by numerical solution of the homogenization cell problem (33) and by the Monte Carlo simulations are shown to agree to excellent accuracy. The actual definition used in [231] for the enhanced diffusivity as simulated by the Monte Carlo method over finite time is:

$$\bar{K}_{xx}^{(MC)} = \frac{1}{5}\int_5^{10}\left(\frac{N^{-1}\sum_{j=1}^N (X^{(j)}(t) - x_0)^2}{2t} - 1\right)dt,$$

where $N = 1000$ independent realizations of the tracer paths were simulated. The initial time interval $0 \le t \le 5$ was excluded from the average to reduce contamination by transient effects.

It is evident from Fig. 8 that the slight difference between the mean sweeps $V = (-15,15)$ and $V = (-15.5,15)$ creates an order of magnitude difference between the transport rate for finite Péclet number Pe $\sim 10^2$ after a finite interval of time $t \sim 10$ (in units nondimensionalized with respect to molecular diffusion). Examination of the simulated mean-square displacement as a function of time further revealed that the transient period of adjustment to the homogenized behavior was very rapid, on the order $t \sim 10^{-2}$ and decreasing further as Péclet number is increased [231]. This may be compared with the order unity time of adjustment found for the shear flow with cross sweep discussed in Section 2.3.1. The difference is apparently due to the better mixing properties of the Childress–Soward flow with mean sweep; the velocity field cooperates with the molecular diffusion to accelerate the rate at which a tracer fully samples a period cell and thereby attains its ultimately homogenized behavior [231].

Monte Carlo simulations have also been utilized by Crisanti et al. [77] for flows closely akin to Childress–Soward flows without mean sweep (see Paragraph 2.2.3.1). The simulated diffusivities are found to behave in a manner consistent with maximally enhanced diffusion along the direction of the open channels and minimally enhanced diffusion in the transverse direction where transport
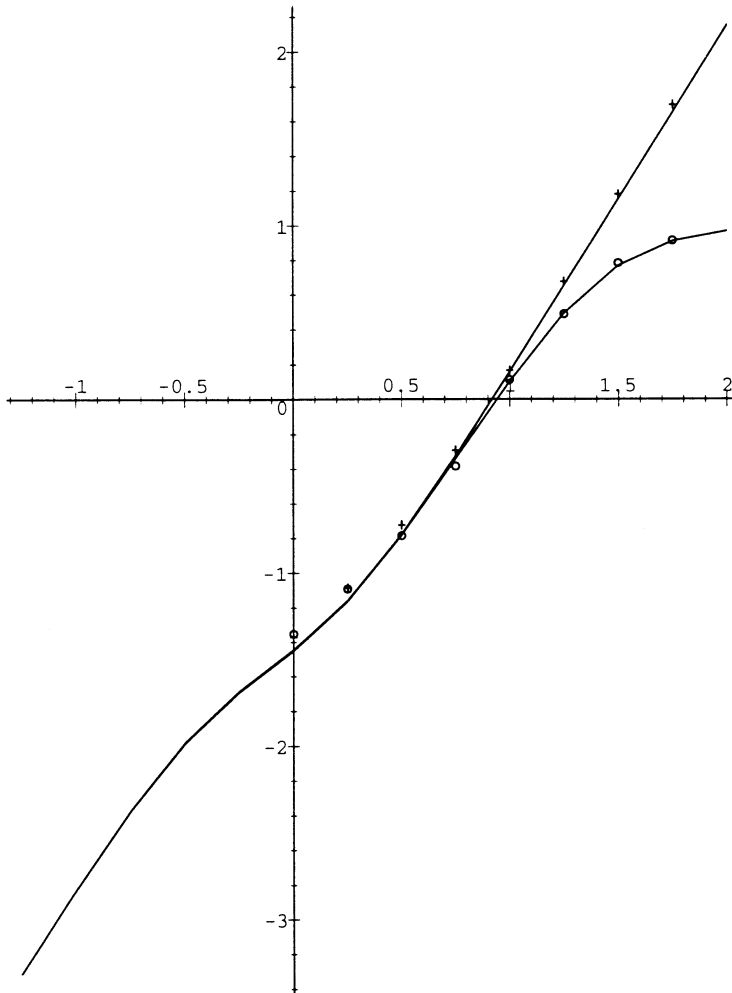
Fig. 8. Log–log plot of enhanced diffusion coefficient $\bar{K}_{xx}$ versus Pe (from [231]). Solid curves: numerical solutions of cell problem from homogenization theory, discrete markers: Monte Carlo simulations. Upper curve and crosses: mean sweep $(-15, 15)^{\dagger}$, lower curve and circles: mean sweep $(-15.5, 15)^{\dagger}$.

is blocked by streamlines. Finally, we note that Rosenbluth et al. [287] employed Monte Carlo simulations to check and extend their analytical high Péclet number predictions for the effective diffusivity of a passive scalar field in a cellular flow (62), which they obtained through matched asymptotic expansions rather than through homogenization theory.

2.4. Random flow fields with short-range correlations

The periodic flows we have been considering so far have a precisely ordered structure. Many flows in nature and in the laboratory, however, are at sufficiently high Reynolds number that

turbulent fluctuations are strongly excited, and these impart a disordered and chaotic character to the flow pattern. A convenient way to approximate the complex spatio-temporal structure of such turbulent flows is by modelling the velocity field as a *random* function. The typical realizations (particular random choices) of velocity fields in such random models display a disordered structure which is quite difficult to achieve through deterministic models. The stochastic nature of random velocity field models is also appropriate because of the unpredictability of the precise microstructure which a turbulent flow will develop in systems where only large-scale information can be observed or specified, as is always the case in practice. We will exclusively consider random *incompressible* flows ($\nabla \cdot \boldsymbol{v}(\boldsymbol{x}, t) = 0$), but will not otherwise insist that the random velocity fields are actual statistical solutions of the Navier–Stokes or Euler hydrodynamic equations. For reference, we provide an appendix in Section 2.4.5 discussing some fundamental definitions, notations, and facts about random functions which we will need throughout this report.

We begin our exploration of the advection of a passive scalar field by a random velocity field by considering two large-scale, long-time rescalings which rigorously lead, in certain asymptotic limits, to effective diffusion equations for the mean passive scalar field (averaged over the statistics of the velocity field). One of these, which we discuss in Section 2.4.1, corresponds to a limit in which the spatial scale of the velocity field is scaled up in proportion to the spatial scale of the passive scalar field. The effective diffusivity in this limit is given by the relatively simple Kubo formula [188]. Next, in Section 2.4.2, we consider the same sort of large-scale, long-time limit of a passive scalar field advected by a steady random velocity field as we did in the context of periodic velocity fields in Section 2.1.2. A similar homogenized description results, provided that the velocity field has sufficiently short-ranged correlations so that a strong separation can exist between the observed macroscale and the spatial scale of the velocity field fluctuations [12]. Throughout Section 3, we will explore examples of random shear flows which have strong long-range correlations which violate the conditions for the applicability of the homogenization theory, and the tracer motion is explicitly shown in such examples to proceed superdiffusively at long times.

Stieltjes measure formulas and variational principles for the effective diffusivity, analogous to those presented for periodic flows in Section 2.1.4, will be developed for steady, homogenous random fields in Section 2.4.3. In Section 2.4.4, we discuss the application of the homogenization theory to some example random flows.

2.4.1. Kubo theory

Before presenting the homogenization theory for random velocity fields, we consider another type of large-scale, long-time asymptotic rescaling which also leads to an effective diffusion equation, but with a much simpler formula for the effective diffusivity. We will express this rescaling in terms of dimensional functions and variables.

We consider a given homogenous, stationary, mean zero, incompressible random velocity field $\boldsymbol{v}(\boldsymbol{x}, t)$. We rescale the passive scalar field to large scales and long times

$$T^{(\tilde{\delta})}(\boldsymbol{x}, t) \equiv \tilde{\delta}^{-d} T(\tilde{\delta}\boldsymbol{x}, \tilde{\delta}^2 t) ,$$

with $\tilde{\delta} \to 0$, and simultaneously rescale the length scale of the random velocity field to remain on the same order as that of the passive scalar field:

$$\boldsymbol{v}^{(\tilde{\delta})}(\boldsymbol{x}, t) = \boldsymbol{v}(\tilde{\delta}\boldsymbol{x}, t) .$$

This rescaling of the length scale of the velocity field distinguishes the present asymptotic rescaling from that leading to homogenization theory; see Section 2.4.2 below. In particular, $\tilde{\delta}$ is not the ratio between the spatial scales of the velocity and passive scalar fields; it may rather be thought of as the ratio between some fixed reference scale and the common scale of the velocity and passive scalar field. The rescaled advection–diffusion equation reads

$$\partial T^{(\tilde{\delta})}(\boldsymbol{x}, t)/\partial t + \tilde{\delta}^{-1}\boldsymbol{v}(\boldsymbol{x}, \tilde{\delta}^{-2}t) \cdot \nabla T^{(\tilde{\delta})}(\boldsymbol{x}, t) = \kappa \Delta T^{(\tilde{\delta})}(\boldsymbol{x}, t) ,$$
$$T^{(\tilde{\delta})}(\boldsymbol{x}, t = 0) = T^{(\tilde{\delta})}(\boldsymbol{x}) . \tag{78}$$

We now seek a simplified description for the mean statistics $\langle T^{(\tilde{\delta})}(\boldsymbol{x}, t) \rangle$ in the limit that $\delta \to 0$; angle brackets denote a statisical average over all randomness. The general obstacle to obtaining an effective equation for the mean passive scalar density is the difficulty in evaluating the average of the nonlinear term $\langle \boldsymbol{v} \cdot \nabla T \rangle$ in terms of $\langle T \rangle$ or other simple statistical objects (see Section 1). As $\tilde{\delta} \to 0$, however, one can hope to approximate

$$\langle \tilde{\delta}^{-1}\boldsymbol{v}(\boldsymbol{x}, \tilde{\delta}^{-2}t) \cdot \nabla T^{(\tilde{\delta})}(\boldsymbol{x}, t) \rangle$$

accurately by accounting for the velocity field in some averaged way, since there is a strong separation between the *time* scales characterizing the rate of change of the velocity field and the passive scalar field. To have any hope of achieving this program, the original velocity field must have some sufficiently strong decorrelation in time. In particular, $\boldsymbol{v}(\boldsymbol{x}, t)$ cannot be steady or have very long-term memory. In mathematical terminology, the velocity field $\boldsymbol{v}(\boldsymbol{x}, t)$ must have certain *mixing* properties in time [143].

Provided that the unscaled velocity field $\boldsymbol{v}(\boldsymbol{x}, t)$ does obey certain mixing and other technical regularity conditions, it can be shown [44,159,262] that for bounded and sufficiently smooth initial data $T_0(\boldsymbol{x})$, the passive scalar field $T^{(\tilde{\delta})}(\boldsymbol{x}, t)$ converges uniformly over finite intervals of (rescaled) time to a nontrivial limit

$$\lim_{\tilde{\delta} \to 0} T^{(\tilde{\delta})}(\boldsymbol{x}, t) = \bar{T}(\boldsymbol{x}, t)$$

which obeys an effective diffusion equation

$$\partial \bar{T}(\boldsymbol{x}, t)/\partial t = \nabla \cdot (\mathscr{K}^* \nabla \bar{T}(\boldsymbol{x}, t)) ,$$
$$\bar{T}(\boldsymbol{x}, t = 0) = T_0(\boldsymbol{x}) , \tag{79}$$

with effective diffusion tensor

$$\mathscr{K}^* = \mathscr{I} + \mathscr{K}_{\text{Kubo}}$$

given by the *Kubo formula* [188]

$$\mathscr{K}_{\text{Kubo}} = \int_0^\infty \tilde{\mathscr{R}}(\boldsymbol{0}, t)\,\mathrm{d}t ,$$
$$\tilde{\mathscr{R}}(\boldsymbol{x}, t) = \langle \boldsymbol{v}(\boldsymbol{x}' + \boldsymbol{x}, t' + t) \otimes \boldsymbol{v}(\boldsymbol{x}', t') \rangle . \tag{80}$$

The matrix $\mathscr{K}_{\text{Kubo}}$ is guaranteed, by general properties of correlation functions ([341], Section 4), to be non-negative definite, and therefore represents an enhanced diffusivity. Note that the Kubo

diffusivity $\mathscr{K}_{\mathrm{Kubo}}$ depends only the amplitude of the velocity field and its integrated temporal structure; there is no dependence on the spatial structure of the random field $\boldsymbol{v}(\boldsymbol{x},t)$.

Kubo formally argued this result for the case of a purely time-dependent random velocity field $\boldsymbol{v} = \boldsymbol{v}(t)$ and no molecular diffusion in his pioneering paper [188]. In this case the spatial rescaling of the velocity field is trivial, and one concludes from the above that the long-time asymptotics of the mean passive scalar field in a spatially uniform velocity field with short-ranged temporal correlations is, under appropriate conditions, governed by some positive effective diffusivity, even in the absence of molecular diffusion. Stratonovich [313] formulated the more general result stated above for the case of random velocity fields with spatio-temporal fluctuations, and Khas'minskii [159] was the first to provide a rigorous derivation of these asymptotics, though under somewhat restrictive conditions on the random velocity field model. Later work widened the applicability of Khas'minskii's theorem to a broader class of random velocity fields (see [44,262], and the references in [134]). We note these theorems are generally stated without accounting for molecular diffusion, but their proofs can be easily extended to include it.

Note that the Kubo theory requires no fundamental restriction (other than regularity) on the spatial structure of the velocity field, and thus can be applied under certain circumstances to velocity fields with long-range spatial correlations. It has indeed been shown [15] that a slightly generalized form of Kubo theory describes the large-scale, long-time behavior of the mean passive scalar field in a certain natural class of random velocity field models with qualitative features similar to those of fully developed turbulence. We discuss this point briefly in Paragraph 3.4.3.3.

As with homogenization theory, we must remember that Kubo theory is a long-time asymptotic theory, and the description of the evolution of the passive scalar field by an effective diffusion is only valid at sufficiently long times. Over finite time intervals, the passive scalar field may behave in a radically different way. For example, very simple models can be formulated for which the passive scalar field has an effectively negative diffusion over finite time intervals (see Section 3.4.4 and [18,131,141]). Also, Kubo theory crucially requires that the velocity field not have long-range memory. Superdiffusion can result from random, purely time-dependent velocity fields with long-range temporal correlations [18], as we will demonstrate in Section 3.1.2.

We finally remark that the asymptotically rescaled advection–diffusion equation (78) can also be interpreted as describing a limit in which the correlation time of the velocity field is very fast compared to the advection time scale, without any large-scale, long-time rescaling. We discuss this perspective in Paragraph 4.1.3.1.

2.4.2. Homogenization theory for random flows

We now revisit the large-scale, long-time rescaling of the passive scalar field introduced in the context of periodic velocity fields in Section 2.1.2 and apply it to the case of advection by a *steady, random, incompressible, homogenous* velocity field. In this rescaling, the velocity field is held fixed while the length scale of the initial passive scalar field is made large relative to the length scales characterizing the random velocity field. A simplified, homogenized description of the passive scalar is sought in the asymptotic limit, with the idea that over large scales, the random velocity field ought to have some averaged bulk effect. There is, however, an important distinction between periodic and random velocity fields that comes into play here. Periodic velocity fields have a well-defined, single length scale which can be definitely separated by a factor δ from the large length scale characterizing the passive scalar field. Random velocity fields, on the other hand, can

in general have a continuum of actively excited scales which can moreoever extend to arbitrarily large scales. Homogenization requires the notion that the velocity field fluctuates on much smaller scales than the passive scalar field, and this may never happen in a meaningful sense under a formal large-scale, long-time rescaling (10) of the passive scalar field if the velocity field has strong long-range correlations.

A simple and general criterion for the applicability of a homogenized diffusive behavior for the passive scalar field on large scales and long times was formulated in [12] in terms of the finiteness of the following *Péclet number* defined for random velocity fields:

$$\text{Pe} \equiv \kappa^{-1} \left(\int_{\mathbb{R}^d} \frac{\text{Tr}\,\hat{\mathscr{R}}(\boldsymbol{k})}{4\pi^2 |\boldsymbol{k}|^2} \right)^{1/2}, \quad \mathrm{d}\boldsymbol{k} = \kappa^{-1} \left(\frac{1}{2\pi^2} \int_0^\infty E(k) k^{-2} \,\mathrm{d}k \right)^{1/2}, \tag{81}$$

where $\hat{\mathscr{R}}$ is the spectral density of the velocity field:

$$\hat{\mathscr{R}}(\boldsymbol{k}) = \int_{\mathbb{R}^d} \mathrm{e}^{-2\pi \mathrm{i} \boldsymbol{k} \cdot \boldsymbol{x}} \mathscr{R}(\boldsymbol{x}) \,\mathrm{d}\boldsymbol{x} \;,$$

$$\mathscr{R}(\boldsymbol{x}) = \langle \boldsymbol{v}(\boldsymbol{x}' + \boldsymbol{x}) \otimes \boldsymbol{v}(\boldsymbol{x}') \rangle \;,$$

and

$$E(k) = \frac{1}{2} \int_{S^{d-1}} \text{Tr}\,\hat{\mathscr{R}}(k\hat{\boldsymbol{\varpi}}) \,\mathrm{d}\hat{\boldsymbol{\varpi}}$$

is the energy spectrum (integrated over spherical shells of constant wavenumber). It is readily checked that if the random velocity field has fluctuations sharply concentrated near a single length scale L_v, then the Péclet number (81) is proportional to $L_v \langle |\boldsymbol{v}|^2 \rangle^{1/2} / \kappa$, which is comparable to the definition (7) of Péclet number for a periodic velocity field.

A finite value of the Péclet number is equivalent to a sufficiently weak distribution of energy at low wavenumbers (large scales), which implies that the random velocity field's spatial correlations are sufficiently short ranged. In particular, a characteristic length scale

$$L_v = \kappa \text{Pe} / \langle |\boldsymbol{v}|^2 \rangle^{1/2} \tag{82}$$

can be associated to any random velocity field with finite Péclet number; L_v formally describes the largest length scale of the velocity field with substantial energy. An infinite value of the Péclet number may be viewed as a manifestation of strong long-range correlations; examples of such flows will be studied in Section 3.

It was shown in [12] that a rigorous homogenized large-scale, long-time description of the passive scalar field advected by a random velocity field is possible whenever the Péclet number is finite. We shall present this homogenized theory in terms of variables and functions nondimensionalized in a similar way as in Section 2.1.1, using now the length scale (82) and time scale L_v^2/κ. The nondimensionalized advection–diffusion equation reads

$$\partial T(\boldsymbol{x}, t)/\partial t + \text{Pe}\,\boldsymbol{v}(\boldsymbol{x}) \cdot \nabla T(\boldsymbol{x}, t) = \varDelta T(\boldsymbol{x}, t) \;,$$

$$T(\boldsymbol{x}, t = 0) = \delta^d T_0(\delta \boldsymbol{x}) \;,$$

where δ denotes a ratio between the length scale L_v of the random velocity field and the length scale L_T of the initial passive scalar field.

Defining the rescaled passive scalar field as before (10),

$$T^{(\delta)}(x, t) \equiv \delta^{-d} T(\delta x, \delta^2 t) ,$$

we obtain the following advection–diffusion equation, rescaled to large spatial scales and long times

$$\partial T^{(\delta)}(x, t)/\partial t + \delta^{-1} \mathrm{Pe}\, v\left(\frac{x}{\delta}\right) \cdot \nabla T^{(\delta)}(x, t) = \varDelta T^{(\delta)}(x, t) ,$$

(83)

$$T^{(\delta)}(x, t = 0) = T_0(x) .$$

For incompressible random, homogenous, ergodic velocity fields with finite values of the Péclet number (81), the following homogenization theorem can be established.

2.4.2.1. Homogenized effective diffusion equation for random velocity fields with short-range correlations. In the long time, large-scale limit, the rescaled passive scalar field converges to a finite limit

$$\lim_{\delta \to 0} T^{(\delta)}(x, t) = \bar{T}(x, t) ,$$

(84)

which satisfies an effective diffusion equation

$$\frac{\partial \bar{T}(x, t)}{\partial t} = \nabla \cdot (\mathscr{K}^* \nabla \bar{T}(x, t)) ,$$

(85a)

$$\bar{T}(x, t = 0) = T_0(x) ,$$

(85b)

with constant, positive-definite, symmetric diffusivity matrix $\mathscr{K}^*$. This effective diffusivity matrix can be expressed as

$$\mathscr{K}^* = \mathscr{I} + \bar{\mathscr{K}} ,$$

where $\mathscr{I}$ is the identity matrix (representing the nondimensionalized molecular diffusion) and $\bar{\mathscr{K}}$ is a nonnegative-definite *enhanced diffusivity* matrix which represents the additional diffusivity due to the random flow. The enhanced diffusivity matrix $\bar{\mathscr{K}}$ can be computed as follows. Let $\chi(x)$ be the (unique) random field with the following properties:

- $\chi(0) = 0$,
- $\nabla \chi(x)$ is a homogenous, random tensor field with $\langle \|\nabla \chi(x)\|^2 \rangle < \infty$,
- χ solves the following random elliptic equation on $\mathbb{R}^d$ (in unscaled coordinates):

$$\mathrm{Pe}\, v(x) \cdot \nabla \chi(x) - \varDelta \chi(x) = -\mathrm{Pe}\, v(x) .$$

(86)

Then the components of the enhanced diffusivity matrix may be expressed as

$$\bar{\mathscr{K}}_{ij} = \langle \nabla \chi_i \cdot \nabla \chi_j \rangle , \tag{87}$$

where the angle brackets denote an ensemble average over the statistics of the velocity field.

A homogenization theorem of this form was established by Avellaneda and the first author [12], using the framework of homogenization of equations with random coefficients developed by Papanicolaou and Varadhan [264], and by Oelschläger [256] using a somewhat different probabilistic approach. Some additional technical conditions required in these proofs were later removed by Fannjiang and Papanicolaou [98].

The finite Péclet number condition for the homogenization theorem is essential. Explicit shear flow examples [10] rigorously demonstrate that when the Péclet number (81) is infinite, the mean passive scalar field will generally not be described by an effective diffusion equation at large scales and long times; see Section 3. The finite Péclet number condition for the applicability of the homogenization theorem for random velocity fields cannot therefore be weakened unless some explicit reference is made to the flow geometry.

The homogenization theorem for random fields is very similar to that which was stated for periodic velocity fields in Section 2.1.2. Indeed, modulo some technicalities, "periodicity" has simply been converted to "statistical homogeneity", and averages over the period cell have been replaced by ensemble averages over the velocity field. Indeed, the homogenization theorem for steady, periodic velocity fields can be essentially embedded into the random homogenization theorem by defining a homogenous random field as periodic velocity field with the origin of the period lattice uniformly distributed over a fixed period cell. A homogenization theorem for spatio-temporal random velocity fields may be found in [245,244].

2.4.2.2. Comparison between Kubo theory and homogenization theory for random velocity fields. Before moving on to develop the homogenization theory for random velocity fields, we pause to compare it to the Kubo theory presented in Section 2.4.1. The principal differences in the asymptotic setup are that

- the Kubo theory rescales the spatial scale of the velocity field in tandem with the spatial scale of the passive scalar field, while the homogenization scaling leaves the velocity field fixed, and leads to a strong formal separation of the spatial scales of the velocity and passive scalar field;
- the homogenization theory is formulated for steady velocity fields, whereas the Kubo theory relies crucially on sufficiently rapid decorrelation of the velocity field in time.

The Kubo and homogenization theories may therefore be viewed as complementary coarse-grained averaging theories. The effective averaging in homogenization theory of steady random velocity fields with short-range correlations occurs because a large spatial volume contains many regions between which the velocity fluctuations are essentially independent. Therefore, any coarse volume will sample and average over the full statistics of the velocity field, assuming it is ergodic with short-ranged correlations. Under the Kubo rescaling, on the other hand, the spatial scale of the velocity field is scaled up along with the coarse scale of the passive scalar field, so there is no averaging over space. Instead, the effective averaging occurs because a coarse-grained time interval can be broken up into many subintervals over which the velocity field fluctuations are essentially

independent, provided that the random velocity field has sufficiently strong mixing (forgetting) properties as a function of time. We can therefore associate the homogenization theory of steady random velocity fields to spatial averaging, and the Kubo theory to temporal averaging. This explains why the homogenization theory requires short-range correlations in space, but no temporal decorrelation, whereas the Kubo theory requires short-range correlations in time (through the mixing assumption), but not necessarily any spatial decorrelation.

One interesting question is why the Kubo effective diffusivity formula (80) is so much simpler than the homogenized effective diffusivity formula (87). The answer is that spatial averaging by a tracer is much more complex than temporal averaging. Indeed, the temporal coordinate of a tracer marches in a trivial linear manner as time proceeds, whereas the variation of its spatial coordinate depends intricately on the properties of the velocity field. Under Kubo rescaling, the velocity field varies slowly in space but rapidly in time, so the fluctuations in a tracer's velocity come primarily from the intrinsic (Eulerian) temporal decorrelation of the velocity field, rather than due to the tracer's motion across the velocity field. Indeed, the tracer effectively feels a velocity field which is (locally) constant in space but fluctuating in time. Therefore, the averaged motion of the tracer may, in the asymptotically rescaled Kubo limit, be simply expressed in terms of time averages of the statistics of the velocity field (80). A tracer moving in a steady flow, on the other hand, samples the velocity field in a nonuniform way; it will, for example, spend a disproportionate amount of time near stagnation points. Hence, the homogenized effect of the steady velocity field felt by the tracer cannot be expressed in terms of a straightforward volume average of the velocity field. The effective bulk averaging of the tracer transport in homogenization theory is instead intricately dependent on the velocity microstructure and the effects of molecular diffusion, as expressed through the cell problem (86).

2.4.3. Alternative representations for effective diffusivity in random flows

A Stieltjes integral representation and some variational principles can be formulated for the effective diffusivity of a passive scalar field in a random velocity field with short-range correlations, in analogy to the periodic velocity field case discussed in Paragraph 2.1.4.1. The formulas have a similar appearance in both the periodic and random settings, though their derivation is more technically involved in the random case.

2.4.3.1. Stieltjes integral representation. The effective diffusivity $\mathscr{K}^*$ of the passive scalar field in a steady random velocity field with $\mathrm{Pe} < \infty$ was shown by Avellaneda and the first author [9,12] to be expressible as a Stieltjes integral,

$$\hat{e} \cdot \bar{\mathscr{K}} \cdot \hat{e} = \mathrm{Pe}^2 \|\boldsymbol{v} \cdot \hat{e}\|_{-1}^2 \int_{-\infty}^{\infty} \frac{\mathrm{d}\rho_v}{1 + \mathrm{Pe}^2 \mu^2} \tag{88}$$

with respect to a certain measure $\mathrm{d}\rho_v$ which is nonnegative and normalized to have total integral equal to one. The Stieltjes integral formula (88) is formally identical to that for the periodic case (41); only the definition of its components are modified. For example, the definition of the Sobolev norm $\|\cdot\|_{-1}$ in the prefactor involves now an average over the random ensemble of velocity fields rather than over a period cell (40). Most importantly, the operator $\mathscr{A}^V$ defined by

$$\mathscr{A}^V \boldsymbol{g} = \nabla \Delta^{-1}((\boldsymbol{V} + \boldsymbol{v}(\boldsymbol{x})) \cdot \boldsymbol{g})$$

which arises in the formal derivation of the Stieltjes integral representation is now a random operator acting on homogenous random fields with finite variance defined over $\mathbb{R}^d$. The measure $d\rho_v$ which appears in the Stieltjes integral representation is consequently no longer a discrete measure concentrated on a countable number of points, but is instead generally a continuous distribution (with possibly some discrete components). Therefore, the Stieltjes integral representation will not generally be reducible to a discrete sum (39) as in the periodic case.

Moreover, the support of $d\rho_v$ may be unbounded, in which case, Eq. (88) implies that a small Péclet number expansion of the effective diffusivity will be divergent for *all* Péclet number. The work of Kraichnan [181] suggests that this does indeed occur for velocity fields with Gaussian statistics. The Stieltjes integral representation therefore represents in these cases a rigorous resummation of a formal perturbative power series with zero radius of convergence [9,11]. We stress, however, that this rigorous resummation is valid only when the notion of an effective, homogenized diffusivity is itself meaningful, i.e. when there is a strong separation of scales between the velocity and passive scalar field. Passive scalar transport in fully developed turbulence, in particular, cannot be handled in this manner (see Section 3.4.3).

As in the periodic case, the existence of the Stieltjes integral representation implies that certain Padé approximants can be built from the coefficients of a formal (but divergent) small Péclet number series which rigorously bound the effective diffusivity at all Péclet numbers. Criteria for maximal and minimal diffusivity are more difficult to formulate for the case of random velocity fields due to the loss of discreteness of the measure $d\rho_v$ appearing in the Stieltjes integral representation formula (88). Generalizations of the Stieltjes integral representation to time-dependent random velocity fields with $\text{Pe} < \infty$ were derived by Avellaneda and Vergassola [20]; the modification is parallel to that of the periodic case discussed in Paragraph 2.1.4.1 (see in particular Eq. (42)).

2.4.3.2. Variational principles. The effective diffusivity in a homogenous random field can be represented through a variational principle (47) just as in the periodic case. The only differences are that:

- the trial functions g are now homogenous random fields defined on $\mathbb{R}^d$, with $g - \hat{e}$ a generalized gradient of a homogenous random field with finite variance, and
- the average of the functional $|g|^2 + \text{Pe}^2 g \cdot \mathscr{K} \cdot g$ over the period cell is replaced by an average over the statistical ensemble of the random velocity field.

The original variational formulation for homogenous random velocity fields was derived by Avellaneda and the first author in [12]. Other types of variational principles for random velocity fields, particularly with a cellular structure, were later put forth by Fannjiang and Papanicolaou [99]. These variational principles can be used to obtain rigorous bounds and estimates for the effective diffusivity in random velocity fields [12,99] in a similar way to periodic velocity fields, but they are a bit more difficult to implement in practice since the fundamental spatial domain is infinite space rather than a compact period cell [99].

2.4.4. Examples of effective diffusivity for random flows

Most of the studies of tracer transport in random velocity fields with short-range correlations appear to focus on flows with vortex or cellular structures, and we mention a few of these here.

Avellaneda and the first author [12] derived an exact formula for the effective diffusivity in a flow consisting of a random tiling of two-dimensional space by a family of circular vortices of various sizes but common shape and direction of rotation. The special structure of this random flow permitted the reductionof the cell problem (86) to an exactly solvable, radially symmetric PDE on a single disk. It was found in this way that the the effective diffusivity scales as $Pe^{1/2}$ at high Péclet number, just as in the case discussed in Section 2.2.3 where the vortices are arranged as periodic cells.

Avellaneda et al. [19] studied two other kinds of random vortex models, in which vortices of fixed shape and size were thrown down onto the plane according to a random Poisson process, either with a common or randomly chosen orientation. The effective diffusivity in these flows increased as a function of the vortex density, but was only enhanced by a factor of 2.5 at the highest density simulated, with $Pe = 100$. An approximate Lagrangian analysis (see Section 3.1.3) of these random vortex flows is also offered in [19].

Isichenko et al. [144] formulated an interesting conjecture, based on some scaling laws from percolation theory, that the effective diffusivity in a generic (or "common-position") random, homogenous, flow with short-range correlations should scale at high Péclet number as $Pe^{10/13}$. Using variational principles along with some scaling hypotheses from percolation theory, Fannjiang and Papanicoloau [99] verify this result for certain flows obtained by a random perturbation of the canonical steady cellular flow (62). These authors [99] also study tracer transport in randomized checkerboard flows (in which the flow in each cell is randomly turned on or off).

2.4.5. Appendix: Random velocity fields

An extensive and accessible treatment for the rigorous formulation of random functions may be found in [341,342]. We restrict ourselves here to formally setting forth some elementary notions which we will use throughout our discussion of random velocity fields. For concreteness, we will introduce the definitions of various aspects of random functions in the context of random velocity fields, but they clearly apply to other random functions, such as the passive scalar field.

A random function may be described quite simply as a random variable taking values in some given function space. In practice, the probability measure on the function space is described implicitly through a sufficiently precise specification of the statistical properties of the random function.

A generic way of describing a random function, such as the random velocity field $v(x, t)$, is to present all its *finite-dimensional distributions* and to declare v to be separable. A finite-dimensional distribution of $v(x, t)$ is just the (joint) probability law for the values of v at a given finite collection of points. Knowing all the finite-dimensional distributions is equivalent to a rule for computing

$$\text{Prob}\{v(x^{(j)}, t^{(j)}) \in A_j, j = 1, \ldots, N\}$$

for every finite collection of space–time points $\{(x^{(j)}, t^{(j)})\}_{j=1}^N$ and Borel subsets A_j of the range space of F. If one wishes to prescribe these, the rules must obey some simple consistency conditions ([41], Section 36). The separability condition is technical ([41], Section 38), but in practice means that we want the realizations of v to be as nice as possible, given the finite-dimensional distributions.

Random functions defined over a multidimensional spatial domain (and possibly time) are often referred to as *random fields*, and we will use this terminology hereafter.

2.4.5.1. Homogenous and stationary random fields. Many of the random fields arising in our models have statistical space–time symmetries, and we now define the most basic of these. A more detailed discussion may be found in ([341], Ch. 4).

A random field $v(x, t)$ is called:

- *stationary* if all finite-dimensional distributions are invariant under time translation:

$$\text{Prob}\{v(x^{(j)}, t^{(j)}) \in A_j, j = 1, \dots, N\} = \text{Prob}\{v(x^{(j)}, t^{(j)} + t') \in A_j, j = 1, \dots, N\}$$

for any real t'.

- *homogenous* if all finite-dimensional distributions are invariant under rigid translations in space:

$$\text{Prob}\{v(x^{(j)}, t^{(j)}) \in A_j, j = 1, \dots, N\} = \text{Prob}\{v(x^{(j)} + x', t^{(j)}) \in A_j, j = 1, \dots, N\}$$

for any $x' \in \mathbb{R}^d$.

Colloquially, a homogenous random field looks statistically the same at every point of space, and a stationary random field looks statistically the same at every moment of time.

Another important statistical symmetry which we will discuss in Section 4 is *isotropy*, which is statistical equivariance under arbitrary rotations and reflections. We refer to ([341], Section 22) for a detailed discussion of the meaning and implications of statistical isotropy for a random field.

2.4.5.2. Mean and two-point correlation function. Two fundamental statistical functions associated to a random field are the *mean* $\mu(x, t) = \langle v(x, t) \rangle$ and the *two-point correlation tensor* $\tilde{\mathcal{R}}(x, x', t, t') = \langle v(x, t) \otimes v(x', t') \rangle$, where angle brackets denote statistical averages. So long as there is no danger of ambiguity with reference to higher-order correlation functions, we will often refer to the "two-point correlation tensor" as simply the "correlation tensor" (or "correlation function" for scalar random fields). The arguments of the correlation tensor (function) will be called *observation points* (or sites, locations).

When $v(x, t)$ is a homogenous, stationary, random field, then all statistical descriptors, including the mean statistics $\langle v(x, t) \rangle$ and the two-point correlation function $\langle v(x, t) \otimes v(x', t') \rangle$ must be invariant under space and time translation. The mean must therefore be constant, and the two-point correlation function must depend only on the differences between the space and time coordinates of the observation points:

$$\langle v(x, t) \otimes v(x', t') \rangle = \tilde{\mathcal{R}}(x - x', t - t') .$$

2.4.5.3. Spectral density. The structure of a homogenous, stationary, random field is in some ways more directly expressed in terms of the *Fourier transform* of the correlation tensor

$$\hat{\tilde{\mathcal{R}}}(k, \omega) = \int_{\mathbb{R}^d} \int_{-\infty}^{\infty} e^{-2\pi i(k \cdot x + \omega t)} \tilde{\mathcal{R}}(x, t) \, dt \, dx \tag{89}$$

than in the correlation tensor itself. We shall call $\hat{\tilde{\mathcal{R}}}(k, \omega)$ the *spectral density tensor* of the random field. For a scalar random field, the spectral density tensor is just a scalar function.

An important theorem due to Khinchine states that the class of correlation tensors of homogenous, stationary random fields coincides with the class of tensor functions for which the Fourier transform is everywhere a non-negative definite, Hermitian matrix ([341], Section 9). This means that for any homogenous, stationary random field, the spectral density tensor $\hat{\tilde{\mathcal{R}}}(\mathbf{k}, \omega)$ is guaranteed to be a non-negative-definite, Hermitian matrix for each $\mathbf{k}$ and ω.

It is often convenient to condense the spectral density tensor of the velocity field $\mathbf{v}(\mathbf{x}, t)$ by integrating over shells of constant wavenumber $|\mathbf{k}|$; this produces the *spatio-temporal energy spectrum*:

$$\tilde{E}(k, \omega) = \frac{1}{2} \int_{S^{d-1}} \operatorname{Tr} \hat{\tilde{\mathcal{R}}}(k\hat{\omega}, \omega) \, d\hat{\omega} \ ,$$

where S^{d-1} is the $(d-1)$-dimensional sphere of unit radius. This function specifies the density of energy $E = \frac{1}{2}\langle|\mathbf{v}|^2\rangle$ in wavenumber-frequency space: the amount of energy contained in the band $k \pm \Delta k$, $\omega \pm \Delta\omega$ is $\int_{k-\Delta k}^{k+\Delta k}\int_{\omega-\Delta\omega}^{\omega+\Delta\omega} E(k, \omega) \, dk \, d\omega$. The usual "energy spectrum" $E(k)$ is the integral of the spatio-temporal energy spectrum over frequency space,

$$E(k) = \int_{-\infty}^{\infty} \tilde{E}(k, \omega) \, d\omega \ ,$$

and describes the statistical spatial structure of the velocity field at any given moment of time.

The full spectral density tensor $\hat{\tilde{\mathcal{R}}}(\mathbf{k}, \omega)$ provides a more detailed resolution of the random field $\mathbf{v}(\mathbf{x}, t)$ into fluctuations of various wavenumbers $\mathbf{k}$ and frequencies ω, including correlations between various components of the velocity field ([341], Sections 9, 22.1 and 22.2).

2.4.5.4. Gaussian random fields. *Gaussian random fields* are the extension of Gaussian random variables to the random function setting. By definition, all finite-dimensional distributions of a Gaussian random field are Gaussian. Gaussian random fields are therefore completely described by their mean and correlation tensor [341,342]. Homogenous, stationary, Gaussian random fields $\mathbf{v}(\mathbf{x}, t)$, may also be defined through their spectra, using the Khinchine theorem ([341], Section 9). One simplify chooses an arbitrary constant mean and an arbitrary spectral density tensor $\hat{\tilde{\mathcal{R}}}(\mathbf{k}, \omega)$ which is everywhere a non-negative definite, Hermitian matrix such that the entries of $\hat{\tilde{\mathcal{R}}}(\mathbf{k}, \omega)$ and $\hat{\tilde{\mathcal{R}}}(-\mathbf{k}, -\omega)$ are complex conjugates of one another. Then, by the Khinchine theorem, there exists a well-defined Gaussian random field with the specified constant mean and correlation tensor

$$\tilde{\mathcal{R}}(\mathbf{x}, t) = \int_{\mathbb{R}^d}\int_{-\infty}^{\infty} e^{2\pi i(\mathbf{k}\cdot\mathbf{x} + \omega t)} \hat{\tilde{\mathcal{R}}}(\mathbf{k}, \omega) \, d\omega \, d\mathbf{k} \ .$$

3. Anomalous diffusion and renormalization for simple shear models

In Section 2, we have discussed some general mathematical theories for the computation of the effective diffusion of a passive scalar field at large scales and long times. The underlying theory relies on the velocity field being periodic or having short-range correlations so that a strong scale separation between velocity and passive scalar scales can exist. While such theories can work well for moderately turbulent flows with sufficiently simple spatial structures, they may not furnish

a good description for tracer diffusion in a fully developed turbulent flow at high Reynolds number. As we shall discuss in more detail in Section 3.4.3, fully developed turbulent flows are characterized by strong spatio-temporal correlations extending over a wide range of scales, all the way up to the scale of the external forcing. In many applications particularly in atmospheric science [78,196], this forcing scale is on the same order of magnitude as the macroscales on which scientists wish to explicitly describe the flow. Consequently, there is no clean separation between the active scales of the velocity field and the scales of observational interest. Homogenization theory may not therefore be adequate to describe the macroscale passive scalar dynamics in these situations.

The development of simplified effective equations for the large-scale passive scalar statistics is, however, of particular practical importance in the numerical simulation of transport processes in highly turbulent environments. It is often not possible, even on the largest contemporary super-computers, to explicitly resolve all the active scales of turbulence [154]. A scheme is therefore needed for assessing the effects of the continuum of energetic but unresolved turbulent small scales of motion on the resolved scales, without having to compute them in full detail. The simplest modelling strategies account for the unresolved small scales by replacing the molecular diffusivity with a larger "eddy diffusivity". The value of this eddy diffusivity may be estimated by some ad hoc procedure such as mixing length arguments or through approximate, analytical theories based on perturbation expansions in a small parameter [182], ideas from renormalization group (RNG) theory [227,243,300,344], or simplifying assumptions concerning higher-order correlations between the velocity and scalar field [31,196]. It has been pointed out by several authors [166,182,286], however, that such an eddy diffusivity model may not be sufficient to capture the effects of the unresolved scales of the velocity field when they are not well separated from the cutoff scale. More complex effective large-scale equations for the passive scalar field have been proposed based on the renormalization group [286] or perturbation expansions [166], often resummed according to various renormalized perturbation theories from field theory [177,227,285]. These equations are typically nonlocal in space and time, reflecting large-scale interactions mediated by the unresolved small scales [286] and/or memory effects coming from the significant spatio-temporal correlations of the unresolved scales [166,177,285]. The investigation of the relative merits and shortcomings of these various approximate closure theories for turbulent diffusion is still very much an active area of research [227].

In response to the above issues, Avellaneda and the first author [10,14] have developed a mathematically rigorous theory for turbulent transport in a class of *Simple Shear Models* in which the velocity field has a stratified geometry:

$$\boldsymbol{v}(\boldsymbol{x}, t) = \boldsymbol{v}(x, y, t) = \begin{bmatrix} w(t) \\ v(x, t) \end{bmatrix}.$$

The *shearing* component $v(x, t)$ is taken as a homogenous and stationary, mean zero random field, and the spatially uniform transverse *sweeping* component $w(t)$ is taken as a stationary random process with possibly nonzero mean. The case of no cross sweep $w(t) = 0$ was analyzed in [10], and the case of a constant mean cross sweep $w(t) \equiv \bar{w}$ was studied in [14,141]. The inclusion of randomness in $w(t)$ in the present work is new.

The virtue of the Simple Shear Model is that the tracer trajectory equations may be exactly integrated for all times, as we saw in Section 2.3.1 for the case of deterministic, periodic velocity

fields. In the present case of random velocity fields, these formulas still provide a representation of the tracer position in terms of explicit random variables which are open to mathematical analysis from a variety of angles [10,14,18,141,207,233]. The random tracer trajectories maintain a very rich and subtle statistical behavior [10,14,141], as will be demonstrated throughout Section 3. The Simple Shear Model therefore provides a means of studying various nontrivial aspects of turbulent diffusion in a precise manner. Versions of shear flow models also have been utilized to study horizontal mixing in the ocean [347].

While the mathematical analysis of the Simple Shear Model relies heavily on the special geometric structure, it can include several statistical features of a realistic turbulent flow, such as spatial correlations extending over a wide range of scales along with a reasonable temporal structure. Moreover, many flow fields in geophysical applications do have an underlying shear structure. We will discuss another turbulent diffusion model in Section 4 which instead drastically simplifies the temporal correlation structure of the random velocity field, but permits a more general geometry [152,179]. Our purpose in investigating these simplified models is that through unambiguous computations and analysis, we can obtain insight concerning subtle physical features of turbulent transport which might be missed by crude reasoning on a "realistic" turbulent velocity field model. Throughout Section 3 we will examine a rich variety of Simple Shear flows with an emphasis on describing flows which generate *anomalous diffusion* of tracers, and on identifying the physical mechanisms responsible. By anomalous diffusion, we mean statistical tracer motion which departs from the standard situation in which its coarse-scale, long-time behavior resembles an ordinary Brownian motion. We will also at times mention some finite-time anomalies in which the tracer acts as if it had a temporarily negative diffusion coefficient (Sections 3.4.4 and 3.5.1).

Exactly solvable models also provide excellent test problems [13,17,300] for assessing the strengths and weaknesses of the approximate closure theories mentioned above which seek to furnish simplified descriptions of turbulent diffusion on the macroscale. We will briefly discuss this use of simplified models in Section 7.

Overview of Section 3: We will approach the study of the Simple Shear Model through submodels of increasing complexity. First we consider in Section 3.1 the *Random Sweeping Model* in which $v(x,t) = 0$, and the tracer is advected only by the time-dependent random field $w(t)$. Even in this extremely simplified model, the tracer motion can behave anomalously, depending on the long-range (low-frequency) statistical characterization of $w(t)$. We classify the various forms of anomalous diffusion, and discuss their origin on a heuristic level. We then show from a Lagrangian viewpoint how this intuition gleaned from the Random Sweeping Model can be applied to understand qualitatively the circumstances under which anomalous tracer diffusion may arise in general flows. This theme will be invoked repeatedly in later subsections as we interpret the mathematically derived turbulent diffusion formulas in the Simple Shear model.

Next, in Section 3.2, we develop the *Random Steady Shear* (RSS) Model, in which the shear field is taken as a random steady flow $v(x,t) = v(x)$ with Gaussian statistics and correlation function

$$\langle v(x')v(x' + x)\rangle \equiv R(x) \equiv \int_{-\infty}^{\infty} E(|k|)\,e^{2\pi ikx}\,dk \;,$$

with

$$E(k) \sim A_E|k|^{1-\varepsilon} \tag{90}$$

at low wavenumbers k. Such a velocity field could model flow through a stratified porous medium. The exponent $\varepsilon < 2$ measures the strength of the long-range correlations of velocity field. As ε increases towards $\varepsilon = 2$, the long-range spatial correlations become more pronounced. We concentrate on how the transport of tracers along the shearing direction y depends on the long-range spatial structure of $v(x)$, the presence of molecular diffusion, and various types of cross sweeps $w(t)$. Following [10,141], we derive exact formulas for the mean-square tracer displacement along the shear and analyze their physical content.

The effects of temporal fluctuations in the shear flow $v(x,t)$ are studied within the *random spatio-temporal shear* (RSTS) Model in Section 3.3. We take $v(x,t)$ to be statistically stationary in time, with the idea of qualitatively mimicking turbulent flows which have reached a quasi-equilibrium state in response to some statistically stationary external driving and internal viscous dissipation. Motivated by the inertial-range theory of turbulence (see, for example, [320]), we associate a wavenumber-dependent correlation time $\tau(k)$ to shear flow fluctuations with spatial wavenumber k, where $\lim_{k \to 0} \tau(k) \sim A_\tau |k|^{-z}$. The exponent $z \geq 0$ describes how slowly the large scales (low wavenumbers) of the shear flow vary in time; $z \to \infty$ corresponds to a steady limit in which the large scales are frozen, whereas $z = 0$ describes the opposite limit in which arbitrarily large scales decorrelate at a uniformly rapid rate. We explore how the temporal structure of the large scales, as described by z, influences the shear-parallel transport of tracers.

We next consider the full probability distribution function (PDF) for the shear-parallel motion of a single tracer, which is equivalent to the description of the evolution of the mean $\langle T(x,y,t) \rangle$ of the passive scalar field density. For velocity fields with sufficiently localized spatial correlations, the homogenization theory discussed in Section 2 shows that the PDF for the position of a single tracer approaches a Gaussian distribution at long times. Equivalently, the mean statistics are governed by an ordinary diffusion equation with an enhanced diffusion coefficient. In Section 3.4, we demonstrate through explicit examples how the PDF for a tracer can forever deviate strongly from a Gaussian distribution in Simple Shear Models with sufficiently strong long-range correlations [10]. A related feature is that the large-scale, long-time evolution of the mean statistics is not described by a standard diffusion PDE, but rather by a nonlocal diffusion equation. This anomalous large-scale long-time behavior actually manifests itself in a broad range of models with a nearly stratified structure [16].

In Section 3.4.3 we develop a modification of the Simple Shear Model which permits the study of velocity fields with a statistically self-similar *inertial range* of scales $L_K \ll r \ll L_0$, an important feature manifest in real fully developed turbulence [10,14]. According to Kolmogorov's theory [169], the energy spectrum within the inertial range of wavenumbers $L_0^{-1} \ll k \ll L_K^{-1}$ scales as $k^{-5/3}$. This is largely confirmed by experimental data [307], though some question remains whether there are "intermittency corrections" [34,309] which alter the exponent slightly from 5/3. The $k^{-5/3}$ scaling of the energy spectrum formally corresponds to a value of $\varepsilon = 8/3$ in the Simple Shear Model (see Eq. (90)), but the cutoff of this scaling on the low wavenumber (infrared) end at L_0^{-1} is essential for the total energy to be finite and the flow to be well-defined in the standard sense. Kolmogorov theory also predicts that the decorrelation times for the turbulent fluctuations in the inertial range scales as $\tau(k) \sim k^{-2/3}$, corresponding to a $z = 2/3$ value in the RSTS Model. A competing point of view [319] suggests instead the value $z = 1$. We modify the RSTS Model to permit the study of velocity fields with scalings corresponding to such values of ε and z by introducing an explicit infrared cutoff [10,14]. We then formulate the problem of computing

effective large-scale equations for the mean passive scalar density in the presence of such a turbulent shear flow, and concretely indicate some of the inherent difficulties. Large-scale effective equations for the mean passive scalar density in the Simple Shear Model have in fact been rigorously derived by Avellaneda and the first author [10,14], and they display a rich variety of qualitative structure depending on the value of the scaling exponents ε and z. We briefly mention some of the findings of these rigorous renormalization computations.

Up to this point in the paper, we have for the most part concentrated on describing the statistical motion of a single tracer and the intrinsically related evolution of the mean passive scalar density $\langle T(\mathbf{x}, t) \rangle$. These dynamics are strongly determined by the large-scale features of the turbulent system, simply because these are the most energetic in most realistic circumstances. In Sections 3.5 and 4, we shift our focus to the small-scale fluctuations of the passive scalar field. These are intimately related to the dynamics of the separation between *pairs* of tracers. While the large-scale properties of the passive scalar field are of more obvious observational and applied physical interest, the small-scale features are crucial in estimating the size of clouds of pollutants [78,132] and the progress of mixing processes and combustion in turbulent environments [43,339]. Moreover, the small-scale statistics of turbulent systems are of particular theoretical interest because they are thought to exhibit a variety of *universal* features which are independent of the particular large-scale configuration (see [309]).

We explicitly examine in Section 3.5 various aspects of the small-scale passive scalar statistics in the Simple Shear Model in the absence of molecular diffusion ($\kappa = 0$). We lay the foundations of our study with the development of an exact equation for the *pair-distance function* introduced by Richardson [284], which describes the PDF for the separation of a pair of tracers. From the pair-distance function, we can deduce some important properties about the evolution of *interfaces* between regions in which the passive scalar field is present or absent. The way in which these interfaces wrinkle plays a crucial role in turbulent combustion and mixing [43,310,305,339]. We characterize the roughness of interfaces through their fractal dimension [215], which may be explicitly computed within the Simple Shear Model. We relate the exact results to experimental measurements and other theoretical work, and state some open problems concerning the inclusion of the effects of molecular diffusion. Our study of the small-scale features of the passive scalar field in a turbulent flow continues in Section 4 with the analysis of a different simplified turbulent diffusion model.

3.1. Connection between anomalous diffusion and Lagrangian correlations

Before analyzing the statistical tracer motion in the Simple Shear Model, we set up a general framework for the discussion of anomalous tracer diffusion. We define the terminology we shall use in Section 3.1.1. Next, we provide an extremely simple example of anomalous diffusion in the *Random sweeping Model*, which consists of a spatially uniform random flow fluctuating in time (Section 3.1.2). Finally, we emphasize in Section 3.1.3 that tracer motion is determined by the statistics of its *Lagrangian velocity*, and show how it is connected to but different from the velocity field defined in the Eulerian (laboratory) frame of reference [317]. The Lagrangian perspective provides a basis for the intuitive understanding of the exact mathematical formulas which we will develop for the simple shear models in Sections 3.2 and 3.3.

3.1.1. Qualitative classes of anomalous diffusion

To fix vocabulary, we say that the tracer motion (usually along a certain direction) is:

- *Ballistic* if the mean-square displacement is growing quadratically in time, corresponding to coherent unidirectional motion.
- *Diffusive* if the mean-square displacement is growing linearly in time, corresponding to "normal" behavior of a tracer which executes a mean zero, random back and forth motion, with sufficiently rapid decorrelation of its velocity in time. (This is of course the category in which Brownian motion, due to molecular diffusion alone, falls.)
- *Trapped* if the mean-square displacement remains bounded for all time.
- *Superdiffusive* if the mean-square displacement is growing faster than linearly in time.
- *Subdiffusive* if the mean-square displacement is growing at a sublinear rate.

Note that according to these definitions, "ballistic" is a subcategory of superdiffusive, and "trapped" is a subcategory of subdiffusive. We will endeavor, however, to be explicit when ballistic or trapped behavior actually occurs.

Other forms of anomalous diffusion will be described through rigorous examples in Section 3.4. One is the decrease of the mean-square tracer displacement over a certain time interval, so that the effective diffusivity is (temporarily) negative (Section 3.4.4). Therefore, even if an effective equation for the mean statistics can be derived in such flows, it will be ill-posed over some time interval. This phenomenon creates difficulties for conventional numerical Monte Carlo schemes (see Section 6) for turbulent diffusion. Another interesting way in which anomalous diffusion manifests itself is through the higher order statistics. We discuss in Sections 3.4.1 and 3.4.2 an explicit, nontrivial class of examples in which the tracer displacement is neither Gaussian nor self-averaging at large times, in strong contrast to tracers in flows for which the homogenization theory of Section 2 is valid.

3.1.2. Anomalous diffusion in the random sweeping model

To provide a concrete illustration of the variety of anomalous diffusion behavior possible for a tracer, we define the extremely simple yet fundamental *Random Sweeping Model*. The velocity field in this model is defined to be a spatially uniform flow which fluctuates randomly in time according to a stationary, Gaussian random process. For the sake of simplicity of notation and coherence with the turbulent diffusion models to be discussed in Sections 3.2 and 3.3, we shall restrict attention to the case in which the velocity field always points along a single direction, and the spatial domain is two-dimensional. Then the random velocity field in the *Random Sweeping Model* is defined:

$$\boldsymbol{v}(\boldsymbol{x}, t) = \boldsymbol{v}(x, y, t) = \begin{bmatrix} w_f(t) \\ 0 \end{bmatrix},$$

where $w_f(t)$ is a stationary, Gaussian random process with mean zero and correlation function:

$$R_w(t) \equiv \langle w_f(t') w_f(t + t') \rangle . \tag{91}$$

Such a model was considered by Kubo [188] as an example of how randomly fluctuating velocity fields can act as effective diffusion processes when viewed on large scales and long times. A more

general Random Sweeping Model for arbitrary dimensions without the constraint that the velocity field point along a single direction was analyzed in great detail in [18]. We will present some pertinent results here.

We will find it convenient to express the correlation function in terms of the *power spectrum* $E_w(\omega)$ of the velocity field:

$$R_w(t) = \int_{-\infty}^{\infty} e^{2\pi i \omega t} E_w(|\omega|) \, d\omega = 2 \int_{0}^{\infty} \cos(2\pi \omega t) E_w(|\omega|) \, d\omega \;. \tag{92}$$

The power spectrum $E_w(\omega)$ describes precisely the spectral density of the energy $\frac{1}{2}\langle |w_f(t)|^2 \rangle$ resolved with respect to frequency. That is, $\int_{\omega - \Delta\omega}^{\omega + \Delta\omega} E_w(\omega) \, d\omega$ is the amount of energy residing within the frequency band $\omega \pm \Delta\omega$. The power spectrum is a manifestly non-negative function, which in our applications we assume quite reasonably to be smooth (see Paragraph 2.4.5.3).

Consider the location $(X(t), Y(t))$ of a tracer particle advected by the Random Sweeping Model flow, first without molecular diffusion $\kappa = 0$. Starting from position (x_0, y_0), the (random) tracer position at later times is given by

$$X(t) = x_0 + \int_{0}^{t} w_f(s) \, ds \;,$$

$$Y(t) = y_0 \;.$$

The displacement $X(t) - x_0$ along the sweeping direction is a mean zero Gaussian random variable, since it is a linear functional of the mean zero Gaussian random process $w_f(t)$. Consequently, it is completely described by its variance, which is nothing but the mean-square tracer displacement along the x direction:

$$\sigma_X^2(t) = \langle (X(t) - x_0)^2 \rangle = \int_{0}^{t}\int_{0}^{t} \langle w_f(s) w_f(s') \rangle \, ds \, ds' = \int_{0}^{t}\int_{0}^{t} R_w(s - s') \, ds \, ds'$$

$$= 2 \int_{0}^{t} (t - s) R_w(s) \, ds \;, \tag{93}$$

where the last equality used a change of variables and the fact that, by its very definition (91), $R_w(t)$ is an even function. Eq. (93) manifestly relates the turbulent diffusion of the tracer to the statistical correlations of the sweeping velocity field $w_f(t)$. Strong and persistent correlations are clearly associated with rapid diffusion.

It is quite convenient mathematically to express the mean-square displacement in terms of the power spectrum of the sweeping velocity field. Substituting Eq. (92) into Eq. (93) and performing the integration over s, we obtain

$$\sigma_X^2(t) = 4 \int_{0}^{\infty} E_w(\omega) \frac{1 - \cos 2\pi \omega t}{4\pi^2 \omega^2} \, d\omega \;. \tag{94}$$

The qualitative long-time behavior $\sigma_X^2(t)$ depends sensitively on the nature of the low frequency component of $w_f(t)$, as we now describe. Suppose that the power spectrum is smooth for $\omega > 0$, absolutely integrable, and has power law behavior near $\omega = 0$

$$E_w(\omega) = A_{E,w} \omega^{-\beta} \psi_w(\omega) \;. \tag{95}$$

Here, $A_{E,w}$ is a positive constant and $\psi_w(\cdot)$ is a smooth function on the positive real axis with $\psi_w(0) = 1$ and $|\psi'_w(0)| < \infty$. To ensure integrability, the exponent β must be a real number less than 1. We will see that the long-time behavior of the tracer can then be categorized as diffusive, superdiffusive, or subdiffusive according to the value of this exponent. Note that all power spectra with finite low-frequency limits are included within the class $\beta = 0$.

3.1.2.1. Diffusive sweep. Consider first the case $\beta = 0$, corresponding to the generic case of a finite, nonzero distribution of energy at the lowest wavenumbers. By changing integration variables $\omega \to \omega t$ in Eq. (94) and passing to the $t \to \infty$ limit via Lebesgue's dominated convergence theorem ([288], Section 4.4), we find that

$$\lim_{t \to \infty} \sigma_X^2(t) \sim 2K_x^* t \,,$$

with the positive constant

$$K_x^* = \frac{1}{2} A_{E,w} = \int_0^\infty R_w(s) \, \mathrm{d}s \,. \tag{96}$$

This formula shows that, on long time scales, the random velocity fluctuations serve to induce an effective diffusion of the tracer with the ordinary linear growth of the mean-square displacement. The effective large-scale diffusivity is given by the constant K_x^*, which is just the integral of the correlation function of the velocity field. Because the tracer displacement is always Gaussian distributed, all its higher moments scale in the same way as those of ordinary diffusion processes. The PDF for the tracer position, or equivalently, the mean statistics, therefore exactly satisfy a diffusion equation with diffusivity constant K_x^* on large space–time scales [18].

The $\beta = 0$ class of Random Sweeping Model velocity fields comprises the simplest (and original) example of Kubo's theory [188] for how transport by a randomly fluctuating, mean zero velocity field induces an effective diffusion on large scales (see Section 2.4.1). We emphasize that the standard diffusion of Kubo type arises in the Random Sweeping Model when the velocity field has the "generic" property that its integrated correlation function is nonzero and finite

$$0 < \int_0^\infty R_w(s) \, \mathrm{d}s < \infty \,, \tag{97}$$

which is exactly equivalent to $\beta = 0$ in Eq. (95). For other values of β, the condition (97) fails, and the tracer will diffuse *anomalously* on long time scales, as we now show.

3.1.2.2. Superdiffusive sweep. For the exponent values $0 < \beta < 1$, the power spectrum diverges at low frequencies, corresponding to an infinite value of $\int_0^\infty R_w(s) \, \mathrm{d}s$. This means that the velocity field exhibits a very long-term memory. Changing variables $\omega \to \omega t$ in Eq. (94) and using the dominated convergence theorem to evaluate the long-time limit results in the following asymptotic formula:

$$\lim_{t \to \infty} \sigma_X^2(t) \sim (2/(1 + \beta))K_x^* t^{1 + \beta} \,, \tag{98}$$

where the positive constant in the prefactor may be expressed:

$$K_x^\sharp = \frac{1}{2} A_{E,w} \pi^{\beta - (1/2)} \frac{\Gamma((1-\beta)/2)}{\Gamma((2+\beta)/2)} , \qquad (99)$$

and Γ is the standard Gamma function [195]. The tracer motion is *superdiffusive* because $\sigma_X^2(t)$ grows faster than linearly at long times. Because the tracer motion is Gaussian in the Random Sweeping Model, it can be shown [18] that the mean passive scalar density satisfies a time-dependent diffusion equation:

$$\partial \langle T(x,y,t) \rangle / \partial t = D_{w_f}(t) \partial^2 \langle T(x,y,t) \rangle / \partial x^2 ,$$
$$\langle T(x,y,t=0) \rangle = \langle T_0(x,y) \rangle , \qquad (100)$$

where the effective diffusion coefficient

$$D_{w_f}(t) \equiv \frac{1}{2} \frac{d\sigma_X^2(t)}{dt}$$

diverges in time as

$$D_{w_f}(t) \sim K_x^\sharp t^\beta . \qquad (101)$$

3.1.2.3. Subdiffusive sweep. For exponent values $\beta < 0$, the power spectrum $E_w(\omega)$ vanishes at the origin. We consider in this paragraph the case in which $-1 < \beta < 0$. A direct asymptotic calculation as in the previous cases produces

$$\lim_{t \to \infty} \sigma_X^2(t) \sim (2/(1+\beta)) K_x^\sharp t^{1+\beta} ,$$

where $K_x^\sharp$ is given by Eq. (99). But now the scaling exponent $1 + \beta$ is between 0 and 1, corresponding to *subdiffusive* motion of the tracer. The mean passive scalar density again satisfies a time-dependent diffusion PDE (100) with effective diffusion coefficient $D_{w_f}(t)$ obeying the law (101), which now decays in time.

The value $\beta = -1$ leads to a logarithmic growth of $\sigma_X^2(t)$.

3.1.2.4. Trapping sweep. Finally, for $\beta < -1$, we can take the $t \to \infty$ limit in (94) directly, without rescaling the integration variable. The oscillatory term vanishes in the $t \to \infty$ limit due to the integrability of $E_w(\omega)\omega^{-2}$ and the Riemann–Lebesgue lemma [172]. There results:

$$\lim_{t \to \infty} \sigma_X^2(t) = K_x^\circ ,$$

where

$$K_x^\circ = \frac{1}{\pi^2} \int_0^\infty E_w(\omega) \omega^{-2} \, d\omega . \qquad (102)$$

The mean-square tracer displacement never exceeds a finite limit, and the tracer is statistically *trapped*. There is no effective long-range transport.

Table 1
Long-time asymptotics of mean-square tracer displacement in Random Sweeping Model, with $\kappa = 0$. Scaling coefficients are given by Eqs. (96), (99) and (102)

Parameter regime	Asymptotic mean square displacement $\lim_{t \to \infty} \sigma_X^2(t)$	Qualitative behavior
$\beta < -1$	$K_x^\circ t^0$	Trapping
$-1 < \beta < 0$	$\frac{2}{1+\beta} K_x^\sharp t^{1+\beta}$	Sub-diffusive
$\beta = 0$	$2K_x^* t$	Diffusive
$0 < \beta < 1$	$\frac{2}{1+\beta} K_x^\sharp t^{1+\beta}$	Super-diffusive

3.1.2.5. Summary. We collect the anomalous diffusion results stated above for the Random Sweeping Model in Table 1.

3.1.2.6. Effects of molecular diffusion. We now briefly consider how the above tracer behavior is modified under the addition of molecular diffusion $\kappa > 0$. The equations of motion now become stochastic:

$$dX(t) = v(t)\,dt + \sqrt{2\kappa}\,dW_x(t) \;,$$

$$dY(t) = \sqrt{2\kappa}\,dW_y(t) \;,$$

where $(W_x(t), W_y(t))$ is a two-dimensional Brownian motion. The interaction between the molecular diffusion and a spatially uniform velocity field is completely linear, and the integrated trajectory equations are

$$X(t) = x_0 + \int_0^t v(s)\,ds + \sqrt{2\kappa} W_x(t) \;,$$

$$Y(t) = y_0 + \sqrt{2\kappa} W_y(t) \;.$$

The mean-square tracer displacement in each direction is modified from Eq. (93) only by the addition of $2\kappa t$ due to the molecular effects

$$\sigma_X^2(t) = 2\kappa t + 2\int_0^t (t - s) R_w(s)\,ds \;,$$

$$\sigma_Y^2(t) = 2\kappa t \;.$$

Molecular diffusion will therefore produce an ordinary diffusive character for all $\beta \leq 0$. The random sweep will have relatively negligible effects at long times when $\beta < 0$, corresponding to the regimes of subdiffusive or trapping behavior due to random sweeping alone. On the other hand, molecular diffusion plays a negligible role in the superdiffusive regime $0 < \beta < 1$ at long times.

The simple additivity of the contributions from turbulent diffusivity and molecular diffusivity is a consequence of the absence of spatial structure in the Random Sweeping Model. We will see that

molecular diffusivity can influence the tracer motion in much more subtle ways when the velocity field has spatial variations, even in some very simple models (see Section 3.2).

3.1.3. Eulerian vs. Lagrangian statistics

The Random Sweeping Model is quite simplistic, yet already gives us some qualitative under-standing of what circumstances can lead to anomalous diffusion in *general* statistically homogenous turbulent diffusion models. Specifically, suppose we are given an arbitrary two-dimensional, incompressible, mean zero, spatially homogenous, statistically stationary random velocity field (which need not be Gaussian)

$$\boldsymbol{v}(x, y, t) = \begin{bmatrix} v_x(x, y, t) \\ v_y(x, y, t) \end{bmatrix}.$$

The equations of motion for the tracer are then

$$\mathrm{d}X(t) = v_x(X(t), Y(t), t)\,\mathrm{d}t + \sqrt{2\kappa}\,\mathrm{d}W_x(t)\,,$$

$$\mathrm{d}Y(t) = v_y(X(t), Y(t), t)\,\mathrm{d}t + \sqrt{2\kappa}\,\mathrm{d}W_y(t)\,.$$

Now, we define the *Lagrangian velocity* of the tracer

$$\boldsymbol{v}^{(\mathrm{L})}(t) = \begin{bmatrix} v_x^{(\mathrm{L})}(t) \\ v_y^{(\mathrm{L})}(t) \end{bmatrix} = \begin{bmatrix} v_x(X(t), Y(t), t) \\ v_y(X(t), Y(t), t) \end{bmatrix}; \tag{103}$$

this is nothing but the random velocity field evaluated at the current location of the tracer. In terms of this Lagrangian velocity, the equations of motion take an exceptionally simple form

$$\mathrm{d}X(t) = v_x^{(\mathrm{L})}(t)\mathrm{d}t + \sqrt{2\kappa}\,\mathrm{d}W_x(t)\,,$$
$$\mathrm{d}Y(t) = v_y^{(\mathrm{L})}(t)\mathrm{d}t + \sqrt{2\kappa}\,\mathrm{d}W_y(t)\,. \tag{104}$$

In fact, these equations are identical to those of the Random Sweeping Model, without the restriction of the velocity pointing in a single direction, and with the *Lagrangian velocity* appearing as the advective term instead of the externally prescribed sweep velocity $w_f(t)$.

The Lagrangian velocity can be shown to be a mean zero, statistically stationary random process; see ([247], Section 9.5) for a formal argument and [270,350] for rigorous derivations. This is *not* a simple consequence of $\boldsymbol{v}(x, y, t)$ being a mean zero, stationary random process, but relies crucially on incompressibility and statistical homogeneity. By repeating the computations in Eq. (93), which did not require $w_f(t)$ to be Gaussian, we obtain the following general formula for the mean-square displacement of a tracer along the coordinate axes:

$$\sigma_X^2(t) \equiv \langle (X(t) - x_0)^2 \rangle = 2 \int_0^t (t - s) R_x^{(\mathrm{L})}(s)\,\mathrm{d}s\,,$$

$$\sigma_Y^2(t) \equiv \langle (Y(t) - y_0)^2 \rangle = 2 \int_0^t (t - s) R_y^{(\mathrm{L})}(s)\,\mathrm{d}s\,. \tag{105}$$

The functions appearing in the integrand are the *Lagrangian correlation functions*:

$$R_x^{(L)}(t) \equiv \langle v_x^{(L)}(t')v_x^{(L)}(t+t') \rangle, \tag{106}$$

$$R_y^{(L)}(t) \equiv \langle v_y^{(L)}(t')v_y^{(L)}(t+t') \rangle.$$

The general formula (105) was originally derived by Taylor [317]. By direct analogy with the analysis presented in the Random Sweeping Model, we can *in principle* categorize whether the tracer motion is, at long times, diffusive, superdiffusive, subdiffusive, or trapped. The main criterion is the low frequency behavior of the power spectra associated to the Lagrangian correlation functions (106). A trivial secondary criterion is the presence of molecular diffusion, which precludes subdiffusive or trapping behavior.

The practical obstacle to a quantitative treatment along these lines, however, is the computation of the Lagrangian correlation function. What is explicitly specified are the so-called *Eulerian* statistics of the velocity field, which are just the probability distributions of the velocity field evaluated at *fixed* points (x, y, t) in the laboratory frame. The Lagrangian velocity, on the other hand, requires the evaluation of the velocity field at the *random* tracer locations $(X(t), Y(t), t)$. It is, in general, extremely difficult to describe quantitative statistical features of the Lagrangian velocity field, such as its correlation function [227,350]. In some sense, it requires us to have already solved the problem of describing the statistics of the tracer position! There are special exceptions of course; the Lagrangian velocity $v_x^{(L)}(t)$ in the Random Sweeping Model is exactly the specified sweeping velocity $w_f(t)$. But in general, we cannot gainfully use Taylor's formula (105) to compute the mean-square displacement quantitatively.

3.1.3.1. Lagrangian intuition. The Lagrangian perspective does provide intuition for the qualitative behavior of a tracer. Based on the results of the Random Sweeping Model in Section 3.1.2 and Taylor's formula (105), we can deduce the following connections between anomalous tracer diffusion (say in the x direction) and properties of the Lagrangian velocity:

- Ordinary diffusion occurs when the correlations of the Lagrangian velocity field are of finite range, in that $\int_0^\infty R_x^{(L)}(s)\,\mathrm{d}s$ is nonzero and finite.
- Superdiffusion is associated with long-range correlations of the Lagrangian velocity field, so that $\int_0^\infty R_x^{(L)}(s)\,\mathrm{d}s$ is a divergent integral.
- Subdiffusion and trapping are associated to oscillations in the Lagrangian velocity, which cause the Lagrangian correlation function to have a substantial negative region (so that $\int_0^\infty R_x^{(L)}(s)\,\mathrm{d}s = 0$).

Though we cannot in general compute $\int_0^\infty R_x^{(L)}(s)\,\mathrm{d}s$, we can often infer, based on the spatio-temporal flow structure, whether the Lagrangian velocity ought to have long-range correlations or oscillations, so that superdiffusion or subdiffusion may be expected. For example, long-range correlations of the Lagrangian velocity of a tracer can generally be associated to flows with long-range spatio-temporal correlations. The connections between long-range spatio-temporal correlations and superdiffusion have been explored in the context of Levy walks by Zumofen et al. [352] and through renormalization group analysis [45] and various forms of probabilistic analysis [47] by Bouchaud and others. We aim here to concentrate on continuum, incompressible, random fluid flow models which can be analyzed unambiguously and which reveal a number of subtle features

concerning anomalous diffusion. In interpreting the exact mathematical results which we present in Sections 3.2 and 3.3, we will refer repeatedly to the qualitative paradigm outlined above.

3.1.3.2. Lagrangian description of standard tracer diffusion. It is helpful in this connection to describe a standard scenario in which the random velocity field gives rise to ordinary diffusive behavior at long times. Suppose the Lagrangian correlation function (of the x component of the tracer motion) can be expressed as

$$R_x^{(L)}(t) = V^2 \rho(t/\tau_L) \,,$$

where $\rho(\cdot)$ is some smooth, rapidly decaying numerical function with $\rho(0) = 1$ and $\int_0^\infty \rho(t)\,dt = 1$. This corresponds to a model in which the Lagrangian velocity has mean-square velocity V, a single, finite Lagrangian correlation time scale τ_L, and no strong oscillatory behavior. We readily find formulas for the mean-square tracer displacement in two asymptotic limits, using Taylor's formula (105)

$$\sigma_x^2(t) \sim \begin{cases} V^2 t^2 & \text{for } 0 \le t \ll \tau_L \,, \\ 2V^2 \tau_L t & \text{for } t \gg \tau_L \,. \end{cases} \tag{107}$$

The initial quadratic growth in t corresponds to a *ballistic* phase in which the mean-square tracer displacement is growing quadratically in time. This can be understood as the effect of a push coherent over the time $t \ll \tau_L$, which steadily moves the tracer in a certain direction at a certain speed. After τ_L, the initial push has become incoherent and the tracer is moving primarily under the influence of another independent fluctuation in the velocity field. Once many of these renewals have occurred, one can see that the motion of the particle will have some properties in common with ordinary Brownian motion, representing the cumulative effect of many independent kicks. Thus, the mean-square displacement grows now linearly instead of quadratically.

Observed over times long compared with the Lagrangian correlation time τ_L, the tracer random velocity field appears to move with an effective diffusivity of $V^2 \tau_L$. The diffusivity naturally increases with the magnitude of the velocity fluctuations V, but also grows with the Lagrangian correlation time τ_L. The latter dependence can be understood from the fact that a particle will make more progress in a time t if its motion is composed of fewer random changes of direction, since there will be fewer cancellation of displacements.

We will use this standard diffusion picture as a benchmark in our discussion of anomalous diffusion behavior in the simple shear models of Sections 3.2 and 3.3.

3.2. Tracer transport in steady, random shear flow with transverse sweep

The first class of flows for which we shall explicitly compute the mean-square tracer displacement is the *Random Steady Shear* (RSS) Model [10,14,141]. The flow is defined in two spatial dimensions as a superposition of a steady random shear flow $v(x)$ and a spatially uniform, possibly random, cross sweep $w(t)$

$$\boldsymbol{v}(\boldsymbol{x}, t) = \boldsymbol{v}(x, y, t) = \begin{bmatrix} w(t) \\ v(x) \end{bmatrix}.$$

The steady shear flow $v(x)$ is taken as a mean zero, Gaussian, homogenous, random field. Its correlation function $R(x)$ and energy spectrum $E(k)$ are related by a Fourier transformation

$$\langle v(x')v(x' + x)\rangle \equiv R(x) \equiv \int_{-\infty}^{\infty} E(|k|)e^{2\pi ikx}\,dk = 2\int_{0}^{\infty} E(k)\cos(2\pi kx)\,dk \ . \tag{108}$$

Note that the energy spectrum here is resolved with respect to spatial wavenumber k rather than with respect to frequency ω; otherwise, it has the same physical meaning as the power spectrum defined in the Random Sweeping Model (Section 3.1.2). We assume the energy spectrum to be smooth for $k > 0$, absolutely integrable, and to behave like a power law at low wavenumbers

$$E(k) = A_E k^{1-\varepsilon}\psi(k) \ , \tag{109}$$

where $\psi(k)$ is a smooth function on $k > 0$ with $\psi(0) = 1$. We will sometimes call ε the *infrared scaling exponent* of the energy spectrum since it describes the low wavenumber properties of $E(k)$. Integrability at $k = 0$ requires $\varepsilon < 2$. Note that energy spectra with finite $k \to 0$ limits correspond to $\varepsilon = 1$. As ε increases, more energy is concentrated at low wavenumbers, corresponding to an increase in the strength of long-range correlations. By considering flows with energy spectra which diverge at low wavenumber ($1 < \varepsilon < 2$), we attempt to gain an understanding of some of the effects of long-range spatial correlations on tracer transport. This is of particular relevance to realistic turbulent diffusion, though we hasten to add that the long-range correlations in a fully developed turbulent flow manifest themselves much more strongly; see Section 3.4.3.

The cross sweep

$$w(t) = \bar{w} + w_f(t)$$

is taken as a superposition of deterministic constant $\bar{w}$ and a mean zero, Gaussian, stationary random field $w_f(t)$ with correlation function

$$R_w(t) \equiv \langle w_f(t')w_f(t' + t)\rangle \ .$$

Note that the fluctuating component of the cross sweep is of exactly the same form as in the Random Sweeping Model of Section 3.1.2. The shear field $v(x)$ and sweep field $w(t)$ are statistically independent of each other.

The stochastic equations of motion for the location of a tracer particle $X(t), Y(t)$ in an RSS Model flow are

$$dX(t) = w(t)\,dt + \sqrt{2\kappa}\,dW_x(t) \ ,$$

$$X(t = 0) = x_0 \ ,$$

$$dY(t) = v(X(t))\,dt + \sqrt{2\kappa}\,dW_y(t) \ ,$$

$$Y(t = 0) = y_0 \ ,$$

where $\{W_x(t), W_y(t)\}$ is a pair of independent Brownian motions. This system of equations can be successively integrated by quadrature:

$$X(t) = x_0 + \int_0^t w(s)\,ds + \sqrt{2\kappa}W_x(t) \,, \tag{110a}$$

$$Y(t) = y_0 + \int_0^t v(X(s))\,ds + \sqrt{2\kappa}W_y(t) \,. \tag{110b}$$

Up to the addition of a constant mean sweep, the statistics of the shear-transverse position, $X(t)$, is just that of a tracer in the Random Sweeping Model which was discussed in Section 3.1.2 and in [18]. We have that $X(t)$ is a Gaussian random process with mean displacement

$$\langle X(t) \rangle = x_0 + \bar{w}t$$

and *cross-shear displacement variance*

$$\sigma_X^2(t) \equiv \langle (X(t) - \langle X(t) \rangle)^2 \rangle = 2\kappa t + 2\int_0^t (t-s)R_w(s)\,ds \,. \tag{111}$$

We concentrate therefore on the shear-parallel motion $Y(t)$ of the tracer. While it can be explicitly represented in the fairly simple form (110b), its statistics are highly nontrivial owing to the nonlinear interaction between the shear velocity field $v(x)$ and the shear-transverse tracer position $X(t)$. For example, $Y(t)$ is not in general a Gaussian random process, even though all random fields ($v(x)$, $X(t)$, and $W_x(t)$) appearing on the right-hand side of Eq. (110b) are Gaussian. We will return to this issue in Section 3.4. Within Section 3.2, we will focus on the (*absolute*) *mean-square shear-parallel displacement*

$$\sigma_Y^2(t) = \langle (Y(t) - y_0)^2 \rangle \,.$$

The mean displacement $\langle Y(t) - y_0 \rangle$ vanishes identically because of the mean zero assumption on $v(x)$.

As we will demonstrate in Paragraph 3.2.6.1, the mean-square displacement along the shear is given by the following formula:

Mean-square shear-parallel tracer displacement for RSS model:

$$\sigma_Y^2(t) = 2\kappa t + 2\int_0^\infty E(k)\Sigma(k,t)\,dk \,, \tag{112a}$$

$$\Sigma(k,t) = 2\int_0^t (t-s)\cos(2\pi k\bar{w}s)\mathrm{e}^{-2\pi^2 k^2 \sigma_X^2(s)}\,ds \,. \tag{112b}$$

This formula remains valid when $v(x)$ is non-Gaussian.

Expression (112) explicitly resolves the mean-square displacement along the shear into contributions from fluctuations of various wavenumbers. The function $\Sigma(k,t)$, which we will call the *shear-displacement kernel*, contains the effects of cross-shear transport due to the deterministic mean flow $\bar{w}$, the fluctuating velocity field $w_f(t)$, and molecular diffusion κ. The random cross-shear motion is accounted for by $\sigma_X^2(t)$; see Eq. (111). The shear-displacement kernel $\Sigma(k,t)$ may be interpreted as the response of $\sigma_Y^2(t)$ to the presence of a component $A\cos(2\pi kx) + B\sin(2\pi kx)$ of the

random shear velocity field along with any cross-shear transport processes, where A and B are a pair of standard, independent Gaussian random variables (zero mean, unit variance). The actual random shear flow may be thought of as a superposition of independent random fluctuations of various wavenumbers k, with amplitude given by $\sqrt{2E(k)}$. Since these fluctuations are independent and do not act across the gradient of the velocity field, the shear-parallel tracer motion $Y(t)$ may be expressed as a superposition of independent contributions coming from each wavenumber k of the shear velocity field $v(x)$. This will be a useful heuristic perspective in interpreting the exact mathematical results.

Some general observations are already apparent. For $w(t) = 0$ and $\kappa = 0$, we have no cross-shear motion ($\bar{w} = \sigma_X^2(t) = 0$) so the shear-displacement kernel is simply

$$\Sigma(k,t) \equiv t^2 \ ,$$

and the mean-square displacement along the shear grows quadratically in time

$$\sigma_Y^2(t) = 2t^2 \int_0^\infty E(k)\,\mathrm{d}k = \langle v^2\rangle t^2 \ ,$$

signalling ballistic motion in the shear-parallel direction. This is readily understood: with no cross-shear motion, tracers stay on the original striated streamlines of the shear flow and proceed at the constant (but random) velocity $v(x_0)$ of the streamline on which they were originally situated. Much richer behavior arises when tracers do move across the shear flow streamlines due to molecular diffusion κ and/or the sweeping velocity $w(t)$, thereby breaking up the monotonic motion along the streamlines of the shear. This is reflected in the suppression of the shear-displacement kernel $\Sigma(k,t)$ (112b) through an oscillatory term due to the mean sweep and an exponential damping factor due to random cross-shear motion. We note moreover that the suppression effects become weaker at low wavenumber k. Hence, if there is sufficient energy in the low-wavenumber modes, we may expect that the shear-parallel transport is dominated by them, particularly at long times.

In what follows, we will develop these ideas in detail, through exact formulas and accompanying explanations of the relevant physical mechanisms. We will find that the shear-parallel tracer motion can have a wide variety of long-time behaviors, depending on the nature of the shear-transverse tracer motion $X(t)$ and on the strength of the long-range correlations of the random velocity field $v(x)$.

We shall first consider in turn the individual effects of each cross-shear motion on tracer transport along the shear: molecular diffusion in Section 3.2.1, a constant deterministic cross sweep $w(t) = \bar{w}$ in Section 3.2.2, and a purely random cross sweep $w(t) = w_f(t)$ in Section 3.2.3. They will be compared in Section 3.2.4, and collective effects will be discussed in Section 3.2.5.

After presenting these asymptotic results and some heuristic discussion, we indicate the means of their derivation in Section 3.2.6.

3.2.1. Effects of molecular diffusion

We first consider tracer motion along a random steady shear when molecular diffusion is active ($\kappa > 0$) and there is no cross sweep velocity $w(t) = 0$. This problem has been considered in the context of the flow of groundwater through a stratified porous medium [119,223]; in these

applications κ represents local dispersion coefficients of the medium rather than microscopic diffusion. The general results presented here were derived in [10]. The mean-square cross-shear displacement is just

$$\sigma_X^2(t) = 2\kappa t \;,$$

and the general formula (112) can be simplified to the following expression:

$$\sigma_Y^2(t) = 2\kappa t + 2\int_0^\infty E(k)\Sigma_\kappa(k, t)\,\mathrm{d}k \;,$$

$$\Sigma_\kappa(k, t) = t^2 F_1(t/\tau_\kappa(k)) \;.$$

We use here a specially defined universal function:

$$F_1(u) \equiv 2(\mathrm{e}^{-u} + u - 1)/u^2 \;,$$

and a natural wavenumber-dependent time scale

$$\tau_\kappa(k) \equiv (4\pi^2\kappa k^2)^{-1} \;, \tag{113}$$

which we will call the κ-*persistence* time scale. The important properties of $F_1(u)$ for our purposes are that it approaches a constant value 1 at small u, and that it decays for large positive u like $2u^{-1}$. Matheron and de Marsily [223] obtain an alternative formula for $\sigma_Y^2(t)$ in terms of the Laplace transform of the correlation function $R(x)$, and present some numerical plots indicating the growth of $\sigma_Y^2(t)$ over finite time intervals. We focus now on the long time asymptotics of $\sigma_Y^2(t)$.

Recalling that the shear-displacement kernel $\Sigma_\kappa(k, t)$ represents the influence of fluctuations of wavenumber k on the shear-parallel tracer transport, we see that the contribution of wavenumber k is ballistic for $t \ll \tau_\kappa(k)$ and diffusive for $t \gg \tau_\kappa(k)$

$$\Sigma_\kappa(k, t) \sim \begin{cases} t^2 & \text{for } t \ll \tau_\kappa(k) \;, \\ K_\kappa(k)t & \text{for } t \gg \tau_\kappa(k) \;. \end{cases}$$

The asymptotic shear-parallel tracer diffusivity due to a normalized mode of wavenumber k is

$$K_\kappa(k) \equiv \lim_{t\to\infty} \Sigma_\kappa(k, t)/2t = 1/4\pi^2\kappa k^2 \;. \tag{114}$$

This can be understood physically through the Lagrangian perspective developed in Section 3.1.3, where $\tau_\kappa(k)$ plays the role of a Lagrangian correlation time for the shear-parallel transport contribution from random shear fluctuations of wavenumber k. The persistent motion of the tracer toward a given direction along a steady shear flow is broken up over time by the molecular diffusion, which allows the tracer to hop across streamlines. Since the shear flow has zero mean, the tracer will be stochastically buffeted from streamlines carrying it one way to streamlines carrying it the other. The shear-parallel Lagrangian velocity of the tracer will consequently decorrelate on a time scale on the order of the time it takes for molecular diffusion to move the tracer across one wavelength $\sim k^{-1}$ of the fluctuation. This is readily computed to have the parameteric scaling $\sim (k^{-2})/\kappa$, which is identical to $\tau_\kappa(k)$ up to numerical constant. This justifies the interpretation of

$\tau_\kappa(k)$ as the Lagrangian correlation time due to the molecular diffusion across the streamlines. And, consistently with the general heuristic picture outlined in Paragraph 3.1.3.2, the tracer displacement due to the fluctuation of wavenumber k is ballistic for shorter times and diffusive for longer times. Moreover, the asymptotic diffusivity $K_\kappa(k)$ is proportional to (in fact equal) to the Lagrangian correlation time $\tau_\kappa(k)$. Therefore, the tracer motion induced by a single wavenumber k of the steady shear flow completely follows the paradigm of standard diffusion.

Summing up the contributions from all wavenumbers in the shear flow is quite subtle, however, because the Lagrangian correlation time $\tau_\kappa(k)$ diverges as $k \to 0$. This is clearly physical: it takes much longer for molecular diffusion to break up the coherent shear-parallel tracer transport of large wavelength fluctuations. Because of the slow decorrelation of the low wavenumber modes, it is *not* necessarily true that the tracer transport is asymptotically diffusive at long times, even though the contribution from each individual wavenumber $k > 0$ does eventually become diffusive. The long-time limiting behavior of the tracer motion along the shear depends crucially on the low wavenumber properties of the random shear spectrum, or equivalently, the strength of the long-range correlations in the shear flow. A careful asymptotic calculation, indicated in Section 3.2.6 and originally by [10], reveal the results reported in Table 2. The preconstants of the scaling laws are

$$K_\kappa^* = \kappa + 2\int_0^\infty E(k)K_\kappa(k)\, dk \ ,$$

$$K_\kappa^\sharp = -\Gamma\left(-\frac{\varepsilon}{2}\right)A_E(4\pi^2\kappa)^{-(2-\varepsilon)/2} \ . \tag{115}$$

As we see, for $\varepsilon < 0$, the steady shear flow has sufficiently weak long-range correlations so that at long times, the shear-parallel tracer motion behaves diffusively with finite effective diffusion constant K_κ^* obtained by simply integrating the long time effective single-mode diffusivities (114)

$$K_\kappa(k) \equiv \lim_{t\to\infty} \Sigma_\kappa(k,t)/2t = \tau_\kappa(k) = 1/4\pi^2\kappa k^2$$

against twice the energy spectral density. Results of this type with a similar formula for enhanced diffusivity were pioneered by Taylor [318]. The particular result noted here was originally derived by Gelhar et al. [119], and can be seen to be a natural extension of the effective diffusivity of

Table 2
Long-time asymptotics of mean-square tracer displacement along the shear in Random Steady Shear Model, with $\kappa > 0$, $\bar{w} = w_f(t) = 0$. Scaling coefficients are given by Eq. (115)

Parameter regime	Asymptotic mean square displacement $\lim_{t\to\infty} \sigma_Y^2(t)$	Qualitative behavior
$\varepsilon < 0$	$2K_\kappa^* t$	Diffusive
$0 < \varepsilon < 2$	$\frac{4}{2+\varepsilon}K_\kappa^\sharp t^{1+\varepsilon/2}$	Superdiffusive

a periodic shear flow (51). An important class of shear velocity fields which fall in the class $\varepsilon < 0$ are those with wavenumbers excited only above some threshold $k_{\min} > 0$, i.e., $E(k) = 0$ for $0 \leq k < k_{\min}$. Velocity fields given by a finite superposition of random sinusoidal oscillations are a particular example.

For $0 < \varepsilon < 2$, the long-range correlations in the shear flow are sufficiently strong to cause this simple picture to break down. The tracer's motion is dominated for arbitrarily large times t by fluctuations of very large scales with $\tau_\kappa(k) \gtrsim t$, which act coherently and persistently on the tracer. These produce a long-term memory in the Lagrangian velocity of a tracer particle and give rise to a superdiffusive transport for exactly the same reason as we discussed in Section 3.1.3. Put another way, for $0 < \varepsilon < 2$, the cross-shear transport induced by Brownian motion is not fast enough to completely break up the coherent advection by the strong, large-scale shear fluctuations. This is reflected in the fact that the effective diffusion constant K_κ^* for $\varepsilon < 0$ would diverge if used for $\varepsilon > 0$. Note moreover that this division between diffusive and superdiffusive behavior is in exact accord with the rigorous homogenization criterion described in Section 2.4.2; the Péclet number (81) of the random shear flow with energy spectrum (109) is finite precisely when $\varepsilon < 0$.

It is interesting to note that superdiffusion arises for quite typical shear velocity fields, namely those with finite $k \to 0$ limits of the energy density $E(k)$ (which correspond to $\varepsilon = 1$). These are precisely those random velocity fields for which the integral of the correlation function is finite and positive

$$0 < \int_0^\infty R(x)\,\mathrm{d}x < \infty \ . \tag{116}$$

That superdiffusion could occur in steady shear flows of this type was suggested by Gelhar et al. [119] and precisely demonstrated by Matheron and de Marsily [223]. A special example of a steady random shear flow with $\varepsilon = 1$ which has been considered by Mazo and Van den Broeck [225] and others [46,279,280,353,354] consists of infinite array of parallel channels of common width, with a constant random velocity along each channel chosen independently to be $\pm v_0$ with equal probability. (The criterion (116) is manifestly satisfied by this and any other random shear flow with a finite-range, purely nonnegative correlation structure.) An explicit formula for $\sigma_Y^2(t)$ valid for all finite times is derived in [225], from which an asymptotic $t^{3/2}$ scaling may be read off. The authors [46,279] furnished the following physical-space heuristic explanation for the $\sigma_Y^2(t) \sim t^{3/2}$ superdiffusive scaling law: The molecular diffusion across the channels causes a tracer to sample $\sim t^{1/2}$ channels over a time interval t, so the tracer spends a typical time $\sim t^{1/2}$ in each channel. Consequently, the total mean-square displacement over a time interval t is the number of channels explored $\sim t^{1/2}$ multiplied by the mean-square displacement produced by each channel $\sim (t^{1/2})^2 = t$. Phrased more generally, the reason for the anomalous diffusion is that the number of different channels sampled grows sublinearly in time, so there is a long-term memory effect due to preferential resampling of channels previously visited.

Viewing the scaling exponent v in $\sigma_Y^2(t) \sim t^v$ as an order parameter, we can say that there is a formal phase transition [126] in the long-time tracer behavior with respect to the infrared scaling exponent ε of the energy spectrum. The phase transition occurs at $\varepsilon = 0$; below this value $v = 1$, and above this value, v bifurcates continuously to the curve $v = (\varepsilon + 2)/2$. We indicate this graphically in Fig. 9. At the phase transition value $\varepsilon = 0$ itself, there are logarithmic corrections.
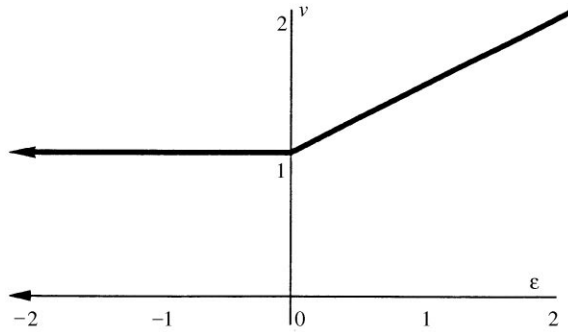
Fig. 9. Scaling exponent v in $\sigma_Y^2(t) \sim t^v$ as a function of ε in Random Steady Shear Model with $\kappa > 0$, $\bar{w} = w_f(t) = 0$.

Finally, we note that the long-time tracer behavior is singular in limit of zero molecular diffusion; the scaling coefficients (115) diverge as $\kappa \to 0$. The reason for the drastic difference between $\kappa = 0$ and κ small is that tracers are permanently stuck on their original streamline in the former case, but can over time move arbitrarily far across the shear in the latter case, no matter how small κ is.

3.2.2. Effects of constant cross sweep

We now consider the effects of a deterministic sweeping of tracers across streamlines, as manifested by a constant (in space and time) mean drift $w(t) = \bar{w} \neq 0$ across the random, steady shear $v(x)$

$$v(x, y, t) = \begin{bmatrix} \bar{w} \\ v(x) \end{bmatrix}. \tag{117}$$

The behavior of a tracer in such a flow was studied in detail by Horntrop and the first author [141]. We consider for now the case without molecular diffusion.

Then $\sigma_X^2(t) = 0$, and the formula for the mean-square tracer displacement along the shear may be written

$$\sigma_Y^2(t) = 2 \int_0^\infty E(k) \Sigma_{\bar{w}}(k, t) \, dk ,$$

$$\Sigma_{\bar{w}}(k, t) = t^2 F_2(t/\tau_{\bar{w}}(k)) .$$

We have defined another universal function

$$F_2(u) \equiv 2(1 - \cos u)/u^2 ,$$

and a wavenumber-dependent time scale

$$\tau_{\bar{w}}(k) \equiv (2\pi k \bar{w})^{-1} , \tag{118}$$

which we call the $\bar{w}$-persistence time scale. It plays a role similar to $\tau_\kappa(k)$ in Section 3.2.1, with some important distinctions due to the lack of randomness of the sweep $\bar{w}$. As we shall see, $\tau_{\bar{w}}(k)$ has some but not all of the standard properties of a (wavenumber-dependent) Lagrangian correlation time.

The time scale $\tau_{\bar{w}}(k)$ does have the same property as $\tau_\kappa(k)$ in measuring *persistence* of the tracer motion, in that $\tau_{\bar{w}}(k)$ describes the time scale on which the cross sweep $\bar{w}$ disrupts the ballistic motion due to a random oscillatory mode of wavenumber k in the shear velocity field. Indeed, over times $t \ll (k\bar{w})^{-1}$, the tracer motion is predominantly unidirectional. Over longer times $t \gtrsim (k\bar{w})^{-1}$, the tracer is dragged by the mean sweep across several wavelengths of the oscillating shear flow, so the tracer motion assumes an oscillatory character along the shear rather than a ballistic one. The key point of departure of the present model from the standard diffusion picture enunciated in Paragraph 3.1.3.2 is that each fluctuation of the shear flow with wavenumber k contributes an *oscillatory*, rather than a *diffusive* component to the shear-parallel tracer motion at times long compared to the natural $\bar{w}$-persistence time scale $\tau_{\bar{w}}(k)$. This is reflected in the fact that the shear-displacement kernel $\Sigma_{\bar{w}}(k,t)$ is, for each k, a bounded oscillatory function of time. We therefore call $\tau_{\bar{w}}(k)$ a Lagrangian *persistence* time scale, which is a more generally applicable notion than a Lagrangian correlation time scale. In Section 3.2.4, we will compare and contrast the above described behavior of the kernel associated to a constant mean sweep, $\Sigma_{\bar{w}}(k,t)$, with those arising from other cross-transport mechanisms.

We note now that the mean-square displacement in a statistically homogenous, random steady shear flow with constant cross sweep is given by the same formula as in the Random Sweeping Model (94), except that ω is replaced by $k\bar{w}$ in the kernel, and the energy spectrum resolved with respect to wavenumber appears instead of the energy spectrum resolved with respect to frequency. This is readily understood from the formula (110b) for the shear-parallel tracer motion, which for $\kappa = 0$ and $w(t) = \bar{w}$ reads

$$Y(t) = y_0 + \int_0^t v(x_0 + \bar{w}s)\,\mathrm{d}s \ .$$

The Lagrangian velocity of the tracer is therefore exactly $v(x_0 + \bar{w}t)$, which is manifestly a mean zero, statistically stationary random process, just as the sweeping field $w_f(t)$ in the Random Sweeping Model. We can therefore immediately deduce the long-time asymptotics of the mean-square displacement across the shear from the results of the Random Sweeping Model (see Table 1 and [141]); these are displayed in Table 3. The scaling coefficients are

$$K_{\bar{w}}^* = \tfrac{1}{2} A_E \bar{w}^{-1} \ , \tag{119a}$$

$$K_{\bar{w}}^\sharp = \tfrac{1}{2} A_E \pi^{\varepsilon - (3/2)} \bar{w}^{\varepsilon - 2} \Gamma((2 - \varepsilon)/2)/\Gamma((1 + \varepsilon)/2) \ , \tag{119b}$$

$$\mathrm{K}_{\bar{w}}^\circ = \frac{1}{\pi^2 \bar{w}^2} \int_0^\infty E(k) k^{-2}\,\mathrm{d}k \ . \tag{119c}$$

The long-time tracer behavior is a smooth function of ε as it varies over $0 < \varepsilon < 2$, even though it falls into different qualitative categories. There is however, a phase transition at $\varepsilon = 0$ between trapping behavior and subdiffusive behavior (Fig. 10). This is manifested both in the sharp change in the scaling exponent, and in the fact that the long time tracer motion depends on the whole energy spectrum for $\varepsilon < 0$ through K_x° (see Eq. (119c)), whereas only the infrared parameters A_E and ε appear in the preconstants for $\varepsilon > 0$.

The simplicity of the Random Steady Shear model with constant cross sweep and the wide variety of resulting tracer behavior make this model an excellent candidate for testing numerical

Table 3
Long-time asymptotics of mean-square tracer displacement along the shear in Random Steady Shear Model, with $\kappa = 0$, $w(t) = \bar{w} \neq 0$ (from [141]). Scaling coefficients are given by (119)

Parameter regime	Asymptotic mean square displacement $\lim_{t \to \infty} \sigma_Y^2(t)$	Qualitative behavior
$\varepsilon < 0$	$K_{\bar{w}}^{\circ} t^0$	Trapping
$0 < \varepsilon < 1$	$\frac{2}{\varepsilon} K_{\bar{w}}^{\sharp} t^{\varepsilon}$	Sub-diffusive
$\varepsilon = 1$	$2 K_{\bar{w}}^{*} t$	Diffusive
$1 < \varepsilon < 2$	$\frac{2}{\varepsilon} K_{\bar{w}}^{\sharp} t^{\varepsilon}$	Super-diffusive
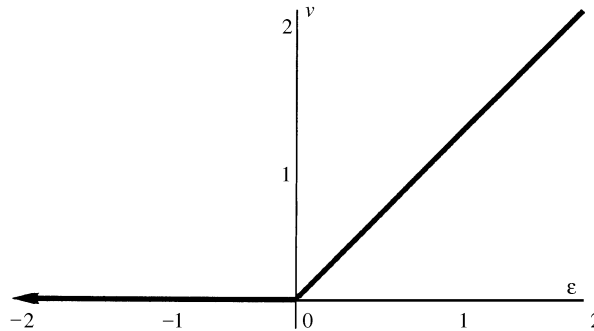
Fig. 10. Scaling exponent v in $\sigma_Y^2(t) \sim t^v$ as a function of ε in Random Steady Shear Model with $\bar{w} \neq 0$, $\kappa = w_f(t) = 0$.

methods for simulating turbulent diffusion. It has been applied toward this end in [83], and we present an extensive discussion in Section 6.2.

3.2.2.1. Streamline analysis. Consideration of the streamlines of the steady velocity field gives a pictorial way to understand how the cross sweep $\bar{w}$ impedes diffusion along the shear flow (see Section 2.2). Without a cross flow, the streamlines of the shear are of course straight lines parallel to the x_2 axis. The effect of the velocity field alone is to transport any tracer along its own streamline forever along a single direction.

When a nonzero cross sweep is added $\bar{w} \neq 0$, the streamlines display a more interesting behavior. We define the stream function $\Psi(x, y)$ of the resulting incompressible steady flow in the standard way:

$$\boldsymbol{v}(x, y) = \begin{bmatrix} \bar{w} \\ v(x) \end{bmatrix} = \begin{bmatrix} -\dfrac{\partial \Psi(x, y)}{\partial y} \\ \dfrac{\partial \Psi(x, y)}{\partial x} \end{bmatrix}.$$

An obvious solution is

$$\Psi(x, y) = -\bar{w} y + \tilde{\Psi}(x) , \tag{120}$$

where

$$\mathrm{d}\tilde{\Psi}(x)/\mathrm{d}x = v(x) \ . \tag{121}$$

As $v(x)$ is a homogenous, mean zero, Gaussian random process, it may be expressed as a stochastic Fourier integral ([341], Section 9)

$$v(x) = \int_{-\infty}^{\infty} \mathrm{e}^{2\pi \mathrm{i}kx}\sqrt{E(|k|)}\,\mathrm{d}\tilde{W}(k) \ , \tag{122}$$

where the integration measure is complex white noise, which is a Gaussian random quantity with the formal properties

$$\mathrm{d}\tilde{W}(-k) = \overline{\mathrm{d}\tilde{W}(k)} \ ,$$

$$\langle \mathrm{d}\tilde{W}(k) \rangle = 0 \ ,$$

$$\langle \mathrm{d}\tilde{W}(k)\mathrm{d}\tilde{W}(k') \rangle = \delta(k + k')\,\mathrm{d}k\,\mathrm{d}k'$$

(An overbar denotes complex conjugation.) The stochastic Fourier integral expresses $v(x)$ as a continuum limit of a sum of independent random Fourier modes, with amplitudes weighted by the square root of their energy density. It is readily checked that $v(x)$ defined by Eq. (122) is a mean zero, Gaussian random process with correlation function in agreement with Eq. (108).

Now, it is tempting to define $\tilde{\Psi}(x)$ as

$$\tilde{\Psi}(x) = \int_{-\infty}^{\infty} \mathrm{e}^{2\pi \mathrm{i}kx}\frac{\sqrt{E(|k|)}}{2\pi \mathrm{i}k}\,\mathrm{d}\tilde{W}(k) = \frac{\sqrt{A_E}}{2\pi \mathrm{i}}\int_{-\infty}^{\infty} \mathrm{e}^{2\pi \mathrm{i}kx}\mathrm{sgn}(k)|k|^{-(1+\varepsilon)/2}\sqrt{\psi(|k|)}\,\mathrm{d}\tilde{W}(k) \ , \tag{123}$$

so that Eq. (121) is formally satisfied. For the stochastic Fourier integral (123) to be well-defined, however, the integrand must be square-integrable [341]. The division by k introduces a possible singularity at $k = 0$, which is square-integrable only for $\varepsilon < 0$.

For this range of infrared scaling exponents, we have successfully defined a good stream function $\Psi(x, y)$ by Eqs. (120) and (123). In particular, when $\varepsilon < 0$, $\tilde{\Psi}(x)$ is a real, homogenous, Gaussian random field with finite variance:

$$\langle \tilde{\Psi}^2(x) \rangle = \int_{-\infty}^{\infty} |\sqrt{A_E}\,\mathrm{sgn}(k)(2\pi \mathrm{i})^{-1}|k|^{-(1+\varepsilon)/2}\sqrt{\psi(|k|)}|^2\,\mathrm{d}k = \frac{A_E}{4\pi^2}\int_{-\infty}^{\infty} |k|^{-1-\varepsilon}\psi(|k|)\,\mathrm{d}k < \infty \ .$$

Now, the streamlines are given by level sets of the stream function

$$\Psi(x, y) = -\bar{w}y + \tilde{\Psi}(x) = C \ , \tag{124}$$

or equivalently

$$y = \tilde{\Psi}(x)/\bar{w} + (C/\bar{w}) \ . \tag{125}$$

Since $\tilde{\Psi}(x)$ is a homogenous random field with finite variance, the shear-parallel displacement of the streamline, y, is randomly distributed, but smoothly and with finite variance. There are no large excursions off to infinity (almost surely), and the streamlines are blocked in a statistical sense along

the shearing direction. Because we are not including molecular diffusion at the moment, tracers follow the streamlines, and will consequently remain trapped along the shearing direction for $\varepsilon < 0$.

When $0 < \varepsilon < 2$, these arguments no longer hold (due to the singularity of the integral (123) at $k = 0$); it is not possible to define a statistically homogenous stream function with bounded variance. The streamlines instead wander off to infinity, yielding subdiffusive, diffusive, or super-diffusive behavior on large scales and long times.

3.2.3. Effects of temporally fluctuating cross sweep

The third and final mechanism of cross-shear transport which we will consider is that of a randomly fluctuating, spatially uniform, mean zero velocity field $w_f(t)$:

$$\boldsymbol{v}(x, y, t) = \begin{bmatrix} w_f(t) \\ v(x) \end{bmatrix} .$$

The shear-transverse component of the velocity field $w_f(t)$ is taken to be a mean zero, Gaussian, stationary, random process with correlation function:

$$R_w(t) \equiv \langle w_f(t') w_f(t + t') \rangle = 2 \int_0^\infty \cos(2\pi\omega t) E_w(|\omega|) \, \mathrm{d}\omega .$$

We assume the power spectrum of the random sweeping is smooth for $\omega > 0$, absolutely integrable, and has the same form as that assumed in the Random Sweeping Model discussed in Section 3.1.2

$$E_w(\omega) = A_{E,w} |\omega|^{-\beta} \psi_w(|\omega|) . \tag{126}$$

Here, $A_{E,w} > 0$, $\beta < 1$, and $\psi_w(\cdot)$ is a smooth function on the non-negative real axis with $\psi_w(0) = 1$ and $|\psi_w'(0)| < \infty$.

The mean-square displacement of a tracer across the shear due to the random sweeping is given by Eq. (93)

$$\sigma_X^2(t) \equiv \langle (X(t) - x_0)^2 \rangle = 2 \int_0^t (t - s) R_w(s) \, \mathrm{d}s .$$

We saw in Section 3.1.2 that the exponent β determines the long-time behavior of the tracer motion in the x direction:

$$\lim_{t \to \infty} \sigma_X^2(t) \sim \begin{cases} \frac{2}{1+\beta} K_x^\sharp t^{1+\beta} & \text{for } -1 < \beta < 1 , \\ K_x^\circ & \text{for } \beta < -1 , \end{cases} \tag{127}$$

where

$$K_x^\sharp = \tfrac{1}{2} A_{E,w} \pi^{\beta - (1/2)} \Gamma((1 - \beta)/2)/\Gamma((2 + \beta)/2) ,$$

$$K_x^\circ = \frac{1}{\pi^2} \int_0^\infty E_w(\omega) \omega^{-2} \, \mathrm{d}\omega .$$

To avoid needless complications, we will not treat the phase transition value $\beta = -1$, in which logarithms arise.

The mean-square displacement of a tracer along the shear is obtained by setting $\kappa = \bar{w} = 0$ in Eqs. (112a) and (112b)

$$\sigma_Y^2(t) = 2\int_0^\infty E(k)\Sigma_{w_f}(k,t)\,dk\ ,$$

$$\Sigma_{w_f}(k,t) = 2\int_0^t (t-s)e^{-2\pi^2 k^2 \sigma_x^2(s)}\,ds\ . \tag{128}$$

We see that the random cross sweeping decorrelates the tracer motion along the shear through the exponentially decaying factor. It acts in a manner quite similar to molecular diffusion in buffeting tracers randomly onto different streamlines of the pure shear flow; indeed, the case of pure molecular diffusion is recovered by simply setting $\sigma_X^2(t) = 2\kappa t$. The random cross sweeping, however, can have a variety of long-time scaling behavior, depending on its low-frequency scaling exponent β. The shear-parallel transport depends sensitively on the effectiveness of the random cross sweep, as illustrated in Table 4, which displays the long time asymptotics of $\sigma_Y^2(t)$ for various parameter values. The scaling coefficients are

$$K_{w_f}^* = 2\int_0^\infty E(k)K_{w_f}(k)\,dk\ , \tag{129}$$

$$K_{w_f}^\sharp = \frac{\Gamma((2-\varepsilon)/2)A_E}{((\varepsilon(1+\beta)/2)-\beta)}\left(\frac{1+\beta}{4\pi^2 K_x^\sharp}\right)^{(2-\varepsilon)/2}\ ,$$

$$K_{w_f}^\bullet = 2\int_0^\infty E(k)e^{-2\pi^2 k^2 K_x^\circ}\,dk\ ,$$

where

$$K_{w_f}(k) \equiv \lim_{t\to\infty}\frac{\Sigma_{w_f}(k,t)}{2t} = \int_0^\infty e^{-2\pi^2 k^2 \sigma_x^2(s)}\,ds \tag{130}$$

is the asymptotic shear-parallel diffusivity contribution from a normalized mode of wavenumber k. These results are derived in Paragraph 3.2.6.3.

Table 4
Long-time asymptotics of mean-square tracer displacement along the shear in Random Steady Shear Model, with $\kappa = 0$, $w(t) = w_f(t) \neq 0$. Scaling coefficients are given by (129)

Parameter regime		Asymptotic mean square displacement $\lim_{t\to\infty}\sigma_Y^2(t)$	Qualitative behavior
$-1 < \beta < 1$	$\varepsilon < \dfrac{2\beta}{1+\beta}$	$2K_{w_f}^* t$	Diffusive
	$\dfrac{2\beta}{1+\beta} < \varepsilon < 2$	$\dfrac{4}{2+\varepsilon-\beta(2-\varepsilon)}K_{w_f}^\sharp t^{1+\varepsilon/2-\beta(2-\varepsilon)/2}$	Superdiffusive
$\beta < -1$	$\varepsilon < 2$	$K_{w_f}^\bullet t^2$	Ballistic

Consider first the case in which the mean-square displacement across the shear grows unboundedly with time ($-1 < \beta < 1$). The value $\beta = 0$ corresponds to a diffusive cross sweep, and the behavior of $\sigma_Y^2(t)$ is much the same at long times as it is for the case of molecular diffusion; see Section 3.2.1. In particular, there is a phase transition at $\varepsilon = 0$, below which the tracer displacement along the shear is diffusive, and above which it grows superdiffusively as $\sigma_Y^2(t) \sim K_{w_f}^\sharp t^{1+\varepsilon/2}$. As β is varied within the range $-1 < \beta < 1$, the situation is qualitatively the same. The key changes are that

- The phase transition value between superdiffusive and diffusive shear-parallel transport is shifted to $\varepsilon = 2\beta/(1+\beta)$.
- The superdiffusive scaling exponent is modified to $1 + \varepsilon/2 - \beta(2-\varepsilon)/2$.

These are indicated graphically in Fig. 11.

We note that increasing β increases the strength of the low-frequency, long-range temporal correlations in the sweep, and thus increases the rate at which the tracer is swept across the streamlines. We see that an increase of β is associated with an increase in the range of values of ε for which the shear-parallel transport is diffusive rather than superdiffusive, and is also associated with a depression of the scaling exponent in the superdiffusive regime. This explicitly demonstrates that an increase in the strength of cross-shear transport decreases the rate of shear-parallel transport. The reason is simply that the Lagrangian correlation time for the tracer motion along the shear will be reduced if it is swept across the shear at a faster rate; see Section 3.1.3. One can associate the Lagrangian correlation time in the present model with a natural w_f-persistence time $\tau_{w_f}(k)$ for each wavenumber k in the shear by the implicit relation

$$\sigma_X^2(\tau_{w_f}(k)) = (2\pi^2 k^2)^{-1} \ .$$

This is suggested mathematically by the exponential damping term in Eq. (128), and physically (up to numerical factor) by the typical time taken to cross one wavelength $\sim k^{-1}$ of the shear flow. For low wavenumbers k, which have the longest Lagrangian decorrelation times and therefore often dominate the long-time asymptotics of tracer motion, we can use the
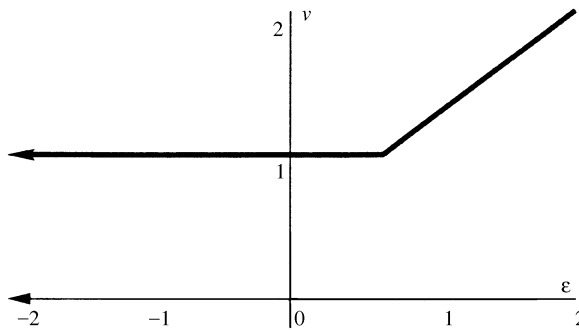

Fig. 11. Scaling exponent v in $\sigma_Y^2(t) \sim t^v$ as a function of ε in Random Steady Shear Model with $w_f(t) \neq 0$, $\kappa = \bar{w} = 0$. The value $\beta = 1/2$, corresponding to a random cross sweep which induces superdiffusive cross-shear transport, is used in this drawing. Varying β slides the transition value horizontally along $v = 1$.

asymptotic formula (127) to obtain

$$\lim_{k \to 0} \tau_{w_f}(k) \sim C_{w_f}(K_x^\sharp k^2)^{-1/(1+\beta)} \,, \tag{131}$$

where C_{w_f} is an unimportant numerical constant. The rate of divergence of the Lagrangian correlation time $\tau_{w_f}(k)$ is shallower when β increases and the cross-sweep transport is more effective, as we claimed. It can be checked that the asymptotic single-mode diffusivity $K_{w_f}(k)$ is on the order of $\tau_{w_f}(k)$, as would be expected by the standard Lagrangian analysis (Paragraph 3.1.3.2).

The case $\beta < -1$ has a distinctive character. The low-frequency component of the random sweep is so weak in this regime that the tracer motion across the shear is trapped. Thus, at long time scales, the tracer remains statistically localized about its original streamline, and therefore exhibits permanent memory effects. In fact, the Lagrangian correlation time associated to each wavenumber is effectively infinite. Consequently, the shear-parallel transport is ballistic, in accordance with the cartoon Lagrangian description in Section 3.1.3.

It is interesting to note that the scaling coefficient $K_{w_f}^\bullet$ for the ballistic regime depends on the energy spectrum at all wavenumbers, a feature in common with the diffusive regime and distinct from the superdiffusive regime. The reason is that *each* mode of the shear flow has an infinite Lagrangian correlation time associated to it due to the trapped cross shear transport. Hence, the contribution of even large wavenumbers remains ballistic at arbitrarily long times, and never becomes subdominant to the total ballistic scaling.

3.2.4. Comparison of effects of various cross-shear transport processes

We now make some general observations regarding the competing effects of cross-shear transport due to molecular diffusion κ (Section 3.2.1), a constant cross sweep $\bar{w}$ (Section 3.2.2), or a randomly fluctuating cross sweep $w_f(t)$ (Section 3.2.3).

First of all, we have noticed that shear velocity fields with long-range correlations (ε relatively large) can exhibit superdiffusive shear-parallel transport for all cross-shear transport mechanisms considered. The reason is that the mode-by-mode contribution to the shear-parallel tracer motion has an effective Lagrangian persistence time scale diverging at low wavenumber. When there is enough energy in the low wavenumber modes, the total motion of the tracer also has an infinite Lagrangian persistence time, so the standard diffusive situation of Paragraph 3.1.3.2 does not apply.

Another trend which can be observed is the fact that shear-parallel transport is generally diminished as cross-shear transport becomes more efficient. This was demonstrated explicitly in Section 3.2.3 by consideration of how the long-time asymptotics of $\sigma_Y^2(t)$ depend on the exponent β characterizing the low-frequency behavior of the randomly fluctuating cross sweep $w_f(t)$. The sense in which this qualitative trend is supported by all cases considered is that the superdiffusive regime of exponent values ε shrinks as the cross-shear transport becomes more rapid. Indeed, the superdiffusive regime is minimal ($1 < \varepsilon < 2$) for the case of a constant (ballistic) cross sweep, and expands smoothly for a randomly fluctuating cross sweep as β is decreased so that the cross-shear transport is superdiffusive, then diffusive, then subdiffusive, then trapped. Moreover, the case of a constant cross sweep can be thought of as a limit with $\beta \nearrow 1$ of the randomly fluctuating cross sweep insofar as superdiffusive tracer motion is concerned. Specifically, as $\beta \nearrow 1$, the boundary

value between diffusive and superdiffusive behavior, $2\beta/(1 + \beta)$, and the superdiffusive scaling exponent $1 + \varepsilon/2 - \beta(2 - \varepsilon)/2$ for the randomly fluctuating cross sweep tend to the values 1 and ε, respectively, which are those corresponding to a constant cross sweep (cf. Figs. 10 and 11).

There is, however, a strong distinction between the case of a constant cross sweep and the case of a random cross-shear transport (whether by molecular diffusion or by a randomly fluctuating cross sweep) insofar as subdiffusive tracer behavior is concerned. There is no subdiffusive nor trapping regime for random cross-shear transport, whereas these do exist with a constant cross sweep when the energy spectrum of the shear flow vanishes at the origin. The reason for the distinction may be understood by a consideration of the contribution $\Sigma(k, t)$ of a single mode of wavenumber k of the random shear fl

the two. Therefore, the more rapid cross-shear transport process will determine the character of the long-time asymptotics of the shear-parallel transport. Note that the above superposition laws indicate that the scaling exponent for $\sigma_Y^2(t)$ is always the smaller of the exponents associated to each individual, active random cross-shear transport mechanism operating in isolation.

When the tracer motion is superdiffusive, the scaling *coefficient* in the asymptotics for $\sigma_Y^2(t)$ will depend only the dominant cross-shear mechanism. But when the tracer motion is diffusive, the effective diffusion coefficient will generally depend on all cross-shear transport processes involved.

It must always be kept in mind that long-time asymptotic results are only valid when t is larger than all relevant time scales, and that there may in practice be important finite time corrections. For example, even though the effects of molecular diffusion will eventually dominate those of a subdiffusive cross sweep $w_f(t)$, there may well be a long intermediate interval of time over which the cross-shear transport is dominated by the effects of the fluctuating cross sweep, because κ is typically small relative to the macroscopic units of the system. Therefore, the shear-parallel transport may, in such a case, exhibit the scaling associated to a subdiffusive cross sweep for a while (Table 4), then ultimately cross over to the asymptotic scaling associated to the effects of molecular diffusion (Table 2).

3.2.5.2. Superposition of constant cross sweep with random cross-shear transport process. The situation is more subtle when a constant cross sweep $\bar{w}$ is superposed with a random cross-shear transport process (κ or $w_f(t)$). On the one hand, it is true that the fastest cross-shear transport mechanism (in the present case, $\bar{w}$) determines whether the tracer motion is superdiffusive, and if so, how its mean-square displacement scales in time. Therefore, the superdiffusive regime is $1 < \varepsilon < 2$ and has the same scaling law as for a constant cross sweep with no other random mechanisms (Table 3). But for $\varepsilon < 1$, we must take into account the fact that the random cross-shear transport will break up the coherence present when the constant cross sweep is acting alone. Therefore, when the constant cross sweep $\bar{w}$ is superposed with molecular diffusion κ and/or random cross-shear fluctuations $w_f(t)$ with $-1 < \beta < 1$, the subdiffusive and trapping regimes ($\varepsilon < 1$) become diffusive.

We now explicitly illustrate some of these subtle effects of superposition by reporting some basic formulas, worked out in detail in [141], for the mean-square shear-parallel transport for the case in which a constant cross sweep $\bar{w} \neq 0$ and molecular diffusion $\kappa \neq 0$ are both present. We take $w_f(t) = 0$ for this discussion.

The mean-square displacement of the tracer along the shear is given by the following formula [141], specialized from Eq. (112)

$$\sigma_Y^2(t) = 2\kappa t + 2\int_0^\infty E(k)\Sigma_{\kappa,\bar{w}}(k,t)\,\mathrm{d}k \ , \tag{132a}$$

$$\Sigma_{\kappa,\bar{w}}(k,t) = t^2 F_3\left(\frac{t}{\tau_\kappa(k)}, \frac{t}{\tau_{\bar{w}}(k)}\right) . \tag{132b}$$

Here, $F_3(u, u')$ is the following universal function

$$F_3(u, u') = 2\left[\frac{u}{u^2 + u'^2} - \frac{(1 - \mathrm{e}^{-u}\cos u')(u^2 - u'^2) + 2uu'\mathrm{e}^{-u}\sin u'}{(u^2 + u'^2)^2}\right], \tag{133}$$

Table 5
Long-time asymptotics of mean-square tracer displacement along the shear in Random Steady Shear Model, with $\kappa > 0$, $\bar{w} \neq 0$, $w_f(t) = 0$. Scaling coefficients are given by Eq. (134)

Parameter regime	Asymptotic mean square displacement $\lim_{t \to \infty} \sigma_Y^2(t)$	Qualitative behavior
$\varepsilon < 1$	$2K_{\kappa,\bar{w}}^* t$	Diffusive
$\varepsilon = 1$	$2K_{\kappa,\bar{w}}^{\prime *} t$	Diffusive
$1 < \varepsilon < 2$	$\frac{2}{\varepsilon} K_{\kappa,\bar{w}}^{\sharp} t^{\varepsilon}$	Superdiffusive

and

$$\tau_{\kappa}(k) = (4\pi^2 \kappa k^2)^{-1} ,$$

$$\tau_{\bar{w}}(k) = (2\pi \bar{w} k)^{-1}$$

are the Lagrangian persistence times associated to the molecular diffusion and to the constant cross sweep, respectively. A more compact formula for $\sigma_Y^2(t)$ in terms of the Laplace transform of the velocity correlation function $R(x)$ was derived by Matheron and de Marsily [223]; the spectral representation has been developed here because of its flexibility in handling randomly fluctuating components $w_f(t)$ in the cross sweep. Some numerical plots of $\sigma_Y^2(t)$ over finite intervals of time for special choices of correlation functions $R(x)$ can be found in [223].

The long-time asymptotics of $\sigma_Y^2(t)$ are worked out rigorously in [141], and the results displayed in Table 5. The scaling coefficients are

$$K_{\kappa,\bar{w}}^* = \kappa + 2 \int_0^{\infty} E(k) K_{\kappa,\bar{w}}(k) \, \mathrm{d}k , \tag{134}$$

$$K_{\kappa,\bar{w}}^{\prime *} = \kappa + K_{\kappa,\bar{w},\varepsilon=1}^{\sharp} + 2 \int_0^{\infty} E(k) K_{\kappa,\bar{w}}(k) \, \mathrm{d}k ,$$

$$K_{\kappa,\bar{w}}^{\sharp} = \frac{A_E \pi^{\varepsilon-3/2} \Gamma((2-\varepsilon)/2)}{2\Gamma((1+\varepsilon)/2)} ,$$

where

$$K_{\kappa,\bar{w}}(k) \equiv \lim_{t \to \infty} \frac{1}{2t} \Sigma_{\kappa,\bar{w}}(k,t) = \frac{\tau_{\kappa}^{-1}(k)}{\tau_{\kappa}^{-2}(k) + \tau_{\bar{w}}^{-2}(k)} = \frac{\kappa}{4\pi^2 \kappa^2 k^2 + \bar{w}^2} \tag{135}$$

is the asymptotic diffusivity contributed by a single normalized Fourier mode of the shear flow.

These results have some interesting relations to the asymptotics for a random steady shear flow with either molecular diffusion κ or a constant cross sweep $\bar{w}$ acting individually (see Sections 3.2.1 and 3.2.2, respectively). First, we note that the superdiffusive regime and scalings are identical to those in which $\bar{w} \neq 0$ but $\kappa = 0$. This is in accordance with the general principle described above that the fastest cross-shear transport mechanism determines whether the tracer behaves super-diffusively, and if so, how. Recall that if the random shear flow has the generic property

$0 < \int_0^\infty R(x)\,dx < \infty$ (which corresponds to $\varepsilon = 1$), then the mean-square tracer displacement along the shear grows superdiffusively in time in the presence of molecular diffusion but with no cross sweep: $\sigma_Y^2(t) \sim t^{3/2}$. The addition of a constant cross sweep $\bar{w}$ restores a diffusive character to the shear-parallel transport, as was noted by Matheron and de Marsily [223] in a hydrological context. One way to understand this for the case of the independent channel models of [46,279,353] is that a mean sweep across the channels destroys the oversampling of old channels. Over a time interval t, a tracer samples only $O(\sqrt{t})$ different channels if it only moves diffusively across channels, but will sample a full $O(t)$ different channels when a constant cross-drift is added [47].

A second outcome of the combination of molecular diffusion with the constant cross sweep is the elimination of the subdiffusive and trapping regimes which were present when $\bar{w} \neq 0$ but $\kappa = 0$. This is *not* simply because molecular diffusion contributes an independent shear-parallel diffusive transport process. Indeed, even if molecular diffusion were only to act across the shear, the only change to the asymptotics stated above is that the *additive* κ term in the scaling constants $K_{\kappa,\bar{w}}^*$ and $K_{\kappa,\bar{w}}'^*$ would disappear. The fundamental reason the subdiffusive and trapping behavior disappears is that the addition of molecular diffusion randomizes the cross-shear transport, and disrupts the coherent cross-shear motion which produces the persistent oscillations of the Lagrangian velocity. Interestingly, the boundary between the diffusive and superdiffusive regimes is located at $\varepsilon = 1$, as for the case of pure constant cross sweep, but manifests a sharp phase transition as for the case of pure molecular diffusion (Fig. 12). (Recall that the diffusive–superdiffusive transition is smooth for the case of a pure constant cross sweep.)

We finally remark upon the need for mathematical care which the current example demonstrates. Note that the asymptotic mode-by-mode diffusivity $K_{\kappa,\bar{w}}(k)$ (135) is a bounded function. Consequently, if one were to blindly compute $\lim_{t\to\infty} \sigma_Y^2(t)/2t$ by moving the $t \to \infty$ limit under the integral over k in Eq. (132a), one would arrive at a finite answer for all $\varepsilon < 2$, which would coincide with a naive extrapolation of formula (52) for the effective diffusivity in a periodic shear flow to the case of a random shear flow. It would be incorrect to conclude, however, that this result described the asymptotic shear-parallel diffusivity for $1 \leq \varepsilon < 2$. The commutation of the $t \to \infty$ limit with the integral over k is patently invalid for this range of parameters, and leads to a misleading and incorrect result. The reason is a subtle nonuniform convergence of the integrand to its asymptotic limit at small wavenumbers; a formally transient contribution to the integral is in fact significant or
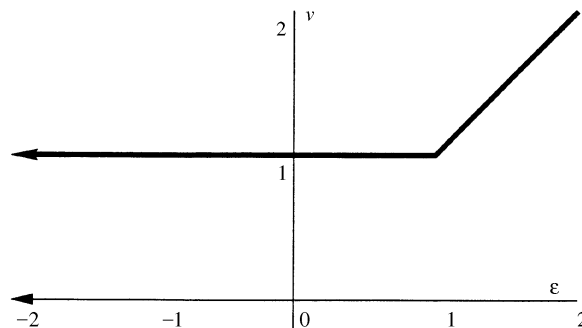

Fig. 12. Scaling exponent ν in $\sigma_Y^2(t) \sim t^\nu$ as a function of ε in Random Steady Shear Model with $\kappa > 0$, $\bar{w} \neq 0$, $w_f(t) = 0$.

dominant for $1 \leq \varepsilon < 2$. Mathematically correct computations of the asymptotic diffusivity can be ensured by proper application of the dominated convergence theorem to interchange limits and integration and by explicit accounting of the troublesome nonuniformities at small wavenumber. We illustrate this procedure in Paragraph 3.2.6.3 below; see [141] for the rigorous computation of the asymptotic results just discussed.

3.2.6. Derivation

We now indicate how the exact asymptotic formulas for the mean-square tracer displacement in the Random Steady Shear flow are mathematically obtained. First, we derive the fundamental formula (112) for the mean-square tracer displacement at all finite times. Next, we indicate in general terms how the long-time asymptotics may be deduced both heuristically and rigorously from this formula. We provide details for the case of a randomly fluctuating cross sweep $w_f(t)$; the other cases have been thoroughly addressed in previous publications [10,141].

3.2.6.1. Derivation of general formula. The mean-square tracer displacement of a tracer along the shear may be written in the following primitive form using the integrated equations for the tracer trajectories (110)

$$\sigma_Y^2(t) \equiv \langle (Y(t) - y_0)^2 \rangle \, , \tag{136a}$$

$$Y(t) - y_0 = \int_0^t v(X(s)) \, ds + \sqrt{2\kappa} W_y(t) \, , \tag{136b}$$

$$X(t) = x_0 + \int_0^t w(s) \, ds + \sqrt{2\kappa} W_x(t) \, . \tag{136c}$$

Using the mutual independence of $v(x)$ and $W_y(t)$ and the fact they each have mean zero, we may write

$$\sigma_Y^2(t) = 2\kappa \langle (W_y(t))^2 \rangle + \int_0^t \int_0^t \langle v(X(s))v(X(s')) \rangle \, ds \, ds'$$

$$= 2\kappa t + \int_0^t \int_0^t \langle R(X(s) - X(s')) \rangle \, ds \, ds' \, . \tag{137}$$

The remaining averaging is over the statistics of $W_x(t)$ and $w(t)$, which determine $X(t)$. Invoking the spectral representation (108) for the correlation function $R(t)$ of the shear velocity field, we write

$$\sigma_Y^2(t) = 2\kappa t + \int_0^t \int_0^t \int_{-\infty}^\infty E(|k|) \langle e^{2\pi i k(X(s) - X(s'))} \rangle \, dk \, ds \, ds' \, . \tag{138}$$

Now, $X(s) - X(s')$ is the random tracer displacement between times s and s'. By statistical homogeneity and stationarity of the advection processes, this must have the same statistics as the tracer displacement over a general time interval $s - s'$

$$\delta X(s - s') \, .$$

Furthermore, as can be checked from Eq. (110a), this is an integral of a Gaussian random process and therefore a Gaussian random variable. Its characteristic function is therefore readily evaluated:

$$\langle e^{2\pi ik(X(s)-X(s'))}\rangle = \langle e^{2\pi ik\delta X(s-s')}\rangle = e^{2\pi ik\langle\delta X(s-s')\rangle - 2\pi^2 k^2 \sigma_X^2(|s-s'|)} = e^{2\pi ik\bar{w}(s-s') - 2\pi^2 k^2 \sigma_X^2(|s-s'|)} ,$$

where

$$\sigma_X^2(t) \equiv \langle (X(t) - \langle X(t)\rangle)^2\rangle = 2\kappa t + 2\int_0^t (t-s)R_w(s)\,ds .$$

Substituting this equation into Eq. (138), we complete the derivation

$$\sigma_Y^2(t) = 2\kappa t + \int_0^t\int_0^t\int_{-\infty}^{\infty} E(|k|)e^{2\pi ik\bar{w}(s-s') - 2\pi^2 k^2 \sigma_X^2(|s-s'|)}\,dk\,ds\,ds'$$

$$= 2\kappa t + 2\int_0^t\int_0^t\int_0^{\infty} E(k)\cos(2\pi k\bar{w}(s-s'))e^{-2\pi^2 k^2 \sigma_X^2(|s-s'|)}\,dk\,ds\,ds'$$

$$= 2\kappa t + 4\int_0^{\infty}\int_0^t (t-s)E(k)\cos(2\pi k\bar{w}s)e^{-2\pi^2 k^2 \sigma_X^2(s)}\,ds\,dk .$$

This may be rewritten in the form stated in Eqs. (112a) and (112b)

$$\sigma_Y^2(t) = 2\kappa t + 2\int_0^{\infty} E(k)\Sigma(k,t)\,dk , \tag{139a}$$

$$\Sigma(k,t) = 2\int_0^t (t-s)\cos(2\pi k\bar{w}s)e^{-2\pi^2 k^2 \sigma_X^2(s)}\,ds . \tag{139b}$$

3.2.6.2. General asymptotic considerations. The long-time limit of Eqs. (139a) and (139b) may be computed through consideration of the behavior of the shear-displacement kernel $\Sigma(k,t)$. We first discuss the asymptotics on a heuristic level, then indicate how to make these arguments rigorous. Subsequently, we will provide a detailed computation of the asymptotic shear-parallel transport rate when a randomly fluctuating cross sweep $w_f(t)$ is active.

For a given superposition of cross-shear transport processes, there is a naturally defined Lagrangian persistence time $\tau_L(k)$ associated to transport by the shear mode with wavenumber k. Expressions for $\tau_L(k)$ for various cross-shear transport mechanisms were given in Eqs. (113), (118) and (131). When multiple cross-shear transport processes are present, $\tau_L(k)$ is taken as the smallest of the corresponding persistence time scales. For the moment, we will discuss only random cross-shear transport processes (κ and $w_f(t)$); the presence of a constant cross sweep $\bar{w} \neq 0$ requires some special consideration, and we return to it later. When $t \ll \tau_L(k)$, the contribution of the shear mode of wavenumber k is ballistic, and

$$\Sigma(k,t) \approx t^2 \quad \text{for } 0 \leq t \ll \tau_L(k) .$$

The shear-parallel transport due to shear fluctuations of wavenumber k becomes diffusive for $t \gg \tau_L(k)$, and

$$\Sigma(k,t) \approx 2K(k)t \quad \text{for } t \gg \tau_L(k) \ ,$$

$$K(k) \equiv \lim_{t \to \infty} \Sigma(k,t)/2t \ .$$

This corresponds, for a fixed wavenumber k, to the generic situation described in Paragraph 3.1.3.2.

The Lagrangian persistence time $\tau_L(k)$ generally decreases with k and diverges as $k \to 0$, because a tracer must move far across the shear before the persistent motion due to long-wavelength (low k) modes of the shear is broken up. We can therefore define a time-dependent wavenumber scale $k_{db}(t)$ as the inverse function of $\tau_L(k)$, and this will demarcate a gradual transition between low-wavenumber modes which each contribute ballistically ($0 \leq k \lesssim k_{db}(t)$) and the modes which each contribute diffusively ($k_{db}(t) \ll k$). The diffusive-ballistic transition wavenumber $k_{db}(t)$ shrinks to zero as $t \to \infty$, and there are essentially two possibilities

- The total effect of all the modes of the shear is to induce an ordinary diffusive behavior with effective diffusivity equal to the integral of the asymptotic diffusivity $K(k)$ contributed by each normalized mode, weighted by the energy spectrum

$$\sigma_Y^2(t) = 2K^* t \ , \tag{140a}$$

$$K^* = \kappa + 2 \int_0^\infty E(k)K(k)\, dk \ . \tag{140b}$$

This situation prevails when the energy spectrum $E(k)$ is sufficiently weak near the origin (ε sufficiently small) so that the contribution from the low-wavenumber ballistic modes $0 \leq k \lesssim k_{db}(t)$ is negligible.
- There is sufficient energy at low wavenumbers k (ε sufficiently large) so that the collective contribution from the low-wavenumber ballistic modes $0 \leq k \lesssim k_{db}(t)$ produces superdiffusive transport. In this case, the asymptotics of $\sigma_Y^2(t)$ are determined only by the low-wavenumber characteristics of $E(k)$; the diffusive contribution from high wavenumbers is negligible.

There is also an intermediate case in which the contribution from the ballistic modes $0 \leq k \lesssim k_{db}(t)$ contributes a linear function of t, so that the shear-parallel transport is diffusive, but with an extra term in the formula for the enhanced diffusivity (140b). An explicit example of this special case, which we discuss no further here, arises at the phase transition value $\varepsilon = 1$ for a random shear flow with constant cross sweep $\bar{w} \neq 0$ and molecular diffusion $\kappa > 0$; see Table 5.

Rigorous approach. To decide mathematically whether the total shear-parallel transport is diffusive or superdiffusive, one first derives a bound of the following form on the shear-displacement kernel

$$|\Sigma(k,t)| \leq C\tau_L(k)t \ , \tag{141}$$

where C is some numerical constant. This can be done through integration by parts in Eq. (139b) or by direct consideration of the damped exponential. Then one can use this equality along with the

dominated convergence theorem ([288], Section 4.4) to prove that if

$$\int_0^\infty E(k)\tau_L(k)\,dk \,<\, \infty \ ,\tag{142}$$

then $\sigma_Y^2(t)$ grows linearly in time with effective diffusion coefficient given by Eqs. (140a) and (140b). When Eq. (142) is violated, this indicates that the ballistic behavior of the modes $k \lesssim k_{db}(t)$ is producing a nonuniformity near $k = 0$. To compute the contribution from this region, one rescales the integration wavenumber to $k' = k/k_{db}(t)$. We illustrate this procedure explicitly below.

A mathematically equivalent approach [141] to computing the asymptotics of $\sigma_Y^2(t)$ is to posit general space–time rescalings $\widetilde{Y}(\tilde{t}) = \alpha Y(\tilde{t}/\rho(\alpha)^2)$ and to choose $\rho(\alpha)$ in such a way that $\widetilde{Y}(\tilde{t})$ approaches a finite nontrivial limit as $\alpha \to 0$.

We emphasize that our continual appeal to the dominated convergence theorem to justify our computations in what follows is not simply an exercise in mathematical pedantry. As we pointed out through a counterexample at the end of Paragraph 3.2.5.2, it is patently wrong to say that ordinary diffusion occurs with diffusion coefficient K^* whenever the expression (140b) for this quantity is finite. Discrepancies between this formal quantity and the true asymptotics of $\sigma_Y^2(t)$ can and do arise from a formally transient contribution to the integral which is however quantitatively significant or dominant at long times. By establishing bounds for which the dominated convergence theorem applies, we ensure that the transient terms do not contribute significantly. Transient contributions which are important can, in the present context, be isolated and evaluated by an appropriate rescaling of the integration variables. This will be explicitly illustrated in our detailed presentation of the long-time asymptotics of $\sigma_Y^2(t)$ for the case of a randomly fluctuating cross sweep $w_f(t)$ below.

Subtle features of constant cross sweep. We now mention how the above discussion is modified in the presence of a constant cross sweep $\bar{w} \neq 0$.

If the only cross-shear transport mechanism is the constant cross-sweep ($\bar{w} \neq 0$, $\kappa = 0$, $w_f(t) = 0$), then the single-mode contribution is trapped, rather than diffusive, in the long time limit. That is, for each $k > 0$, $\Sigma(k, t)$ is a bounded function of t. Therefore, the long-time limit of $\sigma_Y^2(t)$ is trapping when the energy spectrum is sufficiently weak at low wavenumber ($\varepsilon < 0$) so that dominated convergence applies. The shear-displacement kernel for the case of a purely constant cross sweep $\Sigma(k, t) = \Sigma_{\bar{w}}(k, t)$ can be written in terms of elementary functions, thereby permitting a completely explicit and direct analysis (see Section 3.2.2 and [141]).

When the constant cross sweep is superposed upon another random transport mechanism, the Lagrangian persistence time as we have defined it is $\tau_L(k) = \tau_{\bar{w}}(k) = (2\pi\bar{w}k)^{-1}$, but there is an additional important time scale which we call the *randomization time* $\tau_r(k)$. This is the time scale over which the phase of the oscillations of the Lagrangian velocity is forgotten due to the presence of the random component of the cross-sweep. It may be equated to the shortest Lagrangian persistence time scale of the random processes included, which is just the time taken for the randomness to give the cross-shear tracer location an uncertainty equal to the wavelength k^{-1} of the shearing mode under consideration. It is readily checked that for all random cross-shear transport mechanisms considered, $\tau_L(k) = \tau_{\bar{w}}(k) \ll \tau_r(k)$ at small k. The contribution $\Sigma(k, t)$ to the shear-parallel transport is ballistic for $t \ll \tau_L(k)$, trapped subsequently for an intermediate interval

$\tau_L(k) \ll t \ll \tau_r(k)$ due to oscillations in the Lagrangian velocity, then diffusive $t \gg \tau_r(k)$ when the random cross-shear processes finally become effective and destroy the phase coherence of the Lagrangian velocity oscillations. One notable consequence of the long intermediate interval of trapping behavior at low wavenumber k is that the asymptotic diffusivity $K(k)$ contributed by a single normalized shear mode is much less than $\tau_L(k)$, in contrast to the typical behavior indicated for Lagrangian velocities with a single relevant time scale discussed in Paragraph 3.1.3.2. (See in particular Eq. (135).)

3.2.6.3. Derivation of asymptotics for case of randomly fluctuating cross sweep. Detailed derivations for the long-time asymptotics of $\sigma_Y^2(t)$ may be found in the published literature for the case of pure molecular diffusion [10], pure constant cross sweep [141], and a superposition of a constant cross sweep with molecular diffusion [141]. We provide here an explicit derivation of the long-time behavior of $\sigma_Y^2(t)$ for the case of a fluctuating cross sweep $w_f(t)$, with no deterministic component ($\bar{w} = 0$) and no molecular diffusion ($\kappa = 0$). The superposition of these extra cross-shear transport mechanisms can be handled through the general plan of attack outlined above, but we do not provide the details here.

For $\kappa = 0$ and $\bar{w} = 0$, the formula (139) for the shear-parallel mean-square displacement may be written

$$\sigma_Y^2(t) = 2 \int_0^\infty E(k) \Sigma_{w_f}(k, t) \, dk \,, \tag{143a}$$

$$\Sigma_{w_f}(k, t) = 2 \int_0^t (t - s) e^{-2\pi^2 k^2 \sigma_X^2(s)} \, ds \,, \tag{143b}$$

where the cross-shear displacement variance is expressed in terms of the correlation function $R_w(t)$ of $w_f(t)$ as

$$\sigma_X^2(t) \equiv \langle (X(t) - x_0)^2 \rangle = 2 \int_0^t (t - s) R_w(s) \, ds \,.$$

Recall that the energy spectrum $E(k)$ of the shear flow and the power spectrum $E_w(\omega)$ of the random cross-sweep are assumed to be smooth on the positive real axis, absolutely integrable, and of the following forms:

$$E(k) = A_E |k|^{1-\varepsilon} \psi(|k|) \,,$$

$$E_w(\omega) = A_{E,w} |\omega|^{-\beta} \psi_w(|\omega|) \,,$$

where $\beta < 1$, $\varepsilon < 2$, $A_E > 0$, $A_{E,w} > 0$, and $\psi_w(\cdot)$ and $\psi(\cdot)$ are each smooth function on the positive real axis with $\psi_w(0) = \psi(0) = 1$.

We know from Section 3.1.2 that

$$\lim_{t \to \infty} \sigma_X^2(t) \sim \begin{cases} \frac{2}{1+\beta} K_x^\sharp t^{1+\beta} & \text{for } -1 < \beta < 1 \,, \\ K_x^\circ & \text{for } \beta < -1 \,, \end{cases} \tag{144}$$

where

$$K_x^{\sharp} = \frac{1}{2} A_{E,w} \pi^{\beta - (1/2)} \frac{\Gamma((1 - \beta)/2)}{\Gamma((2 + \beta)/2)} \; ,$$

$$K_x^{\circ} = \frac{1}{\pi^2} \int_0^{\infty} E_w(\omega) \omega^{-2} \, d\omega \; .$$

Weak sweeping regime. We dispense first with the case $\beta < -1$. Here the cross-shear fluctuations are trapped, and the Lagrangian persistence time $\tau_L(k) = \tau_{w_f}(k)$ is effectively infinite for each wavenumber. Consequently, every mode contributes forever ballistically

$$\lim_{t \to \infty} t^{-2} \Sigma_{w_f}(k, t) = \lim_{t \to \infty} 2 \int_0^1 (1 - u) e^{-2\pi^2 k^2 \sigma^2_x(tu)} \, du = 2 \int_0^1 (1 - u) e^{-2\pi^2 k^2 K_x^{\circ}} \, du = e^{-2\pi^2 k^2 K_x^{\circ}} \; .$$

Moreover, $t^{-2} \Sigma(k, t)$ is uniformly bounded by unity, and we may therefore take the $t \to \infty$ limit under the integral over wavenumber by the dominated convergence theorem and conclude

$$\lim_{t \to \infty} \sigma_Y^2(t) \sim 2t^2 \int_0^{\infty} E(k) \lim_{t \to \infty} t^{-2} \Sigma_{w_f}(k, t) \, dk \sim 2t^2 \int_0^{\infty} E(k) e^{-2\pi^2 k^2 K_x^{\circ}} \, dk \; ,$$

as indicated in Table 4.

Diffusive regime. We now turn to the more interesting cases in which $-1 < \beta < 1$ and the tracer travels ever farther across the shear streamlines. The single-mode normalized contribution $\Sigma_{w_f}(k, t)$ is then asymptotically diffusive

$$\lim_{t \to \infty} \Sigma_{w_f}(k, t) \sim 2 K_{w_f}(k) t \; ,$$

$$K_{w_f}(k) = \int_0^{\infty} e^{-2\pi^2 k^2 \sigma^2_x(s)} \, ds \; .$$

We are therefore led to consider situations in which the total shear-parallel transport $\sigma_Y^2(t)$ is diffusive. By noting the asymptotics of $\sigma_X^2(t)$ in Eq. (144), we can bound $\Sigma_{w_f}(k, t)$ as follows

$$0 \leq \Sigma_{w_f}(k, t) \leq C_1 \tau_{w_f}(k) t \; , \tag{145}$$

where $\tau_{w_f}(k)$ is some positive, decreasing function with low-wavenumber asymptotics

$$\tau_{w_f}(k) \sim C_{w_f} (K_x^{\sharp} k^2)^{-1/(1 + \beta)} \; , \tag{146}$$

where C_1 and C_{w_f} are some positive numerical constants depending on β but not on k nor t. The dominating function $\tau_{w_f}(k)$ obeys the same properties as the Lagrangian w_f-persistence time, and we identify it symbolically as such.

The dominated convergence theorem allows us to conclude that provided

$$\int_0^{\infty} E(k) \tau_{w_f}(k) \, dk < \infty \; , \tag{147}$$

the long-time shear-parallel transport is diffusive

$$\lim_{t \to \infty} \sigma_Y^2(t) \sim 2K_{w_f}^* t ,$$

$$K_{w_f}^* = 2 \int_0^\infty E(k) K_{w_f}(k) \, dk .$$

The condition (147) is satisfied whenever $\varepsilon < 2\beta/(1 + \beta)$, and we thereby obtain the results for the diffusive regime stated in Table 4.

Superdiffusive regime. We next consider the regime $2\beta/(1 + \beta) < \varepsilon < 2$ where the above argument fails due to the nonuniform convergence of $E(k)\Sigma_{w_f}(k, t)$ to $2K_{w_f}(k)E(k)t$ near $k = 0$. (Here we do not treat the transition value $\varepsilon = 2/(1 + \beta)$ which involves logarithmic corrections.) According to the general considerations discussed above, we should expect that $\sigma_Y^2(t)$ grows superlinearly and is dominated at large time by low wavenumbers $0 \le k \lesssim k_{db}(t)$, where

$$k_{db}(t) = \left(\frac{4\pi^2 K_x^\#}{1 + \beta} \right)^{-1/2} t^{-(1+\beta)/2}$$

is the inverse function to Eq. (146) (up to an unimportant numerical factor). We will therefore zoom in on this region by rescaling the integration variable in Eqs. (143a) and (143b) to

$$q = k/k_{db}(t) \tag{148}$$

First, for technical reasons, we separate the formula (143a) for $\sigma_Y^2(t)$ as follows

$$\sigma_Y^2(t) = \bar{\sigma}_Y^2(t) + \tilde{\sigma}_Y^2(t) ,$$

$$\bar{\sigma}_Y^2(t) = 2 \int_0^{k_1} E(k) \Sigma_{w_f}(k, t) \, dk ,$$

$$\tilde{\sigma}_Y^2(t) = 2 \int_{k_1}^\infty E(k) \Sigma_{w_f}(k, t) \, dk ,$$

where k_1 is an arbitrary positive cutoff wavenumber. The contribution $\tilde{\sigma}_Y^2(t)$ is clearly (at most) diffusive since the range of active k is bounded below by $k_1 > 0$. We can therefore neglect $\tilde{\sigma}_Y^2(t)$ if $\bar{\sigma}_Y^2(t)$ is superdiffusive, and we now show this is indeed the case.

Rescaling $\bar{\sigma}_Y^2(t)$ according to Eq. (148), we obtain

$$\bar{\sigma}_Y^2(t) = 2k_{db}(t) \int_0^{k_1/k_{db}(t)} E(qk_{db}(t)) \Sigma_{w_f}(qk_{db}(t), t) \, dq . \tag{149}$$

Now, it is readily shown that

$$\lim_{t \to \infty} t^{-2} \Sigma_{w_f}(qk_{db}(t), t) = \lim_{t \to \infty} 2 \int_0^1 (1 - u) \, e^{-2\pi^2 q^2 k_{db}^2(t) \sigma_X^2(tu)} \, du = 2 \int_0^1 (1 - u) e^{-q^2 u^{1+\beta}} \, du .$$

The finiteness of this limit reflects the fact that we have zoomed in on the low wavenumbers $k \lesssim qk_{db}(t)$ for which the mode-by-mode contribution $\Sigma_{w_f}(k, t)$ to the shear-parallel tracer motion is

ballistic. The long-time limit of the other factor in the integrand is described by

$$\lim_{t \to \infty} (k_{db}(t))^{\varepsilon - 1} E(k_{db}(t)q) = A_E q^{1 - \varepsilon} ,$$

since $\lim_{t \to \infty} k_{db}(t) = 0$.

Now, we would like to evaluate the $t \to \infty$ limit of $\bar{\sigma}_Y^2(t)$ in Eq. (149) by taking the $t \to \infty$ limits of the integrands and the upper cutoff. To do this, we first establish the uniform bounds

$$0 \le t^{-2} \Sigma_{w_f}(q k_{db}(t), t) \Theta(k_1/k_{db}(t) - q) \le \frac{C_2}{1 + q^{2/(1 + \beta)}} , \tag{150a}$$

$$0 \le k_{db}^{\varepsilon - 1}(t) E(k_{db}(t)q) \Theta(k_1/k_{db}(t) - q) \le C_3 q^{1 - \varepsilon} , \tag{150b}$$

where C_2 and C_3 are constants independent of k and t (but possibly depending on the fixed cutoff k_1), and $\Theta(\cdot)$ is the Heaviside function

$$\Theta(q) = \begin{cases} 1 & \text{if } q > 0 , \\ 0 & \text{if } q < 0 , \\ \frac{1}{2} & \text{if } q = 0 . \end{cases} \tag{151}$$

Inequality (150a) follows from Eq. (145) and the easy bound $0 \le \Sigma_{w_f}(k, t) \le t^2$; inequality (150b) is a consequence of the low wavenumber asymptotics of $E(k)$.

Using Eqs. (150a) and (150b) and the fact that $q^{1 - \varepsilon}(1 + q^{2/(1 + \beta)})^{-1}$ is an absolutely integrable function on $q \in [0, \infty)$ for $2\beta/(1 + \beta) < \varepsilon < 2$, we can apply the dominated convergence theorem to conclude that

$$\begin{aligned} \lim_{t \to \infty} \bar{\sigma}_Y^2(t) &\sim 2 k_{db}^{2 - \varepsilon}(t) t^2 \int_0^\infty \lim_{t \to \infty} (k_{db}^{\varepsilon - 1}(t) E(q k_{db}(t))(t^{-2} \Sigma_{w_f}(q k_{db}(t), t)) \, dq \\ &= 2 k_{db}^{2 - \varepsilon}(t) t^2 \int_0^\infty A_E q^{1 - \varepsilon} \left(2 \int_0^1 (1 - u) e^{-q^2 u^{1 + \beta}} \, du \right) dq \\ &= \frac{4}{2 + \varepsilon - \beta(2 - \varepsilon)} K_{w_f}^{\sharp} t^{1 + \varepsilon/2 - \beta(2 - \varepsilon)/2} , \end{aligned} \tag{152}$$

where

$$K_{w_f}^{\sharp} = (2 + \varepsilon - \beta(2 - \varepsilon)) A_E \left(\frac{4\pi^2 K_x^{\sharp}}{1 + \beta} \right)^{(\varepsilon - 2)/2} \int_0^1 (1 - u) \int_0^\infty q^{1 - \varepsilon} e^{-q^2 u^{1 + \beta}} \, dq \, du .$$

By a change of variables $p = q^2 u^{1 + \beta}$, the integral may be evaluated exactly in terms of Gamma functions [195], leading to the expression for $\sigma_Y^2(t)$ in the superdiffusive regime displayed in Table 4.

3.3. Tracer transport in shear flow with random spatio-temporal fluctuations and transverse sweep

We next explore the effects of introducing temporal fluctuations into the random shear flow v

$$\boldsymbol{v}(x, y, t) = \begin{bmatrix} w(t) \\ v(x, t) \end{bmatrix} .$$

This model will be referred to as the *Random Spatio-Temporal Shear Model* (RSTS) Model. The cross-shear sweeping flow $w(t)$ is defined with the same properties as in the Random Steady Shear Model of Section 3.2.

The random spatio-temporal shear flow $v(x, t)$ is assumed to be a Gaussian, homogenous, stationary, mean zero random field. We now need to describe v by a correlation function depending on space and time

$$\tilde{R}(x, t) \equiv \langle v(x', t')v(x + x', t + t') \rangle \ .$$

As in the steady case, we define the velocity correlation function through its Fourier transform,

$$\tilde{R}(x, t) = \int_{-\infty}^{\infty} \int_{-\infty}^{\infty} e^{2\pi i(kx + \omega t)} \tilde{E}(k, \omega) \, d\omega \, dk \ . \tag{153}$$

The *spatio-temporal energy spectrum* $\tilde{E}(k, \omega)$ appearing here resolves the energy of the fluid simultaneously into spatial wavenumber and temporal frequency;

$$\int_{k - \Delta k}^{k + \Delta k} \int_{\omega - \Delta \omega}^{\omega + \Delta \omega} \tilde{E}(k, \omega) \, d\omega \, dk$$

is the amount of energy associated to fluctuations with spatial wavenumbers $k \pm \Delta k$ and temporal frequencies $\omega \pm \Delta \omega$. The spatio-temporal energy spectrum $\tilde{E}(k, \omega)$ is necessarily a nonnegative function with $\tilde{E}(k, \omega) = \tilde{E}(-k, -\omega)$. (See Paragraph 2.4.5.3.) For the sake of simplifying some formulas, we shall restrict attention to random flows which are statistically invariant under time reversal, so that $\tilde{R}(x, t) = \tilde{R}(x, -t)$ and consequently $\tilde{E}(k, \omega) = \tilde{E}(k, -\omega)$. This requirement excludes random travelling wave motion. With this extra condition, we can express the velocity correlation function entirely in terms of the energy at nonnegative wavenumbers and frequencies

$$\tilde{R}(x, t) = 4 \int_0^{\infty} \int_0^{\infty} \cos(2\pi(kx + \omega t)) \tilde{E}(k, \omega) \, d\omega \, dk \ .$$

By definition, the energy spectrum $E(k)$ (resolved with respect to spatial wavenumber) is just the integral over frequencies of the spatio-temporal energy spectrum

$$E(|k|) = \int_{-\infty}^{\infty} \tilde{E}(k, \omega) \, d\omega = 2 \int_0^{\infty} \tilde{E}(k, \omega) \, d\omega \ .$$

We shall make the same assumptions on the energy spectrum $E(k)$ as we did for a steady random shear flow in Section 3.2. Namely, $E(k)$ is assumed to be smooth on $k > 0$ and absolutely integrable, with

$$E(k) = A_E k^{1 - \varepsilon} \psi(k) \ , \tag{154}$$

where $\varepsilon < 2$, $A_E > 0$ and $\psi(k)$ is a smooth function on the positive real axis with $\psi(0) = 1$.

We are left to describe the behavior of $\tilde{E}(k, \omega)$ with respect to ω. To this end, we shall assume that the fluctuations of any given wavenumber k decay on a *single* wavenumber-dependent time scale $\tau(k)$. Mathematically, this implies that

$$\tilde{E}(k, \omega) = E(|k|)\phi_k(\omega\tau(|k|))\tau(|k|) \ ,$$

where the $\{\phi_k(\cdot), 0 < k < \infty\}$ is a family of nondimensional even functions with $\int_{-\infty}^{\infty} \phi_k(\omega') \, d\omega' = 1$.

The important point is that ω only appears in the combination $\omega\tau(k)$. We shall call $\tau(k)$ the *Eulerian correlation time scale* since it describes the rate of decay of (a single wavenumber component of) the velocity field as observed at a fixed point, as in the Eulerian perspective. (See Section 3.1.3) It is to be contrasted with the *Lagrangian persistence time* $\tau_L(k)$, introduced in Section 3.2, for the rate of decay of the Lagrangian velocity (due to fluctuations of wavenumber k) observed by a moving tracer in the flow. The Lagrangian and Eulerian correlation times coincide when the tracer moves purely along the streamlines of the shear flow, but the Lagrangian persistence time will be shorter in the presence of a cross sweep $w(t)$ or molecular diffusion which transports the tracer across streamlines.

We will assume that

- $\tau(k)$ is a decreasing, smooth function of k, with

$$\lim_{k \to 0} \tau(k) \sim A_\tau k^{-z} , \tag{155}$$

  with $A_\tau > 0$ and $0 \leq z < \infty$.
- $\phi_k(\varpi)$ are even, nonnegative, smooth functions of both ϖ and k, and obey a mild, uniform bound

$$0 \leq \phi_k(\varpi) \leq \frac{C_\phi}{1 + |\varpi|^\gamma} , \tag{156}$$

  with $0 < C_\phi < \infty$ and $\gamma > 1$. Moreover, we assume that $\phi_0(0) > 0$, meaning that the spatio-temporal random shear has some nontrivial zero frequency component at low wavenumbers.

It is quite satisfactory to consider the special case with $\tau(k) \equiv A_\tau k^{-z}$ and $\phi_k(\cdot) \equiv \phi_0(\cdot)$. Our purpose in stating the assumptions in greater generality is solely to emphasize that it is only the low-wavenumber properties of $\tilde{E}(k, \omega)$ which determine whether the tracer motion along the shear has an anomalous diffusion law, and if so, what that law is.

The reason we demand that $\tau(k)$ decrease with k is that fluctuations at higher wavenumbers (smaller spatial scales) naturally have faster dynamics than those of lower wavenumbers. Note that the Eulerian correlation time scale diverges more severely in the low wavenumber limit as z increases. Since the low wavenumbers often play a central role in determining the long-time behavior of a tracer, we can expect that the $z \to \infty$ limit should exhibit features in common with a random steady shear flow. This will be borne out in what follows. In the other extreme $z = 0$, the low wavenumbers decorrelate at a uniformly finite time. This may be viewed as a rapid decorrelation limit in a weak sense; we will discuss turbulent diffusion models with rapid decorrelations in a strong sense in Section 4.

A decreasing, power law dependence for the Eulerian decorrelation time scale $\tau(k)$ is natural for describing the self-similar inertial range of scales in fully developed turbulence at a high Reynolds number. As we shall discuss in Section 3.4.3, the standard Kolmogorov theory for the inertial range statistics of a turbulent velocity field corresponds formally to $\varepsilon = 8/3$ and $z = 2/3$ in the Random Spatio-Temporal Shear (RSTS) Model defined above. The value $\varepsilon = 8/3$ is actually outside the admissible domain $\varepsilon < 2$ of infrared scaling exponents allowed in the present model because it would result in an infinite amount of energy residing at small wavenumbers. We will discuss in Sections 3.4.3 and 3.5 how the RSTS Model can be extended to incorporate an inertial range of scales.

At the present, we will restrict attention to the mean-square displacement $\sigma_Y^2(t) \equiv \langle (Y(t) - y_0)^2 \rangle$ of a tracer along the shear in the RSTS Model with $\varepsilon < 2$ and $z \geq 0$. An exact formula for this quantity is obtained in Paragraph 3.3.6.1:

Mean-Square Shear-Parallel Tracer Displacement for RSTS Model

$$\sigma_Y^2(t) = 2\kappa t + 4 \int_0^\infty \int_0^\infty \tilde{E}(k,\omega)\tilde{\Sigma}(k,\omega,t)\,\mathrm{d}\omega\,\mathrm{d}k\ , \tag{157a}$$

$$\tilde{\Sigma}(k,\omega,t) = 2 \int_0^t (t-s)\cos(2\pi k\bar{w}s)\cos(2\pi\omega s)\mathrm{e}^{-2\pi^2 k^2 \sigma_X^2(s)}\,\mathrm{d}s\ . \tag{157b}$$

This formula remains valid when $v(x,t)$ is non-Gaussian. Note that it properly reduces to the formula (112) when the spatio-temporal energy spectrum has the form $\tilde{E}(k,\omega) = E(k)\delta(\omega)$ associated to a steady random shear flow.

The shear-displacement kernel $\tilde{\Sigma}(k,\omega,t)$ represents the response of $\sigma_Y^2(t)$ to the presence of a component

$$A\cos(2\pi kx)\cos(2\pi\omega t) + B\cos(2\pi kx)\sin(2\pi\omega t)$$
$$+\ C\sin(2\pi kx)\cos(2\pi\omega t) + D\sin(2\pi kx)\sin(2\pi\omega t)$$

in the random shear flow, where A, B, C, and D are independent, standard Gaussian random variables. The formula for $\tilde{\Sigma}(k,\omega,t)$ differs from that of its counterpart $\Sigma(k,\omega,t)$ (112b) for the steady shear flow only in the presence of an oscillatory term $\cos(2\pi\omega s)$ in the integrand, naturally manifesting the temporal fluctuations of the shear flow.

An alternate formula for $\sigma_Y^2(t)$, which is at first perhaps easier to understand, involves the *spectral temporal correlation function* $\check{E}(k,t)$, which provides an intermediate representation between the full physical space spatio-temporal correlation function $\tilde{R}(x,t)$ and the spatio-temporal spectrum $\tilde{E}(k,\omega)$

$$\tilde{R}(x,t) = \int_{-\infty}^\infty \mathrm{e}^{2\pi\mathrm{i}kx}\check{E}(k,t)\,\mathrm{d}k = 2\int_0^\infty \cos(2\pi kx)\check{E}(k,t)\,\mathrm{d}k\ ,$$
$$\check{E}(k,t) = \int_{-\infty}^\infty \mathrm{e}^{2\pi\mathrm{i}\omega t}\tilde{E}(k,\omega)\,\mathrm{d}\omega = 2\int_0^\infty \cos(2\pi\omega t)\tilde{E}(k,\omega)\,\mathrm{d}\omega\ . \tag{158}$$

As such, $\check{E}(k,t)$ describes the temporal correlations of turbulent shear modes of wavenumber k in terms of the physical time variable; $\check{E}(k,t=0)$ is simply equal to $E(k)$. The mean-square shear-parallel displacement can be expressed in terms of $\check{E}(k,t)$ by formula similar to Eqs. (112a) and (112b) in the RSS Model

$$\sigma_Y^2(t) = 2\kappa t + 4\int_0^\infty \int_0^t (t-s)\cos(2\pi k\bar{w}s)\mathrm{e}^{-2\pi^2 k^2 \sigma_X^2(s)}\check{E}(k,s)\,\mathrm{d}s\,\mathrm{d}k\ . \tag{159}$$

For the special case of a steady shear flow, $\check{E}(k,t) \equiv E(k)$. We will work here with the representation (157), since it cleanly separates the influence of the particular shear flow structure $\tilde{E}(k,\omega)$ from a kernel $\tilde{\Sigma}(k,\omega,t)$ which depends only on the active cross-shear transport mechanisms. In Section 3.5, we will make use of a semi-spectral representation similar to Eq. (159).

We will consider the long-time behavior of $\sigma_Y^2(t)$ in the RSTS Model in a manner parallel to our study of the Random Steady Shear Model in Section 3.2. First, we consider in Section 3.3.1 the motion of a tracer in the randomly fluctuating shear flow with no molecular diffusion and no cross sweep. Next, we consider separately the effects when molecular diffusion κ (Section 3.3.2), a constant cross sweep $\bar{w}$ (Section 3.3.3), or a randomly fluctuating cross sweep $w_f(t)$ (Section 3.3.4) are added to the fluctuating shear flow. The qualitative scaling behavior for $\sigma_Y^2(t)$ in each case may be classified into three categories determined by the exponents ε and z characterizing the low-wavenumber (infrared) scaling behavior of the energy spectrum $E(k)$ and the Eulerian correlation time $\tau(k)$. These will be graphically described by *phase diagrams*, indicating the regions of the (ε, z) diagram associated to each type of qualitative scaling behavior.

In Section 3.3.5, we discuss how the shear-parallel transport of a tracer behaves under superpositions of the various cross-shear transport mechanisms. It turns out that the superposition rules are completely straightforward here; the subtleties discussed in Section 3.2.5 for the Random Steady Shear Model are absent here. The method of derivation for all the results in the RSTS Model is indicated in Section 3.3.6.

3.3.1. Tracer behavior in absence of cross-shear transport

We begin by considering the rather simple case of a tracer in a random shear flow with spatio-temporal fluctuations with no molecular diffusion ($\kappa = 0$) or cross sweep ($w(t) = 0$). A tracer then forever stays on its original streamline, and its Lagrangian velocity is the same as the Eulerian velocity observed at any given point on that streamline. Consequently, the tracer behaves exactly as in the Random Sweeping Model; the spatial structure of the shear flow is irrelevant. The long-time asymptotics of the shear-parallel tracer displacement could be worked out as in Section 3.1.2 by considering the low-frequency behavior of the energy spectrum of the velocity resolved with respect to temporal frequency, which can be expressed as $\int_0^\infty \tilde{E}(k, \omega)\,dk$. We will, however, proceed in a fashion which better maintains continuity with our analysis of the Random Steady Shear Model in Section 3.2 and our later discussion of the RSTS Model where the spatial structure of the shear plays a crucial role.

For $\kappa = w(t) = 0$, the shear-displacement kernel $\tilde{\Sigma}(k, \omega, t)$ in Eq. (157b) takes the simple, wavenumber-independent form,

$$\tilde{\Sigma}_0(k, \omega, t) = t^2 F_2(2\pi\omega t) , \tag{160}$$

$$F_2(\varpi) \equiv 2(1 - \cos \varpi)/\varpi^2 .$$

It is readily seen that the tracer displacement due to a single random spatio-temporal Fourier mode of the shear with wavenumber k and frequency ω is ballistic for short times $t \ll \omega^{-1}$ and trapped for long times $t \gg \omega^{-1}$. The long-time trapping behavior is a consequence of the exact periodicity of the tracer motion induced by a mode with a single frequency ω. We can expect from these considerations that shear-parallel tracer transport will be dominated at long times by contributions from low frequency modes.

In the RSTS Model, we are always assuming that a *continuous* spectrum of frequencies are associated to any given spatial wavenumber k, and that this spectrum of frequencies is nonvanishing at $\omega = 0$ at least for small k. We will therefore never see trapping behavior for the tracer in the total random spatio-temporal shear flow. Our heuristic discussion therefore becomes a bit more

direct if we break up the shear-parallel transport into contributions from a shear mode of a single wavenumber k, with temporal fluctuations coming from all frequencies, rather than disintegrating the motion into modes of single wavenumber and single frequency.

We accordingly rewrite Eqs. (157a) and (157b) as an integral of the energy spectrum $E(k)$ against a kernel $\Sigma_{\phi,0}(k,t)$ which has already accounted for the temporal structure of the fluctuating shear flow

$$\sigma_Y^2(t) = 2\int_0^\infty E(k)\Sigma_{\phi,0}(k,t)\,\mathrm{d}k \ , \tag{161a}$$

$$\Sigma_{\phi,0}(k,t) \equiv 2\int_0^\infty \tilde{\Sigma}_0(k,\omega,t)\phi_k(\omega\tau(k))\tau(k)\,\mathrm{d}\omega \ . \tag{161b}$$

With Eq. (160), it is clear that $\Sigma_{\phi,0}(k,t)$ may be expressed as

$$\Sigma_{\phi,0}(k,t) = t^2 F_\phi(t/\tau(k)) \ ,$$

$$F_\phi(u) \equiv 2\int_0^\infty F_2(2\pi u\varpi)\phi_k(\varpi)\,\mathrm{d}\varpi \ . \tag{162}$$

This representation reflects the fact that the temporal fluctuations of a single wavenumber mode k of the velocity field has a characteristic time scale $\tau(k)$. Since the Lagrangian velocity coincides with the Eulerian velocity in the present instance, the Lagrangian persistence time $\tau_L(k)$ of the tracer is readily identified with $\tau(k)$. According to the standard intuition of Paragraph 3.1.3.2, we therefore expect that the shear-parallel tracer displacement due to a single wavenumber k of the shear is ballistic for $t \ll \tau(k)$ and diffusive for $t \gg \tau(k)$, with effective diffusion coefficient proportional to the product of $\tau(k)$ and the mean-square velocity of the shear mode. This is borne out mathematically by Eq. (162), provided that $\phi_k(\varpi)$ is nonvanishing in a neighborhood of $\varpi = 0$. We do indeed assume that this is the case in the RSTS Model for at least sufficiently small k, and for our heuristic discussion we will assume for simplicity that this is true for all k.

We will now apply this qualitative perspective to understand the long-time asymptotics of the mean-square shear-parallel displacement $\sigma_Y^2(t)$. The exact results, as computed rigorously according to the prescription in Section 3.3.6, appear in Table 6. The scaling coefficients which appear may be expressed as follows:

$$\tilde{K}_0^* = \int_0^\infty \tilde{E}(k,0)\,\mathrm{d}k = \int_0^\infty E(k)\tau(k)\phi_k(0)\,\mathrm{d}k \ , \tag{163a}$$

$$\tilde{K}_0^\sharp = z^{-1}\pi^{(2\varepsilon+z-4)/2z}\frac{\Gamma((2-\varepsilon)/2z)}{\Gamma((\varepsilon+3z-2)/2z)}A_E A_\tau^{(2-\varepsilon)/z}\int_0^\infty \varpi^{(\varepsilon-2)/z}\phi_0(\varpi)\,\mathrm{d}\varpi \ . \tag{163b}$$

In contrast to the Random Sweeping Model, there is no subdiffusive or trapping behavior here because $\tilde{E}(k,\omega=0)$ is by assumption positive for small k, so the velocity of a streamline always has a nonvanishing zero frequency limit. We observe that the diffusion coefficient $\tilde{K}_0^*$ in the diffusive regime only depends on the zero frequency modes of the shear flow. We stress that this does not imply that the tracer behavior is therefore the same as in the Random Steady Shear Model. In a steady shear flow, the spatio-temporal energy spectrum is *singularly* concentrated at $\omega = 0$,

Table 6
Long-time asymptotics of mean-square tracer displacement along the shear in Random Spatio-Temporal Shear Model, with $\kappa = \bar{w} = w_f(t) = 0$. Scaling coefficients are given by Eq. (163)

Parameter regime		Asymptotic mean square displacement $\lim_{t \to \infty} \sigma_Y^2(t)$	Qualitative behavior
$z \geq 0$	$\varepsilon < 2 - z$	$2\tilde{K}_0^* t$	Diffusive (D)
$z \geq 0$	$2 - z < \varepsilon < 2$	$\dfrac{2z}{2z + \varepsilon - 2}\tilde{K}_0^{\sharp} t^{(2z + \varepsilon - 2)/z}$	Superdiffusive (SD-ω)

namely $\tilde{E}(k, \omega) = E(k)\delta(\omega)$, and the shear-parallel tracer motion is ballistic in the absence of cross-shear transport. In the Random Spatio-Temporal Shear Model, the diffusive shear-parallel tracer transport (for $\varepsilon + z < 2$) comes from the *continuous* distribution of energy at low frequencies.

To understand the criterion $\varepsilon + z < 2$ for diffusive behavior, we formally sum up the shear-parallel transport contributions from each wavenumber k. A straightforward argument generalized from the discussion of the RSS Model in Paragraph 3.2.6.2 suggests that the statistical tracer motion should, at long times, be diffusive and characterized by a diffusion coefficient on the order of the integral of the diffusivities contributed by each mode, provided that

$$\int_0^\infty E(k)\tau_L(k)\,dk \tag{164}$$

is finite. For the present case of no cross-shear transport mechanisms, $\tau_L(k) = \tau(k)$, the Eulerian correlation time for each spatial Fourier mode of the random shear. The finiteness of expression (164) is determined by the behavior of the integrand near $k = 0$; integrability at high wavenumbers is ensured by the physical assumption that $\tau(k)$ decreases with k. At small k, the Eulerian correlation time $\tau(k) \sim A_\tau k^{-z}$. Recalling that $E(k) \sim A_E k^{1-\varepsilon}$ for small k, we see that the criterion that Eq. (164) be finite is just $\varepsilon + z < 2$, which is exactly the diffusive regime described in Table 6. Note moreover that since $\phi_k(0)$ is an order unity dimensionless constant (with a possible but unimportant mild variation with k), the formula for the shear-parallel diffusivity (163a) states that the asymptotic diffusivity contributed by a normalized mode of wavenumber k (with prescribed temporal fluctuations) is proportional to the Lagrangian correlation time $\tau_L(k)$. This is in agreement with the general relation which we have seen to hold in standard diffusive situations (see Paragraph 3.1.3.2 and Section 3.2). For $\varepsilon + z > 2$, the shear-parallel tracer motion is superdiffusive because the product $E(k)\tau_L(k)$ diverges too strongly at low wavenumber.

The two regimes of long-time behavior of $\sigma_Y^2(t)$ are indicated on a phase diagram in Fig. 13. Such phase diagrams are two-dimensional versions of the pictures of phase transitions with respect to the single parameter ε which we presented for the RSS Model in Section 3.2. Each regime of qualitatively different long-time behavior for $\sigma_Y^2(t)$ may be viewed as a "phase" with a distinct algebraic law for the long-time scaling exponent of $\sigma_Y^2(t)$. The boundaries between these phases correspond to phase transitions, and are associated with more complicated formulas for the long-time behavior of $\sigma_Y^2(t)$. We shall not present the special formulas characterizing the phase
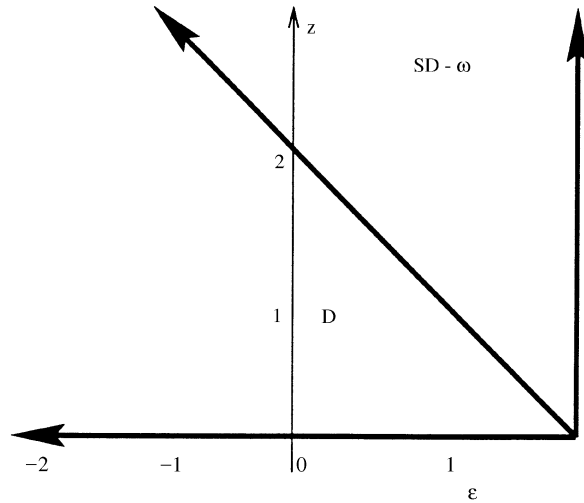
Fig. 13. Phase diagram for long-time asymptotics of $\sigma_Y^2(t)$ in Random Spatio-Temporal Shear Model with $\kappa = \bar{w} = w_f(t) = 0$.

boundaries, as these would be a distraction from our main endeavor on developing physical insight from the simplified model.

We see from the phase diagram that when $z = 0$, corresponding to a finite correlation time of the low wavenumber modes, the shear-parallel tracer motion is diffusive for any energy spectrum $E(k)$. To facilitate later discussion, We label the diffusive regime with the symbol D and the other regime with the symbol SD-ω, indicating a superdiffusive tracer behavior determined by temporal fluctuations of the shear flow.

3.3.2. Effects of molecular diffusion

We now consider the effects of positive molecular diffusion $\kappa > 0$ on the shear-parallel transport of a tracer. We continue for the moment to assume no cross sweep ($w(t) = 0$). The shear-displacement kernel (157b) may then be expressed in the closed form

$$\sigma_Y^2(t) = 2\kappa t + 4 \int_0^\infty \int_0^\infty \tilde{E}(k,\omega) \tilde{\Sigma}_\kappa(k,\omega,t) \, d\omega \, dk \;, \tag{165a}$$

$$\tilde{\Sigma}_\kappa(k,\omega,t) = t^2 F_3(t/\tau_\kappa(k), 2\pi \omega t) \;, \tag{165b}$$

where $\tau_\kappa(k) = (4\pi^2 \kappa k^{-1})^{-1}$ is the Lagrangian persistence time associated to molecular diffusion, and the universal, dimensionless function F_3 is defined in Eq. (133). Upon integration over the frequency variables, we discover that the shear-parallel tracer motion due to each spatial wavenumber k is naturally determined by the time scales $\tau_\kappa(k)$ and $\tau(k)$, corresponding to the decorrelation mechanisms due to molecular diffusion across the shear and temporal fluctuations of the shear flow, respectively.

The long-time behavior of the mean-square shear-parallel displacement, obtained from a rigorous asymptotic computation of Eqs. (165a) and (165b), is classified according to the parameter

Table 7
Long-time asymptotics of mean-square tracer displacement along the shear in Random Spatio-Temporal Shear Model, with $\kappa > 0$, $\bar{w} = w_f(t) = 0$. Scaling coefficients are given by Eq. (166)

Parameter regime		Asymptotic mean square displacement $\lim_{t \to \infty} \sigma_Y^2(t)$	Qualitative behavior
$0 \leq z \leq 2$	$\varepsilon < 2 - z$	$2\tilde{K}_\kappa^* t$	Diffusive (D)
$z \geq 2$	$\varepsilon < 0$		
$0 \leq z < 2$	$2 - z < \varepsilon < 2$	$\dfrac{2z}{2z + \varepsilon - 2}\tilde{K}_0^\sharp t^{(2z+\varepsilon-2)/z}$	Superdiffusive (SD-ω)
$z > 2$	$0 < \varepsilon < 2$	$\dfrac{4}{2 + \varepsilon}K_\kappa^\sharp t^{1+\varepsilon/2}$	Superdiffusive (SD-κ)

values ε and z in Table 7. The coefficients appearing in the scaling laws are as follows

$$\tilde{K}_\kappa^* = \kappa + 4\int_0^\infty \int_0^\infty \tilde{E}(k,\omega)\tilde{K}_\kappa(k,\omega)\,\mathrm{d}\omega\,\mathrm{d}k\;, \tag{166a}$$

$$\tilde{K}_0^\sharp = z^{-1}\pi^{(2\varepsilon+z-4)/2z}\frac{\Gamma((2-\varepsilon)/2z)}{\Gamma((\varepsilon+3z-2)/2z)}A_E A_\tau^{(2-\varepsilon)/z}\int_0^\infty \varpi^{(\varepsilon-2)/z}\phi_0(\varpi)\,\mathrm{d}\varpi\;, \tag{166b}$$

$$K_\kappa^\sharp = -\Gamma\!\left(-\frac{\varepsilon}{2}\right)A_E(4\pi^2\kappa)^{-(2-\varepsilon)/2}\;, \tag{166c}$$

where

$$\tilde{K}_\kappa(k,\omega) = \lim_{t\to\infty}\frac{\tilde{\Sigma}_\kappa(k,\omega,t)}{2t} = \frac{\tau_\kappa^{-1}(k)}{\tau_\kappa^{-2}(k) + (2\pi\omega)^2} = \frac{\kappa k^2}{4\pi^2\kappa^2 k^4 + \omega^2} \tag{167}$$

is the asymptotic diffusivity due to a single spatio-temporal Fourier mode of the shear with wavenumber k and frequency ω. The three regimes of long-time behavior of $\sigma_Y^2(t)$ are also indicated on a phase diagram in Fig. 14. We shall now explain on a heuristic level why the phase diagram takes the form it does.

There are two natural time scales associated to the tracer motion due to each spatial wavenumber of the shear flow: an Eulerian temporal decorrelation time $\tau(k)$ due to temporal fluctuations of the shear flow and a decorrelation time $\tau_\kappa(k)$ due to molecular diffusion buffeting the tracer across the shear flow. One therefore naturally associates a Lagrangian persistence time of the tracer motion $\tau_L(k)$ with the smaller of these two time scales. The same standard argument as was given in Section 3.3.1 indicates that diffusive or superdiffusive behavior should result according to whether $\tau_L(k)E(k)$ is integrable or not-integrable at $k = 0$. (See the discussion around Eq. (164).)

The Lagrangian persistence time $\tau_L(k)$ is set by the smaller of $\tau(k)$ and $\tau_\kappa(k)$. As $\tau(k) \sim k^{-z}$ for small k and $\tau_\kappa(k) \sim k^{-2}$, we see that for $z < 2$, Lagrangian persistence time for the low wavenumber modes is determined by the Eulerian correlation time scale $\tau(k)$, and molecular diffusion has a negligible effect. Consequently, the criterion for diffusive behavior for $z < 2$ should be expected to
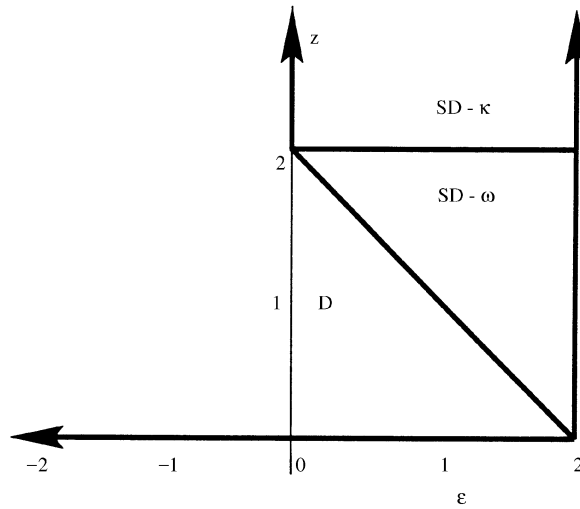
Fig. 14. Phase diagram for long-time asymptotics of $\sigma_T^2(t)$ in Random Spatio-Temporal Shear Model with $\kappa > 0$ and $\bar{w} = w_f(t) = 0$.

be the same as that for a random shear flow with spatio-temporal fluctuations and no molecular diffusion: $\varepsilon + z < 2$ (see Section 3.3.1). This is confirmed in the phase diagram (Fig. 14). Moreover, when this diffusivity condition is violated for $z < 2$, the resulting asymptotic superdiffusive behavior is exactly the same as for the case of a shear flow with spatio-temporal fluctuations and no molecular diffusion. The reason is that superdiffusion is determined solely by the low wavenumber modes of the shear flow, and we have noted that molecular diffusion is asymptotically irrelevant for such modes relative to the intrinsic temporal decorrelation of the shear flow. We have therefore identified the region $0 \leq z < 2$, $\varepsilon + z > 2$ as the same SD-ω regime introduced in Section 3.3.1.

A complementary situation arises for the portion of the phase diagram corresponding to $z > 2$, for which molecular diffusion plays the dominant role at low wavenumber. The criterion for diffusivity, $\varepsilon < 0$, is identical to that for transport in a *steady* random shear flow with molecular diffusion. We also note from Table 7 that the long-time tracer behavior for $z > 2$, $\varepsilon > 0$ is identical to the superdiffusive regime $\varepsilon > 0$ for a random *steady* shear flow with molecular diffusion (cf. Section 3.2.1). The temporal fluctuations of the shear flow are not manifested in any way in this regime, because they are asymptotically irrelevant for the low wavenumbers driving the super-diffusive tracer motion. We call the phase region $z > 2$, $\varepsilon > 0$ the SD-κ regime, indicating superdiffusive tracer behavior with molecular diffusion as the dominant Lagrangian decorrelation mechanism.

All told, we may understand the phase diagram (Fig. 14) for shear-parallel tracer transport in an RSTS flow with $\kappa > 0$ as a gluing together of a portion of the phase diagram (Fig. 13) for an RSTS flow with $\kappa = 0$ and a portion of the phase diagram for an RSS flow with $\kappa > 0$. The former applies for $0 \leq z < 2$, and the latter for $z > 2$; the dividing line $z = 2$ is determined by the balance at low wavenumbers between the decorrelation time scale $\tau(k)$ due to temporal fluctuations of the shear flow and the decorrelation time scale $\tau_\kappa(k)$ set by diffusion across streamlines due to molecular diffusion.

There is a similar subtlety in the formula for the diffusivity constant in terms of the single spatio-temporal mode diffusivities (167) as in the RSS Model with molecular diffusion and a constant cross sweep. Namely, the single-mode diffusivity does not obey the standard relation of being proportional to the Lagrangian persistence time of a single spatio-temporal shear mode, which here would be identified as $\min(\tau_\kappa(k), \omega^{-1})$. The reason for this aberrant behavior is that the retardation of the tracer's net motion due to temporal fluctuations of a shear mode with a single frequency is periodic and coherent. Integration over the frequency variables, however, produces a formula for the diffusivity in terms of the energy spectrum which does conform to standard Lagrangian intuition. Specifically,

$$\tilde{K}^*_\kappa = \kappa + 2 \int_0^\infty E(k) K_{\phi,\kappa}(k) \, \mathrm{d}k \; ,$$

$$K_{\phi,\kappa}(k) = 2 \int_0^\infty \tilde{K}_\kappa(k,\omega) \, \phi_k(\omega \tau(k)) \, \tau(k) \, \mathrm{d}\omega = \tau(k) \int_0^\infty \frac{2\kappa k^2}{4\pi^2 \kappa^2 k^4 + \omega^2} \, \phi_k(\omega \tau(k)) \, \mathrm{d}\omega \; ,$$

and the diffusivity $K_{\phi,\kappa}(k)$ due to a single wavenumber k (with the full spectrum of temporal fluctuations) is approximately proportional to $\tau_L(k) = \min(\tau_\kappa(k), \tau(k))$. A related fact is that the $\kappa \to 0$ limit of the asymptotic diffusivity $\tilde{K}_\kappa(k,\omega)$ of a single spatio-temporal Fourier mode behaves singularly in the $\kappa \to 0$ limit, reflecting the change from diffusive to ballistic ($\omega = 0$) or trapped ($\omega > 0$) behavior. Integration over frequencies regularizes the limit however: the $\kappa \to 0$ limit of $K_{\phi,\kappa}(k)$ converges to $\frac{1}{2}\tau(k)\phi_k(0)$. Therefore, as $\kappa \to 0$, the diffusion constant $\tilde{K}^*_\kappa$ smoothly approaches the limiting value $\tilde{K}^*_0$ (163a) characterizing the case of no molecular diffusion.

3.3.3. Effects of constant cross sweep

We next consider the effects of a constant cross sweep $w(t) = \bar{w} \neq 0$ on the shear-parallel transport of a tracer in an RSTS flow, with no molecular diffusion. The shear-displacement kernel can again be expressed in closed form

$$\tilde{\Sigma}_0(k,\omega,t) = \tfrac{1}{2}t^2(F_2(2\pi(\omega + \bar{w}k)t) + F_2(2\pi(\omega - \bar{w}k)t)) \; ,$$

$$F_2(u) \equiv 2(1 - \cos u)/u^2 \; .$$

It is interesting to note that, for a fixed wavenumber k, a strong contribution to the shear-parallel tracer motion comes from frequencies $\omega \approx \bar{w}k$. This is in contrast to the general situation without a mean cross sweep $\bar{w}$, for which the shear-displacement kernel typically decays with ω away from $\omega = 0$. The presence of the mean sweep $\bar{w}$ creates a type of "resonance" with spatio-temporal shear modes for which $\omega - \bar{w}k = 0$. These resonant modes have a component which appears steady from the point of view of a tracer swept across the shear at speed $\bar{w}$, and consequently contribute ballistically to the shear-parallel tracer motion for all times. The off-resonance modes $\omega - \bar{w}k \neq 0$, on the other hand, each contribute an oscillatory, trapped motion in the long-time limit. It is thus natural to expect that the long-time behavior of $\sigma_Y^2(t)$ should be dominated by the modes along the resonance line $\omega = \bar{w}k$. Note that since energy is distributed continuously in wavenumber-frequency space, the ballistic contribution of single spatio-temporal Fourier modes along the resonance line does not imply ballistic transport of the total random shear flow.

The long-time asymptotic behavior of $\sigma_Y^2(t)$ is described in Table 8 and the phase diagram in Fig. 15. The scaling coefficients are given by

$$\tilde{K}_w^* = \int_0^\infty \tilde{E}(k, \bar{w}k)\,\mathrm{d}k = \int_0^\infty E(k)\tau(k)\phi_k(\bar{w}k\tau(k))\,\mathrm{d}k , \tag{168a}$$

$$\tilde{K}_0^\sharp = z^{-1}\pi^{(2\varepsilon+z-4)/2z}\frac{\Gamma((2-\varepsilon)/2z)}{\Gamma((\varepsilon+3z-2)/2z)}A_E A_\tau^{(2-\varepsilon)/z}\int_0^\infty \varpi^{(\varepsilon-2)/z}\phi_0(\varpi)\,\mathrm{d}\varpi , \tag{168b}$$

$$K_{\bar{w}}^\sharp = \frac{1}{2}A_E\pi^{\varepsilon-3/2}\bar{w}\Gamma((2-\varepsilon)/2)/\Gamma((1+\varepsilon)/2) . \tag{168c}$$

Table 8
Long-time asymptotics of mean-square tracer displacement along the shear in Random Spatio-Temporal Shear Model, with $\bar{w} \neq 0$, $\kappa = w_f(t) = 0$. Scaling coefficients are given by Eq. (168)

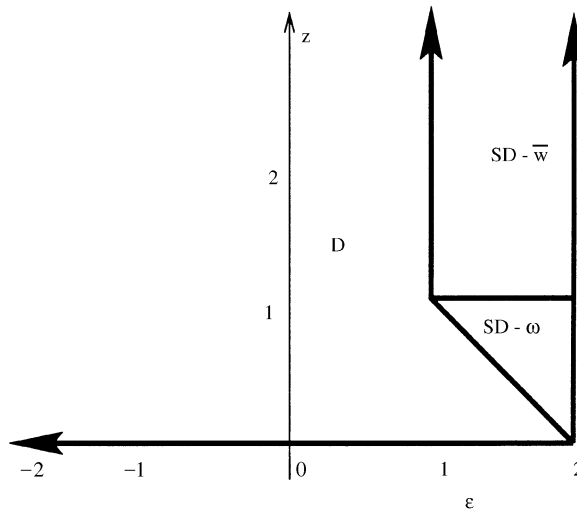| Parameter regime		Asymptotic mean square displacement $\lim_{t\to\infty}\sigma_Y^2(t)$	Qualitative behavior
$0 \leq z \leq 1$	$\varepsilon < 2 - z$	$2\tilde{K}_w^* t$	Diffusive (D)
$z \geq 1$	$\varepsilon < 1$		
$0 \leq z < 1$	$2 - z < \varepsilon < 2$	$\dfrac{2z}{2z+\varepsilon-2}\tilde{K}_0^\sharp t^{(2z+\varepsilon-2)/z}$	Superdiffusive (SD-ω)
$z > 1$	$1 < \varepsilon < 2$	$\dfrac{2}{\varepsilon}K_{\bar{w}}^\sharp t^\varepsilon$	Superdiffusive (SD-$\bar{w}$)

Fig. 15. Phase diagram for long-time asymptotics of $\sigma_Y^2(t)$ in Random Spatio-Temporal Shear Model with $\bar{w} \neq 0$ and $\kappa = w_f(t) = 0$.

We note that, in the diffusive regime, the diffusion coefficient is indeed determined by the energy spectrum along the resonance line $\omega = \bar{w}k$, as suggested by our previous discussion.

The phase boundaries may again be explained by simple consideration of the behavior of the Lagrangian persistence time $\tau_L(k)$. In the present case, it is the minimum of the Eulerian correlation time $\tau(k)$ of the shear flow and the sweeping persistence time $\tau_{\bar{w}} = (2\pi\bar{w}k)^{-1}$. For $0 \leq z < 1$, the low-wavenumber modes of the shear-parallel transport are dominated by the temporal decorrelation of the shear flow, and the effects of the cross sweep $\bar{w}$ are asymptotically negligible. Consequently, the phase diagram and behavior of the superdiffusive regime for $0 \leq z < 1$ is identical to the case of an RSTS flow with no cross sweep (Section 3.3.1). On the other hand, for $z > 1$, the low-wavenumber contribution to the tracer motion is limited primarily by the sweeping across streamlines. Upon comparison with the results of Section 3.2.2, we see that for $z > 1$, the boundary $\varepsilon = 1$ marking the onset of the superdiffusive regime, as well as the tracer behavior within the superdiffusive regime, are the same as those for the case of a constant cross sweep in a *steady* random shear flow. We label the regime $\varepsilon > 1$, $z > 1$ the SD-$\bar{w}$ regime, within which $\sigma_Y^2(t)$ grows superdiffusively according to a law depending only on $\bar{w}$ and the low-wavenumber behavior of $E(k)$, but not on the temporal fluctuations of the shear.

One important distinction between the long-time asymptotic shear-parallel transport with a constant cross sweep for $z > 1$ in the RSTS model from that of the RSS model is that the tracer motion is never subdiffusive or trapping. The reason is that the spatio-temporal fluctuations of the shear flow break up the phase coherence of the shear-parallel transport from individual spatial Fourier modes k, so the long-time contribution from each wavenumber k becomes diffusive rather than trapped. We saw a similar phenomenon when molecular diffusion was superposed on a constant cross sweep in the RSS Model; see Paragraph 3.2.5.2. Crucial to the obliteration of the subdiffusive and trapping regimes is the assumption that the spatio-temporal energy spectrum $\tilde{E}(k, \omega)$ is nonzero for $k > 0$ and small. Random shear flows violating these conditions can give rise to subdiffusive shear-parallel tracer transport. Other types of anomalous behavior can also arise if energy is singularly concentrated at certain wavenumbers and frequencies, but we shall not explore these issues in any further detail here.

One unusual feature of the present situation is that the contribution from wavenumber k to the diffusion constant $\tilde{K}_{\bar{w}}^*$ in the D regime is not proportional to $\tau_L(k) \sim \tau_{\bar{w}}(k)$ for wavenumbers k for which sweeping effects dominate ($\tau_{\bar{w}}(k) \ll \tau(k)$). The reason can be traced to the fact that the interaction of a pure, constant cross sweep with a shear mode of a single wavenumber k induces a shear-parallel *trapping* motion at long times. Therefore, the asymptotic diffusivity must rely somehow on the phase-randomizing effects of the random temporal fluctuations of the shear flow, even though the sweeping acts faster to break up the persistent motion of the tracer. The single-mode diffusivity in the RSS Model with $\kappa > 0$, $\bar{w} \neq 0$, and $w_f(t) = 0$ suffers from a similar anomaly, as we discussed briefly in Paragraph 3.2.5.2.

3.3.4. Effects of temporally fluctuating cross sweep

Just as for the Random Steady Shear Model, a mean zero, randomly fluctuating cross sweep $w(t) = w_f(t)$ influences the shear-parallel transport in the RSTS Model in a manner similar to molecular diffusion, but with a wide range of behavior depending on the exponent β describing the

Table 9
Long-time asymptotics of mean-square tracer displacement along the shear in Random Spatio-Temporal Shear Model, with $w_f(t) \neq 0$, $\kappa = \bar{w} = 0$. Scaling coefficients are given by Eq. (169)

Parameter regime		Asymptotic mean square displacement $\lim_{t \to \infty} \sigma_Y^2(t)$	Qualitative behavior
For $-1 < \beta < 1$:			
$0 \leq z \leq \dfrac{2}{1+\beta}$	$\varepsilon < 2 - z$	$2\tilde{K}_{w_f}^* t$	D
$z \geq \dfrac{2}{1+\beta}$	$\varepsilon < \dfrac{2\beta}{1+\beta}$		
$0 \leq z < \dfrac{2}{1+\beta}$	$2 - z < \varepsilon < 2$	$\dfrac{2z}{2z + \varepsilon - 2}\tilde{K}_0^\sharp t^{(2z + \varepsilon - 2)/z}$	SD-ω
$z > \dfrac{2}{1+\beta}$	$\dfrac{2\beta}{1+\beta} < \varepsilon < 2$	$\dfrac{4}{2 + \varepsilon - \beta(2 - \varepsilon)}K_{w_f}^\sharp t^{1 + \varepsilon/2 - \beta(2 - \varepsilon)/2}$	SD-w_f
For $\beta < -1$:			
$z \geq 0$	$\varepsilon < 2 - z$	$2\tilde{K}_{w_f}'^* t$	D
$z \geq 0$	$2 - z < \varepsilon < 2$	$\dfrac{2z}{2z + \varepsilon - 2}\tilde{K}_0^\sharp t^{(2z + \varepsilon - 2)/z}$	SD-ω

low-frequency scaling of its power spectrum

$$R_w(t) \equiv \langle w_f(t')w_f(t + t') \rangle = 2\int_0^\infty \cos(2\pi\omega t)E_w(|\omega|)\, d\omega ,$$

$$E_w(\omega) = A_{E,w}\omega^{-\beta}\psi_w(\omega) .$$

The long-time behavior of the mean-square shear-parallel tracer displacement $\sigma_Y^2(t)$ in an RSTS flow with randomly fluctuating cross sweep $w_f(t)$ is detailed in Table 9 and in the phase diagram in Fig. 16. The preconstants appearing in the asymptotic scaling laws have the following expressions:

$$\tilde{K}_{w_f}^* = 4\int_0^\infty \int_0^\infty \tilde{E}(k, \omega)\tilde{K}_{w_f}(k, \omega)\, dk\, d\omega , \tag{169}$$

$$\tilde{K}_0^\sharp = z^{-1}\pi^{(2\varepsilon + z - 4)/2z}\frac{\Gamma((2 - \varepsilon)/2z)}{\Gamma((\varepsilon + 3z - 2)/2z)}A_E A_\tau^{(2 - \varepsilon)/z}\int_0^\infty \varpi^{(\varepsilon - 2)/z}\phi_0(\varpi)\, d\varpi ,$$

$$K_{w_f}^\sharp = \frac{\Gamma((2 - \varepsilon)/2)A_E}{(\varepsilon(1 + \beta)/2 - \beta)}\left(\frac{1 + \beta}{4\pi^2 K_x^\sharp}\right)^{(2 - \varepsilon)/2} ,$$

$$\tilde{K}_{w_f}'^* = \int_0^\infty \tilde{E}(k, 0)e^{-2\pi^2 k^2 K_x^\circ}\, dk = \int_0^\infty E(k)\tau(k)\phi_k(0)e^{-2\pi^2 k^2 K_x^\circ}\, dk .$$
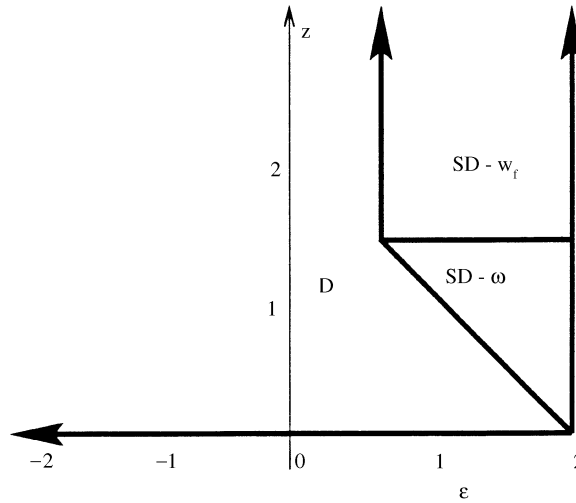
Fig. 16. Phase diagram for long-time asymptotics of $\sigma_Y^2(t)$ in Random Spatio-Temporal Shear Model with $w_f(t) \neq 0$ and $\kappa = \bar{w} = 0$. The value $\beta = 1/2$, corresponding to a random cross sweep which induces superdiffusive cross-shear transport, is used in this drawing. Varying β simply slides the "triple point" of intersection of the phase boundaries along the $\varepsilon + z = 2$ line.

In the D regime for $-1 < \beta < 1$, the single wavenumber-frequency mode contribution to the diffusivity constant is

$$\tilde{K}_{w_f}(k, \omega) \equiv \lim_{t \to \infty} \frac{\tilde{\Sigma}_{w_f}(k, \omega, t)}{2t} = \int_0^\infty \cos(2\pi\omega s) \mathrm{e}^{-2\pi^2 k^2 \sigma_X^2(s)} \, \mathrm{d}s \ .$$

A rigorous derivation of these results is presented in detail in Paragraph 3.3.6.2.

We see the same qualitative structure of the phase diagram here in Fig. 16, for $-1 < \beta < 1$, as for the case of molecular diffusion or a constant cross sweep acting in concert with a randomly fluctuating spatio-temporal shear flow (cf. Figs. 14 and 15). The phase diagram may be analyzed in exactly the same manner through consideration of the Lagrangian persistence time $\tau_L(k)$ of the low wavenumber modes. Here it is the minimum of the Eulerian correlation time $\tau(k) \sim k^{-z}$ and the w_f-persistence time $\tau_{w_f}(k) \sim k^{-2/(1+\beta)}$; see Eq. (131). For $0 \leq z < 2/(1 + \beta)$, the intrinsic decorrelation of the random shear determines the shear-parallel tracer motion due to low-wavenumber shear modulations, and the phase diagram and superdiffusive scaling laws are indifferent to the presence of $w_f(t) \neq 0$. On the other hand, for $z > 2/(1 + \beta)$, the random sweeping $w_f(t)$ sets the decorrelation rate of the shear-parallel tracer motion, and the superdiffusive regime along with its boundary take the same form as in the Random Steady Shear Model (see Section 3.2.3). We label the superdiffusive regime within this portion of the phase diagram the SD-w_f regime. Varying β from 0 to 1 increases the cross-shear transport from diffusive to superdiffusive to almost ballistic, and the phase diagrams and superdiffusive scaling exponents for $\sigma_Y^2(t)$ correspondingly interpolate between those associated to molecular diffusion κ acting across the shear (Section 3.3.2) to those

associated with a constant sweep $\bar{w}$ across the shear (Section 3.3.3). The diffusivity constant $\tilde{K}^*_{w_f}$ in the D regime may be heuristically understood in terms of the contributions from modes of various wavenumbers and frequencies in a similar fashion to the case in which molecular diffusion is the cross-shear transport mechanism (Section 3.3.2).

For $\beta < -1$, the cross-shear motion is trapped, and consequently never competes with the temporal fluctuations of the shear in determining the tracer dynamics due to low wavenumber components of the shear. The phase diagram and superdiffusive scaling laws are consequently identical for all z to those for the case in which there is no cross-shear transport (see Section 3.3.1). The trapping cross sweep does have a mild influence on the diffusion constant within the diffusive regime.

3.3.5. Superposition of cross-shear transport mechanisms

For the RSTS Model, the behavior of shear-parallel transport under a combination of cross-shear transport processes is simple to describe. The phase diagram, along with the scaling laws for the indicated superdiffusive regimes, are exactly those corresponding to the mechanism which moves the tracer across the shear most rapidly (at long times). Therefore, any time that a mean cross sweep $\bar{w} \neq 0$ is active, the phase diagram appears as in Fig. 15, and the asymptotic behavior of $\sigma_Y^2(t)$ in superdiffusive regimes is insensitive to any other cross-shear transport mechanisms which may be present. Similarly, if $\bar{w} = 0$ but a superdiffusive ($0 < \beta < 1$) random cross sweep $w_f(t)$ is active, then the phase diagram and superdiffusive scaling laws are just as described in Section 3.3.4, whether or not molecular diffusion is present or not. Molecular diffusion, in like manner, dominates randomly fluctuating cross sweeps $w_f(t)$ with subdiffusive or trapping behavior.

It should be noted that in any case, the diffusion coefficient in the diffusive regime D will depend on all cross-shear transport mechanisms present.

Another way to summarize the above results is that the criterion for superdiffusive shear-parallel tracer motion, and the asymptotic behavior of $\sigma_Y^2(t)$ in the superdiffusive regime, depend only on the low-wavenumber behavior of the energy spectrum $E(k) \sim A_E |k|^{1-\varepsilon}$ and the low-wavenumber behavior of the Lagrangian persistence time $\tau_L(k)$. The Lagrangian persistence time is in turn determined by the shortest of the individual persistence times ($\tau(k)$, $\tau_\kappa(k)$, $\tau_{\bar{w}}(k)$, and $\tau_{w_f}(k)$) which correspond to active processes. Diffusive behavior results when $E(k)\tau_L(k)$ is integrable at low wavenumber. The region of superdiffusive behavior may from this argument be deduced to be the intersection of the superdiffusive regions associated to each cross-shear transport process acting separately.

With the assumptions of the RSTS Model, there is never any subdiffusive or trapped shear-parallel tracer motion, and the associated subtlety in the RSS Model concerning superposition of cross-shear transport mechanisms is not an issue (see Paragraph 3.2.5.2). We emphasize that this is a consequence of the assumption that energy is distributed continuously in wavenumber-frequency space, with some nontrivial contribution at low frequencies and wavenumber. This is illustrated by the behavior of the shear-displacement kernel $\tilde{\Sigma}(k, \omega, t)$ when $\bar{w} \neq 0$ in the limit in which the random components of the cross shear motion vanish, i.e. $\kappa \to 0$ and $w_f(t) \to 0$. For any fixed $k \neq 0$ and ω, the long-time asymptotics of $\tilde{\Sigma}(k, \omega, t)$ behaves singularly in this limit, just in the RSS Model. The integration against the spatio-temporal spectrum $\tilde{E}(k, \omega)$ satisfying the assumptions of the RSTS Model, however, completely regularizes the limit in which the random cross-shear components vanish. Irregular limiting behavior of the type described in the Random Steady Shear Model

can result for random shear flows with spatio-temporal fluctuations which do not satisfy the basic assumptions of the RSTS Model.

3.3.6. Derivations

We indicate here how to establish the results concerning the statistics of shear-parallel tracer motion in the RSTS Model which were stated throughout Section 3.3. First, we derive the basic formula (157) for $\sigma_Y^2(t)$ at finite times. Next, we illustrate in detail how the long-time asymptotics of $\sigma_Y^2(t)$ can be rigorously computed for the case in which only a randomly fluctuating cross sweep is present (as in Section 3.3.4). We finally sketch without details how to compute the long-time asymptotics of $\sigma_Y^2(t)$ with general cross-shear transport mechanisms.

3.3.6.1. Derivation of general formula.
The derivation of formula (157) proceeds in exactly the same way as in the Random Steady Shear Model (see Paragraph 3.2.6.1), except that the time dependence of the shear velocity field must be accounted for. We start with the following modification of formula (137)

$$\sigma_Y^2(t) = 2\kappa \langle (W_y(t))^2 \rangle + \int_0^t \int_0^t \langle v(X(s), s)v(X(s'), s') \rangle \, ds \, ds'$$

$$= 2\kappa t + \int_0^t \int_0^t \langle \tilde{R}(X(s) - X(s'), s - s') \rangle \, ds \, ds' \, ,$$

which is obtained by simply replacing $v(X(s))$ in the trajectory equation (136b) for $Y(t)$ with $v(X(s), s)$.

Substituting the spectral representation (153) for $\tilde{R}(x, t)$ into this last expression, we have

$$\sigma_Y^2(t) = 2\kappa t + \int_0^t \int_0^t \int_{-\infty}^{\infty} \int_{-\infty}^{\infty} \tilde{E}(k, \omega) \langle e^{2\pi i k(X(s) - X(s'))} \rangle e^{2\pi i \omega(s - s')} \, d\omega \, dk \, ds \, ds' \, .$$

The remaining average may now be computed in the same way as in Paragraph 3.2.6.1:

$$\sigma_Y^2(t) = 2\kappa t + \int_0^t \int_0^t \int_{-\infty}^{\infty} \int_{-\infty}^{\infty} \tilde{E}(k, \omega) e^{2\pi i k\bar{w}(s - s') - 2\pi^2 k^2 \sigma_X^2(|s - s'|)} e^{2\pi i \omega(s - s')} \, d\omega \, dk \, ds \, ds' \, .$$

Using finally the four-way symmetry $\tilde{E}(k, \omega) = \tilde{E}(k, -\omega) = \tilde{E}(-k, \omega) = \tilde{E}(-k, -\omega)$ which is a consequence of the assumed time reversal symmetry of the shear flow, we can condense the wavenumber-frequency integration to the first quadrant

$$\sigma_Y^2(t) = 2\kappa t + 4 \int_0^t \int_0^t \int_0^{\infty} \int_0^{\infty} \tilde{E}(k, \omega) \cos(2\pi k\bar{w}(s - s')) \cos(2\pi \omega(s - s'))$$

$$\times e^{-2\pi^2 k^2 \sigma_X^2(|s - s'|)} \, d\omega \, dk \, ds \, ds'$$

$$= 2\kappa t + 8 \int_0^t \int_0^{\infty} \int_0^{\infty} \tilde{E}(k, \omega)(t - s) \cos(2\pi k\bar{w}s) \cos(2\pi \omega s) e^{-2\pi^2 k^2 \sigma_X^2(s)} \, d\omega \, dk \, ds \, .$$

Reversing the order of integration and decomposing the formula into an explicit integration against the shear-displacement kernel $\tilde{\Sigma}(k, \omega, t)$, we arrive at the desired formula (157)

$$\sigma_Y^2(t) = 2\kappa t + 4 \int_0^\infty \int_0^\infty \tilde{E}(k, \omega) \tilde{\Sigma}(k, \omega, t) \, d\omega \, dk , \tag{170a}$$

$$\tilde{\Sigma}(k, \omega, t) = 2 \int_0^t (t - s) \cos(2\pi k \bar{w} s) \cos(2\pi \omega s) e^{-2\pi^2 k^2 \sigma_X^2(s)} \, ds . \tag{170b}$$

3.3.6.2. Derivation of asymptotics for case of randomly fluctuating cross sweep. We present here a rigorous computation of the long-time asymptotics for $\sigma_Y^2(t)$ for the case considered in Section 3.3.4 in which $w_f(t) \neq 0$, $\kappa = 0$, and $\bar{w} = 0$. The general finite-time formula (170) specializes to

$$\sigma_Y^2(t) = 4 \int_0^\infty \int_0^\infty \tilde{E}(k, \omega) \tilde{\Sigma}_{w_f}(k, \omega, t) \, d\omega \, dk , \tag{171a}$$

$$\tilde{\Sigma}_{w_f}(k, \omega, t) = 2 \int_0^t (t - s) \cos(2\pi \omega s) e^{-2\pi^2 k^2 \sigma_X^2(s)} \, ds , \tag{171b}$$

where

$$\sigma_X^2(t) \equiv \langle (X(t) - x_0)^2 \rangle = 2 \int_0^t (t - s) R_w(s) \, ds ,$$

$$R_w(t) \equiv \langle w_f(t') w_f(t + t') \rangle = 2 \int_0^\infty \cos(2\pi \omega t) E_w(|\omega|) \, d\omega ,$$

$$E_w(\omega) = A_{E,w} \omega^{-\beta} \psi_w(\omega) .$$

This is the case for which we also presented a detailed derivation for the Random Steady Shear Model in Paragraph 3.2.6.2. The general procedure is similar in spirit, though the extra integration over the frequency variable creates the need for some extra work.

We shall first deal with the range of exponent values $-1 < \beta < 1$ for which the random cross sweep produces unbounded motion across the shear. The effects of a trapping cross sweep ($\beta < -1$) is handled separately at the end.

Diffusive regime. For $-1 < \beta < 1$, the long-time asymptotics of the shear-displacement kernel are diffusive

$$\lim_{t \to \infty} \tilde{\Sigma}_{w_f}(k, \omega, t) \sim 2 \tilde{K}_{w_f}(k, \omega) t ,$$

$$\tilde{K}_{w_f}(k, \omega) = \int_0^\infty \cos(2\pi \omega s) e^{-2\pi^2 k^2 \sigma_X^2(s)} \, ds . \tag{172}$$

We now show that for the range of parameters defining the D regime in Fig. 16, the shear-parallel tracer motion is described by a finite diffusion coefficient given by the integral of the single-mode

diffusivity against the spatio-temporal energy spectrum

$$\lim_{t \to \infty} \sigma_Y^2(t) \sim 2\tilde{K}_{w_f}^* t ,$$

$$\tilde{K}_{w_f}^* = 4 \int_0^\infty \int_0^\infty \tilde{E}(k, \omega) \tilde{K}_{w_f}(k, \omega) \, d\omega \, dk . \tag{173}$$

To do this, we need only show that $t^{-1}\tilde{\Sigma}_{w_f}(k, \omega, t)$ is bounded uniformly in time by a function which is integrable against $\tilde{E}(k, \omega)$, and then apply the dominated convergence theorem. Noting that $|\tilde{\Sigma}_{w_f}(k, \omega, t)| \leq \tilde{\Sigma}_{w_f}(k, 0, t) = \Sigma_{w_f}(k, t)$, we can utilize the bound (145) obtained in our previous analysis in the RSS Model

$$|\tilde{\Sigma}_{w_f}(k, \omega, t)| \leq C_1 \tau_{w_f}(k) t .$$

Here $\tau_{w_f}(k)$ is some positive, decreasing function with the low-wavenumber asymptotics (146)

$$\tau_{w_f}(k) \sim C_{w_f}(K_x^\sharp k^2)^{-1/(1+\beta)} , \tag{174}$$

and may be thought of as the Lagrangian w_f-persistence time. The constant $K_x^\sharp$ is defined in Eq. (129); $\{C_j\}$ and C_{w_f} are positive numerical constants which do not depend on k, ω, or t.

Next we establish a second bound

$$|\tilde{\Sigma}_{w_f}(k, \omega, t)| \leq C_2 \omega^{-1} t , \tag{175}$$

with positive numerical constant C_2 depending only on β. We first integrate $\tilde{\Sigma}_{w_f}(k, \omega, t)$ by parts

$$\tilde{\Sigma}_{w_f}(k, \omega, t) = 2\omega^{-1} t \int_0^t e^{-2\pi^2 k^2 \sigma_X^2(s)} \sin(2\pi\omega s) \left[(2\pi t)^{-1} + \pi k^2 \frac{d\sigma_X^2(s)}{ds} \left(1 - \frac{s}{t} \right) \right] ds . \tag{176}$$

As stated in Eq. (144), $\lim_{s \to \infty} \sigma_X^2(s) \sim 2K_x^\sharp/(1+\beta)s^{1+\beta}$. It may be verified through an integration by parts of the formula

$$\frac{d\sigma_X^2(s)}{ds} = \int_0^t R_w(s) \, ds = \int_0^\infty A_{E,w} |\omega|^{-\beta} \psi_w(|\omega|) \frac{\sin 2\pi\omega t}{2\pi\omega} \, d\omega$$

that the derivative has the naturally expected bound

$$|d\sigma_X^2(s)/ds| \leq C_3 K_x^\sharp (1 + s^\beta)$$

for $-1 < \beta < 1$ and some positive numerical constant C_3 depending only on β. Using these facts about $\sigma_X^2(s)$ and its derivative, the desired bound (175) follows from Eq. (176).

We therefore have that

$$|\tilde{\Sigma}_{w_f}(k, \omega, t)| \leq C_4 \min(\tau_{w_f}(k), \omega^{-1}) t . \tag{177}$$

This sensibly generalizes the natural bounds (141) which one obtains in the RSS Model, since $\min(\tau_{w_f}(k), \omega^{-1})$ acts as a Lagrangian persistence time for the shear-parallel tracer motion associated to a fluctuation of a single wavenumber and frequency.

We make even stronger contact with the analysis of the RSS Model when we perform the integration of Eqs. (171a) and (171b) over frequency. Recalling that the spatio-temporal spectrum in the RSTS Model has the form

$$\tilde{E}(k, \omega) = E(k)\phi_k(\omega\tau(k))\tau(k) \,,$$

we can write

$$\sigma_Y^2(t) = 2 \int_0^\infty E(k)\Sigma_{\phi, w_f}(k, t)\, dk \,, \tag{178a}$$

$$\Sigma_{\phi, w_f}(k, t) = 2 \int_0^\infty \tilde{\Sigma}_{w_f}(k, \omega, t)\phi_k(\omega\tau(k))\tau(k)\, d\omega \,. \tag{178b}$$

The kernel $\Sigma_{\phi, w_f}(k, t)$ may be interpreted as the mean-square shear-parallel displacement of a tracer due to a single normalized random Fourier mode of wavenumber k (with temporal fluctuations at all frequencies); it directly generalizes the RSS shear-displacement kernel $\Sigma_{w_f}(k, t)$. Using the assumed bound (156) on $\phi_k(\cdot)$ along with Eq. (177), we infer the following bound:

$$|\Sigma_{\phi, w_f}(k, t)| \le C_5 \min(\tau_{w_f}(k), \tau(k))t \,. \tag{179}$$

Realizing that $\min(\tau_{w_f}(k), \tau(k))$ represents the Lagrangian persistence time $\tau_L(k)$ of spatial wavenumber k, we see that this directly generalizes the physically motivated bounds (141) we obtained for the RSS shear-displacement kernel. With Eq. (179) and the dominated convergence theorem, we have demonstrated a rigorous version of the criterion

$$\int_0^\infty \tau_L(k)E(k)\, dk < \infty \tag{180}$$

for ordinary diffusive growth of $\sigma_Y^2(t)$ at long times. We have only proven it here for the special case $\kappa = \bar{w} = 0$, but as we shall discuss below, it holds rigorously for $\kappa \ne 0$ and $\bar{w} \ne 0$ as well, provided that $\tau_L(k)$ is interpreted in the appropriate fashion. We have already indicated in Section 3.3.4 how Eq. (180) defines the boundaries of the diffusive regime D in the phase diagram in Fig. 16.

Superdiffusive regimes. For values of ε and z outside the closure of the D regime, the integral in Eq. (180) diverges at low wavenumber. We therefore expect superdiffusion which is driven by the low wavenumber modes of the shear flow, and zoom in on this region with a strategy similar to that developed for the RSS Model in Section 3.2.6. We introduce a wavenumber cutoff k_1 and frequency cutoff ω_1, and separate the formula (171a) into a low wavenumber-frequency piece $\bar{\sigma}_Y^2(t)$ and the remainder $\tilde{\sigma}_Y^2(t)$:

$$\sigma_Y^2(t) = \bar{\sigma}_Y^2(t) + \tilde{\sigma}_Y^2(t) \,,$$

$$\bar{\sigma}_Y^2(t) = 4 \int_0^{k_1} \int_0^{\omega_1} \tilde{E}(k, \omega)\tilde{\Sigma}_{w_f}(k, \omega, t)\, d\omega\, dk \,,$$

$$\tilde{\sigma}_Y^2(t) = 4 \iint_{k \ge k_1 \text{ or } \omega \ge \omega_1} \tilde{E}(k, \omega)\tilde{\Sigma}_{w_f}(k, \omega, t)\, d\omega\, dk \,.$$

The contribution $\tilde{\sigma}_Y^2(t)$ is clearly at most diffusive by Eq. (177), since it has no contribution from modes with both small ω and small k.

We next rescale $\bar{\sigma}_Y^2(t)$ by

$$q = k/k_{db}(t)$$

where $k_{db}(t)$ scales with the inverse function to the Lagrangian persistence time $\tau_L(k)$ at small k. (For the motivation, see our discussion in Paragraph 3.2.6.2 in the context of the RSS Model.) Noting that

$$\lim_{k\to 0} \tau_L(k) = \lim_{k\to 0} \min(\tau_{w_f}(k), \tau(k))$$

$$\sim \begin{cases} \tau_{w_f}(k) \sim C_{w_f}(K_x^\# k^2)^{-1/(1+\beta)} & \text{for } z > 2/(1+\beta) , \\ \tau(k) \sim A_\tau k^{-z} & \text{for } 0 \le z < 2/(1+\beta) , \end{cases}$$

we choose

$$k_{db}(t) = \begin{cases} \left(\dfrac{4\pi^2 K_x^\#}{1+\beta}\right)^{-1/2} t^{-(1+\beta)/2} & \text{for } z > 2/(1+\beta) , \\[2mm] A_\tau^{1/z} t^{-1/z} & \text{for } 0 \le z < 2/(1+\beta) . \end{cases}$$

(Numerical prefactors in $k_{db}(t)$ have been chosen for convenience.) Because the frequency variable ω appears in Eqs. (178a) and (178b) in conjunction with the single time scale $\tau(k)$ with $\tau(k) \sim A_\tau k^{-z}$ at small wavenumbers, it is natural (and actually quite necessary) to rescale the frequency variable along with the wavenumber variable according to

$$\varpi = \omega/\omega_{db}(t) , \tag{181a}$$

$$\omega_{db}(t) \equiv A_\tau^{-1}(k_{db}(t))^z . \tag{181b}$$

Note that $\omega_{db}(t) = t^{-1}$ for $z < 2/(1+\beta)$, where the decorrelation of the shear flow fluctuations itself is dominant at low wavenumbers.

Performing the rescalings indicated above, we obtain

$$\bar{\sigma}_Y^2(t) = 4k_{db}(t)\omega_{db}(t)\int_0^{k_1/k_{db}(t)} \int_0^{\omega_1/\omega_{db}(t)} \tilde{E}(qk_{db}(t), \varpi\omega_{db}(t))\tilde{\Sigma}_{w_f}(qk_{db}(t), \varpi\omega_{db}(t), t)\, d\varpi\, dq . \tag{182}$$

The rescaled shear-displacement kernel in the integrand converges, for each fixed q and ϖ to a finite multiple of t^2 in the long-time limit, reflecting the fact that the modes in the band $k \lesssim k_{db}(t)$, $\omega \lesssim \omega_{db}(t)$ are still contributing ballistically:

$$\lim_{t\to\infty} t^{-2}\tilde{\Sigma}_{w_f}(qk_{db}(t), \varpi\omega_{db}(t), t) = \begin{cases} 2\int_0^1(1-u)e^{-q^2 u^{1+\beta}}\, du & \text{for } z > 2/(1+\beta) , \\ (1-\cos 2\pi\varpi)/(2\pi^2\varpi^2) & \text{for } 0 \le z < 2/(1+\beta) . \end{cases}$$

The long-time limit of the rescaled spatio-temporal energy spectrum in the integrand may be expressed through the low-wavenumber asymptotics of $\tilde{E}$:

$$\lim_{t\to\infty} \tilde{E}(qk_{db}(t), \varpi\omega_{db}(t)) = \lim_{t\to\infty} E(qk_{db}(t))\,\phi_{qk_{db}(t)}(\varpi\omega_{db}(t)\,\tau(qk_{db}(t)))\tau(qk_{db}(t))$$

$$\sim A_E(qk_{db}(t))^{1-\varepsilon}\phi_0(\varpi\omega_{db}(t)A_\tau(qk_{db}(t))^{-z})\,A_\tau(qk_{db}(t))^{-z}$$

$$= (k_{db}(t))^{1-\varepsilon-z}A_E A_\tau q^{1-\varepsilon-z}\phi_0(\varpi q^{-z})\ .$$

To deduce the limit of the integral (182) as the integral of the limit of the integrand, we establish uniform integrable bounds on the integrand. From the inequality (177) and $|\tilde{\Sigma}_{w_f}(k, \omega, t)| \le 2t^2$, we can deduce that

$$|t^{-2}\tilde{\Sigma}_{w_f}(qk_{db}(t), \varpi\omega_{db}(t), t)\Theta(k_1/k_{db}(t) - q)\Theta(\omega_1/\omega_{db}(t) - \varpi)| \tag{183}$$

$$\le \begin{cases} \dfrac{C_6}{1 + q^{2/(1+\beta)}} & \text{for } z > 2/(1+\beta)\ , \\[2ex] \dfrac{C_7}{1 + \varpi} & \text{for } 0 \le z < 2/(1+\beta)\ , \end{cases} \tag{184}$$

where Θ is the Heaviside function (151). The low wavenumber asymptotics $E(k) \sim A_E k^{1-\varepsilon}$ and $\tau(k) \sim A_\tau k^{-z}$ along with the uniform bound (156) on $\phi_k(\cdot)$ imply

$$(k_{db}(t))^{-(1-\varepsilon-z)}\tilde{E}(qk_{db}(t), \varpi\omega_{db}(t))\Theta(k_1/k_{db}(t) - q)\Theta(\omega_1/\omega_{db}(t) - \varpi)$$

$$\le C_8 q^{1-\varepsilon-z}/(1 + |\varpi q^{-z}|^\gamma)\ , \tag{185}$$

where $\gamma > 1$. The bounds provided by the product of the right-hand sides of Eqs. (183) and (185) are indeed absolutely integrable over $0 \le q \le \infty$, $0 \le \varpi \le \infty$, provided that (ε, z) fall within the interior of either of the superdiffusive regimes indicated in Fig. 16. The dominated convergence theorem thus guarantees that we may safely evaluate the long-time limit of Eq. (182) by replacing the integrand by its long-time limit.

Within the SD-w_f regime, defined by the inequalities

$$z > 2/(1+\beta), \qquad 2\beta/(1+\beta) < \varepsilon < 2\ ,$$

we obtain

$$\lim_{t\to\infty} \sigma_Y^2(t) \sim \lim_{t\to\infty} \bar{\sigma}_Y^2(t) \sim 4k_{db}(t)\omega_{db}(t)t^2 k_{db}^{1-\varepsilon-z}(t)$$

$$\times \int_0^\infty \int_0^\infty A_E A_\tau q^{1-\varepsilon-z}\phi_0(\varpi q^{-z})\left(2\int_0^1 (1-u)e^{-q^2 u^{1+\beta}}\,\mathrm{d}u\right)\mathrm{d}\varpi\,\mathrm{d}q$$

$$= 4k_{db}^{2-\varepsilon}(t)t^2 \int_0^\infty A_E q^{1-\varepsilon}\left(2\int_0^1 (1-u)e^{-q^2 u^{1+\beta}}\,\mathrm{d}u\right)\int_0^\infty \phi_0(\varpi)\,\mathrm{d}\varpi\,\mathrm{d}q$$

$$= 2k_{db}^{2-\varepsilon}(t)t^2 \int_0^\infty A_E q^{1-\varepsilon}\left(2\int_0^1 (1-u)e^{-q^2 u^{1+\beta}}\,\mathrm{d}u\right)\mathrm{d}q\ .$$

We used $\int_0^\infty \phi_0(\varpi)\,d\varpi = \frac{1}{2}\int_{-\infty}^\infty \phi_0(\varpi)\,d\varpi = \frac{1}{2}$ in the last equality. We thereby arrive at the same long-time asymptotic expression for $\bar\sigma_Y^2(t)$ as in the RSS Model; see Eq. (152). This rigorously proves that the long-time asymptotics of $\sigma_Y^2(t)$ in the SD-w_f regime is unaffected by the presence of temporal fluctuations in the shear flow.

For the SD-ω regime in Fig. 16, defined by

$$0 < z \le 2/(1+\beta), \qquad 2 - z < \varepsilon < 2 ,$$

we compute instead

$$\lim_{t\to\infty} \sigma_Y^2(t) \sim \lim_{t\to\infty} \bar\sigma_Y^2(t) \sim 4k_{db}(t)\omega_{db}(t)t^2 k_{db}^{1-\varepsilon-z}(t)\int_0^\infty$$

$$\times \int_0^\infty A_E A_\tau q^{1-\varepsilon-z}\phi_0(\varpi q^{-z})\frac{1-\cos 2\pi\varpi}{2\pi^2\varpi^2}\,d\varpi\,dq$$

$$= \frac{2z}{2z+\varepsilon-2}\tilde K_0^\sharp t^{(2z+\varepsilon-2)/z} ,$$

where

$$\tilde K_0^\sharp = \frac{(2z+\varepsilon-2)}{z}\pi^{-2}A_E A_\tau^{(2-\varepsilon)/z}\int_0^\infty\int_0^\infty q^{1-\varepsilon-z}(1-\cos 2\pi\varpi)\varpi^{-2}\phi_0(\varpi q^{-z})\,d\varpi\,dq$$

$$= \frac{(2z+\varepsilon-2)}{z}\pi^{-2}A_E A_\tau^{(2-\varepsilon)/z}z^{-1}\int_0^\infty\int_0^\infty p^{(\varepsilon-2)/z}(1-\cos 2\pi\varpi)\varpi^{(2-\varepsilon-3z)/z}\phi_0(p)\,d\varpi\,dp$$

$$= z^{-1}\pi^{(2\varepsilon+z-4)/2z}\frac{\Gamma((2-\varepsilon)/2z)}{\Gamma((\varepsilon+3z-2)/2z)}A_E A_\tau^{(2-\varepsilon)/z}\int_0^\infty p^{(\varepsilon-2)/z}\phi_0(p)\,dp .$$

This is exactly what is stated in Table 9 and Eq. (169).

Weak sweeping regime. We finally treat the case in which the randomly fluctuating cross sweep $w_f(t)$ produces only trapped motion across the shear ($\beta < -1$). The following calculation will also be valid for the special case of no cross sweep $w_f(t) = 0$ (and no other cross-shear transport mechanisms), thereby yielding the results stated in Section 3.3.1 as a by-product.

To understand how to proceed, we notice that for no cross sweep ($\sigma_X^2(t) = 0$), the shear-displacement kernel in Eq. (171b) has the explicit form

$$\tilde\Sigma_{w_f}(k,\omega,t) = \tilde\Sigma_0(k,\omega,t) = t^2 F_2(2\pi\omega t) ,$$

$$F_2(\varpi) = \frac{2(1-\cos\varpi)}{\varpi^2} . \tag{186}$$

In particular, the shear-parallel tracer displacement generated by a single wavenumber-frequency mode with $\omega \ne 0$ is oscillatory and trapped. This suggests that most of the tracer action at long times will come from low frequency modes, and the rescaling $\varpi = \omega t$ is suggested to zoom in on them. We follow this strategy also if a trapping cross sweep $w_f(t)$ is present, since we can expect that this should only produce a weak perturbation of the case of no cross-shear transport.

We thereby arrive at the following expression for $\sigma_Y^2(t)$:

$$\sigma_Y^2(t) = 4t^{-1} \int_0^\infty \int_0^\infty \tilde{E}(k, \varpi t^{-1}) \tilde{\Sigma}_{w_f}(k, \varpi t^{-1}, t) \, d\varpi \, dk .$$

The long-time limit of the rescaled shear-displacement kernel has a clean form when the cross sweep $w_f(t)$ is trapped:

$$\lim_{t \to \infty} t^{-2} \tilde{\Sigma}_{w_f}(k, \varpi t^{-1}, t) = 2 \lim_{t \to \infty} \int_0^1 (1-u) \cos(2\pi \varpi u) e^{-2\pi^2 k^2 \sigma_X^2(tu)} \, du$$

$$= 2 \int_0^1 (1-u) \cos(2\pi \varpi u) e^{-2\pi^2 k^2 K_x^\circ} \, du = e^{-2\pi^2 k^2 K_x^\circ} F_2(2\pi \varpi) .$$

We used the fact (144) that $\sigma_X^2(t)$ has the finite long-time limit K_x° for $\beta < -1$. The rescaled spatio-temporal energy spectrum clearly converges to its zero-frequency limit:

$$\lim_{t \to \infty} \tilde{E}(k, \varpi t^{-1}) = \tilde{E}(k, 0) .$$

With $|\tilde{\Sigma}_{w_f}(k, \varpi t^{-1}, t)| \leq t^2$ and $\tilde{E}(k, \varpi t^{-1}) \leq C_9 E(k) \tau(k) \sim_{k \to 0} C_9 A_E A_\tau k^{1-\varepsilon-z}$ (due to the uniform bound (156) on ϕ_k), we can apply the dominated convergence theorem when $\varepsilon + z < 2$ to deduce

$$\lim_{t \to \infty} \sigma_Y^2(t) = 4t \int_0^\infty \int_0^\infty \tilde{E}(k, 0) e^{-2\pi^2 k^2 K_x^\circ} F_2(2\pi \varpi) \, d\varpi \, dk = 2t \int_0^\infty e^{-2\pi^2 k^2 K_x^\circ} \tilde{E}(k, 0) \, dk ,$$

where we have used the integral formula $\int_0^\infty F_2(2\pi \varpi) \, d\varpi = \frac{1}{2}$. This covers the diffusive regime D.

For $\varepsilon + z > 2$, there is a nonintegrable divergence of the limiting integrand at $k = 0$, so we rescale the wavenumber along with the frequency variable

$$q = k/k_{db}(t) .$$

Since the Lagrangian persistence time $\tau_L(k)$ is clearly just the Eulerian correlation time $\tau(k)$ of the shear flow, and $\tau(k) \sim A_\tau k^{-z}$ for low wavenumbers, an appropriate choice of the rescaling is

$$k_{db}(t) = A_\tau^{1/z} t^{-1/z} .$$

Note that the indicated wavenumber and frequency rescaling is the same as that in the SD-ω regime described above in our discussion of the case of random sweeps with $-1 < \beta < 1$. Under this rescaling, the random cross sweeping there became asymptotically irrelevant in the long time limit; the same clearly must be true when the cross sweep is trapping. Therefore, the long-time asymptotics of $\sigma_Y^2(t)$ obeys the SD-ω scaling law for $\varepsilon + z > 2$ when the random cross sweep motion is trapping.

3.3.6.3. Sketch of general derivation of asymptotics. We have just computed in detail the asymptotic results presented in Section 3.3.4 for the shear-parallel transport in the presence of a randomly fluctuating cross sweep $w_f(t)$ and no molecular diffusion $\kappa = 0$ or mean cross sweep $\bar{w} = 0$. We covered, as a special case of a trapping cross sweep, the derivation of the results of Section 3.3.1

where no cross-shear transport process is active. The approach developed above extends easily to handle $\kappa \neq 0$; indeed molecular diffusion may be treated in the above analysis in exactly the same way as a diffusive cross sweep ($\beta = 0$). Therefore, only the case of a nonzero mean cross sweep remains to be discussed. We shall simply sketch how to modify the above approach to compute the asymptotics for $\sigma_Y^2(t)$ when $\bar{w} \neq 0$.

First of all, if no other cross-shear transport process is active ($\kappa = w_f(t) = 0$), as in our discussion in Section 3.3.3, then the shear-displacement kernel takes the explicit form

$$\tilde{\Sigma}_{\bar{w}}(k, \omega, t) = \tfrac{1}{2}t^2[F_2(2\pi(\omega - \bar{w}k)t) + F_2(2\pi(\omega + \bar{w}k)t)] \,,$$

$$F_2(\varpi) = 2(1 - \cos(\varpi))/\varpi^2 \,.$$

This is essentially just a sum of Doppler shifts of the kernel $\tilde{\Sigma}_0(k, \omega, t)$ in Eq. (186) for the case of no cross-shear transport. The single-mode wavenumber-frequency contributions away from the resonance line $\omega = \bar{w}k$ are trapped, so the main contribution to the total shear-parallel transport at long times comes only from modes near this resonance line. The asymptotics of $\sigma_Y^2(t)$ are therefore computed by rescaling the frequency variable in Eqs. (170a) and (170b) as $\omega = \bar{w}k + \varpi t^{-1}$, and then proceeding similarly as in our discussion of a trapping cross sweep above. This will work out the D and SD-ω regime in Fig. 15. Within the SD-$\bar{w}$ regime, only the low wavenumbers are relevant at long times, and the effects of the cross sweep dominate those of the temporal fluctuations in the shear flow. The wavenumber-frequency rescaling must therefore be chosen in accordance with the fact that the effective Lagrangian persistence time is $\tau_L(k) = \tau_{\bar{w}}(k) = (2\pi\bar{w}k)^{-1}$, namely

$$k_{db}(t) = (2\pi\bar{w}t)^{-1}, \qquad \omega_{db}(t) = A_\tau^{-1}(k_{db}(t))^z \,.$$

When a mean cross sweep is superposed with molecular diffusion κ or a randomly fluctuating cross sweep $w_f(t)$, the only substantial change is that the frequency variable should not be rescaled in the computation within the D regime. The reason is that the random component of the cross shear-transport will render $\tilde{\Sigma}(k, \omega, t)$ diffusive at all nonzero wavenumbers and frequencies, so the whole wavenumber-frequency domain contributes to the effective diffusion constant.

For the benefit of the reader interested in some of the mathematical details of the computation, we remark that the rigorous asymptotic computation of $\sigma_Y^2(t)$ with $\bar{w} \neq 0$ is more arduous than in the $\bar{w} = 0$ case presented in detail above. There are transient contributions in the integral representation (170) for $\sigma_Y^2(t)$ which cannot be controlled by a uniform, time-independent bounding function. Their contribution must instead be separately estimated and shown to be subdominant. This can be accomplished with sufficient care, but we do not present these details here because it would require too much space.

3.4. Large-scale effective equations for mean statistics and departures from standard eddy diffusivity theory

We now shift our focus from the description of the mean-square displacement of a single tracer to the mean concentration of tracers (or other passive scalar quantity). These points of view are related in that the mean passive scalar density $\langle T(\boldsymbol{x}, t) \rangle$ evolving from a concentrated source at $\boldsymbol{x}_0$ is exactly equal to the full probability distribution function (PDF) for the location $\boldsymbol{X}(t)$ of a single tracer starting from $\boldsymbol{x}_0$ [164]. The mean passive scalar density $\langle T(\boldsymbol{x}, t) \rangle$ is therefore determined not

only by the mean-square displacement of a single tracer, but by the higher order statistics of its motion as well.

We recall that it is not possible in general to obtain a closed PDE for $\langle T(x,t) \rangle$ by naively averaging the advection–diffusion equation

$$\partial T(x,t)/\partial t + v(x,t) \cdot \nabla T(x,t) = \kappa \Delta T(x,t) \,,$$

because of the statistically nonlinear coupling between $v(x,t)$ and $T(x,t)$. We did show through homogenization theory in Section 2, however, that for certain periodic velocity fields and random velocity fields with short-range correlations, the mean passive scalar density does obey an effective diffusion equation at large scales and long times. Namely, if the initial data is rescaled to vary on large scales:

$$T_0^{(\delta)}(x) \equiv T_0(\delta x)$$

(with $\delta > 0$ small), then the mean of the resulting passive scalar field $T^{(\delta)}(x,t)$ converges under a *diffusive* rescaling,

$$\bar{T}(x,t) = \lim_{\delta \to 0} \langle T^{(\delta)}(x/\delta, t/\delta^2) \rangle \,. \tag{187}$$

This large-scale, long-time limit is in these cases the unique solution of a constant-coefficient diffusion equation

$$\partial \bar{T}(x,t)/\partial t = \nabla \cdot (\mathscr{K}^* \nabla \bar{T}(x,t)), \qquad \bar{T}(x,t=0) = T_0(x) \,, \tag{188}$$

where $\mathscr{K}^*$ is a constant, symmetric, positive-definite matrix depending on the velocity field $v(x,t)$ and the molecular diffusivity κ, and can be obtained from the solution of an associated "cell problem" (86).

It can be shown, using the arguments in the appendices to [10,14], that such a homogenized description holds throughout the diffusive regimes in both the Random Steady Shear Model (Section 3.2) and the Random Spatio-Temporal Shear Model (Section 3.3), at least when $\kappa > 0$ and the cross sweep velocity $w(t)$ is a (zero or nonzero) deterministic constant. It is an open problem whether the Simple Shear Models do or do not adhere to a homogenized description at large scales and long times within the diffusive regimes when $\kappa = 0$ or a randomly fluctuating cross sweep $w_f(t)$ is present.

We explore now some ways in which the effective diffusivity picture is altered when the velocity field has long-range spatial correlations which violate the conditions needed to apply standard homogenization theory. The Simple Shear Models developed in Sections 3.2 and 3.3 will be used for explicit illustrations. First of all, the diffusively linked rescaling of space and time in (187) clearly will not do for superdiffusive regimes. Instead, the large-scale, long-time behavior is captured by an appropriate choice of rescaling function $\rho(\delta)$ which vanishes as $\delta \to 0$, and for which

$$\bar{T}(x,t) = \lim_{\delta \to 0} \left\langle T^{(\delta)}\left(\frac{x}{\delta}, \frac{t}{\rho^2(\delta)}\right) \right\rangle$$

has a nontrivial limit. Diffusive rescaling corresponds to $\rho(\delta) = \delta$.

As we shall see in Sections 3.4.1 and 3.4.2, the rescaled (or "renormalized") limit $\bar{T}(\boldsymbol{x}, t)$ of the mean passive scalar field cannot in general be expressed as the solution of a (local) PDE [10,16]. Therefore, we sometimes utilize the more general framework of Green's functions. Because of the linearity of the advection–diffusion equation and the prevailing assumption that the initial passive scalar data is independent of the statistics of the velocity field, we can always express the mean of passive scalar statistics as an integral of the mean initial data against some kernel, or Green's function, $P^{(t)}$:

$$\langle T^{(\delta)}(\boldsymbol{x}, t) \rangle = \int_{\mathbb{R}^d} P^{(t)}(\boldsymbol{x}, \boldsymbol{x}') \langle T_0^{(\delta)}(\boldsymbol{x}') \rangle \, \mathrm{d}\boldsymbol{x}' . \tag{189}$$

When the velocity field is statistically homogenous, as we shall assume here, the Green's function only depends on the difference between the spatial locations of the "source" and the "target", and we can express $P^{(t)}(\boldsymbol{x}, \boldsymbol{x}')$ more simply as $P^{(t)}(\boldsymbol{x} - \boldsymbol{x}')$. The reason we write the Green's function in this way is that $P^{(t)}(\boldsymbol{x})$ is exactly the probability distribution function (PDF) of the displacement $\boldsymbol{X}(t) - \boldsymbol{x}_0$ of a single tracer. The renormalized mean statistics are described by a renormalized Green's function

$$\bar{T}(\boldsymbol{x}, t) = \int_{\mathbb{R}^d} \bar{P}^{(t)}(\boldsymbol{x} - \boldsymbol{x}') \langle T_0(\boldsymbol{x}') \rangle \, \mathrm{d}\boldsymbol{x}' ,$$

and this renormalized Green's function characterizes the long-time asymptotic PDF for the displacement of a single tracer:

$$\bar{P}^{(t)}(\boldsymbol{x}) = \lim_{\delta \to 0} \delta^{-1} P^{(t/\rho^2(\delta))} \left(\frac{\boldsymbol{x}}{\delta} \right). \tag{190}$$

The renormalized Green's function associated with the homogenized PDE (188) is the standard Gaussian heat kernel:

$$\bar{P}^{(t)}(\boldsymbol{x}) = \frac{\mathrm{e}^{-\boldsymbol{x} \cdot (\mathscr{K}^*)^{-1} \cdot \boldsymbol{x}/4t}}{(4\pi t)^{d/2} (\mathrm{Det}\, \mathscr{K}^*)^{1/2}} ,$$

reflecting the fact that the tracer displacement relaxes to a Gaussian distribution at long times.

In Section 3.4.1, we present the long-time, large-scale limit of a passive scalar field evolving under the Random Steady Shear (RSS) model with positive molecular diffusion $\kappa > 0$. For the parameter range $0 < \varepsilon < 2$, the tracer motion is superdiffusive and an anomalous scaling $\rho(\delta) = \delta^\nu$, $\nu \neq 1$ is needed to obtain a finite limit. The associated large-scale, long-time Green's function may be represented as the average of an explicit functional of Brownian motion, but is not the solution to any (local) PDE [10]. Moreover, as we shall discuss in Section 3.4.2, this anomalous Green's function behavior persists when these steady shear flows are perturbed by a general class of short-ranged *two-dimensional* random flows [16].

In Section 3.4.3 we modify the Random Spatio-Temporal Shear (RSTS) model to include an important feature of real-world turbulence at high Reynolds number: a self-similar *inertial range* of scales. We discuss some issues pertaining to the computation of effective large-scale passive scalar behavior in high Reynolds number turbulent flows in the context of these shear flow models, and report on the results of some rigorous work along these lines [10,14]. Finally, in Section 3.4.4 we

provide some explicit examples in which the Green's function for the mean passive scalar density solves a time-dependent diffusion equation in which the diffusion coefficient is negative over finite time intervals.

3.4.1. Large-scale, long-time Green's functions in steady random shear flow

We return to the Random Steady Shear Flow Model from Section 3.2, with no cross sweeping flow:

$$
\boldsymbol{v}(x, y, t) = \begin{bmatrix} 0 \\ v(x) \end{bmatrix},
$$

where the random shear flow $v(x)$ has energy spectrum (109), in which the low wavenumber asymptotics of $E(k)$ are given by $\lim_{k \to 0} E(k) \sim A_E k^{1 - \varepsilon}$ with $\varepsilon < 2$. Molecular diffusion $\kappa > 0$ is assumed to be active.

We computed in Section 3.2.1 that the shear-parallel tracer displacement $\sigma_Y^2(t) = \langle (Y(t) - y_0)^2 \rangle$ is diffusive for $\varepsilon < 0$ and superdiffusive for $0 < \varepsilon < 2$; see Table 2. We now consider aspects of the full probability distribution function (PDF) $P^{(t)}(x, y)$ of the tracer displacement at long time, as reflected in the renormalized Green's function (190).

3.4.1.1. Diffusive regime. For the diffusive regime $\varepsilon < 0$, the condition

$$
\int_0^\infty \frac{E(k)}{k^2} \, dk < \infty
$$

is satisfied, and the homogenization theory for incompressible velocity fields with short-range correlations applies (see Section 2.4.2). Consequently, the renormalized Green's function (with diffusive rescaling $\rho(\delta) = \delta$) is a Gaussian:

$$
\bar{P}^{(t)}(x, y) = \frac{\exp(-(x^2/4\kappa t) - (y^2/4K_\kappa^* t))}{4\pi \sqrt{\kappa K_\kappa^* t}}, \tag{191}
$$

where the diffusivity in the x direction is the bare molecular value κ, whereas the diffusivity in the y direction is the turbulence-enhanced value K_κ^* stated in Eq. (115). The mean passive scalar density therefore rigorously satisfies an ordinary, constant-coefficient diffusion equation when rescaled to large scales and long times as in Eq. (187):

$$
\frac{\partial \bar{T}(x, y, t)}{\partial t} = \kappa \frac{\partial^2 \bar{T}(x, y, t)}{\partial x^2} + K_\kappa^* \frac{\partial^2 \bar{T}(x, y, t)}{\partial y^2},
$$

$$
\bar{T}(x, y, t = 0) = T_0(x, y).
$$

Moreover the behavior of a single tracer is *self-averaging* for $\varepsilon < 0$, in that the large-scale, long-time PDF of a tracer, conditioned on a single realization of the velocity field, is (almost) always identical to the asymptotic Gaussian distribution (191) characterizing the ensemble-averaged behavior [16]. In other words, the tracer's motion in (almost) any given environment effectively samples the statistics of the entire ensemble after some finite time.

3.4.1.2. Superdiffusive regime. The behavior of a tracer in a random shear flow with $0 < \varepsilon < 2$ has many anomalies which contrast sharply with this simple homogenized picture. Recall that the "typical" class of random shear flows with finite energy at low wavenumbers correspond to $\varepsilon = 1$, and belong to this anomalous class. First of all, we have shown in Section 3.2.1 that the shear-parallel tracer motion is superdiffusive for $0 < \varepsilon < 2$:

$$\lim_{t \to \infty} \sigma_Y^2(t) \sim \frac{4}{2 + \varepsilon} K_\kappa^\sharp t^{1 + \varepsilon/2} \;,$$

where the constant $K_\kappa^\sharp$ is described in Eq. (115). The appropriate rescaling of time to capture the large-scale behavior of the tracer displacement in Eq. (190) is therefore $\rho(\delta) = \delta^{2/(2 + \varepsilon)}$. Under this space–time rescaling, the diffusive tracer motion along the x direction is negligible, and it factors out of the renormalized Green's function as a delta function:

$$\bar{P}^{(t)}(x, y) = \delta(x)\bar{P}_Y^{(t)}(y) \;.$$

One could of course retain the cross-shear dynamics by choosing an anisotropic scaling of space, but our interest here is only on the PDF for the tracer displacement along the shear, which at long times is described by $\bar{P}_Y^{(t)}(y)$.

An explicit formula for this renormalized Green's function was derived rigorously in [10]:

$$\bar{P}_Y^{(t)}(y) = \left\langle \frac{\exp\left[-\dfrac{y^2}{4(2/(2 + \varepsilon))K_\kappa^\sharp \alpha t^{1 + \varepsilon/2}} \right]}{\sqrt{4\pi(2/(2 + \varepsilon))K_\kappa^\sharp \alpha t^{1 + \varepsilon/2}}} \right\rangle_\alpha . \tag{192}$$

The outer brackets denote an expectation over the random variable

$$\alpha \equiv \frac{2^{\varepsilon/2 - 2}}{\Gamma(-(\varepsilon + 2)/2)} \int_0^1 \int_0^1 F_\varepsilon(W(s) - W(s')) \, ds \, ds' \;,$$

where $W(t)$ is a standard Brownian motion. The function $F_\varepsilon(y)$ appearing in the integral is given by

$$F_\varepsilon(y) = \int_{-\infty}^\infty e^{iqy} |q|^{1 - \varepsilon} \, dq = \begin{cases} C_\varepsilon \dfrac{\mathrm{sgn}(y)}{|y|^{2 - \varepsilon}} & \text{for } 0 < \varepsilon < 1 \text{ or } 1 < \varepsilon < 2 \;, \\ C_{\varepsilon = 1}\delta(y) & \text{for } \varepsilon = 1 \;, \end{cases}$$

where

$$C_\varepsilon = \begin{cases} -\sqrt{\dfrac{2}{\pi}}\sin\left(\dfrac{(1 - \varepsilon)\pi}{2}\right)\Gamma(2 - \varepsilon) & \text{for } 0 < \varepsilon < 1 \text{ or } 1 < \varepsilon < 2 \;, \\ \dfrac{1}{\sqrt{2\pi}} & \text{for } \varepsilon = 1 \;. \end{cases}$$

Without the ensemble average over α, the renormalized Green's function $\bar{P}_Y^{(t)}(y)$ would be a Gaussian distribution. But the averaging over α implies that $\bar{P}_Y^{(t)}(y)$ is in fact the probability distribution for a *mixture* of (mean zero) Gaussian random variables, and is therefore necessarily a broader-than-Gaussian distribution (see Paragraph 5.2.2.1). That is, the tracer is more likely to make large

excursions along the shear, relative to its root-mean-square displacement, than a Gaussian random process with the same mean-square displacement law would. Through analytical considerations and numerical simulations, Zumofen et al [353,354] identify the source of non-Gaussianity more specifically as coming from the variability in the *range* of the Brownian motion across the shear.

The renormalized Green's function given by Eq. (192) cannot be represented as the solution to a PDE of diffusion type or even any local PDE of the form

$$\partial \bar{P}_Y^{(t)}(y)/\partial t = Q(\partial/\partial y)\bar{P}_Y^{(t)}(y) \, ,$$

where $Q(\cdot)$ is a polynomial. Therefore, we say that the renormalized mean statistics $\bar{T}(x, y, t)$ obey a *nonlocal* equation within the regime $0 < \varepsilon < 2$.

One appealing formulation of this nonlocal equation for $\bar{T}(x, y, t)$ uses the notion of a random diffusivity. The conditional Green's function

$$\bar{P}_Y^{(t)}(y|\alpha) \equiv \frac{\exp\left[-\dfrac{y^2}{4(2/(2 + \varepsilon))K_\kappa^\sharp \alpha t^{1 + \varepsilon/2}} \right]}{\sqrt{4\pi(2/(2 + \varepsilon))K_\kappa^\sharp \alpha t^{1 + \varepsilon/2}}} \tag{193a}$$

is the fundamental solution of the constant coefficient diffusion equation

$$\partial \bar{P}_Y^{(t)}(y|\alpha)/\partial t = K_\kappa^\sharp \alpha t^{\varepsilon/2} \, \partial^2 \bar{P}_Y^{(t)}(y|\alpha)/\partial y^2 \, , \tag{193b}$$

$$\bar{P}_Y^{(t = 0)}(y|\alpha) = \delta(y) \tag{193c}$$

with diffusion coefficient $K_\kappa^\sharp \alpha$. Therefore, the renormalized Green's function may be viewed as an average over solutions to constant-coefficient diffusion equations with a random factor α appearing in the diffusivity. The behavior of the PDF of α as a function of ε is discussed in [10].

While Eq. (192) is an explicit representation of the renormalized Green's function, it would be interesting to identify some properties of $\bar{P}^{(t)}(y)$, such as the form of the tail region $y^2 \gg K_\kappa^\sharp t^{(1 + \varepsilon/2)}$, in a more transparent manner. Some numerical simulations and formal large deviation arguments [46,280,353], as well as some partial exact results from a quantum mechanical analogy [194] suggest that, for $\varepsilon = 1$, the tails of the renormalized Green's function have a stretched exponential form

$$\lim_{|y|/K_\kappa^\sharp t^{(2 + \varepsilon)/4} \to \infty} \bar{P}_Y^{(t)}(y) \sim t^{-(2 + \varepsilon)/4} \exp(-(|y|/t^{(2 + \varepsilon)/4})^\delta) \, ,$$

with $\delta = \frac{4}{3}$ and possibly some power-law prefactor in the large parameter. It would be interesting to rigorously derive such a result using the method of large deviations [331], and to describe the shape of the tails of $\bar{P}^{(t)}(y)$ as a function of ε. We note that explicit quantitative expressions for several moments of the renormalized Green's function for $\varepsilon = 1$ may be extracted from the exact finite-time formulas in [353,354] for the moments of the shear-parallel displacement in a limiting version of the independent channel model with infinitely thin channels.

Departure from self-averaging. This representation of the renormalized Green's function suggests, but does not prove, that at long times, the squared tracer displacement along the shear in a single realization may grow as $t^{1 + \varepsilon/2}$, but with a realization-dependent prefactor. In other words, the motion of a single tracer may not be self-averaging, in that the behavior of a typical single

realization does not resemble the ensemble-averaged behavior. This issue has been explored in more depth by [46,280] for a random shear flow which takes the form of an array of independent channels, as discussed in Section 3.2.1. These models have energy spectra which are finite at the origin and so belong to the class $\varepsilon = 1$.

Bouchaud et al. [46,280] demonstrated that the motion of a single tracer is not self-averaging for the independent stratified channel model by computing the quantity

$$\lim_{t \to \infty} \langle \langle Y(t) - y_0 \rangle_W^2 \rangle_v \sim (\sqrt{2} - 1)(4A_E/3\sqrt{\pi\kappa})t^{3/2} . \tag{194}$$

This is to be compared with the formula for the mean-square displacement for $\varepsilon = 1$:

$$\lim_{t \to \infty} \sigma_Y^2(t) \equiv \lim_{t \to \infty} \langle (Y(t) - y_0)^2 \rangle = (4A_E/3\sqrt{\pi\kappa})t^{3/2} . \tag{195}$$

To interpret Eq. (194), note first that $M_Y(t|v, y_0) = \langle Y(t) - y_0 \rangle_W$ is the mean displacement of a tracer, averaged over Brownian motion but in a fixed realization of the random shear environment and fixed starting location y_0. This random variable $M_Y(t|v, y_0)$ describes exactly the displacement of the center of mass of a cloud of tracers initially concentrated at the specified point y_0, then subsequently moving in a common random shear environment but with independent Brownian motions. Clearly, $M_Y(t|v, y_0)$ has mean zero when averaged over all random shear configurations $v(x)$.

The important point of the above results is that the displacement of the center of mass of the cloud, in a given realization of the random shear environment, will be of the same order of magnitude as the typical displacement of a tracer. On the other hand, the mean tracer concentration density, averaged over the ensemble of random shears, will have its center of mass fixed at y_0 and spread symmetrically about it. Therefore, the evolution of an initially concentrated cloud observed in a given environment does not resemble the ensemble-averaged behavior, and we therefore say that the evolution of a concentrated cloud (and also of a single tracer) is not self-averaging. This conclusion is also reached from a different direction for any value of ε with $0 < \varepsilon < 2$ in [10], in which it is demonstrated that the renormalized Nth order moments of the rescaled passive scalar field $\delta^{-1}T(x/\delta, y/\delta, t/\rho^2(\delta))$ do not coincide with $\bar{T}^N(x, y, t)$. The loss of self-averaging may be attributed to the long-range correlations of the Lagrangian tracer velocity which arise due to sufficiently strong long-range spatio-temporal correlations in the random shear flow.

This violation of self-averaging for an initially concentrated cloud lends some support to the idea that the tracer may indeed behave at long times in a given realization as if it had a time-dependent diffusivity $K_\kappa^\sharp \alpha t^{\varepsilon/2}$ with a random factor α, as suggested by the representation (193). It would be interesting to determine whether this random diffusivity picture is literally valid.

3.4.2. Persistence of non-Gaussian Green's function for nearly stratified steady flows

We next report on some work which indicates the robustness of the anomalous renormalized Green's function (192) under perturbations of the Random Steady Shear Model. As we now discuss, this renormalized Green's function actually characterizes the large-scale, long-time behavior of the statistics of a tracer in a rather broad class of random steady flows with an approximately stratified structure.

First of all, the assumption of Gaussian statistics of the random shear flow can be considerably relaxed. It has been demonstrated rigorously in [14], that the long-time PDF of a tracer position converges to Eq. (192) for several classes of non-Gaussian shear models with energy spectra as in Eq. (109). Included in these classes of non-Gaussian models is the independent channel model [46,279,353] discussed in Section 3.2.1 and shear flow versions of models with translational disorder as studied in [12,19,167]. In effect, there is a central limit theorem in operation as the tracer explores its random environment.

Secondly, Avellaneda and the first author established [16] that renormalized Green's functions of the form (192) arise generically for a class of steady random velocity fields which are "nearly stratified", in the sense that they have the structure

$$v(x, y) = \begin{bmatrix} 0 \\ v(x) \end{bmatrix} + u(x, y)$$

of a Gaussian homogenous random steady shear flow $v(x)$ with energy spectrum (109) perturbed by a two-dimensional random homogenous velocity field

$$u(x, y) = \begin{bmatrix} u_x(x, y) \\ u_y(x, y) \end{bmatrix}$$

of the type with short-range correlations discussed in Section 2. More precisely, the random perturbation field $u(x, y)$ is assumed to be periodic in y (with period 1) and statistically homogenous along the x direction, and the Fourier transform of its correlation tensor,

$$\hat{\mathscr{R}}_m(k) \equiv \int_{-\infty}^{\infty} \int_0^1 e^{-2\pi i(kx + my)} \mathscr{R}(x, y)\, dy\, dx \ ,$$

$$\mathscr{R}(x, y) \equiv \langle v(x', y')v(x' + x, y' + y) \rangle$$

is assumed to satisfy the condition

$$\sum_{m=0}^{\infty} \int_{-\infty}^{\infty} \frac{\|\hat{\mathscr{R}}_m(k)\|}{k^2 + m^2}\, dk < \infty \ .$$

This last condition guarantees that $u(x, y)$ obeys the conditions for homogenization theory, so that the statistical motion of a tracer due to the perturbation field $u(x, y)$ alone would be Gaussian and diffusive at long times. Note that $u(x, y)$ is allowed to be a deterministic, periodic flow as a special case.

The superposition of the random shear with the two-dimensional perturbation $u(x, y)$ corresponds to flow in a stratified heterogenous porous medium, with the perturbations $u(x, y)$ varying only over short wavelengths. Intuitively, we expect the solution of the equations of motion for the tracer

$$dX(t) = u_x(X(t), Y(t))\, dt + \sqrt{2\kappa}\, dW_x(t) \ ,$$

$$dY(t) = v(X(t))\, dt + u_y(X(t), Y(t))\, dt + \sqrt{2\kappa}\, dW_y(t)$$

to behave as follows: on a coarse scale, the cross-shear component of the path, $X(t)$, will approach (statistically) a Brownian motion. In this case, the cross-shear transport would be of diffusive type, and from our discussion in Sections 3.2.1 and 3.2.3, the random shear should produce superdiffusive scaling $\sigma_Y^2(t) \sim t^{1+\varepsilon/2}$ for $0 < \varepsilon < 2$. The contribution from u_y to the shear-parallel transport can be expected to be diffusive, and thus negligible relative to the contribution from the random shear. Therefore, the tracer in this nearly stratified system should behave in much the same way as in the Random Steady Shear Model with molecular diffusion, and the renormalized Green's function, using the same rescaling function $\rho(\delta) = \delta^{2/(2+\varepsilon)}$, should be of the same form (192). One change, however, is that the presence of the perturbation field $u_x(x, y)$ will enhance the cross-shear motion so that the effective shear-transverse diffusion constant at long time will be some value K_x^* greater than the bare molecular value κ. The factors of κ appearing in the formula for the renormalized Green's function stem from the shear-transverse diffusion, so they should self-consistently be replaced by the enhanced shear-transverse diffusivity K_x^*.

This picture is rigorously justified in [16]. Moreover, the effective shear-transverse diffusivity K_x^* can be obtained by solving a cell problem in the sense of homogenization theory, as in Section 2. Namely, let $\chi_x(x, y)$ be a suitable solution of

$$\kappa \Delta \chi_x(x, y) - u_x(x, y) \frac{\partial \chi_x(x, y)}{\partial x} - [v(x) + u_y(x, y)] \frac{\partial \chi_x(x, y)}{\partial y} = u_x(x, y) \ .$$

Then K_x^* is given by

$$K_x^* = \kappa (1 + \langle |\nabla \chi_x|^2 \rangle) \ .$$

The proof hinges on showing that an effective separation of scales between the diffusive cross-shear motion $X(t)$ and the superdiffusive shear-parallel motion $Y(t)$ exists. Namely, the superposition models should have the property that the $X(t)$ motion achieves its asymptotic statistical behavior on a time scale which is short with respect to the time scale on which superdiffusion occurs. Moreover, a crucial ingredient in this self-consistency argument is that sample-to-sample fluctuations in the velocity statistics should not affect the $X(t)$ motion; that is, the cross-shear motion should be completely self-averaging.

Some of the above technical assumptions can be relaxed without a change in the conclusion; see [16] for full details. It is also shown in that paper how the superdiffusive space–time scaling of the renormalized Green's function may be calculated for nearly stratified flows through a *rigorous* diagrammatic resummation of a perturbation expansion of the advection–diffusion equation with respect to the advective term. There is also interesting theoretical and computational work by Avellaneda et al. [8] with non-Gaussian eddy diffusivity equations for special steady random velocity fields defined by the "Manhattan grid".

3.4.3. Renormalized Green's functions for turbulent shear flows with very long-range spatio-temporal correlations

We have so far been considering tracer transport in a variety of random shear velocity fields, and found that the character of the long-range spatial and temporal correlations in the velocity field play a crucial role in determining the long-time behavior of an immersed tracer. Fully developed turbulent velocity fields at high Reynolds number have very strong long-range spatio-temporal correlations, and we have seen from explicit shear flow examples that tracers can exhibit a variety

of subtle and anomalous behavior in such flows. Long-range correlations are manifested in fully developed turbulence in a distinctive way: a wide range of scales, known as the *inertial range*, over which the velocity field exhibits statistical self-similarity. We first describe this feature, then seek to mimic it within our general class of Gaussian random shear flows.

3.4.3.1. Inertial range of fully developed turbulent flow. The inertial range was first predicted theoretically by Kolmogorov [169] in 1941 as a characteristic of a fully developed turbulent system which is maintained in a statistically stationary state (or "quasi-equilibrium") through external forcing at some characteristic length scale L_0 and dissipation by viscosity v. Kolmogorov utilized an intuitive picture of turbulence, introduced by Richardson [284], in which energy cascades from the relatively large scales at which it is injected down to ever smaller scales until viscous dissipation of energy ultimately sets in. The cascade process arises from nonlinear interactions between various turbulent velocity fluctuations, or "eddies", which tear apart large-scale structures into smaller ones. Kolmogorov introduced the key hypothesis that, away from boundaries, the small-scale structure of the flow should be largely independent of the large scale details, due to the mixing nature of the cascade. More precisely, he hypothesized that the only information communicated from the large scales is the rate of energy injection, which must be equal to the rate of energy dissipation $\bar{\varepsilon}$ in a statistically stationary state. The small-scale statistics $r \ll L_0$ of turbulence are therefore said to be *universal* in the Kolmogorov theory, since they do not depend on any of the large scale details other than the overall energy flux. From this universality hypothesis he deduced the existence of a distinguished length scale $L_K = (v^3/\bar{\varepsilon})^{1/4}$, which we will call the *Kolmogorov dissipation length scale*. He hypothesized that viscosity v plays an important role only on scales smaller than or comparable to L_K; on larger scales $r \gg L_K$, the velocity statistics should be independent of v. The Kolmogorov dissipation length scale L_K scales with Reynolds number Re as $L_0 \mathrm{Re}^{-3/4}$, so at sufficiently large Reynolds number there exists an *inertial range* of scales $L_K \ll r \ll L_0$ within which the velocity field statistics should depend only on the scale of interest r and the energy dissipation rate $\bar{\varepsilon}$.

From these hypotheses and dimensional analysis follows the Kolmogorov's "two-thirds law":

$$\langle |\boldsymbol{v}(\boldsymbol{x} + \boldsymbol{r}, t) - \boldsymbol{v}(\boldsymbol{x}, t)|^2 \rangle = \tilde{C}_K \bar{\varepsilon}^{2/3} |\boldsymbol{r}|^{2/3} \quad \text{for } L_K \ll |\boldsymbol{r}| \ll L_0 \;, \tag{196}$$

where $\tilde{C}_K$ is a universal numerical constant. The fact that the mean-square velocity difference over a distance r vanishes at a slower rate than r^2 implies that the velocity fluctuations are not smooth when viewed with a resolution within the inertial range of scales. The velocity field is in fact a fractal field [215,305] on scales within the inertial range. We return to this fractal aspect of turbulence in Sections 3.5 and 6.

It is often convenient to formulate the Kolmogorov theory in terms of the spectral density of energy $E(k)$ in wavenumber space. This energy spectrum is defined for general multidimensional flows with the same physical meaning as in our models with scalar random fields: $\int_{k-\Delta k}^{k+\Delta k} E(k') \, \mathrm{d}k'$ is the energy of the velocity field which would be measured if all fluctuations were filtered out except those with wavevector magnitudes within the band $k \pm \Delta k$ (see Paragraph 2.4.5.3). By analogous arguments, or through Fourier scaling, one arrives at Kolmogorov's "five-thirds law":

$$E(k) = C_K \bar{\varepsilon}^{2/3} k^{-5/3} \quad \text{for } L_0^{-1} \ll k \ll L_K^{-1} \;. \tag{197}$$

The universal numerical constant C_K appearing in this law is called the *Kolmogorov constant*. When the Reynolds number is large, the regime of power law scaling extends over a range of wavenumbers proportional to $Re^{3/4}$. This means that the velocity fluctuations are active and self-similar over a wide range of scales. The Kolmogorov inertial range scaling predictions (197) and (196) are quite well established experimentally, with a Kolmogorov constant $C_K \approx 1.5$ (see [307] for a review).

Another consequence of Kolmogorov's theory is the association of an *eddy turnover time* scale

$$\tau_e(k) = \bar{\varepsilon}^{-1/3} k^{-2/3} \tag{198}$$

to each inertial-range wavenumber k. This is just the natural advective time scale of an eddy of size k^{-1}, with velocity on the order of $\bar{\varepsilon}^{1/3} k^{-1/3}$. It may also be thought of as an estimate for the time it takes for an inertial range eddy to be torn up into smaller eddies. According to the Kolmogorov hypotheses, the eddy turnover time is the only relevant time scale for an inertial range eddy, and so the spatio-temporal energy spectrum must have the following universal inertial-range form:

$$\tilde{E}(k, \omega) = E(k)\phi(\omega\tau_e(k))\tau_e(k) = C_K \bar{\varepsilon}^{1/3} k^{-7/3} \phi(\omega\bar{\varepsilon}^{-1/3} k^{-2/3}) \quad \text{for } L_0^{-1} \ll k \ll L_K^{-1}, \tag{199}$$

where $\phi(\cdot)$ is a universal, nonnegative function with $\int_{-\infty}^{\infty} \phi = 1$. This complete spatio-temporal Kolmogrov inertial-range theory is much more difficult to assess empirically. A competing theory for the temporal dynamics for the inertial range will be mentioned below.

Mathematical modelling of spatio-temporal spectrum of Kolmogorov type. For the moment, we proceed to construct a mathematical model for an energy spectrum which contains an inertial range conforming to Kolmogorov's theory. The inertial range is described by Eq. (199), and we must only specify the form of $\tilde{E}(k, \omega)$ outside the self-similar scaling range. At very large wavenumbers $k \gg L_K^{-1}$, the velocity fluctuations are rapidly dissipated by viscosity, and the energy spectrum decays rapidly. The energy spectrum must vanish at sufficiently small wavenumbers $k \ll L_0^{-1}$ because of the finite size of the system.

We are therefore motivated to define the following model for the spatio-temporal energy spectrum corresponding to a turbulent flow with a Kolmogorov inertial range:

$$\tilde{E}(k, \omega) = E(k)\tau(k)\phi(\omega\tau(k)), \tag{200a}$$

where

$$E(k) = C_K \bar{\varepsilon}^{2/3} k^{-5/3} \psi_0(kL_0)\psi_\infty(kL_K), \tag{200b}$$

$$\tau(k) = \tau_e(k) = \bar{\varepsilon}^{-1/3} k^{-2/3}. \tag{200c}$$

The new parameters and auxiliary functions appearing here have the following meaning and properties:

- ψ_0 is the infrared (low wavenumber) cutoff, a smooth, nonnegative function on the positive real axis vanishing in a neighborhood of the origin,
- ψ_∞ is the ultraviolet (high wavenumber) cutoff, a smooth, nonnegative function on the positive real axis, decaying faster than any power, with $\psi_\infty(k') = 1 + O(k'^2)$ near the origin,
- $\phi(\varpi)$ describes the temporal component, and is assumed to be a non-negative, bounded, smooth, even function, decaying at least as fast as $|\varpi|^\gamma$ for some $\gamma > 1$. Moreover, we demand that $\phi(0) > 0$ and $\int_{-\infty}^{\infty} \phi(\omega')\,d\omega' = 1$.

The model assumes that the velocity field statistics continue to be isotropic on the large scales, which certainly is not true; but we are not attempting to account for system-dependent large-scale features of the velocity field here. Also, $\tau(k)$ should cross over to a different dependence on wavenumber outside the inertial range, but there is little point in introducing this extra complexity here. To maintain the parlance of physical discussions of turbulence, we will sometimes refer to L_0 as the "integral length scale" of the velocity field, though in our model it differs from the technical definition [320] of this term by a constant of order unity in the high Reynolds number limit.

We can build a simple shear model with a Kolmogorov type inertial range by simply defining a Gaussian random shear flow $v(x, t)$ using the spatio-temporal energy spectrum (200) through the formula (153). It can be checked explicitly that such the velocity differences will exhibit the Kolmogorov inertial range scaling:

$$\langle(v(x' + x, t) - v(x', t))^2\rangle = \tilde{C}_K \bar{\varepsilon}^{2/3}|x|^{2/3} \quad \text{for } L_K \ll x \ll L_0 \;,$$

for some universal constant $\tilde{C}_K$ proportional to C_K. Of course, such a shear model differs geometrically from fully developed turbulence in that the latter is usually modelled as statistically isotropic. The shear model has the advantage, however, of being mathematically tractable in the context of turbulent diffusion, and we will see that it sheds light on a number of physically relevant issues regarding the effects of a wide inertial range on turbulent diffusion.

The reader will note the formal similarity between the Kolmogorov model spectrum (200) and the Random Spatio-Temporal Shear (RSTS) Model in Section 3.3 with parameter values $\varepsilon = 8/3$ and $z = 2/3$. The key difference is that the power law scaling of the Kolmogorov energy spectrum has $\varepsilon > 2$, and is cut off at the low wavenumber L_0^{-1}. This cutoff is essential for the energy

$$E = \frac{1}{2}\langle(v(x, t))^2\rangle = \int_0^\infty E(k)\,dk$$

to be finite; the $L_0 \to 0$ limit is singular.

We will next widen the spatio-temporal energy spectrum model for fully developed turbulence from the strict Kolmogorov picture (200) to include intermittency corrections and alternate theories for the temporal correlations. This will motivate the consideration of modified RSTS models with more general values of $\varepsilon > 2$ and $z > 0$.

Intermittency corrections. Although the Kolmogorov form for the spatial energy spectrum $E(k)$ mentioned above agrees quite well with experimental data, it is of theoretical interest to consider a more general self-similar inertial-range power law behavior of the form

$$E(k) = C_K \bar{\varepsilon}^{2/3} k^{-5/3}(kL_0)^{\alpha_1}(kL_K)^{\alpha_2} \quad \text{for } L_0^{-1} \ll k \ll L_K^{-1} \;. \tag{201}$$

Here, the asymptotically small parameters $(kL_0)^{-1}$ and (kL_K) are permitted to enter the inertial-range asymptotic form via power laws with exponents α_1 and α_2, which if nonzero, are referred to as *anomalous exponents*. In the terminology of Barenblatt [24,25], Kolmogorov's hypothesis (200) is completely self-similar with respect to the inertial range limit while the more general hypothesis (201) is *incompletely* self-similar. The anomalous exponents will always be assumed to satisfy

$$-\tfrac{4}{3} < \alpha_1 + \alpha_2 < \tfrac{2}{3} \;, \tag{202}$$

which ensures that energy is concentrated at low wavenumber, dissipation is concentrated at high wavenumber, and a physical-space self-similar inertial range scaling regime exists within $L_K \ll r \ll L_0$.

In real-world turbulence, the issue of anomalous scaling is much more important in discussions of higher-order statistics of the velocity field than in the second-order statistics (as reflected in $E(k)$) [309]. There remain, however, suggestions [34,72] that the inertial range form of the energy spectrum may have "intermittency corrections" of the form (201), with $\alpha_2 = 0$ and α_1 small (on the order of 0.03). A different incomplete self-similarity hypothesis for the inertial-range has recently been formulated [26], but we will not consider it here. Our purpose is only to introduce the flavor of anomalous corrections to inertial range scaling into our shear flow models, and examine their effects on turbulent diffusion.

In the presence of intermittency corrections, the natural eddy turnover time $\tau_e(k)$, defined as the ratio of the length scale k^{-1} and velocity scale of the eddy, is altered from the Kolmogorov definition (198). The mean-square velocity of an inertial-range eddy of length scale k^{-1} scales as $E(k)k$, so with Eqs. (200a), (200b) and (200c), we define the eddy turnover time in the presence of intermittency corrections as

$$\tau_e(k) = \frac{k^{-1}}{\sqrt{C_K \bar{\varepsilon}^{2/3} k^{-2/3} (kL_0)^{\alpha_1} (kL_K)^{\alpha_2}}} = C_K^{-1/2} \bar{\varepsilon}^{-1/3} k^{-2/3} (kL_0)^{-\alpha_1/2} (kL_K)^{-\alpha_2/2} \ . \tag{203}$$

Alternative temporal decorrelation theories. Whether the eddy turnover time $\tau_e(k)$ truly sets the decorrelation rate of inertial range eddies has come into question, starting with some papers of Kraichnan [176] and Tennekes [319]. It is pointed out that beyond the inertial breakdown of eddies, the velocity field observed at a given point will see a decorrelating influence from the *sweeping* of eddies by strong, large-scale velocity components. The influence of an eddy of wavenumber k on a given point in space will, according to this notion, effectively cease once the eddy is carried away through advection by large scale eddies. An estimate for this *sweeping time* scale is

$$\tau_s(k) = (v_0 k)^{-1} \ , \tag{204}$$

where v_0 is the single-point root-mean-square magnitude of the turbulent velocity field. If we extrapolate the Kolmogorov inertial-range scaling of the velocity of eddies, we would expect v_0 to typically be on the order of $\bar{\varepsilon}^{1/3} L_0^{1/3}$, in which case the sweeping time $\tau_s(k)$ would be shorter than the eddy turnover time $\tau_e(k)$. This would appear to suggest that sweeping is the dominant decorrelation mechanism, so that the eddy correlation time $\tau(k)$ should be set equal to $\tau_s(k)$ instead of $\tau_e(k)$ in the inertial range of wavenumbers. The same conclusion holds true in the presence of intermittency corrections, as will be clear when we nondimensionalize later.

Whether the sweeping effect really has this decorrelating influence has not been conclusively decided; we refer the reader to [60,273,345] for theoretical, numerical, and experimental investigations along this line. We only wish to mention this issue here, but will not dwell on it. To cover both possibilities, we will simply assume that $\tau(k)$, the correlation time of an eddy of wavenumber k, has some scaling law:

$$\tau(k) = A_\tau k^{-z} \ ,$$

where $z > 0$ and A_τ is some positive constant. The exponent $z = 2/3$ corresponds to the strict Kolmogorov theory, and $z = 1$ corresponds to the decorrelation by large-scale sweeping. Because we have embedded both possibilities into our model, we can draw distinctions concerning how the passive scalar statistics will differ under these two competing hypotheses. Our results are only guaranteed to be true for the model flows considered, but one can hope to obtain some understanding for the physical mechanisms and qualitative effects at work, and consider which of these may apply in more general situations. We note that for a shear flow, there is no direct physical mechanism for decorrelation by large-scale sweeping unless a cross-shear sweep, such as $w_f(t)$, is present.

3.4.3.2. Basic considerations concerning large-scale effective diffusivity. To illustrate some of the issues involved in computing the effective evolution of a passive scalar field in a turbulent flow, we construct a cartoon model founded on shear flows. We will refer to this model as the *Random Spatio-Temporal Shear flow with Inertial Range*, or RSTS-I Model for short. The velocity field is taken to be a parallel superposition of a two-dimensional steady, large-scale mean shear flow $U(x)$ and a turbulent small-scale component $v(x, t)$, with a temporally fluctuating cross sweep $w_f(t)$:

$$\boldsymbol{v}(x, z, t) = \begin{bmatrix} w_f(t) \\ U(x) + v(x, t) \end{bmatrix} . \tag{205}$$

The cross-sweep $w_f(t)$ will be modelled as a mean zero, Gaussian, stationary random process as in the Random Sweeping Model of Section 3.1.2, with

$$R_w(t) \equiv \langle w_f(t')w_f(t + t') \rangle = 2 \int_0^\infty \cos(2\pi\omega t)E_w(|\omega|)\,d\omega \;,$$

$$E_w(\omega) = A_{E,w}\omega^{-\beta}\psi_w(\omega) \;.$$

The turbulent shear flow $v(x, t)$ is a Gaussian, homogenous, stationary, mean zero random field with correlation function

$$\tilde{R}(x, t) \equiv \langle v(x', t')v(x + x', t + t') \rangle = \int_{-\infty}^\infty \int_{-\infty}^\infty e^{2\pi i(kx + \omega t)}\tilde{E}(k, \omega)\,dk\,d\omega$$

and spatio-temporal energy spectrum $\tilde{E}(k, \omega)$ taken to be of the high Reynolds number form, with intermittency corrections, discussed above:

$$\tilde{E}(k, \omega) = E(|k|)\tau(|k|)\phi(\omega\tau(|k|)) \;, \tag{206a}$$

$$E(k) = C_K\bar{\varepsilon}^{2/3}k^{-5/3}(kL_0)^{\alpha_1}(kL_K)^{\alpha_2}\psi_0(kL_0)\psi(kL_K) \;, \tag{206b}$$

$$\tau(k) = A_\tau k^{-z} \;. \tag{206c}$$

Finally, the mean shear flow is taken to be either linear or a sinusoid:

$$U(x) = \begin{cases} \gamma x \;, \\ \bar{v}\sin(2\pi x/\bar{L}) \;. \end{cases} \tag{207}$$

It will be helpful to think of the linear shear coefficient γ as the ratio of a certain velocity $\bar{v}$ and length scale $\bar{L}$ characterizing the turbulent system.

The shear-parallel tracer motion due to the mean shear and the turbulent shear field are simply additive, since they do not act across each other's gradient. To better assess their relative magnitude, it is helpful to first nondimensionalize with respect to the (large) scale of the turbulent system.

Nondimensionalization. We think of the mean shear flow $U(x)$, the fluctuating cross-sweep $w_f(t)$, and the turbulent shear flow $v(x, t)$ as being produced by forces of comparable scale. It is therefore natural in our model to equate the mean-square turbulent velocity $v_0 = \langle v^2(x, t) \rangle^{1/2}$ with the velocity scale $\bar{v}$ of the mean flow, and to equate the outer length scale L_0 of the turbulent flow with the length scale $\bar{L}$ of the mean flow. The turbulent fluctuations will then be active over a wide range of scales extending from the system scale $L_0 = \bar{L}$ down to the Kolmogorov dissipation scale L_K. We are assuming a high Reynolds number flow so that $L_K \ll L_0$, and a substantial inertial range exists. Moreover, we equate the magnitude of the cross-sweep velocity $w_f(t)$ with $\bar{v}$ and the time scale of its fluctuations with the natural time macroscale $\bar{L}/\bar{v}$. The initial passive scalar density is assumed to vary on the macroscale $\bar{L}$, and to have total mass M. We then use $L_0 = \bar{L}$, $\bar{v} = v_0$, and M as our reference units for nondimensionalization. This implies that the reference time scale is $\tau_0 = L_0/v_0$.

Temporarily, we will use a superscript $'$ to denote a nondimensionalized variable and a superscript $\circ$ to denote a nondimensionalized function. To nondimensionalize the turbulent shear flow, we note first that

$$v_0^2 = 2 \int_0^\infty E(k) \, dk = c_1 C_K \bar{\varepsilon}^{2/3} L_0^{2/3} (L_K/L_0)^{\alpha_2} , \tag{208}$$

where symbols c_j will denote dimensionless positive numerical constants depending only weakly on Reynolds number in the sense that they approach finite positive limits as $\text{Re} \to \infty$. The constants c_j also depend on the scaling exponents α_1, α_2, and z, and on the dimensionless auxiliary functions ψ_0, ψ_∞, and ϕ. As a consequence of Eq. (208), the energy spectrum may be written in terms of L_0 and v_0 as

$$E(k) = c_1^{-2} v_0^2 L_0^{-2H} k^{-1-2H} \psi_0(kL_0) \psi_\infty(kL_K) , \tag{209}$$

where we have defined the *Hurst exponent* as

$$H = \tfrac{1}{3} - (\alpha_1 + \alpha_2)/2 .$$

The reason we call H the Hurst exponent is that $\langle (v(x' + x) - v(x'))^2 \rangle$ scales self-similarly as $|x|^{2H}$ over the inertial range of scales $L_K \ll x \ll L_0$, and the Hurst exponent is defined in just this way for self-similar (or more properly "self-affine") fractal random fields (see [215,216]). The restriction on the intermittency exponents (202) is equivalent to $0 < H < 1$. From Eq. (209), it follows that the energy spectrum nondimensionalized to large scales takes the appealingly simple form

$$E^\circ(k') = (v_0^{-2} L_0^{-1}) E(k' L_0^{-1}) = c_1^{-2} (k')^{-1-2H} \psi_0(k') \psi_\infty(k' l_K) ,$$

where

$$l_K \equiv L_K/L_0 .$$

It is often desirable to relate this ratio of the Kolmogorov dissipation length scale L_K and the integral length scale L_0 to the Reynolds number:

$$\text{Re} = v_0 L_0 / v$$

characterizing the flow, where v is the kinematic viscosity. In the Kolmogorov theory, Re is proportional to $(L_0/L_K)^{4/3}$; this law must however be modified in the presence of intermittency corrections. To compute Re, we need an expression for v in terms of the model parameters. This is obtained by using the definition of the mean energy dissipation rate $\bar{\varepsilon}$

$$\bar{\varepsilon} \equiv v \left\langle \left| \frac{\partial v(x,t)}{\partial x} \right|^2 \right\rangle = 4\pi^2 v \int_0^\infty k^2 E(k)\, dk \ .$$

Substituting Eq. (206b) into this expression, we find

$$v = c_2 C_K^{-1} \bar{\varepsilon}^{1/3} L_K^{4/3} (L_K/L_0)^{\alpha_1} \ .$$

The Reynolds number is now computed to scale with $l_K \equiv L_K/L_0$ as follows:

$$\text{Re} = c_3 C_K^{3/2} l_K^{-4/3 - \alpha_1 + \alpha_2/2} \ . \tag{210}$$

We now only need to nondimensionalize the eddy decorrelation time $\tau(k)$. To estimate how A_τ relates to the system scale, we consider the two natural cases in which $\tau(k)$ is the eddy turnover time $\tau_e(k)$ (203) or the sweeping time $\tau_s(k)$ (204). Using Eq. (208), we can express these time scales as

$$\tau_e(k) = c_1^{1/2} L_0^H v_0^{-1} k^{-1+H}, \tag{211a}$$

$$\tau_s(k) = v_0^{-1} k^{-1} \ , \tag{211b}$$

and their large-scale nondimensionalizations are

$$\tau_e^\circ(k') = (v_0/L_0)\tau_e(k' L_0^{-1}) = c_1^{1/2} k'^{-1+H} \ ,$$

$$\tau_s^\circ(k') = (v_0/L_0^{-1})\tau_s(k' L_0^{-1}) = k'^{-1} \ .$$

Since $\tau(k)$ is supposed to generalize the behavior of these natural sweeping times, we can take its nondimensionalized form as

$$\tau^\circ(k') = k'^{-z} \ ;$$

we do not bother with a possible order unity preconstant.

We can finally write the spatiotemporal energy spectrum, nondimensionalized to the system space–time scales L_0 and $\tau_0 = L_0/v_0$, dropping the $'$ and $\circ$ superscripts, as

$$\tilde{E}(k, \omega) = E(|k|)\tau(|k|)\phi(\omega\tau(|k|)) \ , \tag{212a}$$

$$E(k) = c_1^{-2} k^{-1-2H} \psi_0(k)\psi(k l_K) \ , \tag{212b}$$

$$\tau(k) = k^{-z} \ , \tag{212c}$$

where l_K may be related to the Reynolds number through Eq. (210).

The nondimensionalization of the mean shear flow (207) is directly seen to be

$$U(x) = \begin{cases} x \\ \sin(2\pi x) \ . \end{cases} \tag{213}$$

Since the cross-sweep $w_f(t)$ is assumed to vary also on the same scales, its nondimensionalized correlation function $R_w(t)$ has amplitude and scale of variation both of order unity. The nondimensionalized initial data $T_0(x, y)$ is similarly an order unity function.

The molecular diffusion coefficient, nondimensionalized to the macroscale, may be identified as the inverse of the *Péclet number*,

$$\mathrm{Pe} = L_0 v_0 / \kappa \ .$$

This definition of Péclet number is consistent with the one used in Section 2.4 (see Eq. (81)), up to a factor which approaches a constant of order unity in the high Reynolds number limit.

Challenges of modelling effective large-scale passive scalar behavior. We can now write down the advection–diffusion equation, nondimensionalized with respect to the system length macroscale L_0 and time macroscale τ_0:

$$\frac{\partial T(x, y, t)}{\partial t} + w_f(t) \frac{\partial T(x, y, t)}{\partial x} + U(x) \frac{\partial T(x, y, t)}{\partial y} + v(x, t) \frac{\partial T(x, y, t)}{\partial y} = \mathrm{Pe}^{-1} \Delta T(x, y, t) \ , \tag{214}$$

$$T(x, y, t = 0) = T_0(x, y) \ .$$

The nondimensionalized mean flow $U(x)$ is given by Eq. (213), the nondimensionalized spatio-temporal energy spectrum of the turbulent shear flow $v(x, t)$ is given by Eqs. (212a), (212b) and (212c), and the nondimensionalized correlation function $R_w(t)$ of the random cross sweep $w_f(t)$ is an order unity function. A key observation from this nondimensionalization is that the advective processes due to both the mean and turbulent components of the flow are of order unity with respect to the system macroscales. The Reynolds number enters only in the energy spectrum (212b) through the nondimensionalized Kolmogorov dissipation scale l_K and weakly through the non-dimensional preconstant c_1. On the other hand, the Péclet number Pe can often be large in fully developed flows, making the molecular contribution formally subdominant (away from boundaries) to the turbulent advection in Eq. (214). We know, however, from our discussions in Sections 2 and 3 that the presence of even a small amount of molecular diffusion can have subtle effects on large-scale passive scalar transport in certain flow configurations.

A key goal of turbulence modelling is obtaining an effective equation for the mean concentration density $\langle T(x, y, t) \rangle$ which is at least approximately valid on the system scale. One wishes to account for the important effects which the random fluctuations have on the system scale, without resolving the fluctuations explicitly in detail. We can make some partial progress toward this end in the presently stated model, because we can exactly compute the effective diffusivity of a single tracer, defined as half the time rate of change of its variance in position (along a given direction). The effective diffusivity in the cross-shear direction is determined by the sweeping (111):

$$D_x(t) \equiv \frac{1}{2} \frac{\mathrm{d} \langle \sigma_x^2(t) \rangle}{\mathrm{d}t} = \mathrm{Pe}^{-1} + \int_0^t R_w(s) \, \mathrm{d}s \ .$$

The effective diffusivity along the shearing direction is obtained by simply summing the contributions of molecular diffusion, the mean shear flow, and the random shear flow, taking into account the cross-shear transport:

$$D_y(t) \equiv \frac{1}{2}\frac{\mathrm{d}\langle \sigma_X^2(t)\rangle}{\mathrm{d}t} = \mathrm{Pe}^{-1} + \bar{D}_y(x,t) + \tilde{D}_y(t) \ .$$

A linear mean shear flow $U(x) = x$ contributes a shear-parallel diffusivity [31,258]:

$$\bar{D}_{y,\mathrm{lin}}(t) = \mathrm{Pe}^{-1}t^2 + t\int_0^t (t-s)R_w(s)\,\mathrm{d}s \ , \tag{215}$$

whereas a sinusoidal mean shear flow $U(x) = \sin 2\pi x$ contributes

$$\bar{D}_{y,\mathrm{sin}}(x_0, t) = \frac{1}{2}\int_0^t e^{-2\pi^2\sigma_X^2(s)}\,\mathrm{d}s - \frac{1}{2}(\cos 4\pi x_0)e^{-2\pi^2\sigma_X^2(t)}$$

$$\times \int_0^t \exp\left[-2\pi^2\left(\sigma_X^2(s) + 4\mathrm{Pe}^{-1}s + 2\int_0^t\int_0^s R_w(s'-s'')\,\mathrm{d}s'\,\mathrm{d}s''\right)\right]\mathrm{d}s$$

$$- \frac{1}{2}(\sin^2 2\pi x_0)\,e^{-2\pi^2\sigma_X^2(t)}\int_0^t e^{-2\pi^2\sigma_X^2(s)}\,\mathrm{d}s \ , \tag{216}$$

both of which may be computed by a generalization of the method presented in Section 2.3.1. Finally, the effective diffusion due to the turbulent shear fluctuations (157) is

$$\tilde{D}_y(t) = \kappa + 4\int_0^\infty\int_0^\infty \tilde{E}(k,\omega)\tilde{K}(k,\omega,t)\,\mathrm{d}\omega\,\mathrm{d}k \ ,$$

$$\tilde{K}(k,\omega,t) = \int_0^t e^{-2\pi^2k^2\sigma^2_x(s)}\cos(2\pi\omega s)\,\mathrm{d}s \ . \tag{217}$$

All these effective diffusivities are time-dependent and of order unity in units nondimensionalized to the macroscale. Observe, however, that the diffusivity along a linear mean shear (215) grows unboundedly in time whereas the diffusivity due to a sinusoidal mean shear (216) saturates to a finite positive value for large nondimensional times $t \gg 1$. The turbulent diffusivity (217) also saturates to a finite value for $t \gg 1$ by virtue of the energy spectrum having a low wavenumber cutoff at a length scale of order unity in nondimensionalized units; see Eqs. (212a), (212b) and (212c).

It is also important to note that the mean position of a tracer will respond to the presence of a mean shear. For a linear mean shear flow,

$$V_Y(t) \equiv \mathrm{d}\langle Y(t)\rangle/\mathrm{d}t = x_0 \ ,$$

whereas for a sinusoidal mean shear flow,

$$V_Y(t) \equiv \mathrm{d}\langle Y(t)\rangle/\mathrm{d}t = \sin 2\pi x_0\, e^{-2\pi^2\sigma_X^2(t)} \ .$$

The mean tracer velocity in this latter cases rapidly decays, and the mean tracer displacement saturates to a finite value.

Now, it may be tempting to formulate an advection–diffusion equation for the mean passive scalar field $\langle T(x, y, t)\rangle$ of the form

$$\frac{\partial\langle T(x, y, t)\rangle}{\partial t} + V_Y(t)\frac{\partial\langle T(x, y, t)\rangle}{\partial y} = D_x(t)\frac{\partial^2\langle T(x, y, t)\rangle}{\partial x^2} + D_y(x, t)\frac{\partial^2\langle T(x, y, t)\rangle}{\partial y^2},$$

$$\langle T(x, y, t = 0)\rangle = \langle T_0(x, y)\rangle.$$

Or perhaps one may explicitly retain the mean flow $U(t)$ in the advection, and simply include the turbulent contributions to $D_x(t)$ and $D_y(x, t)$ in the diffusion coefficients in the PDE. Indeed, we saw in Section 2 that effective equations of this type, with time-independent diffusion coefficients, do rigorously describe the effective behavior of the mean passive scalar field on large scales at long times for random flows with short-range correlations. Also, we saw in Section 3.1.2 that the evolution of the mean statistics were precisely described, even in anomalous diffusion regimes, by a time-dependent diffusion equation in the Random Sweeping Model.

In the present situation, however, the reasoning leading to such simplified effective evolution equations for the mean statistics $\langle T(x, y, t)\rangle$ break down. The key difficulty is that the excited scales of turbulent motion extend over a continuous range from the small scale $l_K \sim \mathrm{Re}^{-3/4 + IC}$ (where "IC" denotes intermittency corrections) up to the macroscale of the system. It is on this macroscale that we wish to pose the effective evolution equation, and there is no scale separation between it and the active scales of the turbulence. This is why homogenization theory cannot be directly applied. The failure of separation of scales is particularly acute for turbulence spectra with $\varepsilon > 2$ (which includes the Kolmogorov value $\varepsilon = 8/3$), because these have very strong long range correlations and require the presence of the infrared cutoff $\psi_0(\cdot)$ to keep the energy finite.

Another delicate issue is that the time scale at which the turbulent diffusivity saturates to its asymptotic value is comparable to the natural time-scale associated to the macroscale dynamics. This suggests that any effective turbulent diffusivity should generally be expected to be time-dependent, as in the Random Sweeping Model described in Section 3.1.2. Because of the spatial variability of the shear interacting with the fluctuating cross-sweep, however, the tracer displacements cannot be expected to obey an approximately Gaussian distribution after order unity times. A proper effective evolution equation for $\langle T(x,y,t)\rangle$ therefore need not be a standard diffusion equation with time-dependent diffusivities.

In efforts to address the challenge of modelling the large-scale effects of turbulence active over a wide range of scales, a wide variety of *renormalized perturbation theories* [177,285] involving partial summation of divergent perturbation series which mimic ideas from field theory and renormalization group (R-N-G) theories [300,286,344] inspired from critical phenomena have been proposed. We shall now briefly discuss some rigorous mathematical work concerning effective evolution equations for the mean statistics in a simplifed shear model [10,14] which can be used as a basis for testing the various renormalized perturbation theories [13,17,300].

3.4.3.3. Renormalized Green's functions for random shear flows on large scales within inertial range. Avellaneda and the first author considered the problem of computing the large-scale effective turbulent diffusion for a family of random spatio-temporal shear flows with energy spectra of the type (206), parametrized by scaling exponents ε and z. They found it convenient to nondimensionalize with respect to the Kolmogorov dissipation length scale L_K and dissipation

time scale, rather than with respect to the system macroscales as above. In this formulation, the nondimensionalized value δ^{-1} of the integral length scale L_0 of the turbulent velocity field diverges with Reynolds number: $\delta^{-1} \sim \mathrm{Re}^{3/4 + \mathrm{IC}}$. Since the macroscale of the passive scalar field naturally coincides with the macroscale of the velocity field in most applications, the (nondimensionalized) initial data is rescaled along with the integral length of the velocity field:

$$T_0^{(\delta)}(x, y) \equiv T_0(\delta x, \delta y) \ . \tag{218}$$

The central goal in turbulent diffusion modelling at high Reynolds number is to obtain an effective description of the evolution of $\langle T^{(\delta)}(x, y, t) \rangle$ on the system macroscale in the $\delta \to 0$ limit, where $T^{(\delta)}(x, y, t)$ is the passive scalar field evolving from initial data (218) in a turbulent velocity field with integral length scale δ^{-1}.

The first issue is finding the proper space–time rescaling. Clearly, the nondimensionalized space variable must be rescaled by δ, the macroscale of both the velocity field and the initial data. But unlike standard homogenization theory, the proper time rescaling is not necessarily linked to this spatial rescaling through the usual diffusive relation. Instead, one seeks a more general temporal rescaling function $\rho(\delta)$ for which a finite and nontrivial limit,

$$\bar{T}(x, y, t) \equiv \lim_{\delta \to 0} \left\langle T^{(\delta)}\left(\frac{x}{\delta}, \frac{y}{\delta}, \frac{t}{\rho^2(\delta)}\right) \right\rangle \ ,$$

exists. The usual diffusive rescaling corresponds to $\rho(\delta) = \delta$. Note that the renormalization differs here from that discussed generally at the beginning of Section 3.4 in that the turbulent velocity field also depends on δ, which is equated to its nondimensionalized integral length scale.

Once the proper choice of $\rho(\delta)$ is established, one strives to compute the equation satisfied by $\bar{T}(x, y, t)$. This may be viewed as a generalized "eddy diffusivity" equation for the high Reynolds number limit, since the effect of all the small scales $\delta \lesssim k \lesssim 1$ of the velocity field on the macroscale have been incorporated into an effective equation involving only the large scales. To stress that the equation for $\bar{T}(x, y, t)$ is not always of the form of a standard diffusion equation, we will refer to it by the general appellation of "eddy-renormalized equation". In any event, the fundamental solution to this eddy-renormalized equation may be identified as the renormalized Green's function.

This program has been rigorously carried out for the spatio-temporal shear flow models (206), with zero cross sweep [10] and a constant cross sweep [14]. The effects of molecular diffusion are also taken into account. A variety of possible effective equations arise, depending on the parameters $-\infty < \varepsilon < 4$ and $z > 0$ of the turbulent spatio-temporal energy spectrum, and these can be described by a phase diagram similar to those displayed in Section 3.3. The rigorous renormalization theory for the case of no cross sweep ($w(t) = 0$) involves five distinct phase regions in the ε, z plane. To each phase region corresponds a temporal rescaling function $\rho(\delta) = \delta^\zeta$ with a distinctive algebraic law for the exponent ζ in terms of ε and z, and an eddy-renormalized equation for the mean passive scalar density. It is readily checked that the renormalized mean-square tracer displacement

$$\langle \bar{Y}^2(t) \rangle = \lim_{\delta \to 0} \delta^{-2} \left\langle \left(Y^\delta\left(\frac{t}{\rho^2(\delta)}\right) \right)^2 \right\rangle \ ,$$

scales as $t^{1/\zeta}$. Therefore, as in Section 3.3, the exponent ζ may be viewed as an order parameter describing "phase transitions" across the boundaries of the phase regions. The effective equation within each phase region has a distinctive form, though the coefficients within each region depend smoothly on the parameters ε and z. We will simply sketch the main qualitative points, and later, in Section 3.5.4, illustrate the renormalization procedure itself in the simpler context of the pair distance function.

One phase region in the phase diagram for the renormalized mean passive scalar density corresponds to a situation in which ordinary homogenization theory applies: $\rho(\delta) = \delta$, the eddy-renormalized diffusivity equation for $\bar{T}(x, y, t)$ is an ordinary diffusion equation with a constant, turbulence-enhanced diffusion coefficient (166a), and the renormalized Green's function is Gaussian. This is exactly the region D of Fig. 14 in which the long-range correlations of the velocity field are not strong enough to create anomalous behavior. Note in particular that this diffusive regime lies exclusively outside the parameter range $2 < \varepsilon < 4$ corresponding to velocity fields with a physical-space inertial scaling range.

All the other phase regions support superdiffusion of the passive scalar field ($\zeta < 1$). One of the phase regions for the renormalized mean passive scalar field coincides exactly with the SD-κ phase region of Fig. 14. The renormalized Green's function for this region is exactly the one discussed for a steady random shear flow with $0 < \varepsilon < 2$ in Paragraph 3.4.1.2. Indeed, the decorrelation of shear-parallel transport is set in the SD-κ region by molecular diffusion, and the role of temporal fluctuations in the shear flow plays a negligible role at large space and time scales. It is therefore not surprising that the eddy-renormalized equation coincides over this whole region with that for the steady case. The eddy-renormalized equation corresponding to this non-Gaussian renormalized Green's function is nonlocal. The presence of the infrared cutoff ψ_0 plays no role in the renormalization for the SD-κ phase region, and does not appear in the eddy-renormalized equation.

The situation is a bit more subtle for the other three superdiffusive phase regions. The eddy-renormalized equations for these regions take the form of diffusion equations with constant or time-dependent diffusion coefficients. The presence of molecular diffusion is irrelevant on the large scales for all three of these regions. At the boundaries between the phase regions, the eddy-renormalized equation takes special forms which cross over between those on each side of the boundary. It is very interesting that the analogue of the Kolmogorov spectrum in the shear model occurs at the point $\varepsilon = 8/3$, $z = 2/3$, which lies on the boundary between two of the superdiffusive regimes. In one of these regimes, the Eulerian temporal decorrelation of the velocity field is the dominant influence on the large-scale, long-time tracer transport, and the superdiffusively renormalized Green's function satisfies an effective diffusion equation with diffusion coefficient given by a Kubo formula; see Section 2.4.1. The point $(\varepsilon, z) = (8/3, 1)$ corresponding to the alternative sweeping temporal decorrelation hypothesis falls in this Kubo region. In the other superdiffusive regime adjacent to the Kolmogorov point $(\varepsilon, z) = (8/3, 2/3)$, the temporal dynamics of the velocity field are by contrast completely irrelevant in determining the large-scale, long-time motion of the tracer. This is the regime corresponding to an energy spectrum with intermittency corrections reducing the value of ε (this matches the conventional wisdom for the sign of intermittency corrections, if they exist [34]). More generally, we see that the renormalized mean passive scalar statistics in the RSTS-I Model are very sensitive to intermittency corrections of the Kolmogorov theory. In [15], it was rigorously shown that these features of the phase diagram for the renormalized Green's function near the Kolmogorov point carry over rigorously to random, *isotropic* turbulent flows with spatio-temporal energy spectrum (206).

Note that there is no contradiction in the fact that the renormalized Green's function in the superdiffusive "Kubo" regime is described by an ordinary diffusion equation. The reason for the difference between the superdiffusive space–time scaling relations of the renormalization group and the diffusive space–time scaling of the renormalized equation can be traced to the linking of the infrared cutoff $\psi_0(\delta k)$ defining the energy spectrum with the observation scale δ^{-1}. This infrared cutoff breaks the symmetry of the renormalized equations with respect to the renormalization group of scalings [10]. The sensitivity of the large-scale behavior of the *mean passive scalar density* to the infrared cutoff is consistent with the well-known fact that the mean passive scalar statistics are strongly influenced by the large scales of a turbulent velocity field [196]. For an explicit numerical demonstration in a simple context, the reader may consult [141]. Only second order statistical quantities, such as the "pair distance function" which involve relative diffusion of a pair of tracers, can be expected to exhibit universal behavior which is independent of the details of the large scales. We discuss this issue in greater length in Section 3.5.

The presence of the infrared cutoff in Eqs. (206a), (206b) and (206c) also leads to a departure of the renormalized phase diagram from that presented in Fig. 14 for the mean-square tracer displacement in a random shear flow with no infrared cutoff in the spatio-temporal energy spectrum. Namely, the SD-ω region of Fig. 14 does not renormalize as a single unit with the temporal rescaling $\rho(\delta) \sim \delta^{z/(\varepsilon + 2z - 2)}$. This choice of temporal rescaling leads to a proper high Reynolds number renormalization only for part of the SD-ω region; the rest falls within another phase region (corresponding to the Kubo-like regime) with a distinct temporal rescaling law and sensitive dependence of the renormalized equation on the infrared cutoff.

The effects of the addition of a constant cross sweep to the random spatio-temporal turbulent shear flow (206) are considered in [14]. The renormalization phase diagram is altered in some ways; in particular the phase region corresponding to a nonlocal eddy-renormalized equation is eliminated. The renormalization is unaffected by the constant cross sweep in the vicinity of the Kolmogorov point ($\varepsilon = 8/3$, $z = 2/3$). The eddy-renormalized equations are also shown in [14] to hold without change for a variety of random shear velocity models with energy spectra (206) but non-Gaussian statistics.

The rigorous renormalization theory for the simple shear model [10,14] has been used by Avellaneda and the first author as an unambiguous means of assessing the performance of a variety of R-N-G methods and renormalized perturbation theories for predicting eddy diffusivity [13,17,300]. We summarize some of these findings in Section 7.

3.4.4. Comment on the eddy diffusivity modelling at finite times

In our above discussion concerning the mean passive scalar density, we have focused on the behavior at large scales and long times, which is usually of the main practical interest. There is, however, still an important practical concern regarding the transient period of adjustment to long-time asymptotic behavior, both for observations and for numerical simulations. In particular, if the numerical simulation of the tracer dynamics becomes unstable or inaccurate during any phase of the evolution, a substantial error may be incurred which permanently contaminates results at large times, even if the numerics are well behaved in the large-time asymptotic regime. We point out here some simple, explicit examples in which the tracer exhibits an effective negative diffusivity over some finite interval of time, but eventually settles down to a positive diffusivity at long times. As it is quite difficult for numerical Monte Carlo schemes (see Section 6) to simulate

periods of negative diffusion accurately, one must be on the alert for such a contingency. The appearance of an effective negative diffusivity is not a pathological feature of our mathematical models; Taylor [317] recognized such a phenomenon in chimney smoke experiments by Richardson [283] in 1920.

As was pointed out in [18], negative diffusivity can already be observed in the extremely simple Random Sweeping Model described in Section 3.1.2. Recall that the velocity field is defined to be spatially uniform and directed always along a single direction:

$$\boldsymbol{v}(x, y, t) = \begin{bmatrix} w_f(t) \\ 0 \end{bmatrix} ,$$

with $w_f(t)$ fluctuating in time according to a Gaussian, mean zero, stationary stochastic process. The correlation function of the sweeping field is defined:

$$R_w(t) \equiv \langle w_f(t') w_f(t + t') \rangle .$$

The tracer displacement is at all times a Gaussian random variable, and it can therefore be shown [18] that the mean tracer concentration density $\langle T(\boldsymbol{x}, t) \rangle$ obeys an exact PDE of diffusive type:

$$\partial \langle T(x, y, t) \rangle / \partial t = \kappa \varDelta \langle T(x, y, t) \rangle + D_{w_f}(t) \frac{\partial^2 \langle T(x, y, t) \rangle}{\partial x^2} ,$$

$$\langle T(x, y, t = 0) \rangle = \langle T_0(x, y) \rangle . \tag{219}$$

The effect of the random fluctuations is to augment the diffusivity along the sweeping direction x above its bare molecular value κ by the time-dependent quantity:

$$D_{w_f}(t) \equiv \int_0^t R_w(s) \, \mathrm{d}s . \tag{220}$$

At large times, the enhanced diffusivity $D_{w_f}(t)$ must be nonnegative, but there may well be finite intervals of time over which it is negative. Explicit examples may be found by defining the velocity field $w_f(t)$ through statistically homogenous solutions to a damped and stochastically driven harmonic oscillator problem [18]:

$$\mathrm{d}(\mathrm{d}w_f(t)/\mathrm{d}t) + 2\alpha \, \mathrm{d}w_f(t) + \omega_0^2 w_f(t) \, \mathrm{d}t = A \, \mathrm{d}W(t) , \tag{221}$$

where $\omega_0 > 0$ describes the stiffness of the oscillator, $\alpha > 0$ describes the damping, and $\mathrm{d}W(t)$ is white noise. For the underdamped range of parameters, $\omega_0 > \alpha$, the correlation function has oscillations:

$$R_w(t) = (A^2/4\alpha\omega_0^2)\mathrm{e}^{-\alpha|t|}[\cos(\omega_1 t) + (\alpha/\omega_1)\sin(\omega_1|t|)] ,$$

where $\omega_1 = \sqrt{\omega_0^2 - \alpha^2}$. The criterion for $D_{w_f}(t)$ (220) to be always nonnegative may be shown [141] to be exactly equivalent to the inequality $\omega_0^2 \leq C_1\alpha^2$, where C_1 is a numerical constant which may be computed to be approximately 27.197. Therefore, for sufficiently strong restoring forces on the

oscillations driving the random sweeping ($\omega_0^2/\alpha^2 > C_I$) and sufficiently small κ, there are finite intervals of time over which

$$\kappa + D_{w_J}(t) < 0 \;,$$

and the PDE (219) for the mean passive scalar density is ill-posed.

This fact is not of great concern within the Random Sweeping Model itself, because its simplicity permits the mean statistics $\langle T(x, y, t)\rangle$ to be unambiguously represented in closed form [18], and there is no need to actually solve (219). But the potential for ill-posed behavior does raise practical concerns for numerical simulations in more complex flows where no exact solution is available. When the effective diffusivity becomes negative, approximate PDEs for the mean statistics cannot be numerically integrated by ordinary means, and the numerical simulation of even the mean-square displacement of a tracer faces severe difficulties [140].

An example with nontrivial spatial variations which exhibits ill-posed behavior for the mean passive scalar density can be constructed for the Random Steady Shear (RSS) Model with constant, nonzero cross sweep:

$$\boldsymbol{v}(x, y, t) = \begin{bmatrix} \bar{w} \\ v(x) \end{bmatrix} .$$

The mean passive scalar density in such a flow can be shown to obey a time-dependent diffusion equation of the same form as Eq. (219), except that the time-dependent diffusivity enhancement is in the shearing direction y, and is expressed as

$$D(t) = \int_0^t R(\bar{w}s)\, \mathrm{d}s \;,$$

where $R(x)$ is the correlation function of the Gaussian, homogenous, random shear flow $v(x)$. For a random shear flow $v(x)$ generated as the homogenous solution of a stochastically damped and driven harmonic oscillator (221) (but with spatial rather than temporal variations), it has been similarly shown that for sufficiently strong restoring forces $\omega_0^2/\alpha^2 > C_I \approx 27.197$ and sufficiently small molecular diffusivity κ, the PDE for the mean tracer density $\langle T(x, y, t)\rangle$ is ill-posed over some finite interval of time [141]. In particular, negative diffusion over finite time intervals arises in the degenerate limiting case, studied by Güven and Molz [131], in which the random shear flow $v(x)$ is an undamped periodic oscillation with random phase and the molecular diffusion κ is sufficiently small.

3.5. Pair-distance function and fractal dimension of scalar interfaces

A common theme in the various shear flow examples which have been presented is that the motion of a single tracer is determined to a great extent by the details of the large-scale features of the velocity field. This is particularly true for random velocity fields with long-range correlations characteristic of fully developed turbulence (such as the $2 < \varepsilon < 4$ simple shear models), in which the energy is concentrated at small wavenumbers. In practical situations, this means that the motion of a tracer, and therefore the evolution of the ensemble-averaged mean passive scalar concentration, in a turbulent environment depends strongly on the geometry and the details of the

large-scale stirring. Therefore, there can be no single law describing the behavior of a tracer's position in an arbitrary turbulent system.

The situation can be quite different for the *separation* between a pair of tracers in a fully developed turbulent flow with a wide inertial range. The rate of separation between a pair of tracers is not governed by the typical velocity of the flow, but by the *difference* between the velocity at the two tracer locations. Therefore, a turbulent eddy with large size relative to the separation between the two tracers will sweep them both with roughly the same velocity, and contribute to their *relative* motion only through its velocity gradient (primarily the strain component). Recall that in the Kolmogorov picture, the root mean square velocity of a turbulent eddy of length scale L in the inertial range scales as $L^{1/3}$. Therefore, an inertial range eddy of size L large compared to the separation ℓ of a tracer pair will contribute to the *absolute* motion of either of them (or their center of mass) in proportion to $L^{1/3}$, but will contribute to their *relative* motion in proportion to $L^{1/3}(\ell/L) \sim \ell L^{-2/3}$. Consequently, large-scale eddies are seen to dominate the absolute motion of a tracer, but to contribute little to their relative motion (separation). In other words, the process of separation of a tracer pair can be expected to be insensitive to large-scale details so long as the separation remains small compared to the system size.

By noting that inertial-range eddies on scales small compared to the distance between the tracers contribute their full velocity to the relative tracer motion, we arrive at the following heuristic principle: When the tracer pair separation lies within the inertial range of scales of a fully developed turbulent flow, its evolution should be primarily governed by inertial-range eddies of size comparable to the momentary separation. As we have discussed in Section 3.4.3, the statistics of a turbulent velocity field well within the inertial range of scales is thought to have a number of *universal* properties which are independent of many of the details of the physical system. Combining the previous two statements, we see that the separation $\ell(t)$ between a pair of tracers may obey universal laws as it evolves through the inertial range of scales. The most famous proposed universal relation of this type is Richardson's law [252,253,284] $\langle \ell^2(t) \rangle \sim t^3$, which has been observed in a wide variety of laboratory experiments [248,258,261,315] and numerical simulations using synthetic turbulent velocity fields (see Section 6 of this review and [86,109,291,351]). Like the Kolmogorov theory of turbulence, universal inertial-range theories for turbulent diffusion in multidimensional velocity fields with realistic spatio-temporal structure are based on extra physical assumptions which do not follow directly from the advection–diffusion equation.

As we have seen in Sections 3.2, 3.3 and 3.4, many mechanisms and subtleties of turbulent diffusion can be explored in a clear and unambiguous fashion in shear flows. Here, we will mathematically investigate universal inertial-range aspects of turbulent diffusion in shear flows, using the family of models with reasonably realistic spatio-temporal energy spectra introduced in Paragraph 3.4.3.2. For simplicity in exposition, we will not consider any active cross-shear transport processes, so the only decorrelation of the Lagrangian tracer motion is due to the temporal fluctuations of the random shear flow itself. It is consequently a little more direct to work here with the spectral temporal correlation function $\check{E}(k,t)$ defined earlier in Eq. (158) instead of the spatio-temporal energy spectrum $\widetilde{E}(k,\omega)$. The function $\check{E}(k,t)$ describes the temporal correlation structure of the shear modes of wavenumber k, and is related to the physical-space correlation function $\widetilde{R}(x,t)$ and the spatio-temporal correlation function $\widetilde{E}(k,\omega)$ through the Fourier transform relations (158).

The representation of the RSTS-I Model (206) in terms of $\breve{E}(k,t)$ reads

$$\tilde{R}(x,t) = \int_{-\infty}^{\infty} \breve{E}(|k|,t)e^{2\pi ikx}\,\mathrm{d}k = 2\int_0^{\infty} \breve{E}(k,t)\cos(2\pi kx)\,\mathrm{d}k \;, \tag{222a}$$

$$\breve{E}(k,t) = E(|k|)\hat{\phi}(t/\tau(|k|)) \;, \tag{222b}$$

$$E(k) = A_E k^{-1-2H}\psi_0(kL_0)\psi_\infty(kL_K) \;, \tag{222c}$$

$$\tau(k) = A_\tau k^{-z} \;, \tag{222d}$$

where $\hat{\phi}(u)$ is just the Fourier transform of $\phi(\varpi)$ in Eqs. (206a), (206b) and (206c). We have collected the various constant prefactors into the single coefficient A_E. The cutoff functions ψ_0 and ψ along with $\hat{\phi}$ are smooth functions on the positive real axis with the assumed technical properties listed under (200). The exponent H characterizing the inertial-range scaling exponent of the energy spectrum is formally related to the infrared scaling exponent ε used in the RSTS Model in Section 3.3 by $H = (\varepsilon - 2)/2$. The appropriate parameter range for which a universal scaling range arises in real space is $0 < H < 1$, or $2 < \varepsilon < 4$. The value with $H = 1/3$ (and $z = 2/3$) corresponds to Kolmogorov-type statistics. It is easily checked that the heuristic considerations suggesting universal inertial-range behavior for pair separation formally apply throughout the range $0 < H < 1$. By "universal inertial-range behavior" in the context of this family of mathematical models for turbulence, we mean statistical behavior which depends only on parameters describing the inertial range (A_E, ε, and z), but not on viscous-scale or large-scale properties (L_0, L_K, ψ_0, ψ_∞). We also by no means imply that these laws are universal with respect to flow geometry; the anisotropic geometry of the shear flow can of course lead to departures in the specific appearance of certain laws from their formulation for statistically isotropic flows. For example, the mean-square pair separation will be found in Paragraph 3.5.2.1 to grow in the inertial range according to a power law with exponent different from that appearing in Richardson's t^3 law for isotropic turbulence, even for Kolmogorov values of the exponents $H = 1/3$ and $z = 2/3$. We will return to Richardson's t^3 law later when we discuss an exactly solvable statistically isotropic mathematical model (Paragraph 4.2.2.4) and numerical methods for accurately simulating tracer pair dispersion over a wide inertial range in a synthetic statistically isotropic turbulent flow (Section 6.5).

Our present study of pair separation in the simple shear model begins in Section 3.5.1 with a derivation of an exact solution for the PDF (probability distribution function) of the separation between a pair of tracers in a shear flow with arbitrary spatio-temporal statistics, in the absence of molecular diffusion ($\kappa = 0$). This PDF of the separation will be called the *pair-distance function*, a term introduced by Richardson in his pioneering work on relative diffusion [284]. We show that the pair-distance function satisfies a linear PDE of diffusive type, and indicate an explicit example in which the diffusion coefficient is negative over some finite time interval, leading to ill-posedness [141]. We then specialize in Section 3.5.2 to the Random Spatio-Temporal Shear Models with Inertial Range (RSTS-I) introduced in Section 3.4.3, and show that the pair-distance function has an explicit, universal form on scales well within the inertial range.

We then subsequently utilize the formula for the pair-distance function to study the properties of the boundary of a region marked by a passive scalar quantity as it evolves in an RSTS-I flow in the absence of molecular diffusion $\kappa = 0$. Of particular natural and engineering interest [199,305,339] is the turbulent wrinkling of the interface between the scalar-occupied and the scalar-free region.

The notion of *fractal dimension* [215] provides a useful measure of the geometric convolution of a surface with scale invariance, such as the scalar interface in the inertial range of scales. By combining the explicit formula for the pair-distance function with a mathematical theorem of Orey [259] concerning the fractal dimension of the graph of a Gaussian random process, we compute in Section 3.5.3 the local fractal dimension of the scalar interface in the RSTS-I model within the inertial range of scales. There is also a distinct global fractal dimension describing the roughness of the passive scalar level set above some time-dependent length scale determined by the rate of temporal decorrelations of the shear flow. We next study fully scale-invariant properties of the pair-distance function which emerge after an *isotropic renormalization* to large space and time scales within the inertial range. The fractal dimensions which emerge from the isotropically renormalized passive scalar field are in quite good agreement with experimentally observed fractal dimensions of interfaces in a variety of turbulent systems [305]. We conclude in Section 3.5.5 by posing the open problem of including the effects of molecular diffusion $\kappa > 0$ on the pair-distance function and the fractal dimension of scalar interfaces in the RSTS-I Model. Unambiguous results along these lines could provide useful insights concerning general mathematical and physical theories for fractal dimensions of interfaces in turbulent flows [74,75,128,132,310].

3.5.1. Pair-distance function in shear flow

The *pair-distance function* is defined for our purposes to be the PDF for the separation between a pair of tracers, given a certain initial separation. We will specialize the notation for convenience in our study of pair dispersion in a two-dimensional shear flow with constant cross sweep:

$$\boldsymbol{v}(x, y, t) = \begin{bmatrix} \bar{w} \\ v(x, t) \end{bmatrix}. \tag{223}$$

Here $v(x, t)$ is a homogenous, Gaussian, mean zero random field with correlation function

$$\langle v(x', t') v(x + x', t + t') \rangle = \tilde{R}(x, t) ,$$

and $\bar{w}$ is a deterministic constant (which may be zero). Within Section 3.5.1, we do not specify a particular model for $\tilde{R}(x, t)$.

Consider two tracers released at the points $(x'_0, 0)$ and $(x_0 + x'_0, 0)$ in the random shear flow (223), with no molecular diffusion ($\kappa = 0$). Let $Y_{x'_0}(t)$ and $Y_{x_0 + x'_0}(t)$ denote their y positions at time t. Then we define the pair-distance function $Q^{(t)}(y|x_0)$ as the probability density function satisfying

$$\int_{y_-}^{y_+} Q^{(t)}(y|x_0)\, \mathrm{d}y = \mathrm{Prob}\{y_- \leq Y_{x_0 + x'_0}(t) - Y_{x'_0}(t) \leq y_+\} \tag{224}$$

for all $y_- < y_+$. In words, then, $Q^{(t)}(y|x_0)$ gives the probability density that two tracers with initial shear-transverse separation x_0 will have developed a relative shear-parallel displacement of y at time t.

A few comments on this definition are in order. First, by statistical homogeneity, the statistics of pair separation depends only on the relative position of the tracers, and are therefore independent of x'_0. Furthermore, the constancy of the cross-shear velocity preserves the shear-transverse separation x_0 of the tracers, so there is no need to separately account for the shear-transverse

separation at later times in the pair-distance function. Since there is no variation of the flow along the y direction, there is no loss in taking both tracers to start at $y = 0$; the PDF for pair separation starting from arbitrary locations (x'_0, y'_0) and $(x'_0 + x_0, y'_0 + y_0)$ is obtained straightforwardly from the PDF $Q^{(t)}(y|x_0)$ defined for $y'_0 = y_0 = 0$. Finally, we note that Richardson's original definition [284] of the pair-distance function is more general in a literal sense, but equivalent in essence to the simpler definition used here.

We will now proceed to give an exact formula for the pair-distance function in a general shear flow with constant cross sweep (223). The relative shear-parallel separation is given by the explicit formula (see Eqs. (110a) and (110b))

$$Y_{x_0 + x'_0}(t) - Y_{x'_0}(t) = \int_0^t (v(x_0 + x'_0 + \bar{w}s, s) - v(x'_0 + \bar{w}s, s)) \, ds \ . \tag{225}$$

This expression is an integral over a Gaussian random field, and thus a Gaussian random variable. Since $Q^{(t)}(y|x_0)$ is the probability density for the random variable (225), it is completely determined by the mean and variance of the relative displacement. Since v has mean zero, it is easy to see that

$$\langle Y_{x_0 + x'_0}(t) - Y_{x'_0}(t) \rangle = 0 \ . \tag{226}$$

The variance of the shear-parallel separation can be computed as an integral of the velocity correlation function:

$$\sigma^2_{\Delta Y}(t|x_0) \equiv \langle (Y_{x_0 + x'_0}(t) - Y_{x'_0}(t))^2 \rangle = \int_0^t \int_0^t \langle (v(x_0 + x'_0 + \bar{w}s, s) - v(x'_0 + \bar{w}s, s))$$

$$\times \langle (v(x_0 + x'_0 + \bar{w}s', s') - v(x'_0 + \bar{w}s', s')) \rangle \, ds \, ds' \tag{227}$$

$$= \int_0^t \int_0^t [2R(\bar{w}(s - s'), s - s') - R(-x_0 + \bar{w}(s - s'), s - s')$$

$$- R(x_0 + \bar{w}(s - s'), s - s')] \, ds \, ds' \ . \tag{228}$$

Then the pair-distance function can then be expressed as the following Gaussian:

$$Q^{(t)}(y|x_0) = \frac{\exp[-y^2/(2\sigma^2_{\Delta Y}(t|x_0))]}{\sqrt{2\pi\sigma^2_{\Delta Y}(t|x_0)}} \ . \tag{229}$$

It is instructive to note that $Q^{(t)}(y|x_0)$ satisfies a diffusion PDE:

$$\frac{\partial Q^{(t)}(y|x_0)}{\partial t} = D_\Delta(x_0, t) \frac{\partial^2 Q^{(t)}(y|x_0)}{\partial y^2} \ , \tag{230}$$

$$Q^{(0)}(y|x_0) = \delta(y) \ .$$

The initial condition comes from the fact that at time $t = 0$, the tracers have a deterministically zero displacement. The time-dependent diffusion coefficient $D(x, t)$ is obtained by differentiating Eq. (227):

$$D_\Delta(x_0, t) \equiv \tfrac{1}{2} \partial \sigma^2_{\Delta Y}(t|x_0)/\partial t \ . \tag{231}$$

A simple way to derive the diffusion equation (230) is to compute the characteristic function of Eq. (225), which is just the Fourier transform of the pair-distance function:

$$\hat{Q}^{(t)}(k|x_0) \equiv \langle \exp(2\pi i k(Y(x+x',t) - Y(x',t))) \rangle = \exp(-2\pi^2 k^2 \sigma_{\Delta Y}^2(t|x_0)) , \qquad (232)$$

and to note that it satisfies the Fourier transform of Eq. (230).

3.5.1.1. Possible ill-posedness of pair-distance PDE. While the pair-distance function has been shown to always obey a fairly simple, time-dependent diffusion equation, the PDE (230) is not necessarily well-posed. It is shown in [141] that for the case of a steady shear flow ($v(x,t) = v(x)$ and $\tilde{R}(x,t) = R(x)$), this PDE is well-posed for all time $t > 0$ and initial separations x_0 if and only if one of the following two conditions holds:

- there is no cross sweep $\bar{w} = 0$, or
- the velocity correlation function $R(x)$ is a nonincreasing function of x on $0 < x < \infty$.

If both of these conditions are violated, then the formal diffusion coefficient $D_\Delta(t|x_0)$ is negative for some values of x_0 and t, leading to an ill-posed problem for $Q^{(t)}(y|x_0)$.

Explicit examples of a random shear velocity fields giving rise to ill-posedness for the pair-distance function may be found within the class of statistically homogenous solutions to a damped and stochastically driven harmonic oscillator problem [141]:

$$d(dv(x)/dx) + 2\alpha \, dv(x) + k_0^2 v(x) \, dx = A \, dW(x) ,$$

where $k_0 > 0$ describes the stiffness of the oscillator, $\alpha > 0$ describes the damping, $A > 0$ is the driving amplitude, and $dW(x)$ is white noise. We introduced this stochastic model before in Section 3.4.4. For the underdamped range of parameters, $k_0 > \alpha$, the correlation function has oscillations:

$$R(x) = (A^2/4\alpha k_0^2) e^{-\alpha|x|} [\cos(k_1 x) + (\alpha/k_1)\sin(k_1|x|)] ,$$

with $k_1 = \sqrt{k_0^2 - \alpha^2}$. Thus by the general fact quoted above from [141], the formal diffusion coefficient $D_\Delta(x_0, t)$ is negative over some range of values of x_0 and t whenever the oscillations exceed the damping. Note that $D_\Delta(x_0, t)$ is just half the rate of the mean-square shear-parallel tracer separation; its negativity implies time intervals over which the tracers are actually decreasing their separation on average.

Of course, for the present model we have an exact expression (229) for the pair-distance function so the ill-posedness of the PDE (230) does not thwart our analytical progress here. The potential for ill-posed behavior of the relative tracer displacement, as explicitly demonstrated in our simple model, however does raise practical concerns for numerical integration of tracer trajectories in more complex flows where no exact solution is available [140].

3.5.2. Inertial range behavior of the pair-distance function in the simple shear model

We will now study the pair-distance function in detail when the random shear flow is an RSTS flow with an inertial range and no cross sweep ($w(t) = 0$).

Substituting the expression (222) for the spatio-temporal correlation function of this velocity field into the general formula for the mean-square shear-parallel separation (227) with $\bar{w} = 0$, we have

$$
\begin{aligned}
\sigma_{\Delta Y}^2(t|x_0) &= \int_0^t \int_0^t \int_{-\infty}^{\infty} 2(1 - \cos(2\pi k x_0)) E(|k|) \hat{\phi}\left(\frac{s - s'}{\tau(|k|)}\right) dk \, ds \, ds' \\
&= 4t^2 \int_0^{\infty} (1 - \cos(2\pi k x_0)) E(k) \Phi(t/\tau(k)) \, dk \\
&= 4t^2 \int_0^{\infty} (1 - \cos(2\pi k x)) A_E k^{-1-2H} \psi_0(k L_0) \psi_\infty(k L_K) \Phi(t A_\tau^{-1} k^z) \, dk .
\end{aligned}
\tag{233}
$$

We have defined

$$
\Phi(u) = \frac{2}{u^2} \int_0^u (u - u') \hat{\phi}(u') \, du'
\tag{234}
$$

and used a change of variables to re-express the double time integral in the second equality above. We collect here some basic properties of Φ which will be useful in our later analysis of $\sigma_{\Delta Y}^2(t|x_0)$:

$$
\Phi(0) = 1 ,
\tag{235a}
$$

$$
\lim_{u \to \infty} \Phi(u) \sim \phi(0) u^{-1} ,
\tag{235b}
$$

$$
|\Phi(u)| \leq C_\Phi / (1 + |u|) ,
\tag{235c}
$$

where C_Φ is some finite positive constant. These results follow from the Fourier relation between $\hat{\phi}(u)$ and $\phi(\varpi)$, and the assumed properties of $\phi(\varpi)$ stated near Eq. (156).

It is instructive at this point to compare and contrast the formulas we have developed for the mean-square *relative* displacement $\sigma_{\Delta Y}^2(t|x_0)$ between a pair of tracers and the mean-square *absolute* displacement $\sigma_Y^2(t)$ of a single tracer along the shear. We represent the latter using formula (159) for the special case in which there is no cross-shear transport and $\check{E}(k, t)$ is given by Eq. (222b):

$$
\sigma_Y^2(t) = 2t^2 \int_0^{\infty} A_E k^{-1-2H} \psi_0(k L_0) \psi_\infty(k L_K) \Phi(t A_\tau^{-1} k^z) \, dk .
\tag{236}
$$

The formulas for the absolute and relative tracer displacements differ in only two regards: a multiplicative factor of 2, and the appearance of a factor $(1 - \cos 2\pi k x_0)$ in the integrand for $\sigma_{\Delta Y}^2(t|x_0)$. The prefactor of 2 simply reflects the fact that the mean-square relative distance between two tracers undergoing some independent statistical motion will simply be the sum of their individual absolute mean-square displacements. There is, however, a definite coupling between the motion of two tracers in our model due to the spatial correlations of the shear flow. The effects of this coupling are completely contained in the factor $(1 - \cos 2\pi k x_0)$.

For $k \ll 1/x_0$, this factor is small $(O((k x_0)^2))$, reflecting the fact that the motion of two tracers due to a shear mode with wavenumber k is highly correlated when their cross-shear separation x_0 is much less than the wavelength k^{-1}. Their relative velocity is on the order of their cross-shear

separation x_0 multiplied by the *gradient* of the shear mode, which is proportional to k times the root-mean-square velocity of the shear mode. The rate of relative mean-square separation due to a shear mode of wavenumber $k \ll 1/x_0$ is thus depressed by a factor of $(kx_0)^2$ from the absolute mean-square displacement of either tracer. The exact formula (233) for $\sigma_{\Delta Y}^2(t|x_0)$ thereby explicitly manifests the general principle that the low wavenumber modes contribute weakly to the process of tracer separation on small scales (see our discussion at the beginning of Section 3.5).

For shear modes with high wavenumbers $k \gg 1/x_0$, the spatial correlation factor $1 - \cos 2\pi k x_0$ is generally of order unity. The effect of the cosine becomes negligible when integrated over a sufficiently wide band of wavenumbers k, due to incoherent phase cancellation. Therefore, any wide band of random shear modes with wavenumbers $k \gg 1/x_0$ contribute essentially independently to the motion of each tracer in a pair with cross-shear separation x_0.

We now proceed to study the inertial-range behavior of $\sigma_{\Delta Y}^2(t|x_0)$ for the parameter range $0 < H < 1$. By this we mean that the (constant) shear-transverse separation satisfies $L_K \ll x_0 \ll L_0$; the shear-parallel separation has no influence on the tracer dynamics in our shear flow model. We may straightforwardly take the asymptotic inertial-range limit in Eq. (233), and the integral scale and dissipation scale cutoffs disappear:

$$\sigma_{\Delta Y,I}^2(t|x_0) \equiv \lim_{x_0/L_K \to \infty, x_0/L_0 \to 0} \sigma_{\Delta Y}^2(t|x_0) = 4t^2 \int_0^\infty (1 - \cos(2\pi k x_0)) A_E k^{-1-2H} \Phi(t A_\tau^{-1} k^z) \, dk \ . \quad (237)$$

This is mathematically justified by the dominated convergence theorem after a rescaling of the integration variable $q = kx_0$, owing to the boundedness of the function Φ and the integrability of the function $(1 - \cos 2\pi q) q^{-1-2H}$ over $q \in [0, \infty)$. Therefore, we have expressed the relative mean-square displacement of tracers on scales within the inertial range purely in terms of inertial range quantities; there is no dependence on either the integral or dissipation length scales. The same is true for the full pair-distance function $Q_I^{(t)}(y|x_0)$ for inertial-range separations of x_0, since it is determined entirely by $\sigma_{\Delta Y,I}^2(t|x_0)$ (see (229)). The pair-distance function is therefore truly universal in the inertial range of scales in the RSTS-I Model.

In contrast, we remark that the mean-square absolute displacement of a single tracer $\sigma_Y^2(t)$ depends vitally on the factor $\psi_0(kL_0)$. Taking $L_0 \to \infty$ in Eq. (236) would give an infinite value for $\sigma_Y^2(t)$, simply because the total energy of the shear flow would become infinite. Energy spectra with inertial ranges ($0 < H < 1$) are therefore said to manifest an *infrared divergence*. A direct consequence is that the motion of a single tracer in a turbulent flow is strongly sensitive to the large-scale structure of the flow. The reason that the relative tracer displacement has a finite inertial-range limit, notwithstanding the infrared divergent energy spectrum, is that low wavenumber shear modes contribute quite weakly to the separation process due to their small gradients. Mathematically, this is manifested by the factor $(1 - \cos(2\pi k x_0))$ in Eq. (233), which contributes a factor k^2 to tame the infrared divergence k^{-1-2H} at small k.

The ability to remove the Kolmogorov dissipation length cutoff $\psi(kL_K)$ from Eq. (233) is less subtle; it is simply a consequence of the "ultraviolet convergence" of energy spectra with inertial range.

The heuristic component of our above discussion concerning absolute and relative tracer motion in a high Reynolds number shear flow can be generalized through similar scaling arguments to isotropic turbulence. The exact mathematical formulas, however, are special to shear flows. These

Table 10
Long-time asymptotics of mean-square relative tracer displacement along the shear within Inertial Range of Random Spatio-Temporal Shear Model. Scaling coefficients are given by Eq. (238)

Parameter regime		Asymptotic mean square displacement $\lim_{t \to \infty} \sigma^2_{\Delta Y, \parallel}(t \mid x_0)$	Phase region
$z \geq 0$	$0 < H < \dfrac{2-z}{2}$	$2 \tilde{K}^*_\Delta \lvert x_0 \rvert^{2H+z} t$	R-1
$z \geq 0$	$\dfrac{2-z}{2} < H < 1$	$\dfrac{z}{z+H-1} \tilde{K}^\sharp_\Delta \lvert x_0 \rvert^2 t^{2(z+H-1)/z}$	R-2

permit us to examine various aspects pertaining to tracer dynamics within the inertial range of scales in much more detail than is generally possible, as will be shown in what follows.

3.5.2.1. Evolution of relative separation between a fixed pair of tracers. The long-time asymptotics of the mean-square shear-parallel tracer pair separation $\sigma^2_{\Delta Y}(t)$ are described in Table 10, with scaling coefficients

$$\tilde{K}^*_\Delta = 2 \int_0^\infty (1 - \cos(2\pi k x_0)) \phi(0) A_E A_\tau k^{-1-2H-z} \, \mathrm{d}k = 2\pi^{2H+z+1/2} \frac{-\Gamma(-H-z/2)}{\Gamma(H+(z+1)/2)} A_\tau A_E \phi(0) \,,$$

(238a)

$$\tilde{K}^\sharp_\Delta = \frac{8\pi^2(z+H-1)}{z^2} A_E A_\tau^{(2-2H)/z} \int_0^\infty u^{(2-2H-z)/z} \Phi(u) \, \mathrm{d}u \,.$$

(238b)

These results are very similar to those found for the mean-square shear-parallel displacement of a single tracer in an RSTS flow with no cross shear transport (Section 3.3.1), and the method of derivation is very similar. One only needs to account for the extra factor $(1 - \cos 2\pi k x_0)$, and we remark only on the changes this produces.

First of all, the integrand for the long time relative diffusivity (238a) in the linear growth regime (R-1 in Fig. 17) is peaked at $k \sim x_0^{-1}$, rather than at the lowest wavenumbers where energy is concentrated. This reflects the idea discussed at the beginning of Section 3.5 that relative diffusion is driven primarily by velocity fluctuations (eddies) with wavelength comparable to the current tracer separation. This notion, however, is violated in the present model when the correlation time diverges sufficiently rapidly at low wavenumber, in which case the long-time relative diffusion is driven at a superlinear rate by these slow, low wavenumber shear modes (regime R-2 in Fig. 17). Care is therefore required in analyzing this regime at long times and large but finite integral length scales L_0; the limits $t \to \infty$ and $L_0 \to \infty$ do not commute. In our present discussion, we are always assuming that L_0 is extremely large so that the limit $L_0 \to \infty$ is appropriately taken first.

Note that when the temporal correlation times of the shear modes are chosen as the natural eddy turnover times so that $z = 1 - H$ (see Eq. (211a)), the relative diffusion is always linear and driven primarily by modes of wavenumber $k \sim x_0^{-1}$. This includes the Kolmogorov values
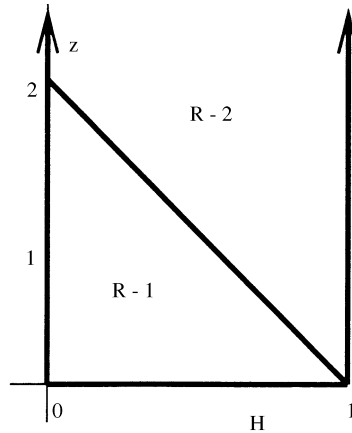
Fig. 17. Phase diagram for long-time asymptotics of $\sigma_{\Delta Y}^2(t)$ in Random Spatio-Temporal Shear Model with Inertial Range, no cross shear transport. This phase diagram also applies to the local fractal dimension of level sets of $T(x, y, t)$ (see Paragraph 3.5.3.2).

$H = 1/3$, $z = 2/3$. These results for the Random Spatio-Temporal Shear Model contrast strongly with Richardson's law predicting a t^3 growth of $\sigma_{\Delta Y}^2(t)$ for relative diffusion through the inertial range of scales in isotropic turbulence. The shear geometry destroys a fundamental premise in the similarity argument [252,253] behind Richardson's law: the initial pair separation x_0 is never forgotten because the shear turbulence does not act along the x direction. Therefore, the most relevant turbulent eddies driving the separation of the tracer pair are those with wavelengths comparable to the initial separation x_0, rather than to the current separation scale.

3.5.3. Fractal dimension of scalar interfaces

In this subsection, we will apply the exact formulas for the pair-distance function which we worked out in Sections 3.5.1 and 3.5.2 to provide a measure of smoothness of level sets of the passive scalar density $T(x, y, t)$. This is of practical importance in determining mixing rates. Consider first two initially distinguishable fluids, such as a salty fluid and a freshwater fluid, a dyed fluid and an undyed fluid, or a warm fluid and a cold fluid which are brought together to mix. If effects such as buoyancy and chemical reactions between the fluids can be neglected, then the evolution of the fluid mixture may be expressed in terms of a passive scalar field $T(x, y, t)$ which reflects the local concentration density of one fluid or the other. For example, in the above-mentioned examples, $T(x, y, t)$ could be chosen as salinity, dye concentration, and temperature, respectively. After a suitable rescaling and translation of physical units, one may characterize the initial state of the passive scalar field by $T_0(x, y) \equiv 1$ in the region occupied by the first fluid, $T_0(x, y) \equiv 0$ in the region occupied by the second fluid, and $T_0(x, y) \equiv \frac{1}{2}$ at the initial interface. If we neglect molecular diffusion for the moment, then the passive scalar concentration density is unchanged along Lagrangian trajectories, so the fluid is characterized thereafter by mobile regions where $T(x, y, t) \equiv 1$ and $T(x, y, t) \equiv 0$ separated by the level set $T(x, y, t) = \frac{1}{2}$ demarcating the evolving interface between the two fluids. The action of molecular diffusion will smooth the variation of $T(x, y, t)$ across the fluid interface, but it is readily seen that the level set $T(x, y, t) = \frac{1}{2}$

still provides a good representation for the location of the interface between the fluids where mixing is occurring, particularly when the Péclet number is large so that the interface region is thin.

One major feature of turbulent diffusion is that it roughens interfaces on small scales both within the inertial range and the viscous range [54,305]. This is in strong contrast to the smoothing nature of molecular diffusion. The source of the difference is the interface structure created by spatial correlations in turbulent velocity fields. Only when viewed on scales large compared to the largest correlation length of the velocity field do these undulations blur out, and the mixing action of turbulent diffusion appear to be smoothing. The reason that molecular diffusion is smoothing on all scales is that its correlation length is strictly zero, so all scales are large enough for the mixing to appear smoothing!

The turbulent wrinkling of the fluid interface permits the fluids to contact each other over a greater surface area than if it were a flat plane as in laminar flow conditions. This increases the flux of temperature, salinity, dye, etc., across the interface, and speeds the process of mixing.

Another context in which level sets of a scalar field are of great practical interest is in the progress of diffusion flames in turbulent combustion [305,339]. A diffusion flame is characterized by the fact that the fuel and the oxidant are supplied separately, and the flame appears at the boundary of the fuel and oxidant zones where the necessary molecular mixing takes place. When the reaction rate is large compared with the diffusion coefficients of the chemical species involved, the flame can be idealized as an infinitesimally thin surface where all the reaction takes place. From the physical equations governing the combustion process one can deduce that at the flame front the temperature $T(x, y, t)$ attains its maximum value corresponding to the adiabatic stoichiometric temperature T_c (for the algebraic details of the derivation consult [339]). Therefore the location of the diffusion flame can be characterized by the level surface $T(t, x, y) = T_c$, under the approximation that the flame front is infinitesimally thin. If the combustion is occurring in a turbulent environment, the flame surface will be wrinkled into a larger surface area, thereby increasing the speed at which the flame burns through the fuel [339]. In combustion, the temperature field is not a *passive* scalar field, but one might to a first approximation suppose that the wrinkling of the interface may be governed by a similar process. Indeed, laboratory measurements indicate that diffusion flames have a quantitatively similar small-scale geometry to that of passive scalar interfaces, provided that certain conditions are met [305]. We mention here that the first author with Souganidis have studied the enhanced flame speed in premixed turbulent combustion with the effects of nonlinear reaction and diffusion, as well as small-scale turbulence [90,88,89,211–213]. In particular, [212,213] contain a rigorous analysis of renormalized flame fronts in a steady shear flow with an inertial range of scales.

In the above examples, the extent of mixing and burning enhancements relies sensitively on the degree of wrinkling of the flame front. We now discuss one way of quantifying this wrinkling.

3.5.3.1. Elements of fractal theory. In a high Reynolds number flow, the small-scale turbulent fluctuations have a self-similar statistical structure over a wide inertial range of scales. It is reasonable to expect that the small-scale contortions of the scalar interface produced by these inertial range eddies will also exhibit a self-similar structure over a subregion of the inertial range of scales where molecular diffusion is formally negligible relative to advection. A useful framework for describing objects with a statistical scaling invariance is *fractal geometry* [215]. The roughness of such fractal objects can be quantitatively represented through the notion of *fractal dimension*. For

an extensive discussion of theory and applications of fractal geometry, see [215]. Here we state only the essentials for our purposes.

The intuitive notion of fractal dimension is a measure of how well a set fills up space. There are several ways to define and compute fractal dimensions of an object A; these yield identical results under certain caveats [217,218]. A useful operational definition that can be computed efficiently in practice [305] is that of *local box-counting dimension* $d_{L,B}$. One partitions the ambient space $\mathbb{R}^d$ in which the object resides into boxes of size δ, and counts how many boxes N_δ intersect the object. The local box-counting dimension of A is then defined as

$$d_{L,B} \equiv \lim_{\delta \to 0} \log N_\delta / \log \delta^{-1}. \tag{239}$$

This local box-counting dimension clearly coincides with the ordinary Euclidean dimension of any smooth, rectifiable object. But it also assigns a useful geometric dimension to very rough curves, such as the graph of Brownian motion $W(t)$ versus time, which has $d_{L,B} = 1.5$ (see [215]). The fractional value of this dimension indicates that the small-scale wrinkles in the Brownian graph cause it to have space-filling properties intermediate between that of a curve and of a solid region in a plane. Curves of arbitrary local box-counting fractal dimension from 1 to the dimension of the embedding space can be constructed [215]; greater values indicate wilder local fluctuations.

When we speak of the fractal dimension of a physical entity like a front, we do not mean the technical fractal dimension of the front, defined by the behavior on the smallest scales. We are rather interested in the structure of the curve over some finite range of scales with both an upper and lower cutoff, particularly ranges of self-similarity such as the inertial range. For these purposes, the size of the boxes δ in the definition of the local box-counting dimension must be restricted to lie within the range of desired scales. When the front possesses approximate self-similarity over a substantial portion of this range, then a graph of $\log N_\delta$ versus $\log \delta^{-1}$ will produce points lying nearly along a straight line. A more robust and meaningful assessment of the fractal dimension of the front on this range of scales is obtained in empirical measurements [305] through the slope of the best-fit line, rather than through a literal implementation of Eq. (239).

In our mathematical analysis, we have computed the second-order statistics after having taken the limit of zero Kolmogorov dissipation length and no molecular diffusion, so there is no lower limit to the inertial range behavior of the passive scalar interface. We can therefore equate the fractal dimension for the inertial range in our model with that computed from a $\delta \to 0$ mathematical limit. To this end, we will appeal to a theorem of Orey [259].

If $(x, f(x))$ is the graph of a statistically homogenous Gaussian random field, and

$$c_1|x|^{2\alpha} \le \langle (f(x' + x) - f(x))^2 \rangle \le c_2|x|^{2\alpha} \tag{240a}$$

for $|x| \ll 1$ and positive constants c_1, c_2, then for almost every realization, this graph has (Hausdorff) fractal dimension

$$d_{L,H} = 2 - \alpha . \tag{240b}$$

The definition of the *Hausdorff* fractal dimension referred to in this theorem is somewhat technical, and we refer the reader to [249] for a complete discussion. It suffices for our discussion to note that the Hausdorff fractal dimension coincides with the more intuitive local box-counting dimension in

standard situations [215]. There are caveats and counterexamples to this statement [218,332] which we do not wish to dwell on here, since we see no reason why they should arise in our application to passive scalar interfaces produced in a shear flow. We will therefore simply refer to the Hausdorff dimension as the *local fractal dimension* d_L. The adjective "local" is important, however, since the scalar level set in the RSTS-I Model exhibits a crossover to a different self-similar structure at large scales which is characterized by a different fractal dimension, as we will explain in detail later.

The exponent α appearing in Eq. (240a) is just the Hurst exponent of the graph [215], and acts as a Hölder exponent for almost every realization of the random graph [1]. Smooth random curves have Hurst exponent $\alpha = 1$, and fractal dimension d_L equal to their topological dimension of unity. Rougher random curves have smaller Hurst exponents α and, according to Eq. (240b), larger values of fractal dimension d_L.

3.5.3.2. Local fractal dimension of passive scalar level sets. We now show how the local fractal dimension of passive scalar level sets on the inertial range of scales may be exactly computed in the RSTS-I model through the exact formula for the pair-distance function in the inertial range and Orey's theorem (240). We assume that the level set of $T(x, y, t)$ of interest is initially a flat line lying along $y = 0$. Because there is no molecular diffusion, the level set at any later time is simply given by the image of the initial level set $y = 0$ under the (random) mapping of Lagrangian tracers induced by the motion of the shear flow. (This follows mathematically from the method of characteristics applied to the first order PDE which results from setting $\kappa = 0$ in the advection-diffusion PDE.) Therefore, the scalar level set of interest at time t is described by the graph

$$(x, Y_x(t)) \,,$$

where

$$Y_x(t) = \int_0^t v(x, s)\, \mathrm{d}s$$

is the y position at time t of the tracer starting from $(x, 0)$ at time zero.

Now, $Y_x(t)$ is a statistically homogenous Gaussian random field in x, since it is just a time integral over the statistically homogenous Gaussian random field $v(x, t)$. In Section 3.5.2, we computed that, within the inertial range of scales,

$$\langle (Y_{x+x'}(t) - Y_{x'}(t))^2 \rangle \equiv \sigma^2_{\Delta Y, \mathrm{I}}(t|x) = 4t^2 \int_0^\infty (1 - \cos(2\pi kx)) A_E k^{-1-2H} \Phi(t A_\tau^{-1} k^z)\, \mathrm{d}k \,. \qquad (241)$$

Since the passive scalar level set is the graph of a homogenous Gaussian random field, we can compute its local fractal dimension from the small x asymptotics of this quantity, using Orey's theorem. The results are presented in Table 11. The phase diagram coincides with that for the relative mean-square displacement $\sigma^2_{\Delta Y, \mathrm{I}}(t|x_0)$ (Fig. 17).

The small x asymptotics of the integral appearing in Eq. (241) are computed as follows. Within Region R-2, one can simply replace $(1 - \cos 2\pi kx)$ by its small x limit $2\pi^2 k^2 x^2$, and appeal to the dominated convergence theorem using the fact (235c) that $(1 + u)\Phi(u)$ is a bounded function.

Table 11
Local fractal dimension of scalar level sets within inertial range of scales in Random Spatio-Temporal Shear Model

Parameter regime		Local fractal dimension d_L	Phase region
$z \geq 0$	$0 < H < \dfrac{2-z}{2}$	$d_L = 2 - H - \dfrac{z}{2}$	R-1
$z \geq 0$	$\dfrac{2-z}{2} < H < 1$	$d_L = 1$	R-2

Dominated convergence using this approach would fail in Region R-1, and one must instead rescale integration variables $q = k|x|$, yielding

$$\langle (Y_{x+x'}(t) - Y_{x'}(t))^2 \rangle \equiv \sigma^2_{\Delta Y, \mathrm{I}}(t|x)$$

$$= 4t^2|x|^{2H} \int_0^\infty (1 - \cos(2\pi q)) A_E q^{-1-2H} \Phi(tA_\tau^{-1}q^z|x|^{-z}) \, dq \; .$$

If $z = 0$, then this quantity is clearly proportional everywhere to $|x|^{2H}$, yielding a fractal dimension $d_L = 2 - H = 2 - H - z/2$. For $z \geq 0$, one must use the large-argument asymptotics (235b) of Φ. To establish that the limiting value of the integral is obtained by replacing the Φ factor in the integrand by its asymptotic limit, we apply the dominated convergence theorem to the integral multiplied by $|x|^{-z}$, using the bound (235c).

Note from Table 11 that an increase of the exponent z at fixed value of H results in a smoother interface; we next explain the physical reason for this. We must first of all note that, for the purposes of local smoothness, it is clearly the dynamics of the small scales (large wavenumbers) which play the dominant role. The temporal decorrelation rate of the shear modes scales as $A_\tau(k) = A_\tau k^{-z}$ in the RSTS-I Model, so that the temporal correlations of high wavenumbers are weaker as z increases. That is, $z \to \infty$ implies very rapid decorrelation of high wavenumbers whereas $z \to 0$ corresponds to a slow decorrelation. This is the opposite of the statement made in Section 3.3 concerning the relation of z to the low wavenumber dynamics. One physical implication of Table 11, therefore, is that the passive scalar level sets become smoother as the temporal correlations of the high wavenumber velocity fluctuations decay more rapidly.

To understand this, consider first the case of a steady shear flow. This can be incorporated in our analysis by setting $\hat{\phi}(u) \equiv 1$, which renders the temporal decorrelation factor Φ in Eq. (241) to be simply equal to unity. It is then readily seen that

$$\langle (Y_{x+x'}(t) - Y_{x'}(t))^2 \rangle \equiv \sigma^2_{\Delta Y, \mathrm{I}}(t|x) = 4t^2|x|^{2H} \int_0^\infty (1 - \cos(2\pi k)) A_E k^{-1-2H} \, dk \; ,$$

so that by Orey's theorem, the scalar level sets would have a local fractal dimension $d_L = 2 - H$. This also coincides with the fractal dimension resulting from slow decorrelation of the high wavenumbers at a constant rate ($z = 0$). We see that the fractal structure of the velocity field is directly impressed upon the scalar interface; the Hurst exponent of the interface is exactly the Hurst

exponent H of the velocity field. Suppose now that $z > 0$ so that the rate of decorrelation increases unboundedly at high wavenumbers. This means that after any finite time t, the velocity fluctuations at sufficiently high wavenumber $k \gg (A_\tau/t)^{1/z}$ will have passed through many correlation times. The structure of the scalar interface viewed in the corresponding range of scales $|x| \ll (A_\tau/t)^{-1/z}$ is therefore the result of many roughly independent pushes in time. The temporal fluctuations in the small-scale advection serve to at least partially wash out the influence of the fractal spatial structure of the velocity field on the interface, leading to a smaller interface fractal dimension than in the steady case. The rapid temporal fluctuations of the small-scale velocity components appear to produce a self-averaging, smoothing effect. This is somewhat reminiscent of molecular diffusion, which serves to smooth interfaces and has microscopically small spatio-temporal correlations. For $z > 2 - 2H$, the high wavenumber shear velocity modes fluctuate rapidly enough in time to produce smooth passive scalar level sets.

3.5.3.3. Global fractal dimension of passive scalar level sets. Our above physical description of how temporal correlations influence the roughening of the scalar interface by the turbulent shear flow applies only in the time-dependent range of scales $|x| \ll (A_\tau/t)^{-1/z}$. Here the wrinkling of the scalar interface has an anisotropically self-similar (or *self-affine* [216]) structure which coincides with the long-time asymptotic reported in Table 10:

$$\langle (Y_{x+x'}(t) - Y_{x'}(t))^2 \rangle \equiv \sigma^2_{\Delta Y,1}(t|x)$$

$$\sim \begin{cases} 2\tilde{K}_\Delta^* |x|^{2H+z} t & \text{if } z \geq 0, \ 0 < H < \dfrac{2-z}{2} \\ \dfrac{z}{z+H-1} \tilde{K}_\Delta^\sharp |x|^2 t^{2(z+H-1)/z} & \text{if } z \geq 0, \ \dfrac{2-z}{2} < H < 1 \end{cases} \quad \text{for } |x| \ll (A_\tau/t)^{-1/z} .$$

On the other hand, for $|x| \gg (A_\tau/t)^{-1/z}$, it can be shown directly by rescaling the integration variable $q = kx$ in Eq. (241) that

$$\langle (Y_{x+x'}(t) - Y_{x'}(t))^2 \rangle \equiv \sigma^2_{\Delta Y,1}(t|x) \sim K_\Delta^* t^2 |x|^{2H} \quad \text{for } |x| \gg (A_\tau/t)^{-1/z} , \tag{242a}$$

$$K_\Delta^\sharp = 2\pi^{2H+1/2} \frac{-\Gamma(-H)}{\Gamma(H+\frac{1}{2})} A_E , \tag{242b}$$

which is identical to what a steady random shear velocity field would produce ($\hat{\phi}(u) \equiv 1$). That is, the scalar interface has a distinct anisotropically self-similar structure for $|x| \ll (A_\tau/t)^{-1/z}$ and for $|x| \gg (A_\tau/t)^{-1/z}$, provided $z > 0$. The crossover length scale

$$L_c(t) \equiv (A_\tau/t)^{-1/z} \tag{243}$$

describes the spatial scale below which the interface has settled statistically into its long-time asymptotic structure and above which the interface has not yet substantially felt the effects of temporal decorrelation of the shear flow.

The scalar level set can therefore be described as having two fractal dimensions: a local fractal dimension d_L given in Table 11 for the structure on small scales $|x| \ll L_c(t)$, and a global fractal dimension

$$d_G = 2 - H \tag{244}$$

(by formal analogy with Eqs. (240a) and (240b)) on sufficiently large scales $|x| \gg L_c(t)$. The strict computation of Hausdorff fractal dimension by Orey's theorem (240) involving the $x \to 0$ limit will always focus on the small scales and produce the local fractal dimension. For the case where $z = 0$ (wavenumber-independent decorrelation time scale $\tau(k) = A_\tau$), there is no crossover between fractal dimensions; the passive scalar level set is, for all times, exactly (anisotropically) self-similar with a single fractal dimension $d_L = d_G = 2 - H$:

$$\langle (Y_{x+x'}(t) - Y_{x'}(t))^2 \rangle \equiv \sigma_{\Delta Y,1}^2(t|x) = 4t^2 |x|^{2H} \int_0^\infty (1 - \cos(2\pi k)) A_E k^{-1-2H} \Phi(t/A_\tau) \, dk \ .$$

3.5.3.4. Comparison of model fractal dimensions with experimental results. We pause now to relate the fractal dimensions computed for the passive scalar level sets in our RSTS-I model to the local box-counting fractal dimensions measured within the inertial range of scales in laboratory turbulence. At the Kolmogorov point ($H = 1/3$, $z = 2/3$), the local fractal dimension is $d_L = 4/3$ while the global fractal dimension is $d_G = 5/3$. These values agree extremely well with fractal dimensions computed by Sreenivasan and coworkers using box-counting on two-dimensional section images obtained in a variety of dyed turbulent flows using laser-induced fluorescence [272,305]. In particular, they find a common fractal dimension of 1.36 ± 0.05 for the *interface* between the dyed turbulent and un-dyed quiescent region in jets, wakes, mixing layers, and boundary layers [271], and a fractal dimension of 1.67 ± 0.04 for level sets of the dye concentration within the *interior* of the dyed turbulent region [75]. The interface fractal dimension from these experiments is very close to the value 1.35 observed by Lovejoy to govern the boundary of cloud and rain areas over three decades of scales [199].

We hasten to mention that the agreement between the experiments and the model predictions is not direct. In particular, the experiments do not report a crossover of fractal dimensions within the inertial-convective range for a single passive scalar level set; the different values reported correspond to fractal dimensions in different parts of the flow. We only wish to point out that the numerical fractal dimensions computed in the model do appear in the real world. The model may be suggesting, though, that the reason for observing different fractal dimensions for different level sets may have something to do with the temporal dynamics of the turbulent flow; we come back to this point in Paragraph 3.5.5.2.

3.5.4. Fractal dimension of scalar interfaces after isotropic renormalization

We will now consider large-scale, long-time properties of the pair-distance function within the inertial range of scales. We proceed via a renormalization process similar to that used for the mean passive scalar density in Section 3.4.3, with the important distinction that the integral length scale has already been removed to infinity, and need not be linked with the spatial rescaling. Recall that the presence of an integral length scale is necessary for analysis of the mean passive scalar density to prevent an infrared divergence of energy. The pair-distance function, however, filters the effects of large-scale fluctuations so that the low-wavenumber cutoff can be removed from consideration forthwith.

We therefore simply need to rescale the spatial arguments $x_0 \to x_0/\lambda$, $y \to y/\lambda$, and the time variable $t \to t/\rho(\lambda)$ in the pair-distance function in a suitably linked fashion so that a nontrivial

limiting "fixed point"

$$\bar{Q}^{(t)}(y|x_0) = \lim_{\lambda \to \infty} \lambda^{-1} Q_1^{(t/\rho(\lambda))}\left(\frac{y}{\lambda}\bigg|\frac{x_0}{\lambda}\right) \tag{245}$$

is achieved. Since the pair-distance function is a PDF for the spatial location of the tracer along the shear direction y, we have also rescaled its amplitude by λ^{-1} to preserve the law of total probability

$$\int_{-\infty}^{\infty} Q_1^{(t)}(y|x_0)\,\mathrm{d}y = 1$$

throughout the renormalization.

We note that the inertial-range pair-distance function enjoys an exact scaling invariance

$$Q_1^{(t)}(y|x_0) = (\beta(\lambda))^{-1} Q_1^{(t/\rho(\lambda))}\left(\frac{y}{\beta(\lambda)}\bigg|\frac{x_0}{\lambda}\right), \tag{246a}$$

with

$$\begin{aligned} \rho(\lambda) &= \lambda^z, \\ \beta(\lambda) &= \lambda^{z+H}. \end{aligned} \tag{246b}$$

This may be directly checked from the explicit formula for the pair-distance function (see Eq. (229)) and

$$Q_1^{(t)}(y|x_0) = \frac{\exp(-y^2/(2\sigma_{\Delta Y,\mathrm{I}}^2(t|x_0)))}{\sqrt{2\pi\sigma_{\Delta Y,\mathrm{I}}^2(t|x_0)}},$$

$$\sigma_{\Delta Y,\mathrm{I}}^2(t|x_0) = 4t^2 \int_0^{\infty} (1 - \cos(2\pi k x_0)) A_E k^{-1-2H} \Phi(t A_\tau^{-1} k^z)\,\mathrm{d}k.$$

The scaling invariance (246) is anisotropic except when $z + H = 1$, whereas the renormalization (245) involves an isotropic rescaling. In the case where $H + z = 1$, the rescaling (246b) may be used for the renormalization, and the renormalized pair-distance function $\bar{Q}^{(t)}(y|x_0)$ will coincide with $Q_1^{(t)}(y|x_0)$. For the other cases, the renormalized pair-distance function will differ from the "bare" pair-distance function $Q_1^{(t)}(y|x_0)$.

One key feature of the renormalized pair-distance function is that it will enjoy an isotropic scaling invariance defined by the renormalization group leading to it

$$\bar{Q}^{(t)}(y|x_0) = \lambda^{-1} \bar{Q}^{(t/\rho(\lambda))}\left(\frac{y}{\lambda}\bigg|\frac{x_0}{\lambda}\right) \quad \text{for all } \lambda > 0.$$

A crucial fact behind this statement is that the renormalization does not affect any other fundamental length scales; the renormalized mean passive scalar density discussed in Paragraph 3.4.3.3 does not necessarily enjoy a similar scaling invariance because the integral length scale is rescaled along with space [10,14,141].

The present renormalization of the pair-distance function is quite similar in spirit to the renormalization group in critical phenomena [126,204]. In that context, the Hamiltonian for the

Table 12
Properties of pair distance function and fractal dimension of level sets under isotropic renormalization within inertial range of scales in Random Spatio-Temporal Shear Model

Parameter regime		Temporal rescaling function $\rho(\lambda)$	Renormalized mean-square relative displacement $\bar{\sigma}_{\Delta Y}^2(t\|x_0)$	Fractal dimension $\bar{d}$	Phase region
$z \geq 0$	$0 < H < 1 - z$	λ^{2-2H-z}	$2\tilde{K}_{\Delta}^*\|x_0\|^{2H+z}t$	$2 - H - z/2$	R-I1
$z \geq 0$	$1 - z < H < 0$	λ^{1-H}	$K_{\Delta}^{\sharp}\|x_0\|^{2H}t^2$	$2 - H$	R-I2
$z \geq 0$	$H = 1 - z$	λ^{1-H}	$\sigma_{\Delta Y,\mathrm{I}}^2(t\|x_0)$	$2 - H - z/2$	Boundary

microscopic physics is coarse-grained in a certain scale-invariant fashion to produce a Hamiltonian purported to give a macroscopic picture of the physical system under consideration. In the coarse-graining procedure, certain physical quantities need to be rescaled by some power law, and one initially leaves the exponents unspecified. One discovers, however, that only for special values of these *critical exponents* does the renormalization procedure tend toward a nontrivial macroscopic Hamiltonian. For these special values, the limiting Hamiltonian is itself scale-invariant and fixed under successive application of the renormalization group. Such a Hamiltonian is thus naturally called a *fixed point* (of the renormalization group flow). We can similarly view $\bar{Q}^{(t)}(y|x_0)$ as a fixed point of the renormalization defined by Eqs. (246a) and (246b).

3.5.4.1. Results of renormalization. In Table 12, we report the *unique* temporal rescaling power law $\rho(\lambda)$ necessary for the isotropic renormalization to converge to a nontrivial fixed point, as well as the properties of the resulting renormalized pair-distance function $\bar{Q}^{(t)}(y|x)$. The Gaussian form of the pair-distance function is preserved under the renormalization, so $\bar{Q}^{(t)}(t|x)$ is completely characterized in all cases by the renormalized mean-square relative displacement

$$\bar{\sigma}_{\Delta Y}^2(t|x_0) \equiv \lim_{\lambda \to 0} \lambda^2 \sigma_{\Delta Y,\mathrm{I}}^2\left(\frac{t}{\rho(\lambda)}\bigg|\frac{x_0}{\lambda}\right) .$$

One may directly write the pair-distance function as

$$\bar{Q}^{(t)}(y|x_0) = \frac{\exp(-y^2/(2\bar{\sigma}_{\Delta Y}^2(t|x_0)))}{\sqrt{2\pi\bar{\sigma}_{\Delta Y}^2(t|x_0)}} ,$$

or equivalently as the solution of a diffusion equation

$$\frac{\partial \bar{Q}^{(t)}(y|x_0)}{\partial t} = \bar{D}_{\Delta}(x_0, t)\frac{\partial^2 \bar{Q}^{(t)}(y|x_0)}{\partial y^2} ,$$

$$\bar{Q}^{(0)}(y|x_0) = \delta(y) .$$

with renormalized relative diffusion coefficient

$$\bar{D}_{\Delta}(x_0, t) \equiv \frac{1}{2}\frac{\partial \sigma_{\Delta Y}^2(t|x_0)}{\partial t} . \tag{247}$$
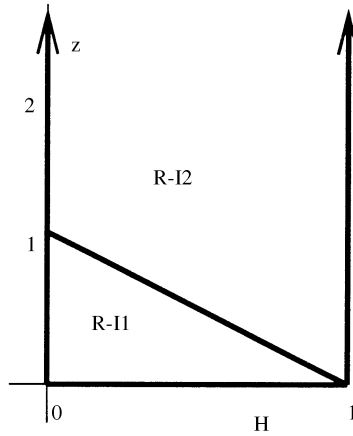
Fig. 18. Phase diagram for renormalized pair distance function in Random Spatio-Temporal Shear Model with Inertial Range, no cross shear transport.

The scaling laws for $\bar{\sigma}^2_{\Delta Y}(t|x_0)$ have coefficients given by Eqs. (238a) and (242b). In each case, the renormalized pair-distance function self-consistently enjoys an isotropic scaling invariance corresponding to the rescalings in the renormalization which produced it:

$$\bar{Q}^{(t)}(y|x_0) = \lambda^{-1}\bar{Q}^{(t/\rho(\lambda))}\left(\frac{y}{\lambda}\bigg|\frac{x_0}{\lambda}\right).$$

The renormalized behavior of the pair-distance function has some sharply different features on either side of the phase boundary $H + z = 1$, drawn in Fig. 18. The formulas for the renormalized relative mean-square displacement $\bar{\sigma}^2_{\Delta Y}(t|x_0)$ and the fractal dimension $\bar{d}$ jump discontinuously across the phase boundary. We now explain why this happens, then derive the results stated in Table 12.

It is readily checked that Region R-I1 has the same properties as the long-time asymptotics of Region R-1 in the phase diagram before renormalization presented in Fig. 17. The reason is that for this range of parameters, the appropriate temporal rescaling function $\rho(\lambda)$ is such that $\lambda L_c(t/\rho(\lambda)) \to \infty$ as $\lambda \to 0$, where $L_c(t)$ is the crossover length defined in Eq. (243). Consequently, the isotropic renormalization zooms in on the passive scalar level set structure below the crossover length, where it has settled down to its long-time asymptotic statistics and is governed by the local fractal dimension d_L reported in Table 11. Note that Region R-I1 of Fig. 18 lies entirely within Region R-1 of Fig. 17.

Region R-I2, on the other hand, corresponds to temporal rescalings in which $\lambda L_c(t/\rho(\lambda)) \to 0$, so that the isotropic renormalization zooms in on the structure of the passive scalar set on scales above the crossover. Here, the effects of temporal fluctuations of the velocity field are not felt; the passive scalar level set is evolving as in a steady shear flow. The fractal dimension characterizing the renormalized fixed point is given in Region R-I2 by the global value $d_G = 2 - H$; see the discussion around Eq. (244).

The discontinuity of the behavior of the renormalized fixed point across the phase boundary $H + z = 1$ is thereby shown to result from a jump between zooming in on the level set structure above and below the crossover length $L_c(t)$.

On the phase boundary $H + z = 1$ itself, the unrenormalized pair-distance function within the inertial range $Q_I^{(t)}(y|x_0)$ obeys the exact isotropic scaling symmetry

$$Q_I^{(t)}(y|x_0) = \lambda^{-1} Q_I^{(t/\rho(\lambda))}\left(\frac{y}{\lambda}\bigg|\frac{x_0}{\lambda}\right)$$

for $\rho(\lambda) = \lambda^{2-2H-z}$, and therefore persists unchanged under the isotropic renormalization: $\bar{Q}^{(t)}(y|x_0) = Q_I^{(t)}(y|x_0)$. The renormalized mean-square relative tracer displacement $\bar{\sigma}_{\Delta Y}^2(t|x_0)$ and the renormalized relative diffusion coefficient $\bar{D}_\Delta(t|x_0)$ remain equal to their bare values $\sigma_{\Delta Y,I}^2(t|x_0)$ (237) and $\frac{1}{2}(\partial\sigma_{\Delta Y,I}^2(t|x_0))/(\partial t)$, which do not have a simple scaling form in x_0 and t.

Interestingly, the phase boundary $H + z = 1$ for the renormalized pair-distance function is exactly the locus of parameters for RSTS-I models with temporal correlations dictated by the natural eddy turnover time scale (see 211a). In particular, the Kolmogorov point ($H = 1/3$, $z = 2/3$) falls on the phase boundary. One interesting implication of this in the model is that the fractal dimension of the level set on large scales within the inertial range is very sensitive to perturbations of the exponents H and z from the exact Kolmogorov exponents, since the fractal dimension $\bar{d}$ jumps discontinuously across the phase boundary. In particular, while the Kolmogorov point itself is associated with a level set fractal dimension of $\bar{d} = 4/3$, a small perturbation of H or z can give rise to a fractal dimension of $\bar{d} = 5/3$.

3.5.4.2. Renormalization computation.

We first of all seek the scaling law $\rho(\lambda)$ for which

$$\bar{Q}^{(t)}(y|x_0) \equiv \lim_{\lambda \to 0} \lambda^{-1} Q_I^{(t/\rho(\lambda))}\left(\frac{y}{\lambda}\bigg|\frac{x_0}{\lambda}\right)$$

is nontrivial, i.e., neither zero nor infinity. We will operate under the assumption that $\rho(\lambda)$ must be a power law,

$$\rho(\lambda) = \lambda^\zeta$$

with $\zeta > 0$; we leave it to the reader to verify that there is in fact no other suitable scaling for the renormalization. In the course of our computation, it will be seen that the scaling exponent ζ is uniquely determined by H and z. From the explicit formula (229) for the pair-distance function, we see that our task is equivalent to finding the scaling law $\rho(\lambda)$ so that

$$\bar{\sigma}_{\Delta Y}^2(t|x_0) \equiv \lim_{\lambda \to 0} \lambda^2 \sigma_{\Delta Y,I}^2\left(\frac{t}{\rho(\lambda)}\bigg|\frac{x_0}{\lambda}\right)$$

is nontrivial. The renormalized pair distance function will then be simply

$$\bar{Q}^{(t)}(y|x_0) = \frac{\exp(-y^2/(2\bar{\sigma}_{\Delta Y}^2(t|x_0)))}{\sqrt{2\pi\bar{\sigma}_{\Delta Y}^2(t|x_0)}}. \tag{248}$$

Now, by a rescaling of the integration variable in Eq. (237), we have the following expression for the renormalized mean-square relative tracer displacement:

$$\bar{\sigma}_{\Delta Y}^2(t|x_0) = \lim_{\lambda \to 0} 4A_E \rho^{-2}(\lambda)\lambda^{2-2H}t^2|x_0|^{2H}J_\Phi\left(\lambda^z\rho^{-1}(\lambda)\frac{t}{A_\tau|x_0|^z}\right), \tag{249a}$$

$$J_\Phi(u) \equiv \int_0^\infty (1 - \cos(2\pi q))q^{-1-2H}\Phi(uq^z)\,dq . \tag{249b}$$

We now try various choices of rescaling $\rho(\lambda) = \lambda^\zeta$, and see for which values of H and z a nontrivial limit is self-consistently produced. We will find that only one choice of ζ will work for each (H, z). It is helpful to separately consider three possible cases: $\zeta = z$, $\zeta > z$, and $0 < \zeta < z$.

$\zeta = z$: When $\zeta = z$, the argument of J_Φ in Eq. (249a) remains fixed as $\lambda \to 0$, and therefore a nontrivial renormalized limit requires that the prefactors balance, i.e., $\rho(\lambda) = \lambda^{1-H}$. Since $\rho(\lambda) = \lambda^\zeta = \lambda^z$ is assumed, self-consistency requires that $z = 1 - H$, which is exactly the phase boundary in Fig. 18. Here, the renormalization leaves $\sigma_{\Delta Y,1}^2(t|x_0)$ fixed, which is not surprising because the scaling invariance (246) which this quantity enjoys is isotropic for $z = 1 - H$.

$\zeta > z$: For temporal rescalings with $\zeta > z$, the argument of J_Φ in (249a) diverges as $\lambda \to 0$. We therefore require the large u asymptotics of $J_\Phi(u)$:

$$\lim_{u \to \infty} J_\Phi(u) \sim \phi(0)u^{-1}\int_0^\infty (1 - \cos(2\pi q))q^{-1-2H-z}\,dq$$

$$= \tfrac{1}{2}\pi^{2H+z+1/2}\frac{-\Gamma(-H-z/2)}{\Gamma(H+(z+1)/2)}\phi(0)u^{-1} , \tag{250}$$

which follows formally from the large argument asymptotics (235b) of Φ, provided that $H < 1 - z/2$ so that the integral appearing in the middle expression is finite. The dominated convergence theorem in conjunction with Eq. (235c) guarantees (250) rigorously in this case. Therefore, for $\zeta > z$,

$$\bar{\sigma}_{\Delta Y}^2(t|x_0) = \lim_{\lambda \to 0} 2A_E\lambda^{2-2H-z-\zeta}t|x_0|^{2H+z}\phi(0)A_\tau\pi^{2H+z+1/2}\frac{-\Gamma(-H-(z/2))}{\Gamma(H+(z+1)/2)} ,$$

and the existence of a nontrivial limit requires that we choose $\zeta = 2 - 2H - z$. Self-consistency with the assumption $\zeta > z$ means that this scaling can only work when $H < 1 - z$, which is just Region R-I1 in Fig. 18. The other required condition in the computation, $H < 1 - \frac{z}{2}$, is automatically satisfied within Region R-I1, and therefore the renormalization developed here is indeed valid for that regime of parameters.

$\zeta < z$: When $\zeta < z$, the argument of J_Φ in Eq. (249a) converges to zero, and we need instead the small argument asymptotics:

$$\lim_{u \to 0} J_\Phi(u) = \int_0^\infty (1 - \cos(2\pi q))q^{-1-2H}\,dq = \tfrac{1}{2}\pi^{2H+(1/2)}\frac{-\Gamma(-H)}{\Gamma(H+\frac{1}{2})},$$

which follows from Eq. (235a) and the boundedness of Φ. The renormalized limit of the mean-square relative tracer displacement then takes the form

$$\bar{\sigma}_{\Delta Y}^2(t|x_0) = \lim_{\lambda \to 0} 2A_E \lambda^{2-2H-2\zeta} t^2 |x_0|^{2H} \pi^{2H+(1/2)} \frac{-\Gamma(-H)}{\Gamma(H+\frac{1}{2})} \ .$$

A nontrivial limit requires that we choose $\zeta = 1 - H$, and self-consistency with $\zeta < z$ means that this renormalization is valid precisely for Region R-I2.

Self-similarity and fractal dimension of renormalized passive scalar field. Having computed the appropriate rescaling $\rho(\lambda)$ and renormalized mean-square shear-parallel displacement $\bar{\sigma}_{\Delta Y}^2(t|x_0)$ for each value of H and z, we obtain the renormalized pair distance function from Eq. (248). Its scaling invariance under the isotropic rescaling defining the renormalization group can be directly checked. The renormalization preserves the Gaussianity of the graph describing the level set of the passive scalar field initially lying along $y = 0$, so the fractal dimension of this level set for the renormalized passive scalar field may be obtained from Orey's theorem. The exponent α to be used in Eq. (240) is readily read off from the formulas for $\bar{\sigma}_{\Delta Y}^2(t|x_0)$, which have pure power law scaling in x_0. This concludes the derivation of the results stated in Table 12.

3.5.5. Open problem: fractal dimension of scalar interfaces with small but nonvanishing molecular diffusivity

The simple methodology used to compute the rich inertial-range behavior of the pair-distance function and the passive scalar level set fractal dimensions in Section 3.5 has relied fundamentally on the neglect of molecular diffusion. Its inclusion significantly complicates matters. Instead of Eq. (225), we would have (for no cross sweep $\bar{w} = 0$)

$$Y_{x_0 + x'_0}(t) - Y'_{x_0}(t) = \int_0^t (v(x_0 + x'_0 + \sqrt{2\kappa}W_x(s), s) - v(x'_0 + \sqrt{2\kappa}W_x(s), s)) \, ds + \sqrt{2\kappa}W_y(t) \ ,$$

where $(W_x(t), W_y(t))$ is a Brownian motion. The appearance of $W_x(s)$ in the argument of $v(x, s)$ destroys the Gaussianity, and thereby the resulting development of the pair-distance function hinging on this property. Nonetheless, there are more sophisticated tools available for handling the effects of molecular diffusion on a spatio-temporal random shear flow in a mathematically rigorous fashion [10,14]. Furthermore, any moments of the pair distance function with diffusion can be treated explicitly by following the procedure utilized in Section 3.2.

We pose as an open problem the mathematical examination of the properties of the pair-distance function and the structure of passive scalar level sets within the inertial-convective range of scales in the RSTS-I Model when molecular diffusion is present but weak compared to the large scale turbulent advection (high but finite Péclet number). By inertial-convective range of scales, we mean the portion of the inertial range over which the effects of molecular diffusion are *formally* subdominant to turbulent diffusion, in the sense that $\kappa \ll \tau_L(x)\langle(\delta v(x))^2\rangle$, where $\langle(\delta v(x))^2\rangle \sim A_E |x|^{2H}$ denotes the mean-square velocity fluctuation measured over a distance x across the shear and $\tau_L(x) \sim \min(x^2/\kappa, A_\tau x^z)$ is an approximate Lagrangian correlation time associated to this scale. The inertial-convective range can be equivalently defined as the asymptotic regime

$$L_K, L_d \ll x \ll L_0$$

where L_d is a length scale above which molecular diffusion is formally subdominant to turbulent advection (see Paragraph 4.3.3.1).

Since we are concerned with scales $x \gg L_d$, the effects of molecular diffusion might naively be assumed to be negligible. The limit of vanishing molecular diffusion, however, has a number of singular features which require it to be studied carefully [74]. For example, without molecular diffusion, a sharp interface between distinct fluids will forever remain sharp, while any molecular diffusion, however small, will smooth the variation of the passive scalar field across the interface. The thickness of the resulting front can be expected to be on the order of L_d, which is very small compared to the scales of interest, but the geometric structure along the front at all length scales could be significantly affected by the fact that the passive scalar field has been smoothed across the front. The fractal dimension of passive scalar level sets within the inertial-convective range of scales may therefore well assume different values in the presence of molecular diffusion than those computed in Section 3.5.3 for $\kappa = 0$.

Experimental measurements [271,272] of the fractal dimensions of interfaces generally involve flows such as wakes and jets and layers, wherein the large-scale shear in these flows is directed along the coarse-grained interface. The passive scalar level set emanating from $y = 0$ which we considered in Section 3.5.3 on the other hand gets hit head-on by the shear flow. To bring the model closer to the experimental setup, it would be preferable to consider the fractal dimension of a passive scalar level set evolving from $x = 0$. For $\kappa = 0$, such a level set remains forever straight, but for $\kappa > 0$, the interaction of molecular diffusion and the shear will wrinkle it. An interesting question is how the fractal dimensions of the level sets evolving from $x = 0$ and $y = 0$ compare to each other when $\kappa > 0$.

The inclusion of the effects of molecular diffusion into the RSTS-I Model would put it in a position to interact with various physical and mathematical theories which have been put forth concerning the fractal dimension of passive scalar level sets over the inertial-convective range of scales. We briefly mention some of these now, along with some questions concerning them raised by the RSTS-I Model as developed here.

3.5.5.1. Theories and bounds for fractal dimensions of passive scalar level sets. Several theories have been put forward to explain either the observed fractal dimension of $1.36 \pm 0.05 \approx 4/3$ for scalar level sets at turbulent interfaces [271] or the dimension $1.67 \pm 0.04 \approx 5/3$ for scalar level sets immersed well within a turbulent fluid [75]. That the fractal dimension of the interface between dyed and non-dyed region of a turbulent flow should be 4/3 (modulo intermittency corrections) has been argued in several ways. One, offered independently by Sreenivasan et al. [235,310] and by Gouldin [128]), proceeds from the experimental observation that the flux of dye across the interface depends only on the large-scale parameters and not on molecular diffusivity, which demands that the interface must increasingly contort itself to provide the surface area to maintain this constant flux as the Péclet number is increased. Another approach, due to Hentschel and Procaccia [132], analyzes Richardson's pair-distance function in the limit of zero molecular diffusion by positing a diffusion PDE for this quantity with relative diffusivity depending as a power law on current tracer separation and elapsed time. If the exponents for the relative diffusivity are chosen in accordance with Kolmogorov–Obukhov completely self-similar theory, then the fractal dimension of any level set as computed from the pair-distance function and the assumption that Eqs. (240a) and (240b) holds also for non-Gaussian graphs produces $d = 4/3$.

More recently, Constantin et al. [75] have predicted an interface fractal dimension of

$$d = 1 + H \quad \text{(interface)} , \tag{251}$$

based on a certain rigorous mathematical bound they derived and some further assumptions concerning the sharpness of this upper bound and the nature of turbulent velocity fluctuations near the interface. The parameter H is, as usual, the Hurst exponent characterizing the inertial-range spatial structure of the velocity field. For Kolmogorov turbulence, $H = 1/3$, and the theory (251) predicts an interface fractal dimension of 4/3. The interface fractal dimension formula (251) also follows from a direct generalization of the phenomenological arguments of [235,310]. There is some interesting experimental data in [75] showing fairly good agreement with the prediction (251) for various moderate Reynolds number experiments in which the inertial-range is not fully developed but characterized in some effective sense by a Reynolds-number-dependent Hurst exponent $0 \leq H(\text{Re}) < 1/3$.

Mandelbrot [214,215] suggested a simple possible reason for why a passive scalar level set in a fully turbulent region should have fractal dimension 5/3: almost every level set of a two-dimensional self-similar (or more properly, self-affine) Gaussian fractal random field with Hurst exponent α has fractal dimension $2 - \alpha$. Passive scalar fluctuations in the inertial-convective range of scales within a statistically homogenous region of turbulence are thought to have Hurst exponent $H_T = 1/3$, both from similarity theory [76,254] and from experimental measurements [308]; see Paragraph 4.3.4.1 for further discussion. If the passive scalar field were Gaussian, it would then follow that their level sets would have fractal dimension 5/3. The passive scalar fluctuations in the inertial-convective range of scales are however, known to be highly non-Gaussian [309]. Constantin et al. [75], on the other hand, deduce from a rigorous estimate an upper bound

$$d \leq \tfrac{1}{2}(3 + H) \quad \text{(within homogenous turbulence)} \tag{252}$$

for the fractal dimension of a passive scalar level set immersed in a homogenous turbulent flow with velocity Hurst exponent H. If this upper bound is assumed to be sharp, then a fractal dimension of 5/3 is predicted for the Kolmogorov value $H = 1/3$. We note that, strictly speaking, the fractal dimension upper bound (252) applies to a short time average of the level set, rather than an instantaneous level set. A rigorous sufficient condition for Eq. (252) to be sharp was obtained in [74]; unfortunately it is difficult to decide in practice whether this technical condition holds. We emphasize that the rigorous mathematical theory of [74,75] includes the effects of small but nonvanishing molecular diffusivity.

3.5.5.2. Questions raised by the RSTS-I Model concerning theories for fractal dimension of scalar level sets. It would be interesting to compare some of these theories with exact results from the RSTS-I Model, once the effects of molecular diffusion were properly taken into account. As it stands, the exact fractal dimensions deduced from the simplified model with $\kappa = 0$ conflict rather sharply with the conclusions of some of these theories. For example, the model predicts that both local and global fractal dimensions should decrease with the Hurst exponent of the velocity field, H, whereas the above theories predict an increase for passive scalar level sets both at turbulent interfaces (251) and within a region of homogenous turbulence (252). Moreover, one readily checks from Table 11 and Eq. (244) that the mathematical upper bound (252) for passive scalar level sets is violated by

both local and global fractal dimension in the RSTS-I Model for sufficiently small values of H. We emphasize that, in and of itself, this is no contradiction because the above mathematical and physical theories all assume the presence of a small amount of molecular diffusion (except for [132]). It does, however, motivate the computation of effects of molecular diffusion in the RSTS-I Model to address questions such as: Do the inertial-convective range fractal dimensions change to fall in line with the theoretical predictions and inequalities? If not, can the physical mechanism creating the disagreement be identified? Might there be subtle issues concerning the time averaging of level sets used in the derivation of the upper bound (252) in [75]? Is the technical condition from [74] which establishes the sharpness of Eq. (252) satisfied in the RSTS-I Model?

One possible objection to the relevance of the RSTS-I Model to these theories is the strong anisotropy of the model. Indeed, this prevents quantitative comparison with [132], which relies on the isotropy of the turbulence in its analysis. But the other theories are formulated in a quite general way which should apply to anisotropic situations. We have also noted above that experimental measurements [271,272] are performed in settings with strong large-scale anisotropic shear.

We recall finally our discussion in Section 3.5.3 in which we demonstrated the strong relevance of the temporal correlation structure of the RSTS-I flow in determining the fractal dimension of scalar level sets. First of all, the local fractal dimension depends on the value of z, with more rapid decay of the correlation time at high wavenumber (z large) leading to smoother scalar level sets. Secondly, the scalar level sets exhibit two regimes of different self-similarity which are determined by the relative scales which have strongly or barely felt the effects of temporal fluctuations. Of the above-mentioned theories, however, only [132] makes explicit reference to the temporal correlation structure of the velocity field. The mathematical inequalities of [74,75] may depend implicitly on the velocity temporal structure through their assumptions about the degree of (Hölder) smoothness of the passive scalar field and on their temporal averaging of scalar level sets. It would be interesting to know whether the qualitative effects of temporal structure on the passive scalar sets in the RSTS-I Model persist when $\kappa > 0$. If so, the following questions could be pursued: Do the mathematical and physical theories apply for the RSTS-I Model as both Hurst exponent H and temporal scaling exponent z are varied? If not, can they be modified to explicitly account for the nature of the temporal correlations in the velocity field? Could the difference between the fractal dimension of passive scalar interfaces and level sets in fully turbulent regions be due to a difference in the local temporal structure of the turbulence?

4. Passive scalar statistics for turbulent diffusion in rapidly decorrelating velocity field models

In Section 3, we studied tracer transport in a velocity field model with a simplified shear flow geometry. For such a flow, the nonlinearity of the trajectory equations simplifies to the point that they may be integrated by quadrature, leading to an explicit statistical expression for the location of a tracer particle at any moment of time. We could then proceed directly to analyze a rich variety of behavior for the statistical motion of a tracer particle in response to various properties of the environment.

In this section, we will consider a complementary simplification which again permits a tractable analysis of the tracer trajectories. Rather than restricting the geometrical structure of the flow, we

will prescribe a convenient statistical structure. Namely, the velocity field will be taken to be a mean zero, homogenous, stationary Gaussian random field with no memory

$$\langle \boldsymbol{v}(\boldsymbol{x}, t) \otimes \boldsymbol{v}(\boldsymbol{x} + \boldsymbol{r}, t + \tau) \rangle \equiv \mathscr{R}_{s}(\boldsymbol{r}) \delta(\tau) \, ,$$

where the tensor $\mathscr{R}_{s}(\boldsymbol{r})$ describes the spatial correlation structure, and the Dirac delta function describes the temporal correlation structure. For clarity, in this paper we shall call this the *Rapid Decorrelation in Time* (RDT) model. It is also known in the literature as the "delta-correlated" model, the "white-noise" model, or the "Kraichnan model" after one of its original proposers [179]. (Kazantsev [152] independently suggested such a model for a magnetohydrodynamic turbulent flow.)

The key simplification afforded by the Rapid Decorrelation in Time model is that each of the tracer particles in such a flow undergoes an effective Brownian motion. Unlike an ordinary Fickian diffusion process, the Brownian motions of a collection of particles moving simultaneously in the flow are coupled to one another. Through the standard relation between the mean of a passive scalar field and the equations of motion for a single tracer particle (see, for example, [185,196], or [244]), it follows that the mean $\langle T(\boldsymbol{x}, t) \rangle$ obeys a closed diffusion PDE. That is, the moment closure problem [227] is averted in the RDT model. One can go further and write down a closed equation of diffusion type for the equal-time, second-order passive scalar correlation function

$$\langle T(\boldsymbol{x}, t) T(\boldsymbol{x}', t) \rangle \, ,$$

a fundamental statistic reflecting the small-scale spatial structure of the passive scalar field. In fact, as first shown by the first author [206], the equal-time correlation functions of all orders

$$\left\langle \prod_{j=1}^{N} T(\boldsymbol{x}^{(j)}, t) \right\rangle$$

obey diffusion equations with variable coefficients. Hence, the statistical spatial structure of the passive scalar field in the RDT model is represented precisely through the solutions to *deterministic* PDEs. There is no need to handle random variables explicitly.

Overview of Section 4

RDT model setup: The diffusion equations for the mean passive scalar density and second-order correlation function are presented in Section 4.1. The mean passive scalar density in the RDT model obeys a standard constant-coefficient diffusion equation (255); the effect of the velocity field is simply to boost the diffusivity constant. Therefore, we shall focus for the most part on the second-order passive scalar correlation function. In the RDT model, it obeys a variable coefficient diffusion PDE (256) which admits some explicit special solutions showing how the small-scale fluctuations of the passive scalar field respond to the turbulent velocity field. To illuminate the behavior of the passive scalar field fluctuations, we only consider statistically homogenous systems. We furthermore restrict attention to fluctuations with length scales much smaller than the integral length of the velocity field. The main physical aspects are most clearly seen in asymptotic regimes in which the passive scalar statistics exhibit *universal* features independent of particular model details, and we shall concentrate our attention on these regimes.

Evolution through the inertial range: In Section 4.2, we examine the evolution of the passive scalar correlation function over time intervals during which the correlation length of the passive scalar fluctuations lies within the inertial range of scales. In this asymptotic regime, the passive scalar

correlation function obeys some *universal* laws which depend only on the inertial-range scaling law for the turbulent energy spectrum. We first consider, in Section 4.2.1, the rate of decay of the passive scalar variance $\langle (T(\boldsymbol{x},t))^2 \rangle$ with time in a turbulent shear flow of the type discussed in Section 3, but with a delta-correlated temporal structure. The passive scalar variance is an analogue of the energy of the velocity field, and is just the value of the second-order correlation function at coinciding points. For a turbulent flow with short-range spatial correlations, the passive scalar variance decays according to a power law with an exponent equal to that describing dissipation by molecular diffusion alone; only the decay rate is enhanced due to the turbulent activity. On the other hand, in a turbulent flow with long-range spatial correlations, the passive scalar variance decays anomalously at long times according to a more rapidly vanishing power law. We obtain an exact expression for the evolution of the passive scalar variance by relating the variable-coefficient diffusion equation satisfied by the passive scalar correlation function to an associated quantum-mechanical Schrödinger equation. The potential function appearing in this Schrödinger equation reflects the spatial correlations of the turbulent shear flow.

Next, in Section 4.2.2, we consider a statistically isotropic turbulent flow with long range correlations, and develop a self-similar solution which describes the evolution of the passive scalar correlation function through the inertial range of scales. From the form of this solution, we will deduce the anomalous relative diffusion of a pair of tracers while they are separated by a distance lying within the inertial range of scales. The mean-square distance between the particles grows according to a superlinear power law, rigorously manifesting a version of Richardson's law [284] for the RDT model which reflects the acceleration of diffusion as the particles separate. We illustrate this dispersion of a pair of tracer particles over several decades through a Monte Carlo numerical simulation. The explicit self-similar solution indicates another interesting contrast between the decay of passive scalar fluctuations under the influence of a turbulent flow and under ordinary molecular diffusion. Whereas rough fluctuations are smoothed out by molecular diffusion, the self-similar spatial correlations in a turbulent flow actually introduce a rough fractal structure which spreads out in space even as the passive scalar field is decaying in amplitude.

Statistically stationary state of driven passive scalar: In Section 4.3, we turn to the statistics of a passive scalar field which is advected by an RDT turbulent flow, dissipated by molecular diffusion, and directly driven by a "pumping" field $f(\boldsymbol{x},t)$ representing external agitation:

$$\frac{\partial T(\boldsymbol{x},t)}{\partial t} + \boldsymbol{v}(\boldsymbol{x},t)\cdot\nabla T(\boldsymbol{x},t) = \kappa\varDelta T(\boldsymbol{x},t) + f(\boldsymbol{x},t) \,,$$

$$T(\boldsymbol{x},t=0) = T_0(\boldsymbol{x}) \,.$$

In the RDT model, the pumping is represented as a mean zero, Gaussian, homogenous random field with a delta-correlated temporal structure, and a spatial structure characterized by a single large length scale L_f:

$$\langle f(\boldsymbol{x},t)f(\boldsymbol{x}+\boldsymbol{r},t+\tau)\rangle = \varPhi(\boldsymbol{r})\delta(\tau) \,. \tag{253}$$

With pumping, the advection–diffusion equation has both driving and damping. The passive scalar field may then be expected to settle down after a suitable period of time to a statistically stationary state in which production of new fluctuations by the pumping is balanced by destruction via

molecular dissipation. Sometimes we will refer to such a statistically stationary state as a "quasi-equilibrium", with the "quasi" prefix distinguishing the strongly damped and driven equilibrium described here from ordinary thermal equilibrium.

For pumping of the form (253), the mean and correlation functions of the passive scalar function still obey closed equations of diffusion type (with an inhomogeneity arising from the pumping) (Section 4.3.1). The statistically stationary state is characterized by the steady solutions to these equations. The mean of this state is zero by symmetry, but the correlation function of the passive scalar field in quasi-equilibrium:

$$P_2^*(\boldsymbol{r}) \equiv \langle T(\boldsymbol{x},t) T(\boldsymbol{x}+\boldsymbol{r},t) \rangle_*$$

will reflect the spatial structure of the passive scalar field set up by the input of fluctuations at large scales and dissipation at small scales. The asterisks decorating the above expression indicate that the statistics of the passive scalar field are to be taken as those of the quasi-equilibrium state, which inherits statistical homogeneity from its environment. For the case in which the velocity and pumping field is statistically isotropic, Kraichnan [179] showed how the correlation function of the passive scalar field could be represented via quadrature in terms of the functions $\mathcal{R}_s(\boldsymbol{x})$ and $\Phi(\boldsymbol{x})$ characterizing the spatial correlations of the velocity and pumping fields (Section 4.3.2).

We shall be particularly interested in the *small-scale* spatial structure of the quasi-equilibrium passive scalar field, which one might expect to display *universal* features independent of the particulars of the large scale pumping or the large-scale structure of the velocity field. The second-order statistics of the small scales do indeed exhibit universal behavior in the RDT model, but we hasten to mention that there does appear to be some sensitivity to the large scale velocity field in real turbulent flows [306,309]. Some striking features of the small-scale statistics are brought out in the *passive scalar spectrum* $E_T(k)$, which resolves the strength of the passive scalar fluctuations as a function of their wavenumber k and parallels the energy spectrum for the velocity field.

Perhaps the most interesting feature of $E_T(k)$ is that it can support a variety of universal self-similar scaling regimes at high wavenumbers. These are analogous to the Kolmogorov $k^{-5/3}$ inertial-range scaling of the energy spectrum of a turbulent velocity field at high Reynolds number (see Paragraph 3.4.3.1). Theoretical predictions for three different scaling regimes in the passive scalar spectrum $E_T(k)$ have been proposed from a number of directions [28,29,76,120,254]. Like the Kolmogorov prediction, each of these theories predicts a universal scaling law for $E_T(k)$ within some range of wavenumbers, provided the physical conditions are such that the delimiting wavenumbers are sufficiently widely separated. Though each theory has some experimental data which purportedly support it, none are unequivocally confirmed and some are under active controversy. Moreover, in one range of scales (the inertial-diffusive regime), two competing theories predict different scaling laws, and experiments have not decided the issue definitively.

We will utilize the RDT model to investigate the nature of scaling regimes of the passive scalar spectrum, with a view to making contact with the real-world issues when we can. First, in Section 4.3.3, we report the rigorous existence of three universal scaling regimes in the passive scalar spectrum in the RDT model, corresponding to those predicted for the real world. Two of these scaling laws were computed by Kraichnan [179,183]. Then, in Section 4.3.4, we examine whether straightforward adaptations of the approximate real-world theories to the RDT model make the correct predictions. The theories based on Kolmogorov-type dimensional analysis produce the correct scaling predictions for two of the regimes. In the inertial-diffusive regime,

where naive dimensional analysis is insufficient to produce a unique prediction, we find that the theory of Batchelor, Howells, and Townsend [29] carries over successfully to the RDT model, but the theory of Gibson [121] does not.

Higher-order statistics: Finally, in Section 4.4, we survey some recent work concerning the higher order quasi-equilibrium statistics of the passive scalar field in the RDT model. We focus particular attention on the passive scalar structure functions

$$S_N^*(r) \equiv \langle (T(\boldsymbol{x} + \boldsymbol{r}) - T(\boldsymbol{x}))^N \rangle \,,$$

and the issue of whether they display *anomalous scaling* properties in the inertial-convective range. By anomalous scaling is meant that the structure functions have a power law form

$$S_N^*(r) \propto r^{\zeta_N}$$

over a common interval of scales r much larger than the dissipation scales and much smaller than the macroscopic system scale, but that the exponents have a nontrivial relation, i.e.

$$\zeta_{2N} \neq N\zeta_2 \,.$$

This phenomenon is often called an instance of "small-scale intermittency" or "inertial range intermittency", as it reflects a tendency for the passive scalar fluctuations on these scales to burst to large values from time to time with a much greater frequency than would arise from a Gaussian random field.

We shall state some theories for the values of the exponents ζ_{2N} in the RDT model [64,116,183,343], often with conflicting predictions. The predictions are compared to the results of some recent numerical simulations in some simplified settings where accurate resolution is possible and unambiguous anomalous scaling can be demonstrated [33,334].

In Section 5, we will utilize a variant of the RDT model to study *large-scale* intermittency of the passive scalar field.

4.1. Definition of the rapid decorrelation in time (RDT) model and governing equations

First we restate in Section 4.1.1 the definition of the RDT model and indicate a sound mathematical interpretation of the Gaussian, delta-correlated velocity field. Then, in Section 4.1.2 we develop the diffusion PDEs for the mean and second-order correlation function of the passive scalar field, and remark on their structure. The equation for the second-order correlation function will be studied through applications in Sections 4.2 and 4.3. We discuss in Section 4.1.3 the sense in which the RDT model describes the limiting behavior of the passive scalar field in a velocity field with short but finite correlation time relative to the time scales characterizing advection. While the RDT model equations do in fact describe a particular short correlation time limit of a broad class of velocity fields, we illustrate through a cautionary example that other limiting nontrivial passive scalar dynamics can be realized. Finally, in Section 4.1.4, we define the particular form of the velocity spatial correlation function we will use in applications.

4.1.1. Definition of model

The velocity field $\boldsymbol{v}(\boldsymbol{x}, t)$ is formally defined in the Rapid Decorrelation in Time (RDT) model as an incompressible, Gaussian, homogenous, stationary, random field with mean zero and

second-order correlation function

$$\langle \boldsymbol{v}(\boldsymbol{x},t) \otimes \boldsymbol{v}(\boldsymbol{x}+\boldsymbol{r}, t+\tau)\rangle = \mathscr{R}_{s}(\boldsymbol{r})\delta(\tau) . \tag{254}$$

The tensor-valued function $\mathscr{R}_{s}(\boldsymbol{r})$ describes the spatial structure of the velocity field; incompressibility implies $\nabla \cdot \mathscr{R}_{s}(\boldsymbol{r}) \equiv 0$ (see [341], Section 22.4). One readily observes that the velocity field so defined is not an ordinary random field, since the variance of such a field is infinite. This divergence of the mean-square velocity is necessary for a nontrivial advection in a model with zero correlation time.

Random fields with delta correlations arise naturally in a variety of simplified physical models, and they can be given a clear mathematical meaning as generalized, or distribution-valued, random fields (see [118] or [341], Ch. 24,25). The complication in the current context is the appearance of such a random field as a coefficient in the advection–diffusion PDE

$$\partial T(\boldsymbol{x},t)/\partial t + \boldsymbol{v}(\boldsymbol{x},t) \cdot \nabla T(\boldsymbol{x},t) = \kappa \varDelta T(\boldsymbol{x},t) ,$$

$$T(\boldsymbol{x}, t=0) = T_0(\boldsymbol{x}) .$$

We can avoid the difficulty of making sense of the solution of a PDE with random, distribution-valued coefficients by reformulating the mathematical problem in terms of the *flow* of the fluid. That is, we can specify the mapping of the location of fluid elements from one time to another, and not make explicit reference to the velocity field. The RDT velocity field induces a random *Brownian flow* of the fluid, in which every fluid element undergoes a Brownian motion, but the motions of different fluid elements are correlated with one another according to the spatial structure tensor $\mathscr{R}_{s}(\boldsymbol{r})$ [189]. A Brownian flow makes rigorous mathematical sense of a fluid flow with a Gaussian, delta-correlated velocity field just as mathematical Brownian motion makes sense out of the evolution of a particle with a Gaussian, delta-correlated velocity. Through the mathematical framework of a Brownian flow, one can make rigorous sense of the advection of a passive scalar field in the RDT velocity field and derive all the results in this section without having to deal directly with the distribution-valued velocity field itself. We only wish to indicate that a rigorous formalism is possible, though we will not dwell on it here. The reader may consult [185] or [349] for the technical implementation of these ideas.

4.1.2. Closed equations for mean and correlation function of passive scalar field

Though the RDT velocity field model is limited in simulating physical reality through its lack of inertia or memory effects, it has the virtue of having closed equations for the mean and correlation functions of the passive scalar field. The usual turbulence moment closure problem [227] does not arise in the RDT model. Thus, one has the opportunity for much more precise mathematical analysis of the passive scalar field statistics than is generally possible. In particular, one can study the advection of a passive scalar field in a velocity field with long-range spatial correlations and an inertial range of self-similar behavior.

We can think of the Simple Shear Model and RDT Models as complementary simplified models which permit a mathematical study of various aspects of turbulent diffusion in velocity fields. The Simple Shear Model restricts the geometry of the flow, but permits an arbitrary specification of the spatio-temporal statistics. The RDT Model assumes a special (and unphysical) temporal structure, but permits a multi-dimensional flow geometry with an arbitrary specification of the spatial statistics.

We will present the PDEs for the mean and second-order correlation function of the passive scalar field in turn. The fact that closed equations could be written down for these statistical functions was first pointed out by Kraichnan [179] and Kazantsev [152] through formal arguments. Since then, these equations have been derived in several contexts by various techniques, some mathematical and rigorous [185,206,208,246,244,349] and some formal [95,117,164].

4.1.2.1. Mean passive scalar density. In the RDT model, the mean passive scalar field $\langle T(\boldsymbol{x},t)\rangle$ obeys an ordinary diffusion equation with enhanced coefficient:

$$\partial\langle T(\boldsymbol{x},t)\rangle/\partial t = \nabla\cdot((\kappa\mathscr{I} + \tfrac{1}{2}\mathscr{R}_{\mathrm{s}}(\boldsymbol{0}))\nabla\langle T(\boldsymbol{x},t)\rangle) \ ,$$

$$\langle T_0(\boldsymbol{x},t=0)\rangle = \langle T_0(\boldsymbol{x})\rangle \ . \tag{255}$$

Here $\mathscr{I}$ denotes the identity matrix, and $\mathscr{R}_{\mathrm{s}}(\boldsymbol{r})$ is the spatial structure tensor of the velocity field; see Eq. (254). $\mathscr{R}_{\mathrm{s}}(\boldsymbol{0})$ is a nonnegative-definite tensor since $\langle \boldsymbol{v}(\boldsymbol{x}',t)\otimes\boldsymbol{v}(\boldsymbol{x}',t)\rangle = \mathscr{R}_{\mathrm{s}}(\boldsymbol{0})\delta(t)$.

For a statistically isotropic velocity field, $\mathscr{R}_{\mathrm{s}}(\boldsymbol{0})$ will simply be a multiple of the identity, say $\mathscr{R}_{\mathrm{s}}(\boldsymbol{0}) = R_0\mathscr{I}$, with $R_0 > 0$, and one can simply say the scalar diffusion constant for the mean passive scalar density is enhanced from κ to $\kappa + \tfrac{1}{2}R_0$. The turbulent enhancement R_0 is simply a measure of the strength of the velocity field, which may be formally thought of as the product of the (very small) velocity correlation time and the (very large) single-point velocity variance. (Smooth the delta function in the expression (254) over a very small time interval τ_{c} to see this). This is in agreement with what Taylor's formula for the turbulent diffusivity would produce in the zero correlation time limit (Section 3.1.3).

The reason that the mean passive scalar density obey a simple diffusion equation is that the trajectory of a single tracer particle in the RDT model is given as a sum of two independent Brownian motions: one with diffusivity κ from molecular diffusion, and one with diffusivity $\tfrac{1}{2}R_0$ from advection by the RDT velocity field. The superposition of these independent motions produces an effective Brownian motion with diffusivity $\kappa + \tfrac{1}{2}R_0$. The equation for the mean passive scalar density then follows from its relation to the statistics of a single tracer trajectory (see Section 3.4).

None of these comments should lead the reader to conclude that the white noise velocity field leads to trivial behavior for the passive scalar. It is only the mean passive scalar density (or equivalently, the statistics of the motion of a single tracer) which has this simple effective behavior. When we turn to statistics of the fluctuations, the situation is much more interesting.

4.1.2.2. Second-order passive scalar correlation function. Until now, we have focused for the most part on the behavior of the mean concentration of the passive scalar, or equivalently, the motion of a single tracer particle. (An exception was in our discussion of the pair-distance function and fractal interfaces in Section 3.5.) We wish in this section to focus on the nature of the fluctuations of the passive scalar field. This is particularly relevant when considering the transport of dangerous quantities (pollutants or hazardous chemicals). In these cases one is more interested in the probability of the passive scalar density exceeding some certain safety threshold, rather than simply the (presumably) very low mean value. (See for example the environmental science books [78,265].) Knowledge of the statistics of the fluctuations are important in general geophysical and engineering applications, as they give information about how rapidly a passive scalar becomes "well-mixed"

in a turbulent fluid and about the rate of growth of a cloud of passive scalar released into a turbulent environment, as we saw in Section 3.5.

From a fundamental physical viewpoint, the statistics of the fluctuations of the passive scalar field reveal much more about the small-scale structure of the velocity field than the mean does. This is particularly interesting in fully developed turbulence, which we shall be considering, in which the turbulent velocity field has its energy distributed over a wide range of scales. The mean passive scalar density is most sensitive to the large-scale fluctuations of the velocity field, in which most of the energy resides (see Section 3.5). The effects of the small-scale velocity fluctuations are manifested primarily in the small-scale passive scalar fluctuations. This is particularly interesting in physical turbulence theory, where the statistics of the velocity fluctuations on small scales are at least approximately *universal*. That is, while the large-scale structure of a turbulent velocity field depends strongly on the system configuration (pipe flow, jet flow, shear flow, boundary layer flow), the small scales have several common features in these different settings. (See [309] for a recent review.) One might expect the passive scalar fluctuations on small scales to be universal as well. It is thus of interest to discover to what extent this is true, and, furthermore, to describe these universal statistics of the passive scalar field.

A fundamental statistic of the passive scalar field from which one can determine some basic properties about the spatial structure of the fluctuations is the (equal-time) *second-order passive scalar (PS) correlation function*:

$$\langle T(\boldsymbol{x}, t) T(\boldsymbol{x}', t) \rangle .$$

For simplicity, we shall assume that the passive scalar field is a statistically homogenous random field with mean zero, so that in particular, the second-order PS correlation function depends only on time and the relative displacement of the observation points $\boldsymbol{x} - \boldsymbol{x}'$:

$$P_2(\boldsymbol{r}, t) \equiv \langle T(\boldsymbol{x}, t) T(\boldsymbol{x} + \boldsymbol{r}, t) \rangle .$$

We will discuss the evolution of the passive scalar variance,

$$P_2(\boldsymbol{0}, t) = \langle (T(\boldsymbol{x}, t))^2 \rangle ,$$

which gives the simplest measure of the amplitude of the passive scalar fluctuations, in an RDT model with shear flow geometry in Section 4.2.1. Subsequently, we elaborate upon the spatial structure of the passive scalar field revealed by the full second-order PS correlation function in an isotropic RDT model. These analyses are possible due to the fact that in the RDT model, the PS correlation function obeys a closed PDE, which we now present.

We shall assume that the passive scalar field is at all times a mean zero, statistically homogenous random field; the self-consistency of this assumption is easily checked. Then the second-order passive scalar correlation function $P_2(\boldsymbol{r}, t) \equiv \langle T(\boldsymbol{x} + \boldsymbol{r}, t) T(\boldsymbol{x}, t) \rangle$ obeys the following variable-coefficient diffusion PDE:

Evolution of second-order passive scalar correlation function

$$\frac{\partial P_2(\boldsymbol{r}, t)}{\partial t} = \nabla \cdot ((2\kappa \mathscr{I} + \mathscr{D}_s(\boldsymbol{r})) \nabla P_2(\boldsymbol{r}, t)) ,$$

$$P_2(\boldsymbol{r}, t = 0) = P_2^0(\boldsymbol{r}) . \tag{256}$$

The function $P_2^0(r)$ is just the correlation function of the initial data:

$$P_2^0(r) \equiv \langle T_0(x)T_0(x+r) \rangle \ .$$

The turbulent contribution to the diffusivity of $P_2(r,t)$ is given by the tensor

$$\mathscr{D}_s(r) = \mathscr{R}_s(0) - \tfrac{1}{2}(\mathscr{R}_s(r) + \mathscr{R}_s^\dagger(r)) \ . \tag{257}$$

We call this tensor $\mathscr{D}_s(r)$ the *velocity structure tensor*. It is just (half) the correlation tensor of the velocity *differences* at locations with relative spatial separation r:

$$\tfrac{1}{2}\langle(v(x+r,t+\tau) - v(x,t))\otimes(v(x+r,t+\tau) - v(x,t))\rangle = \mathscr{D}_s(r)\delta(\tau) \ , \tag{258}$$

as may be checked by expansion of the binomial product and the definition (254) for the velocity correlation tensor $\mathscr{R}_s(r)$. It is readily seen that $\mathscr{D}_s(r)$ is a nonnegative definite tensor for each r.

Connection with relative diffusivity. The appearance of the velocity structure tensor as the enhanced turbulent diffusivity in Eq. (256) may be understood through the well-known connection between the evolution of the second-order correlation function (of a statistically homogenous random field) and the *relative* diffusion of a pair of tracer particles. This connection parallels that between the mean passive scalar density and the absolute diffusion of a single tracer trajectory; further discussion may be found, for example, in [164]. Here it suffices to observe that *if* the passive scalar correlation function obeys a diffusion equation, as it does in the RDT model, then the diffusion coefficient of the PDE corresponds exactly to the *relative diffusivity* of a pair of tracer particles. That is, in the RDT model, if $X^{(1)}(t)$ and $X^{(2)}(t)$ denote the random tracer trajectories for particles starting at $x^{(1)}$ and $x^{(2)}$ at time 0, then under the current conditions of statistical homogeneity:

$$\frac{1}{2}\frac{d}{dt}\langle(X^{(1)}(t) - X^{(2)}(t))\otimes(X^{(1)}(t) - X^{(2)}(t))\rangle\Big|_{t=0} = 2\kappa\mathscr{I} + \mathscr{D}_s(x^{(1)} - x^{(2)}) \ .$$

In particular, the rate of growth of the mean-square distance between a pair of tracers momentarily separated at time 0 by displacement vector $r = x^{(1)} - x^{(2)}$ is

$$\frac{1}{2}\frac{d}{dt}\langle|X^{(1)}(t) - X^{(2)}(t)|^2\rangle\Big|_{t=0} = 2d\kappa + \mathrm{Tr}\,\mathscr{D}_s(r) \ . \tag{259}$$

The first term arises from the independent Brownian motions which the tracers undergo due to molecular diffusion. The second contribution to the relative diffusivity is proportional to the mean-square velocity *difference* at two points displaced by r. Due to spatial correlations in the velocity field, this mean-square velocity difference will start at zero for zero displacement, and generally grow as the displacement is increased, and saturate at some constant value when the displacement greatly exceed the correlation length of the velocity field. Turbulent diffusion is thus more effective at separating tracers which are farther apart than those which are closer together.

The RDT model explicitly reflects Richardson's hypothesis that the relative diffusivity should depend only on the current separation of the particles [284]. Richardson deduced that this feature can give rise to a strongly superlinear rate of growth of the mean-square separation of a pair of tracers in a turbulent flow. We shall discuss this issue at more length in Section 4.2.2. Batchelor

[27] suggests that the relative diffusivity should actually depend on the time since the tracer release in real-world turbulent diffusion. As the RDT model velocity field has no memory, this consideration does not arise here. The reader may refer to [132] for a nice unifying discussion of Richardson's and Batchelor's ideas.

We have thus far indicated why the enhanced diffusion of the PS correlation function $P_2(r,t)$ is given by $\mathscr{D}_s(r)$, provided that $P_2(r,t)$ obeys a diffusion equation. The fact that $P_2(r,t)$ obeys a (variable-coefficient) diffusion equation in the first place relies mathematically on the fact that a pair of tracer particles in the RDT model undergo a coupled Brownian motion. The coupling is due to spatial correlations in the flow, and is completely described by the tensor $\mathscr{D}_s(r)$.

4.1.2.3. Dependence of passive scalar mean and correlation function on velocity field spatial structure.
We mentioned above the general fact that the mean passive scalar density is sensitive primarily to the large-scale features of the velocity field, and that the small-scale structure of the velocity field is much more strongly reflected in the fluctuations of the passive scalar field. The RDT model brings this out quite clearly.

The mean passive scalar density $\langle T(x,t) \rangle$ obeys an ordinary diffusion equation (255), with the diffusivity enhanced by the nonnegative definite tensor $\mathscr{R}_s(0)$ associated to the absolute strength (i.e., the single-point variance) of the velocity field. In turbulence, most of the energy is contained in the largest scales of the velocity field, so $\mathscr{R}_s(0)$ primarily depends upon the macroscopic features of the velocity field. On the other hand, in a statistically homogenous setting, the second-order PS correlation function $P_2(r,t) = \langle T(x,t)T(x+r,t) \rangle$ evolves according to a variable coefficient diffusion PDE. The diffusivity tensor is enhanced by the velocity structure tensor $\mathscr{D}_s(r)$, which describes velocity differences separated by arbitrary distances r. Thus, the second-order statistics of a statistically homogenous passive scalar field will be directly sensitive to the small-scale spatial structure of the velocity field.

We will explore in Sections 4.2 and 4.3 how universal small-scale features of the velocity field are transmitted to universal small-scale features of the passive scalar field in the RDT model.

4.1.3. Velocity field model with two distinct short correlation time limits
Before proceeding with the applications of the RDT model, we wish to remark upon the domain of its validity. Certainly, the equations apply for the Gaussian delta-correlated velocity field (or its mathematical interpretation as a Brownian flow). One might further ask, though, in what sense the RDT model equations also furnish an asymptotic description of the statistics of a passive scalar field advected by a velocity field with a finite but short correlation time relative to the advection time scales. While the RDT model does describe a *particular* limit with short correlation time of a large class of random velocity fields, we will present an example of a velocity field for which two different short correlation time limits can be taken. The mean and correlation function of the passive scalar field converge in one limit to solutions of the RDT model equations, and converge in the other limit to solutions of spatially nonlocal pseudo-differential equations (Eqs. (264) and (265)). Thus, the possibility of writing closed diffusion equations for the passive scalar statistics is not merely a consequence of the correlation time being very short relative to the advection time scales.

4.1.3.1. Central limit rescaling. We state first a positive way in which the RDT model describes a certain short correlation time limit: If one is given a (generally non-Gaussian) random velocity field $v(x, t)$ satisfying suitable mixing and regularity conditions, then under the particular rescaling

$$v^{(\varepsilon)}(x, t) \equiv \varepsilon^{-1/2} v(x, t/\varepsilon) , \tag{260}$$

the statistics of the passive scalar field advected by $v^{(\varepsilon)}(x, t)$ converge as $\varepsilon \to 0$ to the solutions of the RDT model equations [53,185]. Note that the particular rescaling in Eq. (260) is of a "central limit" type, and is moreover mathematically equivalent to (but somewhat conceptually distinct from) the Kubo rescaling discussed in Section 2.4.1. Over an order unity time interval, the advection process formally becomes a sum of a large number $N \sim O(\varepsilon^{-1})$ of roughly uncorrelated, mean zero, identically distributed pushes with duration $\delta\tau \sim O(\varepsilon)$ and displacement magnitude $\delta|x| \sim |v^{(\varepsilon)}|\delta\tau \sim O(\varepsilon^{1/2}) \sim O(N^{-1/2})$. We may say therefore that a "central limit theorem in the environment" holds; that is, as $\varepsilon \to 0$, the non-Gaussian velocity field $v^{(\varepsilon)}(x, t)$ acts more and more like a Gaussian, rapidly decorrelating velocity field as far as passive scalar advection is concerned. The result that central limit scaling of a broad class of velocity fields gives rise to passive scalar dynamics described by diffusion equations is in accord with the well-known fact that central limit scaling of discrete random walks generally leads to continuum processes with diffusive behavior, such as Brownian motion ([102], Section 14.6).

4.1.3.2. An explicit alternative short correlation time limit. The limit theorem stated above may tempt one to conclude that the RDT model universally describes the advection of a passive scalar field by a velocity field with very short correlation time. That is, one might suppose that the specification that the RDT velocity field is Gaussian is gratuitous, since the equations of the RDT model also describe the short correlation time limit of a large class of non-Gaussian models. In fact, we now show by example that there exist limits in which the velocity correlation time scale is much smaller than the advection time scale, but which do not give rise to the RDT model equations for the passive scalar statistics.

For this purpose, we use a *simple shear Poisson blob* velocity field model, introduced by Avellaneda and the first author in [14]. The velocity field is taken as a random two-dimensional shear flow:

$$v(x, y, t) = \begin{bmatrix} 0 \\ v(x, t) \end{bmatrix} .$$

The random field $v(x, t)$ is defined as

$$v(x, t) = \sum_n \Psi(x - \xi_n, t - \tau_n)$$

where (ξ_n, τ_n) denumerates a space–time Poisson process of unit intensity [151], and Ψ is some smooth, compactly supported "blob" structure function with zero integral:

$$\int_{-\infty}^{\infty} \int_{-\infty}^{\infty} \Psi(x, t) \, dx \, dt = 0 . \tag{261}$$

That is, the velocity field is a superposition of the blob functions distributed according to a space–time Poisson process. It has mean zero and a finite correlation function:

$$\tilde{R}(x,t) \equiv \langle v(x',t')v(x'+x,t'+t)\rangle = \int_{-\infty}^{\infty}\int_{-\infty}^{\infty} \Psi(x',t')\Psi(x'+x,t'+t)\,\mathrm{d}x'\,\mathrm{d}t' \; .$$

We now define two families of Poisson blob velocity field models generated from the given Poisson blob velocity field under two different rescalings, each describing a different limit process in which the correlation time becomes small. The family of velocity fields under *central limit rescaling* is defined:

$$v_{\mathrm{CL}}^{(\varepsilon)}(x,t) = \sum_n \varepsilon^{-1/2}\Psi(x-\xi_n^{(\varepsilon)},(t-\tau_n^{(\varepsilon)})/\varepsilon) \; , \tag{262}$$

where the intensity of the Poisson process $(\xi_n^{(\varepsilon)},\tau_n^{(\varepsilon)})$ is taken as ε^{-1}. It can be shown that this definition is statistically equivalent to the rescaling (260).

The family of velocity field models generated under the *fixed intensity* rescaling of the original Poisson blob model is defined:

$$v_{\mathrm{FI}}^{(\varepsilon)}(x,t) = \sum_n \varepsilon^{-1}\Psi(x-\xi_n,(t-\tau_n)/\varepsilon) \; , \tag{263}$$

with the intensity of the Poisson process (ξ_n,τ_n) fixed at unity and the amplitude of the blob functions rescaled from the prototype Ψ more strongly than in the central limit rescaling.

At $\varepsilon = 1$, both families coincide with the unscaled Poisson blob velocity field:

$$v(x,t) = \sum_n \Psi(x-\xi_n,t-\tau_n) \; ,$$

where the Poisson process (ξ_n,τ_n) has unit intensity. As $\varepsilon \to 0$, the second-order correlation function of each rescaled family approaches the same delta-correlated form:

$$\lim_{\varepsilon\to 0} \langle v_{\mathrm{CL}}^{(\varepsilon)}(x',t')v_{\mathrm{CL}}^{(\varepsilon)}(x'+x,t'+t)\rangle = \lim_{\varepsilon\to 0} \langle v_{\mathrm{FI}}^{(\varepsilon)}(x',t')v_{\mathrm{FI}}^{(\varepsilon)}(x'+x,t'+t)\rangle = \tilde{R}_s(x)\delta(t) \; ,$$

$$\tilde{R}_s(x) \equiv \int_{-\infty}^{\infty} \tilde{R}(x,t)\,\mathrm{d}t \; .$$

Moreover, both rescalings give rise to a limit in which the correlation time is $\mathrm{O}(\varepsilon)$ and short compared with the advection time scale $\propto 1/\langle(v^{(\varepsilon)}(x,t))^2\rangle^{1/2} \sim \mathrm{O}(\varepsilon^{1/2})$.

Now we define $T_{\mathrm{CL}}^{(\varepsilon)}(x,y,t)$ and $T_{\mathrm{FI}}^{(\varepsilon)}(x,y,t)$ to be the random passive scalar fields solving the advection-diffusion equation with rescaled velocity fields $v_{\mathrm{CL}}^{(\varepsilon)}(x,t)$ and $v_{\mathrm{FI}}^{(\varepsilon)}(x,t)$, respectively. In accordance with the above discussion, under central limit rescaling, the passive scalar statistics converge to those governed by the RDT model. Thus, as $\varepsilon \to 0$, the mean $\langle T_{\mathrm{CL}}^{(\varepsilon)}(x,y,t)\rangle$ and the correlation function $\langle T_{\mathrm{CL}}^{(\varepsilon)}(x',y',t)T_{\mathrm{CL}}^{(\varepsilon)}(x'+x,y'+y,t)\rangle$ converge to solutions of the diffusion equations associated to an RDT model velocity field $\tilde{v}(x,t)$ with correlation function $\langle \tilde{v}(x',t')\tilde{v}(x'+x,t'+t)\rangle = \tilde{R}_s(x)\delta(t)$.

On the other hand, one can show [186] that the mean $\langle T_{\mathrm{FI}}^{(\varepsilon)}(x, y, t)\rangle$ and correlation function $\langle T_{\mathrm{FI}}^{(\varepsilon)}(x', y', t)T_{\mathrm{FI}}^{(\varepsilon)}(x' + x, y' + y, t)\rangle$ of the family generated by fixed intensity rescaling converge as $\varepsilon \to 0$ to finite limits $\bar{P}_{1,\mathrm{FI}}(x, y, t)$ and $\bar{P}_{2,\mathrm{FI}}(x, y, t)$ which solve *pseudo-differential equations*:

$$\frac{\partial \bar{P}_{1,\mathrm{FI}}(x, y, t)}{\partial t} = \kappa \Delta \bar{P}_{1,\mathrm{FI}}(x, y, t) + U_{1,\mathrm{FI}}\left(\frac{\partial}{\partial y}\right)\bar{P}_{1,\mathrm{FI}}(x, y, t) ,$$

$$\bar{P}_{1,\mathrm{FI}}(x, y, t = 0) = \langle T_0(x, y)\rangle , \tag{264}$$

and

$$\frac{\partial \bar{P}_{2,\mathrm{FI}}(x, y, t)}{\partial t} = 2\kappa \Delta \bar{P}_{1,\mathrm{FI}}(x, y, t) + U_{2,\mathrm{FI}}\left(x, \frac{\partial}{\partial y}\right)\bar{P}_{1,\mathrm{FI}}(x, y, t) ,$$

$$\bar{P}_{2,\mathrm{FI}}(x, y, t = 0) = \langle T_0(x', y')T_0(x' + x, y' + y)\rangle . \tag{265}$$

The pseudo-differential operators are specified by

$$U_{1,\mathrm{FI}}(k) = \int_{-\infty}^{\infty} (\mathrm{e}^{-2\pi \mathrm{i}k\bar{\Psi}(\xi)} - 1)\,\mathrm{d}\xi ,$$

$$U_{2,\mathrm{FI}}(x, k) = \int_{-\infty}^{\infty} (\mathrm{e}^{-2\pi \mathrm{i}k(\bar{\Psi}(x + \xi) - \bar{\Psi}(\xi))} - 1)\,\mathrm{d}\xi ,$$

with

$$\bar{\Psi}(x) \equiv \int_{-\infty}^{\infty} \Psi(x, t)\,\mathrm{d}t .$$

Since $U_{1,\mathrm{FI}}(k)$ and $U_{2,\mathrm{FI}}(x, k)$ are, in general, transcendental functions of k, the mean and correlation function of the limiting passive scalar field under the fixed intensity rescaling cannot be expressed as solutions of PDEs. Their governing equations are intrinsically nonlocal.

The upshot is that under central limit rescaling, a central limit theorem "in the environment" applies, and the trajectories of tracer particles begin to resemble a coupled Brownian motion as the correlation time becomes short. But in the short correlation limit of the Poisson blob model which produces a distinct limiting behavior, the tracer trajectories retain a Poissonian character and do not converge to Brownian motions. The validity of the RDT model equations specifically requires that the tracers diffuse according to Brownian motion processes with no Poissonian components.

Put another way, in the short correlation time limit under central limit rescaling (262), the Poisson blob velocity field acts on the tracer trajectories like a *Gaussian* random, delta-correlated velocity field, whereas under fixed intensity rescaling, it acts on the tracer trajectories like a *non-Gaussian* delta-correlated velocity field and the RDT model equations do not apply. These examples are due to the second author and further discussion may be found in [185,186].

4.1.4. Energy spectra with inertial range for RDT model

Thus far, we have discussed the RDT model in a general manner; for applications we must specify the spatial correlation tensor $\mathcal{R}_{\mathrm{s}}(x)$ appearing in the velocity correlation function:

$$\langle v(x, t)\otimes v(x + r, t + \tau)\rangle = \mathcal{R}_{\mathrm{s}}(r)\delta(\tau) .$$

As usual, we define the velocity correlation function through its spectrum. For simplicity and continuity with our discussion in Section 3, we consider first the case where the RDT velocity field is a simple two-dimensional shear flow

$$\boldsymbol{v}(x, y, t) = \begin{bmatrix} 0 \\ v(x, t) \end{bmatrix},$$

so that the velocity correlation function is simply described by a scalar function:

$$\langle v(x', t')v(x' + x, t' + t)\rangle = R_s(x)\delta(t) . \tag{266}$$

Then we write the spatial correlation function in terms of its spectral density:

$$R_s(x) = \int_{-\infty}^{\infty} e^{2\pi ikx}\tilde{E}(|k|)\,dk = 2\int_0^{\infty} \cos(2\pi kx)\tilde{E}(k)\,dk .$$

Please note that even though $\tilde{E}(k)$ depends only on wavenumber, it is really the *spatio-temporal energy spectrum* $\tilde{E}(k, \omega)$ discussed in Section 3.3. It is simply independent of the frequency variable ω, as is characteristic of delta-correlated "white noise" processes.

We would like to simulate a fully developed turbulent flow as closely as possible with the RDT model velocity field, but of course we must respect the short correlation time inherent in the model. A natural way to produce such a model, given our discussion in Paragraph 4.1.3.1, is to start with a velocity field model with a reasonable spatio-temporal energy spectrum $\tilde{E}(k, \omega)$, and then pass to a short correlation time limit through the central limit rescaling (260). Thus, we posit a spatio-temporal energy spectrum corresponding to the Kolmogorov similarity hypotheses stated in Paragraph 3.4.3.1, in which the energy spectrum has the inertial range form $E(k) \approx C_K\bar{\varepsilon}^{2/3}k^{-5/3}$ and the correlation time of an inertial range velocity fluctuation of wavenumber k scales as $\tau_e(k) \approx \bar{\varepsilon}^{-1/3}k^{-2/3}$. The spatio-temporal energy spectrum is then constructed from these quantities as follows (199):

$$\begin{aligned}
\tilde{E}(k, \omega) &= E(k)\phi(\omega\tau_e(k))\tau_e(k) \\
&= C_K\bar{\varepsilon}^{2/3}k^{-5/3}\psi_0(kL_0)\psi_\infty(kL_K)\phi(\omega\bar{\varepsilon}^{-1/3}k^{-2/3})(\bar{\varepsilon}^{-1/3}k^{-2/3}) \\
&= C_K\bar{\varepsilon}^{1/3}k^{-7/3}\phi(\omega\bar{\varepsilon}^{-1/3}k^{-2/3})\psi_0(kL_0)\psi_\infty(kL_K) ,
\end{aligned}$$

where L_0 is the integral length scale, L_K is the Kolmogorov dissipation length scale, C_K is the Kolmogorov constant, ψ_0 and ψ_∞ are infrared and ultraviolet cutoffs, respectively, and ϕ is the temporal structure function ($\int_{-\infty}^{\infty}\phi(\omega)\,d\omega = 1$). Performing the central limit rescaling

$$\boldsymbol{v}^{(\varepsilon)}(\boldsymbol{x}, t) \equiv \varepsilon^{-1/2}\boldsymbol{v}(\boldsymbol{x}, t/\varepsilon)$$

induces the following rescaling of the spatio-temporal energy spectrum:

$$\tilde{E}^{(\varepsilon)}(k, \omega) = \tilde{E}(k, \varepsilon\omega) .$$

Passing to the $\varepsilon \to 0$ limit, we see that the RDT model velocity field induced by a central limit rescaling of a Kolmogorov-type turbulent model is specified by the spatio-temporal energy spectrum:

$$\tilde{E}_{\text{RDT}}(k) = C_K\phi(0)\bar{\varepsilon}^{1/3}k^{-7/3}\psi_0(kL_0)\psi_\infty(kL_K) .$$

We note that in the RDT model, after central limit rescaling, the Kolmogorov spectrum formally corresponds to the exponent 7/3.

As we did in Section 3, we imbed this particular spectrum in a more general family of models with the same qualitative features:

$$\tilde{E}(k) = A_E k^{-1-2H} \psi_0(kL_0) \psi_\infty(kL_K) , \tag{267}$$

and we have dropped the "RDT" suffix. The parameter $H < 1$ describes the inertial-range scaling, with $H = 2/3$ corresponding to the central limit rescaling of Kolmogorov velocity field, and A_E is some prefactor of appropriate dimensions. We will be most interested in the case $0 < H < 1$, which describe velocity fields with long-range spatial-correlations typical of turbulence ($2 < \varepsilon < 4$ in the parameterization of Section 3). If we imagine replacing the delta function in Eq. (266) by a smooth approximation, then the parameter H would be exactly the *Hurst exponent* ([215], Section 27) characterizing the fractal spatial structure of the velocity field in the inertial-range of scales (see Eq. (269) and subsequent discussion). The Hurst exponent of a true Kolmogorov velocity field is 1/3; the reason the value $H = 2/3$ arises from a central limit of this velocity field is because fluctuations decorrelate in time at a wavenumber-dependent rate.

One can specify similar turbulent spectra for velocity fields with multi-dimensional geometry through the use of tensors, and the general remarks above persist without change. We shall in particular construct a multi-dimensional velocity field with isotropic statistics in Paragraph 4.2.2.1.

4.2. Evolution of the passive scalar correlation function through an inertial range of scales

We now utilize the explicit PDE (256) for the second-order passive scalar correlation function in the RDT model to explore the statistical evolution of passive scalar fluctuations. It is clear from the diffusive form of the equation that, in general, the amplitude of the fluctuations in a freely evolving passive scalar field will be damped, and the typical length scale of the fluctuations will increase due to turbulent spreading. It is instructive to examine a situation in which a universal description is possible. We thus consider a fully developed turbulent flow with well-developed inertial range, and focus on a time interval during which the predominant length scale of the fluctuations lies within the inertial range and is much larger than the length scale of the initial disturbance. In such an asymptotic regime, one might plausibly expect that most of the details about the initial structure of the PS correlation function are irrelevant, and that the dynamics are driven primarily by the inertial-range turbulent fluctuations which have universal, self-similar properties. We will see that this is indeed the case in the RDT model. The asymptotic regime just described is the same as that for which we computed fractal dimensions of scalar interfaces in Section 3.5. Another theme we will emphasize is the distinction between the action of turbulent diffusion and bare molecular diffusion on the passive scalar field, particularly when the turbulent velocity field has very strong long-range correlations ($H > 0$).

We first revisit turbulent diffusion in a shear flow, now with rapid decorrelation in time, and derive formulas for the rate of dissipation of the passive scalar fluctuations as they evolve through the inertial range of scales (Section 4.2.1). When the velocity field has long-range spatial correlations typical of fully developed turbulence, the amplitude of the passive scalar fluctuations will decay anomalously according to a power law with the exponent differing from that corresponding to ordinary diffusion. The methodology involves the relation of solutions of the RDT model

diffusion PDE to an associated quantum mechanics Schrödinger problem with potential related to the spatial structure of the shear flow [206]. This strategy will play a central role in the derivation of results concerning large-scale passive scalar intermittency in a closely related model to be discussed in Section 5.

Next, in Section 4.2.2, we investigate more extensively the spreading of passive scalar fluctuations through the inertial range of scales in an *isotropic* RDT model. A completely self-similar solution for the second-order PS correlation function may be obtained in this asymptotic regime, and from it we may deduce the rate of decay of the passive scalar variance, the rate at which the length scales of the fluctuations grow with time, and the fractalizing (roughening) properties of turbulent diffusion.

4.2.1. Anomalous decay of passive scalar fluctuations

We begin our study of passive scalar fluctuations in the RDT model with a two-dimensional RDT shear flow with statistics described in Section 4.1.4. The RDT model equation (256) for the second-order PS correlation function $P_2(x, y, t) = \langle T(x', y', t)T(x' + x, y' + y, t)\rangle$ can then be expressed in terms of scalar functions:

$$\partial P_2(x, y, t)/\partial t = 2\kappa \Delta P_2(x, y, t) + D_s(x)\partial^2 P_2(x, y, t)/\partial y^2 \ ,$$

$$P_2(x, y, t = 0) = P_2^0(x, y) \ , \tag{268}$$

with the turbulent diffusion coefficient given by

$$D_s(x) = R_s(0) - R_s(x) \ .$$

Note that this PDE is very similar to the PDE for the pair-distance function in a turbulent shear flow which we derived in Section 3.5.1. Indeed, it is a general fact that the second order PS correlation function and pair-distance function satisfy the same PDE (see for example [185] or [196]). The PDE derived in Section 3.5.1 permitted nontrivial temporal correlations, while here we have accounted for the presence of molecular diffusivity. Including both effects simultaneously is a more challenging and interesting task, as we indicated at the end of Section 3.5.

Now, we describe the behavior of the passive scalar correlation function $P_2(x, y, t)$ as it evolves through the inertial range of scales. For such a regime to exist, we must have that $L_K \ll L_0$ and that the length scale L of the passive scalar correlation function satisfies $L_K \ll L \ll L_0$. As we indicated in Section 3.5.1, the $L_0 \to \infty$ limit may be directly taken in Eq. (268) for all $H < 1$. Even though the spatial correlation function of the velocity field $R_s(x)$ for $0 < H < 1$ approaches infinity in this limit, these divergences cancel in the expression for $D_s(x)$, and

$$\bar{D}_s(x) \equiv \lim_{L_0 \to \infty} D_s(x) = 2A_E \int_0^\infty (1 - \cos(2\pi kx))k^{-1-2H}\psi_\infty(kL_K)\,dk$$

is finite.

Having taken the $L_0 \to \infty$ limit, we then need to restrict our attention to time scales sufficiently large so that the length scale of the PS correlation function is much larger than both L_K and its initial length scale. We do this through a large-space, long-time rescaling chosen so that the asymptotic evolution PS correlation function is faithfully and finitely expressed in terms of these

rescaled variables. We call this rescaling an "inertial range renormalization"; in the language of the renormalization group we are looking for rescalings leading to a nontrivial "fixed point". A similar renormalization was carried out for a spatio-temporal shear flow in Section 3.5.4, but we will not enforce isotropy of the renormalization group here. The qualitative character of the renormalization depends on whether $H < 0$ or $H > 0$. We shall consider each case in turn, first deriving the PDE describing the inertial-range evolution of the PS correlation function and then computing the rate of decay of the passive scalar variance $\langle (T(x, y, t))^2 \rangle = P_2(0, 0, t)$. Further details may be found in the original work [206], and the statements presented here can be verified rigorously through the Feynman-Kac representation developed in that paper.

4.2.1.1. Inertial range renormalization for $H < 0$. In the parameter regime with $H < 0$, the turbulent velocity field does not have very strong long-range correlations, and the turbulent diffusion coefficient $\bar{D}_s(x)$ approaches a finite limit as the spatial scale x becomes arbitrarily large:

$$\lim_{x \to \infty} \bar{D}_s(x) = \bar{R}_s(0) = 2 \int_0^\infty A_E k^{-1-2H} \psi_\infty(k L_{\mathbf{K}}) \, dk .$$

Thus, the inertial-range evolution for the PS correlation function may be described by the standard diffusive renormalization:

$$P_2^{(\lambda)}(x, y, t) = \lambda^{-2} P_2 \left(\frac{x}{\lambda}, \frac{y}{\lambda}, \frac{t}{\lambda^2} \right) .$$

The limiting function $\bar{P}_2(x, y, t) \equiv \lim_{\lambda \to 0} P_2^{(\lambda)}(x, y, t)$ (which may be viewed as a fixed point of the renormalization) obeys a constant-coefficient diffusion PDE with enhanced diffusion coefficient along the shearing direction:

$$\frac{\partial \bar{P}_2(x, y, t)}{\partial t} = 2\kappa \frac{\partial^2 \bar{P}_2(x, y, t)}{\partial x^2} + (2\kappa + \bar{R}_s(0)) \frac{\partial^2 \bar{P}_2(x, y, t)}{\partial y^2} ,$$

$$\bar{P}_2(x, y, t = 0) = M_2^0 \delta(x) \delta(y) ,$$

where $M_2^0 = \int_{\mathbb{R}^2} P_2^0(x, y) \, dx \, dy$. The renormalized PS correlation function $\bar{P}_2(x, y, t)$ thus assumes a standard (but anisotropic) Gaussian form. In particular, the variance $\langle (\bar{T}(x, y, t))^2 \rangle$ of the renormalized passive scalar field $\bar{T}(x, y, t)$ decays according to a power law with the same exponent as it would under molecular diffusion alone:

$$\langle (\bar{T}(x, y, t))^2 \rangle = \bar{P}_2(0, 0, t) = M_2^0 (4\pi)^{-1} (2\kappa + \bar{R}_s(0))^{-1/2} (2\kappa)^{-1/2} t^{-1} .$$

For the case $H < 0$ just discussed, the only role of the random velocity field in the decay of the passive scalar variance is to decrease the coefficient through the term $\bar{R}_s(0)$.

4.2.1.2. Inertial range renormalization for $H > 0$. Turbulence typically has very long-range spatial correlations, however, and corresponds to the class $H > 0$ which we now discuss. The standard diffusive renormalization fails in this case to produce a finite limiting inertial-range behavior, because the turbulent diffusion coefficient $\bar{D}_s(x)$ diverges as $x \to \infty$:

$$\lim_{|x| \to \infty} \bar{D}_s(x) = D^I |x|^{2H} . \tag{269}$$

The numerical coefficient in Eq. (269) is given by

$$D^I = 2A_E \int_0^\infty (1 - \cos(2\pi k))k^{-1-2H}\,\mathrm{d}k = -A_E \pi^{2H+1/2}\frac{\Gamma(-H)}{\Gamma(H+\frac{1}{2})},$$

where $\Gamma(\cdot)$ is the Gamma function [195]. The power law growth of $\bar{D}_s(x)$ in Eq. (269) manifests the property that, within the inertial range of scales, the turbulent separation of particles becomes stronger and stronger as their relative distance increases.

To capture the behavior of the PS correlation function through the inertial range of scales, we must renormalize according to the following prescription [206]:

$$P_2^{(\lambda)}(x,y,t) \equiv \lambda^{-2-H}P_2\left(\frac{x}{\lambda}, \frac{y}{\lambda^{1+H}}, \frac{t}{\lambda^2}\right). \tag{270}$$

With Eq. (269), one then readily checks that the renormalized inertial-range limit $\bar{P}_2(x,y,t) \equiv \lim_{\lambda \to \infty} P_2^{(\lambda)}(x,y,t)$ obeys the variable-coefficient diffusion PDE:

$$\frac{\partial \bar{P}_2(x,y,t)}{\partial t} = 2\kappa\frac{\partial^2 \bar{P}_2(x,y,t)}{\partial x^2} + D^I|x|^{2H}\frac{\partial^2 \bar{P}_2(x,y,t)}{\partial y^2},$$

$$\bar{P}_2(x,y,t=0) = M_2^0\delta(x)\delta(y). \tag{271}$$

The inertial-range limit which we have just derived is *completely self-similar* in the terminology of Barenblatt [25]. All length scales have disappeared in this asymptotic regime, and the only remnant of the initial data is the total spatial integral of the initial PS correlation function, M_2^0, which is an exactly conserved quantity. A related fact is the invariance of the PDE (271) under the rescalings defining the renormalization (270). Therefore, in the RDT model under discussion, the second order PS correlation function is universal and scale-invariant within the inertial range of scales, when the random velocity field has very long range correlations $H > 0$. We will examine the self-similarity properties of the passive scalar correlation function in an isotropic version of the RDT model in Section 4.2.2. Here, we shall simply examine the rate of decay of the variance of the renormalized passive scalar field $\langle \bar{T}(x,y,t)^2 \rangle$, and show that it decays anomalously with a power law $t^{-1-H/2}$.

The fact that the turbulent flow is a shear flow along the y direction puts the PDE (271) for $\bar{P}_2(x,y,t)$ in a form well suited for a partial Fourier transform in the y variable [206]:

$$\hat{\bar{P}}_2(x,k,t) = \int_{-\infty}^\infty \mathrm{e}^{2\pi i k y}\bar{P}_2(x,y,t)\,\mathrm{d}y.$$

The resulting PDE for $\hat{\bar{P}}_2(x,k,t)$ takes the form of a quantum mechanical Schrödinger equation (in imaginary time):

$$\frac{\partial \hat{\bar{P}}_2(x,k,t)}{\partial t} = 2\kappa\frac{\partial^2 \hat{\bar{P}}_2(x,k,t)}{\partial x^2} - 4\pi^2 D^I k^2|x|^{2H}\hat{\bar{P}}_2(x,k,t),$$

$$\hat{\bar{P}}_2(x,k,t=0) = M_2^0\delta(x). \tag{272}$$

Since the effective potential function $4\pi^2 D^I k^2 |x|^{2H}$ grows sufficiently rapidly as $|x| \to \infty$, the operator on the right-hand side has pure point spectrum [323], and the solution to Eq. (272) may be represented as a superposition of orthonormal eigenfunctions corresponding to "bound states" of the corresponding quantum mechanical system. This is in contrast with the situation for $H < 0$, in which the effective potential would be a constant function, and the quantum mechanical operator would correspond to a free particle and have purely continuous spectrum.

Define now $\{\psi_j(x)\}$ to be the normalized eigenfunctions of a nondimensionalized Schrödinger operator corresponding to the right-hand side of Eq. (272):

$$-\frac{\mathrm{d}^2 \psi_j(x)}{\mathrm{d}x^2} + |x|^{2H} \psi_j(x) = \mu_j \psi_j(x) \, ,$$

$$\int_{-\infty}^{\infty} (\psi_j(x))^2 \, \mathrm{d}x = 1 \, .$$

We only need to account for the even real eigenfunctions due to the parity invariance of the potential and the evenness of our initial data. The "energy" eigenvalues are $\mu_1 < \mu_2 < \mu_3 < \cdots$, and $\mu_1 > 0$ is guaranteed by the positivity of the potential. Through the rescaling:

$$\tilde{\psi}_j(x) = (2\pi^2 D^I k^2)^{1/(4+4H)} \kappa^{-1/(4+4H)} \psi_j((2\pi^2 D^I k^2)^{1/(2+2H)} \kappa^{-1/(2+2H)} x) \, ,$$

$$\tilde{\mu}_j = 2\kappa^{H/(H+1)} (2\pi^2 D^I k^2)^{1/(H+1)} \mu_j \, ,$$

the eigenfunction expansion of the solution to Eq. (272) reads

$$\hat{\bar{P}}_2(x, k, t) = \sum_{j=1}^{\infty} \mathrm{e}^{-\tilde{\mu}_j t} \tilde{\psi}_j(x) \int_{-\infty}^{\infty} \tilde{\psi}_j(x) \delta(x) \, \mathrm{d}x = \sum_{j=1}^{\infty} \mathrm{e}^{-\tilde{\mu}_j t} \tilde{\psi}_j(x) \tilde{\psi}_j(0) \, .$$

Now, the passive scalar variance is determined by this partial Fourier transform as follows:

$$\langle (\bar{T}(x, y, t))^2 \rangle = \hat{\bar{P}}_2(0, 0, t) = \int_{-\infty}^{\infty} \hat{\bar{P}}_2(0, k, t) \, \mathrm{d}k \, .$$

We compute this quantity by expressing $\hat{\bar{P}}_2(x, k, t)$ in terms of the parameter-free eigenfunctions and eigenvalues $\psi_j(x)$ and μ_j:

$$\langle (\bar{T}(x, y, t))^2 \rangle = \int_{-\infty}^{\infty} \hat{\bar{P}}_2(0, k, t) \, \mathrm{d}k = \int_{-\infty}^{\infty} \sum_{j=1}^{\infty} (2\pi^2 D^I k^2)^{1/(2+2H)} \kappa^{-1/(2+2H)} |\psi_j(0)|^2$$

$$\times \exp(-2\kappa^{H/(H+1)}(2\pi^2 D^I k^2)^{1/(H+1)} \mu_j t) \, \mathrm{d}k = C_H \kappa^{-(H+1)/2} (2\pi^2 D^I)^{-1/2} t^{-(H+2)/2} \, ,$$

where the numerical constant:

$$C_H = 2^{-(H+2)/2} (H+1) \Gamma((H+2)/2) \sum_{j=1}^{\infty} \mu_j^{-(H+2)/2} |\psi_j(0)|^2 \, .$$

In particular, we see that the passive scalar variance decays through the inertial range according to an anomalous power law $t^{-(H+2)/2}$ for $H > 0$, whereas for $H < 0$, the passive scalar variance decays

according to the ordinary diffusive power law t^{-1}. Note that the passive scalar variance decays more rapidly at long times due to the presence of long-range correlations ($H > 0$), and that the decay rate is self-consistent with the self-similar inertial range scaling (270) of the amplitude and time argument of the PS correlation function. As we will see more clearly in Section 4.2.2, the faster decay is due to the rapid dispersal of the passive scalar fluctuations by the energetic long-wavelength fluctuations of the turbulent flow.

4.2.2. Self-similar spreading of passive scalar fluctuations

For the rest of Section 4, we will explore further issues concerning the passive scalar correlation function within the context of an RDT model with statistical isotropy, i.e., no preferred direction. This is a natural geometry for describing "generic" fully developed turbulence, particularly since the small-scale fluctuations may be expected in many circumstances to be insensitive to the large scale configuration. The assumption of statistical isotropy furthermore simplifies the mathematical analysis by reducing the dimensionality of the diffusion PDE (256) for the PS correlation function. This affords us the possibility of describing the second order passive scalar statistics in a rather explicit fashion. Here we give a complete description of the PS correlation function during the same "inertial-range" phase of evolution just considered for the shear RDT model, during which the length scale of the passive scalar fluctuations lies within the inertial range of scales and is much larger than the length scale of the initial disturbance.

We begin by defining the correlation function for the isotropic RDT velocity field through a spatio-temporal energy spectrum with inertial-range scaling, and conduct an inertial-range renormalization in the same manner as we did for the shear RDT model. The PDE describing the renormalized PS correlation function is then exactly solved, and we read off from this solution some properties concerning the evolution of passive scalar fluctuations and the separation of a pair of particles on length scales within the inertial range.

4.2.2.1. Setup for isotropic RDT model. As the velocity field is now multi-dimensional (with $d = 2$ or 3 denoting the spatial dimension), its correlations must be described by a tensor rather than a scalar function. The general relation between the correlation tensor and the scalar spatio-temporal energy spectrum (k) describing the strength of the velocity fluctuations at various wavenumbers k is given by (see [341], Sections 9 and 22):

$$\langle \boldsymbol{v}(\boldsymbol{x}', t') \otimes \boldsymbol{v}(\boldsymbol{x} + \boldsymbol{x}', t + t') \rangle \equiv \mathscr{R}_{\mathrm{s}}(\boldsymbol{x})\delta(t) \,,$$

$$\mathscr{R}_{\mathrm{s}}(\boldsymbol{x}) = \int_{\mathbb{R}^d} \mathrm{e}^{2\pi \mathrm{i} \boldsymbol{k} \cdot \boldsymbol{x}} (\mathscr{I} - \hat{k} \otimes \hat{k}) \frac{2\tilde{E}(|\boldsymbol{k}|)}{(d-1)A_{d-1}|\boldsymbol{k}|^{d-1}} \, \mathrm{d}\boldsymbol{k} \,. \tag{273}$$

The tensor factor $\mathscr{I} - \hat{k} \otimes \hat{k}$, where $\mathscr{I}$ is the identity matrix and $\hat{k} = \boldsymbol{k}/|\boldsymbol{k}|$, is a projection which enforces incompressibility. The constant A_{d-1} is the area of the $(d-1)$-dimensional sphere. We take the same inertial-range form of the spatio-temporal energy spectrum as that which we have been using for a shear geometry:

$$\tilde{E}(k) = A_E k^{-1-2H} \psi_0(kL_0) \psi_\infty(kL_{\mathbf{K}}) \,.$$

Because of statistical isotropy and incompressibility, the turbulent diffusion tensor $\mathcal{D}_s(\boldsymbol{r}) = \mathcal{R}_s(\boldsymbol{0}) - \mathcal{R}_s(\boldsymbol{r})$ appearing in Eq. (256) may be expressed in terms of a scalar function of a single variable ([341], pp. 380–383):

$$\mathcal{D}_s(\boldsymbol{r}) = D_{s\parallel}(r)\hat{r} \otimes \hat{r} + D_{s\perp}(r)(\mathcal{I} - \hat{r} \otimes \hat{r}) \,,$$

$$D_{s\perp}(r) = \frac{(r^{d-1}D_{s\parallel}(r))'}{(d-1)r^{d-2}} \,. \tag{274}$$

$D_{s\parallel}(r)$ is half the mean-square *longitudinal* velocity difference, and $D_{s\perp}(r)$ is half the mean-square *lateral* velocity difference observed at two points separated by a distance r.

If we assume that the passive scalar statistics are initially statistically isotropic, then by symmetry the passive scalar statistics remain statistically isotropic, and the PS correlation function may be expressed for all time as a function of a single space variable $r = |\boldsymbol{r}|$ and a single time variable:

$$\langle T(\boldsymbol{x},t)T(\boldsymbol{x}+\boldsymbol{r},t)\rangle = P_2(|\boldsymbol{r}|,t) \,,$$

$$\langle T_0(\boldsymbol{x})T_0(\boldsymbol{x}+\boldsymbol{r})\rangle = P_2^0(|\boldsymbol{r}|) \,.$$

With Eq. (274), we can then write the PDE (256) for the second-order PS correlation function in the following form:

Isotropic evolution of second-order passive scalar correlation function

$$\frac{\partial P_2(r,t)}{\partial t} = \frac{1}{r^{d-1}}\frac{\partial}{\partial r}\left(r^{d-1}(2\kappa + D_{s\parallel}(r))\frac{\partial P_2(r,t)}{\partial r}\right) \,,$$

$$P_2(r,t=0) = P_2^0(r) \,. \tag{275}$$

4.2.2.2. Inertial-range renormalization of isotropic RDT model. Now we are in a position to analyze the evolution of $P_2(r,t)$ through the inertial range of scales through a similar type of renormalization procedure as in our earlier discussion of the shear RDT model. It is readily checked that for $H < 0$, the renormalized PS correlation function obeys, as in the shear case, a constant coefficient diffusion equation with the diffusion coefficient enhanced by the presence of the random velocity field. The PS correlation function thus assumes a standard Gaussian shape and spreads and decays according to ordinary diffusive laws.

We shall focus on the case of very long-range correlations $H > 0$, which exhibits more interesting behavior and has qualitative similarities to real-world turbulence. By taking $L_0 \to \infty$ and renormalizing the PS correlation function according to the law:

$$P_2^{(\lambda)}(r,t) = \lambda^{-d}P_2(r/\lambda, t/\lambda^{2-2H}) \,,$$

we find formally that the inertial range limit $\bar{P}_2(r,t) \equiv \lim_{\lambda \to 0}P_2^{(\lambda)}(r,t)$ obeys the PDE

$$\frac{\partial \bar{P}_2(r,t)}{\partial t} = \frac{1}{r^{d-1}}\frac{\partial}{\partial r}\left(D_L^I r^{2H+d-1}\frac{\partial P_2(r,t)}{\partial r}\right) \,,$$

$$\bar{P}_2(r,t=0) = \frac{M_2^0}{A_{d-1}r^{d-1}}\delta(r) \,. \tag{276}$$

We have used the fact that within the inertial range of scales, $D_{s\|}(r)$ grows as a power law

$$\lim_{L_0/r \to \infty, r/L_K \to \infty} D_{s\|}(r) = D_L^I r^{2H} ,$$

$$D_L^I = \frac{2\Gamma(-H)\Gamma(d/2)}{\Gamma((2+2H+d)/2)} \pi^{2H+2} A_E .$$

The inertial-range limit for the isotropic RDT model is completely self-similar, just as for the shear RDT model in Section 4.2.1. The only memory of the initial data is the spatial integral of the initial PS correlation function

$$M_2^0 = \int_0^\infty A_{d-1} r^{d-1} P_2^0(r) \, \mathrm{d}r .$$

Rigorous verification of this complete self-similarity and of the convergence of the passive scalar correlation function to the solution of Eq. (276) under the inertial-range renormalization is more subtle than in the shear case; see [208] for some positive mathematical results and a discussion.

4.2.2.3. Exact solution of renormalized PDE. We now proceed with the development of an exact solution for the renormalized PS correlation function $\bar{P}_2(r, t)$, from which we will be able to deduce a number of properties concerning the statistics of passive scalar fluctuations as they evolve through the inertial range of scales.

The assumption of statistical isotropy has reduced the complexity of the PDE (276) for $\bar{P}_2(r, t)$ to the point that it can be solved by dimensional analysis [24]. There are three independent dimensions: length, time, and the passive scalar density. Five different parameters and variables appear in the PDE defining $\bar{P}_2(r, t)$, so by general principles of dimensional analysis [24,25], we can re-express the PDE in terms of $5 - 3 = 2$ dimensionless variables. One natural way to choose these dimensionless variables is to nondimensionalize the dependent quantity $\bar{P}_2$ and one of the independent variables (say r) with respect to the remaining variables and parameters (t, D_L^I and M_2^0). Thus, we define the nondimensional quantities:

$$\xi = \frac{r}{(D_L^I t)^{1/(2-2H)}} ,$$

$$Q_H = \frac{\bar{P}_2}{M_2^0 (D_L^I t)^{-d/(2-2H)}} .$$

As dimensional analysis guarantees, the PDE (276) is equivalent to an ODE for the nondimensionalized function $Q_H = Q_H(\xi)$:

$$-\frac{d}{2-2H} Q_H(\xi) - \frac{1}{2-2H} \xi \frac{\mathrm{d}Q_H(\xi)}{\mathrm{d}\xi} = \xi^{1-d} \frac{\mathrm{d}}{\mathrm{d}\xi} \left(\xi^{2H+d-1} \frac{\mathrm{d}Q_H(\xi)}{\mathrm{d}\xi} \right) . \tag{277}$$

This ODE is to be solved with the auxiliary condition

$$\int_0^\infty Q_H(\xi) A_{d-1} \xi^{d-1} \, \mathrm{d}\xi = 1 , \tag{278}$$

which expresses the fact that the spatial integral of the correlation function $\bar{P}_2(r, t)$ is conserved and equal to its value M_2^0 at time $t = 0$.

This ODE problem may be exactly solved by quadrature. After multiplying Eq. (277) through by ξ^{d-1}, it becomes a perfect derivative:

$$\frac{d}{d\xi}\left(\xi^{2H+d-1}\frac{dQ_H(\xi)}{d\xi} + \frac{\xi^d Q_H(\xi)}{2 - 2H}\right) = 0 .$$

Integrating once, we have

$$\xi^{2H+d-1}\frac{dQ_H(\xi)}{d\xi} + \frac{\xi^d Q_H(\xi)}{2 - 2H} = C,$$

and it is readily checked that the integration constant C must vanish for the integral in Eq. (278) to be finite. The remaining first-order ODE is thus separable and easily integrated to give

$$Q_H(\xi) = C_H \exp\left(-\frac{\xi^{2-2H}}{(2 - 2H)^2}\right) . \tag{279}$$

The normalization constant C_H must be chosen so that Eq. (278) holds; this gives

$$C_H = \frac{\Gamma(d/2)}{2 \pi^{d/2} (2 - 2H)^{(d+H-1)/(1-H)}\Gamma(d/(2 - 2H))} .$$

Re-expressing this result in the original dimensional variables through Eq. (277), we obtain the following.

Exact solution for the renormalized passive scalar correlation function:

$$\bar{P}_2(r, t) = \frac{M_2^0}{(D_L^I t)^{d/(2-2H)}} Q_H\left(\frac{r}{(D_L^I t)^{1/(2-2H)}}\right), \tag{280}$$

with Q_H given by Eq. (279) for $H > 0$.

4.2.2.4. Inertial-range properties of passive scalar fluctuations and relative diffusion of particle pairs. With this exact solution, we can read off several features concerning the evolution of the passive scalar fluctuations on length scales which lie within the inertial-range and are much larger than the correlation length scale of the initial passive scalar field. First, we see that, as with the shear RDT model in Section 4.2.1, the passive scalar variance decays anomalously for $H > 0$:

$$\langle T(x, y, t)^2\rangle \sim \bar{P}_2(0, t) \sim t^{-d/(2-H)} .$$

Under ordinary diffusive decay, the scaling exponent would be $-d/2$, corresponding to slower decay of variance.

We now proceed to use the explicit form of the shape of the PS correlation function to infer properties of relative tracer diffusion and the roughness of the passive scalar field.

Relative tracer diffusion. Below we will see that the length scale of the passive scalar fluctuations grows with time in proportion to $t^{1/(2-2H)}$. Our discussion of this property will be facilitated by the general relation between the second order PS correlation function and the probability distribution

for the relative separation of a pair of tracer particles ([196], Section 8.5). In the present case, $\bar{P}_2(|\boldsymbol{r}|, t)$ is proportional to the probability distribution over $\mathbb{R}^d$ of the relative displacement $\boldsymbol{r}$ of a pair of tracers at large times t for which the tracer separation distance $\rho_{\mathrm{rel}}(t)$ is statistically concentrated within the inertial range of scales and is much larger than the initial separation. The constant of proportionality is M_2^0, the integral of the initial PS correlation function.

The fact that the length scale of the correlation function scales as $t^{1/(2-2H)}$ means precisely, then, that the typical relative separation between a pair of tracers grows in time proportionally to $t^{1/(2-2H)}$ as they evolve through the inertial range. In particular, the mean-square relative tracer displacement may be computed as

$$\langle \rho_{\mathrm{rel}}(t)^2 \rangle = (M_2^0)^{-1} \int_{\mathbb{R}^d} |\boldsymbol{x}|^2 P_2(|\boldsymbol{x}|, t)\, \mathrm{d}\boldsymbol{x} = (M_2^0)^{-1} \int_0^\infty r^2 (A_{d-1} r^{d-1} P_2(r, t))\, \mathrm{d}r = C_R (D_L^I t)^{1/(1-H)}$$

with the numerical constant given by

$$C_R = (2 - 2H)^{2/(1-H)} \frac{\Gamma((d+2)/(2-2H))}{\Gamma(d/(2-2H))}\ .$$

Under ordinary diffusion, the mean-square displacement grows linearly with time. The presence of the rapidly decorrelating velocity field with very long-range spatial correlations ($H > 0$) causes particles to separate within the inertial range at a more rapid rate. In fact, the exponent of the power law of the relative separation becomes arbitrarily large as $H \to 1$.

In 1926, Richardson [284] predicted a law of this type for real-world turbulent diffusion as a consequence of the increase of relative diffusivity of a pair of tracers with separation distance. Through a fitting of available data from observation of balloon motion, Richardson found the relative diffusivity to scale as the 4/3 power of the separation distance and postulated a PDE of a form similar to that which we have been discussing Eq. (276) with $H = 2/3$. Solving the equation, Richardson deduced that the mean-square separation of a pair of tracers should grow as t^3. Richardson's prediction has found a good amount of numerical and experimental confirmation, as we shall later discuss in Section 6. Here, we can say that Richardson's reasoning is exactly valid for a Gaussian velocity field with rapid decorrelation in time. Furthermore, with the central limit rescaling discussed above (267), the familiar Kolmogorov spectrum corresponds in the RDT model exactly to the value $H = 2/3$!!

As a concrete illustration of this theoretical result, we present in Fig. 19 the results of a numerical Monte Carlo simulation of the relative dispersion of a pair of tracers in a rapidly decorrelating, isotropic velocity field with Hurst exponent $H = 1/3$. Through use of a multiwavelet method [84,85], which will be discussed later in Section 6, the numerically synthesized random velocity field supports a wide inertial range extending from scales 3×10^{-2} to 10^6. For all times plotted, the tracer separation lies well within the inertial range of the simulated velocity field.

In the upper plot, we see that the root-mean-square relative tracer displacement $\langle \rho_{\mathrm{rel}}(t)^2 \rangle^{1/2}$ settles down to the predicted $t^{3/4}$ power law growth over two decades of spatial scales. We plot the logarithmic derivative of the mean-square relative displacement $\mathrm{d}\langle \rho_{\mathrm{rel}}(t)^2 \rangle/\mathrm{d}\ln t$ as a function of time in the lower part of the figure as a more stringent test of the apparent power law behavior. The theoretically predicted scaling behavior corresponds to a constant logarithmic derivative of 3/2, and indeed the numerically computed logarithmic derivative hovers quite closely to this value after
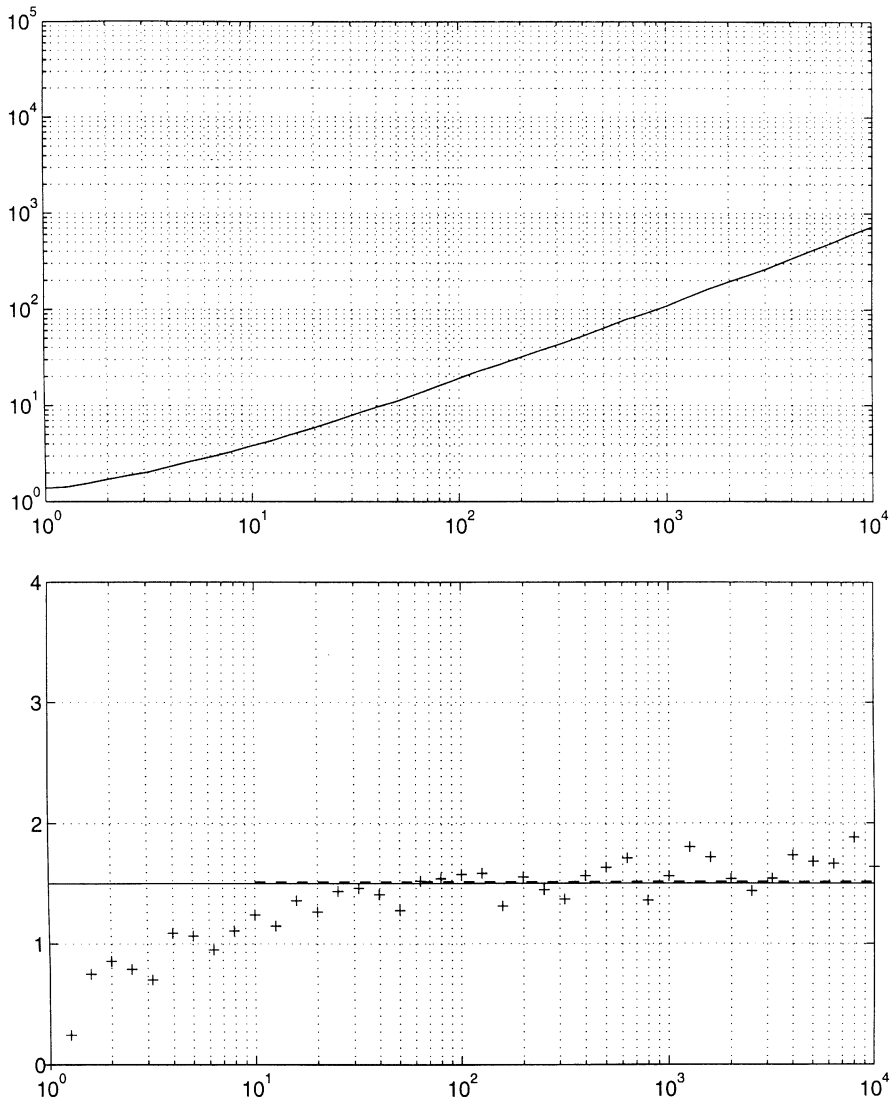
Fig. 19. Monte Carlo simulation of tracer pair dispersion through inertial range of isotropic, rapidly decorrelating velocity field with $H = 1/3$. Upper graph: log–log plot of root-mean-square tracer separation as a function of time. Lower graph: logarithmic derivative of the mean-square relative separation as a function of time.

an initial transient period. Besides producing a manifest realization of the inertial-range asymptotic theory for relative tracer diffusion in the RDT model, these numerical results also demonstrate the capacity of the underlying Monte Carlo method to generate accurate statistical scaling behavior over several decades. This is not an easy task, as we shall discuss in Section 6.

Thus far, we have discussed only the variance of the relative displacement of a pair of tracers, but our exact solution $\bar{P}_2(r, t)$ in fact gives the full probability density function (PDF) for this

random quantity. The relative displacement between two tracers undergoing independent Brownian motion is described by a Gaussian PDF. From Eq. (280), we see that when a pair of tracers are separated within the inertial range of scales of an isotropic RDT velocity field with long range correlations $H > 0$, their relative displacement has a PDF which has a broader-than-Gaussian shape. That is, the PDF decays more slowly at large values than a Gaussian with the same mean and variance does. The tangible manifestation of a random quantity with a broader-than-Gaussian PDF is an unusually high probability for large fluctuations. The reason why the relative tracer displacement should exhibit large fluctuations within the inertial range can be understood from a positive feedback effect arising from the fact that turbulent diffusion is more effective in separating particles the further apart they already are. If a random fluctuation causes a pair of particles momentarily to be separated by a distance greater than average, then they will be predisposed to be separated even more rapidly at later times.

Turbulent roughening of passive scalar field: We draw a final contrast between molecular diffusion and turbulent diffusion from the isotropic RDT model through a consideration of the smoothness of the passive scalar field. One measure of this smoothness, viewed on the inertial range of scales, is given by the behavior of the *structure function* of the renormalized passive scalar field $\bar{T}(\boldsymbol{x}, t)$:

$$\bar{S}_2(|\boldsymbol{r}|, t) = \langle (\bar{T}(\boldsymbol{x} + \boldsymbol{r}, t) - \bar{T}(\boldsymbol{x}, t))^2 \rangle$$

as $\boldsymbol{r} \to \boldsymbol{0}$. Noting that this quantity is nothing other than $2(\bar{P}_2(0, t) - \bar{P}_2(|\boldsymbol{r}|, t))$, we have from the exact solution (280) that

$$\bar{S}_2(r, t) = \frac{2C_H M_2^0}{(D_L^I t)^{d/(2-2H)}} \left(1 - \exp\left(-\frac{r^{2-2H}}{(2-2H)^2 D_L^I t} \right) \right).$$

One now readily checks that there exist positive numerical constants C_-, C_+, and r_0 so that

$$C_- \frac{r^{2-2H}}{(D_L^I t)^{(d+2-2H)/(2-2H)}} \leq \langle (\bar{T}(\boldsymbol{x} + \boldsymbol{r}, t) - \bar{T}(\boldsymbol{x}, t))^2 \rangle \leq C_+ \frac{r^{2-2H}}{(D_L^I t)^{(d+2-2H)/(2-2H)}}$$

over the expanding region

$$0 \leq r \leq r_0 (D_L^I t)^{1/(2-2H)}.$$

The structure function of a smooth, isotropic random field vanishes as $O(r^2)$ for small r, but we see that the structure function of $\bar{T}(\boldsymbol{x}, t)$ vanishes according to a slower power law as $r \to 0$, indicating a rough fractal structure of the passive scalar field in the inertial range of scales. Moreover, this fractal structure spreads to larger length scales as time evolves. The formal fractal Hurst exponent of this passive scalar field structure is $1 - H$, but because the passive scalar field is non-Gaussian, we cannot use Orey's theorem (discussed in Paragraph 3.5.3.1) to say this exponent characterizes the fractal structure of individual realizations.

Under ordinary molecular diffusion, sharp features are damped out and the passive scalar field would appear smooth on any given length scale ℓ after a sufficiently large time $\sim \ell^2/\kappa$. On the other hand, turbulent diffusion by an isotropic, rapidly decorrelating velocity field *creates* a rough fractal structure on the passive scalar field over an increasing band of scales within the inertial-range even as the amplitude of the fluctuations decay. As we have discussed in Section 3.5 in the context of scalar interfaces, the reason for this distinction is the long-range correlations of the

turbulent velocity field. Through advection, the fractal inertial-range spatial structure of the velocity field is impressed upon the passive scalar field. We note from our results of Section 3.5 that the rapid decorrelation limit smooths out the passive scalar level sets on the inertial range of scales in a *shear* flow. We see here, by contrast, that rough fractal structure persists throughout the inertial range of scales of the passive scalar field in an isotropic turbulent flow, even when it decorrelates rapidly in time.

4.3. Scaling regimes in spectrum of fluctuations of driven passive scalar field

In Section 4.2, we have discussed some physical characteristics of the diffusion and free decay of passive scalar fluctuations advected by a turbulent RDT model velocity field. For large times during which the length scale of the fluctuations passed through the inertial range of scales, we were able to describe a number of universal properties of the passive scalar field. Another situation in which one may hope to observe universal features in the passive scalar field is in a damped and driven statistically stationary state analogous to that of a fully developed turbulent velocity field. That is, we envision some external mechanisms stirring the fluid and agitating the passive scalar field at some large length scales. This directly creates large wavelength (small wavenumber) fluctuations in the velocity and passive scalar field, which then break up into smaller scale (higher wavenumber) fluctuations through nonlinear interactions. Sufficiently small fluctuations are damped out by viscosity and molecular diffusion. One can generally expect that if the driving is applied in a statistically steady fashion, that the turbulent system will achieve a *statistically stationary state* in which the input of energy at large scales is balanced by dissipation at very small scales, and the statistics of the velocity and passive scalar field settle down to a time-independent form. For conciseness, we will often refer to such a statistically stationary state as "quasi-equilibrium", with the "quasi-" prefix differentiating the present strongly damped and driven statistical equilibrium from a thermal equilibrium system weakly coupled to its surroundings.

We recall that for the velocity field, Kolmogorov formulated the well-known hypotheses that (see Paragraph 3.4.3.1 and [169,196]):

1. the statistics of the velocity fluctuations and wavenumbers much greater than those characterizing the driving should be independent of the large scales, and that
2. if the system is driven sufficiently strongly (Reynolds number is high enough) so that there is a wide separation between the scale of the driving L_0 and the scale of dissipation L_K, then the dynamics of the velocity field well within the intervening inertial-range of scales is completely self-similar and independent of both the large scales and viscosity. From this follows the famous $k^{-5/3}$ prediction for the energy spectrum in the inertial range of wavenumbers $L_K^{-1} \ll k \ll L_0^{-1}$.

These hypotheses have been largely confirmed with important provisos; see [309] for a recent review of theoretical and experimental developments. Here we shall only be concerned with these basic concepts, particularly as they apply to the structure of the *passive scalar field* in the statistically stationary, damped and driven state described above.

The passive scalar field responds directly to the turbulent fluctuations in the velocity field. As the statistics of the velocity field are believed to be universal to some degree on scales well below the scale L_0 at which the turbulence is driven, it is natural to suppose that the passive scalar fluctuations should also be universal at small scales. Furthermore, one might expect there to exist

self-similar *scaling regimes* for the spectrum of passive scalar fluctuations just as the energy spectrum of the velocity field exhibits the Kolmogorov $k^{-5/3}$ scaling in the inertial range. Indeed various theories have been formulated predicting a variety of passive scalar spectral scaling regimes over certain asymptotic ranges of wavenumbers [28,29,76,120,254]. None of the theoretical predictions for the scaling regimes of the velocity or passive scalar spectra makes use of the exact PDEs describing the physics. Mathematically understanding the statistics of the velocity field as a solution to the Navier–Stokes equations with random initial data is extremely difficult due to the nonlinearity. Even solving for the passive scalar statistics advected by a random velocity field with finite correlation time is a challenging problem.

The RDT model, however, provides us an opportunity to study directly the connection between the exact advection–diffusion PDE and the scaling regimes of the passive scalar spectrum, as first observed by Kraichnan [179,183]. If the random external driving of the passive scalar field is Gaussian and delta-correlated in time, then exact, closed evolution equations can still be written for the mean passive scalar density and correlation function of the passive scalar field (Section 4.3.1). The statistics of the passive scalar field in quasi-equilibrium are given as steady solutions of these equations. In a statistically isotropic environment, the quasi-equilibrium second-order PS correlation function may be represented by an explicit quadrature formula in terms of the spatial structure of the turbulent velocity field and driving (Section 4.3.2). The passive scalar spectrum is then expressed as a Fourier transform of this explicit formula. Through asymptotic analysis of these exact formulas, three different scaling regimes in the passive scalar spectrum can be rigorously shown to exist in the RDT model under suitable conditions (Section 4.3.3). These scaling regimes correspond qualitatively to those predicted for a realistic turbulent system, and we shall use the exact results of the RDT model to comment upon some of the approximate real-world theories, particularly those under current controversy (Section 4.3.4).

4.3.1. RDT model with driving

4.3.1.1. Model of large-scale driving force. To establish a statistically stationary state of the passive scalar field, we introduce an external driving, or "pumping", field $f(\mathbf{x}, t)$ as a source/sink term in the advection–diffusion equation:

$$\partial T(\mathbf{x}, t)/\partial t + \mathbf{v}(\mathbf{x}, t) \cdot \nabla T(\mathbf{x}, t) = \kappa \Delta T(\mathbf{x}, t) + f(\mathbf{x}, t) ,$$

$$T(\mathbf{x}, t = 0) = T_0(\mathbf{x}) .$$

For the RDT model, we shall assume that the pumping field is a mean zero, Gaussian, random, homogenous, stationary, random field which is delta-correlated in time:

$$\langle f(\mathbf{x}, t) f(\mathbf{x} + \mathbf{r}, t + \tau) \rangle = \Phi(\mathbf{r}) \delta(\tau) , \tag{281}$$

where $\Phi(\mathbf{r})$ is the (scalar) spatial correlation function of the pumping field.

This is admittedly quite artificial from a physical perspective. First of all, it is rather difficult to envision a system in which an external agency is directly introducing heat or concentration fluctuations homogenously throughout the bulk of the fluid. One would more naturally suppose that the external sources and sinks are confined to the boundary or some localized region. The rapidly decorrelating temporal structure is also inappropriate for a macroscale driving; it is

assumed in order to achieve closed equations for the passive scalar statistics. Nonetheless, we have the freedom to choose the spatial structure $\Phi(r)$ to correspond to pumping on a large length scale L_f, in which case the RDT model pumping field at least provides a cartoon for the generation of large-scale passive scalar fluctuations due to external driving.

Specifically, we define the pumping correlation function through its spectrum $E_f(k)$, which plays the analogous role of the energy spectrum for the random velocity field:

$$\Phi(r) = \int_{\mathbb{R}^d} e^{2\pi i k \cdot r} \frac{E_f(|k|)}{A_{d-1}|k|^{d-1}} \, dk ,$$

We choose for the pumping spectrum $E_f(k)$ a smooth form which is maximized at wavenumber $k = L_f^{-1}$, vanishes for $k \leq \frac{1}{2}L_f^{-1}$, and decays rapidly for $k \gg L_f^{-1}$. Note that we are assuming isotropic pumping statistics.

4.3.1.2. RDT model equations with pumping. The assumption of a delta-correlated pumping preserves the closure properties of the RDT model for a freely advected passive scalar field. Eq. (255) for the mean passive scalar density $\langle T(x,t) \rangle$ is unchanged because the pumping has mean zero. Thus, we may and do self-consistently assume the passive scalar field has mean zero for all time. The diffusion equation (256) for the second-order PS correlation function is modified only through the addition of an inhomogeneous term $\Phi(r)$ representing the effects of the pumping.

Evolution of second-order correlation function for driven passive scalar

$$\frac{\partial P_2(r,t)}{\partial t} = \nabla \cdot ((2\kappa \mathcal{I} + \mathcal{D}_s(r))\nabla P_2(r,t)) + \Phi(r) ,$$

$$P_2(r,t=0) = P_2^0(r) .$$

$$(282)$$

With the driving included in this way in the RDT model, we can search for solutions corresponding to a quasi-equilibrium state for the passive scalar field, in which the statistics of the passive scalar field are time-independent. In particular, the quasi-equilibrium second-order PS correlation function $P_2^*(r) \equiv \langle T(x,t)T(x+r,t) \rangle_*$ is a steady solution of Eq. (282). The asterisks decorating ensemble averages and statistical functions indicate that the statistics are those corresponding to quasi-equilibrium. Because of the dissipation provided by molecular diffusivity, all solutions with sufficient spatial decay will approach a unique statistically stationary state at long times.

We note here an important relation implied by Eq. (282) for the quasi-equilibrium passive scalar dissipation rate $\bar{\chi} = 2\kappa \langle (\nabla T(x,t))^2 \rangle_*$. This is just the rate at which the passive scalar variance $\langle (T(x,t))^2 \rangle$ would decay in the absence of external driving, as is readily checked (not just for the RDT model) by multiplying the undriven advection–diffusion equation by $T(x,t)$ and averaging. In a statistically stationary state, the passive scalar dissipation rate is exactly balanced by the rate at which passive scalar fluctuations are introduced into the system by the external driving. For the RDT model, this can be quantified:

$$\bar{\chi} = \Phi(0) ,$$

as follows by realizing that $\bar{\chi} = -2\kappa \Delta P_2^*(r)|_{r=0}$ and evaluating the steady form of Eq. (282) at $r = 0$.

4.3.1.3. Alternative driving through linear background passive scalar profile. Before proceeding with our analysis of the model we have just set up, we pause to mention that another way to introduce driving into the advection–diffusion equation is to impose a linear background profile on the passive scalar field through the initial data [156,277]: $T_0(\mathbf{x}) = \mathbf{g} \cdot \mathbf{x}$. This linear profile will persist in time and the turbulence will interact with it to perpetually drive fluctuations of the passive scalar field about this background profile, eventually leading to a nontrivial statistically stationary state of the passive scalar field. A background linear profile with a mean gradient for the passive scalar field is rather natural for stratified fluids in a geophysical setting, and can be readily arranged in the laboratory [127,145]. It is not difficult to show [185] that all the results that we will derive here for the passive scalar spectrum of the statistically stationary state of the passive scalar field driven by external pumping of the form (281) carry over to the case where passive scalar fluctuations are driven instead by turbulent interaction with a background linear passive scalar profile. One need only equate $L_f = L_0$ and the passive scalar dissipation rate $\bar{\chi}$ in the formulas with $g^2 R_0$, where the constant R_0 is a measure of the strength of the turbulent fluctuations: $R_0 = (1/d)\mathrm{Tr}R_s(\mathbf{0})$.

4.3.2. Exact quadrature solution for quasi-equilibrium passive scalar correlation function

Now, the model we have adopted has isotropic pumping and velocity statistics, so by symmetry and uniqueness of solutions, the quasi-equilibrium passive scalar field must also be statistically isotropic. Hence, the quasi-equilibrium second-order PS correlation function is radial $P_2^*(\mathbf{r}) = P_2^*(|\mathbf{r}|)$, and Eq. (282) simplifies to a one-dimensional ODE:

$$r^{1-d}\frac{\mathrm{d}}{\mathrm{d}r}\left((2\kappa + D_{\|}(r))r^{d-1}\frac{\mathrm{d}P_2^*(r)}{\mathrm{d}r}\right) = -\Phi(r) \ . \tag{283}$$

The boundary conditions that go with this second-order differential equation on the positive real axis $r \in [0, \infty)$ are:

- $P_2^*(r)$ is continuous and finite near $r = 0$, reflecting finite variance of the passive scalar fluctuations,
- $P_2^*(r)$ decays to zero as $r \to \infty$ since the passive scalar field is uncorrelated at large enough distances.

Eq. (283) can be solved exactly by quadrature, with the integration constants determined by the boundary conditions:

Exact solution for quasi-equilibrium passive scalar correlation function

$$P_2^*(r) = \int_r^\infty r'^{-d+1}\frac{\int_0^{r'}r''^{d-1}\Phi(r'')\,\mathrm{d}r''}{2\kappa + D_{\|}(r')}\,\mathrm{d}r' \ . \tag{284}$$

This formula was derived by Kraichnan [183]. Its importance is that it gives an exact formula for the passive scalar correlation function in terms of the velocity and pumping correlation functions, and that it was deduced in a precise fashion from the advection–diffusion equation. One could proceed to study the properties of this PS correlation function [183,185], but we will concentrate our attention on a related function, the *passive scalar spectrum*, which reveals the small-scale structure of the passive scalar field in a clearer fashion.

4.3.3. Passive scalar spectral scaling regimes in RDT model

The (radial) *passive scalar (PS) spectrum* $E_T(k)$ is defined to be the spectral resolution of the variance of the passive scalar field $\langle (T(\mathbf{x},t))^2 \rangle_*$ with respect to wavenumber magnitude k ([320], pp. 280–281). That is, $E_T(k)$ measures the strength of the fluctuations of wavenumber k, and $\int_0^\infty E_T(k)\,\mathrm{d}k = \langle (T(\mathbf{x},t))^2 \rangle_*$. Its relation to the passive scalar field is essentially the same as that of the energyspectrum to the velocity field. Not only is the PS spectrum an object with appealing theoretical meaning, but it is closely related to what experimentalists actually measure when observing a signal from a turbulent system. (In most experiments, measurements are taken only along a single line, and thus a "one-dimensional passive scalar spectrum" is recorded. This is closely related to the radial passive scalar spectrum discussed when the turbulence is statistically isotropic. (See ([320], Ch. 8) for further discussion.)

The radial PS spectrum $E_T(k)$ can be computed from the Fourier transform of the passive scalar correlation function

$$\hat{P}_2^*(\mathbf{k}) = \int_{\mathbb{R}^d} \mathrm{e}^{-2\pi i k \cdot x} P_2^*(\mathbf{x})\,\mathrm{d}\mathbf{x} \ . \tag{285}$$

For the statistically isotropic case of interest in this section, $\hat{P}_2^*(\mathbf{k}) = \hat{P}_2^*(|\mathbf{k}|)$ and the PS spectrum can be simply expressed:

$$E_T(k) = A_{d-1} k^{d-1} \hat{P}_2^*(k) \ . \tag{286}$$

Through Eqs. (284)–(286), we have an exact integral formula for the PS spectrum $E_T(k)$, which we can analyze for our specific choice of velocity and pumping statistics.

We will in particular look for universal scaling regimes analogous to the Kolmogorov $k^{-5/3}$ inertial-range law for the energy spectrum of the velocity field. Recall that this self-similar region fell within an asymptotic regime intermediate to the fundamental wavenumbers L_0^{-1} at which energy is fed into the fluid, and L_K^{-1} above which energy is strongly dissipated by viscosity. By general intermediate asymptotic principles [25], we can also anticipate self-simliar scaling regimes in the PS spectrum at wavenumbers well-separated from the fundamental wavenumbers characterizing the passive scalar field.

To proceed, we shall first identify in Paragraph 4.3.3.1 the fundamental length scales (and associated wavenumbers) characterizing the quasi-equilibrium passive scalar field. Next, in Paragraphs 4.3.3.2 and 4.3.3.3, we report three possible PS spectrum scaling regimes which rigorously arise in the RDT model when certain fundamental length scales are sufficiently widely separated. We will compare the exact self-similar scaling forms of the RDT model PS spectrum with the predictions of approximate theories for real-world turbulent systems in Section 4.3.4.

4.3.3.1. Fundamental length scales and wavenumbers.
There are four natural length scales which partially characterize the passive scalar field, both in the RDT model and in the real world. Two length scales are inherited from the advecting turbulent velocity field: the integral length scale L_0 at which the fluid is driven, and the Kolmogorov dissipation length scale L_K below which velocity fluctuations are strongly damped by viscosity. Next, we have the correlation length L_f of the pumping field, which sets the (large) length scale at which passive scalar fluctuations are externally introduced. Finally, it is natural to identify a passive scalar dissipation length scale L_d, analogous to the Kolmogorov dissipation scale of the velocity field, at which convection and diffusion effects

are in balance. Below such a scale, diffusive effects rapidly damp passive scalar fluctuations, and above L_d, the passive scalar dynamics are convection-dominated and molecular diffusion effects are formally negligible.

To see how this scale should be determined in the RDT model, recall from Eq. (259) that the relative diffusion rate of two particles separated by distance $|r|$ is $2\kappa + \mathrm{Tr}\,\mathscr{D}_s(r)$. The contribution from the turbulent diffusion, $\mathrm{Tr}\,\mathscr{D}_s(r)$, is proportional to the mean-square fluid velocity difference between the particles, and generally grows as a function of $|r|$. (By isotropy $\mathrm{Tr}\,\mathscr{D}_s(r)$ is independent of the orientation of r.) It thus becomes appropriate to define L_d as the length scale at which relative turbulent diffusion and molecular diffusion are in balance: $2\kappa = \mathrm{Tr}\,\mathscr{D}_s(L_d\hat{e})$, where $\hat{e}$ is a unit vector.

Let us now discuss how the various length scales are typically ordered. In general, turbulent systems, L_0 and L_f are large length scales characteristic of the macroscopic system size, whereas the Kolmogorov velocity dissipation length L_K and the passive scalar dissipation length L_d are considerably smaller:

$$L_K, L_d < L_0, L_f .$$

The disparity between the length scales is often several orders of magnitude. Now, we will be considering the passive scalar structure on scales small compared with the scale of the driving, so the ordering of L_0 and L_f will not concern us. The relation between the velocity and passive scalar dissipation lengths is more interesting.

The relative magnitude of these dissipation length scales is set by the *Schmidt number* Sc of the fluid, which is the ratio of the kinematic viscosity v of the fluid to the molecular diffusivity κ of the passive scalar:

$$\mathrm{Sc} = v/\kappa . \tag{287}$$

This ratio is called the Prandtl number Pr when the passive scalar field corresponds to weak temperature fluctuations, but we will generally use the term "Schmidt number". Note that the Schmidt number measures the relative effectiveness of *microscopic* fluid momentum transport relative to microscopic passive scalar transport.

A common situation for transport of light particles or heat in ordinary fluids like air (Pr ≈ 0.7) is for the Schmidt number to be order unity. In this case, $L_d \sim L_K$ because the efficiency of microscopic momentum and passive scalar transport are comparable, and the length scales at which the microscopic effects become relevant are about the same. Another fairly prevalent situation is that of high Schmidt number, for which the passive tracer is diffused much less effectively than the momentum of the fluid. The transport of heavy dyes or complex fluorocarbons with large molecular weights as utilized in contemporary laser-induced flourescence measurements (Sc $\sim 10^3$) provide important practical examples. In these situations, $L_d \ll L_K$ because one must go to much smaller scales than L_K to feel the relatively feeble influence of molecular diffusion. The third possibility of low Schmidt number exists in some exotic cases like electron plasmas (Pr $\sim 10^{-1}$) and thermal fluctuations in liquid mercury (Pr ≈ 0.02). The regime $L_d \gg L_K$ occurs at low Schmidt number, because the molecular diffusion becomes relevant at a larger length scale than viscosity.

To each of the four physical length scales just discussed, we naturally associate their corresponding wavenumber for the purpose of discussing the PS spectrum $E_T(k)$: $k_0 = L_0^{-1}$, $k_K = L_K^{-1}$, $k_f = L_f^{-1}$, and $k_d = L_d^{-1}$.

4.3.3.2. Passive scalar spectral scaling regimes. Subject to the natural ordering of the length scales discussed above, three natural intermediate asymptotic regimes where one may expect self-similar scaling of the passive scalar spectrum are suggested. These regimes, which we now enumerate, have meaning in both the real world and the RDT model.

- *inertial-convective regime*:

$$k_0, k_f \ll k \ll k_K, k_d .\tag{288}$$

  This is present in the case of a wide separation between the system macroscale and dissipation microscales (high Reynolds number and high Péclet number). Passive scalar fluctuations on this range are driven by inertial-range turbulent eddies, and molecular diffusion plays a subdominant role.

- *viscous-convective (high Schmidt number) regime*:

$$k_0, k_f, k_K \ll k \ll k_d .\tag{289}$$

  This is present when $Sc \gg 1$, and there is no strict need for a high Reynolds number or an extended inertial range. Fluctuations of the passive scalar on these scales are too fine to be driven directly by the active scales of turbulence; they are rather produced by straining by velocity field gradients. Molecular diffusion is ostensibly unimportant in the dynamics of the passive scalar in this range of scales since $k \ll k_d$.

- *inertial-diffusive (low Schmidt number) regime*:

$$k_0, k_f, k_d \ll k \ll k_K .\tag{290}$$

  This is present when $Sc \ll 1$ and $Re \gg 1$. Molecular diffusion now transports the passive scalar more effectively than the turbulence, but the passive scalar field is still suffering deformations from the inertial-range eddies of the turbulent velocity field.

The convention in the above discussion is that a regime is called inertial or viscous according to whether the wavenumber k is on the inertial $k_0 \ll k \ll k_K$ or viscous $k \gg k_K$ range of scales, and is called convective or diffusive according to whether the dynamics are formally convection-dominated $k \ll k_d$ or diffusion dominated $k \gg k_d$. There is of course also a viscous-diffusive regime $k \gg k_d, k_K, k_0, k_f$ but the PS spectrum falls off very rapidly at these very high wavenumbers and does not exhibit scaling.

In the RDT model, the form of the passive scalar spectrum in each of the three above-mentioned asymptotic regimes may be rigorously computed, and is presented in Table 13. In each case, a scaling law emerges, with the prefactor consisting of the fundamental physical parameters:

- The passive scalar dissipation rate, $\bar{\chi}$.
- The parameter A_E describing the amplitude of the inertial-range turbulent eddies (recall $\widetilde{E}(k) \sim A_E k^{-1-2H}$ for $k_0 \ll k \ll k_K$).
- The *small-scale strain rate γ* which describes the dynamics of the passive scalar field in the viscous range of scales $r \ll L_K$ (or $k \gg k_K$). The relative turbulent diffusion of tracers separated by such a small distance comes primarily through straining by gradients of inertial-range eddies. The definition for the strain rate which we adopt here is

$$\gamma \equiv (\mathrm{d}/\mathrm{d}t)\ln\langle |\boldsymbol{X}^{(1)}(t) - \boldsymbol{X}^{(2)}(t)|^2 \rangle^{1/2},$$

where $X^{(1)}(t)$ and $X^{(2)}(t)$ denote the locations of two tracers separated by a distance $|X^{(1)}(t) - X^{(2)}(t)| \ll L_K$, and the effects of molecular diffusion are omitted in this computation. In the RDT model, γ is related to the energy spectrum through

$$\gamma^{-1} = 16 d\pi^2 \int_0^\infty \tilde{E}(k) k^2 \, dk .$$

The dimensionless numerical constants appearing in the formulas have the values:

$$C_{IC} = \frac{2H^2}{\pi^2 d} B(d/2, 1 + H) B(d/2, 1 - H) ,$$

$$C_{VC} = (d + 2)/d, \qquad C_{ID} = 1/8 d\pi^2$$

where $B(\cdot, \cdot)$ denotes the special beta functions [195].

The scaling forms for the inertial-convective and viscous-convective regime were formally computed by Kraichnan [179,183]. Rigorous derivations for all scaling regimes may be found in [185].

4.3.3.3. Complete self-similarity of passive scalar spectral scaling regimes. One immediate observation from the exact scaling laws presented in Table 13 is that they are all *completely self-similar* in the terminology of Barenblatt [25]. That is, in each asymptotic regime of wavenumbers presented above, the PS spectrum depends only on physical parameters which are obviously relevant for that range of scales. There is no dependence on physical parameters associated to remote length scales, and no "anomalous scaling" of the PS spectrum. (See Section 4.4 for further discussion on this topic.)

In all the regimes, the PS spectrum depends on the passive scalar dissipation rate $\bar{\chi}$. This quantity measures the flux of passive scalar "energy" which is injected at low wavenumbersand travels up to high wavenumbers where it is dissipated. $\bar{\chi}$ simply sets the amplitude of the PS spectrum. In addition to $\bar{\chi}$, the PS spectrum in the inertial-convective regime depends only on the local wavenumber k and the parameter A_E which measures the strength of the inertial-range eddies. This is exactly the set of parameters which one would expect to appear in the inertial-convective

Table 13
Universal scaling regimes for passive scalar spectrum in RDT model

Asymptotic regime	$E_T(k)$
Inertial-convective $k_f, k_0 \ll k \ll k_K, k_d$	$C_{IC} \bar{\chi} A_E^{-1} k^{2H-3}$
Viscous-convective $k_f, k_0, k_K \ll k \ll k_d$	$C_{VC} \bar{\chi} \gamma^{-1} k^{-1}$
Inertial-diffusive $k_f, k_0, k_d \ll k \ll k_K$	$C_{ID} A_E \bar{\chi} \kappa^{-2} k^{-3-2H}$

asymptotics of the PS spectrum, where the inertial-range eddies play a dominant role, and molecular diffusivity is negligible. Similarly, the viscous-convective form of the PS spectrum depends only on $\bar{\chi}$, k, and γ, the strain rate characterizing the advective effects of the velocity field in the viscous range of scales. Finally, the inertial-diffusive regime depends on four parameters $\bar{\chi}$, k, A_E, and κ, because the inertial-range eddies are the predominant cause of distortions on this range of scales, and molecular diffusivity is playing a strong role. Thus, the passive scalar spectrum in each of the ranges reported depends only on the parameters which one would naively expect.

It turns out, therefore, that the kind of reasoning which Kolmogorov used to formulate his $k^{-5/3}$ inertial-range scaling prediction works *correctly* in the RDT model when applied to the inertial-convective and viscous-convective range of scales. One simply hypothesizes which parameters should be naturally relevant in each of these ranges of wavenumbers, applies dimensional analysis, and finds that only a unique scaling combination of these parameters is dimensionally self-consistent. One would thereby arrive at the scaling laws presented in Table 13, except of course that the numerical constants C_{IC} and C_{VC} would not be determined by this approach. Obukhov [254] and Corrsin [76] independently formulated such a similarity theory for the inertial-convective regime in a real-world turbulent system. The inertial-diffusive regime, on the other hand, involves too many parameters which have a priori relevance so that dimensional analysis alone will not produce a unique scaling prediction.

4.3.4. Connections to theory and experiments concerning real-world scaling regimes

We wish now to use the exact results for the scaling regimes of the passive scalar spectrum in the RDT model as a point of reference for discussing some physical theories formulated for analogous scaling regimes in the real world. Recall that we could impose a fairly realistic spatial structure on the turbulent RDT model; the primary deficiency in the model is the lack of memory in the velocity field. Thus, we can anticipate qualitative similarities in the PS spectral scaling regimes in the real world and the RDT model, but there will of course be quantitative discrepancies due to the different temporal structures. We will probe the *ideas* behind the physical theories for the real world to see if they can be successfully adapted to the RDT model.

We now briefly discuss each of the passive scalar scaling regimes in turn. We present the main theoretical predictions for the real-world PS spectrum, and summarize their experimental status. Then we indicate whether these theories can be adapted to the RDT model, and if so, whether they predict the correct scaling law. Details can be found in [185].

4.3.4.1. Inertial-convective regime.

The prediction for the inertial-convective regime of the passive scalar spectrum in the real world is based on Kolmogorov-type dimensional analysis, and was formulated independently by Obukhov [254] and Corrsin [76]. It reads

$$E_T(k) \approx C_{OC}\bar{\chi}\bar{\varepsilon}^{-1/3}k^{-5/3} \quad \text{for } k_0, k_f \ll k \ll k_K, k_d ,$$

where $\bar{\varepsilon}$ is the energy dissipation rate and the other parameters have the same physical meaning as in the RDT model. C_{OC} is supposed to be a universal numerical constant, called the Obukhov–Corrsin constant.

A number of experiments over the last three decades have reported a decade or two of $k^{-5/3}$ scaling behavior in flows with sufficiently large Reynolds numbers, with fairly consistent values of the reported Obukhov–Corrsin constant near 0.4. A recent review of the data for the

inertial-convective regime from experiments may be found in [308]. In this paper, it is pointed out that the Reynolds number (based on the Taylor microscale) required to see a $k^{-5/3}$ scaling region is approximately 50 in isotropic flows, but about 1000 for anisotropic flows. Experiments conducted in anisotropic settings which report departures from $k^{-5/3}$ scaling in the inertial-convective range [81,145,242] may simply have too low a Reynolds number to manifest the universal Obukhov–Corrsin behavior.

There are still some unexplained mysteries, however. The $k^{-5/3}$ law seems to be more robust than it should be. In particular, it sometimes arises in flows for which the inertial-convective scales are not locally isotropic [113,236,306]. Moreover, the $k^{-5/3}$ scaling in the PS spectrum can extend over a range larger than that for which the velocity field exhibits inertial-range $k^{-5/3}$ scaling. Indeed, a $k^{-5/3}$ scaling in the PS spectrum is reported in some cases where the Reynolds number is insufficient for the velocity field to have any $k^{-5/3}$ inertial range at all! [145,309] Although the prediction of the Obukhov–Corrsin similarity theory appears to be well borne out by experiments, the *reason* behind the $k^{-5/3}$ scaling is not satisfactorily understood.

The Obukhov–Corrsin inertial-convective scaling prediction has a good deal of formal similarity to that of the RDT model:

$$E_T^{\mathrm{OC}}(k) \approx C_{\mathrm{IC}} \bar{\chi} A_E^{-1} k^{2H-3} \quad \text{for } k_0, k_{\mathrm{f}} \ll k \ll k_{\mathrm{K}}, k_{\mathrm{d}} .$$

The strength of the inertial range eddies is measured by the energy dissipation rate $\bar{\varepsilon}$ in the real world and by A_E in the RDT model (see Section 4.1.4). The dimensional analysis reasoning behind the Obukhov–Corrsin prediction works perfectly in the RDT model. Consequently, a number of other simple heuristic considerations (based on spectral flux considerations, for example) will also automatically predict the correct inertial-convective scaling form in the RDT model, provided they only involve the inertial-range form of the turbulent energy spectrum and the passive scalar dissipation rate!

4.3.4.2. Viscous-convective (*high Schmidt number*) *regime.* The PS spectrum was predicted by Batchelor [28] to have the following viscous-convective scaling form in a real turbulent system:

$$E_T^{\mathrm{B}}(k) \approx \bar{\chi}/\gamma k \quad \text{for } k_{\mathrm{K}} \ll k \ll k_{\mathrm{d}} . \tag{291}$$

He argued, based on empirical considerations, that it would be sufficient to consider the passive scalar dynamics on this range of scales in a *steady* uniform strain flow, and deduced Eq. (291) where γ is the maximum strain rate. Kraichnan [179] investigated the effect of fluctuations in the velocity field through consideration of his Rapid Decorrelation in Time model, arriving at the same prediction as Batchelor, up to a numerical multiplicative constant (see Table 13). Chertkov et al. [65] generalize the prediction of a k^{-1} law to finite correlation times as well by reducing the problem to that of the stretching of lines by a spatially uniform straining field in the presence of weak molecular diffusion. We see thus that there exists strong theoretical support for a k^{-1} viscous-convective scaling of the PS spectrum. Note that the scaling law (291) could also be predicted (up to numerical constant) through an accounting of the obviously relevant parameters and simple dimensional analysis, in a fashion entirely parallel to the Obukhov–Corrsin theory for the inertial-convective regime.

Until recently, the k^{-1} scaling prediction also enjoyed experimental confirmation for a number of passive physical quantities in various turbulent systems [123,129,251,271]. Some of these

findings [123,129,251] were later criticized [113,242], however, and some recent high Schmidt number experiments [171,242,338] fail to find k^{-1} spectral scaling despite their ability to resolve the viscous-convective scales. The viscous-convective k^{-1} scaling law is thus under current controversy.

4.3.4.3. Inertial-diffusive (low Schmidt number) regime. As we mentioned before, in the inertial-diffusive regime there are too many "obviously relevant" parameters to predict a unique scaling law by an assumption of complete self-similarity, as was possible in the other regimes previously discussed. There is in fact a controversy over the scaling exponent in the inertial-diffusive range. Batchelor et al. (BHT) [29] argue through an approximate consideration of the passive scalar dynamics in Fourier space, that the passive scalar spectrum (for a turbulent velocity field with realistic temporal correlations) has the following inertial-diffusive scaling form:

$$E_T^{\text{BHT}}(k) = (C_{\text{K}}/16d\pi^4)\bar{\chi}\bar{\varepsilon}^{2/3}\kappa^{-3}k^{-17/3} \quad \text{for } k_{\text{d}} \ll k \ll k_{\text{K}} , \tag{292}$$

where C_{K} is the Kolmogorov constant ($E(k) \approx C_{\text{K}}\bar{\varepsilon}^{2/3}k^{-5/3}$ for $k_0 \ll k \ll k_{\text{K}}$). A competing theory by Gibson [121], which argues that the small-scale strain rate is important for the inertial-diffusive range dynamics, arrives instead at a prediction of a different scaling in a subrange of the inertial-diffusive regime:

$$E_T^{\text{G}}(k) \sim C_{\text{G}}\bar{\chi}\kappa^{-1}k^{-3} \quad \text{for } k_{\text{d}} \ll k \ll k_{\text{B}} ,$$

C_{G} is a numerical constant undetermined by the theory, and k_{B} is the "Batchelor wavenumber", defined as the inverse of the length scale L_{B} at which the molecular diffusion time balances the straining of the velocity field.

Measurements of temperature fluctuations in mercury (Pr ~ 0.02) [73,290], and numerical simulations [56] are consistent with a k^{-3} spectrum for $k_{\text{d}} \ll k \ll k_{\text{B}}$. Furthermore, [56,73] also show evidence for a $k^{-17/3}$ range over $k_{\text{B}} \ll k \ll k_{\text{K}}$. The spectra of both theories decay rapidly and are difficult to measure confidently, however, especially since sufficiently low Schmidt or Prandtl numbers are difficult to achieve experimentally [136,137,196]. Indeed the reported scaling regimes extend over less than a decade. Moreover, it has been pointed out in [22] that apparent but false k^{-3} scaling regimes can result from noisy physical-space observations when the true spectral scaling is steeper (such as $k^{-17/3}$). Finally, the experimental data are too scant to check the predicted dependence of the coefficient of the inertial-diffusive scaling laws on various physical parameters.

In [185], the arguments of the BHT and Gibson theories are examined by the second author in the context of the RDT model. Both the BHT and Gibson theories have versions which appear to be sensibly applicable to the RDT model insofar as the theoretical arguments are concerned. The BHT arguments lead to the correct inertial-diffusive asymptotics for the RDT model:

$$E_T(k) = C_{\text{ID}}A_E\bar{\chi}\kappa^{-2}k^{-3-2H} \quad \text{for } k_{\text{f}}, k_0, k_{\text{d}} \ll k \ll k_{\text{K}} ,$$

$$C_{\text{ID}} = 1/8d\pi^2 .$$

Indeed, the BHT real-world prediction has a strong formal similarity with the exact RDT model result, recalling that A_E in the RDT model plays a similar role as $C_{\text{K}}\bar{\varepsilon}^{2/3}$ in the real world. On the other hand, the adapted version of Gibson's theory fails in the RDT model. The dynamics of the

passive scalar in the inertial-diffusive range of scales does not seem to be signficantly influenced by straining in the RDT model.

This is by no means an invalidation of Gibson's ideas or prediction in a real world setting. Rather it gives us an opportunity to illuminate some ingredients which are essential in the Gibson theory. The straining mechanism envisioned by Gibson has at least a crude analogue in the RDT model, but perhaps the fact that the RDT velocity field is Gaussian and delta-correlated makes the strain ineffective in influencing the inertial-diffusive range passive scalar dynamics. Indeed, numerical simulations [122] indicate that sustained compression events and anomalously long-range straining correlations appear to be necessary for the straining to have a strong effect on these scales. The outcome of the RDT model calculation might then be viewed as an analytical complement to these numerical findings.

Even allowing for this source of discrepancy, there is an assumption made in Gibson's theory which is surprising in light of the exact results of the RDT model. From the premise that straining plays an important role in the passive scalar dynamics in the inertial-diffusive range, Gibson formulates a pair of similarity hypotheses which leads to a prediction for the PS spectrum in a subrange of the inertial-diffusive spectrum which involves fewer parameters than the exact scaling form for the RDT model in this range. Given that the RDT model is a simplification of real world turbulence, this is a puzzling outcome, especially since Gibson's prediction comes not from explicit computation, but from soft self-similarity arguments. Indeed, there seems to be a gap in the logical arguments leading up to the k^{-3} prediction. A full discussion may be found in [185].

4.4. Higher-order small-scale statistics of passive scalar field

It is a remarkable feature of the RDT model that closed linear PDEs can be written not only for the mean passive scalar density and second-order correlation function, but for all higher-order correlation functions

$$P_N(\{\boldsymbol{x}^{(j)}\}_{j=1}^N, t) \equiv \left\langle \prod_{j=1}^N T(\boldsymbol{x}^{(j)}, t) \right\rangle$$

as well. That this could be done in principle was pointed out in [244,246]. The first explicit use of these equations for the study of higher-order statistics of passive scalar fluctuations within the inertial range of scales of a turbulent flow was accomplished by the first author [206] for the case of a freely decaying passive scalar field in a turbulent shear flow. The one-point statistics of the decaying passive scalar (without pumping) were shown to be broader than Gaussian in this setting, and the multipoint statistics within the inertial range were demonstrated to be non-Gaussian.

4.4.1. Anomalous scaling of turbulence structure functions

Kraichnan [183] subsequently proposed that the passive scalar structure functions in quasi-equilibrium

$$S_N^*(r) \equiv \langle (T(\boldsymbol{x} + \boldsymbol{r}, t) - T(\boldsymbol{x}, t))^N \rangle_* \tag{293}$$

should exhibit *anomalous* scaling within the inertial-convective range of scales in the RDT model. By anomalous scaling in this context is meant that

$$S_N^*(r) \propto r^{\zeta_N} \quad \text{for } L_K, L_d \ll r \ll L_0, L_f \,,$$

where the exponents ζ_N are not equal to the values which would be predicted by a complete self-similarity hypothesis [24,25]. A manifestation of anomalous scaling which is observed in experimental inertial-range measurements of both temperature and velocity in high Reynolds number flows with fully developed turbulence [5,309] is that $\zeta_{2N} \neq N\zeta_2$.

As we now explain, the violation of the scaling relation $\zeta_{2N} = N\zeta_2$ implies that the small-scale passive scalar fluctuations both manifest strong non-Gaussianity ("intermittency") and depart strongly from Kolmogorov's and Obukhov's original completely self-similar theory. Using real-world parameters for the moment, the only dimensionally consistent inertial-range asymptotic form of $S_N^*(r)$ which depends purely on the scalar dissipation rate $\bar{\chi}$, the separation distance r, and the energy dissipation rate $\bar{\varepsilon}$ is

$$S_N^*(r) \sim C_N \bar{\chi}^{N/2} \bar{\varepsilon}^{-N/6} r^{N/3} \quad \text{for } L_{\mathrm{K}}, L_{\mathrm{d}} \ll r \ll L_0, L_{\mathrm{f}} , \tag{294}$$

with dimensionless universal constants C_N. The asymptotics (294) correspond to the *normal* scaling relation $\zeta_{2N} = N\zeta_2$. For normal scaling to be violated, some additional parameter must be involved in the inertial-convective range statistics. This extra parameter is expected to be a physical length scale L, which permits the following dimensionally consistent inertial-range anomalous scaling law for the passive scalar structure functions:

$$S_N^*(r) \sim C_N \bar{\chi}^{N/2} \bar{\varepsilon}^{-N/6} r^{N/3} \left(\frac{r}{L}\right)^{\alpha_N} \quad \text{for } L_{\mathrm{K}}, L_{\mathrm{d}} \ll r \ll L_0, L_{\mathrm{f}} , \tag{295}$$

where $\alpha_N = \zeta_N - N/3$ and the $\{C_N\}_{N=1}^\infty$ are a sequence of dimensionless, universal constants. Natural candidates for the length scale L entering the asymptotics are the integral length scale L_0, the pumping length scale L_{f}, the passive scalar dissipation length scale L_{d}, and the Kolmogorov dissipation length scale L_{K}; more exotic possibilities are mentioned in [64]. The current conventional wisdom, based on experimental observations and numerical simulations at various Reynolds numbers, is that $L = L_{\mathrm{f}}$ (and $L = L_0$ for velocity structure functions, but L_0 and L_{f} are typically of the same order.) Hölder inequalities ([288], Section 6.2) imply in this case that $\alpha_{2N} \leq 0$, or equivalently, $\zeta_{2N} \leq N\zeta_2$. We remark that, at least in principle, there could be several length scales appearing as anomalous scaling factors [201]. The inertial-range form (295) is said to be *incompletely self-similar* in the terminology of Barenblatt [24,25], in that the length scale parameter L enters into the asymptotics, but only through a power law, even though it is not an "obviously relevant" parameter in the asymptotic regime of interest. Indeed, the inertial-convective range of values of r is, by definition, far removed from any physical length scale ($L_0, L_{\mathrm{K}}, L_{\mathrm{d}}$, etc.).

One implication of Eq. (295) with $L = L_{\mathrm{f}}$ is that the temperature fluctuations becoming increasingly intermittent (broader-than-Gaussian) on smaller length scales throughout the inertial range since the flatness factors

$$\frac{\langle (T(\boldsymbol{x} + \boldsymbol{r}, t) - T(\boldsymbol{x}, t))^{2N} \rangle}{\langle (T(\boldsymbol{x} + \boldsymbol{r}, t) - T(\boldsymbol{x}, t))^2 \rangle^N} = \frac{S_{2N}^*(r)}{((S_2^*(r))^N} \sim \frac{C_{2N}}{(C_2)^N} \left(\frac{r}{L_{\mathrm{f}}}\right)^{\zeta_{2N} - N\zeta_2} \quad \text{for } L_{\mathrm{K}}, L_{\mathrm{d}} \ll r \ll L_0, L_{\mathrm{f}}$$

diverge as r/L_{f} is made small (since $\zeta_{2N} < N\zeta_2$), whereas they assume constant values $(2N)!/2^N N!$ for Gaussian random fields. The physical mechanism generally believed to underlie this small-scale intermittency in both the velocity and passive scalar fields is a spatially nonuniform transfer of energy or passive scalar variance from large to small scales, producing intricately interlaced regions

of strong and weak turbulent dissipation. A variety of phenomenological cascade models encoding variations of this notion have been proposed to predict the manner in which ζ_N should vary as a function of the order of the moment N; see the references in [309]. None of these models is, however, directly connected to the Navier–Stokes equations or advection–diffusion equation. Indeed, it is still unknown how to derive analytically the inertial-convective scaling laws for the second-order structure function of the passive scalar and velocity fields from the primitive equations, and the higher-order statistics provide an even greater challenge.

The fact that the RDT Model permits closed PDEs to be written for passive scalar correlation functions to all order, however, gives hope that perhaps anomalous inertial-range scaling could be mathematically derived from the basic equations in this model. The second-order structure function can be written as an explicit quadrature using Eq. (284) and the simple relation

$$S_2^*(r) = 2(P_2^*(0) - P_2^*(r))$$

obtained by binomial expansion of the definition of Eq. (293). A direct asymptotic analysis [183] produces the rigorous inertial-convective range scaling formula:

$$S_2^*(r) \sim \frac{2}{d(2 - 2H)}\bar{\chi}(D_L^I)^{-1}r^{2-2H} \quad \text{for } L_d, L_K \ll r \ll L_0, L_f , \tag{296}$$

which is completely self-similar because it only involves the obviously relevant parameters $\bar{\chi}$, D_L^I, and r (see Paragraph 4.3.3.3). The challenge raised in [183,206] is to compute the higher-order structure functions from the basic RDT model equations and to unambiguously demonstrate an anomalous scaling formula such as

$$S_{2N}^*(r) \sim C_{2N}\bar{\chi}^N(D_L^I)^{-N}r^{N(2-2H)}\left(\frac{r}{L}\right)^{\zeta_{2N}-N(2-2H)}$$

$$= C_{2N}\bar{\chi}^N(D_L^I)^{-N}L^{N(2-2H)-\zeta_{2N}}r^{\zeta_{2N}} \quad \text{for } L_d, L_K \ll r \ll L_0, L_f , \tag{297}$$

where the length scale L appearing in the anomalous correction is to be identified and C_N is a universal sequence of constants. Of course, the truth could be even more complicated than Eq. (297) through, say, the anomalous appearance of multiple length scales, a nonuniversal dependence of C_N on details of the pumping, or a dependence of $S_N^*(r)$ on r/L which does not reduce to a power law in the inertial-convective range. The problem of anomalous scaling in the RDT model has been since attacked through a wide variety of means, some of which we will briefly summarize in Sections 4.4.2 and 4.4.3. There is some controversy regarding these computations, since different groups proceeding from different assumptions predict conflicting values of the anomalous scaling exponents. A clearcut demonstration of anomalous scaling proceeding directly from the basic governing equations without additional assumptions has thus far only been accomplished in further simplified versions of the RDT Model. We briefly discuss this work in Section 4.4.5, after reporting the results of some numerical simulations in Section 4.4.4.

4.4.2. Exact equations for scalar structure functions in RDT model

We now describe three basic mathematically exact representations for the passive scalar structure functions $S_N^*(r)$ which have been used as the basis of quantitative investigations of anomalous scaling.

4.4.2.1. Representation through solution of the closed PDE. The first proceeds by expressing $S_N^*(r)$ via binomial expansion of Eq. (293) as a sum of Nth-order quasi-equilibrium PS correlation functions

$$P_N^*(\{x^{(j)}\}) \equiv \left\langle \prod_{j=1}^{N} T(x^{(j)}, t) \right\rangle_* ,$$

with spatial arguments $\{x^{(j)}\}_{j=1}^{N}$ evaluated at either x or $x + r$. These quasi-equilibrium PS correlation functions in turn obey a recursively solvable, linear system of elliptic PDEs:

$$M_N P_N^*(x^{(1)}, \ldots, x^{(N)}) = - \sum_{1 \le m < n \le N} \Phi((x^{(m)} - x^{(n)})/L_f) P_{N-2}^*(\{x^{(j)}\}_{j \ne m,n}) , \qquad (298)$$

where $P_0^* \equiv 1$, $P_{-1}^* = 0$ and the elliptic operators M_N have the form

$$M_N \equiv \kappa \sum_{j=1}^{N} \Delta_j - \sum_{1 \le j < j' \le N} \nabla_j \cdot (\mathscr{D}_s(x^{(j)} - x^{(j')}p) \cdot \nabla_{j'}) . \qquad (299)$$

The subscripts on the differential operators indicate the label of the observation point $x^{(j)}$ on which they act. The velocity structure tensor $\mathscr{D}_s(r)$ was defined in Eq. (257), and we assume it to have the same wide inertial-range structure as defined in Paragraph 4.2.2.1. The PDE (298) is accompanied by some large-scale boundary condition or decay condition to render the problem well-posed. Of course, we really want to identify P_N^* with the long-time asymptotic solution of the evolution equation obtained by adding a $\partial/\partial t$ operator to the left-hand side of Eq. (298). Various mathematical [185,206,208,244,246,349] and formal [95,117,164,198,295] derivations of Eq. (298) and special cases thereof have been offered.

Though the equations are explicit, this description of the PS structure functions involves a number of subtleties and technical difficulties in any practical computation with $N > 2$. First of all, the fundamental PDE (298) is of very high dimension. The symmetries implied by the statistical homogeneity and isotropy of all the random fields help only somewhat [64]. The structure of the differential operator M_N also poses analytical difficulties; the components of the variable coefficient tensor $\mathscr{D}_s(x^{(j)} - x^{(j')})$ vary from zero when the observation points coincide ($x^{(j)} = x^{(j')}$) to large quantities of order $D_L^I L_0^{2H}$ when the observations points are well separated ($|x^{(j)} - x^{(j')}| \gtrsim L_0$). The expression of the structure function in terms of the correlation function has the unfortunate feature of weights of mixed sign; for example,

$$S_4^*(r) = 2P_4^*(x,x,x,x) - 8P_4^*(x+r,x,x,x) + 6P_4^*(x+r,x+r,x,x) . \qquad (300)$$

This means that one must be cautious about assuming that dominant contributions to P_N^* are dominant contributions to the structure function $S_N^*(r)$; there are cancellations possible. Deducing the inertial-convective asymptotics of $S_N^*(r)$ also involves some technical delicacy. Because we are concerned with $r \gg L_d$, one may wish to remove molecular diffusion from consideration, but note that the structure function involves evaluation of the multipoint correlation functions P_N^* in regions where points coalesce and the molecular diffusion operators dominate some of the turbulent diffusion operators. It has been rigorously shown [92,93] that Eq. (298) does have a $\kappa \to 0$ limit which behaves regularly in the space of mean-square integrable functions (L^2). Since the structure function involves evaluation of P_N^* at special points, however, this regularity result does not rule out

singular or subtle behavior of $S_N^*(r)$ in the $\kappa \to 0$ limit. To our knowledge, there are not any other rigorous results concerning the properties of solutions to the PDE (298).

4.4.2.2. Single radial variable representation. Since $S_N^*(r)$ is a function of a single variable, it is natural to want to work with equations of one variable rather than the delicate many-dimensional PDEs described above. This is in fact the approach adopted in Kraichnan's paper [183], in which he deduces a relatively simple equation for $S_{2N}^*(r)$:

$$\frac{1}{r^{d-1}}\frac{\mathrm{d}}{\mathrm{d}r}\left(r^{d-1}D_{\|}(r)\frac{\mathrm{d}S_{2N}^*(r)}{\mathrm{d}r}\right) = \kappa J_{2N}(r) \,, \tag{301a}$$

where

$$J_{2N}(r) \equiv 2N\langle(\delta T(\boldsymbol{r}))^{2N-1}H(\delta T(\boldsymbol{r}))\rangle \,. \tag{301b}$$

In this last expression,

$$\delta T(\boldsymbol{r}) \equiv T(\boldsymbol{x} + \boldsymbol{r}) - T(\boldsymbol{x})$$

(for any choice of $\boldsymbol{x}$, by spatial homogeneity), and

$$H(\delta T(\boldsymbol{r})) \equiv 2\langle \varDelta_r(\delta T(\boldsymbol{r}))|\delta T(\boldsymbol{r})\rangle \tag{301c}$$

is defined as the expected value of $2\varDelta_r(\delta T(\boldsymbol{r}))$, conditioned upon a given value of the scalar increment $\delta T(\boldsymbol{r})$. (The function $H(\delta T(\boldsymbol{r}))$ is akin to, but more complicated than, the *conditional dissipation rate* [268] which will be discussed in Paragraph 5.4.1.1.) The differential equation (301) for the structure function can be deduced from Eq. (298), but a more direct route proceeds through the Fokker–Planck equation for the probability density function (PDF) for the passive scalar increment $\delta T(\boldsymbol{r})$ [184]. The main drawback to the one-dimensional representation (301) of the structure functions is that it is not fully closed; $J_{2N}(r)$ cannot be expressed in terms of $S_{2N}^*(r)$ in any known exact way.

4.4.2.3. Representation through Lagrangian trajectories. Finally, the passive scalar structure functions $S_{2N}^*(r)$ may be expressed in terms of the statistical trajectories of $2N$ tracers initially distributed at two points separated by a distance r. Indeed, for any velocity field model, the passive scalar correlation function $P_N(\{\boldsymbol{x}^{(j)}\}, t)$ of any order N may be precisely related to the joint statistics of the Lagrangian trajectories of N tracers starting from $\{\boldsymbol{x}^{(j)}\}_{j=1}^N$ and moving simultaneously through the random flow [36,62,115,185]. The simplification afforded by the RDT model is that the tracer trajectories obey (coupled) stochastic differential equations with deterministic coefficients [108,185]. The advantage to this Lagrangian approach is that one must analyze a finite system of stochastic ordinary differential equations rather than a PDE. On the other hand, one must explicitly deal with random processes and study the parametric dependence of the tracer trajectory statistics on the initial separation distance r. Some authors [23,62] set up their Lagrangian framework in terms of functional integrals instead of stochastic differential equations.

4.4.3. Calculation of anomalous scaling exponents in RDT model

A large number of theoretical approaches, based on additional assumptions or formal approximations, have been proposed which permit a tractable computation yielding quantitative

predictions for the anomalous scaling exponents of the PS structure functions in the RDT model. Unfortunately, the results produced from some of the approximate methods disagree with one another. We shall now briefly summarize some of the main lines of this theoretical research.

4.4.3.1. Closure by linear ansatz for $H(\delta T(\mathbf{r}))$. Kraichnan [183] put forth a simple closure proposal for Eq. (301) which is equivalent [184] to assuming that $H(\delta T(\mathbf{r}))$ is a linear function of $\delta T(\mathbf{r})$ (multiplied by a uniquely determined function of r). This implies that $J_{2N}(r)$ is proportional to $NS_{2N}^*(r)$ times a function of r which is independent of N. If $S_{2N}^*(r)$ has an inertial-convective scaling law of the form (297), it then follows that the scaling exponents must satisfy the following anomalous law:

$$\zeta_{2N} = \frac{1}{2}\sqrt{4Nd\zeta_2 + (d - \zeta_2)^2} - \frac{1}{2}(d - \zeta_2) \ . \tag{302}$$

Note that the exponent ζ_{2N} is proportional to $\sqrt{N}$ for large N, rather than a linear function of N as in the case of normal scaling. Fairhall et al. [95] supported Kraichnan's closure hypothesis through the formal derivation of "fusion rules" [202] for how a scaling exponent characterizing the inertial-convective range scaling properties of the multipoint correlation function $P_{2N}^*(\{\mathbf{x}^{(j)}\})$ is related to its local behavior when two or more of the spatial arguments are made to coalesce. These authors also argued that $L = L_f$ was the only length scale which could self-consistently enter the anomalous scaling formula (297). Other analytical support for the anomalous scaling law (302), proceeding from deeper assumptions about nice behavior of certain statistical functions, was given in [184].

4.4.3.2. Perturbative analyses. A series of later works by various groups attacked the computation of the scaling exponents through various perturbation expansions in the PDE (298). Leading order anomalous deviations of the exponents ζ_{2N} from normal scaling were calculated in the asymptotic limits of small Hurst exponent [35,116,275] $H \to 0$, large dimensionality [63,64] $d \to \infty$, and large Hurst exponent [278] $H \to 2$. We note that the large d expansion is motivated by the representation of the differential operator M_N for large d in terms of $N(N - 1)/2$ distances between its various arguments, which takes the form of a sum of a relatively simple differential operator of order d^2 and a more complicated differential operator of order d. A common theme of these perturbative calculations is that they seek "zero-mode" solutions $Z_N(\{\mathbf{x}^{(j)}\})$ of M_N, by which is meant that $M_N Z_N$ approximately vanishes when the observation points $\{\mathbf{x}^{(j)}\}_{j=1}^N$ all have separations within the inertial-convective range of scales, and is some unspecified but regular function otherwise. The idea is that a particular solution with normal scaling can be subtracted from P_N^* to cancel (to leading order) the inhomogeneity on the right-hand side of Eq. (298) when the separations between the observation points all fall within the inertial-convective range. Each zero mode for a given order N is then assumed to have inertial-range scaling characterized by a single exponent, which is computed by perturbation about some limit in which the homogenous solutions of M_N can be explicitly constructed. An argument based on either crude matching or continuity with the unperturbed limit [64,116] is then made to show that a certain zero mode provides the dominant contribution to the structure function S_N^* and determines its inertial-convective scaling exponent ζ_N. The general conclusion is that there is anomalous scaling for the passive scalar structure

function of the form (297), with the length scale $L = L_f$. The Kolmogorov dissipation length L_K is set equal to zero from the start in all these works, and anomalies with respect to the scalar dissipation length scale L_d are thought not to occur based on rough matching arguments to small scales indicating sufficiently regular behavior of P_N^* as L_d is made small relative to the largest separation between the observation points, even when some points coalesce [64]. The results from the perturbation theories are mutually consistent with each other in their domains of overlap, but contradict the law (302) for the scaling exponents deduced from the hypothesis of the linearity of $H(\delta r)$.

These perturbation theory analyses of zero modes have recently been interpreted in terms of the statistics of Lagrangian tracer trajectories by Bernard et al. [36] as well as Gat and Zeitak [115]. The zero modes are associated to statistical "shape" configurations of a finite number of Lagrangian tracers which relax slowly in time to their asymptotic shapes [36,115]. A large dimension $d \to \infty$ perturbation analysis carried out directly on the stochastic equations of motion for the Lagrangian tracers [115] recovers the same results as the $d \to \infty$ perturbation theory based on zero modes of the PDE's for the PS correlation functions [63,64].

We finally mention a perturbative approach for $H \to 0$ pursued within a renormalization group framework by Adzhemyan et al. [2], which recovers the results of the anomalous scaling predictions from the perturbative zero mode analyses in [35,116,275].

4.4.3.3. Theories predicting constant asymptote of anomalous scaling exponent. A distinct theory, motivated by studiesof the randomly driven Burgers equation [267], has been offered by Yakhot [343]. This work puts forth an approximate closure for the Fokker–Planck PDE for the probability density function (PDF) for the scalar increment $\delta T(r)$, and seeks a solution for this PDF with a scale-invariant form over the region

$$L_d, L_K \ll |r| \ll L_0, \qquad |\delta T(r)| \ll \langle T^2(x) \rangle^{1/2} .$$

The resulting prediction is that the passive scalar structure functions $S_{2N}^*(r)$ exhibit normal scaling ($\zeta_{2N} = N\zeta_2$) up to some value N_c, after which the scaling exponents remain approximately constant, asymptoting to a finite value $\lim_{N \to \infty} \zeta_{2N} = \zeta_\infty$. This prediction does not agree with either Eq. (302) or the results of the perturbation theories. The discrepancy with the latter is attributed in [343] to assumptions in that work which are not uniformly valid over all H and d and which require modification in the asymptotic regimes considered by the perturbation theories.

The conclusion in [343] that the structure function scaling exponents ζ_{2N} should asymptote to a constant for large N is supported for $\frac{1}{2} < H < 1$ by asymptotic "instanton" calculations of Chertkov [62] and Balkovsky and Lebedev [23], though all three papers disagree as to the value of this constant and other quantitative details. The instanton procedure, put forth in a general turbulence context in [96], seeks to describe the tails of the PDF (and thereby the high-order moments) of statistical quantities such as $\delta T(r)$ through a functional path-integral formalism inspired by the mathematical theory of quantum mechanics. A similar quantum mechanical analogy had previously been exploited by the first author in [206] to analyze higher-order passive scalar correlation functions in a random shear flow. The high-order moments in the instanton formalism are governed by a sort of semi-classical limit in which the dominant contributions to the functional integral are determined by saddle points in function space of a certain action functional $I(\delta T)$. These saddle points correspond in the quantum mechanical analogy to classical trajectories and are sometimes referred to as instantons; in turbulence applications, the instantons represent

certain motions of Lagrangian fluid elements. The identification of the instanton formally indicates the physical process responsible for the shape of the tails of the PDF of $\delta T(r)$ and the intermittency in structure functions of very large order. Completely different physical processes, however, may play the dominant role in producing intermittency of passive scalar structure functions of accessibly low order [61]. The saddle-point equations are generally much too difficult to solve in general, and one typically proceeds by constructing special approximate instanton solutions, arguing by some auxiliary means which of these should be the dominant contribution, and assessing whether fluctuations about the instanton solutions are relevant [62,96]. Another approach is to seek to solve the instanton equations in some perturbative limit, such as large dimension $d \to \infty$ [23].

4.4.3.4. Discussion of approximate theoretical approaches. All of the above analytical arguments for anomalous scaling of the passive scalar structure functions involve a number of assumptions of varying degrees of plausibility which are difficult to verify with full confidence. Anomalous scaling is an inherently subtle subject, and may well involve the violation of certain "reasonable" beliefs. Indeed, some of the above theories produce conflicting predictions for the anomalous scaling exponents, and it is still unclear which of the theories' plausible assumptions fail and why. Some possibilities are suggested in [114]. The situation would clearly be clarified by some unambiguous results involving no assumptions subject to dispute.

4.4.4. Empirical assessment of theoretical predictions concerning anomalous scaling

The usual means of testing physical theories are difficult to apply to the issue of anomalous scaling in the RDT model. As we have indicated in Paragraph 4.4.2.1, the fundamental equations (298) for the high-order passive scalar correlation functions in the RDT model are very difficult to quantitatively analyze in a mathematically rigorous fashion, and we are not aware of any such work which bears directly on the anomalous scaling of the scalar structure functions $S_N^*(r)$. Comparison with experiments is not really feasible, since the RDT model velocity field has unphysical temporal correlations, though we note that Ching et al. [69,70] found some support for the hypothesis [95,183,184] that $H(\delta T(r))$ is a linear function of $\delta T(r)$ in a real turbulent wake. An accurate numerical solution of the closed PDEs (298) for $N > 2$ is too expensive for modern machines both due to the high-dimensionality and the wide range of scales which must be resolved. (Gat et al. [114] and Pumir [276] solve numerically for the scaling exponent characterizing the zero modes of Eq. (298) for $N = 3$, and find good agreement with the $H \to 0$ and $H \to 1$ perturbation theories. While this work is instructive, it still involves the introduction of additional assumptions and does not *directly* compute the PS structure functions.)

Direct numerical simulation (DNS) of the passive scalar advection–diffusion equation with a rapidly decorrelating velocity field is difficult even in $d = 2$ dimensions due to the need to handle the rapid temporal fluctuations, resolve a wide range of spatial scales, and to collect statistics with sufficient quality to compute the higher order scalar structure functions $S_N^*(r)$ accurately as r varies throughout the wide inertial-convective range [61,340,334]. Some DNS studies have been conducted by Kraichnan et al. [61,184] and Fairhall et al. [94], in which a two-dimensional velocity field is constructed by rapidly sweeping a superposition of two *steady* random velocity fields past each other. The spatial structure of the steady component fields is generated by a hierarchical version of the Fourier method which is discussed in Section 6.2.2. The DNS studies [61,94,184] show

qualitative agreement with the predictions of Kraichnan's linear closure ansatz for structure functions up through order 10 and Hurst exponents ranging from 0.3 to 0.75, but there are some statistically significant quantitative discrepancies. The function $H(\delta T(r))$ obtained from this data is indeed approximately linear for $|\delta T(r)| \gtrsim (S_2^*(r))^{1/2}$, but manifests a noticable bump for $|\delta T(r)| \lesssim (S_2^*(r))^{1/2}$ [184]. This particular finding is in qualitative agreement with one prediction of Yakhot's anomalous scaling theory [343], and could indicate a possible departure from the more general fusion rules formulated for the RDT model [95,202] as well as Kraichnan's linear closure hypothesis. The scaling exponents, even of the fourth-order structure function, are shown in [61] to be very sensitive to slight changes in $H(\delta T(r))$ from a linear form. Unfortunately, some of the asymptotic regimes studied by perturbation theories are not amenable to DNS studies: the $d \to \infty$ and $N \to \infty$ limits are inaccessible for obvious reasons [61], and the quality of scaling within the inertial-convective range is seriously degraded as $H \to 0$ because the diffusion length L_d invades the inertial range [33,340].

A more efficient means of numerically computing the passive scalar structure functions in the RDT model, realized and developed by Frisch et al. [108] (and independently proposed in [115]), is the Monte Carlo numerical simulation of the tracer trajectories (see Section 6). The passive scalar structure functions $S_{2N}^*(r)$ can be numerically computed at any value r by a Monte Carlo simulation of $2N$ particles, starting from $N + 1$ different initial clusterings at two locations separated by a distance r. The computational advantage of this trajectory-based approach is that one need only track a finite system of stochastic differential equations with deterministic coefficients rather than resolve a PDE on a full spatial grid. One ostensible drawback is the need to repeat the simulations to compute $S_{2N}^*(r)$ for each new value of r. Frisch et al. [108] however circumvent this expense by noting that the inertial-convective scaling exponent ζ_{2N} of the structure function (297) can be obtained by observing the scaling with respect to the length scale L breaking complete self-similarity, which is widely believed to be the pumping length scale L_f. The other main concern, in common all Monte Carlo simulations, is the need to simulate a large number of independent realizations so that good statistics can be obtained [115]. The fourth-order structure function was computed in [108] by simulating millions of tracer trajectories in $d = 3$ dimensions, with the Hurst exponent of the velocity field ranging from $H = 0.1$ up to values very near $H = 1$. The method was validated by comparison of the simulated second-order structure function against the exactly known result (see Section 4.3.2). The numerically computed scaling exponents of the fourth order structure function depart strongly from the prediction (302) of Kraichnan's linear closure ansatz. (The disagreement is not as bad for values $H \approx 1$ which were previously computed by direct numerical simulations of the advection–diffusion equation [94,184].) The numerical result from Monte Carlo simulations for the fourth-order structure function with $H = 0.1$ is roughly consistent with the prediction of the $H \to 0$ theory, but this limit could not be resolved numerically.

4.4.5. Anomalous scaling in further simplified versions of RDT model

In an effort to obtain clear and unambiguous results regarding several controversial issues regarding anomalous scaling in the RDT model, some researchers have studied related models which are simpler to analyze. Vergassola and Mazzino [334] realized that a one-dimensional version of the RDT model could be sensibly formulated, provided that the incompressibility condition on the velocity field is removed. The velocity field is chosen to be delta-correlated in time with an inertial-scaling range just like the RDT shear flow in Section 4.1.4, except that the velocity

is directed along the x-axis rather than transverse to it. One may worry that the removal of incompressibility may fundamentally change the character of the model, but the rapid fluctuations of the velocity field help to mitigate compressibility effects. Indeed, it may be shown by a quadrature computation that the second-order passive scalar structure function $S_2^*(r)$ scales in the 1-D RDT model as r^{2-2H} in the inertial-convective range of scales, just as in the incompressible RDT model. The one-dimensional advection–diffusion equation with a rapidly decorrelating velocity field was numerically simulated by [334] for $H = \frac{1}{2}$ using a pseudo-spectral code, producing clean scaling behavior for $S_2^*(r)$, $S_4^*(r)$, and $S_6^*(r)$ over one to two decades of scales. The scaling exponents obtained from the slope of log-log plots exhibited anomaly ($\zeta_{2N} \neq N\zeta_2$). The values of these scaling exponents were found moreover to agree well at $H = \frac{1}{2}$ with a Padé approximation constructed from the small Hurst exponent expansion technique in [35,116] adapted to the 1-D compressible analogue of Eq. (298).

Vergassola [333] also considered an RDT model version of the kinematic dynamo equations for the magnetic field, and showed that the second-order structure function in this model already possesses an anomalous scaling exponent ζ_2 in the sense that it is not related to H by standard dimensional analysis considerations (as it is in Eq. (296)). He derived an exact expression ζ_2 as a function of H, and showed that it was consistent in the $H \to 0$ limit with a prediction based on a small Hurst exponent expansion [35,116] for the scaling exponent of the zero modes of a closed equation for the correlation function analogous to Eq. (298). These results provide some support for the anomalous scaling predictions based on expansions of the Hurst exponent [35,116,278], but the reason for the disagreement with the competing theory [95,183,184] based on the linearity of $H(\delta T(\mathbf{r}))$ remains to be clarified [114].

We finally make mention of an RDT "shell model" of Benzi et al. [33,340] in which Fourier space is discretized into geometrically distributed shells, and the nonlinear advective interaction between velocity and passive scalar Fourier shell modes is truncated to nearest neighbors. The Fourier components of the passive scalar correlation functions then satisfy band-diagonal systems of ordinary differential equations with respect to time. The equations for the second- and fourth-order correlation functions can be solved numerically, with the result that the second order structure function $S_2^*(r)$ scales normally in the inertial-convective range with exponent $\zeta_2 = 2 - H$ whereas the fourth order structure function $S_4^*(r)$ scales anomalously [340]. Direct Monte Carlo simulations of the advection–diffusion equations in the RDT shell model confirm these conclusions [340]. Stability analysis of the equations for the PS correlation functions shows that the effects of molecular diffusion and large-scale pumping have negligible effects in the RDT shell model on the scaling properties of the passive scalar correlation function deep within the inertial-convective range [33]. This is in agreement with the conventional wisdom for the continuous RDT model [64,95]. However, the insensitivity to molecular diffusion in the RDT shell model is not uniform in the $H \to 0$ limit, because the scalar dissipation length scale L_d strongly invades the inertial range [33].

4.4.6. Other applications of RDT model to higher-order scalar statistics

The simplification of the temporal structure in the RDT model permit a number of other issues concerning the small-scale structure of the passive scalar field to be examined quantitatively. We refer the reader to the papers [164,292,295] wherein statistical properties of the gradient and level set contours of the passive scalar field are studied in an RDT velocity field without an inertial range.

5. Elementary models for scalar intermittency

Small-scale intermittency, of the type just discussed in Section 4.4, has been a recognized feature of turbulence since 1962, when Kolmogorov [170] and Obukhov [255] modified the original 1941 turbulence theory to account for its effects. The small-scale intermittency in both the velocity and advected scalar fields in a turbulent flow is typically associated with the patchiness and irregularity of regions of strong vorticity and scalar gradients [72,309]. Statistics which involve evaluation of the turbulent field at two closely spaced points are sensitive to small-scale intermittency, and can exhibit anomalous scaling with respect to Reynolds number or separation distance between the observation points.

Single-point recordings, on the other hand, measure the total fluctuation coming from all scales, and are dominated by contributions from the large scale fluctuations because they have the larger amplitude. They are therefore insensitive to small-scale intermittency. It was long thought that, at sufficiently high Reynolds number, the single-point measurements of the velocity field and of the passive scalar field in homogenous turbulence ought to exhibit the Gaussian statistics typical of noisy processes with many degrees of freedom. Indeed, nearly Gaussian behavior for these quantities was observed in several experiments [106,311,316,324,326] dating back to 1947.

An intriguing development came in the late 1980s with the report that single-point temperature measurements in a Rayleigh–Benard convection cell experiment at the University of Chicago exhibited large fluctuations with greater frequency than what would arise from a Gaussian distribution [55,135]. More precisely, the single-point *probability density function* (PDF) $p_T(\rho)$ for the temperature T, defined by

$$\text{Prob}\{a < T < b\} = \int_a^b p_T(\rho)\,\mathrm{d}\rho$$

was found to decay only exponentially $\sim C_1 e^{-C_2|\rho|}$ for large values of ρ, and not like a Gaussian $\sim C_1 e^{-C_2\rho^2}$. Broad tails in the single-point PDF indicate unusual activity occurring at the large scales, such as large random coherent structures amidst the turbulent "noise". This property of large fluctuations in the single-point statistics of a turbulent flow occurring with a significantly super-Gaussian probability is therefore often referred to as *large-scale intermittency*. To understand how this might come about, recall that in a Rayleigh–Benard convection cell, the lower face of a cube of fluid is maintained at a temperature hotter than that of the upper face, while the side walls are insulated. When the applied temperature differential is significantly strong, the temperature profile becomes unstable to a large-scale convection rolling pattern, with hot fluid rising on one side of the cell and cold fluid descending on the other [293]. Superposed on this mean circulation are turbulent fluctuations, and one may envision the large-scale intermittency of the measured temperature as coming from the occasional passage of ascending (descending) plumes of hot (cold) fluid past the probe [135]. Another striking feature about the temperature PDF measured in this experiment beyond its exponential tails is its universality with respect to Rayleigh number (a nondimensionalized measure of the vigor of buoyant convection relative to dissipative processes).

These findings stimulated theoretical inquiry into whether the departure of the temperature from Gaussian behavior was due to the complex flow and velocity–temperature interactions in the

convection cell, or whether it might arise more generally. Pumir et al. [277] analyzed a phenomenological turbulent mixing model, and predicted that exponential tails should be observed in the PDF of a *passive* scalar advected by a moderate Reynolds number flow when a constant mean scalar gradient is imposed by the boundary conditions. That is, neither buoyancy nor a wide inertial range ought to be necessary for the appearance of large-scale scalar intermittency. Sinai and Yakhot [298] considered the general evolution of a freely decaying passive scalar in a statistically stationary velocity field (with no mean scalar gradient imposed). Through a closure approximation, they predicted that the scalar PDF would develop broad, *algebraic tails* ($p_T(\rho) \sim C_1 \rho^{-\beta}$ for large ρ) in the long time limit.

These theoretical developments in turn prompted experimental investigation of the statistics of temperature fluctuations small enough in magnitude to be considered passive. Gollub and coworkers [127,191] conducted an experiment directly suggested in [277]. A weak temperature differential was applied to opposite sides of a desktop cell in which the fluid was stirred by a oscillating grid. For Reynolds numbers $\sim 10^3$, the temperature displays broad exponential tails in its PDF, while the turbulent velocity field has a short inertial range and a Gaussian PDF. Meanwhile, Jayesh and Warhaft [146,147] studied the PDF of the temperature and velocity in a wind tunnel with grid-generated turbulence. A mean temperature gradient is impressed on the flow only at the inlet, and the velocity and temperature fluctuations decay freely in the tunnel. Despite the differences from the setup of Gollub et al., similar results were found: at comparable Reynolds number, the velocity PDF quickly relaxes to a Gaussian form, while the temperature PDF exhibits broad exponential tails far downstream of the grid. The temperature PDF in both experiments, however, reverts to a Gaussian form if the Reynolds number does not exceed some moderate value. Jayesh and Warhaft also observed Gaussian behavior for the temperature when a mean temperature gradient is *not* impressed on the flow.

Large eddy [237,238] and direct numerical simulations [91,111,153,155], which were pursued even earlier and in a different spirit than the above-mentioned laboratory experiments, also indicate a similar variety of both Gaussian and non-Gaussian behavior for turbulently advected active and passive scalars. We shall quickly review some of the main results from physical and numerical experiments in Section 5.1.

In order to investigate some of the issues regarding large-scale passive scalar intermittency raised by the above-mentioned laboratory and numerical experiments, the first author designed a turbulent diffusion model for which the single-point passive scalar PDF could be computed exactly [207]. The velocity field in this *Random Uniform Jet* model was taken as a superposition of two parallel uniform shear flows, one with deterministic variation in time modelling a mean flow, and the other with random and rapid fluctuations modelling the effects of moderate Reynolds number turbulence. Beyond the specification of the form of the velocity field, no further assumptions are introduced; the advection–diffusion equation can be analyzed in its exact form. Though the model velocity field is relatively simple, the single-point statistics of the advected passive scalar field display a rich behavior. For example, the scalar PDF approaches a Gaussian or non-Gaussian form at long times, depending on the dynamics of the mean shear flow. The long-time limiting shape of the scalar PDF is universal in a restricted sense: it depends on three parameters involving only the large-scale features of the initial data and one parameter involving both the flow parameters and the large-scale features of initial data. We will present the Random Uniform Jet model in Section 5.2, and point to some qualitative connections between its findings and the results

of numerical and laboratory experiments. This discussion draws from the original paper [207] and subsequent elaborations by McLaughlin and the first author [233] and by Resnick [282].

Further issues concerning passive scalar intermittency were studied by Bronski and McLaughlin [51] in a variation of the Random Uniform Jet model in which the random shear flow is taken to be periodic, rather than uniform, in space. While this *Random, Spatially Periodic Shear* model is not exactly solvable in the same sense as the original Random Uniform Jet model, the passive scalar PDF can still be analyzed in the long-time limit through precise asymptotic expansions. The results of these direct computations can be compared with the predictions of homogenization theory (see Section 2), which applies rigorously in a certain long-time asymptotic limit in which the initial data is simultaneously rescaled to larger scales. As we shall discuss in Section 5.3, the scalar PDF in the Random, Spatially Periodic Shear model displays substantial qualitative differences from the homogenized description when evaluated at large but finite times with the initial data varying on a large but *fixed* length scale [51]. This is the appropriate limit procedure for studying the long-time characteristics of a particular system, and its departures from homogenization theory indicate some subtleties about the nature of the limit process involved in the latter.

We conclude in Section 5.4 with a brief discussion of some other recent theoretical studies which shed light on other aspects of large-scale passive scalar intermittency beyond those present in the exactly solvable simple models described above. Most of this work is based upon phenomenological or formal approximations, in contrast to the exact analysis of the basic advection–diffusion equation presented in Sections 5.2 and 5.3.

5.1. Empirical observations

As we have mentioned in the introduction, the PDF of a turbulently advected scalar has been empirically found to have exponential tails in some circumstances and to be Gaussian in others. It would be interesting to establish criteria classifying the ingredients and parameter ranges associated with large-scale scalar intermittency, but much more investigation appears necessary. (See [147] for the suggestion of such a criterion, which however does not appear to explain the results of [238] and [316].) The physical experiments and direct and large eddy numerical simulations do at least suggest, though, that the shape of the scalar PDF depends on the following features and parameters:

1. whether the turbulence is driven or freely decaying [153,238],
2. whether buoyancy effects are important [55,135,155,238],
3. the presence of a mean scalar gradient [147],
4. the presence of a mean shear flow (compare [147,316]),
5. Reynolds number [147,191],
6. the relative magnitude of the integral length scale of the velocity field and the correlation length of the passive scalar field [191,311],
7. the time at which the scalar is measured when it is freely decaying.

With regard to the last point, the scalar PDF in some freely decaying turbulent systems exhibits strong skewness [311] or broad tails [91] for a while, but slowly relaxes to a Gaussian distribution after a long time.

We are not aware of any positive experimental results concerning the universality of the scalar PDF other than those reported in the Chicago convection experiments [55], but there does not seem to have been much systematic investigation in this direction.

5.2. An exactly solvable model displaying scalar intermittency

We shall now introduce a simplified turbulent diffusion model in which the scalar PDF can be exactly analyzed without the need for any further ad hoc approximations or assumptions. Within the model, we will be able to characterize precisely the conditions under which the scalar PDF displays Gaussian or non-Gaussian features, and touch on the issues 4, 6 and 7 listed in Section 5.1. We can also describe the extent to which the limiting shape of the PDF in the long-time limit is universal.

5.2.1. Random uniform jetmodel

For our mathematical investigation of passive scalar intermittency, we consider velocity field models from a class of three-dimensional jet flows:

$$
\boldsymbol{v}(\boldsymbol{x}, t) = \boldsymbol{v}(x, y, z, t) = \begin{bmatrix} 0 \\ \gamma_{\mathrm{m}}(t)z + \gamma_{\mathrm{r}}(t)V_{\mathrm{r}}(x) \\ 0 \end{bmatrix}. \tag{303}
$$

Here, $V_{\mathrm{r}}(x)$ is a deterministic spatial profile, $\gamma_{\mathrm{m}}(t)$ is a deterministic function of time, and $\gamma_{\mathrm{r}}(t)$ is a stationary, Gaussian random function of time with mean zero and correlation function:

$$
\langle \gamma_{\mathrm{r}}(t)\gamma_{\mathrm{r}}(t + \tau) \rangle = R(\tau) \, .
$$

The velocity field is directed only in the single direction y, and is composed of a deterministic shear flow $\gamma_{\mathrm{m}}(t)z$ and a random shear flow $\gamma_{\mathrm{r}}(t)V_{\mathrm{r}}(x)$ varying in transverse directions. The deterministic component $\gamma_{\mathrm{m}}(t)z$ is supposed to model a mean shearing motion which responds to some regular, external forcing. The random component $V_{\mathrm{r}}(x)\gamma_{\mathrm{r}}(t)$ represents a *spatially coherent* motion with random temporal fluctuations, qualitatively modelling an excited instability in the fluid flow. The class of models (303) thereby mimics some features of a flow with a moderate Reynolds number not far above the onset of the turbulent activity. To model a high-Reynolds number jet flow, we could superpose a further shear velocity field with random spatio-temporal fluctuations over a wide inertial range of scales (as in Section 3). The empirical evidence suggests, however, that the issue of passive scalar intermittency is already interesting for moderate Reynolds number flows [147,191].

We will consider the evolution of passive scalar initial data of the form

$$
T_0(x, y, z) = \bar{T}_0(x, y) + \tilde{T}_0(x, y) \, ,
$$

where $\bar{T}_0(x, y)$ is a deterministic mean profile and $\tilde{T}_0(x, y)$ is a mean zero, homogenous, Gaussian random field of fluctuations about this profile, with correlation function

$$
P_2^0(x, y) = \langle \tilde{T}_0(x', y')\tilde{T}_0(x' + x, y' + y) \rangle = \int_{\mathbb{R}^2} \mathrm{e}^{2\pi \mathrm{i}(\eta x + ky)} \hat{P}_2^0(\eta, k) \, \mathrm{d}\eta \, \mathrm{d}k \, . \tag{304}
$$

If the mean profile is nontrivial, it will be assumed to have a finite nonzero integral:

$$\bar{M}_0 = \int_{\mathbb{R}^2} \bar{T}_0(x, y)\, \mathrm{d}x\, \mathrm{d}y \neq 0 \ . \tag{305}$$

If random fluctuations are present in the initial data, their spectrum $\hat{P}_2^0(\eta, k)$ will be assumed to have the following low-wavenumber asymptotics:

$$\lim_{\eta \to 0, k \to 0} \hat{P}_2^0(\eta, k) \sim |k|^{-\alpha} \phi(\eta, k) \ , \tag{306}$$

where $\phi(\eta, k)$ is a smooth function with $\phi(0, 0)$ finite and positive. The restriction that the initial data vary only in the x and y directions eases the complexity of the formulas; all the qualitative features we shall discuss carry over to case in which the initial data also varies in the z direction [207,233].

We will presently consider a *uniform* profile for the random shear ($V_r(x) = x$), and prescribe the random temporal fluctuations $\gamma_r(t)$ to be either

- a *white noise process*, with correlation function

$$R(\tau) = A_0 \delta(\tau) \ , \tag{307}$$

  or

- a superposition of *Ornstein–Uhlenbeck processes*, with correlation function

$$R(\tau) = \sum_{j=1}^{M} A_j \mathrm{e}^{-\tau/\tau_j} \ . \tag{308}$$

The $\{\tau_j\}_{j=1}^N$ are the correlation time scales of the Ornstein–Uhlenbeck processes, while A_0 and $\{A_j\}_{j=1}^N$ determine the amplitude of the associated shear flows. The white noise process may be thought of as a certain rapid decorrelation limit of the Ornstein–Uhlenbeck process ($\tau_j \to \varepsilon\tau_j$ and $A_j \to \varepsilon^{-1}A_j$ with $\varepsilon \to 0$).

The passive scalar field will evolve freely in the statistically stationary turbulent velocity just defined, and no mean scalar gradient nor boundary conditions are imposed. The advection–diffusion model we have just defined will be called the *Random Uniform Jet* model:

$$\frac{\partial T(x, y, z, t)}{\partial t} + (\gamma_m(t)z + \gamma_r(t)x)\frac{\partial T(x, y, z, t)}{\partial y} = \kappa \Delta T(x, y, z, t) \ ,$$

$$T(x, y, z, t = 0) = \bar{T}_0(x, y) + \tilde{T}_0(x, y) \ . \tag{309}$$

The assumptions made concerning the spatial profile of the shear and the temporal dynamics permit the single-point statistics $\langle T^N(x, y, t) \rangle$ of the passive scalar field to be expressed by explicit quadrature formulas. Later, in Section 5.3, we shall consider a periodic spatial profile $V_r(x)$ for the random shear.

We present the large-scale scalar intermittency properties of the Random Uniform Jet model in Section 5.2.2 and qualitatively relate them to the empirical observations. The derivation of these results, in which the passive scalar correlation functions are represented through the solutions of

quantum-mechanical Schrödinger equations, will be sketched in Section 5.2.3. In the present case, these Schrödinger equations describe precisely the motion of a system of particles subject to a harmonic oscillator potential, and may be solved in fully explicit form through Mehler's formula [296]. This methodology was developed by the first author [207] and extended together with McLaughlin [233] for the white noise temporal structure of the random shear. Resnick [282] generalized the analysis to handle the Ornstein–Uhlenbeck temporal stucture.

5.2.2. Exact results for models and relation to physical themes

Despite the relative simplicity of the Random Uniform Jet model (309), the PDF $p_T^{(x,y,z,t)}(\cdot)$ for the single-point passive scalar statistics:

$$\text{Prob}\{a \le T(x, y, z, t) \le b\} = \int_a^b p_T^{(x, y, z, t)}(\rho)\, \mathrm{d}\rho$$

displays a variety of interesting features. First, the scalar PDF has a

- *broader-than-Gaussian distribution at all finite times* $0 < t < \infty$ and spatial locations, when the initial data is a mean zero, Gaussian, homogenous random field.

In the long-time limit, the scalar PDF will become concentrated at zero because of dissipative processes, but it will converge to a nontrivial *shape* (independent of spatial location (x, y, z)) which exhibits the following features:

- *broader-than-Gaussian tails* when the mean shear flow $\gamma_m(t)z$ is weak or absent,
- *a Gaussian distribution* when the mean shear flow $\gamma_m(t)z$ is sufficiently persistent,
- *dependence on the relative magnitude of initial velocity and passive scalar length scales* (as measured by the parameter α in Eq. (306)), with the PDF becoming more Gaussian as the long-range correlations in the initial data become stronger,
- *permanent skewness with memory* of the sign of the integral of the mean initial scalar profile, $\bar{M}_0$,
- *a phase transition with respect to the parameter* α when the initial data has both deterministic and random components,
- *dependence on molecular diffusivity* at the phase transition value $\alpha = 3/4$,
- *universality with respect to small-scale features of initial data*,
- *universality with respect to the random temporal correlation structure of the velocity field*, whether it be a white noise process or a superposition of Ornstein–Uhlenbeck processes.

The fact that our exactly solvable model produces scalar intermittency with this wide range of features makes it an attractive candidate for testing approximate closure schemes [269]. We shall now elaborate upon the above results for the model, and connect them with the experimental and numerical findings presented in Section 5.1.

5.2.2.1. Finite-time intermittency.
Suppose that the initial data is purely a mean zero, homogenous, Gaussian random field $T_0(x, y) = \tilde{T}_0(x, y)$. Then, when $\gamma_r(t)$ is white noise in time, one can show through explicit formulas that the scalar PDF $p_T^{(x,y,z,t)}(\cdot)$ is broader-than-Gaussian at all finite positive times [207]. That is, the flatness factor

$$F(x, y, z, t) \equiv \frac{\langle (T(x, y, z, t))^4 \rangle}{\langle (T(x, y, z, t))^2 \rangle^2}$$

strictly exceeds the Gaussian value of 3 for all $(x, y, z) \in \mathbb{R}^3$ and $0 < t < \infty$. A similar result can be rigorously deduced through the analysis of quantum mechanical analogies (see Section 5.2.3) when the shear flow profile $V_r(x)$ is periodic in space (Section 5.3 and [51]) or contains a more general spatio-temporal randomness [206].

Fefferman [101] pointed out that broader-than-Gaussian scalar PDFs should in fact arise at finite times for quite general models with *random* advection and molecular diffusion, when the initial data is a mean zero, homogenous, Gaussian random field. His argument sharpens some related observations of Kimura and Kraichnan [162]. Observe first that since the advection–diffusion equation is linear:

$$\partial T(\mathbf{x}, t)/\partial t + \mathbf{v}(\mathbf{x}, t) \cdot \nabla T(\mathbf{x}, t) = \kappa \Delta T(\mathbf{x}, t) ,$$

$$T(\mathbf{x}, t = 0) = T_0(\mathbf{x}) ,$$

we may represent its solution as the integral of the initial data against a Green's function $p^{(t)}(\mathbf{x}, \mathbf{x}')$:

$$T(\mathbf{x}, t) = \int_{\mathbb{R}^d} p^{(t)}(\mathbf{x}, \mathbf{x}') T_0(\mathbf{x}') \, \mathrm{d}\mathbf{x}' .$$

The Green's function appearing here is random because it depends on the random velocity field $\mathbf{v}$. Consider now a solution of the advection–diffusion equation which is conditioned upon a particular realization of the velocity field $\mathbf{v}$ chosen from the statistical ensemble. This *conditioned passive scalar field*, which we denote $T(\mathbf{x}, t|\mathbf{v})$, is expressible as the integral of the initial data against a deterministic Green's function, since the velocity field is fixed at a given realization. Being a deterministic linear functional of the mean zero, Gaussian random field $T_0(\mathbf{x})$, the conditioned passive scalar field $T(\mathbf{x}, t|\mathbf{v})$ must also be a mean zero, Gaussian random field. The original, unconditioned passive scalar field $T(\mathbf{x}, t)$ can therefore be described as a random mixture of the mean zero, Gaussian random fields $T(\mathbf{x}, t|\mathbf{v})$.

We now show that this implies that $T(\mathbf{x}, t)$ must have a broader-than-Gaussian single point PDF at all space–time points, unless the *conditional passive scalar variance*

$$\sigma_T^2(\mathbf{x}, t; \mathbf{v}) \equiv \langle T(\mathbf{x}, t|\mathbf{v})^2 \rangle_0$$

is independent of the particular realization of the velocity field $\mathbf{v}$ which is held fixed in the average over the initial data. Recall our convention that the suffix "0" on the expectation brackets indicate an averaging *only* over the statistics of the initial data, while a suffix "v" will indicate an average only over the velocity statistics. (We assume these are statistically independent.)

Note first that $\langle T(\mathbf{x}, t) \rangle = \langle \langle T(\mathbf{x}, t|\mathbf{v}) \rangle_0 \rangle_v = \langle 0 \rangle_v = 0$. The flatness factor of the passive scalar field may then be written:

$$F(\mathbf{x}, t) \equiv \frac{\langle (T(\mathbf{x}, t) - \langle T(\mathbf{x}, t) \rangle)^4 \rangle}{\langle (T(\mathbf{x}, t) - \langle T(\mathbf{x}, t) \rangle)^2 \rangle^2} = \frac{\langle T^4(\mathbf{x}, t) \rangle}{\langle T^2(\mathbf{x}, t) \rangle^2} = \frac{\langle \langle T^4(\mathbf{x}, t|\mathbf{v}) \rangle_0 \rangle_v}{\langle \langle T^2(\mathbf{x}, t|\mathbf{v}) \rangle_0 \rangle_v^2} .$$

Because $T(\mathbf{x}, t|\mathbf{v})$ is a Gaussian random field for each fixed realization of $\mathbf{v}$, we have

$$\langle T^4(\mathbf{x}, t|\mathbf{v}) \rangle_0 = 3 \langle (T(\mathbf{x}, t|\mathbf{v}))^2 \rangle_0^2 = 3(\sigma_T^2(\mathbf{x}, t; \mathbf{v}))^2 .$$

Therefore,

$$F(\mathbf{x}, t) = 3 \frac{\langle (\sigma_T^2(\mathbf{x}, t; \mathbf{v}))^2 \rangle_v}{\langle \sigma_T^2(\mathbf{x}, t; \mathbf{v}) \rangle_v^2} \ .$$

But by the simplest moment inequality

$$\frac{\langle (\sigma_T^2(\mathbf{x}, t; \mathbf{v}))^2 \rangle_v}{\langle \sigma_T^2(\mathbf{x}, t; \mathbf{v}) \rangle_v^2} \geq 1 \ ,$$

with equality holding only when the functional of the random velocity field, $\sigma_T^2(\mathbf{x}, t; \mathbf{v})$, has zero variance, i.e., behaves deterministically. We have shown that the passive scalar field will have a broader-than-Gaussian distribution at all space–time points $(\mathbf{x}, t)$ for which $\sigma_T^2(\mathbf{x}, t; \mathbf{v})$ has some nontrivial dependence on $\mathbf{v}$.

Therefore, the question of finite-time intermittency reduces to the question of whether the conditional variance of the passive scalar field at a certain location depends on the particular realization of the velocity field. If the velocity field were deterministic or absent, then there tautologically would be only one realization of the velocity field, and the passive scalar field must be exactly Gaussian at all times. On the other hand, if the passive scalar field were advected by an arbitrary incompressible random velocity field with no molecular diffusion, then the passive scalar field is simply advected along characteristics. Consequently, in every realization of the velocity field, the single-point scalar PDF will everywhere be identical to that of the homogenous, Gaussian random initial data $T_0(\mathbf{x})$. Hence, as was also shown by Kimura and Kraichnan [162], the passive scalar field arising from homogenous, Gaussian random initial conditions will remain Gaussian unless both random advection and molecular diffusion are active.

While these transport mechanisms in isolation always preserve Gaussianity of the initial, homogenous, random passive scalar field, their *interaction* generically will produce intermittent passive scalar fields at all finite times. Consider, for example, the Random Uniform Jet Model, in which the random component of the velocity field is the stochastic process $\gamma_r(t)$ multiplying a uniform shear flow spatial structure. Scalar intermittency will arise provided that the conditional variance of the passive scalar field $\sigma_T^2(\mathbf{x}, t; \mathbf{v})$ depends on the particular realization of $\gamma_r(t)$. This is clearly true: the shear flow interacts with the molecular diffusion to produce enhanced diffusion [31,258], and in each realization of the random shear, the mean-square displacement of a tracer along the shear is

$$D_r(t|\gamma_r) = 2\kappa \int_0^t \int_0^t \gamma_r(s) \min(s, s') \gamma_r(s') \, ds \, ds' \ , \tag{310}$$

as follows from computations similar to those described in Section 2.3.1. The greater the resulting transport, the more rapidly the passive scalar fluctuations will average out and their variance decrease.

In general, velocity fields with regions of stronger strains and shears give rise to more effective diffusion of the passive scalar field and consequently faster dissipation of the passive scalar variance than those with gentler gradients. Thus, in a generic random velocity field model in which the realizations of the statistical ensemble have different shearing and straining behavior, one can expect broader-than-Gaussian scalar PDF's at all finite space-time locations $(\mathbf{x}, t)$, when the initial

passive scalar field is a mean zero, homogenous, Gaussian random field. The assumption of statistical homogeneity is, in fact, inessential.

Note that the argument just presented does *not* suggest that the scalar PDF should generally remain broader-than-Gaussian in the long-time limit. The passive scalar variance $\sigma_T^2(\mathbf{x}, t) = \langle \sigma_T^2(\mathbf{x}, t; \mathbf{v}) \rangle_v = \langle T^2(\mathbf{x}, t) \rangle$ will decay to zero as $t \to \infty$, so one must consider instead the *normalized conditional variance*:

$$\Sigma_T^2(\mathbf{x}, t; \mathbf{v}) \equiv \sigma_T^2(\mathbf{x}, t; \mathbf{v}) / \sigma_T^2(\mathbf{x}, t) .$$

By the same arguments as above, the scalar PDF approaches a broader-than-Gaussian shape in the long-time limit when $\Sigma_T^{2*}(\mathbf{x}; \mathbf{v}) \equiv \lim_{t \to \infty} \Sigma_T^2(\mathbf{x}, t; \mathbf{v})$ is a nontrivial functional of the random velocity field, and will asymptotically become Gaussian when $\Sigma_T^{2*}(\mathbf{x}; \mathbf{v})$ is almost surely a deterministic constant (which must be unity). Intuitively, we might associate relaxation to a Gaussian distribution ($\Sigma_T^{2*}(\mathbf{x}) \equiv 1$) with flows in which the passive scalar field has a "self-averaging property," so that the long-time properties of the passive scalar field are the same in each individual realization of the velocity field. But it is not clear how to decide which case holds for a general, given nontrivial model.

For the Random Uniform Jet Model, we can actually compute the moments of the scalar PDF through explicit formulas, and thereby directly characterize when the scalar PDF is Gaussian or broader-than-Gaussian in the long-time limit.

5.2.2.2. Gaussianity and non-Gaussianity of the asymptotic scalar PDF. As we have just discussed, the single-point passive scalar PDF $p_T^{(x,y,z,t)}(\cdot)$ is broader-than-Gaussian at finite times in the Random Uniform Jet Model. The question of whether this PDF relaxes to a Gaussian in the long-time limit is determined [207] through the long-time behavior of the following function related to the temporal structure of the deterministic mean shear flow $\gamma_{\mathrm{m}}(t)z$:

$$I_{\mathrm{m}}(t) = \kappa \int_0^t \left(\int_0^s \gamma_{\mathrm{m}}(s') \, \mathrm{d}s' \right)^2 \mathrm{d}s .$$

- If $t^{-2} I_{\mathrm{m}}(t)$ is bounded in time, then as $t \to \infty$, the passive scalar PDF $p_T^{(x,y,z,t)}(\cdot)$ converges to a broader-than-Gaussian shape which is completely independent of the mean shear flow,
- If $t^{-2} I_{\mathrm{m}}(t) \to \infty$ as $t \to \infty$, then the passive scalar PDF $p_T^{(x,y,z,t)}(\cdot)$ approaches a Gaussian distribution in the long-time limit.

(If neither of these cases hold, then the passive scalar PDF never settles down to a limit, but forever oscillates in response to variations in the mean shear flow $\gamma_{\mathrm{m}}(t)z$.)

In particular, in the absence of the mean shear flow ($\gamma_{\mathrm{m}}(t) = 0$), the passive scalar PDF in our model converges to a broader-than-Gaussian limiting form in the long-time limit. The addition of a uniform mean shear flow $\gamma_{\mathrm{m}}(t)z$ with $\gamma_{\mathrm{m}}(t)$ a periodic function of time will not influence this limiting distribution. On the other hand, the addition of a steady mean shear flow ($\gamma_{\mathrm{m}}(t)$ a nonzero constant) will cause the passive scalar PDF to relax to a Gaussian form. More generally, the asymptotic scalar PDF will be Gaussian or not according to whether or not the mean shear flow is sufficiently *persistent*, as measured by whether $t^{-2} I_{\mathrm{m}}(t)$ diverges or stays bounded. Large values of $I_{\mathrm{m}}(t)$ correspond to temporal dynamics $\gamma_{\mathrm{m}}(t)$ of the mean shear flow which tend sufficiently strongly toward one direction or the other.

It can be readily checked that the above conclusions hold without change if the mean shear flow were to be given instead by $\gamma_{\mathrm{m}}(t)x$, with its gradient directed parallel to that of the random shear flow $\gamma_{\mathrm{r}}(t)x$.

One might understand why a persistent mean shear flow is associated with Gaussianity of the limiting passive scalar PDF through a "self-averaging effect". From Section 3, we know that molecular diffusion interacts with shear flows to produce enhanced diffusion of the passive scalar field along the direction of the shear. As discussed above, the interaction of the molecular diffusion with the *random* shear flow $\gamma_{\mathrm{r}}(t)x$ is a source of scalar intermittency due to the variability of the resulting shear-enhanced diffusion and dissipation. On the other hand, the interaction of the molecular diffusion with a *deterministic* shear flow will lead to a rapid diffusion along the shearing direction which will tend to average out the passive scalar fluctuations over space in a regular, nonrandom fashion. By a central limit argument, one can expect that this averaging effect will tend to restore Gaussianity to the passive scalar statistics.

This intuition is reflected by the exact criterion concerning $I_{\mathrm{m}}(t)$ described above. This quantity can be rewritten in a form

$$I_{\mathrm{m}}(t) = \kappa \int_0^t \int_0^t \gamma_{\mathrm{m}}(t-s)\min(s,s')\gamma_{\mathrm{m}}(t-s')\,\mathrm{d}s\,\mathrm{d}s' \tag{311}$$

which has a good deal of similarity with the formula for the mean-square tracer displacement along a time-dependent, deterministic uniform shear flow (cf. (310)):

$$\sigma_{Y,\mathrm{m}}^2(t) = 2\kappa \int_0^t \int_0^t \gamma_{\mathrm{m}}(s)\min(s,s')\gamma_{\mathrm{m}}(s')\,\mathrm{d}s\,\mathrm{d}s' \ .$$

The mean-square displacement along a randomly fluctuating shear flow $\gamma_{\mathrm{r}}(t)x$ with white noise correlations can also be calculated by similar means:

$$\sigma_{Y,\mathrm{r}}^2(t) = 2\kappa \int_0^t \int_0^t \min(s,s')\langle\gamma_{\mathrm{m}}(s)\gamma_{\mathrm{m}}(s')\rangle\,\mathrm{d}s\,\mathrm{d}s' = \kappa t^2 \ ,$$

and a quadratic expression in t also results upon averaging the formula (311) for $I_{\mathrm{m}}(t)$ with $\gamma_{\mathrm{r}}(t)$ replacing $\gamma_{\mathrm{m}}(t)$. Therefore, the criterion for whether the asymptotic scalar PDF is Gaussian or not is related in some sense to whether the mean or random shear diffuse the passive scalar field more effectively.

The "Gaussianizing" property of the mean shear revealed in the Random Uniform Jet model might be responsible for the different properties of the temperature observed in wind tunnel experiments by Jayesh and Warhaft [147] and by Tavoularis and Corrsin [316]. In both experiments, a mean temperature gradient is impressed on the fluid at the inlet, after which it freely decays. Jayesh and Warhaft generate turbulence by passing a uniform flow through a grid, whereas Tavoularis and Corrsin introduce a nearly uniform mean shear flow into the tunnel, where turbulence develops due to flow instabilities. In the former experiment, broad tails in the temperature PDF persist far downstream. In the latter, the temperature PDF is very well approximated by a Gaussian, even though the Reynolds number is higher. A satisfactory investigation of this point would of course require a comparison between two experiments in which all conditions are held fixed, other than the presence of the mean shear.

5.2.2.3. Properties of the non-Gaussian asymptotic PDF. From now on, we shall focus on the characterization of the broader-than-Gaussian shape of the scalar PDF which arises in the long-time limit when $t^{-2}I_m(t)$ is bounded. Its asymptotic shape will not depend on the mean shear flow, nor does it depend on whether the random shear is fluctuating in time according to a white noise or Ornstein–Uhlenbeck process. Rather, it depends only on some large-scale features of the initial passive scalar data $T_0(x, y)$. That is, one can define universality classes of the initial data, dependingonly on a few large-scale parameters, so that all initial data belonging to a particular universality class will approach a common broader-than-Gaussian PDF in the long-time limit.

First, we will first separately consider the cases of purely random initial data and purely deterministic initial data. Subsequently, we will examine the long-time form of the scalar PDF when the initial data has both deterministic and random components. Finally, we describe the universality properties of the long-time scalar PDF shape in a little more detail.

Purely random initial data. If the initial data is a mean zero, homogenous, Gaussian random field $T_0(x, y) = \tilde{T}_0(x, y)$, then by linearity of the advection–diffusion equation, the scalar PDF will have a symmetric form with mean zero at all times. The simplest characterization of the shape of the long-time asymptotic scalar PDF is thus the (first) flatness factor:

$$F^* = \lim_{t \to \infty} \frac{\langle T^4(x, y, z, t) \rangle}{\langle T^2(x, y, z, t) \rangle^2} \ .$$

A Gaussian PDF has a flatness of 3, while the flatness of the asymptotic scalar PDF in the Random Uniform Jet model is given by the explicit formula [233]:

$$\tilde{F}_\alpha^* = 3 \frac{\int_{\mathbb{R}^2} \dfrac{|k^{(1)}|^{-\alpha} |k^{(2)}|^{-\alpha} ((k^{(1)})^2 + (k^{(2)})^2)^{1/4}}{(\sinh \sqrt{(k^{(1)})^2 + (k^{(2)})^2})^{1/2}} \, dk^{(1)} \, dk^{(2)}}{\int_{\mathbb{R}^2} \dfrac{|k^{(1)}|^{-\alpha + 1/2} \, (|k^{(2)}|)^{-\alpha + 1/2}}{(\sinh|k^{(1)}|)^{1/2}(\sinh|k^{(2)}|)^{1/2}} \, dk^{(1)} \, dk^{(2)}} \ . \tag{312}$$

The parameter α appearing here describes the low-wavenumber behavior of the spectrum of the initial passive scalar fluctuations:

$$P_2^0(x, y) = \langle \tilde{T}_0(x', y') \tilde{T}_0(x' + x, y' + y) \rangle = \int_{\mathbb{R}^2} \hat{P}_2^0(\eta, k) \, d\eta \, dk \ ,$$

$$\lim_{\eta \to 0, k \to 0} \hat{P}_2^0(\eta, k) \sim |k|^{-\alpha} \phi(\eta, k) \ ,$$

where $\phi(\eta, k)$ is a smooth function with $\phi(0, 0)$ finite and positive.

One can rigorously show through calculus inequalities [207,233] that the asymptotic flatness $\tilde{F}_\alpha^*$ is greater than 3, and that the asymptotic scalar PDF is therefore strictly broader-than-Gaussian. In Table 14, we report some numerical computed values of $\tilde{F}_\alpha^*$.

The value $\alpha = 0$ is the most natural, since it corresponds to initial data for which

$$0 < \int_{\mathbb{R}^2} P_2^0(x, y) \, dx \, dy < \ \infty \ .$$

Table 14
Flatness of asymptotic scalar PDF in Random Uniform Jet Model (from [233])

α	$\tilde{F}_\alpha^*$
-8.0	265.02
-4.0	22.84
-1.5	6.01
-0.8	4.46
0.0	3.44
0.4	3.16
0.8	3.02

This condition is satisfied for the typical case in which the initial data is predominantly positively correlated, with finite integral length scale. As we see from the table, the flatness for this class of "ordinary" initial data is 3.44, which indicates a scalar PDF which is slightly broader than a Gaussian shape but not as broad as an exponential distribution ($F = 6$).

Varying the parameter α corresponds, in a sense, to varying the ratio between the (initial) length scale of the passive scalar field and the length scale of the velocity field. Now, the length scale of the velocity field in the Random Uniform Jet model is strictly infinite, so one cannot literally define such a length scale ratio. But the parameter α does describe the strength of the large-wavelength (low-wavenumber) fluctuations in the initial data. Clearly, as α increases, the initial data is becoming more strongly correlated over larger length scales. In particular, for $0 < \alpha < 1$, the integral length scale of the initial data is infinite, and one can relate this range of parameter values to situations in which the velocity and passive scalar field have comparable length scales. We see from Table 14 that as the long-range correlations of the passive scalar initial data strengthen ($\alpha \to 1$), the flatness factor approaches the Gaussian value of 3. On the other hand, for negative values of α, the long-wavelength fluctuations of the passive scalar field are depleted, and the passive scalar field is initially correlated on much smaller length scales than the integral length scale of the velocity field. The flatness factor diverges rapidly as α decreases. Indeed, if the spectrum of passive scalar fluctuations vanishes in a neighborhood of the origin (formally, $\alpha = \infty$), the flatness factor is infinite: the asymptotic scalar PDF has algebraic tails [207,233].

The qualitative paradigm we infer from the previous paragraph is that the passive scalar PDF relaxes at long times to an approximately Gaussian distribution when the length scale of the passive scalar field is comparable or greater than that of the velocity field, but that strong scalar intermittency will persist if the passive scalar field is correlated on a much smaller length scale than that of the turbulent velocity field.

From an intuitive standpoint, one can imagine that a turbulent velocity field will be able to effectively mix up a passive scalar field with larger-scale variations and produce a diffusive averaging over a wide area after a sufficient amount of time. A central limit argument suggests that the passive scalar statistics ought to then become Gaussian (see also [162]). On the other hand, when the passive scalar variations occur on scales smaller than that of the velocity field, the mixing is less efficient because the energetic large scales of the flow will mostly drag passive scalar structures around rather than chop them up. The passive scalar field will instead be distorted

through irregular small-scale straining and shearing processes, which are likely to produce or at least preserve intermittent features. This is the situation in Rayleigh–Benard convection cells, where thin plumes of hot fluid rise and cold fluid fall through a relatively regular circulation pattern. In the "hard turbulence" regime, the temperature is found to be intermittent in the central region through which these plumes pass [55,135,155,293]. Temperature is of course not a *passive* scalar in these convection cells, but buoyancy plays no role in the intuitive argument.

Purely deterministic initial data. We now describe some characteristics of the asymptotic scalar PDF which arises from purely deterministic initial data $T_0(x, y) = \bar{T}_0(x, y)$. We assume that the total mass of the initial data is nonzero and finite:

$$\bar{M}_0 \equiv \int_{\mathbb{R}^2} \bar{T}_0(x, y) \, \mathrm{d}x \, \mathrm{d}y \neq 0 \ .$$

In this setting, the single-point PDFs $p_T^{(x,y,z,t)}$ will vary with spatial location and will not necessarily be broader-than-Gaussian at finite times. In the Random Uniform Jet model [233], however, the passive scalar PDF at each point approaches a common and universal broader-than-Gaussian shape with flatness $\bar{F}^* \approx 3.52$. Moreover, the scalar PDF will exhibit a persistent asymmetry, which we may characterize by its *skewness*:

$$\bar{S}(x, y, z, t) \equiv \frac{\langle (T(x, y, z, t) - \langle T(x, y, z, t) \rangle)^3 \rangle}{\langle (T(x, y, z, t) - \langle T(x, y, z, t) \rangle)^2 \rangle^{3/2}} \ .$$

In the long-time limit, the skewness everywhere approaches a common value [233]:

$$\lim_{t \to \infty} \bar{S}(x, y, z, t) = \bar{S}^* \, \mathrm{sgn} \, \bar{M}_0 \ ,$$

where $\bar{S}^* \approx 0.76$. Thus, the passive scalar PDF will forever remember the sign of the mass of the initial data, and will not converge to a symmetric shape.

Persistent skewness of temperature was observed in wind tunnel experiments by Sreenivasan and others [311]. The turbulence is generated by a grid, and temperature fluctuations are introduced by heating wires on the same grid, or another screen downstream. The temperature showed significant skewness relatively far downstream of the heated grid, relaxing to an approximately symmetric distribution only after 40–100 thermal mesh sizes.

Initial data with deterministic and random components. We shall finally discuss the asymptotic shape of the scalar PDF in the long-time limit when the initial data $T_0(x, y) = \bar{T}_0(x, y) + \tilde{T}_0(x, y)$ is a superposition of a mean profile $\bar{T}_0(x, y)$ with random fluctuations $\tilde{T}_0(x, y)$ with the same properties as above. As the advection–diffusion PDE is linear, the passive scalar field arising from this combined initial data will be a simple sum of the individual contributions. Because these summands are statistically correlated, the PDF $p_T^{(x,y,z,t)}(\cdot)$ of the total passive scalar field will, however, not be related to the individual PDFs in such a simple fashion.

Through explicit computations [233], we find that the long-time limit of the passive scalar PDF approaches at every point a common shape, which depends on the parameter α. Its skewness and flatness are as follows:

- If $-\frac{3}{2} < \alpha < 1$, the asymptotic skewness S^* is zero, and the asymptotic flatness is $F^* = \tilde{F}_\alpha^*$, just as in the case of purely random initial data.

- If $\alpha < -\frac{3}{2}$, the asymptotic skewness $S^* = \bar{S}^*$ sgn $\bar{M}_0$ and the asymptotic flatness $F^* = \bar{F}^*$, just as in the case of purely deterministic initial data.
- If $\alpha = -\frac{3}{2}$, then the asymptotic skewness is given by

$$\lim_{t \to \infty} S(x, y, z, t) = S_c^* \text{ sgn } \bar{M}_0 ,$$

$$S_c^* = \frac{C_{31}\bar{M}_0^3 + C_{32}(\kappa/A_0)^{1/4}\bar{M}_0\phi(0,0)}{(C_{21}\bar{M}_0^2 + C_{22}(\kappa/A_0)^{1/4}\phi(0,0))^{3/2}} .$$

The asymptotic flatness is given by

$$\lim_{t \to \infty} F(x, y, z, t) = F_c^* = \frac{C_{41}\bar{M}_0^4 + C_{42}(\kappa/A_0)^{1/4}\bar{M}_0^2\phi(0,0) + C_{43}(\kappa/A_0)^{1/2}(\phi(0,0))^2}{(C_{21}\bar{M}_0^2 + C_{22}\ (\kappa/A_0)^{1/4}\phi(0,0))^2} .$$

The numerical constants appearing in these formulas may be computed by quadrature: $C_{21} \approx 0.27$, $C_{22} \approx 0.50$, $C_{31} \approx 0.10$, $C_{32} \approx 0.74$, $C_{41} \approx 0.25$, $C_{42} \approx 2.55$, and $C_{43} \approx 1.52$. The function $\phi(\eta, k)$ is part of the low-wavenumber description of the spectrum of initial passive scalar fluctuations (306).

We thus see a phase transition in the shape of the scalar PDF in the long-time limit. For $\alpha > -\frac{3}{2}$, the long-wavelength random fluctuations in the initial data are sufficiently strong that they alone determine the long-time skewness and flatness (as well as all the higher-order statistics [233]). For $\alpha < -\frac{3}{2}$, the mean initial scalar profile instead plays the dominant role. At the transition boundary $\alpha = -\frac{3}{2}$, both the mean and fluctuating components of the initial data are relevant. Moreover, for this special value of α, the long-time scalar PDF depends upon an additional parameter:

$$\phi(0,0)\kappa^{1/4}/\bar{M}_0^2 A_0^{1/4}$$

which is irrelevant for all other α. This parameter involves the relative magnitude of the large-scale variations in the mean and random components of the initial data, through $\bar{M}_0$ and $\phi(0,0)$ respectively, and further depends on the strength of the advection A_0 (see Eq. (307)) and of molecular diffusion κ. If the random temporal fluctuations are governed by a superposition of Ornstein–Uhlenbeck processes (308), then A_0 should be replaced by $\sum_{j=1}^{M} A_j\tau_j$.

The reason for the appearance of these factors is that at the special value of $\alpha = -\frac{3}{2}$, the variance of the contribution to the passive scalar field from the deterministic initial data $\bar{T}_0(x, y)$ and from the random initial data $\tilde{T}_0(x, y)$ decay at long times according to power laws $Kt^{-\beta}$, with a common exponent $\beta = 3$ but different prefactors K. The statistics of the total passive scalar field will clearly depend on the relative magnitude of these prefactors, which in turn depends on the relative magnitude of the initial data as well as the advection–diffusion parameters. When $\alpha \neq -\frac{3}{2}$, the contributions from the mean and random components of the initial data decay according to power laws with distinct exponents, and thus one will asymptotically dominate the statistics of their sum.

5.2.2.4. Universality of asymptotic PDF shape. With the results on the long-time limiting form of the passive scalar PDF presented, we review the extent to which its shape is universal. We found

that the skewness and flatness depend in the long-time limit only on the following parameters in the model:

- the boundedness or divergence of the quantity $t^{-2}I_m(t)$, which determined whether the mean shear flow is persistent enough to drive the passive scalar PDF to Gaussianity,
- the parameter α characterizing the strength of the long-wavelength fluctuations of the random initial data (306) (and which roughly represents a ratio of the length scales of the velocity and passive scalar field),
- the sign of mass of the mean profile of initial data $\bar{M}_0 = \int_{\mathbb{R}^2} T_0(x,y)\,dx\,dy$,
- the following combination involving the strength of the random advection, the molecular diffusion, and the relative size of the low-wavenumber components of the mean and random components of the initial data:

$$\phi(0,0)\kappa^{1/4}/\bar{M}_0^2 A_0^{1/4} .$$

This parameter is only relevant when $\alpha = -\frac{3}{2}$, a special value at which the random and mean components of the initial data decay at comparable rates at long times.

(It can be shown that the higher-order statistics depend on this same set of quantities [233].)

The asymptotic shape of the scalar PDF is *universal* with respect to all other features of the model, namely:

- The small-scale features of the initial data, i.e., anything other than the low-wavenumber asymptotics of its Fourier spectrum.
- The temporal correlation structure $\gamma_r(t)$ of the random shear, whether it be governed by a white noise process or a superposition of Ornstein–Uhlenbeck processes [282]. It is of course possible that if $\gamma_r(t)$ has long-range temporal correlations, the asymptotic scalar PDF may be altered.
- The details of the temporal dynamics of the mean shear $\gamma_m(t)$, other than through the criterion involving the single parameter $I_m(t)$ mentioned above.

5.2.3. Derivation of results

The basis for all of the above results concerning the single-point passive scalar PDF in the Random Uniform Jet model is the ability to express the equal-time, multipoint passive scalar correlation functions

$$P_N(\{(x^{(j)}, y^{(j)}, z^{(j)})\}_{j=1}^N, t) \equiv \left\langle \prod_{j=1}^N T(x^{(j)}, y^{(j)}, z^{(j)}, t) \right\rangle$$

to all orders in terms of explicit integrals of elementary functions. In particular, all the single-point moments of the passive scalar field $\langle (T(x,y,z,t))^N \rangle$ can be computed by numerical quadrature.

The derivation of the explicit formulas for the passive scalar statistics will now be illustrated for the case in which the random temporal process $\gamma_r(t)$ is white noise in time, and the initial data varies only in the shearing direction y:

$$T(x, y, z, t = 0) = T_0(y) = \bar{T}_0(y) + \tilde{T}_0(y) . \tag{313}$$

Our presentation will be taken for the most part from the original paper [207]. We will, at the end, indicate Resnick's modification [282] for treating Ornstein–Uhlenbeck temporal dynamics.

The reader may well note that the initial data (313) which we assume for the derivation is not actually a special case of the initial data considered in the main discussion of Section 5.2. (The quantities $\bar{M}_0$ and $\hat{P}_2^0(\eta, k)$ defined by Eqs. (304) and (305) would be infinite because of the absence of decay in the x direction.) One consequence is that the numerical values of the asymptotic skewness and flatness factors which would be computed from the formulas derived below will differ from those presented above. We have opted to present the derivation for initial data varying in the single direction y because it illustrates all the main ideas and yields formulas which are more easily derived than those which arise when the initial data varies in both the x and y direction. The formulas for the latter case may be found in [233].

To ease notation, we will write the coordinates of the observation points as components of a vector:

$$\boldsymbol{x}^{()} = \begin{bmatrix} x^{(1)} \\ x^{(2)} \\ \vdots \\ x^{(N)} \end{bmatrix},$$

(314)

$$\boldsymbol{y}^{()} = \begin{bmatrix} y^{(1)} \\ y^{(2)} \\ \vdots \\ y^{(N)} \end{bmatrix},$$

$$\boldsymbol{z}^{()} = \begin{bmatrix} z^{(1)} \\ z^{(2)} \\ \vdots \\ z^{(N)} \end{bmatrix}.$$

To avoid confusion with our standard use of the symbol $\boldsymbol{x}$ for the vector of spatial coordinates of a single point, we have affixed the superscript "()" as a reminder that the indices of the vectors $\boldsymbol{x}^{()}$, $\boldsymbol{y}^{()}$, and $\boldsymbol{z}^{()}$ run over the labels of the observation points $1, \ldots, N$, and not over spatial directions. In the following derivation, differential operators such as ∇ and $\varDelta$ will always refer to vectors of the type (314).

5.2.3.1. PDE for multipoint correlation functions. As the random component of the Random Uniform Jet flow has white noise correlations in time, the passive scalar multipoint correlation functions of all orders obey closed diffusion equations (see Section 4.4):

$$\frac{\partial P_N(\boldsymbol{x}^{()}, \boldsymbol{y}^{()}, \boldsymbol{z}^{()}, t)}{\partial t} + \gamma_{\mathrm{m}}(t)\boldsymbol{z}^{()} \cdot \nabla_{\boldsymbol{y}^{()}} P_N = \kappa(\varDelta_{\boldsymbol{x}^{()}} + \varDelta_{\boldsymbol{y}^{()}} + \varDelta_{\boldsymbol{z}^{()}})P_N$$

$$+ \frac{1}{2}A_0 \sum_{j,j'=1}^{N} V_{\mathrm{r}}(x^{(j)})V_{\mathrm{r}}(x^{(j')})\frac{\partial^2 P_N}{\partial y^{(j)}\partial y^{(j')}}, \quad P_N(\boldsymbol{x}^{()}, \boldsymbol{y}^{()}, \boldsymbol{z}^{()}, t = 0) = \left\langle \prod_{j=1}^{N} T_0(y^{(j)}) \right\rangle_0.$$

(315)

The advective contribution from the mean velocity field $\gamma_m(t)z$ and the molecular diffusion term can be formally obtained by expanding the time derivative $\partial P_N/\partial t = (\partial/\partial t)\langle \prod_{j=1}^N T(x^{(j)}, y^{(j)}, z^{(j)}, t)\rangle$ and substituting in the advection–diffusion equation. The additional diffusion operator arising from the random white noise advection $V_r(x)\gamma_r(t)$ can be derived through the same techniques as used in the Rapid Decorrelation in Time model (Section 4.4), once one notes that the correlation function of the random shear is

$$\langle (V_r(x)\gamma_r(t))(V_r(x')\gamma_r(t'))\rangle = A_0 V_r(x)V_r(x')\delta(t - t') .$$

Because the random advection is a shear flow, we could alternatively proceed by Fourier transforming the advection–diffusion equation with respect to y, as in Section 3.5. The molecular diffusion term is then handled through the Feynman–Kac formula. This is the approach adopted in the original paper [207].

5.2.3.2. Reformulation as quantum mechanical problem.
We now transform the diffusion PDE (315) for P_N into the form of a Schrödinger equation (in imaginary time) describing the evolution of a system of N quantum-mechanical particles. We defer writing $V_r(x)$ as its linear form x assumed in the Random Uniform Shear layer until later, because the quantum-mechanical formulation holds for general spatial profiles of the random shear.

We begin by isolating the effects of the mean shear $\gamma_m(t)z$ through the definition of a new variable $y' = y - z\Gamma_m(t)$, with

$$\Gamma_m(t) = \int_0^t \gamma_m(s)\,ds , \tag{316}$$

so that (x, y', z) are Lagrangian variables associated to the mean shear flow. In these "mean-Lagrangian" variables, the advection term vanishes:

$$\frac{\partial \tilde{P}_N(\boldsymbol{x}^{()}, \boldsymbol{y}'^{()}, \boldsymbol{z}^{()}, t)}{\partial t} = \kappa(\Delta_{x^{()}} + \Delta_{y'^{()}} + \Delta_{z^{()}})\tilde{P}_N + \kappa\Gamma_m^2(t)\Delta_{y'^{()}}\tilde{P}_N$$

$$+ \frac{1}{2}A_0 \sum_{j,j'=1}^N V_r(x^{(j)})V_r(x^{(j')})\frac{\partial^2 \tilde{P}_N}{\partial y^{(j)}\partial y^{(j')}} , \quad \tilde{P}_N(\boldsymbol{x}^{()}, \boldsymbol{y}'^{()}, \boldsymbol{z}^{()}, t=0) = \left\langle \prod_{j=1}^N T_0(y'^{(j)})\right\rangle_0 . \tag{317}$$

The last two terms of the PDE explicitly indicate the enhanced diffusion along the shearing direction (in mean-Lagrangian coordinates) due to the interaction of the molecular diffusion with the mean shear and to the randomly fluctuating shear. Each of these operators is easily checked to be nonnegative definite.

Note now that neither the initial data nor any coefficients of the PDE depend on $z^{()}$. By symmetry, this implies that the solution is in fact independent of this set of variables: $\tilde{P}_N = \tilde{P}_N(\boldsymbol{x}^{()}, \boldsymbol{y}'^{()}, t)$, and the $\Delta_{z^{()}}$ term may be dropped.

Owing to the special shear structure of the model, we can see that a partial Fourier transform with respect to the $y^{(j)}$ variables would conveniently convert the enhanced diffusion operators into

multiplicative factors. We cannot, however, apply the ordinary Fourier transform when the initial data has homogenous random fluctuations, because then $T_0(y)$ and $\tilde{P}_N$ will not decay at infinity. We must use a more general spectral representation, which for the initial data reads

$$
T_0(y) = \bar{T}_0(y) + \tilde{T}_0(y) \, ,
$$

$$
\bar{T}_0(y) = \int_{\mathbb{R}} \hat{\bar{T}}_0(k) e^{2\pi i k y} \, dk \, ,
$$
(318)

$$
\tilde{T}_0(y) = \int_{\mathbb{R}} \hat{\tilde{T}}_0(k) e^{2\pi i k y} \, d\tilde{W}(k) \, .
$$

The Fourier integral for $\tilde{T}_0(y)$ is a stochastic white noise integral ([341], Section 9), which we already encountered in Paragraph 3.2.2.1. For computational purposes, the white noise differential $d\tilde{W}(k)$ acts as a complex Gaussian random quantity with the formal properties:

$$
d\tilde{W}(-k) = \overline{d\tilde{W}(k)} \, , \qquad \langle d\tilde{W}(k) \rangle = 0 \, , \qquad \langle d\tilde{W}(k) d\tilde{W}(k') \rangle = \delta(k + k') \, dk \, dk' \, .
$$
(319)

(An overbar denotes complex conjugation.) The Fourier coefficient of the random initial data is linked to its spectrum $\hat{P}_2^0(k)$ (304) by the relation

$$
\hat{\tilde{T}}_0(k) = \sqrt{\tilde{P}_2^0(|k|)} \, .
$$

The initial data for the passive scalar multipoint correlation function can now be generally written as a superposition of exponentials:

$$
\tilde{P}_N(\boldsymbol{x}^{()}, \boldsymbol{y}'^{()}, t = 0) = \int_{\mathbb{R}^N} e^{2\pi i \boldsymbol{k}^{()} \cdot \boldsymbol{y}'^{()}} \left\langle \prod_{j=1}^{N} (\hat{\bar{T}}_0(k^{(j)}) \, dk^{(j)} + \hat{\tilde{T}}_0(k^{(j)}) \, d\tilde{W}_j(k)) \right\rangle_0 \, .
$$
(320)

The expectation brackets $\langle \cdot \rangle_0$ denote an average over the initial data, which here just amounts to averaging over the independent complex white noise differentials $\{d\tilde{W}_j(k)\}_{j=1}^N$. This average can be evaluated in general through a cluster expansion and the rules (319). Because of the linearity of the PDE (317), $\tilde{P}_N$ can be represented in a similar fashion to Eq. (320) at all later times:

$$
\tilde{P}_N(\boldsymbol{x}^{()}, \boldsymbol{y}'^{()}, t) = \int_{\mathbb{R}^N} e^{2\pi i \boldsymbol{k}^{()} \cdot \boldsymbol{y}'^{()}} Q_N(\boldsymbol{x}^{()}, \boldsymbol{k}^{()}, t) \left\langle \prod_{j=1}^{N} (\hat{\bar{T}}_0(k^{(j)}) \, dk + \hat{\tilde{T}}_0(k^{(j)}) \, d\tilde{W}_j(k)) \right\rangle_0 \, ,
$$

where Q_N satisfies the Fourier transformed PDE:

$$
\frac{\partial Q_N(\boldsymbol{x}^{()}, \boldsymbol{k}^{()}, t)}{\partial t} = \kappa \Delta_{\boldsymbol{x}^{()}} Q_N - 4\pi^2 \kappa |\boldsymbol{k}^{()}|^2 Q_N - 4\pi^2 \kappa \Gamma_{\mathrm{m}}^2(t) |\boldsymbol{k}^{()}|^2 Q_N - 2\pi^2 A_0 \left(\sum_{j=1}^{N} k^{(j)} V_{\mathrm{r}}(x^{(j)}) \right)^2 Q_N \, ,
$$

$$
Q_N(\boldsymbol{x}^{()}, \boldsymbol{k}^{()}, t = 0) = 1 \, .
$$

The undifferentiated terms with spatially constant coefficients can now be removed by an integrating factor $e^{4\pi^2(I_m(t)+\kappa t)|k^{()}|^2}$, with

$$0 \leqslant I_m(t) = \kappa \int_0^t \Gamma_m^2(s)\,\mathrm{d}s = \int_0^t \left(\int_0^s \gamma_m(s')\,\mathrm{d}s' \right)^2 \mathrm{d}s . \tag{321}$$

Through the above transformations, we find in the end that the passive scalar multipoint correlation function can be represented by

$$P_N(x^{()}, y^{()}, z^{()}, t) = \int_{\mathbb{R}^N} e^{2\pi i k^{()} \bullet (y^{()} - \Gamma_m(t)z^{()})} e^{-4\pi^2|k^{()}|^2(I_m(t)+\kappa t)} \psi_N(x^{()}, k^{()}, t)$$

$$\times \left\langle \prod_{j=1}^N (\hat{\bar{T}}_0(k^{(j)})\,\mathrm{d}k + \hat{\bar{T}}_0(k^{(j)})\,\mathrm{d}W^{(j)}(k)) \right\rangle_0 , \tag{322}$$

where $\Gamma_m(t)$ and $I_m(t)$ are given by Eqs. (316) and (321), respectively, and $\psi_N(x^{()}, k^{()}, t)$ solves the PDE:

$$\frac{\partial \psi_N(x^{()}, k^{()}, t)}{\partial t} = \kappa \Delta_{x^{()}} \psi_N - 2\pi^2 A_0 \left(\sum_{j=1}^N k^{(j)} V_r(x^{(j)}) \right) \psi_N ,$$

$$\psi_N(x^{()}, k^{()}, t = 0) = 1 . \tag{323}$$

Note that the effects of the mean shear have been explicitly accounted for by $\Gamma_m(t)$ and $I_m(t)$ in Eq. (322); ψ_N depends only on the molecular diffusivity and the spatial structure of the random shear. Moreover, the equation for ψ_N has the form of a quantum-mechanical Schrödinger equation (in imaginary time)

$$-\frac{\partial \psi_N(x^{()}, k^{()}, t)}{\partial t} = -\kappa \Delta_{x^{()}} \psi_N + U_N(x^{()}, k^{()}) \psi_N ,$$

$$\psi_N(x^{()}, k^{()}, t = 0) = 1 ,$$

with potential

$$U_N(x^{()}, k^{()}) = 2\pi^2 A_0 \left(\sum_{j=1}^N k^{(j)} V_r(x^{(j)}) \right)^2 .$$

We shall only discuss hereafter the case of purely random initial data ($T_0(y) = \tilde{T}_0(y)$), but the ideas carry over to handle initial data with a deterministic component as well [233]. Because $\hat{\bar{T}}_0(k)$ vanishes, the cluster expansion of $\langle \cdot \rangle_0$ becomes a simple Wick contraction, with the wavenumbers $\{k^{(j)}\}_{j=1}^N$ matched in pairs [207]. We are particularly interested in the single-point moments of the passive scalar field $\langle T^N(x, y, z, t) \rangle$, and for these we find

$$\langle T^{2N+1}(x, y, z, t) \rangle = 0 ,$$

$$\langle T^{2N}(x, y, z, t) \rangle = \frac{(2N)!}{2^N N!} \int_{\mathbb{R}^N} e^{-8\pi^2|k^{()}|^2(I_m(t)+\kappa t)} \psi_{2N}(x^{()R}, k^{()\pm}, t) \prod_{j=1}^N \hat{P}_2^0(k^{(j)})\,\mathrm{d}k^{()} . \tag{324}$$

The arguments $x^{()R}$ and $k^{()\pm}$ of ψ_{2N} are shorthand notation for the following collections of $2N$ variables:

$$
x^{()R} = \begin{bmatrix} x \\ x \\ \vdots \\ x \end{bmatrix},
$$

$$
k^{()\pm} = \begin{bmatrix} k^{(1)} \\ k^{(2)} \\ \vdots \\ k^{(N)} \\ -k^{(1)} \\ -k^{(2)} \\ \vdots \\ -k^{(N)} \end{bmatrix}.
$$

5.2.3.3. Solution of quantum mechanical problem. We have shown how to explicitly represent the moments of the passive scalar field in terms of the solution ψ_N to the quantum-mechanical problem (323). We now insert the explicit form of the random shear profile $V_r(x) = x$ in the Random Uniform Jet model into this equation:

$$
\frac{\partial \psi_N(x^{()}, k^{()}, t)}{\partial t} = \kappa \Delta_{x^{()}} \psi_N - 2\pi^2 A_0 (k^{()} \bullet x^{()})^2 \psi_N \,,
$$

$$
\psi_N(x^{()}, k^{()}, t = 0) = 1 \,. \tag{325}
$$

The potential in the Schrödinger operator on the right-hand side is thus quadratic, corresponding to a certain harmonic oscillator potential for the collective motion of N quantum particles. The potential is effectively one-dimensional, depending only on the weighted sum of the spatial coordinates $k^{()} \bullet x^{()}$, so Eq. (325) can be mapped onto the one-dimensional harmonic oscillator problem:

$$
\frac{\partial \psi(x, t)}{\partial t} = \frac{\partial^2 \psi}{\partial x^2} - x^2 \psi \,,
$$

$$
\psi(x, t = 0) = 1 \,.
$$

An exact solution to this PDE in terms of elementary functions is given by Mehler's formula [296]:

$$
\psi(x, t) = (\cosh(2t))^{-1/2}\, e^{-(1/2)\tanh(2t)x^2} \,.
$$

The solution to the N-particle equation (325) is then expressed in terms of ψ as follows:

$$
\psi_N(x^{()}, k^{()}, t) = \psi((2\pi^2 \kappa^{-1} A_0)^{1/4} |k^{()}|^{-1/2} (k^{()} \bullet x^{()}), \sqrt{2\pi^2 \kappa A_0} |k^{()}| t) \,.
$$

Substitution of this exact solution into Eq. (324) then yields the following exact formulas for the single-point scalar moments:

$$
\langle T^{2N+1}(x,y,z,t)\rangle = 0,
$$
$$
\langle T^{2N}(x,y,z,t)\rangle = \frac{(2N)!}{2^N N!}\int_{\mathbb{R}^N} e^{-8\pi^2|k^{()}|^2(I_m(t)+\kappa t)}(\cosh(2\pi\sqrt{2\kappa A_0}|k^{()}|t))^{-1/2}\prod_{j=1}^{N}\hat{P}_2^0(k^{(j)})\,dk^{()}.
\tag{326}
$$

5.2.3.4. Derivation of properties of scalar PDF. The explicit formula (326) now permits direct analysis of the passive scalar moments in the Random Uniform Jet model. The fact that the scalar PDF is broader-than-Gaussian at finite times follows from the following calculus inequality:

$$
(\mathrm{sech}(|k|))^{1/2} \geq \prod_{j=1}^{N}(\mathrm{sech}(|k^{(j)}|))^{1/2},
$$

as established in [207]. The long-time limit of the flatness factor

$$
F^* = \lim_{t\to\infty}\frac{\langle T^4(x,y,z,t)\rangle}{\langle T^2(x,y,z,t)\rangle^2}
$$

follows from a straightforward asymptotic consideration of Eq. (326):

$$
F^* = \begin{cases} 3 & \text{if } t^{-2}I_m(t) \to \infty \text{ as } t\to\infty, \\ \tilde{F}_\alpha^* > 3 & \text{if } t^{-2}I_m(t) \text{ is bounded}, \end{cases}
$$

where

$$
\tilde{F}_\alpha^* = 3\frac{\displaystyle\int_{\mathbb{R}^2}\frac{|k^{(1)}|^{-\alpha}|k^{(2)}|^{-\alpha}}{(\cosh((|k^{(1)}|^2+|k^{(2)}|^2)^{1/2}))^{1/2}}\,dk^{(1)}\,dk^{(2)}}{\displaystyle\int_{\mathbb{R}^2}\frac{|k^{(1)}|^{-\alpha}}{\cosh(|k^{(1)}|)^{1/2}}\frac{|k^{(2)}|^{-\alpha}}{\cosh(|k^{(2)}|)^{1/2}}\,dk^{(1)}\,dk^{(2)}}.
$$

Recall that α describes the behavior of the initial passive scalar spectrum $\hat{P}_2^0(k)$ near $k=0$ (see Eq. (306)). The flatness factors $\tilde{F}_\alpha^*$ may be readily and accurately evaluated through a numerical quadrature calculation.

The procedure described above for deriving explicit formulas for the single-point moments of the passive scalar field can be generalized to handle initial data varying in the x and z as well as y directions, and with deterministic and random components. The formulas will differ in some details (cf. Eq. (312)); see [207,233] for details.

5.2.3.5. Ornstein–Uhlenbeck temporal fluctuations. We shall finally indicate how exact formulas for the passive scalar statistics can be obtained when the temporal fluctuations $\gamma_r(t)$ are given by a superposition of Ornstein–Uhlenbeck processes, rather than a white noise process as assumed above. Complete details may be found in the thesis of Resnick [282]. To communicate the main

idea, it suffices to consider $\gamma_r(t)$ as a single Ornstein–Uhlenbeck process, with correlation function

$$\langle \gamma_r(t)\gamma_r(t+\tau)\rangle = A_1 e^{-|\tau|/\tau_c} . \tag{327}$$

The process $\gamma_r(t)$ may be described as the solution to the linear stochastic differential equation

$$d\gamma_r(t) = -\tau_c^{-1}\gamma_r(t)\,dt + \sigma_\gamma\,dW_\gamma(t) ,$$

with $W_\gamma(t)$ a standard Brownian motion, $\gamma_r(0)$ a Gaussian random variable with mean zero and variance A_1, and $\sigma_\gamma = (2A_1\tau_c^{-1})^{1/2}$.

As discussed in Section 4, the reason closed equations can be written down for the passive scalar multipoint correlation functions when the velocity field is Gaussian and delta-correlated in time is that the random advection of tracer trajectories can be expressed as coupled Brownian motions. In the Random Uniform Jet model with white noise correlations, for example, the equations of motion for the locations $\{(X^{(j)}(t), Y^{(j)}(t), Z^{(j)}(t))\}_{j=1}^N$ of N tracers are:

$$dX^{(j)}(t) = \sqrt{2\kappa}\,dW_x^{(j)}(t) ,$$

$$dY^{(j)}(t) = \gamma_m(t)Z^{(j)}(t)\,dt + V_r(X^{(j)}(t))\,dW_\gamma(t) + \sqrt{2\kappa}\,dW_y^{(j)}(t) ,$$

$$dZ^{(j)}(t) = \sqrt{2\kappa}\,dW_z^{(j)}(t) ,$$

where $W_\gamma(t)$ and $\{W_x^{(j)}(t), W_y^{(j)}(t), W_z^{(j)}(t)\}_{j=1}^N$ are independent Brownian motions describing the random shear flow and the molecular diffusion, respectively. The diffusion equation (315) follows by the general relation between the statistics of N tracer trajectories and the Nth order passive scalar correlation function (see, for example, [185,244]).

With an Ornstein–Uhlenbeck law for the fluctuating shear, the trajectory equations instead read

$$dX^{(j)}(t) = \sqrt{2\kappa}\,dW_x^{(j)}(t) ,$$

$$dY^{(j)}(t) = \gamma_m(t)Z^{(j)}(t)\,dt + V_r(X^{(j)}(t))\gamma_r(t)\,dt + \sqrt{2\kappa}\,dW_y^{(j)}(t) ,$$

$$dZ^{(j)}(t) = \sqrt{2\kappa}\,dW_z^{(j)}(t) ,$$

$$d\gamma_r(t) = -\tau_c^{-1}\gamma_r(t)\,dt + \sigma_\gamma\,dW_\gamma(t) .$$

Note that these equations are again described in terms of independent Brownian motions $W_\gamma(t)$ and $\{W_x^{(j)}(t), W_y^{(j)}(t), W_z^{(j)}(t)\}_{j=1}^N$, and therefore we can still write down a closed diffusion equation for the passive scalar multipoint correlation function. The main difference from the white noise case is that an extra stochastic differential equation is required to describe the dynamics of $\gamma_r(t)$ in terms of a Brownian motion. This fact manifests itself in the need to introduce an additional variable in the diffusion PDE. Namely, with the random shear fluctuating according to an Ornstein–Uhlenbeck process (327), the passive scalar multipoint correlation function may be expressed as follows [282]:

$$P_N(\boldsymbol{x}^{()}, \boldsymbol{y}^{()}, \boldsymbol{z}^{()}, t) = \int_{\mathbb{R}} \Psi_N(\boldsymbol{x}^{()}, \boldsymbol{y}^{()}, \boldsymbol{z}^{()}, \zeta, t) \frac{e^{-\zeta^2/2A_1}}{\sqrt{2\pi A_1}}\,d\zeta , \tag{328}$$

where Ψ_N satisfies the diffusion equation

$$\frac{\partial \Psi_N(\mathbf{x}^{()}, \mathbf{y}^{()}, \mathbf{z}^{()}, \zeta, t)}{\partial t} + \gamma_m(t)\mathbf{z}^{()} \bullet \nabla_{\mathbf{y}^{()}} \Psi_N + \sum_{j=1}^{N} \zeta V_r(x^{(j)}) \frac{\partial \Psi_N}{\partial y^{(j)}} + \tau_c^{-1} \zeta \frac{\partial \Psi_N}{\partial \zeta}$$

$$= \kappa(\Delta_{\mathbf{x}^{()}} + \Delta_{\mathbf{y}^{()}} + \Delta_{\mathbf{z}^{()}})\Psi_N + \frac{1}{2}\sigma_\gamma^2 \frac{\partial^2 \Psi_N}{\partial \zeta^2},$$

$$\Psi_N(\mathbf{x}^{()}, \mathbf{y}^{()}, \mathbf{z}^{()}, \zeta, t = 0) = \left\langle \prod_{j=1}^{N} T_0(y^{(j)}) \right\rangle_0.$$

The auxiliary variable ζ keeps track of the dynamics of the temporal process $\gamma_r(t)$, and Eq. (328) comes from a weighting with respect to the distribution of $\gamma_r(0)$.

One can now proceed with the same transformations as in the white noise case to represent Ψ_N as follows:

$$\Psi_N(\mathbf{x}^{()}, \mathbf{y}^{()}, \mathbf{z}^{()}, \zeta, t) = \int_{\mathbb{R}^N} e^{2\pi i \mathbf{k}^{()} \bullet (\mathbf{y}^{()} - \Gamma_m(t)\mathbf{z}^{()})} e^{-4\pi^2 |\mathbf{k}^{()}|^2 (I_m(t) + \kappa t)} \psi_N^{(OU)}(\mathbf{x}^{()}, \mathbf{k}^{()}, \zeta, t)$$

$$\times \left\langle \prod_{j=1}^{N} (\hat{\tilde{T}}_0(k^{(j)}) \, \mathrm{d}k + \hat{\tilde{T}}_0(k^{(j)}) \, \mathrm{d}W^{(j)}(k)) \right\rangle_0,$$

where

$$\frac{\partial \psi_N^{(OU)}(\mathbf{x}^{()}, \mathbf{k}^{()}, \zeta, t)}{\partial t} + \tau_c^{-1} \zeta \frac{\partial \psi_N^{(OU)}}{\partial \zeta} = \kappa \Delta_{\mathbf{x}^{()}} \psi_N^{(OU)} + \frac{1}{2}\sigma_\gamma^2 \frac{\partial^2 \psi_N^{(OU)}}{\partial \zeta^2} - \left(2\pi i \zeta \sum_{j=1}^{N} k^{(j)} V_r(x^{(j)})\right) \psi_N^{(OU)},$$

$$\psi_N^{(OU)}(\mathbf{x}^{()}, \mathbf{k}^{()}, \zeta, t = 0) = 1.$$

After a further transformation designed to clear the first derivative term from the PDE,

$$\psi_N^{(OU)}(\mathbf{x}^{()}, \mathbf{k}^{()}, \zeta, t) = \exp[(t + \zeta^2/\sigma_\gamma^2)/2\tau_c] \tilde{\psi}_N^{(OU)}(\mathbf{x}^{()}, \mathbf{k}^{()}, \zeta, t),$$

we arrive at a PDE in quantum-mechanical Schrödinger form

$$\frac{\partial \tilde{\psi}_N^{(OU)}(\mathbf{x}^{()}, \mathbf{k}^{()}, \zeta, t)}{\partial t} = \kappa \Delta_{\mathbf{x}^{()}} \psi_N^{(OU)} + \frac{1}{2}\sigma_\gamma^2 \frac{\partial^2 \tilde{\psi}_N^{(OU)}}{\partial \zeta^2} + \left[-\left(2\pi i \zeta \sum_{j=1}^{N} k^{(j)} V_r(x^{(j)})\right) - \frac{\zeta^2}{2\sigma_\gamma^2 \tau_c^2}\right] \psi_N^{(OU)},$$

$$\tilde{\psi}_N^{(OU)}(\mathbf{x}^{()}, \mathbf{k}^{()}, \zeta, t = 0) = e^{-\zeta^2/(2\sigma_\gamma^2 \tau_c)} \tag{329}$$

In the Random Uniform Jet model $V_r(x) = x$, and the effective potential in the Schrödinger operator,

$$U_N^{(OU)}(\mathbf{x}^{()}, \mathbf{k}^{()}, \zeta) = \left[(2\pi i \zeta \mathbf{k}^{()} \bullet \mathbf{x}^{()}) + \frac{\zeta^2}{2\sigma_\gamma^2 \tau_c} \right],$$

is again a quadratic form which varies only along a single direction in $(\mathbf{x}^{()}, \zeta)$ space. Hence, after a (complex) rotation of coordinates, Eq. (329) may be mapped onto the one-dimensional harmonic oscillator problem, and thus expressed in terms of Mehler's formula. Details and generalizations

may be found in Resnick's thesis [282]. It is also shown there that the long-time limit of the single-point passive scalar moments are independent of whether the random temporal fluctuations $\gamma_r(t)$ are governed by white noise (307) or a superposition of Ornstein–Uhlenbeck processes (308). (One need only equate the quantity A_0 for the white noise case to $\sum_{j=1}^{M} A_j \tau_j$ for a superposition of Ornstein–Uhlenbeck processes.)

5.3. An example with qualitative finite-time corrections to the homogenized limit

We have seen how the exactly solvable Random Uniform Jet model permits the exploration of a number of issues pertaining to large-scale intermittency, such as the degree of universality of the scalar PDF in the long-time limit and the sensitivity to parameters such as the relative length scales of the velocity and passive scalar fields. As the uniform shear velocity field has an infinite length scale, we have up to now only been considering situations in which the length scale of the passive scalar field is small or comparable to the length scale of the velocity field. We shall now modify the spatial structure $V_r(x)$ of the random velocity field in the general jet model (303) to be a *periodic* function, so that we may also study long-time scalar intermittency properties when the length scale of the passive scalar field is much larger than that of the velocity field.

This is a realm in which homogenization theory, as discussed in Section 2, can be applied. Given a velocity field with finite periodicity and/or short-ranged randomness, homogenization theory furnishes a rigorous asymptotic description of the passive scalar field under a large-scale rescaling of the initial data $T_0(x) \to T_0(\varepsilon x)$ and a diffusively linked long-time limit $t \to t/\varepsilon^2$, with $\varepsilon \to 0$. While this is a particularly relevant asymptotic limit to consider in many applications in which the velocity varies on much smaller scales than the scalar field, the real issue is the behavior of the passive scalar field at large but *finite* times and length-scales. The rigorous asymptotic theory guarantees a certain abstract mode of convergence of the rescaled passive scalar statistics to the homogenized limit, but this by no means implies that homogenization theory describes the large-scale, long-time passive scalar statistics in a uniformly approximate way. We examined this question for the mean and variance of the displacement of a single tracer in some deterministic periodic flows in Section 2.3, and did find good agreement with the homogenized description at finite times [231].

The accuracy of the homogenization approximation at finite time for a quite different statistical aspect, the one-point scalar PDF, was explored by Bronski and McLaughlin [51] in a spatially periodic version of the Random Uniform Jet model discussed in Section 5.2. This *Random Spatially Periodic Shear* model will be defined in detail in Section 5.3.1.

In this random velocity field model, two qualitative departures of the scalar PDF from a straightforward homogenization picture emerge. In the Random Spatially Periodic Shear model, the passive scalar statistics become Gaussian in the homogenized large-scale, long-time limit, as one might expect from a central limit argument. The long-time limit of the scalar PDF evolving from initial data with large but *fixed* length scale, however, can become increasingly intermittent with flatness factors diverging in the long-time limit. The disagreement with the homogenized result implies that the limits of long-times $t \to t/\varepsilon^2$ and large-scale variation in the initial data $T_0(x) \to T_0(\varepsilon x)$ do not commute (Section 5.3.2). Moreover, even when the moments of the scalar PDF do approach their Gaussian values in the long-time limit, their convergence is very nonuniform. The relaxation time grows quadratically with the order of the moment, indicating that while the scalar PDF develops a Gaussian core at long times, it will always exhibit broader-than-Gaussian tails

sufficiently far out (Section 5.3.3). The Random, Spatially Periodic Shear model teaches us that the passive scalar statistics evolving from fixed initial data can exhibit qualitative departures from homogenization theory at large but finite times.

The passive scalar statistics in the Random, Spatially Periodic Shear model cannot be represented as fully explicit quadrature expressions in the same way as in the Random Uniform Shear model. Nonetheless, the moments of the single-point scalar PDF at large but finite times may be computed precisely through a perturbation theory applied to quantum-mechanical analogies similar to those discussed in Section 5.2.3. In this way, it can be directly proved that the scalar PDF arising from mean zero, Gaussian, homogenous, random initial data is broader-than-Gaussian at all later finite times. The calculations for this and the other results we shall describe are presented in full detail in [51], and will not be reproduced here other than for a few brief remarks in Section 5.3.4.

5.3.1. Random, Spatially Periodic Shear Model

The *Random, Spatially Periodic Shear* velocity field model considered by Bronski and McLaughlin is a shear flow:

$$\boldsymbol{v}(\boldsymbol{x}, t) = \boldsymbol{v}(x, y, t) = \begin{bmatrix} 0 \\ \gamma_{\mathrm{r}}(t) V_{\mathrm{r}}(x) \end{bmatrix} ,$$

with a deterministic spatial profile $V_{\mathrm{r}}(x)$ of period one (in nondimensionalized units), and white noisetemporal fluctuations:

$$\langle \gamma_{\mathrm{r}}(t) \gamma_{\mathrm{r}}(t + \tau) \rangle = A_0 \delta(\tau) .$$

The profile $V_{\mathrm{r}}(x)$ will be assumed to be suitably normalized; the amplitude of the shear flow will be measured by A_0. Like the Random Uniform Jet model, the Random, Spatially Periodic Shear Flow is an element of the class of general jet models (303), but there is no mean shear, and the z dimension has been omitted. The most fundamental difference between the two models is that the Random Uniform Jet velocity field has an infinite length scale of variation, while the Random, Spatially Periodic Shear flow has finite period length scale. The advection–diffusion equation for the present model reads

$$\frac{\partial T(x, y, t)}{\partial t} + \gamma_{\mathrm{r}}(t) V_{\mathrm{r}}(x) \frac{\partial T(x, y, t)}{\partial y} = \kappa \Delta T(x, y, t) ,$$

$$T(x, y, t = 0) = T_0(y) ,$$

where $T_0(y)$ is a mean zero, Gaussian, homogenous random field, and is assumed for simplicity to only vary in the shearing direction. We shall now consider two types of spectra for the random initial data which will illustrate some possibilities for the long-time behavior of the single-point passive scalar PDF.

5.3.2. Persistent intermittency for initial data with no long-wavelength fluctuations

We shall first show that the long-time limit of the passive scalar field arising from fixed initial data can differ sharply from the homogenized limit in which the long-time limit is linked with a large-scale rescaling of the initial data. Suppose that the initial data $T_0(y)$ is a mean zero,

Gaussian, homogenous, random field with spectrum supported above a fixed, positive wavenumber k_0:

$$P_2^0(y) = \langle T_0(y')T_0(y' + y)\rangle = \int_{\mathbb{R}} e^{2\pi i k y} \hat{P}_2^0(k)\, dk ,$$

$$\hat{P}_2^0(k) \begin{cases} = 0 & \text{for } |k| \leq k_0 , \\ > 0 & \text{for } k > k_0 . \end{cases} \tag{330}$$

We will consider the long-time limiting shape of the single-point scalar PDF.

To diagnose the deviation of this PDF from a Gaussian form, we will use not only the flatness factor $F(x, y, t)$ discussed in Section 5.2, but all the *higher order flatness factors* $F_N(x, y, t)$ as well:

$$F_N(x, y, t) \equiv \frac{\langle (T(x, y, t) - \langle T(x, y, t)\rangle)^{2N}\rangle}{\langle (T(x, y, t) - \langle T(x, y, t)\rangle)^2\rangle^N} = \frac{\langle T^{2N}(x, y, t)\rangle}{\langle T^2(x, y, t)\rangle^N} ,$$

with the last equality holding because the mean passive scalar field vanishes. Note that $F_1(x, y, t) \equiv 1$ and $F_2(x, y, t) = F(x, y, t)$. The values of the flatness factors for a Gaussian distribution is

$$F_N^G = (2N)!/2^N N! .$$

An asymptotic computation for the long-time behavior of the flatness factors yields [51]:

$$F_N(x, y, t) = F_N^G e^{\delta\lambda_N t}[1 + O(A_0\kappa^{-1}k_0^2) + O(e^{-4\pi^2\kappa t})] , \tag{331}$$

with

$$\delta\lambda_N = C_V N(N - 1)A_0^2\kappa^{-1}k_0^4 + O(A_0^3\kappa^{-2}k_0^6)$$

and C_V is a positive numerical constant depending only on the structure of the periodic shear profile $V_r(x)$. For sufficiently small but nonzero k_0, the flatness factors are clearly growing without bound as time progresses, so the passive scalar PDF is approaching a shape with broad algebraic tails.

Initial data of the form (330) also give rise to diverging flatness factors of the scalar PDF in the long-time limit of the Random Uniform Jet model (when the mean shear is weak) (see Section 5.2). There, we could intuitively understand this strong scalar intermittency as arising from an extreme ($\alpha = \infty$) situation in which the passive scalar field is correlated on much smaller scales than the velocity field. This interpretation does not explain the scalar intermittency in the present Random, Spatially Periodic Shear model, because the ratio of the passive scalar length scale k_0^{-1} to the velocity length scale 1 is assumed large! According to our discussion in Section 5.2 as well as the prediction of homogenization theory, we might well have expected the passive scalar statistics to approach a Gaussian distribution when k_0 is taken very small.

The resolution of this seeming paradox is as follows. If we homogenize the passive scalar field by rescaling the initial data $T_0(y) \rightarrow T_0(\varepsilon y)$ and time by $t \rightarrow t/\varepsilon^2$, then the lowest wavenumber of the

initial passive scalar spectrum is decreased as $k_0 \to k_0 \varepsilon$. Formula (331) applies perfectly well as $\varepsilon \to 0$, and with these replacements:

$$\delta \lambda_N(\varepsilon) = C_V N(N-1)\varepsilon^4 A_0^2 \kappa^{-1} k_0^4 + \mathrm{O}(\varepsilon^6 A_0^3 \kappa^{-2} k_0^6) \ .$$

Consequently,

$$\lim_{\varepsilon \to 0} F_N(x, y, t/\varepsilon^2) = \lim_{\varepsilon \to 0} F_N^{\mathrm{G}} \, \mathrm{e}^{\delta \lambda_N(\varepsilon)t/\varepsilon^2}(1 + \mathrm{O}(\varepsilon^2 A_0 \kappa^{-1} k_0^2) + \mathrm{O}(\mathrm{e}^{-4\pi^2 \varepsilon^{-2}\kappa t})) = F_N^{\mathrm{G}} \ .$$

Thus, the homogenized result is indeed consistent with the formula for the flatness factors (331).

The strong qualitative discrepancy between their predictions is due to the fact that homogenized limit *links* the large time with the large space scale of variation of the initial data. In an actual experiment or simulation, however, one is usually interested in *fixing* a large space scale for the initial data, and then looking at the long-time limit. The fact that these limit processes disagree means that the long-time limit does not commute with the limit of large scale spatial variation of the initial data. Homogenization theory studies a *particular* large-scale, long-time limit, which may or may not describe the large-scale, long-time limit of interest in a certain application. We have seen explicitly how the passive scalar statistics may manifest strong and persistent intermittency despite the fact that their homogenized limit is Gaussian.

5.3.3. Non-uniform relaxation to Gaussian PDF for initial data with finite, nonzero intensity of long-wavelength fluctuations

We now present another way in which the long-time statistical behavior of the passive scalar field may differ qualitatively from that predicted by homogenization theory. Suppose the initial, Gaussian, homogenous random passive scalar data has a spectrum $\hat{P}_2^0(k)$ which is smooth and nonvanishing at the origin:

$$P_2^0(y) = \langle T_0(y')T_0(y'+y)\rangle = \int_{\mathbb{R}} \mathrm{e}^{2\pi i k y} \hat{P}_2^0(k) \, \mathrm{d}k \ ,$$

$$\hat{P}_2^0(0) \neq 0 \ .$$

The initial passive scalar data then has fluctuations at arbitrarily large wavelengths, while the velocity field has a fixed period length $L_v = 1$. One may therefore expect that the passive scalar statistics should relax to a Gaussian form in the long-time limit, either by the homogenization result or by letting $k_0 \to 0$ in Eq. (331). A precise calculation shows that indeed, the flatness factors converge to their Gaussian values in the long-time limit:

$$\lim_{t \to \infty} F_N(x, y, t) = F_N^{\mathrm{G}} \ .$$

To examine how rapidly the scalar PDF converges to the asymptotic Gaussian shape in the long-time limit, we keep the leading-order correction [51]:

$$F_N(x, y, t) = F_N^{\mathrm{G}} + \frac{N(N-1)\tilde{C}_V}{\kappa t} + \mathrm{O}(t^{-2}) \ ,$$

where $\tilde{C}_V$ is a positive numerical constant depending on A_0/κ and the periodic velocity field structure $V_r(x)$. (The further $O(t^{-2})$ corrections also depend on the low-wavenumber spectrum of the initial passive scalar data.)

An important observation is that the correction is not uniformly small with respect to the order of the flatness factor N. The time scale needed for $F_N(x, y, t)$ to approach its Gaussian value grows quadratically with the order of the moment N. Thus, at any large but finite time, the low-order flatness factors of the scalar PDF will be close to their Gaussian values, but moments of sufficiently high order ($N \gtrsim \sqrt{\kappa \tilde{C}_V^{-1} t}$) will have significantly super-Gaussian values. Pictorially, this means that the scalar PDF at large times has a Gaussian core with broader-than-Gaussian tails. As time evolves, the broad tails become ever more remote relative to the core, that is, become noticable beginning at an ever-larger number of standard deviations away from the origin. As $t \to \infty$, these broader-than-Gaussian tails get squeezed off to infinity, leaving behind a purely Gaussian limiting distribution. The convergence of the scalar PDF to its homogenized Gaussian limit is thus very nonuniform in the tail regions. This exact result for the present model is consistent with general conclusions drawn by Gao [111] through consideration of a mapping closure approximation to the evolution of the scalar PDF (see Paragraph 5.4.1.1).

We remark that $\tilde{C}_V$ is an increasing, bounded function of the ratio A_0/κ, which characterizes the relative strength of turbulent advection and molecular diffusion, and thus serves as a Péclet number in the Random, Spatially Periodic Shear Model. The finite-time corrections to homogenization theory are thus most evident in this model at high Péclet number.

An instance of slow convergence of higher order flatness factors to their Gaussian values is reported in the direct numerical simulations of Eswaran and Pope [91]. The passive scalar field is initialized as a random field assuming values ± 1 over patches of a specified length scale, and allowed to evolve in a statistically stationary turbulent flow. The second and third order flatness factors $F_2(t)$ and $F_3(t)$ of the scalar PDF relax to their Gaussian values only after 6 to 8 large-scale eddy turnover times, by which point the scalar variance has decayed to a small fraction of its initial value.

5.3.4. Remarks on associated quantum mechanics problem

We close with some brief comments concerning the derivation of the above results. As we showed in Section 5.2.3, the quantum mechanics problems which arise in analysis of the scalar moments $\langle (T(x, y, t))^{2N} \rangle$ in the Random, Spatially Periodic Shear Model involve $2N$ particles and read

$$\frac{\partial \psi_{2N}(\boldsymbol{x}^{()}, \boldsymbol{k}^{()}, t)}{\partial t} = \kappa \Delta_{x^{()}} \psi_{2N}(\boldsymbol{x}^{()}, \boldsymbol{k}^{()}, t) - U_{2N}^{(P)}(\boldsymbol{x}^{()}, \boldsymbol{k}^{()}) \psi_{2N}(\boldsymbol{x}^{()}, \boldsymbol{k}^{()}, t) \ , \tag{332a}$$

$$\psi_{2N}(\boldsymbol{x}^{()}, \boldsymbol{k}^{()}, t = 0) = 1 \ , \tag{332b}$$

with potentials

$$U_N^{(P)}(\boldsymbol{x}^{()}, \boldsymbol{k}^{()}) = 2\pi^2 A_0 \left(\sum_{j=1}^{N} k^{(j)} V_r(x^{(j)}) \right)^2 \ .$$

The solution to the PDE (332) cannot be written in explicit form, as in the Random Uniform Jet model. Instead, one expands $\psi_{2N}(\boldsymbol{x}^{()}, \boldsymbol{k}^{()}, t)$ as a superposition of eigenfunctions of the Schrödinger operators on the right-hand side of Eq. (332a). See [51] for details.

We have been considering above the passive scalar field at large scales at long-times, so the relevant wavenumbers $\boldsymbol{k}^{(\,)}$ are small. The potentials $U_N^{(\mathrm{P})}(\boldsymbol{x}^{(\,)}, \boldsymbol{k}^{(\,)})$ are thus weak, and the eigenfunctions of the Schrödinger operators may be analyzed perturbatively. The exponents $\delta\lambda_N$ describing the extent of scalar intermittency in Eq. (331) arise from a computation of the shifts in the energy of the ground state due to the potential $U_{2N}^{(\mathrm{P})}$ relative to N copies of the potential $U_2^{(\mathrm{P})}$.

One can also study the opposite limit in which the potential becomes very strong (relative to the "kinetic energy" Laplacian term $\kappa\varDelta_{\boldsymbol{x}^{(\,)}}$). In this situation, the particles are well localized near minima of the potential $U_N^{(\mathrm{P})}$, and therefore they effectively feel a quadratic harmonic oscillator potential. One can therefore plausibly replace $U_N^{(\mathrm{P})}$ by a quadratic form obtained by Taylor expansion about the minima; this is known in solid state physics as the "tight-binding approximation" [6]. Two situations in which this tight-binding approximation would be relevant in the Random, Spatially Periodic Shear model are:

- passive scalar initial data with spectrum supported only at wavenumbers $|k| \geq k_0$ as in Eq. (330), but now with $k_0 \gg 1$,
- high Péclet number $\mathrm{Pe} = A_0/\kappa \gg 1$ at times sufficiently short $t \ll (\kappa(1 + \mathrm{Pe}^{-1}))$ so that the passive scalar statistics are still dominated by high-wavenumber fluctuations in the initial data.

The passive scalar statistics under either of these asymptotic conditions ought to at least qualitatively be describable by the Random Uniform Jet model considered above, as the tight-binding approximation results in a quadratic harmonic oscillator potential of the type which arises in that model (see [51] and Section 5.2.3).

5.4. Other theoretical work concerning scalar intermittency

The special structure of the velocity field in the Random Uniform Jet model (Section 5.2) and the Random Spatially Periodic Shear model (Section 5.3) has permitted a detailed and exact analysis of the advected passive scalar statistics, without the need for any ad hoc approximations. These models explicitly elucidate one mechanism by which large-scale scalar intermittency can be created, and indicate some features of a turbulent system which may suppress the intermittency or otherwise influence its nature.

We conclude this section on intermittency by summarizing the main findings of some other recent theoretical studies of non-Gaussian features of the scalar PDF. We first discuss some formal considerations of the passive scalar statistics in a generic turbulent flow, and then turn to the analysis of some discrete, phenomenological, mixing models.

5.4.1. General scalar intermittency considerations

5.4.1.1. Conditional dissipation rate formalism. A main theme in the theoretical investigation of large-scale scalar intermittency has been the variability of the local rate of scalar dissipation. Pope [268] had shown much earlier that, in a statistically spatially homogenous setting, the evolution of the scalar PDF $p_T^{(x,t)}(\rho) = p_T^{(t)}(\rho)$ is described by a PDE:

$$\frac{\partial p_T^{(t)}(\rho)}{\partial t} = -\frac{1}{2}\frac{\partial^2}{\partial\rho^2}(\chi(\rho,t)p_T^{(t)}(\rho)) \, . \tag{333}$$

The only coefficient appearing in this PDE is the *conditional scalar dissipation rate* $\chi(\rho, t) = 2\kappa \langle |\nabla T(\mathbf{x}, t)|^2 | T(\mathbf{x}, t) = \rho \rangle$, which is defined as the statistical average of $2\kappa |\nabla T(\mathbf{x}, t)|^2$, conditioned upon $T(\mathbf{x}, t)$ assuming the particular value ρ. Recall from Paragraph 4.3.1.2 that the full (unconditioned) average $\bar{\chi}(t) = 2\kappa \langle |\nabla T(\mathbf{x}, t)|^2 \rangle$ is the rate at which $\langle (T(\mathbf{x}, t))^2 \rangle$ decays in the absence of external driving.

As discussed previously, the scalar PDF $p_T^{(t)}(\rho)$ can be expected to concentrate at $\rho = 0$ in the long-time limit when the passive scalar field is freely decaying. The *shape* of the PDF in the long-time limit can be studied, however, by normalizing it to zero mean and unit variance. This normalized PDF $p_T^{\sharp(t)}(\rho^\sharp)$ is just the PDF of the quantity

$$T^\sharp(\mathbf{x}, t) = \frac{T(\mathbf{x}, t) - \langle T(\mathbf{x}, t) \rangle}{\langle (T(\mathbf{x}, t))^2 \rangle^{1/2}} \ .$$

Sinai and Yakhot [298] adapted Pope's formalism to describe the evolution of the normalized scalar PDF in terms of the *normalized conditional dissipation rate*

$$\chi^\sharp(\rho^\sharp, t) = \left\langle \frac{2\kappa |\nabla T(\mathbf{x}, t)|^2}{\bar{\chi}(t)} \middle| T^\sharp(\mathbf{x}, t) = \rho^\sharp \right\rangle \ .$$

They furthermore found an explicit solution for the normalized PDF in terms of the normalized conditional dissipation rate in which both are independent of time:

$$p_T^{\sharp(t)}(\rho^\sharp) = C_T \frac{1}{\chi^\sharp(\rho^\sharp)} \exp\left[-\int_0^{\rho^\sharp} \frac{\rho^{\sharp\prime}}{\chi^\sharp(\rho^{\sharp\prime})} \, d\rho^{\sharp\prime} \right] . \tag{334}$$

C_T is a normalization constant. This stationary solution is assumed (without proof) to describe the long-time limiting shape of the one-point PDF of a freely decaying passive scalar field.

If $\chi^\sharp(\rho^\sharp)$ is constant, meaning that the (normalized) local scalar dissipation rate is independent of the (normalized) local value of the passive scalar field, then a Gaussian limiting distribution is indicated. A precise description of the tails of the PDF requires knowledge of the behavior of the normalized conditional scalar dissipation rate $\chi^\sharp(\rho^\sharp)$ for large $\rho^\sharp$, but no useful exact formula for this quantity appears to be available. Sinai and Yakhot suggested a quadratic approximation for $\chi^\sharp(\rho^\sharp)$, which yields *algebraic* tails for the scalar PDF. This is not in agreement with empirical results; see [147] for some discussion.

A more elaborate approximation which permits progress in the conditional dissipation rate formalism is the *mapping closure* procedure developed by Chen et al. [58], wherein the passive scalar field is assumed to be representable as a distortion of a Gaussian random field. Gao [111] finds that within the mapping closure approximation, the conditional dissipation rate $\chi(\rho)$ forever assumes a nontrivial shape with lasting memory of the initial data. Because the passive scalar variance is decaying to zero, however, the *normalized* conditional dissipation rate $\chi^\sharp(\rho^\sharp)$ will approach unity over an interval of $\rho^\sharp$ which expands as $t \to \infty$. Since constancy of the conditional scalar dissipation rate is associated with Gaussianity of the scalar PDF, Gao concludes that the scalar PDF has a Gaussian core with non-Gaussian tails at long-times. The crossover between the Gaussian core and non-Gaussian tails occurs at a *fixed* value of ρ in the *unnormalized* scalar PDF $p_T^{(t)}(\rho)$ but at an ever-increasing value of $\rho^\sharp$ in the *normalized* scalar PDF $p_T^{\sharp(t)}(\rho^\sharp)$. That is, the non-Gaussian features of the PDF are always present, but become increasingly remote relative to

the shrinking variance of the scalar PDF as $t \to \infty$. Therefore, the shape of the scalar PDF does converge to a Gaussian form in the long-time limit, but nonuniformly in the tails. This is consistent with the results reported in Section 5.3.3 for a certain class of initial data in the Random Spatially Periodic Shear model.

5.4.1.2. Lagrangian formalism. In the work described above, departures of the scalar PDF from Gaussianity are attributed to the nonconstancy of the conditional dissipation rate, which appears naturally in some exact formulas and equations (see Eqs. (333) and (334)). This object is a precise measure of the correlation between the local value of the passive scalar field and its gradient, but is quite challenging to model. A more intuitive perspective on how this correlation creates non-Gaussianity of the scalar PDF is set forth by Kimura and Kraichnan [162] through consideration of the history of the scalar field within a Lagrangian fluid element. The value of the scalar field in such a fluid element evolves only through molecular dissipation; advection alone would leave it unchanged. The rate of molecular dissipation in the Lagrangian fluid element depends however, on the local scalar gradient and this *does* depend very strongly on the advection. Regions of strong compressive strain in the flow will build large scalar gradients, and consequently rapid scalar dissipation. Therefore, the value of the scalar field in a Lagrangian fluid element at a time $t > 0$ depends on its initial value and the history of the local fluid straining.

When the scalar field is measured at some given point in the fixed (Eulerian) laboratory frame, one observes the value of the scalar field in the Lagrangian fluid element which happens to be there at the time. If the initial passive scalar field is statistically homogenous (with zero mean), then the originating location of the Lagrangian fluid element is unimportant. Then the measured scalar value will depend only on the initial scalar value (specified by a common PDF) and the strain history of the Lagrangian fluid element which is passing by the probe. The scalar PDF at times $t > 0$ is thus modified from the initial PDF solely because the scalar is dissipated more rapidly in Lagrangian fluid elements in which greater scalar gradients have been generated due to stronger straining by the fluid.

Kimura and Kraichnan illustrate this perspective for a flow in which the velocity field is a spatially uniform straining flow fluctuating randomly in time and the initial scalar data is a homogenous, Gaussian random field. The passive scalar field observed at a given point at later times is shown to be a random mixture of mean zero Gaussian random variables, with variance depending on the realization of the velocity field (or equivalently, the straining history of a fluid element). The scalar PDF is consequently broader-than-Gaussian. We showed in Paragraph 5.2.2.1 through a line of reasoning suggested by Fefferman [101] that this result in fact applies to quite general random flows.

The Lagrangian point of view was utilized by Shraiman and Siggia [295] in their formal approximate analysis of the scalar PDF advected by a single-scale turbulent flow at high Péclet number with a constant mean scalar gradient imposed. Recall from Paragraph 4.3.1.3 that turbulent interaction with a mean scalar gradient provides a means of driving passive scalar fluctuations, so the scalar PDF will settle down at long times to a form with finite variance, in contrast to a freely decaying situation. One might expect scalar intermittency in the presence of a constant mean scalar gradient because the length scale of the scalar fluctuations will be naturally comparable to that of the velocity field. And indeed, Shraiman and Siggia derive exponential tails for the scalar PDF through a representation of the scalar value observed at a given location as

a functional integral over Lagrangian tracer trajectories. The large fluctuations are computed to come predominantly from situations in which a Lagrangian fluid element enjoys an unusually mild strain during its voyage. In particular, the shape of the tails is *not* primarily determined by the most obvious class of events in which a Lagrangian fluid element moves unusually persistently across the scalar gradient, with typical straining along the way (see Section 5.4.2 below). Exponential tails for the scalar PDF in the presence of a constant mean scalar gradient were observed in numerical simulations by Holzer and Siggia [139] in which the two-dimensional velocity field was evolved according to inviscid dynamics truncated to a finite band of Fourier modes.

Another functional integral approach by Falkovich et al. [96] and a Lagrangian formalism based on the analysis of line stretching by Cherktov et al. [65,66] indicate that the scalar PDF exhibits similar exponential tails if the driving of the fluctuations comes from an external, rapidly decorrelating pumping field rather than by turbulent interaction with a background scalar gradient. This conclusion was rigorously established by Bernard et al. [36] for the case in which both the pumping and velocity fields are smooth in space and rapidly decorrelating in time (as in the RDT model described in Section 4.3.1, with Hurst exponent $H = 1$ for the velocity field). Low-strain trajectories are again suggested to be the dominant contributors to the large-scale intermittency of the scalar field [96].

5.4.1.3. Nonlinear mean scalar profiles. Non-Gaussian scalar PDFs can also arise quite simply from Gaussian random initial data when the mean profile is nonlinear or the single-point variance is not constant, as pointed out by Kimura and Kraichnan [162] through theoretical arguments and numerical simulations with a synthetic velocity field. Even without molecular diffusion, the passive scalar value observed at a later time at a given point will in such instances be a mixture of Gaussian random variables with different means and variances, which is not generally Gaussian. One experimental example with a nonlinear initial mean profile is a thermal mixing layer, in which half of the fluid in a wind tunnel is heated to a constant level, with the other half remaining at room temperature. The temperature PDF observed downstream is found to be strongly non-Gaussian at the edges of the evolving turbulent mixing layer [193,203]. Exponential tails have likewise been found in the single-point PDF for the concentration of a dye in jet flow experiments [272].

A situation in which a nonlinear mean scalar profile is imposed through boundary conditions rather than initial data was investigated by Ching and Tu [71] through finite-difference numerical simulations with a single-scale Gaussian random velocity field. They find that both nearly Gaussian and broader-than-Gaussian scalar PDFs can be obtained in the long-time limit, whether the imposed mean scalar profile is linear or nonlinear. They find for all cases considered that the scalar PDF develops broader-than-Gaussian tails at sufficiently high Péclet numbers, in agreement with laboratory experiments [191].

5.4.2. Phenomenological discrete mixing models

As it is difficult to directly analyze the advection–diffusion equation with a general turbulent velocity field model, or to conduct a properly resolved numerical simulation over long-time intervals, some physicists and engineers have invented simplified phenomenological equations for the purposes of studying turbulent diffusion. These phenomenological models seek to capture the essential physics of turbulent advection and molecular diffusion without resolving the full dynamics. Notable among these is the linear eddy model of Kerstein [156]. Though originally developed

for engineering applications, it has been adopted in various forms in the theoretical investigation of large-scale scalar intermittency.

The linear eddy model is formulated on a one-dimensional discrete lattice, imagined to represent a one-dimensional cut through a turbulent flow [156]. Molecular diffusion is implemented directly through a finite-difference discretization of the ordinary diffusion equation, with constant time step. Turbulent advection is represented in the model by random exchanges of the scalar values at different sites. Both the times at which the exchange occurs and the sites affected are prescribed according to a random process with specified mapping structure. A standard numerical implementation of the linear eddy model with a mean scalar gradient imposed produced a scalar PDF with exponential tails [156].

Pumir et al. [277] considered an even simpler phenomenological model in which turbulent mixing is similarly represented by a superposition of a random exchange process and an averaging of neighboring passive scalar values, and showed analytically that exponential tails in the scalar PDF occur in the presence of a mean scalar gradient. Their model was subsequently demonstrated by Holzer and Pumir [138] to be essentially a mean-field approximation to the linear eddy model. These latter authors also formulated a simplified variation of the linear eddy model which can be analytically solved without the need to pass to the mean field limit. Nearly exponential tails in the scalar PDF are again predicted in the presence of a background gradient, and their origin is traced to the Poisson process governing the times at which random exchange events occur in the model. More precisely, the exponential tails of the PDF are associated with events in which a series of random exchanges occur in rapid succession, effectively dragging a parcel of fluid far along the gradient before molecular diffusion has time to equilibrate the associated scalar field to the local value at its new location.

Kerstein and McMurtry [157] introduced another mean field theory of the linear eddy model based on a Langevin approximation, and it again predicts exponential tails in the scalar PDF when a constant mean scalar gradient is present. They also point out that other plausible mean field theories can be constructed which lead to Gaussian tails for the scalar PDF. The exponential tails only come about in the above theories because they are built on the assumption that fluid parcels are transported across the scalar gradient according to a Poisson process. Thus, while these discrete models provide some insight into the nature of turbulent mixing, the mechanism by which they generate scalar intermittency is not general enough to relate directly to real world turbulent diffusion. Indeed, Shraiman and Siggia [295] indicate that scalar intermittency in a continuous turbulent flow is due to events in which Lagrangian fluid elements have a history of low straining. None of the above discrete models account for variability in the strain rate, though Kerstein and McMurtry suggest that its effects can be phenomenologically included in their Langevin mean field theory [157].

Finally, the linear eddy model was used by McMurtry, Gansuage, Kerstein, and Krueger [234] to simulate numerically the statistics of a decaying passive scalar field in statistically stationary turbulence (with no mean scalar gradient imposed). Through appropriate specification of the random exchange events, a high Reynolds number flow with inertial-range scaling properties can be modelled. The flexibility and economy of the linear eddy model permits a study of the effects of both Reynolds number and Schmidt number on the shape of the scalar PDF. It is found that the scalar PDF is not much changed as the model Reynolds number increases beyond 100 (up to 10^4), but that the scalar PDF is very sensitive to variations in the model Schmidt number (over the range $0.1–10^4$).

6. Monte Carlo methods for turbulent diffusion

For the most part, we have been discussing mathematical passive scalar advection models with certain simplifying features which permit exact analysis. These special models play an important role in unambiguously elucidating various fundamental physical aspects of turbulent diffusion. In addressing specific applications and questions concerning complex turbulent flows, however, one wants to investigate tracer transport in a random velocity field model for which exact solutions are not available. It is natural to explore such models through computer simulations.

We discussed simulations of tracer trajectories in deterministic, periodic velocity fields with molecular diffusion in Section 2.3.2. Here we consider in detail the numerical simulation of the motion of tracers in a steady, *random* velocity field $v(x)$. (Examples of numerical simulations of tracers in the opposite extreme of rapidly decorrelating random velocity fields were described earlier in Paragraph 4.2.2.4; also see [108].) A typical problem is the computation of the (absolute) mean-square displacement $\sigma_X^2(t) \equiv \langle |X(t) - x_0|^2 \rangle$ of a tracer, where $X(t)$ is the tracer trajectory and $x_0 = X(t = 0)$. Let us suppose $\kappa = 0$ for simplicity. The statistical average in $\sigma_X^2(t)$ is then an average over the full (usually infinite) ensemble of velocity fields $v(x)$ described by the given statistical model. In a numerical Monte Carlo simulation, this averaging operation is discretized as an average over a finite number N of independent samples generated "pseudo-randomly" using a random number generator on the computational machine [274].

More explicitly, an algorithm for producing a random velocity field $v_{\mathrm{app}}(x)$ is prescribed which approximates $v(x)$ in some statistical sense, but which can be fully described by a finite number of operations involving a finite number of random variables. The N independent realizations $\{v_{\mathrm{app}}^{(j)}\}_{j=1}^N$ of the approximate velocity field are then generated through successive calls to the random number generator. In each of these realizations of the velocity field, the equations of motion for the tracer particle,

$$\mathrm{d}X^{(j)}(t) = v_{\mathrm{app}}^{(j)}(X^{(j)}(t), t)\,\mathrm{d}t , \tag{335}$$

are solved numerically. Finally, a numerical approximation to the mean-square displacement of the tracer as a function of time is obtained by averaging over the finite sample size generated:

$$\sigma_{X,\mathrm{app}}^2(t) = \frac{1}{N} \sum_{j=1}^N |X^{(j)}(t) - x_0|^2 .$$

By the Law of Large Numbers ([102], Ch. 10), $\sigma_{X,\mathrm{app}}^2(t)$ will approximate $\sigma_X^2(t)$ if N is sufficiently large and the discretized random velocity field $v_{\mathrm{app}}(x)$ is a sufficiently accurate approximation to the true velocity field $v(x)$. In principle, the Monte Carlo approach can be used in a similar way to compute numerical approximations to the statistical average of any functional of the particle trajectory.

One can account for the effects of molecular diffusion through the addition of a stochastic term $\sqrt{2\kappa}\,\mathrm{d}W(t)$ to the trajectory equation (335). This requires the generation of additional random variables at each time step, but its treatment is straightforward because this effect has a constant coefficient [163]. To keep focus on the more demanding main issues involving the simulation of the random velocity field, we will ignore molecular diffusion ($\kappa = 0$) for the duration of Section 6. The interested reader can consult Section 2.3.2 for Monte Carlo simulations with periodic velocity fields and $\kappa > 0$.

Overview of Section 6: We begin in Section 6.1 with a brief summary of general accuracy considerations in Monte Carlo simulations. Then, in Section 6.2, we consider a class of three Monte Carlo methods for generating general Gaussian, homogenous, random fields. We assess their utility for turbulent diffusion studies by applying them to the exactly solvable Random Steady Shear (RSS) Model [141], which we discussed in Section 3.2. This model includes flows leading to a wide variety of statistical tracer motion, and thereby provides a simple test for the performance of the Monte Carlo methods in simulating turbulent diffusion under various conditions. Comparison of the numerical simulations with the exact results illustrates certain strengths and inherent limitations of the methods, particularly in properly simulating long-range correlations in the random shear velocity field.

Next, we turn to the numerical simulation of turbulent diffusion in random velocity fields with a statistical self-similarity characteristic of the inertial range of scales of a turbulent flow. We continue in Section 6.3 to consider steady shear flows so that the velocity field is still specified by a random scalar function $v(x)$. We seek to simulate a mean zero, Gaussian random field $v(x)$ which has an inertial-range scaling law:

$$\langle (v(x') - v(x))^2 \rangle = S_v^I |x - x'|^{2H}, \tag{336}$$

with $0 < H < 1$ and a constant prefactor S_v^I, over a wide range of scales. To simulate the wide range of active scales of such a random velocity field efficiently, it is natural to formulate *hierarchical* Monte Carlo schemes in which the random velocity field is expressed as a superposition of independently generated random fields varying on different length scales. We first examine one popular hierarchical simulation method, Successive Random Addition [336], and cite results from a rigorous demonstration [87] that this method is fundamentally incapable of simulating a stationary random field obeying the self-similar scaling (336) with any quantitative accuracy. We next describe a pair of hierarchical Monte Carlo methods using wavelets, introduced by Elliott, Horntrop, and the first author [82,84], which have been shown to be capable of generating a random field $v(x)$ with accurate self-similar scaling (336) over 12 decades of scales. By contrast, previous simulations using (variations of) the nonhierarchical Monte Carlo methods discussed in Section 6.2 have only achieved one to two decades of inertial-range scaling behavior. Moreover, the wavelet-based Monte Carlo methods have low variance (see Section 6.1); 100–1000 sample realizations are sufficient for statistical averages to be computed within a few percent error. We compare the wavelet-based Monte Carlo methods with the Randomization Method, the non-hierarchical Monte Carlo method with the greatest capacity for simulating velocity fields with an extended inertial range, and demonstrate their quantitative accuracy in simulating tracer transport on an exactly solvable model problem.

In Section 6.4, we describe a general method of approximating any statistically isotropic, incompressible, multi-dimensional Gaussian random velocity field as a superposition of Gaussian homogenous random shear flows [85]. In this way, any of the Monte Carlo methods for simulating scalar random fields can be used to simulate statistically isotropic multi-dimensional vector fields as well. We show that this technique can be used with the wavelet-based Monte Carlo methods discussed in Section 6.3 to generate a statistically isotropic, incompressible, two-dimensional Gaussian random velocity field with an inertial range extending over twelve decades of scales.

In Section 6.5, we study tracer pair dispersion in two-dimensional synthetic turbulent velocity fields generated in this manner. Temporal dynamics are induced by sweeping the frozen random

field past the laboratory frame at a constant speed, corresponding to the picture underlying Taylor's hypothesis ([320], p. 253). The mean-square separation between a pair of tracers as it evolves through the inertial range of this synthetic turbulent velocity field is found to obey the classical Richardson's t^3 law

$$\sigma_{\Delta X}^2(t) \equiv \langle |X^{(1)}(t) - X^{(2)}(t)|^2 \rangle \sim t^3$$

over eight decades of spatial scales. We relate these numerical results to experimental findings, other numerical simulations, and some theoretical work.

6.1. General accuracy considerations in Monte Carlo simulations

An examination of the error in the numerically evaluated Monte Carlo average brings out two main practical accuracy concerns in a Monte Carlo simulation. For specificity, we focus on the mean-square tracer displacement $\sigma_X^2(t)$, though these considerations are completely general. The discrepancy between the numerically computed Monte Carlo approximation $\sigma_{X,\mathrm{app}}^2(t)$ and the true $\sigma_X^2(t)$ can be expressed as a sum of:

- a *systematic* error (bias) due to numerical discretization of the velocity field and the trajectory equations, and
- a random *sampling* error because $\sigma_{X,\mathrm{app}}^2(t)$ is computed using a finite number of samples.

Mathematically, let

$$\sigma_{X,\mathrm{app},N=\infty}^2(t) \equiv \langle (X_{\mathrm{app}}(t) - x_0)^2 \rangle_{v_{\mathrm{app}}}$$

be the mean-square tracer displacement as would be computed (in principle) by a complete averaging over all the random variables appearing in the discrete *numerical* approximation $v_{\mathrm{app}}(x)$ of the velocity field. Then we can write the error in the numerical computation of $\sigma_X^2(t)$ as

$$\sigma_X^2(t) - \sigma_{X,\mathrm{app}}^2(t) = E_{\mathrm{sys}}(t) + E_{\mathrm{samp}}(t) \,,$$

$$E_{\mathrm{sys}}(t) = \sigma_X^2(t) - \sigma_{X,\mathrm{app},N=\infty}(t) \,,$$

$$E_{\mathrm{samp}}(t) = \sigma_{X,\mathrm{app},N=\infty}^2(t) - \sigma_{X,\mathrm{app}}^2(t) \,,$$

where $E_{\mathrm{sys}}(t)$ is a deterministic, systematic error, and $E_{\mathrm{samp}}(t)$ is a purely random sampling error. There are two sources of the systematic error $E_{\mathrm{sys}}(t)$:

- the difference between the statistics of the true velocity field $v(x)$ and the numerically specified random velocity field $v_{\mathrm{app}}(x)$ involving only a finite number of random variables, and
- the discretization error in the numerical integration of the tracer trajectories.

The accurate and efficient numerical integration of the tracer trajectory equations (335) requires a suitable (sometimes adaptive) choice of time step. We will not dwell on this technical but important issue here; see [84,86,140] for explicit examples of the kind of considerations involved, particularly when several particles are being simultaneously tracked. We will concentrate here on the issues pertaining to the simulation of the random velocity field $v(x)$. To minimize the systematic error in the numerical approximation of the velocity field, the probability law of $v_{\mathrm{app}}(x)$ should be close in some sense to that of $v(x)$ [163]. For example, the mean and correlation tensor of $v_{\mathrm{app}}(x)$

should approximate that of $v(x)$. If $v(x)$ is a Gaussian random field, then it is often desirable for $v_{app}(x)$ also to be a Gaussian random field.

The random sampling error $E_{samp}(t)$ arises solely because the mean-square tracer displacement is numerically computed using only a finite number of realizations. It has mean zero with respect to the statistics of the numerical scheme, $\langle E_{samp}(t)\rangle_{v_{app}} = 0$, and its variance may be computed as

$$\langle (E_{samp}(t))^2\rangle_{v_{app}} = \left\langle \left(\frac{\sum_{j=1}^{N}|X_{app}^{(j)}(t) - x_0|^2}{N} - \langle |X_{app}(t) - x_0|^2\rangle_{v_{app}}\right)^2\right\rangle = \frac{1}{N}\Sigma^2(|X_{app}(t) - x_0|^2)\ ,$$

where

$$\Sigma^2(|X_{app}(t) - x_0|^2) \equiv \langle(|X_{app}(t) - x_0|^2 - \sigma_{X,app,N=\infty}^2(t))^2\rangle_{v_{app}}$$

is just the variance of the numerical quantity $|X_{app}(t) - x_0|^2$ whose Monte Carlo average we are seeking. The random sampling error therefore decreases as the sample size becomes larger, but at the relatively slow rate $E_{samp}(t) \sim N^{-1/2}$. Typically, the sample size is restricted to moderate values (say, a few thousand or million in turbulent diffusion applications), due to computational cost. Therefore, one would like to minimize $\Sigma^2(|X_{app}(t) - x_0|^2)$ to reduce sampling error. This quantity must perforce be at least on the order of the variance of the true random variable $|X(t) - x_0|^2$ whose mean we are trying to estimate. The practical numerical issue is to avoid numerical approximation schemes which add on a lot of extra variability and lead to excessively large values of the variance, $\Sigma^2(|X_{app}(t) - x_0|^2)$. An intuitive rule of thumb for designing a low variance Monte Carlo method is that each individual realization generated by the numerical scheme should have "typical" properties of the true random velocity field $v(x)$.

We will now proceed to examine various Monte Carlo methods for turbulent diffusion with the above considerations in mind.

6.2. Nonhierarchical Monte Carlo methods

A simple context in which to discuss numerical Monte Carlo methods for turbulent diffusion is the class of steady, two-dimensional shear flows with constant cross sweep $\bar{\omega}$:

$$v(x, t) = v(x, y, t) = \begin{bmatrix} \bar{w} \\ v(x) \end{bmatrix}.$$

Then the numerical simulation of the velocity field reduces to the generation of $v(x)$, a scalar random field of a single variable, which we will further assume to be Gaussian and statistically homogenous, with mean zero and correlation function

$$\langle v(x')v(x' + x)\rangle = R(x)\ .$$

In Section 3.2, we discussed a particular one-parameter family of such flows as part of the Random Steady Shear (RSS) Model [141]. The elements of this model have a simple structure, the mean-square displacement of a tracer in these flows can be expressed by exact analytical formulas, and the tracer motion exhibits a wide variety of anomalous scaling behavior. These three properties make this model an excellent means of assessing the performance of numerical approximation schemes for turbulent diffusion. For convenience, we recapitulate in Section 6.2.1 the definition of

the Random Steady Shear (RSS) Model and the exact formulas for the mean-square displacement of a tracer advected by such flows [141]. We state the numerical values of the parameters used in the Monte Carlo simulations of this model in Paragraph 6.2.1.1.

Several numerical procedures for generating a Gaussian, homogenous random field are directly suggested by two general expressions of the random field in terms of stochastic integrals. We have already encountered the Fourier stochastic integral representation

$$v(x) = \int_{-\infty}^{\infty} e^{-2\pi i k x} E^{1/2}(|k|) \, d\tilde{W}(k) \tag{337}$$

in Paragraph 3.2.2.1. The integration measure $d\tilde{W}(k)$ is a complex Gaussian white noise with the formal properties:

$$d\tilde{W}(-k) = \overline{d\tilde{W}(k)} \,,$$
$$\langle d\tilde{W}(k) \rangle = 0 \,, \tag{338}$$
$$\langle d\tilde{W}(k) \, d\tilde{W}(k') \rangle = \delta(k + k') \, dk \, dk' \,,$$

where an overbar denotes complex conjugation. The integrand $E(k)$ is the energy spectrum of the velocity field:

$$R(x) = \int_{-\infty}^{\infty} e^{-2\pi i k x} E(|k|) \, dk = 2 \int_{0}^{\infty} \cos(2\pi k x) E(k) \, dk \,. \tag{339}$$

The Fourier stochastic integral (337) formally represents the random field as a superposition of independent random fluctuations of various wavenumbers, with the amplitude of each fluctuation proportional to the square root of the energy spectral density at its wavenumber.

One way of numerically simulating the random field $v(x)$ is to truncate this stochastic integral to a finite interval, and discretize it according to a midpoint rule with equispaced grid points. The random field $v(x)$ is thereby expressed as a discrete Fourier transform of a finite set of Gaussian random variables. This direct algorithm, which has been used by Viecelli and Canfield [335] and Voss [336] in the generation of fractal random fields, will be called the (standard) *Fourier Method*. It will be discussed in Section 6.2.2. Variations of this scheme have been adopted by Kraichnan [180] and by Sabelfeld and coworkers [190,240,291], in which the grid points of the discretization of the stochastic integral (337) are chosen *randomly* according to some appropriate probability distribution. We shall refer to the strategy of Sabelfeld's group as the *Randomization Method*, and discuss it in Section 6.2.3.

Another explicit expression for the random field $v(x)$ is given in terms of a physical-space stochastic integral ([341], Section 26.2):

$$v(x) = \int_{-\infty}^{\infty} G(x - r) \, dW(r) = \int_{-\infty}^{\infty} G(r) \, dW(x - r) \,. \tag{340}$$

The integration measure $dW(\cdot)$ is now a real white noise measure, with formal properties:

$$\langle dW(r) \rangle = 0 \,,$$
$$\langle dW(r) \, dW(r') \rangle = \delta(r - r') \, dr \, dr' \,. \tag{341}$$

This white noise is convolved against the function $G(x)$, which is proportional to the inverse Fourier transform of the square root of the energy spectrum:

$$G(x) = \int_{-\infty}^{\infty} e^{-2\pi ikx} E^{1/2}(|k|)\, dk = 2 \int_{0}^{\infty} \cos(2\pi kx) E^{1/2}(k)\, dk \ . \tag{342}$$

The function $G(x)$ provides another real-space description of the spatial correlations of the random field $v(x)$ in addition to the standard correlation function $R(x)$. Like $R(x)$, the function $G(x)$ is even, assumes its maximal value at $x = 0$, and generally decays for large x. The stochastic integral expression (340) represents the random field as a local average of an underlying white noise field on the same physical-space domain. One can intuitively imagine laying down a random white noise field on the real-space domain $\mathbb{R}$, and then computing the random field $v(\cdot)$ at a given point x by summing up the values of the white noise field with weights specified by the value of the function G centered at x. The value of the random field $v(\cdot)$ at any other point x' is obtained by simply moving the weighting function G so that it is centered at x', and then summing as before. For this reason, the real-space expression (340) is often called a "moving-average" representation. Note that the averaging procedure produces nontrivial correlations in $v(\cdot)$ starting from the uncorrelated field $dW(\cdot)$ because the evaluation of $v(\cdot)$ at different points involves the same random values of $dW(\cdot)$; the weighting function is simply centered at different locations.

In a manner parallel to that of the Fourier Method, the real-space stochastic integral expression (340) can be implemented numerically through a straightforward truncation of the integration domain and a midpoint-rule discretization with equispaced grid points. This physical-space based method for simulating the random velocity field will be called the *Moving Average Method*. It was first studied in the thesis of McCoy [228], and we shall treat it in Section 6.2.4. There is no sensible analogue of the Randomization Method in physical space.

For each of the three Monte Carlo methods we have mentioned, the Fourier Method, the Randomization Method, and the Moving Average Method, we will first give some details about their implementation. Then we will discuss their performance for the family of Random Steady Shear Model flows summarized in Section 6.2.1. In this fashion, we will uncover certain inherent numerical artifacts of these methods, and obtain some understanding of circumstances in which they may be expected to perform well or not so well. We find, in particular, that the built-in periodicity of the direct Fourier Method creates strong systematic errors after a certain time (Section 6.2.2). The Randomization Method cures this periodicity problem, and performs quite well when the velocity field has strong, positive long-range correlations so that the tracer's motion is diffusive or super-diffusive. It suffers the drawback, however, that the simulated velocity field can be substantially non-Gaussian. Also, the Randomization Method does not perform as well in the class of test models for which the correlation function of the velocity field has slowly decaying negative tails and the tracer motion is sub-diffusive (Section 6.2.3). In contrast, the Moving Average Method can simulate sub-diffusive and diffusive tracer motion reasonably efficiently, but cannot accurately represent super-diffusive tracer motion because of an intrinsic shortcoming in handling strong long-range correlations in the velocity field (Section 6.2.4). The numerical studies discussed here were originally reported in the thesis of Horntrop [140] and in a paper by Elliott et al. [83].

Each of the methods discussed above can be extended directly to simulate a multi-dimensional, vectorial velocity field by discretizing vector-valued versions ([341], Sections 20–22) of the stochastic integral representations (337) and (340). We will discuss a multi-dimensional version of the Randomization Method in Section 6.4, and will find better results from a less direct multi-dimensional implementation! The methods presented here are also capable, in principle, of simulating non-Gaussian random fields. The stochastic integral representations of the random fields would then involve non-Gaussian random measures $d\tilde{Z}(k)$ and $dZ(r)$ in place of the white noise measures $d\tilde{W}(k)$ and $dW(r)$ ([341], Section 8). Of course, the non-Gaussian random variables in the discretized sums would have to be simulated in some fashion. Here we will restrict our attention to the simulation of Gaussian random fields.

6.2.1. Exact formulas for mean-square tracer displacement in Random Steady Shear Model

In our evaluation of Monte Carlo methods for turbulent diffusion, we will use a specific family of Random Steady Shear (RSS) Model flows with constant cross sweep, which was discussed in detail in Section 3.2.2 and the original paper [141]. The velocity field in this model is a steady, two-dimensional shear flow:

$$\boldsymbol{v}(\boldsymbol{x}, t) = \boldsymbol{v}(x, y, t) = \begin{bmatrix} \bar{w} \\ v(x) \end{bmatrix},$$

where $\bar{w} \neq 0$ and $v(x)$ is a mean zero, Gaussian random field with correlation function

$$R(x) = \langle v(x')v(x + x') \rangle .$$

We now define a special, explicit one-parameter family of correlation functions in terms of their energy spectra:

$$R(x) = \int_{-\infty}^{\infty} e^{-2\pi i k x} E(|k|) \, dk = 2 \int_{0}^{\infty} \cos(2\pi k x) E(k) \, dk , \tag{343a}$$

$$E(k) = (2\pi)^{2-\varepsilon} A_E k^{1-\varepsilon} e^{-2\pi L_K k}, \quad -\infty < \varepsilon < 2 , \tag{343b}$$

where ε is the infrared scaling exponent, A_E is a constant amplitude, and L_K is a dissipation length scale defining the ultraviolet cutoff of the power law scaling at high wavenumber (small spatial scales). The special choice of ultraviolet cutoff made in Eq. (343b) permits the following closed-form expression for the correlation functions [141]:

$$R(x) = 2\Gamma(2-\varepsilon) A_E (L_K^2 + x^2)^{(\varepsilon/2)-1} \cos\left((2-\varepsilon) \arctan\left(\frac{|x|}{L_K} \right) \right) .$$

The form of the correlation function $R(x)$ in the RSS Model for various values of the infrared scaling exponent ε is shown in Fig. 20. A successful Monte Carlo method must generate a velocity field which closely reproduces the correct correlation function, because the mean-square displacement of a tracer particle along the shear $\sigma_Y^2(t) = \langle (Y(t) - y_0)^2 \rangle$ at long times involves an integration of $R(x)$ over a large interval (137):

$$\sigma_Y^2(t) = 2 \int_{0}^{t} (t - s) R(\bar{w}s) \, ds . \tag{344}$$
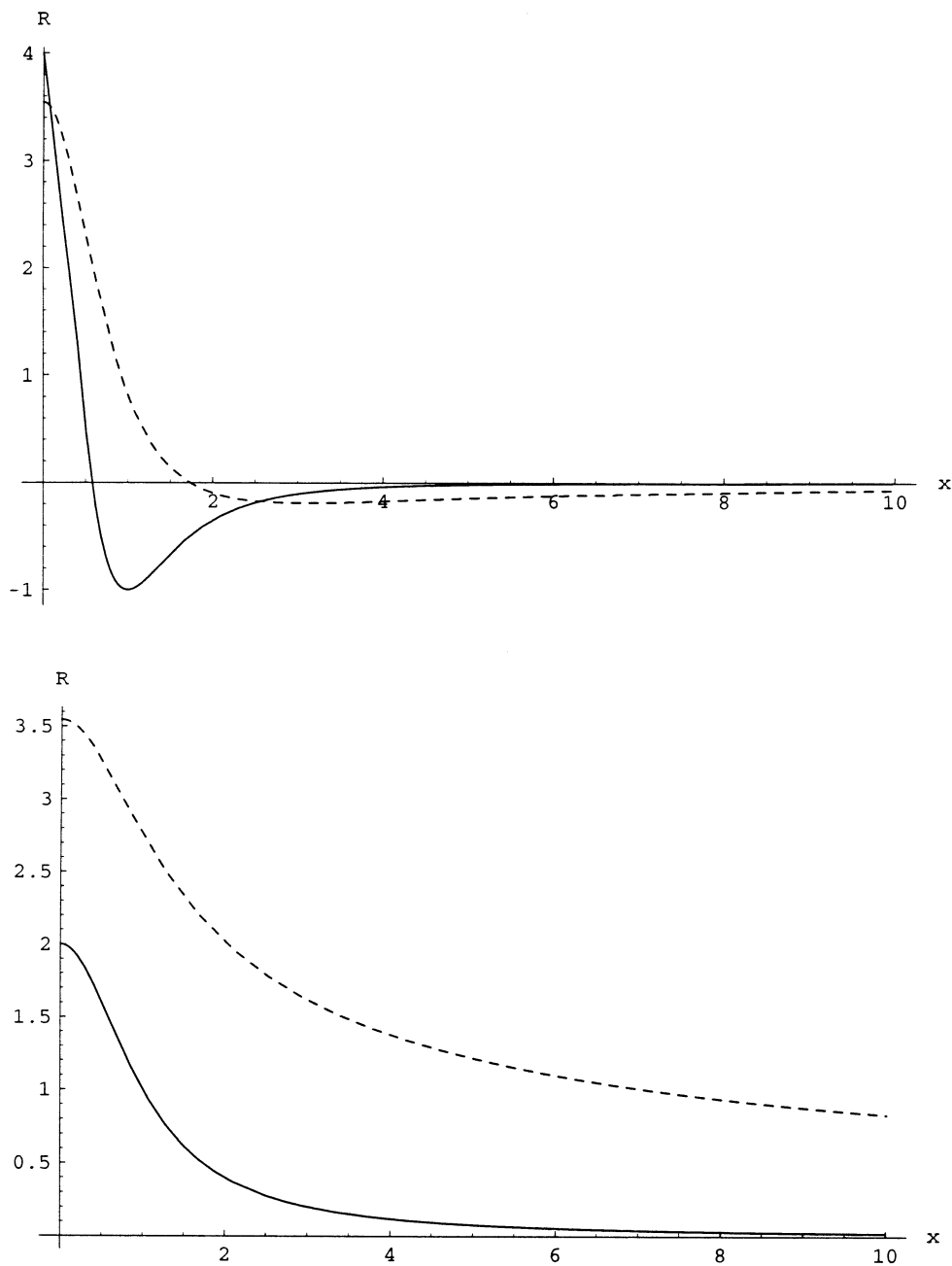
Fig. 20. Plots of the velocity correlation function for the Random Steady Shear (RSS) Model for various values of ε (from [83]). Upper graph: $\varepsilon = -1$ (solid line) and $\varepsilon = \frac{1}{2}$ (dashed line). Lower graph: $\varepsilon = 1$ (solid line) and $\varepsilon = \frac{3}{2}$ (dashed line).

Table 15
Summary of long-time scaling behavior for the mean-square tracer displacement in Random Steady Shear (RSS) Model, with $\bar{w} \neq 0$ and $\kappa = 0$

Parameter regime	Mean square displacement	Qualitative behavior
$\varepsilon < 0$	$\sigma_Y^2(t) \sim t^0$	Trapping
$0 < \varepsilon < 1$	$\sigma_Y^2(t) \sim t^\varepsilon$	Sub-diffusive
$\varepsilon = 1$	$\sigma_Y^2(t) \sim t$	Diffusive
$1 < \varepsilon < 2$	$\sigma_Y^2(t) \sim t^\varepsilon$	Super-diffusive

Two features of $R(x)$ in the RSS Model present challenges to numerical modelling in this regard. First, for $\varepsilon < 1$, the correlation function $R(x)$ has negative tails which decay only algebraically for large $|x|$. Secondly, as $\varepsilon \nearrow 2$, the tails of the correlation function are positive but decay ever more slowly ($R(x) \sim |x|^{\varepsilon-2}$ for $|x| \gg L_K$), reflecting the strong long-range correlations in the velocity field. The RSS Model therefore tests the capacity of Monte Carlo methods to simulate negative correlations and long-range correlations of a random field.

The exact solutions for the mean-square displacement $\sigma_Y^2(t)$ of a tracer in the various RSS Model flows were worked out in Section 3.2 and [141], and we will use these in graphical comparisons with the numerically simulated mean-square tracer displacement. For the purposes of our general discussion, we simply remind the reader in Table 15 of the long-time scaling behavior of $\sigma_Y^2(t)$ for various values of the infrared scaling exponent ε, when the cross sweep is nonzero $\bar{w} \neq 0$ and molecular diffusion is absent $\kappa = 0$. Note the wide range of long-time behavior assumed by the tracer in the RSS Model as the parameter ε is varied. The reason we do not include molecular diffusion is that it would override the sub-diffusive and trapping behavior of the RSS flows for $\varepsilon < 1$. For $\kappa = 0$, the RSS Model can test how faithfully Monte Carlo methods replicate both sub-diffusive and super-diffusive tracer motion.

6.2.1.1. Numerical parameter values in Monte Carlo simulations. In the numerical simulations, the tracer is always started at the origin $(x_0, y_0) = (0, 0)$, and space and time are nondimensionalized so that $L_K = 1$ and $\bar{w} = 1$. The tracer displacement along the shear:

$$Y(t) = \int_0^t v(\bar{w}s)\, \mathrm{d}s$$

is computed in every realization according to a trapezoidal rule with time step sufficiently small ($\Delta t = 0.1$) to resolve the fluctuations in the simulated velocity field $v_{\mathrm{app}}(x)$. The value of $\sigma_Y^2(t) = \langle Y^2(t) \rangle$ is then obtained by averaging over a large number of independent simulations of the velocity field. It has been checked [140] that the error due to the finite time step in the integration of the trajectories is negligibly small relative to the errors arising from the finite sample size in the Monte Carlo average and discrepancies between the statistics of the simulated velocity field $v_{\mathrm{app}}(x)$ and of the true velocity field $v(x)$.

6.2.2. Fourier space-based method

We shall now define the Fourier Method in more detail, and apply it to the RSS Model. We will find inherent limitations of the method in simulating turbulent diffusion [83,140].

6.2.2.1. Derivation of Fourier method. We shall provide two simple derivations of the basic simulation formula for the Fourier Method. One is a direct discretization of the stochastic Fourier integral representation of the random field $v(x)$. The second circumvents the stochastic integral representation, and provides a useful framework for comparing the underpinnings of the Fourier Method with those of the Randomization Method to be discussed in Section 6.2.3.

Discretization of stochastic Fourier integral. A natural means of obtaining numerical schemes is through the truncation and discretization of exact continuum formulas. We apply this approach to the stochastic Fourier integral representation (337)

$$v(x) = \int_{-\infty}^{\infty} e^{-2\pi i k x} E^{1/2}(|k|) \, d\tilde{W}(k)$$

by a Riemann sum approximation over a finite symmetric partition of $2M + 1$ intervals, with equal widths Δk. This partition extends over a finite segment $[-k_{max}, k_{max}]$, with $k_{max} = (M + \frac{1}{2})\Delta k$. Evaluating the integrand at the midpoint of the intervals, we arrive at the following random Riemann–Stieltjes sum for the approximating velocity field:

$$v_{app}(x) = \sum_{j=-M}^{M} e^{-2\pi i j \Delta k x} E^{1/2}(|j|\Delta k)\Delta\tilde{W}_j \,, \tag{345}$$

where the complex random variables $\Delta\tilde{W}_j(k)$ are defined in terms of the complex white noise process:

$$\Delta\tilde{W}_j(k) = \int_{j-\Delta k/2}^{j+\Delta k/2} d\tilde{W}(k) \,.$$

From the formal rules (338) for the statistics of the white noise process, we find that $\{\Delta\tilde{W}_j\}_{j=1}^{M}$ are statistically independent complex Gaussian random variables with the properties:

$$\Delta\tilde{W}_j = \overline{\Delta\tilde{W}_j}, \quad \langle\Delta\tilde{W}_j\rangle = 0, \quad \langle(\Delta\tilde{W}_j)^2\rangle = 0, \quad \langle\Delta\tilde{W}_j\Delta\tilde{W}_j\rangle = \Delta k \,.$$

Also, $\Delta\tilde{W}_0$ is independent of all these variables, and is itself a mean zero, real Gaussian random variable with variance Δk. We can therefore rewrite Eq. (345) as

$$v_{app}(x) = E^{1/2}(0)\Delta\tilde{W}_0 + 2\operatorname{Re}\sum_{j=1}^{M} E^{1/2}(|j|\Delta k)e^{-2\pi i j \Delta k x}\Delta\tilde{W}_j \,,$$

where Re denotes the real part of the following expression. Expanding the complex random variable $\Delta\tilde{W}_j$ into real and imaginary parts, we obtain a concise expression for the approximate velocity field as a discrete random sum of real Fourier modes.

We will call its numerical implementation the *Fourier Method*. The approximate velocity field is written:

$$v_{Four}(x) = \sum_{j=0}^{M} \sqrt{2E(k_j)\Delta k_j}[\xi_j\cos(2\pi k_j x) + \eta_j\sin(2\pi k_j x)] \,, \tag{346}$$

where the wavevectors $k_j = j\Delta k$ denote the locations of the equispaced grid points, and $\Delta k_j = \Delta k$ for $j = 1, \ldots, M$ and $\Delta k_0 = \frac{1}{2}\Delta k$. The $\{\xi_j, \eta_j\}_{j=0}^{M}$ are a collection of independent standard Gaussian random variables (mean zero and unit variance). (If $E(k)$ diverges at $k = 0$, as for the RSS Models with $1 < \varepsilon < 2$, then the $j = 0$ term requires some special treatment.)

The equal spacing of the grid points permits a rapid passage from the set of random Fourier coefficients to the random values of $v_{app}(x)$ on the (equi-spaced) physical space grid through the Fast Fourier Transform ([50], Ch. 18). The Gaussian random coefficients can be simulated by applying a Box–Muller transformation ([163], Section 1.3) to uniformly distributed random variables on the unit interval, which can be supplied by standard computer random number generators.

The Fourier Method with equispaced grid points has been utilized by Voss [336] in the production of fractal sceneries and by Viecelli and Canfield [335] in the simulation of a fully developed turbulent velocity field with about one decade of an inertial range.

An important numerical feature of the Fourier Method is that the simulated random velocity field is periodic with period $(\Delta k)^{-1}$ in every realization. The true velocity field $v(x)$, however, has no such periodicity when the spectrum $E(k)$ is continuous.

Derivation by random Fourier sum ansatz. We now offer another means of arriving at the simulation formula (346) for the Fourier Method which has enough flexibility to yield the simulation formula for the Randomization Method as well. Rather than proceeding deductively from the stochastic Fourier integral representation for the random field $v(x)$, we simply declare that we will seek a finite spectral approximation. We begin by cutting off Fourier space to a finite segment $[0, k_{max}]$, and partitioning this segment into $M + 1$ disjoint intervals, which need not be of equal width (see Fig. 21). We define $k_0 = 0$ and Δk_0 as the width of the interval abutting this point, and take $\{k_j\}_{j=1}^{M}$ as the midpoints and Δk_j as the widths of the remaining intervals comprising the partition, ordered from left to right. We think of k_j as a representative wavenumber from its interval of wavenumber space. We then form a Fourier sum with these wavenumbers:

$$v_{app}(x) = \sum_{j=0}^{M} a_j \cos(2\pi k_j x) + b_j \sin(2\pi k_j x) , \qquad (347)$$

with real, random coefficients $\{a_j\}_{j=0}^{M}$ and $\{b_j\}_{j=0}^{M}$. We wish to choose the probability distribution of these random variables so that $v_{app}(x)$ approximates the random field $v(x)$.

First, $v_{app}(x)$ should be a Gaussian, homogenous random field with mean zero. The fact that linear combinations of mean zero Gaussian random variables are mean zero and Gaussian suggests that $\{a_j, b_j\}_{j=0}^{M}$ should be taken according to a jointly Gaussian distribution with zero mean. By substituting the right-hand side of Eq. (347) into $\langle v_{app}(x')v_{app}(x' + x)\rangle$, and noting that this expression must be independent of x' by statistical homogeneity, we find that the random
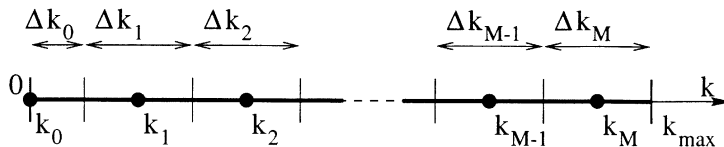
Fig. 21. Partition of a finite segment $[0, k_{max}]$ of Fourier space into $M + 1$ intervals in the Fourier Method.

variables $\{a_j, b_j\}_{j=0}^M$ must all be mutually independent of one another, and that $\langle a_j^2 \rangle = \langle b_j^2 \rangle \equiv v_j^2$ for $0 \leq j \leq M$. We therefore express our random Fourier sum as:

$$v_{\text{app}}(x) = \sum_{j=0}^M v_j [\xi_j \cos(2\pi k_j x) + \eta_j \sin(2\pi k_j x)] , \tag{348}$$

where $\{\xi_j, \eta_j\}_{j=0}^M$ is a collection of independent, standard Gaussian random variables, and $\{v_j\}_{j=0}^M$ are constant amplitudes which we are left to choose.

We pick these amplitudes by requiring that the correlation function

$$R_{\text{app}}(x) = \langle v_{\text{app}}(x') v_{\text{app}}(x' + x) \rangle$$

of $v_{\text{app}}(x)$ approximates the true correlation function (339):

$$R(x) = \langle v(x') v(x' + x) \rangle = 2 \int_0^\infty \cos(2\pi k x) E(k) \, dk . \tag{349}$$

Expanding the double sum and computing the averages in $R_{\text{app}}(x)$, we find that the correlation function of the approximate random field $v_{\text{app}}(x)$ is

$$R_{\text{app}}(x) = \sum_{j=0}^M v_j^2 [\cos(2\pi k_j x') \cos(2\pi k_j (x + x')) + \sin(2\pi k_j x') \sin(2\pi k_j (x + x'))]$$

$$= \sum_{j=0}^M v_j^2 \cos(2\pi k_j x) . \tag{350}$$

A discrete sum of this form can be obtained by a Riemann sum approximation of the integral on the right-hand side of Eq. (349), using the partition defined in Fig. 21:

$$R_{\text{app}}(x) = \sum_{j=0}^M 2 E(k_j) \Delta k_j \cos(2\pi k_j x) . \tag{351}$$

Note that we have implicitly dropped the contribution of the integral from $k \geq k_{\text{max}}$, but this should not be a serious matter if the energy spectrum $E(k)$ decays rapidly for large k and k_{max} is chosen sufficiently large. Upon comparison with Eq. (350), we find that

$$v_j = (2E(k_j) \Delta k_j)^{1/2}$$

will make $v_{\text{app}}(x)$ a consistent approximation to the random field $v(x)$. We arrive therefore at exactly the same Fourier Method simulation formula (346) as before, but the wavenumbers $\{k_j\}_{j=0}^M$ need not be equispaced.

We note from Eqs. (349) and (350) that the energy spectrum of the velocity field simulated by the Fourier Method is the following discrete approximation:

$$E_{\text{app}}(k) = \sum_{j=0}^M E(k_j) \Delta k_j \delta(k - k_j) \tag{352}$$

to the continuous energy spectrum $E(k)$.

There are at least two reasons one might want to choose unequally spaced wavenumbers, even though one thereby loses the possibility of using the fast Fourier transform. First, when the wavenumbers in the discrete sum are equispaced, then all the random Fourier modes are harmonically aligned, and the simulated random field will be exactly periodic (with period k_1^{-1}). This can have undesirable consequences, as we shall explicitly see in the RSS Model application below. Secondly, one may wish to refine the partition of wavenumber space near regions of large values or rapid variation of $E(k)$. In particular, for the RSS Model with $1 < \varepsilon < 2$, $E(k)$ diverges at $k = 0$, and one might want to place extra points near $k = 0$ to improve the accuracy of the simulated velocity field at large scales. In Section 6.2.3 below, we will investigate the effects of using nonuniformly spaced wavenumber grid points k_j within the Randomization Method, wherein these wavenumbers are chosen *randomly*. For our subsequent discussion of the Fourier Method, we restrict attention to equispaced wavenumber grid points $\{k_j\}_{j=0}^{M}$.

We remark that we could also have handled nonuniformly spaced wavenumbers through discretization of the stochastic Fourier integral (337). The present procedure generalizes more readily, however, to allow a random choice of wavenumbers $\{k_j\}_{j=0}^{M}$, as we will discuss in Section 6.2.3.

6.2.2.2. Fourier Method applied to RSS turbulent transport model. Examples of random fields generated by the (equispaced) Fourier Method can be found in the papers of Voss [366] and Viecelli and Canfield [335]. With sufficiently fine wavenumber spacing Δk, the method suffices to produce visually appealing fractal fields [336], with about a decade of statistically self-similar scaling [335]. The authors of each paper complain of the large amount of wavenumbers needed to produce a satisfactory fractal field, and prefer the Successive Random Addition Method, which will be discussed in Section 6.3.1.

We shall examine the practicality of the Fourier Method for the particular application of simulating turbulent transport by trying it in the RSS Model [83,140]. We will emphasize the consequences of the inherent periodicity of the velocity field simulated by the random Fourier Method. These are clearly brought out in a simulation of a sub-diffusive RSS Model ($\varepsilon = \frac{1}{2}$). In Fig. 22, the mean-square tracer displacement is shown for a Monte Carlo simulation for a Fourier sum with $M = 200$ wavenumbers, spaced by $\Delta k = 1/40\pi$, and averaged over 2000 realizations. (The error from truncating the wavenumbers $k \geq k_{\max} = (M + \frac{1}{2})\Delta k \approx 10$ is then less than 0.1%.) We see a systematic downward turning of the Fourier Method simulation from the exact result for times $t \gtrsim 15$. This can readily be traced to the fact that the simulated velocity field has period $1/\Delta k \approx 125$. From the exact formula for the trajectory:

$$Y(t) = \int_0^t v(\bar{w}s)\,\mathrm{d}s \ ,$$

and the fact that $v_{\mathrm{app}}(x)$ has a vanishing coefficient of the $k_0 = 0$ mode, we see that (up to numerical integration error) the simulated value of $\sigma_Y^2(t) = \langle Y^2(t) \rangle$ must also be periodic and vanish at $t = (\bar{w}\Delta k)^{-1} \approx 125$. The true value of $\sigma_Y^2(t)$, on the other hand, continues to grow according to a $t^{1/2}$ power law for $t \gg 1$. The simulated mean-square displacement must therefore turn down from the true solution. The departure becomes noticeable in Fig. 22 after roughly an eighth of a period.
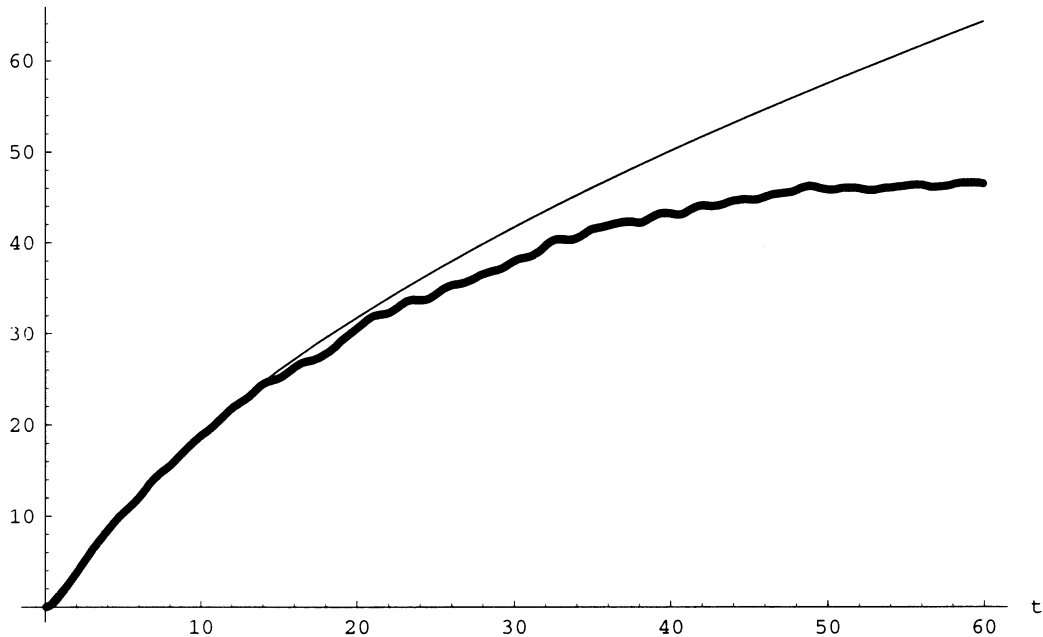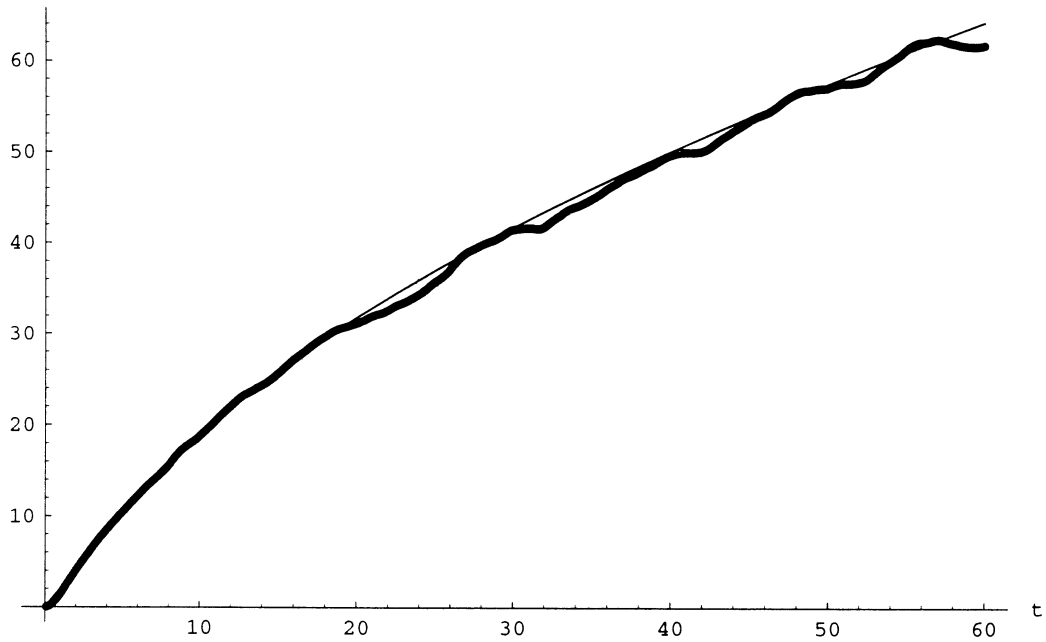
Fig. 22. Mean-square tracer displacement along the shear for RSS Model with $\varepsilon = 1/2$ (from [83]). Thin line: exact formula. Thick line: Fourier Method simulation with $M = 200$ wavenumbers, $\Delta k = 1/40\pi$, and 2000 realizations.

To verify that this discrepancy is due to periodicity effects, and not due to finite sample size or truncation error, the simulation was repeated with $\Delta k = 1/160\pi$ and $M = 800$ wavenumbers. This increases the inherent periodicity of the velocity field and $\sigma_Y^2(t)$ to $160\pi \approx 500$, a factor of 4 greater than before. The results are plotted in Fig. 23. The agreement between the simulated mean-square displacement and the exact result is now good through time $t \lesssim 60$, again an eighth of the artificial period. (The simulated curve starts turning down at times greater than that shown the figure [140].) Therefore, we see that the periodicity of the Fourier Method is a definite obstacle in the accurate simulation of turbulent diffusion over long time scales. To contend with it, one would need to choose a wavenumber spacing so small that the tracer does not cross more than an eighth of the period of the simulated velocity field, and this may require an enormous amount of computational labor, even with the fast Fourier transform. As we shall discuss in Section 6.2.4, the Moving Average Method appears to be a preferable choice for simulating random velocity fields without strong long-range correlations, such as the RSS Model with $\varepsilon = \frac{1}{2}$.

The Fourier Method has a further difficulty when simulating super-diffusive tracer motion in a velocity field with strong long-range correlations. In Fig. 24, we show a simulation of the RSS Model with $\varepsilon = \frac{3}{2}$, with the same choice of other numerical parameters as in Fig. 23. The $j = 0$ term in the random Fourier series (346) is problematic because of the infrared divergence of energy; in the present simulations it is just dropped. We see that the Fourier Method simulation undershoots the exact result even though the plotted times extend only up to an eighth of the artificial period. If we were to somehow retain a nontrivial $j = 0$ term in the random Fourier series (346), the

Fig. 23. Mean-square tracer displacement along the shear for RSS Model with $\varepsilon = \frac{1}{2}$ (from [83]). Thin line: exact formula. Thick line: Fourier Method simulation with $M = 800$ wavenumbers, $\Delta k = 1/160\pi$, and 2000 realizations.
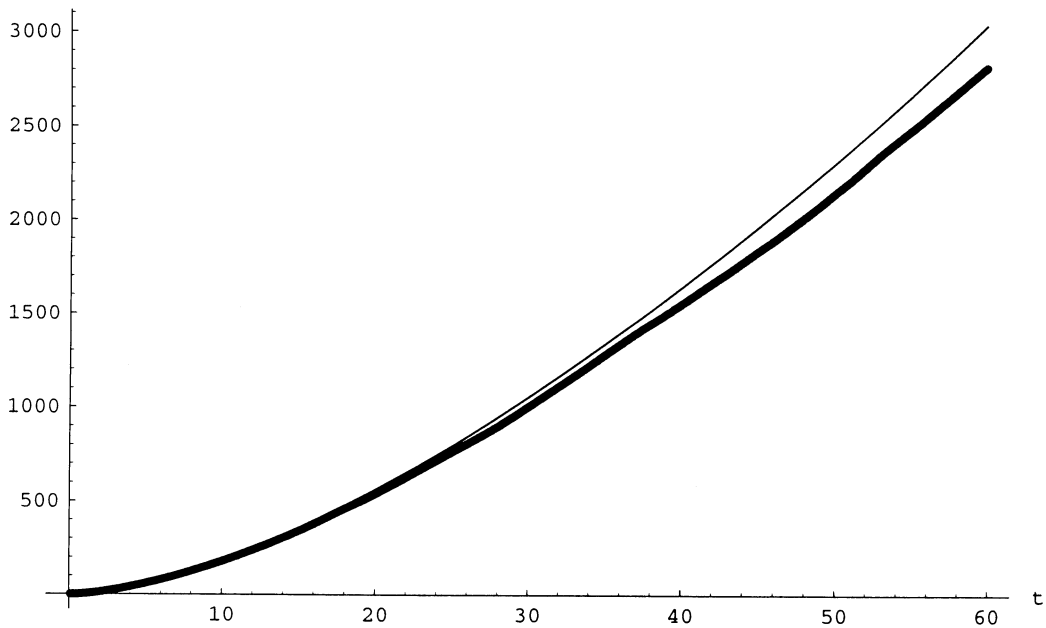
Fig. 24. Mean-square tracer displacement along the shear for RSS Model with $\varepsilon = \frac{3}{2}$ (from [140]). Thin line: exact formula. Thick line: Fourier Method simulation with $M = 800$ wavenumbers, $\Delta k = 1/160\pi$, and 2000 realizations.

mean-square tracer displacement would instead show a ballistic overshoot of the true superdiffusive behavior at long times. The actual superdiffusive behavior of the tracer displacement is very sensitive to the way in which energy is concentrated at low wavenumbers, but the Fourier Method with equispaced grid points cannot adequately resolve the $k^{-1/2}$ singularity in $E(k)$ at $k = 0$. We will see in Section 6.2.3 that appropriately randomizing the wavenumbers in the discrete sum can overcome the deficiencies of the direct Fourier Method for the flows in the RSS Model with long-range correlations ($1 < \varepsilon < 2$).

6.2.2.3. Conclusions regarding Fourier Method. The Fourier Method (with equispaced grid points) has been unambiguously shown to fail in efficiently producing accurate statistics for the motion of a tracer over long-time intervals in the simple RSS Model. The main difficulty is the strong systematic error induced by the artifical periodicity of the simulated flow. The Fourier Method furthermore cannot resolve sufficiently strong long-range correlations when they are present. These deficences are inherent to the Fourier method in general for the simulation of turbulent diffusion. Some better options for various applications will be discussed throughout the remainder of Section 6.

6.2.3. Randomization Method

One way in which various investigators have sought to overcome the numerical artifacts of the equispaced Fourier Method is to choose randomly the wavenumbers $\{k_j\}_{j=1}^{M}$ appearing in the finite Fourier sum approximation:

$$v_{\mathrm{app}}(x) = \sum_{j=1}^{M} a_j \cos(2\pi k_j x) + b_j \sin(2\pi k_j x) \ .$$

For example, Kraichnan [180] deterministically assigned the magnitudes of the wavevectors appearing in a simulated multidimensional velocity field, but selected their direction according to a random uniform distribution on the sphere. Sabelfeld and other scientists at the Computing Center at Novosibirsk [190,240,291] later developed a more substantial variation in which the magnitudes of the wavevectors are also randomly chosen. We shall call this latter algorithm the *Randomization Method*, and apply it to the problem of simulating the turbulent diffusion of a tracer in the RSS Model. We will see that it eliminates the periodicity problem intrinsic to the direct Fourier Method, and performs quite well for the diffusive and super-diffusive class of models $1 \leq \varepsilon < 2$, which include velocity fields with strong long-range correlations. The Randomization Method is not very successful, however, in simulating sub-diffusive tracer motion in the RSS Models with slowly decaying negative correlations ($0 < \varepsilon < 1$).

We shall first define the Randomization Method precisely, then present the results of the simulations in the RSS Model.

6.2.3.1. Definition of Randomization Method. In a manner similar to our second derivation of the Fourier Method (Paragraph 6.2.2.1), the prescription of the random velocity field in the *Randomization Method* begins with a deterministic partition of wavenumber space into M disjoint subintervals $\{I_j\}_{j=1}^{M}$ (Fig. 25). We do not, however, confine the partition to a finite segment; I_M extends all the way to $+\infty$. We now choose a representative wavenumber k_j in each interval according to
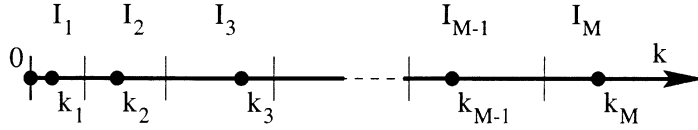
Fig. 25. Partition of the Fourier space into M intervals in the Randomization Method.

a probability density function (PDF) $p_j(k)$ weighted by the energy density $E(k)$:

$$\text{Prob}\{k_j \in A\} = \int_A p_j(k)\, dk,$$

$$p_j(k) = \begin{cases} \dfrac{2E(k)}{v_j^2} & \text{for } k \in I_j, \\ 0 & \text{for } k \notin I_j, \end{cases} \tag{353}$$

where

$$v_j = \left(2\int_{I_j} E(k)\, dk\right)^{1/2}. \tag{354}$$

The random velocity field $v(x)$ is then simulated as a random Fourier sum using these wavenumbers:

$$v_{\text{Rand}}(x) = \sum_{j=1}^{M} v_j[\xi_j \cos(2\pi k_j x) + \eta_j \sin(2\pi k_j x)], \tag{355}$$

where $\{\xi_j, \eta_j\}_{j=1}^{M}$ is a collection of independent standard Gaussian random variables.

Upon comparison with Eq. (346), we see that the random Fourier sum has the same form in the Randomization Method as in the direct Fourier Method. An inessential difference is the particular expression (354) for the amplitudes $\{v_j\}_{j=1}^{M}$; one could consistently use these expressions for the standard Fourier Method as well. The important distinction is that the wavenumbers $\{k_j\}_{j=1}^{M}$ appearing in the sum are chosen randomly within their associated interval in the Randomization Method, rather than at the midpoint as in the Fourier Method.

The amplitudes of the Fourier modes v_j and probability distribution $p_j(k)$ for the wavenumbers which were described in Eqs. (353) and (354) are uniquely specified by insisting that the simulated random field $v_{\text{Rand}}(x)$ have the same covariance as the desired random field $v(x)$, as we now demonstrate. We begin by positing a general random Fourier sum approximation of the same form that arose in our alternate derivation of the Fourier Method (348):

$$v_{\text{app}}(x) = \sum_{j=1}^{M} v_j[\xi_j \cos(2\pi k_j x) + \eta_j \sin(2\pi k_j x)], \tag{356}$$

where $\{\xi_j, \eta_j\}_{j=1}^{M}$ is a collection of independent, standard Gaussian random variables. We further suppose the wavenumbers k_j to be randomly distributed within their intervals I_j. We desire to choose the PDFs $\{p_j(k)\}_{j=1}^{M}$ of these wavenumbers as well as the constant nonnegative amplitudes

v_j so that the correlation function $R_{app}(x)$ of the simulated random field $v_{app}(x)$ approximates the correlation function of $v(x)$,

$$R(x) = \langle v(x')v(x' + x)\rangle = 2\int_0^\infty \cos(2\pi kx)E(k)\,dk\,, \tag{357}$$

as well as possible.

The correlation function of the random Fourier sum (356) may be computed by first averaging over the Gaussian random variables $\{\xi_j, \eta_j\}_{j=1}^M$ as in our derivation of the standard Fourier Method, and then taking another average over the distribution of the wavenumbers $\{k_j\}_{j=1}^M$:

$$R_{app}(x) = \langle v_{app}(x')v_{app}(x' + x)\rangle = \langle\langle v_{app}(x')v_{app}(x' + x)\rangle_{\xi,\eta}\rangle_k$$

$$= \left\langle \sum_{j=1}^M v_j^2 \cos(2\pi k_j x)\right\rangle_k = \sum_{j=1}^M \int_{I_j} \cos(2\pi kx)v_j^2 p_j(k)\,dk\,.$$

(See Eq. (350) for the derivation of the third equality.) Comparing with Eq. (357), we see that in fact we can make $R_{app}(x)$ identically equal to $R(x)$ by choosing $p_j(k) = 2v_j^{-2}E(k)$ for $k \in I_j, j = 1, \dots, M$. The formula for v_j (354) then follows simply from the normalization $\int_{I_j} p_j(k)\,dk = 1$.

6.2.3.2. General comments on the Randomization Method. The above calculation points out another advantage of the Randomization Method over the Fourier Method besides solving the periodicity problem. Whereas the correlation function of the velocity field $v_{Four}(x)$ simulated by the Fourier Method was only a discrete Riemann sum approximation of the true correlation function $R(x)$, the correlation function of the velocity field $v_{Rand}(x)$ simulated by the Randomization Method is exactly $R(x)$. The Randomization Method is therefore free of systematic truncation and discretization errors, at least insofar as second-order statistics are concerned. The reason this is possible is that the wavenumbers $\{k_j\}_{j=1}^M$ are allowed to vary over a continuum, so that an ensemble average can lead to the desired continuous energy spectrum $E(k)$. With fixed wavenumbers, as in the Fourier Method, the simulated spectrum can at best be a discrete approximation to $E(k)$ (352). Improved computational efficiency can be expected for the Randomization Method because of its preferential distribution of wavenumbers toward the most energetic parts of the spectrum. In particular, the Randomization Method should resolve strong concentrations of energy in wavenumber space much better than the equispaced Fourier Method.

However, the Randomization Method does have some drawbacks in practical implementation. First of all, the fast Fourier transform cannot be used because the wavenumbers are not confined to a regular grid. If one is interested in the turbulent transport of a small number of tracers, however, then the random velocity field $v_{Rand}(x)$ need only be evaluated at their momentary positions, so the loss of the fast Fourier transform is of no great concern. A potentially more serious disadvantage is the fact that the velocity field simulated by the Randomization Method is non-Gaussian, due to the randomness of the wavenumbers $\{k_j\}_{j=1}^M$. The single-point PDF of $v_{Rand}(x)$ is Gaussian, but the PDF of any two-point velocity increment $v_{Rand}(x) - v_{Rand}(x')$ is broader-than-Gaussian because such increments are mixtures of mean zero Gaussian random variables of different variances. (See the discussion in Section 5.2.2.) The Gaussianity of the simulated random field can be improved in principle by taking the intervals $\{I_j\}_{j=1}^M$ of the partition sufficiently fine in a certain sense [240,291]. It is not clear, however, whether the improved Gaussianity would require an inordinately large

M in practice, particularly for velocity fields with a wide range of active scales. A more promising approach, suggested by Kraichnan in a multi-dimensional context [180], is to produce $\tilde{M}$ independent approximate velocity fields $\{v_{\mathrm{Rand}}^{(j)}\}_{j=1}^{\tilde{M}}$ of the form (355), and then take the simulated field as a suitably normalized sum:

$$v_{\mathrm{Rand}}(x) = \frac{1}{\sqrt{\tilde{M}}} \sum_{j=1}^{\tilde{M}} v_{\mathrm{Rand}}^{(j)}(x) . \tag{358}$$

The resulting random field $v_{\mathrm{Rand}}(x)$ has mean zero and the appropriate correlation function $R(x)$. Moreover, by the Central Limit Theorem, the statistics of the random field $v_{\mathrm{Rand}}(x)$ will approach a Gaussian form if $\tilde{M}$ is taken sufficiently large. We will return to the issue of non-Gaussianity of the Randomization Method in Section 6.4.

We finally remark that although the Randomization Method has no formal truncation or discretization errors, it does not magically avoid the error incurred in approximating a random field with continuous spectrum by a finite sum of Fourier modes. This source of error rather becomes transferred to the Monte Carlo sampling error. The degree to which the statistics of a finite sample size will accurately resemble those of the entire ensemble depends on how closely the realizations of the simulated random field mimic the properties of the true random field. For example, in a turbulent velocity field with a power law inertial-range spectrum, the number of intervals (M) in the partition of wavenumber space must be chosen sufficiently large to ensure that each simulated velocity field contains a typical distribution of scales [140,291]. A helpful strategy toward this end is to choose the intervals $\{I_j\}_{j=1}^{M}$ of the partition to contain equal amounts of energy:

$$v_j^2 = 2 \int_{I_j} E(k) \, dk = \frac{2}{M} \int_0^\infty E(k) \, dk = \frac{1}{M} \langle (v(x))^2 \rangle .$$

Note that this partition is naturally associated to a Lebesgue integration of the energy spectrum $E(k)$, whereas the equispaced Fourier Method is built from a standard Riemann sum approximation to the integral of $E(k)$.

6.2.3.3. Randomization Method applied to RSS Turbulent Transport Model. The Randomization Method has been used by Sabelfeld and coworkers [190,240,291] to simulate the motion of tracers and pairs of tracers in a fully developed turbulent velocity field with a small inertial range. We will discuss the Randomization Method in this more demanding context later in Section 6.3.2. Here, we apply the Randomization Method to the RSS Model to assess how well it simulates various types of turbulent tracer transport behavior. We are particularly interested in examining the extent to which the Randomization Method alleviates some of the inherent difficulties of the Fourier Method. The results presented here for the Randomization Method originate in the thesis of Horntrop [140]. These simulations adopt a simple incarnation of the Randomization Method, in which the random Fourier series of the simulated velocity field $v_{\mathrm{Rand}}(x)$ consists of 32 wavenumbers chosen independently from $[0, \infty)$, with PDF given by $p_1(k) = 2v_1^{-2}E(k)$ and $v_1^2 = 2\int_0^\infty E(k) \, dk$. For the energy spectra in the RSS Model (343b), the random wavenumbers are then distributed according to a gamma distribution [103], and can be efficiently generated on a computer. In the above general notation, this setup corresponds to taking a trivial partition of wavenumber space

($M = 1$ in Eq. (355)) and building the simulated field by summing up $\tilde{M} = 32$ independent realizations of single-mode velocity fields (see Eq. (358)).

The superiority of the Randomization Method over the Fourier Method is clearly demonstrated in the super-diffusive regime of the RSS Model. In Fig. 26, the mean-squared tracer displacement produced by the Randomization Method for $\varepsilon = \frac{3}{2}$ is indistinguishable from the exact result. The relative error is less than 8% throughout the simulation, and actually settles down to about 1% for $30 \le t \le 200$ [142]. The favorable comparison between the results of the Randomization Method (Fig. 26) and the Fourier Method (Fig. 24) for $\varepsilon = \frac{3}{2}$ becomes even more striking when it is noted that the Randomization Method uses only $\tilde{M} = 32$ wavenumbers (relative to $M = 800$ for the Fourier Method), and the Randomization Method is plotted over a longer time interval. The success of the Randomization Method in simulating super-diffusive tracer motion can be attributed to its (random) selection of wavenumbers over a continuous range, with preferential weighting toward low wavenumbers where the energy is strongly concentrated ($E(k) \approx A_E k^{1-\varepsilon}$ for $k \searrow 0$). At least within the RSS Model, the Randomization Method takes proper account of the long-range correlations in the velocity field which give rise to super-diffusive tracer motion. The periodicity problem of the Fourier Method is also completely avoided. A sufficiently large sample size, however, is necessary to obtain the good agreement observed in Fig. 26. The sampling error becomes quite noticeable if the average involves only 500 independent realizations [140].

The Randomization Method also produces good results for RSS Models with diffusive ($\varepsilon = 1$) and trapping behavior ($\varepsilon < 0$) [140], but does not fare so well in the sub-diffusive regime ($0 < \varepsilon < 1$). In Fig. 27, we see that the simulated tracer motion persistently overshoots the correct behavior for $\varepsilon = \frac{1}{2}$. Evidently, the Randomization Method is not adequately accounting for the slowly decaying negative tail in the correlation function $R(x)$ (see Fig. 20), even with 2000 samples.

One concern which should be addressed when using the Randomization Method is the extent to which the simulated fields deviate from Gaussianity. The ensembles generated in the above simulations did exhibit significantly non-Gaussian sample statistics [140]. This issue plays no role, however, in the simulation of the mean-square tracer displacement in the RSS Model, since this quantity only depends on the second-order statistics of the velocity field (344).

6.2.3.4. Conclusions regarding Randomization Method. The above simulations show the Randomization Method to be a superior variation of the Fourier Method in the simulation of turbulent tracer transport. Its flexible choice of wavenumbers alleviates the periodicity problem and properly incorporates long-range correlations in the simulated velocity field, at least in the RSS Model. The Randomization Method, however, demonstrates some difficulties in simulating random fields which have a correlation function with slowly decaying *negative* tails. One must also be aware that the Randomization Method generally produces random fields with non-Gaussian statistics.

To summarize, the Randomization Method appears to be a good candidate for Monte Carlo simulation of random fields which have long-ranged *positive* correlations. We shall return to it in Section 6.3.2 when we consider the numerical simulation of turbulent velocity fields which have even stronger positive long-range correlations than those present in the super-diffusive RSS Models.

6.2.4. Physical space-based method

The Fourier Method and the Randomization Method presented above are based on the stochastic Fourier integral representation (337) of the random velocity field $v(x)$. The final
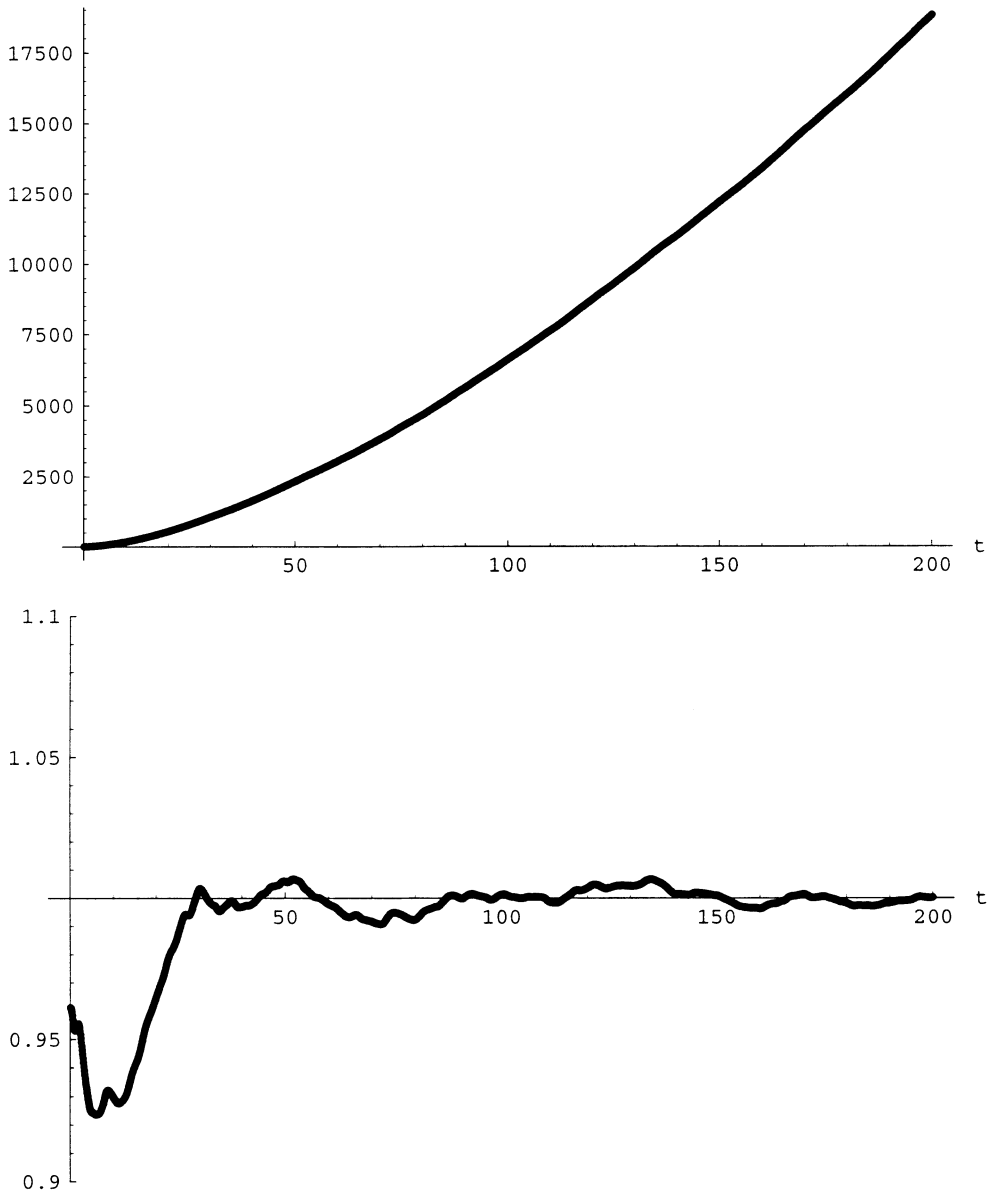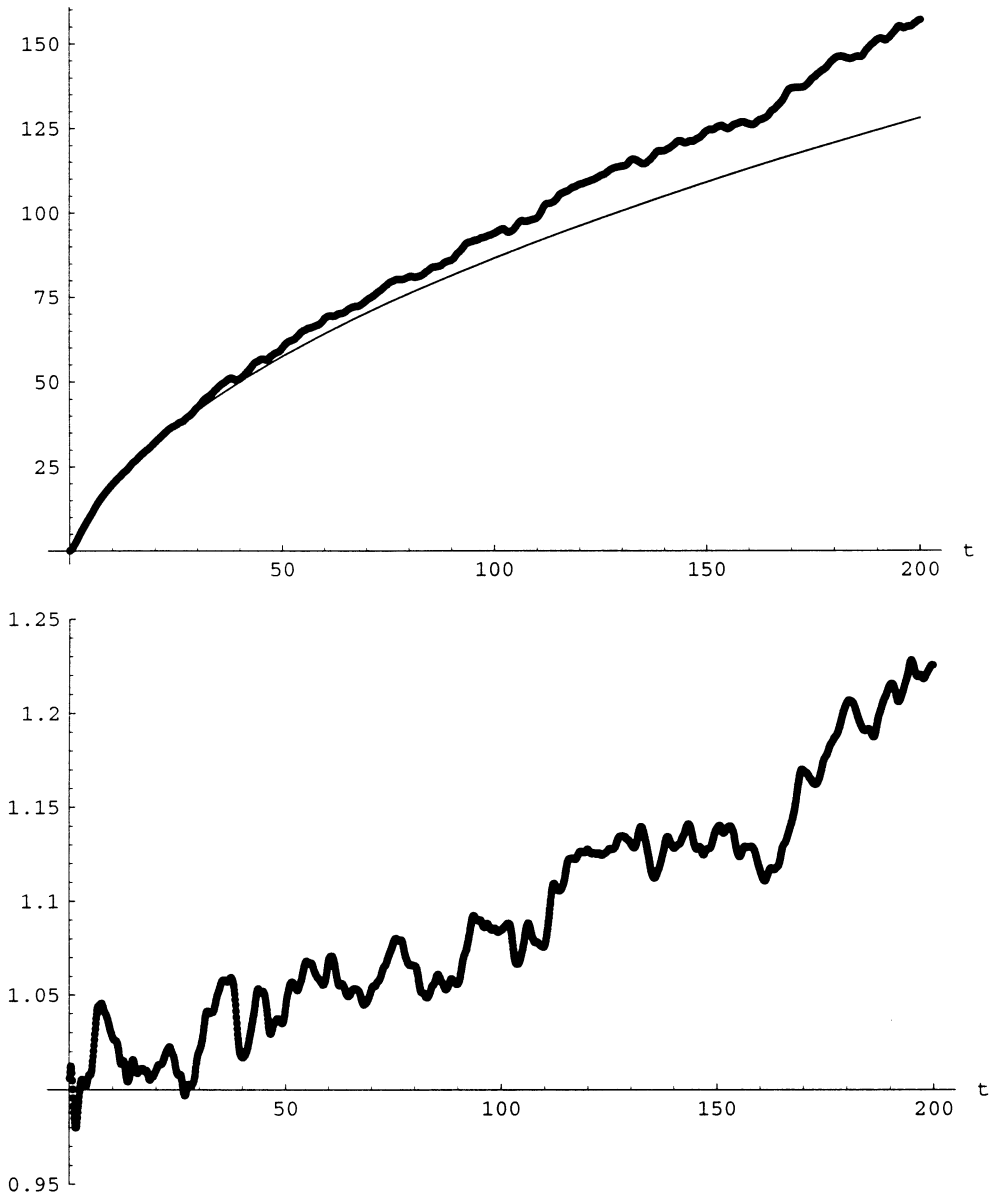
Fig. 26. Mean-square tracer displacement along the shear for RSS Model with $\varepsilon = \frac{3}{2}$ (from [140]). In the upper graph, the thin line describes exact formula whereas the (nearly coincident) thick line describes the Randomization Method simulation with $\tilde{M} = 32$ wavenumbers, and 2000 realizations. The lower graph shows the ratio of the simulated to true mean-square tracer displacement.

nonhierarchical Monte Carlo method for simulating random fields which we will consider is the *Moving Average Method*, the simplest of another class of methods which are derived from the physical-space stochastic integral representation (340) of the random field. After a brief general discussion of the Moving Average Method, we will apply it to the RSS Model and compare the

Fig. 27. Mean-square tracer displacement along the shear for RSS Model with $\varepsilon = \frac{1}{2}$ (from [140]). In the upper graph, the thin line describes exact formula whereas the thick line describes the Randomization Method simulation with $\tilde{M} = 32$ wavenumbers, and 2000 realizations. The lower graph shows the ratio of the simulated to true mean-square tracer displacement.

outcomes with those of the Fourier-spaced methods discussed above [83,140]. We find an intrinsic obstacle for the Moving Average Method in simulating velocity fields with strong long-range correlations. In fact, utilizing it in such situations can lead to ostensibly plausible scaling behavior which is in fact incorrect! The Moving Average Method, however, simulates tracer transport in

those RSS Models without strong long-range correlations ($\varepsilon < 1$) more efficiently than the Fourier method.

In Section 6.3, we will present a *hierarchical* version of the Moving Average Method which performs extremely well in simulating tracer transport in a fractal random field with very strong long-range correlations [84,85].

6.2.4.1. Definition of Moving Average Method. The Moving Average Method is the direct physical-space based analogue of the Fourier Method. It is obtained from the general physical-space stochastic integral representation (340) of the random field $v(x)$:

$$v(x) = \int_{-\infty}^{\infty} G(x - r)\, \mathrm{d}W(r) \tag{359}$$

in much the same way that the Fourier Method was derived from the stochastic Fourier integral representation (337). In Eq. (359), $\mathrm{d}W(\cdot)$ is a real white noise measure with properties stated in Eq. (341), and

$$G(x) = \int_{-\infty}^{\infty} \mathrm{e}^{-2\pi\mathrm{i}kx} E^{1/2}(|k|)\, \mathrm{d}k = 2\int_{0}^{\infty} \cos(2\pi kx) E^{1/2}(k)\, \mathrm{d}k \tag{360}$$

is a symmetric function peaked at the origin.

To implement Eq. (359) numerically, we define a symmetric partition of the real line into intervals of equal width Δx, and use these to construct a Riemann sum approximation (with infinitely many terms) using a midpoint rule discretization:

$$v_{\mathrm{disc}}(x) = \sum_{j=-\infty}^{\infty} G(x - j\Delta r)\, \Delta W_j\,, \tag{361}$$

$$\Delta W_j = \int_{(j-1/2)\Delta r}^{(j+1/2)\Delta r} \mathrm{d}W(r)\,.$$

It is readily checked from Eq. (341) that $\{W_j\}_{j=-\infty}^{\infty}$ is an infinite collection of independent Gaussian random variables with mean zero and variance Δr.

We do not simply truncate Eq. (361) into a fixed, finite sum, as in the Fourier method, because here the magnitude of the integrand peaks at the variable point x. Instead, we specify a *bandwidth* b, and restrict the summation in Eq. (359) to $|j - \lfloor x/\Delta r \rfloor| \le b$, where $\lfloor x \rfloor$ denotes the greatest integer not exceeding x.

This completes the definition of the *Moving Average Method*:

$$v_{\mathrm{MA}}(x) = \sum_{j=\lfloor x/\Delta r \rfloor - b}^{\lfloor x/\Delta r \rfloor + b} G(x - r_j)\xi_j\sqrt{\Delta r}\,, \tag{362}$$

where $\{r_j = j\Delta r\}_{j=-\infty}^{\infty}$ are the equispaced grid points in the integration and $\{\xi_j\}_{j=-\infty}^{\infty}$ is a collection of independent, standard, Gaussian random variables.

Note that the truncation corresponds to an integration over the mobile segment $[\lfloor x \rfloor_{\Delta r} - r_{\max}, \lfloor x \rfloor_{\Delta r} + r_{\max}]$, where $r_{\max} = (b + \frac{1}{2})\Delta r$ and $\lfloor x \rfloor_{\Delta r}$ denotes the grid point r_j lying closest to and left of x.

The Moving Average Method was applied by McCoy [228] in turbulent diffusion simulations. Mandelbrot and Wallis [220–222] and Feder [100] simulated one-dimensional fractal random fields using an analogous algorithm based on a one-sided moving average representation [219].

Note that there is no sensible implementation of the Moving Average Method using random or unequally spaced physical-space grid points r_j, because the computation of the convolution would become extremely complicated. In any case, there is no motivation for randomizing the physical-space grid points. First of all, the Moving Average Method does not suffer from the false periodicity of the equispaced Fourier Method. Secondly, the random field is statistically homogenous in physical space, so there is no need to resolve special regions as there is in Fourier space when the spectrum is strongly concentrated near $k = 0$.

6.2.4.2. General comments on the Moving Average Method. We can already discern a general disadvantage of the Moving Average Method relative to the Fourier-space based methods in that the random field simulated by the Moving Average Method is built out of an infinite number of random variables. To be sure, the restriction of the random field to any finite region refers to only finitely many of these variables. The practical difficulty in simulating turbulent tracer transport is keeping track of the random variables needed to evaluate the velocity field at the current tracer location. When the x position of the tracer moves across a grid point r_j which it has never visited before, then a new independent random variable ξ_{j+b} (or ξ_{j-b}) must be generated to evaluate $v(x)$. But if, as the tracer meanders, its x position turns around and crosses a grid point r_j which it has already visited, then the previously generated value of ξ_{j-b} (or ξ_{j+b}) must be recalled. Consequently, in a standard implementation, one would either need to precompute all the random variables which would be needed over a specified domain, or dynamically store and index all the random numbers generated as the tracer moves into new territory. Computer memory limitations will necessarily restrict the spatial region which the tracer is allowed to explore. An alternative procedure is to utilize a reversible random number generator (such as a linear congruential generator) with an indexing scheme which allows any particular random number ξ_j to be obtained on demand [84]. The sequence of random numbers $\{\xi_j\}_{j=-\infty}^{\infty}$ is not explicitly stored in this implementation, so the memory limitations are averted. Of course, for time-dependent random velocity fields, such considerations become less signficant.

Another disadvantage of the Moving Average Method relative to the Fourier-space-based methods is that the simulated random field $v_{\mathrm{MA}}(x)$ is not precisely statistically homogenous. The statistics of $v_{\mathrm{MA}}(x)$ are generally invariant only under shifts $v_{\mathrm{MA}}(x) \to v_{\mathrm{MA}}(x + h)$ for h an integrable multiple of the grid spacing Δr. The statistics of $v_{\mathrm{MA}}(x)$ do depend, through the weighting factors $G(x - r_j)$, on the location of x relative to the grid points. We will examine this issue in more detail in the context of a much improved, hierarchical version of the Moving Average Method in Section 6.3.2.

A more pressing concern regarding the Moving Average Method is revealed by a comparison of the correlation function of the simulated field with the true correlation function. We find that for

$x = q\Delta r > 0$ and $x' = q'\Delta r$,

$$\langle v_{MA}(x' + x)v_{MA}(x') \rangle = \sum_{j=q+q'-b}^{q+q'+b} \sum_{j'=q'-b}^{q'+b} G((q + q')\Delta r - r_j)G(q'\Delta r - r_{j'})\Delta r \langle \xi_j \xi_{j'} \rangle$$

$$= \sum_{j=q+q'-b}^{q'+b} G(r_{q'-j} + x)G(r_{q'-j})\Delta r = \sum_{j=-b}^{b-q} G(x + r_j)G(r_j)\Delta r \qquad (363)$$

whereas the correlation between the true velocity field at these same points is, from Eqs. (359) and (341):

$$\langle v(x' + x)v(x') \rangle = R(x) = \int_{-\infty}^{\infty} \int_{-\infty}^{\infty} G(x' + x - r)G(x' - r')\langle dW(r) dW(r') \rangle$$

$$= \int_{-\infty}^{\infty} G(x' + x - r)G(x' - r) dr = \int_{-\infty}^{\infty} G(x + r)G(r) dr . \qquad (364)$$

The correlation function (363) of the velocity field $v_{MA}(x)$ is a quadrature approximation of the correlation function (364) of the true velocity field $v(x)$. The most serious difference between the approximate and exact correlation functions is the truncation of integration interval. In fact, for $x > 2r_{max}$, the correlation function of the simulated velocity field vanishes, because the two observation points $x + x'$ and x' make use of disjoint subsets of the random variables $\{\xi_j\}_{j=-\infty}^{\infty}$.

The Fourier Method involved a similar truncation of wavenumber space to a finite segment $[0, k_{max}]$, and this was also reflected in expression (351) for the simulated correlation function $\langle v_{Four}(x' + x)v_{Four}(x') \rangle$. There, the truncation was not a big concern because the energy spectrum $E(k)$ typically decays very rapidly (say, exponentially) at large wavenumber. The moving average weighting function, $G(x)$, however, will not necessarily manifest such rapid decay. In fact, if the velocity field has long-range correlations, these must be reflected in slowly decaying, long-range tails of $G(x)$. The Moving Average Method must be expected to suffer a severe systematic truncation error in such circumstances.

6.2.4.3. Moving Average Method applied to RSS Model. We shall now use the RSS Model to illustrate explicitly that the Moving Average Method's inherent physical-space truncation makes it inadequate in simulating tracer transport in a velocity field with strong long-range correlations (so that $R(x)$ and $G(x)$ have very slow decay) [83,140]. We will find, however, that the Moving Average Method performs relatively efficiently for velocity fields with milder correlations [140]. An earlier study of the Moving Average Method in simulating turbulent diffusion may be found in McCoy's thesis [228]. For the RSS Model simulations presented here, we use a bandwidth $b = 800$ and grid spacing $\Delta r = 0.1$, so that the convolution in the moving average representation is effectively cut off at a distance $r_{max} = (b + \frac{1}{2})\Delta r \approx 80$ from the maximum of the weighting function G.

We consider first the $\varepsilon = 3/2$ RSS model, which has strong long-range correlations and falls in the superdiffusive regime. The effects of the truncation of the moving average representation to a finite bandwidth b in Eq. (362) are already apparent in a plot of the correlation function $R_{MA}(x) = \langle v_{MA}(x')v_{MA}(x' + x) \rangle$ (with $x' = j'\Delta r$) along with the correlation function $R(x) = \langle v(x')v(x' + x) \rangle$ of the true velocity field (Fig. 28). The simulated correlation function $R_{MA}(x)$ is drastically underrepresenting the long-range $r^{-1/2}$ tail of the true correlation function $R(x)$. This reflects the fact that
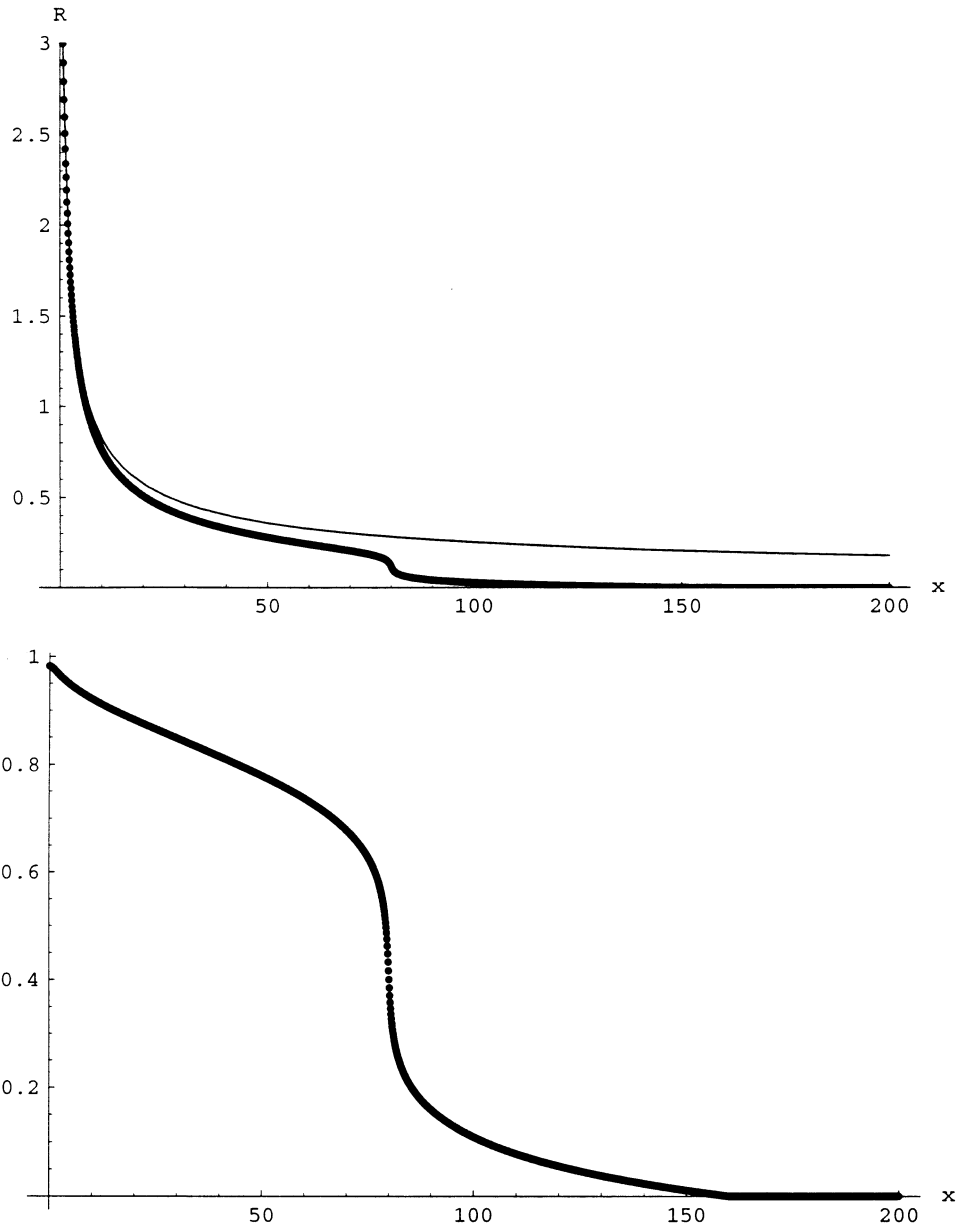
Fig. 28. Correlation function of the velocity field for RSS Model with $\varepsilon = \frac{3}{2}$ (from [83]). In the upper graph, the thin line describes true velocity correlation function $R(x)$, whereas the thick line describes the simulation by the Moving Average Method with bandwidth $b = 800$, grid spacing $\Delta r = 0.1$, and integration cutoff $r_{\max} \approx 80$. The lower graph shows the ratio of the simulated to true velocity correlation function.

correlations on scales large compared to r_{max} have been artificially filtered out. Recall that the exact mean-square displacement $\sigma_Y^2(t)$ of a tracer in the RSS Model is expressible as an integral of $R(x)$ over an interval of length $\bar{w}t$ (344). Therefore, the truncation in the Moving Average Method must necessarily lead to a systematic underprediction of $\sigma_Y^2(t)$ at large time, apart from any additional random errors due to finite sampling in Monte Carlo simulations. An actual simulation of $\sigma_Y^2(t)$ using $N = 2000$ realizations of the velocity field just described, is shown in Fig. 29. The Moving Average Method severely undershoots the correct behavior, and even worse, produces an apparent scaling behavior at long time with the wrong exponent. Note that the error of the Moving Average Method already appears at $t = 40$, when the tracer has only moved across half the width $r_{max} \approx 80$ of the integration window in the convolution. Similar results are found [140] when the bandwidth is increased to $b = 2000\,(r_{max} \approx 200)$. The Moving Average Method is therefore dangerous to use in simulating turbulent diffusion in velocity fields with significant long-range correlations, since it can produce erroneous scaling behavior. Simulations of a one-dimensional fractal random field using a related one-sided Moving Average Method [220–222] with similarly large bandwidths and sample size can also predict incorrect scaling exponents for statistics of the random field itself ([100], Fig. 9.8).

The Moving Average Method, however, performs adequately for the $\varepsilon \leq 1$ RSS Models, in which the tracer motion is diffusive, subdiffusive, or trapped. The subdiffusive motion of a tracer in the $\varepsilon = \frac{1}{2}$ RSS Model can be tracked with reasonable accuracy over a time interval $0 \leq t \lesssim 130$ (Fig. 30), whereas a Fourier Method simulation of comparable cost (described in Fig. 23 and [140])
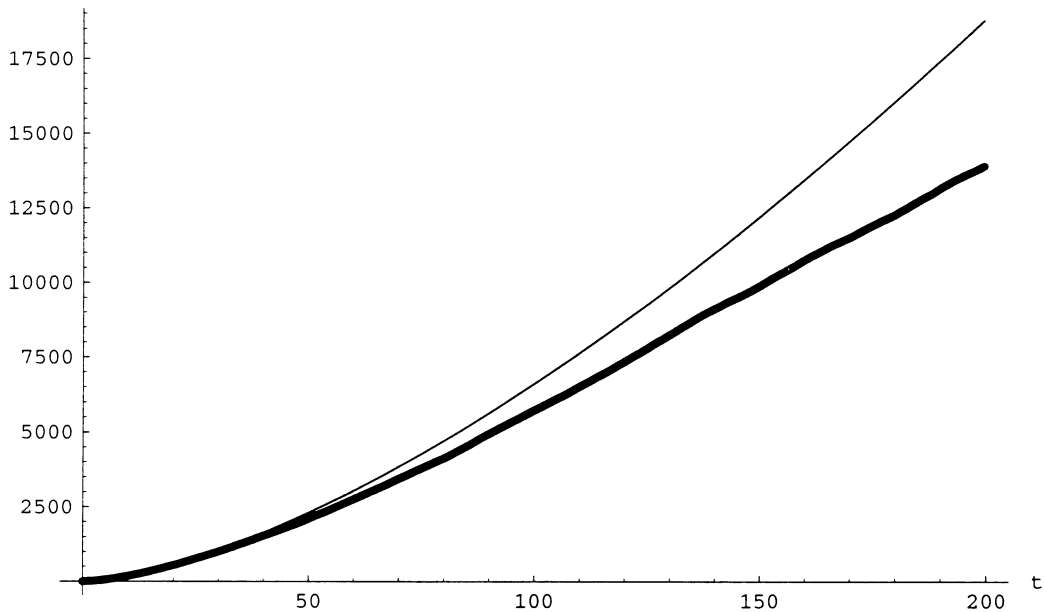
Fig. 29. Mean-square tracer displacement along the shear for RSS Model with $\varepsilon = \frac{3}{2}$ (from [83]). Thin line: exact formula, thick line: Moving Average Method simulation with bandwidth $b = 800$, grid spacing $\Delta r = 0.1$, and integration cutoff $r_{max} \approx 80$.
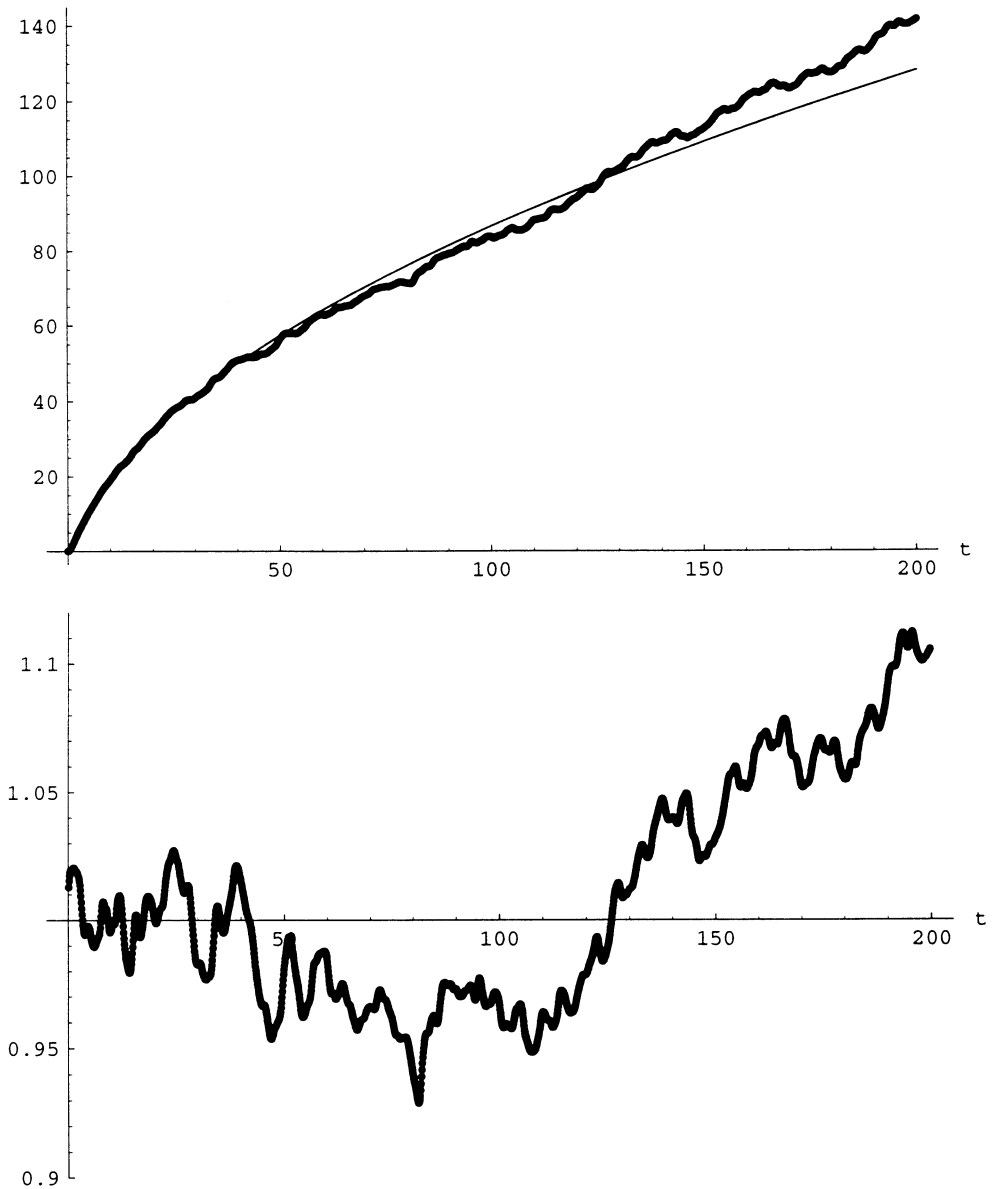
Fig. 30. Mean-square tracer displacement along the shear for RSS Model with $\varepsilon = \frac{1}{2}$ (from [83]). In the upper graph, the thin line describes exact formula, whereas the thick line describes the Moving Average Method simulation with bandwidth $b = 800$, grid spacing $\Delta r = 0.1$, and integration cutoff $r_{max} \approx 80$. The lower graph shows the ratio of the simulated to true mean-square tracer displacement.

starts to systematically turn down due to artificial periodicity after $t \approx 60$. The Randomization Method, on the other hand, had a tendency to overshoot the correct subdiffusive tracer behavior (Fig. 27).

6.2.4.4. Conclusions regarding Moving Average Method. The Moving Average Method intrinsically cannot represent correlations of the velocity field on scales larger than the integration cutoff r_{max}, and this fact can lead to a grossly misleading simulation of the long-time tracer motion in a velocity field with strong long-range correlations. Based on the results for the $1 < \varepsilon < 2$ RSS Models (Figs. 26 and 29), the Randomization Method appears to be a much more economical and accurate Monte Carlo Method for this kind of turbulent diffusion problem. On the other hand, the Moving Average Method performed reasonably well and more efficiently than the Fourier Method for the RSS Models without strong long-range correlations $\varepsilon \leq 1$, in which the tracer motion is diffusive, subdiffusive, or trapped.

The Moving Average Method can be improved significantly by a proper hierarchical formulation, as we shall discuss in Section 6.3.2.

6.3. Hierarchical Monte Carlo methods for fractal random fields

We have analyzed three Monte Carlo methods for the simulation of turbulent diffusion in a class of steady, random shear flows. For the rest of Section 6, we will develop and examine Monte Carlo methods with a view toward simulating tracer motion in synthetic flows with some features in common with fully developed turbulence at high Reynolds number.

One characterizing feature of such flows is the existence of a self-similar inertial range of scales $L_K \ll r \ll L_0$, where L_K is the Kolmogorov dissipation length and L_0 is the integral length scale. A random steady shear flow with such an inertial range was analyzed in Section 3.4.1. Its energy spectrum was expressed as

$$E(k) = A_E k^{1-\varepsilon} \psi_0(kL_0)\psi_\infty(kL_K), \quad 2 < \varepsilon < 4 , \tag{365}$$

where ψ_0 is an infrared cutoff and ψ_∞ is an ultraviolet cutoff. While the energy spectrum has a self-similar form between $L_0^{-1} \ll k \ll L_K^{-1}$ for all $\varepsilon < 4$, it is only for $2 < \varepsilon < 4$ that the velocity field $v(x)$ exhibits statistical self-similarity within an inertial range $L_K \ll r \ll L_0$ in *physical space*. In particular, for $2 < \varepsilon < 4$, the mean-square velocity difference (also called the *structure function* of the velocity field) has the following inertial-range scaling:

$$\langle (v(x' + x) - v(x'))^2 \rangle = S_v^I |x|^{2H} , \tag{366}$$

where $H = (\varepsilon - 2)/2$ is the Hurst exponent, and

$$S_v^I = -2A_E \pi^{1/2 + 2H} \Gamma(-H)/\Gamma(H + \tfrac{1}{2}) . \tag{367}$$

(See Section 4.2.1 for a closely analogous discussion in the context of a random shear velocity field with rapid decorrelation in time.)

Simulation of such a random field faces two main difficulties. First of all, the rapid growth of the mean-square velocity difference (366) with separation x between the observation points manifests the very strong long-range correlation of the velocity field $v(\cdot)$. We saw in Section 6.2 how poorly the Fourier Method and Moving Average Method simulated random fields of the type (365) (with $L_0 = \infty$) for spectral exponents $1 < \varepsilon < 2$, because of their inability to represent accurately the long-range correlations in those fields. The velocity fields with inertial ranges we are now considering ($2 < \varepsilon < 4$) have even higher values of ε, and the long-range correlations become even more pronounced. A further challenge for numerical simulation of these velocity fields is to ensure

that the simulated velocity fields exhibit clean inertial-range scaling (366). This is particularly pertinent to applications in which one is seeking to determine how the inertial-range scaling of the velocity field is reflected in scaling properties of the passive scalar field on length scales within the inertial range. We already considered some of these relations in Section 4 for a velocity field with rapid decorrelation in time. High-quality numerical simulations permit investigations of scaling properties for the passive scalar field in flows with more complex features, as we shall illustrate in Section 6.5.

To keep focus on the two central issues, the very strong long range correlations and the inertial-range scaling properties, we will remove the cutoffs from explicit consideration as much as possible. That is, we formally take the ideal field we are trying to simulate as having a vanishingly small Kolmogorov dissipation length $L_K = 0$ and an infinitely large integral length scale $L_0 = \infty$. This limit, taken at face value, requires some care in interpretation (Section 3.4.1). For the purposes of our discussion of Monte Carlo numerical methods, however, this is of no concern since computer limitations will impose definite upper and lower cutoff length scales to the inertial range of any simulated field. In what follows, it is only important to remember from Section 3.5 that as the cutoffs are removed,

- the velocity *increments* $v(x) - v(x')$ are statistically homogenous, meaning that their PDF depends only on $x - x'$,
- the velocity increments are mean zero Gaussian random variables, with variance converging to the finite inertial-range scaling limit $S_v^I |x - x'|^{2H}$, and
- the statistical dynamics of the *separation* between a pair of tracer particles converges to a well-defined limiting evolution.

We remark for our later discussion in Section 6.4 that these facts remain true for multidimensional velocity fields.

We shall therefore pose the Monte Carlo simulation problem of Section 6.3 as follows. We wish to generate a numerical random (steady shear flow) velocity field $v(x)$ for which the increments $v(x) - v(x')$ are homogenous and Gaussian distributed, with mean zero and variance obeying a specified inertial-range scaling law:

$$\langle (v(x') - v(x))^2 \rangle = S_v^I |x - x'|^{2H} \,, \tag{368}$$

with $0 < H < 1$, over an extensive range of scales. Secondly, we also wish the separation between a pair of tracers advected by such a velocity field to be simulated accurately.

With all the cutoffs removed from explicit consideration, the desired velocity field is in fact a *fractal random field* [215,100]. This simply means that the velocity field enjoys a statistical self-similarity (or, more precisely, *statistical self-affinity* [216]) under dilations. Namely, $v(x) - v(x')$ has the same PDF as $\lambda^{-H}(v(\lambda x) - v(\lambda x'))$, as may be checked from Eq. (368) and the fact that a Gaussian random variable is fully determined by its mean and variance. Fractal random fields have applications in a diversity of fields beyond turbulent diffusion, such as solute transport in groundwater [79], turbulent combustion [339], random topography in statistical physics [100], and many others [215,336]. We remark that the problem of simulating the random, one-dimensional shear velocity field $v(x)$ described above is equivalent to the simulation of a stochastic process known as *fractional Brownian motion* [100,215,219].

Of the nonhierarchical Monte Carlo methods discussed in Section 6.2, the Randomization Method is evidently the best choice for simulating fractal random fields. The Fourier and Moving Average Methods were shown to be incapable of efficiently representing long-range correlations. In Section 6.3.3, we will compare the performance of the Randomization Method with another class of *hierarchical* Monte Carlo methods, which we now introduce.

These hierarchical methods are designed to respect the statistical self-similarity of the fractal random field. The simulated velocity field $v_{app}(x)$ is represented as a superposition of random fields associated to a hierarchy of scales:

$$v_{app}(x) = \sum_{m=m_{min}}^{m=m_{max}} 2^{-mH} v_m(2^m x) \ . \tag{369}$$

Each $v_m(\cdot)$, $m_{min} \leq m \leq m_{max}$ is an independent, identically distributed, mean zero Gaussian random field, which can be computed efficiently. Their precise specification characterizes the particular hierarchical Monte Carlo method. The integers m_{min} and m_{max} represent large scale and small scale cutoffs, as can be seen by noting that if the random fields $\{v_m(\cdot)\}$ have characteristic length scale L, then $v_m(2^m x)$ has characteristic length scale $2^{-m}L$.

In the idealized situation in which the truncation to a finite number of scales may be ignored ($m_{min} = -\infty$ and $m_{max} = +\infty$), any hierarchical method will automatically simulate a velocity field with the discrete scaling symmetry:

$$\langle (v_{app}(x) - v_{app}(x'))^2 \rangle = 2^{-2H} \langle (v_{app}(2x) - v_{app}(2x'))^2 \rangle.$$

Therefore, some of the inertial-range scaling property (368) is built in to the hierarchical method, and this is the main theoretical motivation for representing the simulated velocity field by Eq. (369). It is important to note, however, that the increments of the simulated fractal random field $v_{app}(x)$ are not thereby guaranteed to have the *continuous* scaling symmetry and statistical homogeneity of the increments of the true fractal velocity field $v(x)$.

One intuitively appealing hierarchical Monte Carlo method for generating fractal random fields is the method of *Successive Random Addition* (SRA), developed by Voss [336]. This method has become quite popular in the physics community, due to its speed, efficiency, and flexibility in generating various random fractal surfaces and processes [100,336]. Viecelli and Canfield [335] have moreover shown how to exploit the local recursive nature of SRA to compute rapidly the fractal field at a given point. They therefore suggest SRA as a promising method to apply to the simulation of the turbulent diffusion of a small number of tracers.

Unfortunately, the random fields simulated by SRA have recently been shown to be rigorously inconsistent with the statistical homogeneity and full inertial-range scaling properties of the increments of a truly homogenous fractal random field [87]. We discuss this deficiency of SRA in Section 6.3.1 through explicit and rigorous numerical estimates, which demonstrate that it fails in very practical ways to simulate a truly fractal random field. Of course, this says nothing about its capability of producing qualitatively convincing graphical representations of fractal surfaces and landscapes [100,336]. But to simulate turbulent diffusion in the inertial-range of scales with quantitative precision, the simulated velocity field must have *quantitatively* accurate statistical scaling properties, and SRA is intrinsically incapable of meeting this need.

In Section 6.3.2, we present a pair of hierarchical methods recently developed by the first author with Elliott and Horntrop for the simulation of fractal random fields. The *Multi-Wavelet Expansion*

(*MWE*) *Method* [84] is based on the same physical-space stochastic integral representation (340) as the Moving Average Method discussed earlier. The *Fourier-Wavelet Method* [82] is a Fourier-space based analogue. They are carefully designed to permit efficient local computation of the random field, so that the velocity field $v(x)$ may be evaluated rapidly at whatever positions $x = X^{(j)}(t)$ a small number of tracers happen to be at a certain moment of time. The MWE Method is designed specifically for fractal random fields, while the Fourier-Wavelet method is flexible enough to be applied in more general situations [82].

Some simulations of the velocity field $v(x)$ by the MWE, Fourier-Wavelet, and Randomization Methods are reported in Section 6.3.3. The wavelet approaches are able to generate a high-quality inertial range extending over an unprecedented twelve decades of scales using less than 2500 active computational elements [87,84]. The inertial-range scaling law (368) is accurately reproduced in detail from an average over only 100 or 1000 realizations. Among other things, this stresses the low variance of the wavelet-based Monte Carlo methods. We will explicitly contrast the scaling and homogeneity properties of the random fields generated by the MWE method and SRA method. The Randomization Method is next compared with the wavelet methods. We find that the Fourier-Wavelet Method is the best choice when one wishes to simulate very wide inertial ranges with more than 4–5 decades of scaling behavior, or when it is important for the simulated velocity field to be truly Gaussian. Due to the relatively high fixed overhead of the wavelet methods, the Randomization Method is more computationally efficient when only 4–5 decades of scaling behavior are desired and the statistical quantities of interest do not depend sensitively on the higher order statistics of the velocity field [82]. Finally, we apply the wavelet methods and the Randomization Method to the simulation of the relative turbulent diffusion of a pair of tracers in a steady fractal shear flow for which the exact statistics of the tracer separations can be expressed analytically. The numerical simulations are shown to match closely the exact results.

6.3.1. Successive Random Addition

We begin by formulating the Successive Random Addition (SRA) Method [336] as a hierarchical method as described in Eq. (369). Successive Random Addition constructs a random field by dyadic expansion. By definition, a dyadic rational number x satisfies $x = 2^{-m}n$ for some integers m and n, the *octave* and the *translate*, respectively. For each octave m, SRA constructs a piecewise linear field, $v_m(\cdot)$ as follows. First, at each integer $x = n$, this field is assigned an independent random value $\xi_{m,n}$ drawn from a standard Gaussian distribution (mean zero, unit variance):

$$v_m(n) = \xi_{m,n}, \quad n = 0, \pm 1, \pm 2, \ldots .$$

Next, the method extends $v_m(\cdot)$ to all other points by linear interpolation:

$$v_m(x) = \xi_{m,\lfloor x \rfloor}(1 - [x]) + \xi_{m,\lfloor x \rfloor + 1}[x] .$$

Here $\lfloor x \rfloor$ is the greatest integer less than x, and $[x] = x - \lfloor x \rfloor$ is the fractional part of x. The simulated field is finally built up by summing a suitably rescaled finite collection of such independently generated random fields:

$$v_{\text{SRA}}(x) = \sum_{m=m_{\min}}^{m_{\max}} 2^{-mH} v_m(2^m x) .$$

The SRA algorithm can be readily generalized to multidimensional random fields [100,335,336].

We note that in practice SRA can be implemented in a more efficient way than this literal description [335]. Namely, the computation of $v_{SRA}(x)$ requires the simulation and interpolation of only the two random variables $\xi_{m,n}$ at each octave m which are associated to the dyadic numbers $2^{-m}n$ bracketing x. Our concern here, however, is not with the efficiency of the SRA method, but with the nature of the random field which it would simulate even in the ideal limit in which all errors due to computational constraints can be neglected.

The problem with the SRA method, as explicitly demonstrated in [87], is that it produces a random field with strong deviations from the statistical self-similarity and homogeneity of the increments which a fractal random field is supposed to possess. For the fractal random field $v(x)$, the following scaled variance of velocity fluctuations is an absolute constant

$$\frac{\langle (v(x) - v(x'))^2 \rangle}{|x - x'|^{2H}} = S_v^{\mathrm{I}} ;$$

see Eq. (368). Consistency would require that the corresponding ratio for the random field simulated by SRA:

$$\frac{\langle (v_{SRA}(x) - v_{SRA}(x'))^2 \rangle}{|x - x'|^{2H}} = S_{SRA}^{\mathrm{I}}(x, x')$$

should settle down to approximately constant behavior for appropriately chosen simulation parameters. The function $S_{SRA}^{\mathrm{I}}(x, x')$ however, always has order unity variations as a function of x and x'. This variability in $S_{SRA}^{\mathrm{I}}(x, x')$ is systematic, and *not* due to finite sample sizes; $S_{SRA}^{\mathrm{I}}(x, x')$ as defined is a property of the simulated random field averaged over the full statistical ensemble. Moreover, there is no way to choose the parameters in the algorithm to reduce the variations in $S_{SRA}^{\mathrm{I}}(x, x')$ to a desired tolerance. Substantial variations are present for any finite choice of $m_{\min}$ and $m_{\max}$, and persist in the ideal limit $m_{\min} \to -\infty$, $m_{\max} \to +\infty$. Consequently, the SRA method cannot consistently simulate a fractal random field with statistically homogenous increments. The random field simulated by SRA does not even approximately obey the inertial range scaling law (368) with a constant prefactor. We now summarize some of the results from [87] which quantify the systematic inconsistency of SRA.

Rigorous numerical lower bounds on the variation of $S_{SRA}^{\mathrm{I}}(x, x')$ are obtained by exact evaluation of this function at specially chosen points. The ratio

$$\max S_{SRA}^{\mathrm{I}}(x, x') / \min S_{SRA}^{\mathrm{I}}(x, x')$$

is thereby found strictly to exceed unity for all Hurst exponents $0 < H < 1$, and to exceed 2 for a wide range of Hurst exponents $0.30 < H < 0.85$, including the value $H = 1/3$ associated to a turbulent velocity field with Kolmogorov scaling [87]. These numerical estimates hold not only for finite values of the cutoffs $m_{\min}$ and $m_{\max}$, but remain valid as these cutoffs are removed: $m_{\min} \to -\infty$ and $m_{\max} \to +\infty$. Note that due to the discrete self-similarity of the random field simulated by SRA, $S_{SRA}^{\mathrm{I}}(x, x') = S_{SRA}^{\mathrm{I}}(2x, 2x')$, and the order unity variations in $S_{SRA}^{\mathrm{I}}(x, x')$ occur at every scale.

It might still be conceivable that the variations in $S_{SRA}^{\mathrm{I}}(x, x')$ uncovered by the mathematical analysis are concentrated tightly around special points, and that for most values of (x, x'), the function $S_{SRA}^{\mathrm{I}}(x, x')$ is nearly constant. To demonstrate that this is not the case, we plot in Fig. 31
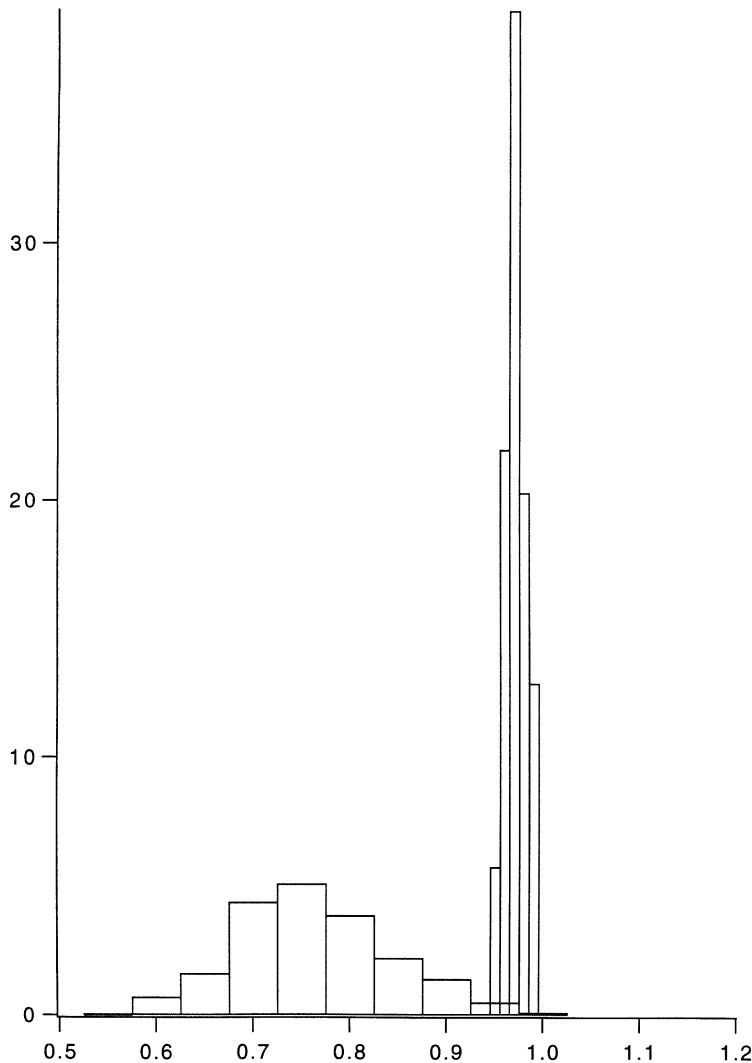
Fig. 31. Distributions for the normalized scaling coefficient for simulations of a fractal random field with Hurst exponent $H = \frac{1}{3}$ (from [87]). The broader distribution plots $S_{SRA}^{I}(x, x')/M_D$ for an ideal random field ($m_{min} = -\infty$, $m_{max} = +\infty$) generated by Successive Random Addition. The thinner distribution plots $S_{MWE}^{I}(x, x')/S_v^{I}$ for a random field generated by the MWE Method (to be discussed in Section 6.3.2) with $M = 40$ scales, wavelet order $\tau = 4$, and bandwidth $b = 5$.

a histogram for $H = \frac{1}{3}$ describing the distribution of $S_{SRA}^{I}(x, x')$ in the ideal case in which cutoffs can be neglected ($m_{min} = -\infty$ and $m_{max} = \infty$) [87]. Recall that $S_{SRA}^{I}(x, x')$ is a statistical quantity fully averaged over the entire statistical ensemble, so these distributions also are associated with the ideal limit in which fluctuations due to finite sampling are negligible. The values of $S_{SRA}^{I}(x, x')$ are normalized in the plot by the exactly computable constant $M_D \equiv \max_{x,x' \in \mathbb{R}^2} S_{SRA}^{I}(x, x')$. The area under the histogram between two points h_1 and h_2 represents the relative area in $(x, x') \in \mathbb{R}^2$ for

which $h_1 \leq S_{\mathrm{SRA}}^{\mathrm{I}}(x, x')/M_D \leq h_2$. By self-similarity, one may equivalently restrict attention to the unit square $0 \leq x, x' \leq 1$. This histogram is calculated numerically from exact discrete summation formulas, evaluated on a 32×32 discrete grid on the unit square [87]. The distribution of the values of the putative scaling coefficient $S_{\mathrm{SRA}}^{\mathrm{I}}(x, x')$ is rather broad. There are no parameters in the SRA algorithm which may be tuned to tighten these distributions so that $S_{\mathrm{SRA}}^{\mathrm{I}}(x, x')$ becomes approximately constant in space. Similar results are found for other values of the Hurst exponent [87].

SRA is therefore demonstrated to be an inconsistent algorithm for generating quantitatively accurate homogenous random fractal fields, both in theoretical and practical terms.

6.3.2. Wavelet approaches

We will next describe a pair of recently developed low variance Monte Carlo methods which can efficiently simulate fractal random fields over a large range of scales [82,84]. These are based on hierarchical discretizations of the basic stochastic representation formulas (340) and (337):

$$v(x) = \int_{-\infty}^{\infty} G(x - r)\, \mathrm{d}W(r) , \tag{370a}$$

$$v(x) = \int_{-\infty}^{\infty} \mathrm{e}^{-2\pi \mathrm{i}kx} E^{1/2}(|k|)\, \mathrm{d}\tilde{W}(k) \tag{370b}$$

through specially designed orthonormal wavelet expansions.

To motivate the introduction of wavelets in these methods, we first discuss the inadequacy of a more primitive hierarchical attempt to improve upon the Moving Average Method. This method and the Fourier Method are based on straightforward, equispaced discretizations of Eqs. (370a) and (370b), and were shown in Section 6.2 to fail seriously in representing long-range correlations in random fields. It is natural to try hierarchical versions of these methods, however, in the simulation of fractal random fields, since a hierarchical structure naturally treats every simulated scale on an approximately evenhanded basis.

Recall that the algorithm for the Moving Average Method was expressed:

$$v_{\mathrm{MA}}(x) = \sum_{j=\lfloor x/\Delta r \rfloor - b}^{\lfloor x/\Delta r \rfloor + b} G(x - r_j)\xi_j\sqrt{\Delta r} ,$$

where $\{r_j = j\Delta r\}_{j=-\infty}^{\infty}$ are the equispaced grid points in the integration and $\{\xi_j\}_{j=-\infty}^{\infty}$ is a collection of independent, standard, Gaussian random variables. The main difficulty of the Moving Average Method was that it could not accurately represent long-range correlations with a reasonable bandwidth b. One way to address this problem is to go back to the exact moving average representation on which the method is based:

$$v(x) = \int_{-\infty}^{\infty} G(x - r)\, \mathrm{d}W(r) , \tag{371}$$

and use the scaling properties of the weighting function $G(\cdot)$ to make a more efficient discrete approximation. For a fractal random field with Hurst exponent H as expressed by the structure function scaling (366), $G(\cdot)$ may be computed from its relation (360) to the energy spectrum $E(k) = A_E k^{-1-2H}$, yielding [84]

$$G(x) = K_H |x|^{H-1/2} , \tag{372}$$

with preconstant

$$K_H = \frac{\pi^{-(2+H)}\Gamma(2+H)}{\Gamma((1+2H)/4)}\sqrt{A_E} \ .$$

(The relation between the prefactor A_E in the energy spectrum and the prefactor in the structure function scaling (366) is given by Eq. (367).) As with all our discussions of fractal random fields, formula (371) with convolution kernel (372) only gives well-defined velocity differences $v(x) - v(x')$. Finite numerical approximations to this moving average formula will necessarily introduce cutoffs and be entirely well-defined.

Now, the weighting function $G(\cdot)$ is very long-ranged; it even grows with distance for $H > \frac{1}{2}$! Based on our numerical demonstrations in Section 6.2.4, we have no hope of representing these long-range correlations with a reasonable bandwidth if we use a straightforward equispaced discretization of the convolution integral (371). The scaling property of $G(\cdot)$, however, suggests a much more economical way of evaluating this integral. Note that the *derivative* of $G(\cdot)$ decreases with distance according to a power law. Thus, it is clearly wasteful to try and integrate Eq. (371) over a large segment with an equispaced partition. The integration step can be made coarser with $|x - r|$ to maintain a given level of accuracy, and the numerical integration interval can thereby be greatly increased without additional cost. More specifically, the self-similarity of the fractal field indicates that the integration step used to resolve correlations on a given scale should be proportional to that length scale. This suggests a hierarchical method in which an integration step $2^j \Delta r$ is used for $2^{j-1}b\Delta r < |x - r| \leq 2^j b\Delta r$, with a suitable positive integer b. Note that this keeps all evaluations on an equispaced grid. While this method will certainly improve upon the Moving Average Method, the bandwidth required for an accurate simulation is still much too large for practical purposes [84].

The underlying idea of using a variable numerical resolution proportional to the length scale being considered is clearly promising, however. What is needed is a more flexible means of constructing a finite hierarchical approximation to the moving average stochastic integral (371), and this is provided by the theory of orthonormal wavelet bases [80]. We will describe how to write the moving average representation as an exact discrete expansion with respect to an orthonormal wavelet family, and discuss the mathematical properties which the wavelet family should have so that finite truncations will be efficient approximations. The Alpert–Rokhlin multi-wavelet bases [3,4] meet the criteria, and their use in the orthonormal expansion produces what we call the Multi-Wavelet Expansion (MWE) Method [84].

We will then discuss the Fourier-Wavelet Method [82], another wavelet-based Monte Carlo method with certain improvements in simplicity, speed, flexibility. It is derived from an analogous orthonormal wavelet expansion in Fourier space using a Meyer wavelet as a "mother wavelet" [80]. While the Fourier-Wavelet Method is formulated in Fourier space, it is not a hierarchical Fourier Method because the simulated random field is not represented as a random Fourier sum. It can be naturally understood as a spectral implementation of an orthonormal wavelet expansion of the moving average representation.

We will only describe the theory and algorithms for the MWE and Fourier-Wavelet Methods here. Some demonstrations of their performance in practice will be given in Section 6.3.3 and throughout the remainder of Section 6.

6.3.2.1. Multi-Wavelet Expansion Method. We begin by showing how the moving average stochastic integral representation (371) may be expressed through an orthonormal basis as a randomly weighted sum of functions. The truncation of this sum permits a "finite element" type of discretization as an alternative to the "finite difference" discretizations of the stochastic integrals which led to the Moving Average Method and the Fourier Method. The MWE Method is based on such an orthonormal expansion using a wavelet basis which we will describe subsequently.

Orthonormal expansion of moving average representation. Let $\{\phi_j\}_{j=0}^\infty$ be a (complete) orthonormal basis for

$$L^2(\mathbb{R}) = \left\{ g \middle| \|g\|_2 = \left(\int_{-\infty}^\infty |g(x)|^2 \, \mathrm{d}x \right)^{1/2} < \infty \right\},$$

the Hilbert space of square integrable complex functions on the real line with inner product

$$(g, h) = \int_{-\infty}^\infty g(x)\overline{h(x)} \, \mathrm{d}x .$$

The orthonormal property means that

$$(\phi_j, \phi_{j'}) = \delta_{jj'} = \begin{cases} 1 & \text{if } j = j' ; \\ 0 & \text{otherwise} . \end{cases}$$

Moreover, any square integrable function $g \in L^2(\mathbb{R})$ can be expanded as a countably infinite and convergent sum of orthonormal basis functions [80]:

$$g = \sum_{j=0}^\infty (g, \phi_j)\phi_j . \tag{373}$$

An orthonormal basis can be used to rewrite any stochastic integral with respect to white noise as an infinite sum of weighted independent standard Gaussian random variables:

$$\int_{-\infty}^\infty g(r) \, \mathrm{d}W(r) = \int_{-\infty}^\infty \sum_{j=0}^\infty (g, \phi_j)\phi_j(r) \, \mathrm{d}W(r) = \sum_{j=0}^\infty (g, \phi_j)\xi_j , \tag{374}$$

where

$$\xi_j = \int_{-\infty}^\infty \phi_j(r) \, \mathrm{d}W(r) .$$

By the properties (341) of real white noise $\mathrm{d}W(r)$, it is easily checked from the orthonormality of the $\phi_j(r)$ that the $\{\xi_j\}_{j=0}^\infty$ is a sequence of independent, standard, real Gaussian random variables (mean zero, variance one). Because Eq. (374) holds for any $g \in L^2$, we can define a general rule for representing the white noise measure in stochastic integrals:

$$\mathrm{d}W(r) = \sum_{j=0}^\infty \xi_j \phi_j(r) , \tag{375}$$

where $\{\phi_j(r)\}_{j=0}^{\infty}$ is an orthonormal basis of $L^2(\mathbb{R})$ and $\{\xi_j\}_{j=0}^{\infty}$ is a collection of independent, standard real Gaussian random variables.

Applying this orthonormal expansion to the moving average representation (371), we obtain

$$v(x) = \int_{-\infty}^{\infty} G(x - r)\,dW(r) = \sum_{j=0}^{\infty} G \star \phi_j(x)\xi_j \,,$$

where the convolution operation is denoted by a star:

$$f \star g(x) = \int_{-\infty}^{\infty} f(x - r)g(r)\,dr \,.$$

Multi-wavelet orthonormal bases. To use the orthonormal expansion to construct a discrete *hierarchical* approximation for $v(x)$, we shall consider *multi-wavelet* orthonormal bases [80]. A multi-wavelet (a generalized wavelet) is a set of functions $\{\phi^{\sigma\tau}\}_{\sigma=1}^{\tau}$ that has the special property that its discrete translates and dilates:

$$\{\phi_{mn}^{\sigma\tau}(x) = 2^{m/2}\phi^{\sigma\tau}(2^m x - n)\,|\,\sigma = 1, \ldots, \tau; \quad m, n = 0, \pm 1, \pm 2, \ldots,\}$$

form an orthonormal basis for $L^2(\mathbb{R})$. We will use the term *wavelet* to refer to a function from a multi-wavelet, although the term usually refers to a single function whose dilates and translates form a basis for $L^2(\mathbb{R})$ [80]. The double subscript notation $\phi_{mn}^{\sigma\tau}(x)$ for dilation and translation is standard for multi-wavelets. The superscript τ denotes the *order* of the multi-wavelet basis. The first subscript m is called the *octave* and the second subscript is called the *translate*. The expansion of the moving average representation in terms of the multi-wavelet basis is written:

$$v(x) = \sum_{\sigma=1}^{\tau} \sum_{m,n=-\infty}^{\infty} G \star \phi_{mn}^{\sigma\tau}(x)\xi_{mn}^{\sigma} \,, \tag{376}$$

where $\{\xi_{mn}^{\sigma}\,|\,\sigma = 1, \ldots \tau;\, m, n = 0, \pm 1, \pm 2, \ldots\}$ is a collection of independent, standard, Gaussian random variables.

Now we make use of the self-similar scaling (372) of the convolution kernel G to write this expansion in an explicitly hierarchical form. By simple rescalings, one can check that

$$G \star \phi_{mn}^{\sigma\tau}(x) = 2^{-mH} G \star \phi^{\sigma\tau}(2^m x - n) \,.$$

Therefore, we have the following hierarchical representation for the random fractal velocity field $v(x)$:

$$v(x) = \sum_{m=-\infty}^{\infty} 2^{-mH} v_m(2^m x) \,, \tag{377a}$$

$$v_m(x) = \sum_{\sigma=1}^{\tau} \sum_{n=-\infty}^{\infty} G \star \phi^{\sigma\tau}(x - n)\xi_{mn}^{\sigma} \,. \tag{377b}$$

We note that for a suitable choice of a multi-wavelet (including the Alpert–Rokhlin multi-wavelet which we will use), the convolution $G \star \phi^{\sigma\tau}$ is perfectly well-defined without cutoffs. The only divergence is in the sum over m, which as usual, will be cut off by any numerical implementation. See [84] for a rigorous mathematical treatment.

The multi-wavelet representation (377) is an exact formula for the fractal random field $v(x)$, equivalent to the moving average representation (371). A numerical implementation will of course require a truncation of the infinite sums over m and n. The cost of such a wavelet-based algorithm will clearly be proportional to the number of terms retained in the sums. We can consequently keep more octaves (more terms in the m summation) at a given cost if we keep fewer terms in the sums over translations (index n). The issue, then, is how to minimize the number of translates which must be summed over in each octave to meet a given accuracy.

Localization of sum over translates. The errors incurred in truncating the sum

$$\sum_{n=-\infty}^{\infty} G\star\phi^{\sigma\tau}(x-n)\xi^{\sigma}_{mn} \tag{378}$$

may appear at first glance to be as devastating as those which result in truncating the physical-space stochastic integral in the moving average representation:

$$v(x) = \int_{-\infty}^{\infty} G(x-r)\,\mathrm{d}W(r)\ .$$

Indeed, this latter expression may be written in a similar form to Eq. (378):

$$v(x) = \sum_{n=-\infty}^{\infty} G\star\chi_{[0,1]}(x-n)\xi_n\ , \tag{379}$$

where

$$\chi_{[0,1]}(x) = \begin{cases} 1 & \text{for } 0 \le x \le 1\ , \\ 0 & \text{otherwise}\ , \end{cases}$$

and $\{\xi_n\}_{n=-\infty}^{\infty}$ is a collection of independent, standard Gaussian random variables. Both Eqs. (378) and (379) involve a sum over convolutions of the slowly decaying (or even increasing!) function $G(\cdot)$. The Moving Average Method is essentially derived by truncating the sum in Eq. (379) (with the step size rescaled to Δr), and we saw in Section 6.2.4 that this led to gross inaccuracies even for large bandwidths.

There is however a crucial difference between the two expressions: Eq. (378) is a convolution of G with multi-wavelets *which we are still free to choose*, whereas the summands in Eq. (379) are completely determined. The success of a wavelet-based Monte Carlo Method relies crucially upon choosing the multi-wavelets $\{\phi^{\sigma\tau}\}^{\tau}_{\sigma=1}$ in an intelligent manner so that $G\star\phi^{\sigma\tau}$ decays rapidly and the sum (378) may be well approximated by only a relatively small number of terms with $n \approx x$. To see what properties the multi-wavelets should have to make this possible, we work out the far-field asymptotics of the convolution [84] by binomially expanding $G(x-r) = G|x-r|^{H-1/2}$ for large x:

$$G\star\phi^{\sigma\tau}(x) \sim C_{\pm}K_H I_Q |x|^{H-(1/2)-Q} \quad \text{as } x \to \pm\infty$$

where $C_{\pm}$ are some explicitly computable combinatorial constants, and Q is the minimal non-negative integer q so that the wavelet moment:

$$I_q \equiv \int_{-\infty}^{\infty} r^q \phi^{\sigma\tau}(r)\,\mathrm{d}r$$

is nonvanishing. The decay of the convolution $G \star \phi^{\sigma \tau}$ is therefore determined by the number of moments I_q which vanish for all wavelets in the multi-wavelet $\{\phi^{\sigma \tau}\}_{\sigma=1}^{\tau}$. We are thus led to look for a multi-wavelet with good moment cancellation properties [37].

The Alpert–Rokhlin basis [3,4] meets our need. For each $\tau \geq 1$, there exists an Alpert–Rokhlin multi-wavelet $\{\phi^{\sigma \tau}\}_{\sigma=1}^{\tau}$ consisting of piecewise polynomial functions supported in the unit interval $[0,1]$ with moments vanishing through order $\tau - 1$:

$$\int_0^1 \phi^{\sigma \tau}(x) x^q \, \mathrm{d}q = 0 \quad \text{for } q = 0, \ldots, \tau - 1 .$$

Their essential properties for our purposes are summarized concisely in [84]. With a larger choice of τ, the convolution $G \star \phi^{\sigma \tau}$ decays more rapidly and fewer terms are needed in the sum over n to meet a specified accuracy. This consideration must be balanced by the cost of maintaining τ different wavelets.

Description of multi-wavelet expansion (MWE) method. According to the analysis in [84], the Alpert–Rokhlin multiwavelet of order $\tau = 4$ is found to be sufficient for accurate simulation for Hurst exponent $H = \frac{1}{3}$, the Kolmogorov value. One now chooses a suitable bandwidth b so that the sum over n is well represented by a sum over $|n - \lfloor x \rfloor| \leq b$, and imposes cutoffs $m_{\min}$ and $m_{\max}$ on the summation over the octaves m in Eq. (377a). By scale invariance, we can generally put $m_{\min} = 0$, and let $m_{\max} = M - 1$, where M is the number of octaves simulated. The *Multi-Wavelet Expansion* (MWE) *Method* then takes the form

$$v_{\mathrm{MWE}}(x) = \sum_{m=0}^{M-1} 2^{-mH} v_{\mathrm{MWE,m}}(2^m x) , \tag{380}$$

$$v_{\mathrm{MWE,m}}(x) = \sum_{n=\lfloor x \rfloor - b}^{\lfloor x \rfloor + b} \sum_{\sigma=1}^{\tau} f_{\mathrm{MWE},\sigma}(x - n) \xi_{mn}^{\sigma} ,$$

$$f_{\mathrm{MWE},\sigma}(x) = G \star \phi^{\sigma \tau}(x) ,$$

where $\{\xi_{mn}^{\sigma} \,|\, \sigma = 1, \ldots, \tau; m = 0, \ldots, M - 1; n = 0, \pm 1, \pm 2, \ldots\}$ is a collection of independent Gaussian standard random variables.

It may be desirable in certain applications to let the bandwidth depend on the octave $b = b_m$; see [84]. In any case, rigorous estimates are available for the error in truncating the summation over n, and these can be used to choose b according to the accuracy desired. Such analysis may be found in the original paper [84]. We note that with the $\tau = 4$ Alpert–Rokhlin multi-wavelet, bandwidths on the order of $b = 5$ are already sufficient to guarantee excellent accuracy [84].

One feature which the Multi-Wavelet Expansion Method shares with the Moving Average Method is its reference to an infinite collection of independent random variables. While only finitely many need to be evaluated to determine $v_{\mathrm{MWE}}(x)$ over any finite region, there is still the practical difficulty of storing and keeping track of the random numbers as they are generated. This problem can be overcome through the use of a reversible random number generator and an indexing scheme exploiting the hierarchical structure of the MWE Method. This procedure, developed and described in [84], completely avoids the enormous memory cost which would be required if the random numbers needed to be precomputed and stored.

We finally remark that the $\tau = 1$ Alpert–Rokhlin multi-wavelet ϕ^{11} is nothing more than the simplest of all wavelets, the Haar wavelet [80]:

$$
\phi^{11}(x) = \begin{cases} -1 & \text{if } 0 < x < \frac{1}{2}, \\ 1 & \text{if } \frac{1}{2} < x < 1, \\ 0 & \text{otherwise}. \end{cases}
$$

It can be checked that the MWE Method using these Haar wavelets is equivalent to the straightforward hierarchical version of the Moving Average Method which we described near the beginning of Section 6.3.2. As only the zeroth-order moment of the Haar wavelet vanishes, the summation over n is not so well localized in this case: $G \star \phi^{11}(x) \sim C_\pm |x|^{H-3/2}$ as $x \to \pm \infty$. Computations in [84] using rigorous truncation error estimates show that to obtain good accuracy, the bandwidth b must be orders of magnitude larger if Haar wavelets were used instead of the $\tau = 4$ Alpert–Rokhlin multi-wavelets. This emphasizes the importance of the choice of multi-wavelet basis in the success of the MWE Method; the fact that it is hierarchical is not sufficient unto itself.

6.3.2.2. Fourier-wavelet method. We now describe the Fourier-Wavelet Method, a variation of the MWE Method which is easier to implement, faster, and more flexible. The Fourier-Wavelet Method is based on the same general orthonormal multi-wavelet expansion (377) as the MWE Method, but is implemented spectrally. As we shall show in a moment, a single *Meyer wavelet* ϕ [80] is sufficient to generate an orthonormal wavelet basis with the desired properties, so we will drop the multi-wavelet indices σ and τ in our discussion of the Fourier-Wavelet Method:

$$
v(x) = \sum_{m,n=-\infty}^{\infty} G \star \phi_{mn}(x)\xi_{mn}, \tag{381}
$$

$$
\phi_{mn}(x) = 2^{m/2}\phi(2^m x - n), \quad m, n = 0, \pm 1, \pm 2, \dots .
$$

The $\{\xi_{mn}\}_{m,n=-\infty}^{\infty}$ is a collection of independent, standard, real Gaussian random variables. For fractal random fields $v(x)$, the power law form of G permits the following self-similar hierarchical expression:

$$
v(x) = \sum_{m=-\infty}^{\infty} 2^{-mH} v_m(2^m x), \tag{382}
$$

$$
v_m(x) = \sum_{n=-\infty}^{\infty} G \star \phi(x - n)\xi_{mn}.
$$

At the end we will show how the Fourier-Wavelet Method can be applied to generate more general random fields without self-similarity properties, but at the moment we focus on fractal random fields.

The Fourier-Wavelet Method departs from the MWE Method in that the convolutions in the sum are handled spectrally. The convolution theorem from Fourier analysis ([50], p. 108) states

that for any square-integrable functions $g, h \in L^2(\mathbb{R})$:

$$g \star h(x) = \mathscr{F}^{-1}(\mathscr{F}g\mathscr{F}h)(x) = \int_{-\infty}^{\infty} e^{-2\pi i kx} \hat{g}(k)\hat{h}(k) \, dk \; ,$$

where hats and the operator $\mathscr{F}$ each denote a Fourier transform:

$$\hat{g}(k) = (\mathscr{F}g)(k) \equiv \int_{-\infty}^{\infty} e^{2\pi i kx} g(x) \, dx \; ,$$

and $\mathscr{F}^{-1}$ denotes the inverse of the Fourier transform:

$$(\mathscr{F}^{-1}\psi)(x) = \int_{-\infty}^{\infty} e^{-2\pi i kx} \psi(k) \, dk \; .$$

Now, from the relation (342), the Fourier transform of $G(x)$ is the square root of the energy spectrum: $(\mathscr{F}G)(k) = E^{1/2}(|k|)$. Defining $\hat{\phi} = \mathscr{F}\phi$, we have

$$G \star \phi(x) = \mathscr{F}^{-1}(E^{1/2}\hat{\phi})(x) \; ,$$

where $E(k)$ is understood here to be extended as an even function to the negative k axis. The orthonormal wavelet expansion (382) may then be written:

$$v(x) = \sum_{m=-\infty}^{\infty} 2^{-mH} v_m(2^m x) \; ,$$

$$v_m(x) = \sum_{n=-\infty}^{\infty} f(x-n)\xi_{mn} \; , \tag{383}$$

$$f(x) = \mathscr{F}^{-1}(E^{1/2}\hat{\phi})(x) \; .$$

This expression for the random field $v(x)$ may also be derived from its stochastic Fourier integral representation (337) by expanding the *complex* white noise $d\tilde{W}(k)$ with respect to the orthonormal basis $\{\hat{\phi}_{mn} = \mathscr{F}\phi_{mn}\}_{m,n=-\infty}^{\infty}$ in a manner similar to Eq. (375) (see [82]). Note that regardless of the method of derivation of Eq. (383), the underlying *wavelet* basis $\{\phi_{mn} = 2^{m/2}\phi(2^m x - n)\}_{m,n=-\infty}^{\infty}$ is defined in physical space. Its Fourier transform is an orthonormal basis by the Plancherel theorem ([50], p. 113), but not (in general) a wavelet basis since the $\{\hat{\phi}_{mn}\}_{m,n=-\infty}^{\infty}$ are not related to each other by dilation and translation.

We now tackle the problem of localizing the summation over n in Eq. (383) from the spectral perspective. What is required is that f decay rapidly. But decay of f in physical space is linked to the smoothness of its Fourier transform $\hat{f} = \mathscr{F}f$. Namely, if

$$|2\pi|^{-p} \int_{-\infty}^{\infty} \left| \frac{d^p \hat{f}(k)}{dk^p} \right| dk = C_p < \infty \; ,$$

then (see [50], p. 117):

$$|f(x)| \le C_p |x|^{-p} \; .$$

We are therefore led to choose the wavelet ϕ so that

$$\hat{f}(k) = E^{1/2}(k)\hat{\phi}(k)$$

has a sufficiently large number of bounded derivatives for the energy spectrum of interest. For the fractral random field currently under consideration, $E(k) = A_E|k|^{-1-2H}$ has a nasty singularity at $k = 0$, but is otherwise smooth. We can therefore guarantee $\hat{f}(k)$ to have p bounded derivatives if the Fourier transform of the wavelet ϕ is compactly supported away from the origin, and has p classical derivatives. The *Meyer wavelet* ϕ based on a pth-order *perfect B-spline* satisfies these properties in an optimal fashion; see [7,80,82] for the details.

Numerical studies in [82] indicate that a second order ($p = 2$) perfect B-spline is a good practical choice in defining the Meyer wavelet ϕ for a fractal random field with $H = \frac{1}{3}$. The *Fourier-Wavelet Method* is then implemented by keeping only a finite number of octaves $m = 0, \ldots, M - 1$ and using the rapid decay of $f(x)$ to approximate the sum over its translates to high accuracy using a reasonable bandwidth b:

$$v_{\text{FW}}(x) = \sum_{m=0}^{M-1} 2^{-mH} v_{\text{FW},m}(2^m x) ,$$

$$v_{\text{FW},m}(x) = \sum_{n=\lfloor x \rfloor - b}^{\lfloor x \rfloor + b} f_{\text{FW}}(x - n)\xi_{mn} , \tag{384}$$

$$f_{\text{FW}}(x) = \mathscr{F}^{-1}(E^{1/2}\hat{\phi})(x) .$$

The $\{\xi_{m,n}; m = 0, \ldots, M - 1; n = 0, \pm 1, \pm 2, \ldots\}$ are standard Gaussian independent random variables. The functions $f_{\text{FW}}(x)$ are evaluated by fast Fourier transform and interpolation. Rigorous estimates for the numerical errors incurred in this computation as well as for the truncation error in the summation over n are given in [82].

Extension of Fourier-Wavelet Method to random fields without self-similarity. One appealing feature of the Fourier-Wavelet Method is that it may be applied without significant change to the simulation of random fields with a wide range of active scales where perhaps the energy spectrum $E(k)$ is not a simple power law. To see this, let us return to the general orthonormal wavelet expansion (381) which did not assume self-similarity of G:

$$v(x) = \sum_{m,n=-\infty}^{\infty} G \star \phi_{mn}(x)\xi_{mn} ,$$

$$\phi_{mn}(x) = 2^{m/2}\phi(2^m x - n), \quad m, n = 0, \pm 1, \pm 2, \ldots .$$

Using the scaling properties of the wavelets, this can always be cast in a hierarchical form:

$$v(x) = \sum_{m=-\infty}^{\infty} v_m(2^m x) , \tag{385a}$$

$$v_m(x) = \sum_{n=-\infty}^{\infty} f_m(x - n)\xi_{mn} , \tag{385b}$$

but the functions f_m do not in general satisfy the scaling relation $f_m(x) = 2^{-mH}f(x)$, which held for fractal random fields with Hurst exponent H. They must instead be computed separately for each m:

$$f_m(x) = G_m \star \phi(x), \qquad G_m(x) = 2^{-m/2}G(2^{-m}x) \,. \tag{386}$$

The spectral representation of these functions is (see Eq. (383))

$$f_m(x) = \mathscr{F}^{-1}(E_m^{1/2}\hat{\phi})(x) \,, \tag{387}$$

$$E_m(k) = 2^m E(2^m k) \,. \tag{388}$$

Localization of the summations of translates of these functions in Eq. (385b) requires that the wavelet ϕ be chosen so that each of the f_m decay rapidly. Viewed in physical space (386), this appears to be a complicated task, but it can be done quite simply in the spectral framework (387). We simply need to ensure that

$$\hat{f}_m(k) = (\mathscr{F}f_m)(k) = E_m^{1/2}(k)\hat{\phi}(k)$$

has sufficiently many bounded derivatives for all octaves m retained in the simulation. The Meyer wavelet based on a pth-order perfect B-spline still works well for this purpose [82]. Because it is compactly supported away from the origin and has p bounded classical derivatives, $\hat{f}_m(k)$ will have p bounded derivatives for any smooth spectrum $E(k)$ which may even have strong algebraic singularities at $k = 0$ and $k = \infty$.

The form of the *Fourier-Wavelet Method* for general random fields can therefore be written:

$$
\begin{aligned}
v_{\mathrm{FW}}(x) &= \sum_{m=0}^{M-1} v_{\mathrm{FW},m}(2^m x) \,, \\
v_{\mathrm{FW},m}(x) &= \sum_{n=\lfloor x \rfloor - b}^{\lfloor x \rfloor + b} f_{\mathrm{FW},m}(x - n)\xi_{mn} \,, \\
f_{\mathrm{FW},m}(x) &= \mathscr{F}^{-1}(E_m^{1/2}\hat{\phi})(x) \,, \\
E_m(k) &= 2^m E(2^m k) \,,
\end{aligned}
\tag{389}
$$

where $\{\xi_{m,n}; m = 0, \ldots, M-1; n = 0, \pm 1, \pm 2, \ldots\}$ is a collection of standard Gaussian independent variables, and ϕ is a Meyer wavelet constructed from a perfect B-spline of order p. Practical choices of p may depend on the application. The functions $f_{\mathrm{FW},m}(x)$ are computed by fast Fourier transform and interpolation.

6.3.2.3. Comparison of the Fourier-Wavelet and Multi-Wavelet Expansion Methods. We have already pointed out one advantage of the Fourier-Wavelet over the Multi-Wavelet Expansion (MWE) Method, in that the Fourier-Wavelet Method is applicable to random fields with general spectra $E(k)$. In localizing the summation over translates of $f_{\mathrm{MWE},\sigma}(x)$ in the MWE Method Eq. (380), a moment cancellation criterion was used to choose the Alpert–Rokhlin multi-wavelet. This criterion arose from a far-field expansion of the specific moving average weighting function $G(x) = K_H|x|^{H-1/2}$ associated to fractal random fields. The criterion used for localizing the summation over the analogous functions $f_{\mathrm{FW},m}(x)$ in the Fourier-Wavelet Method (389), on the other hand, does not rely on specific assumptions about the energy spectrum $E(k)$. Furthermore,

because the Fourier-Wavelet Method is a spectral method, it is compatible with spectral techniques for solving partial differential equations. The MWE Method has no such compatibility with anisotropic spectra generated by solutions of partial differential equations.

The Fourier-Wavelet Method is also much simpler to implement and faster than the MWE Method, as detailed in [82,84].

6.3.3. Comparison of simulation results

We now demonstrate the excellent performance which results from the careful mathematical design of the MWE and Fourier-Wavelet methods. We will also discuss the relative merits of these wavelet-based methods and the nonhierarchical Randomization Method in simulating fractal random fields. First we will focus on the simulation of the random velocity field $v(x)$ itself, and then turn to the simulation of the relative turbulent diffusion of a pair of tracers being swept at a constant rate across a steady, fractal random shear flow.

Recall that a Gaussian fractal random field is characterized by the velocity increment between two points $v(x) - v(x')$ being a mean zero, Gaussian random variable, with variance varying as a power law of the separation distance between the observation points:

$$\langle (v(x) - v(x'))^2 \rangle = S_v^I |x - x'|^{2H} . \tag{390}$$

6.3.3.1. Consistency of Wavelet Methods. The first issue we check is that the wavelet methods will indeed generate random fields with clean scaling behavior in the ideal limit in which finite Monte Carlo sampling error can be ignored. We test whether the rescaled mean-square velocity difference of the velocity field simulated by the MWE method:

$$S_{\text{MWE}}^I(x, x') = \frac{\langle (v_{\text{MWE}}(x) - v_{\text{MWE}}(x'))^2 \rangle}{|x - x'|^{2H}}$$

is indeed approximately constant, as it should be for a consistent approximation to a fractal random field satisfying Eq. (390). We plot in Fig. 31 a histogram of this function for a MWE random field with $M = 40$ octaves, wavelet order $\tau = 4$, and bandwidth $b = 5$ alongside the corresponding histogram for the SRA algorithm with infinitely many octaves [87]. (In the histogram, $S_{\text{MWE}}^I(x, x')$ is normalized by S_v^I rather than a maximum of $S_{\text{MWE}}^I(x, x')$ over the sampled unit square, but as can be seen from the histogram, these values are very nearly the same.) The histogram for the MWE Method is much narrower than that of the SRA Method, showing only a 6% variation of $S_{\text{MWE}}^I(x, x')$ for the sampled values in the square $0 \le x, x' \le 1$. Note that only finitely many octaves are retained for the MWE computation, so the histogram is broadened somewhat by the breakdown of scaling for $|x - x'| \approx 1$, the largest retained scale. Even sharper constancy for $S_{\text{MWE}}^I(x, x')$ can be expected on scales well separated from the cutoffs. In any case, Fig. 31 demonstrates that the MWE Method consistently generates a fractal random field with accurate scaling (390) and homogeneity of its increments in the limit of infinitely many realizations.

6.3.3.2. Simulations of velocity field structure function. A striking feature of the wavelet Monte Carlo methods is their low variance: averaging over an accessibly small number of realizations still produces phenomenally clean statistical scaling. In Fig. 32, we present the numerically computed
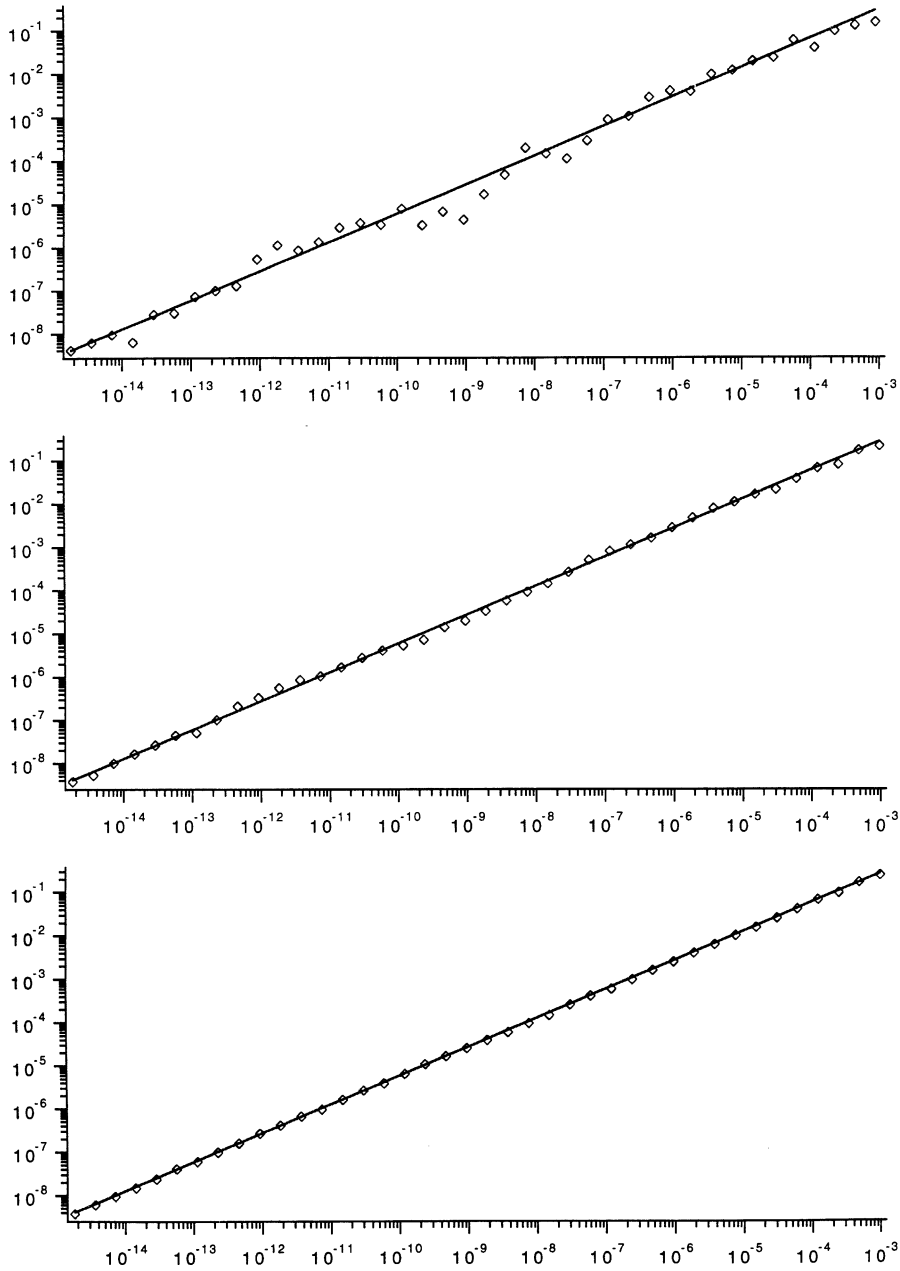
Fig. 32. Monte Carlo simulations for the structure function $S_v(x)$ of a fractal velocity field with Hurst exponent $H = \frac{1}{3}$ using MWE Method with $M = 40$ octaves, wavelet order $\tau = 4$, and bandwidth $b = 5$. The simulated structure functions are plotted with $+$ symbols, computed from averages over 10 (upper graph), 100 (middle graph), and 1000 (lower graph) realizations. The structure function of the true fractal random field is plotted with a solid line (from [87]).

structure function of the velocity field:

$$S_v(x) = \langle (v(x + x') - v(x'))^2 \rangle$$

for $x' = 0$, averaged over 10, 100, and 1000 independent realizations of $H = \frac{1}{3}$ fractal random fields $v(x)$ generated by the MWE method. For all three sample sizes, including the one with only 10 realizations, this structure function obeys a power law with exponent 0.66, in very good agreement with the correct value $2H = \frac{2}{3}$. Moreover, the scaling coefficient $S^{\mathrm{I}}_{\mathrm{MWE}}(x, x')$ remains within 8% of the correct constant value S^{I}_v over the entire 12 decades of scaling. Only 2500 active computational elements are needed to generate each realization. The use of the Alpert–Rokhlin wavelets to localize the computation is crucial to this efficiency. With Haar wavelets, orders of magnitude more wavelets would have to be retained for comparable accuracy [84]. Many more practical numerical details about the MWE method may be found in [84].

The Fourier-Wavelet Method also enjoys great practical success. The plots in Fig. 33 depict the velocity field structure function simulation results using the Fourier-Wavelet Method with $M = 40$ octaves and bandwidth $b = 10$. We observe quite good agreement with the fractal scaling law (390) over nine decades. A log–log least-squares power law fit produces a scaling exponent 0.668 versus a true value of $\frac{2}{3}$, while the fit of the scaling coefficient is 0.635 versus a true value of $S^{\mathrm{I}}_v = 0.639$ in this simulation. The statistics of the sample were shown in [82] to be highly Gaussian, in that the flatness factor of the two-point velocity difference

$$F_{\mathrm{FW}}(x) = \frac{\langle (v_{\mathrm{FW}}(x) - v_{\mathrm{FW}}(0))^4 \rangle}{\langle (v_{\mathrm{FW}}(x) - v_{\mathrm{FW}}(0))^2 \rangle^2}$$

remains within 0.5 of the Gaussian value $F(x) = 3$ over the nine decades of accurate scaling. The deviations from Gaussianity are purely due to finite sample size; the underlying simulation formulas for the wavelet methods describe Gaussian random fields.

Finally, we apply the Randomization Method to the simulation of a fractal random field with a Hurst exponent $H = \frac{1}{3}$ (see Section 6.2.3 for an introduction to the Randomization Method). The Randomization Method makes explicit reference to the energy spectrum, which for the present fractal random field is formally

$$E(k) = A_E |k|^{-5/3} .$$

For the formulas of the Randomization Method to be well defined, the total energy $\int_0^\infty E(k)\,\mathrm{d}k$ must be finite, so we introduce a numerical cutoff:

$$E(k) = 0 \quad \text{for } |k| \leq k_{\min} .$$

We subdivide wavenumber space into $M = 256$ compartments $\{I_j\}_{j=1}^{256}$ containing equal amounts of energy:

$$\int_{I_j} E(k)\,\mathrm{d}k = \frac{1}{M} \int_0^\infty E(k)\,\mathrm{d}k ,$$

and construct the simulated velocity field as a superposition of Fourier modes with one wavenumber selected randomly from each of these $M = 256$ bands. We are thereby able to obtain a random
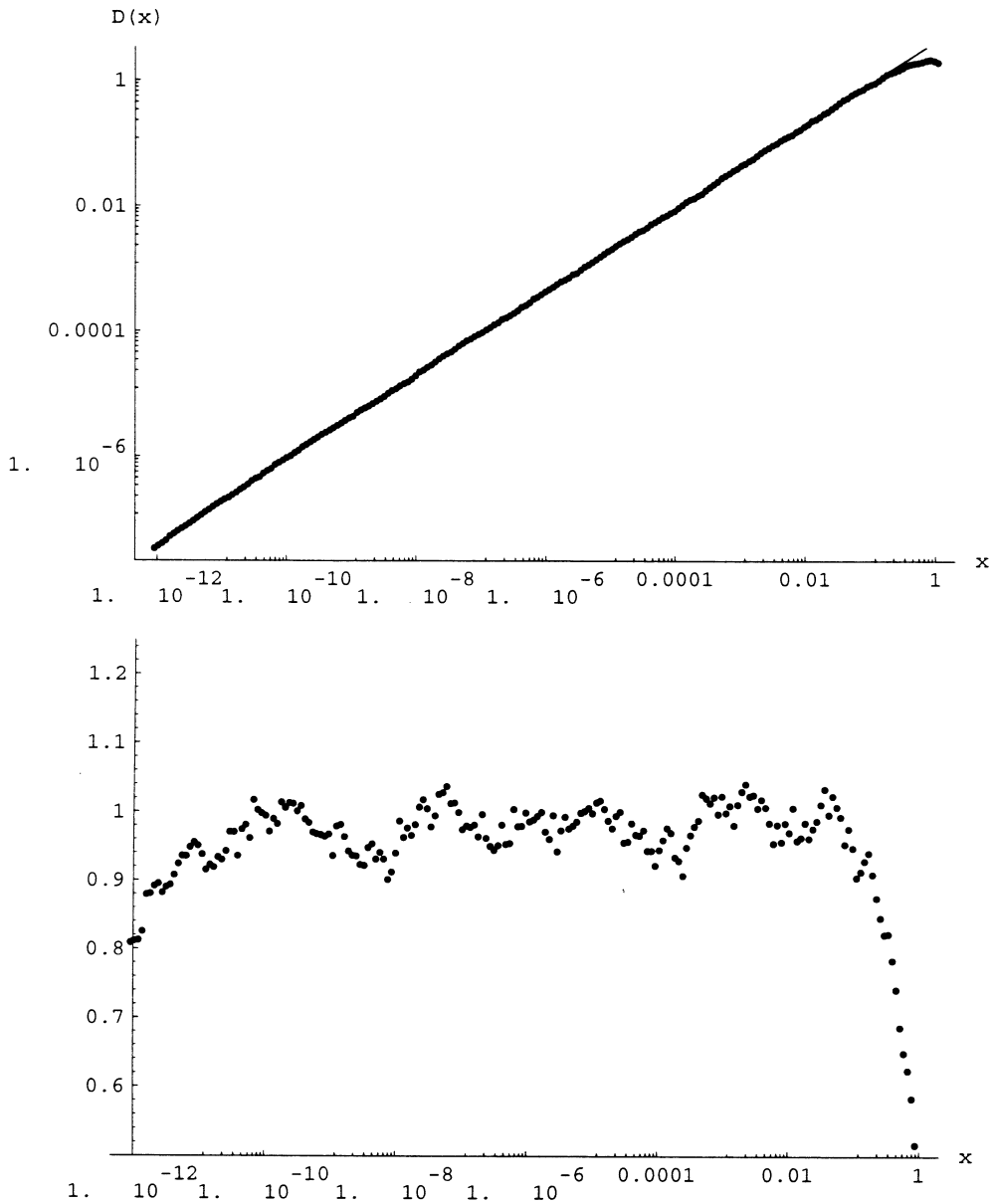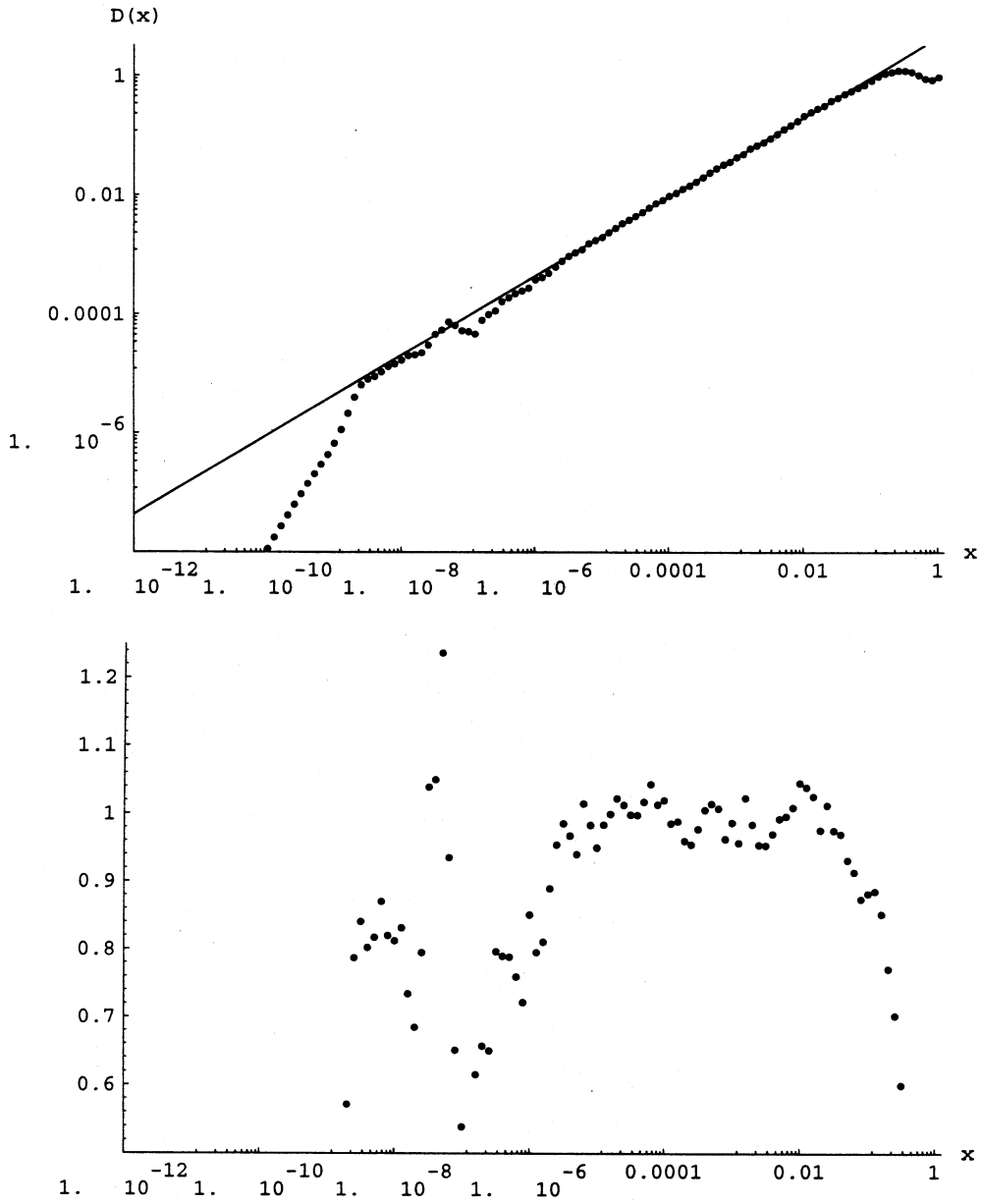
Fig. 33. Monte Carlo simulations for the structure function $S_v(x)$ of a fractal velocity field with Hurst exponent $H = \frac{1}{3}$ using the Fourier-Wavelet Method with $M = 40$ octaves, bandwidth $b = 10$ for 2000 realizations (from [82]). The upper graph shows the simulated structure function as dots and the structure function of the true fractal random field as a solid line. The lower plot shows the ratio of the simulated to the true structure function.

field with roughly 4 decades of accurate scaling behavior in the structure function when averaged over 2000 independent realizations (Fig. 34). Unlike the wavelet methods, the simulation formula for the Randomization Method does not describe a Gaussian random field, so one may well expect significant departures from Gaussianity in the simulated sample. As shown in [82], the flatness

Fig. 34. Monte Carlo simulations for the structure function $S_v(x)$ of a fractal velocity field with Hurst exponent $H = \frac{1}{3}$ using the Randomization Method with $M = 256$ compartments in the partition and 2000 realizations (from [82]). The upper graph shows the simulated structure function as dots and the structure function of the true fractal random field as a solid line. The lower graph shows the ratio of the simulated to the true structure function.

factor computed from the above sample of 2000 fields simulated by the Randomization Method,

$$F_{\text{Rand}}(x) = \frac{\langle (v_{\text{Rand}}(x) - v_{\text{Rand}}(0))^4 \rangle}{\langle (v_{\text{Rand}}(x) - v_{\text{Rand}}(0))^2 \rangle^2},$$

is within 0.5 of the Gaussian value 3 only for the upper three decades of its four decade scaling regime. Over the lowest decade of scaling, the flatness factor becomes very large, and the simulated field on these scales is strongly non-Gaussian. This sort of behavior was also observed for other Randomization Method simulations with other choices of parameters; see [82] for further details and discussion.

6.3.3.3. Simulations of relative tracer diffusion in fractal random steady shear flow. We have seen above that the wavelet Monte Carlo methods and the Randomization Method are each capable of generating random fields with several decades of self-similar scaling behavior. Our particular interest is to apply these methods to simulating tracer motion in velocity fields with wide inertial-ranges. Therefore, it is prudent to check directly that the tracer motion is simulated accurately in an exactly solvable model. Even though we have verified the quality of the simulated velocity fields in several ways, we attempt to understand subtle discrepancies which may have strong cumulative effects on the simulation of tracer motion.

To this end, we introduce an extension of the Random Steady Shear (RSS) Model, which we used as a benchmark problem for nonhierarchical Monte Carlo methods in Section 6.2. As in the RSS Model, we take the velocity field as a two-dimensional steady random shear flow with constant cross sweep:

$$\boldsymbol{v}(\boldsymbol{x}, t) = \boldsymbol{v}(x, y, t) = \begin{bmatrix} \bar{w} \\ v(x) \end{bmatrix},$$

where $v(x)$ is a mean zero, homogenous, Gaussian random field with correlation function expressed through its energy spectrum:

$$R(x) = \langle v(x' + x)v(x') \rangle = \int_{-\infty}^{\infty} E(|k|)e^{2\pi i k x}\, dk = 2\int_0^{\infty} E(k)\cos(2\pi k x)\, dk .$$

In the *Fractal Random Steady Shear* (*FRSS*) Model, we shall choose the steady shear flow as a fractal random field with formal energy spectrum

$$E(k) = A_E |k|^{-1-2H} ,$$

with Hurst exponent $0 < H < 1$. As we mentioned above, there is some technical difficulty in this definition because of the infrared divergence of the energy spectrum at $k = 0$, but in any numerical implementation there will be some effective cutoffs imposed at both large and small wavenumbers. For practical purposes, then, it is only important that the statistical quantities we consider are insensitive to such cutoffs when they are sufficiently remotely separated from the scales of interest. The velocity structure function is one such statistical quantity, and the mean-square relative displacement of a pair of tracers is another; see Section 3.5. The structure functions of the simulated velocity fields have been examined above, and we now turn to the problem of correctly simulating

the mean-square relative displacement of a pair of tracers along the direction of the shear:

$$\sigma_{\Delta Y}^2(t) \equiv \langle (Y^{(1)}(t) - Y^{(2)}(t))^2 \rangle \ .$$

We assume in the following that the cross sweep is nontrivial $\bar{w} \neq 0$, and that there is no molecular diffusion ($\kappa = 0$). By the same methods used in [141] and Section 3.2, one can compute an exact formula for $\sigma_{\Delta Y}^2(t)$ in the FRSS Model [84]:

$$\sigma_{\Delta Y}^2(t) = \frac{S_v^{\mathrm{I}}}{(1 + H)(1 + 2H)|\bar{w}|^2}(|\bar{w}t|^{2 + 2H} + |\Delta x|^{2 + 2H} - \tfrac{1}{2}|\Delta x - \bar{w}t|^{2 + 2H} - \tfrac{1}{2}|\Delta x + \bar{w}t|^{2 + 2H}),$$

(391)

$$S_v^{\mathrm{I}} = -2A_E \pi^{1/2 + 2H}\frac{\Gamma(-H)}{\Gamma(H + \tfrac{1}{2})}$$

Here $\Delta x = X^{(2)}(t) - X^{(1)}(t) = X^{(2)}(0) - X^{(1)}(0)$, and we have assumed that $Y^{(2)}(0) = Y^{(1)}(0)$. In the numerical studies, the Hurst exponent is chosen as the Kolmogorov value $H = \tfrac{1}{3}$, and space and time are nondimensionalized so that $\bar{w} = 1$ and $A_E = 1$. The largest resolved scale (or lowest wavenumber) in the velocity field is taken as 1 in these nondimensionalized units.

In [82,84], it is shown that the mean-square tracer displacement in an FRSS flow simulated by the MWE, Fourier-Wavelet, and Randomization Methods do all closely follow the exact relation over several decades, provided that sufficiently many octaves are included, a sufficiently small integration step size is taken, and a sufficiently large sample size is used in the average. We will simply present a few illustrative results, and refer the reader to [82,84] for a much more thorough exploration and for practical guidelines concerning choices of parameters. Because of the extra expense of integrating particle trajectories, a smaller number of octaves are retained in the simulated velocity field in these validation studies than in the above demonstrations of the capacity of the wavelet methods to simulate velocity fields with extraordinarily wide self-similar inertial ranges (Figs. 32–34).

In Fig. 35, we show that the mean-square relative tracer displacement $\sigma_{\Delta Y}^2(t)$ can be simulated by the MWE Method [84] over five decades of length scales with error never exceeding 3.5%. These results were obtained by averaging over 1000 realizations, with $M = 30$ octaves in the simulated velocity field and a specially chosen octave-dependent bandwidth yielding a total of 792 active wavelets. The integration step size Δt for the particle trajectory is set to a suitable value of one-fifth of the initial separation $x = 100d$ of the tracers. The plot uses units rescaled by the parameter $d = 2^{-25}$; note that the smallest length scale in the velocity field is $2^{1-M} = 2^{-29} = 2^{-4}d$. It is shown in [84] that the dominant contribution to the error comes from the finite sample size. Moreover, in contrast to the systematic errors generated by some of the nonhierarchical Monte Carlo Methods in Section 6.2, the errors in MWE simulations typically fluctuate about zero. Similarly solid results are found for the Fourier-Wavelet Method. With $M = 16$ octaves and bandwidth $b = 10$, the mean-square relative tracer separation $\sigma_{\Delta Y}^2(t)$ can be simulated with 6% accuracy as it increases through a decade of scales [82]. The Randomization Method also gives similar results [82]. Note, however, that as in the RSS Model, $\sigma_{\Delta Y}^2(t)$ depends only on the second order statistics of the velocity field and is thus insensitive to the fact that the Randomization Method generates a velocity field with strong departures from Gaussianity over some length scales.
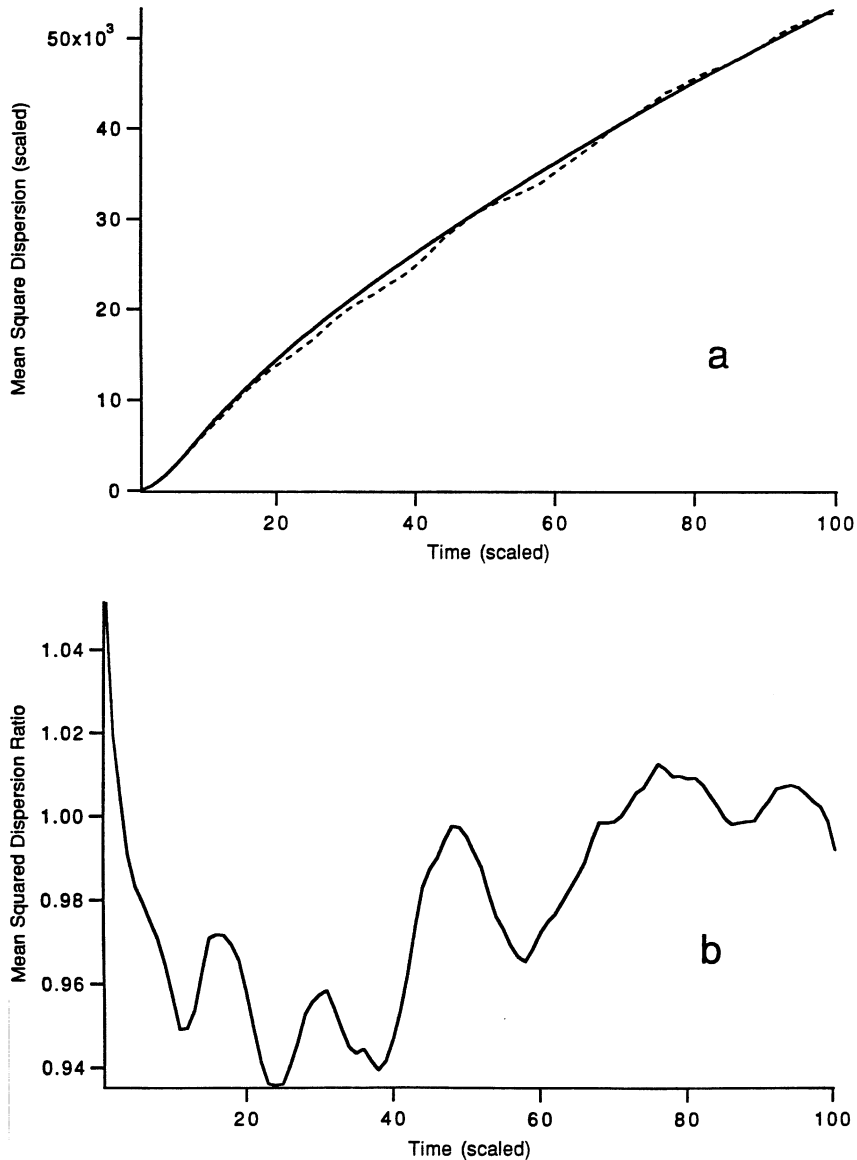
Fig. 35. Monte Carlo simulations for tracer pair dispersion in FRSS Model with Hurst exponent $H = \frac{1}{3}$ using the MWE Method with $M = 30$ octaves, wavelet order $\tau = 4$, a total of 792 wavelets, averaged over 1000 realizations (from [84]). The upper graph compares the simulated relative mean-square tracer displacement $\sigma_{\Delta Y}^2(t)$ (dotted line) with the exact analytical value (solid line). The vertical axis is rescaled by a factor $d = 2^{-25}$, the initial tracer separation is $x = 100d$, and the integration time step $h = 0.2x$. The lower plot displays the ratio of the simulated $\sigma_{\Delta Y}^2(t)$ to its exact value.

6.3.3.4. Relative advantages of wavelet and randomization Monte Carlo methods. Our above discussion is a brief synopsis of the validation studies in [82,84] which demonstrate that the MWE, Fourier-Wavelet, and Randomization Methods are each capable of generating ensembles of steady random shear flows with several decades of inertial-range scaling and sufficient accuracy

for turbulent diffusion simulations. We will now briefly mention some of the relative merits in efficiency and power of these three methods. A more complete discussion may be found in [82].

Both wavelet methods generate fractal random fields of comparable quality. As we discussed in Section 6.3.2, the Fourier-Wavelet Method has some advantages in simplicity, speed, and flexibility over the MWE Method, and we therefore consider it as the wavelet method of choice. The Fourier-Wavelet Method generates random fields which are much closer to Gaussian than those generated by the Randomization Method. Therefore, if the statistical quantities of interest are sensitive to the higher order statistics of the random field, then the Fourier-Wavelet Method is the preferred method. If it is only required that the second-order structure function of the random field exhibit several decades of self-similar scaling, then the decision in using the Fourier-Wavelet method or Randomization Method comes down mostly to computational cost and difficulty which we discuss briefly next.

Being hierarchical and local in nature, the memory cost of the wavelet methods grows only linearly with the number of simulated decades of the fractal random field. The cost of the Randomization Method, on the other hand, is exponential in the number of scaling decades [82]. The wavelet methods, however, have a much higher overhead, and there is a crossover in the relative computational efficiency between the wavelet and Randomization Methods. The rule of thumb enunciated in [82] is that if 4–5 or fewer decades of scaling behavior are needed in the random field, the Randomization Method is more computationally efficient (and simpler to implement). If a wider scaling regime is desired, then the Fourier-Wavelet Method has superior efficiency. To avoid serious memory limitations, it is important that the random numbers in the Fourier-Wavelet Method be generated on demand using a reversible random number generator, as described in [84,85].

6.4. Multidimensional simulations

Thus far, we have been considering one-dimensional random fields, appropriate for turbulent diffusion in random, steady shear flows. General turbulent velocity fields will be multidimensional vector fields, so we need to extend the successful one-dimensional Monte Carlo methods to multiple dimensions.

The Randomization Method has a straightforward multidimensional implementation. One need only partition the multidimensional wavenumber space into compartments and define probability distributions for the wavenumber selected within each according to the same principle as that described for the one-dimensional case in Section 6.2.3. A minor and easily handled complication is that the amplitudes of the Fourier modes are now Gaussian random vectors rather than Gaussian random scalars, and one must account for correlations between the various components of the velocity field ([163], Section 1.4).

Developing a multidimensional version of the wavelet methods appears a bit more daunting. While the abstract wavelet expansions behind both the MWE and Fourier-Wavelet Methods have direct vector-valued analogues, one is faced with the task of choosing a vector-valued wavelet basis which will efficiently localize the computation. Fortunately, there is a simpler approach for the special but important case in which the turbulent velocity field $v(x)$ is Gaussian, incompressible,

and statistically *isotropic* (see Section 4.2.2). Such a velocity field can be well approximated by an appropriate finite superposition of random *shear waves* rotated in various directions, and these random shear waves are in turn built out of one-dimensional Gaussian homogenous random fields [85,208]. This *Rotated Random Shear Wave Approximation* therefore supplies a means of numerically simulating a Gaussian, incompressible, statistically isotropic vector field using any of the Monte Carlo methods for generating one-dimensional Gaussian homogenous random fields described in Sections 6.2 and 6.3.

Elliott and the first author [85] have utilized this idea to construct a numerical approximation of a two-dimensional, Gaussian, isotropic, incompressible fractal random velocity field $v(x)$ out of one-dimensional random shear flows generated by the wavelet methods. The resulting multidimensional synthetic random velocity field inherits the wide scaling ranges generated by the one-dimensional wavelet methods, and 1000 realizations are sufficient to yield nearly Gaussian and isotropic sample statistics. We will mention some explicit numerical validation results from [82,85] in Section 6.4.2. We also briefly discuss the application of the Rotated Random Shear Wave Approximation to the one-dimensional Randomization Method, which in fact produces two-dimensional random velocity fields with statistical properties superior to those generated by the direct multi-dimensional formulation of the Randomization Method indicated above.

We note that incompressibility is not an essential constraint. An arbitrary, Gaussian, statistically isotropic random vector field (which need not be incompressible) can be well approximated by a superposition of one-dimensional random fields through a more general random Radon plane wave decomposition. The interested reader may find the necessary modifications to the Rotated Random Shear Wave Approximation in [85].

6.4.1. Rotated random shear wave approximation

We shall now demonstrate how an incompressible, statistically isotropic, Gaussian random velocity field can be well approximated by a superposition of Gaussian random shear flows pointing in various directions. Let the given incompressible, statistically isotropic, Gaussian random velocity field $v(x)$ have mean zero and correlation tensor $\mathcal{R}(x)$. It can be represented in terms of the (scalar) energy spectrum $E(k)$ in the following way (273):

$$\langle v(x + x') \otimes v(x') \rangle = \mathcal{R}(x) = \int_{\mathbb{R}^d} e^{2\pi i k \cdot x} \frac{2E(|k|)}{(d-1)A_{d-1}|k|^{d-1}} \mathcal{P}(k)\, dk\ . \tag{392}$$

Here A_{d-1} is the area of the unit sphere S^{d-1} in $\mathbb{R}^d$. The tensor $\mathcal{P}(k)$ is the projection operator onto the plane perpendicular to k:

$$\mathcal{P}(k) = \mathcal{I} - (k \otimes k / |k|^2)\ ,$$

and enforces incompressibility of $v(x)$.

Next we introduce some useful notation. The symbol $\hat{e}_j$ in what follows denotes a unit vector in the jth coordinate direction. $\mathcal{U}_{\hat{\omega}} \in SO(d)$ is defined as the unique rotation matrix which maps $\hat{e}_1$ to the unit vector $\hat{\omega} \in S^{d-1}$, and leaves all vectors orthogonal to $\hat{\omega}$ and $\hat{e}_1$ invariant.

The Rotated Random Shear Wave Approximation is motivated by writing the Fourier integral (392) as an iterated integral over the magnitude and direction of the wavevector $\boldsymbol{k}$:

$$\mathscr{R}(\boldsymbol{x}) = \frac{1}{A_{d-1}} \int_{S^{d-1}} \mathscr{R}_{\mathrm{SW},\hat{\varpi}}(\boldsymbol{x}) \, \mathrm{d}\hat{\varpi} \,,$$

$$\mathscr{R}_{\mathrm{SW},\hat{\varpi}}(\boldsymbol{x}) = \int_0^\infty \cos(2\pi k \hat{\varpi} \cdot \boldsymbol{x}) \frac{2E(k)}{d-1} \mathscr{P}(\hat{\varpi}) \, \mathrm{d}k \,. \tag{393}$$

We now observe that $\mathscr{R}_{\mathrm{SW},\hat{\varpi}}(\boldsymbol{x})$ is the correlation tensor of a certain superposition of $d-1$ simple random shear layers all varying along the direction $\hat{\varpi}$ and directed orthogonally to $\hat{\varpi}$ and one another.

Specifically, let $\{v_j(x)\}_{j=2}^d$ be a collection of independent, homogenous, Gaussian random scalar fields with mean zero and common correlation function:

$$\langle v_j(x + x') v_j(x') \rangle = R_1(x) \equiv \int_{-\infty}^\infty \mathrm{e}^{2\pi i k x} \frac{E(|k|)}{d-1} \, \mathrm{d}k = \int_0^\infty \cos(2\pi k x) \frac{2E(|k|)}{d-1} \, \mathrm{d}k \,.$$

Next, we form the canonical *shear wave velocity field* $\boldsymbol{v}_{\mathrm{SW}}(\boldsymbol{x})$ in $\mathbb{R}^d$ varying along the first coordinate direction, with components built from these random fields:

$$\boldsymbol{v}_{\mathrm{SW}}(\boldsymbol{x}) = \sum_{j=2}^d v_j(x_1) \hat{e}_j \,. \tag{394}$$

In $d = 2$ dimensions, $\boldsymbol{v}_{\mathrm{SW}}(\boldsymbol{x})$ is just a standard shear layer. In $d = 3$ dimensions, $\boldsymbol{v}_{\mathrm{SW}}(\boldsymbol{x})$ takes the form of a random planar shear wave, in which the velocity field is directed within planes of constant x_1 and is uniform within each of these shearing planes. The canonical random shear wave $\boldsymbol{v}_{\mathrm{SW}}(\boldsymbol{x})$ is a Gaussian random vector field with mean zero and correlation tensor:

$$\mathscr{R}_{\mathrm{SW}}(\boldsymbol{x}) \equiv \langle \boldsymbol{v}_{\mathrm{SW}}(\boldsymbol{x} + \boldsymbol{x}') \otimes \boldsymbol{v}_{\mathrm{SW}}(\boldsymbol{x}') \rangle = \sum_{j=2}^d R_1(x_1) \hat{e}_j \otimes \hat{e}_j = R_1(x_1)(\mathscr{I} - \hat{e}_1 \otimes \hat{e}_1) = R_1(x_1) \mathscr{P}(\hat{e}_1) \,.$$

Next, we define $\boldsymbol{v}_{\mathrm{SW},\hat{\varpi}}$ as the random shear wave obtained by rotating the vector field $\boldsymbol{v}_{\mathrm{SW}}(\boldsymbol{x})$ (via $\mathscr{U}_{\hat{\varpi}}$) to the definite (deterministic) direction $\hat{\varpi} \in S^{d-1}$:

$$\boldsymbol{v}_{\mathrm{SW},\hat{\varpi}}(\boldsymbol{x}) \equiv \mathscr{U}_{\hat{\varpi}} \boldsymbol{v}(\mathscr{U}_{\hat{\varpi}}^\dagger \boldsymbol{x}) \,.$$

This rotated velocity field is also a mean zero Gaussian random vector field, and its correlation tensor is obtained by the following transformation:

$$\langle \boldsymbol{v}_{\mathrm{SW},\hat{\varpi}}(\boldsymbol{x} + \boldsymbol{x}') \otimes \boldsymbol{v}_{\mathrm{SW},\hat{\varpi}}(\boldsymbol{x}') \rangle = \mathscr{U}_{\hat{\varpi}} \mathscr{R}_{\mathrm{SW}}(\mathscr{U}_{\hat{\varpi}}^\dagger \boldsymbol{x}) \mathscr{U}_{\hat{\varpi}}^\dagger$$

$$= R_1(\hat{e}_1 \cdot \mathscr{U}_{\hat{\varpi}}^\dagger \boldsymbol{x}) \mathscr{U}_{\hat{\varpi}} \mathscr{P}(\hat{e}_1) \mathscr{U}_{\hat{\varpi}}^\dagger = R_1(\hat{\varpi} \cdot \boldsymbol{x}) \mathscr{P}(\hat{\varpi}) = \mathscr{R}_{\mathrm{SW},\hat{\varpi}}(\boldsymbol{x}) \,.$$

Thus, $\mathscr{R}_{\mathrm{SW},\hat{\varpi}}(\boldsymbol{x})$ is exactly the correlation tensor of a Gaussian random shear wave varying along the direction $\hat{\varpi}$.

Since the correlation tensor of the desired statistically isotropic vector field $\boldsymbol{v}(\boldsymbol{x})$ is expressed as an average (393) of $\mathscr{R}_{\mathrm{SW},\hat{\varpi}}(\boldsymbol{x})$ over all directions $\hat{\varpi}$, we are led to the following means of statistically approximating $\boldsymbol{v}(\boldsymbol{x})$ in terms of random shear waves. First choose a set of M_{dir} deterministic

directions $\widehat{\varpi}^{(j)} \in S^{d-1}$, $j = 1, \ldots, M_{\text{dir}}$ at least approximately equally spaced around S^{d-1}. Define the *Rotated Random Shear Wave Approximation*:

$$v_{\text{RRSW}}(x) = \frac{1}{\sqrt{M_{\text{dir}}}} \sum_{j=1}^{M_{\text{dir}}} v_{\text{SW}, \widehat{\varpi}^{(j)}}(x) \, ,$$

where the $\{v_{\text{SW}, \widehat{\varpi}^{(j)}}(x)\}_{j=1}^{M_{\text{dir}}}$ are random shear waves obtained from rotating M_{dir} *statistically independent* realizations of the canonical random shear wave $v_{\text{SW}}(x)$ (394) to the directions $\{\widehat{\varpi}^{(j)}\}_{j=1}^{M_{\text{dir}}}$.

The random velocity field described by this Rotated Random Shear Wave Approximation is a Gaussian random vector field with mean zero and correlation tensor:

$$\mathscr{R}_{\text{RRSW}}(x) \equiv \langle v_{\text{RRSW}}(x + x') \otimes v_{\text{RRSW}}(x') \rangle = \frac{1}{M_{\text{dir}}} \sum_{j=1}^{M_{\text{dir}}} \mathscr{R}_{\text{SW}, \widehat{\varpi}^{(j)}}(x) \, .$$

If the directions $\{\widehat{\varpi}^{(j)}\}_{j=1}^{M_{\text{dir}}}$ are chosen to be roughly equally spaced, then the simulated correlation tensor $\mathscr{R}_{\text{RRSW}}(x)$ is a finite quadrature approximation to formula (393) for the correlation tensor for the true, statistically isotropic, incompressible, Gaussian random velocity field $v(x)$. Since a mean zero Gaussian random field is determined entirely by its correlation tensor, the statistical accuracy of the approximation of the velocity field $v(x)$ by $v_{\text{RRSW}}(x)$ is entirely determined by the explicitly computable error of this finite quadrature approximation. In particular, by suitable choices of directions $\{\widehat{\varpi}^{(j)}\}_{j=1}^{M_{\text{dir}}}$, the velocity field $v_{\text{RRSW}}(x)$ obtained by superposition of random shear waves can be made approximately statistically isotropic.

6.4.2. Numerical implementation of Rotated Random Shear Wave Approximation

The Rotated Random Shear Wave Approximation suggests an immediate way to simulate numerically a given statistically isotropic, incompressible, Gaussian random vector field $v(x)$ with correlation tensor $\mathscr{R}(x)$. Namely, we can use one of the efficient methods discussed in Section 6.3 to generate the independent Gaussian random fields $\{v_j(x)\}_{j=2}^{d}$ which comprise the canonical shear wave $v_{\text{SW}}(x)$ (394). M_{dir} independent realizations of such a shear wave are then rotated to the directions $\{\widehat{\varpi}^{(j)}\}_{j=1}^{M_{\text{dir}}}$ to give $v_{\text{RRSW}}(x)$, which will have mean zero and correlation tensor approximately equal to that of $v(x)$.

The main issue in this multi-dimensional extension of the Monte Carlo Methods is the choice of the set of directions $\{\widehat{\varpi}^{(j)}\}_{j=1}^{M_{\text{dir}}}$. In $d = 2$ dimensions, it is natural and practical to distribute them with equiangular spacing about the unit circle. The task is a bit trickier in $d = 3$ dimensions, since there is no way to distribute more than 20 directions in an exactly equispaced fashion. In either case, the deviation of the simulated field from statistical isotropy can be quantified and bounded by explicit quadrature formulas [85].

We will here give an explicit description of the method of generating an approximately statistically isotropic, incompressible Gaussian velocity field using the Rotated Random Shear Wave Approximation for the case of $d = 2$ dimensions. In this case, the random shear waves $v_{\text{SW}, \widehat{\varpi}}(x)$ are just random shear layers:

$$v_{\text{SW}, \widehat{\varpi}}(x) = \widehat{\varpi}^{\perp} v(\widehat{\varpi} \cdot x) \, ,$$

where

$$\widehat{\varpi}^{\perp} = \begin{bmatrix} -\varpi_2 \\ \varpi_1 \end{bmatrix}$$

is a vector perpendicular to $\widehat{\varpi}$. The approximate velocity field is then symbolically written [85]:

$$\boldsymbol{v}_{\mathrm{RRSL}}(\boldsymbol{x}) = \frac{1}{\sqrt{M_{\mathrm{dir}}}} \sum_{j=1}^{M_{\mathrm{dir}}} \widehat{\varpi}^{\perp(j)} v_j(\widehat{\varpi}^{(j)} \cdot \boldsymbol{x}) \ ,$$

where M_{dir} is the number of directions used, $\{\widehat{\varpi}^{(j)}\}_{j=1}^{M_{\mathrm{dir}}}$ is a collection of unit vectors regularly spaced around the unit circle S^1, and $\{v_j\}_{j=1}^{M_{\mathrm{dir}}}$ is a collection of independent realizations of a random homogenous scalar one-dimensional field with energy spectrum $E(k)$ equal to that of the two-dimensional velocity field $\boldsymbol{v}(\boldsymbol{x})$ being simulated. These random scalar fields can be computed using *any* simulation technique. It is shown in [85] that $M_{\mathrm{dir}} \geq 16$ is needed for the simulated velocity field to be approximately (within 8%) isotropic according to a natural energy criterion, regardless of the method of simulation used for the random scalar fields $\{v_j\}_{j=1}^{M_{\mathrm{dir}}}$.

We now report the results obtained by using the Rotated Random Shear Wave Approximation in conjunction with the Multi-Wavelet Expansion (MWE) Method to simulate a two-dimensional, statistically isotropic, incompressible, fractal Gaussian random field with energy spectrum $E(k) = 2k^{-5/3}$. (We by no means imply that this energy spectrum is appropriate for a high Reynolds number two-dimensional flow in nature.) We will apply this method in Section 6.5 in our numerical study of pair dispersion in a velocity field with a wide inertial range.

The simulation of the scalar fields includes $M = 52$ octaves, and the bandwidth is chosen so that only 10^{-8} of the energy is lost by the truncation [85,84]. The computation uses 46 592 active elements. In Fig. 36, we plot the simulated velocity structure function:

$$S_v(r) = \langle |\boldsymbol{v}(\boldsymbol{x}' + r\hat{e}) - \boldsymbol{v}(\boldsymbol{x}')|^2 \rangle$$

averaged over 10, 100, and 1000 realizations, for $\hat{e}$ directed midway between two of the $M_{\mathrm{dir}} = 32$ directions $\{\widehat{\varpi}^{(j)}\}$ used for the shear layers. The simulated structure function is found to match the exact analytical formula

$$S_v(r) = S_v^{\mathrm{I}} r^{2/3},$$
$$S_v^{\mathrm{I}} = -2\Gamma(-1/3)\pi^{7/6}/\Gamma(5/6)$$

accurately over 12 decades of scales. Only one to two decades of approximate scaling behavior have been achieved in previous simulations of fractal fields in two dimensions by Viecelli and Canfield [335] using Successive Random Addition and the Fourier Method on a 256×256 grid, and in three dimensions by Fung et al. [109] using a variant of Kraichnan's method [180] of randomly directed sinusoidal shear waves with 84 computational elements.

Power law fits to the structure function evaluated along five different directions (including the one plotted in Fig. 36) reveal excellent quantitative accuracy for the MWE-based simulation method. With only 100 realizations, the error in the fitted exponent is never more than 1.1%, and the error in the fitted prefactor S_v^{I} is never more than 6%. Moreover, relative measures of deviations from Gaussianity and isotropy are only a few percent for a sample size of 1000. We refer to [85] for the details of the stringent tests of the quality of the simulated velocity field.
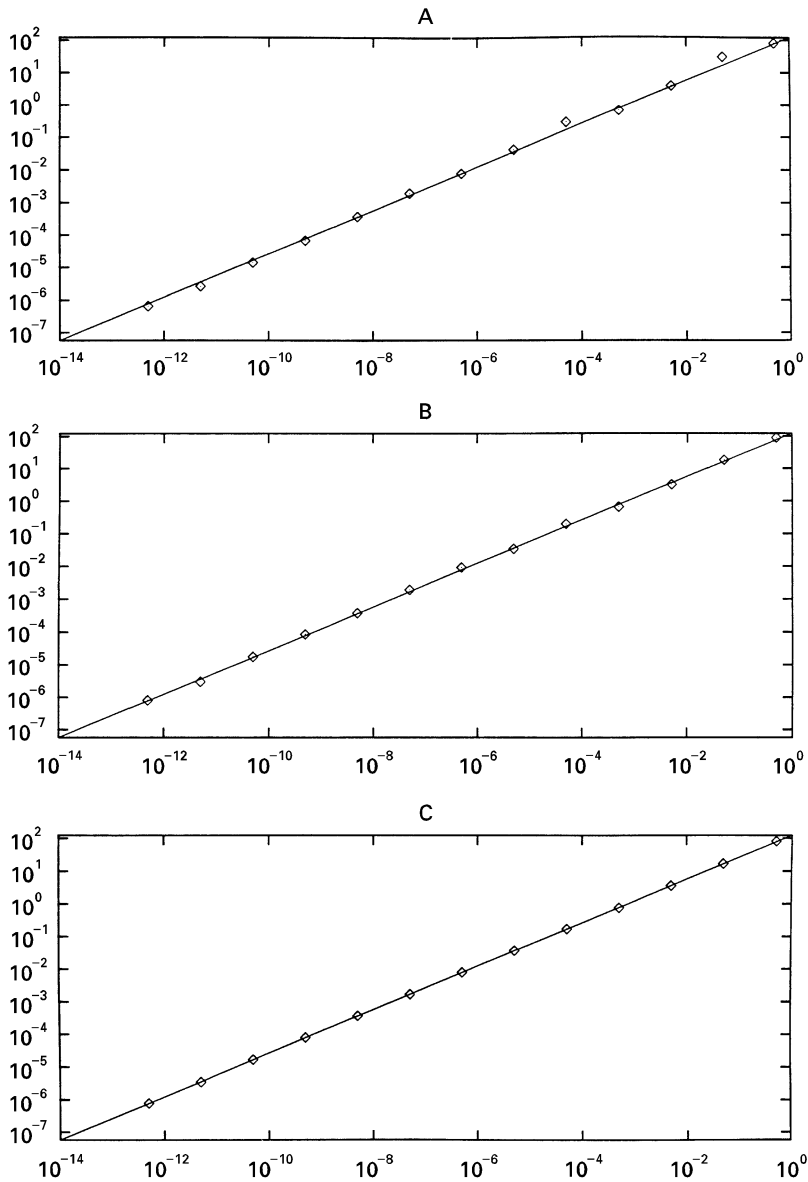
Fig. 36. Structure function of the two-dimensional velocity field with energy spectrum $E(k) = \frac{1}{2}k^{-5/3}$, simulated by the MWE Method ($M = 52$ octaves) with Rotated Random Shear Wave Approximation ($M_{\mathrm{dir}} = 32$ directions). The structure function is evaluated along the radial direction $\theta = \pi/32$. The Monte Carlo statistics for (A) 10, (B) 100, and (C) 1000 realizations are plotted with diamond symbols (from [85]).

The Rotated Random Shear Wave Approximation also works successfully when the one-dimensional scalar fields are simulated by the Fourier-Wavelet Method or the Randomization Method. Details may be found in [82]. We note only that the velocity fields simulated using the Randomization Method in conjunction with the Rotated Random Shear Wave Approximation are smoother and have longer scaling regimes than those simulated by a straightforward generalization

of the Randomization Method to two dimensions [142]. This points out once again that one must pay heed to the relative variance of Monte Carlo Methods in practice, and not just their theoretical accuracy in the asymptotic limit of infinitely many realizations.

Another closely related way of simulating statistically isotropic random vector fields by a super-position of shear waves is to choose the directions $\{\hat{\varpi}^{(j)}\}_{j=1}^{M_{dir}}$ *randomly* from a uniform distribution over the sphere S^{d-1} (see [208]). There would be two main disadvantages to this variation as compared to a regularly spaced, deterministic choice of directions. First, the simulated velocity field would be non-Gaussian. More importantly, the variance of the Monte Carlo Method would be greater, and a larger number of realizations would be required to achieve a desired accuracy.

6.5. Simulation of pair dispersion in the inertial range

We close our section on Monte Carlo methods for turbulent diffusion with a numerical study of the turbulent dispersion of a pair of tracers in a synthetic, statisticallyisotropic turbulent flow with a wide inertial range of scales. We have already analyzed this problem theoretically in two simplified contexts. In Section 3.5, we developed exact formulas for the *pair distance function*, the PDF for the separation between a pair of tracers, in an anisotropic turbulent *shear* flow (with no molecular diffusion). We also derived (following Kraichnan [179]) an explicit PDE in Section 4.2.1 for the pair-distance function in a statistically isotropic velocity field with extremely rapid decorrelations in time; see Eq. (268) and the ensuing discussion. No exact solutions, however, appear available for pair dispersion in multi-dimensional turbulent flows decorrelating at a finite rate. Such a problem is of significant applied interest in engineering and atmosphere-ocean science, since the relative diffusion of a pair of tracers is connected with the growth of the size of a cloud of tracers released in a fluid.

6.5.1. Richardson's law

We concentrate, as in our previous treatments of pair dispersion, on the growth of the separation distance $\ell(t) \equiv |\boldsymbol{X}^{(1)}(t) - \boldsymbol{X}^{(2)}(t)|$ between a pair of tracers as it evolves through a wide inertial range of scales. We will further specialize our attention to the mean-square tracer separation $\sigma_{\Delta X}^2(t) = \langle \ell^2(t) \rangle$ rather than the full pair-distance function. As we mentioned in Section 4.2.1, Richardson [284] empirically observed that the mean-square separation between balloons released into the atmosphere grows according to a cubic power law: $\sigma_{\Delta X}^2(t) \sim t^3$.

Obukhov [252,253] later showed that such a result could be theoretically deduced through an inertial-range similarity hypothesis and dimensional analysis, and formulated it as the following universal inertial-range prediction:

$$\sigma_{\Delta X}^2(t) \approx C_R \bar{\varepsilon} t^3 \quad \text{for } L_K \ll (\sigma_{\Delta X}^2(t))^{1/2} \ll L_0 \ . \tag{395}$$

Here $\bar{\varepsilon}$ is the energy dissipation rate, and C_R represents the universal *Richardson's constant*. The statement (395) is generally referred to as *Richardson's t^3 law*. There has been a large effort to derive this law and predict its associated constant C_R by turbulence closure theories [178,192,200,241,322] and to empirically confirm it and measure C_R through actual experiments [248,258,261,315] and numerical simulations [109,291,351]. We note that Richardson [284] also formulated a considerably stronger statement (see [31]) that the relative diffusivity of a pair of

tracers is proportional to the 4/3 power of their momentary (unaveraged) separation, and this has been called Richardson's 4/3 law. In what follows, we will strictly discuss Richardson's t^3 law.

6.5.2. Monte Carlo simulation of pair dispersion

Here we describe the first numerical experiments, performed by Elliott and the first author [86], which exhibited Richardson's t^3 law over *many* decades of pair separation. Synthetic, two-dimensional incompressible, Gaussian random velocity fields were generated through the Multi-Wavelet Expansion (MWE) Method and the Rotated Random Shear Wave Approximation which we described in Section 6.4.2. Recall that this method is capable of simulating approximate statistically isotropic, incompressible, Gaussian random velocity fields which support an accurately self-similar inertial range:

$$\langle |v(x + r) - v(x)|^2 \rangle = S_v^I r^{2H} , \tag{396}$$

extending over 12 decades of scales. The basic algorithm was validated for applications in turbulent diffusion on an exactly solvable steady shear layer model (see Section 6.3.3), and on an exactly solvable statistically isotropic model in which the velocity field is rapidly decorrelating in time (see Section 4.2.2).

The simulated velocity field $v(x)$ varies only in space, and is frozen in time. Pair dispersion proceeds very differently in a frozen, random two-dimensional velocity field than in realistic, temporally evolving turbulent flows. To introduce temporal fluctuations in the numerical simulation, we sweep the frozen velocity field past the laboratory frame by a constant velocity field w. This corresponds exactly to Taylor's hypothesis ([320], p. 253) for relating experimental time-series measurements to the spatial structure of the turbulence. The tracers are *not* transported by the constant sweep in the numerical simulation, and we also ignore molecular diffusion $\kappa = 0$. The equations of motion for the tracers are then

$$dX^{(j)}(t)/dt = v(X^{(j)}(t) - wt) ,$$

$$X^{(j)}(t = 0) = x_0^{(j)} . \tag{397}$$

Note how the constant sweeping explicitly induces temporal fluctuations in the velocity field seen by the tracers.

It is natural to associate the sweep velocity w with the magnitude of the velocity fluctuations at the largest simulated scale L_u of the inertial range:

$$w \approx \langle ((v(x + L_u \hat{e}) - v(x)) \cdot \hat{e})^2 \rangle^{1/2} . \tag{398}$$

The numerical length scale L_u is roughly equivalent to the integral length scale L_0 in our theoretical studies. As usual, $\hat{e}$ denotes any unit vector. Using the inertial-range relation for the root-mean-square longitudinal velocity difference appearing on the right-hand side of Eq. (398):

$$\langle ((v(x + r) - v(x)) \cdot (r/|r|))^2 \rangle = S_{v,\parallel}^I |r|^{2H} , \tag{399}$$

we are led to set

$$w = \sqrt{S_{v,\parallel}^I} L_u^H .$$

Statistical isotropy (in $d = 2$ dimensions) implies that $S_v^I = (2H + 2)S_{v,\parallel}^I$. Quantities are next nondimensionalized with respect to the length scale L_u and the time scale $L_u/|w|$. In these nondimensionalized units, L_u, w, and $S_{v,\parallel}^I$ are all equal to unity.

6.5.3. Pair separation statistics obtained from Monte Carlo simulation

Here we present the results of the Monte Carlo simulations [86] for the pair separation statistics which utilize the algorithm described above with the Hurst exponent chosen as the Kolmogorov value $H = \frac{1}{3}$. The initial particle separation is chosen as $\ell_0 = 10^{-14}$, which is well within the resolution capabilities of the Monte Carlo algorithm being used. The adaptive time step strategy is described and validated in [86]. Averages are computed over 1024 realizations.

The graph of the root mean-square pair separation $\sigma_{\Delta X}^2(t) = \langle |\Delta X|^2(t) \rangle$ in Fig. 37 indicates a power law behavior after about $t = 100$ and persists for eight decades of pair separation. The
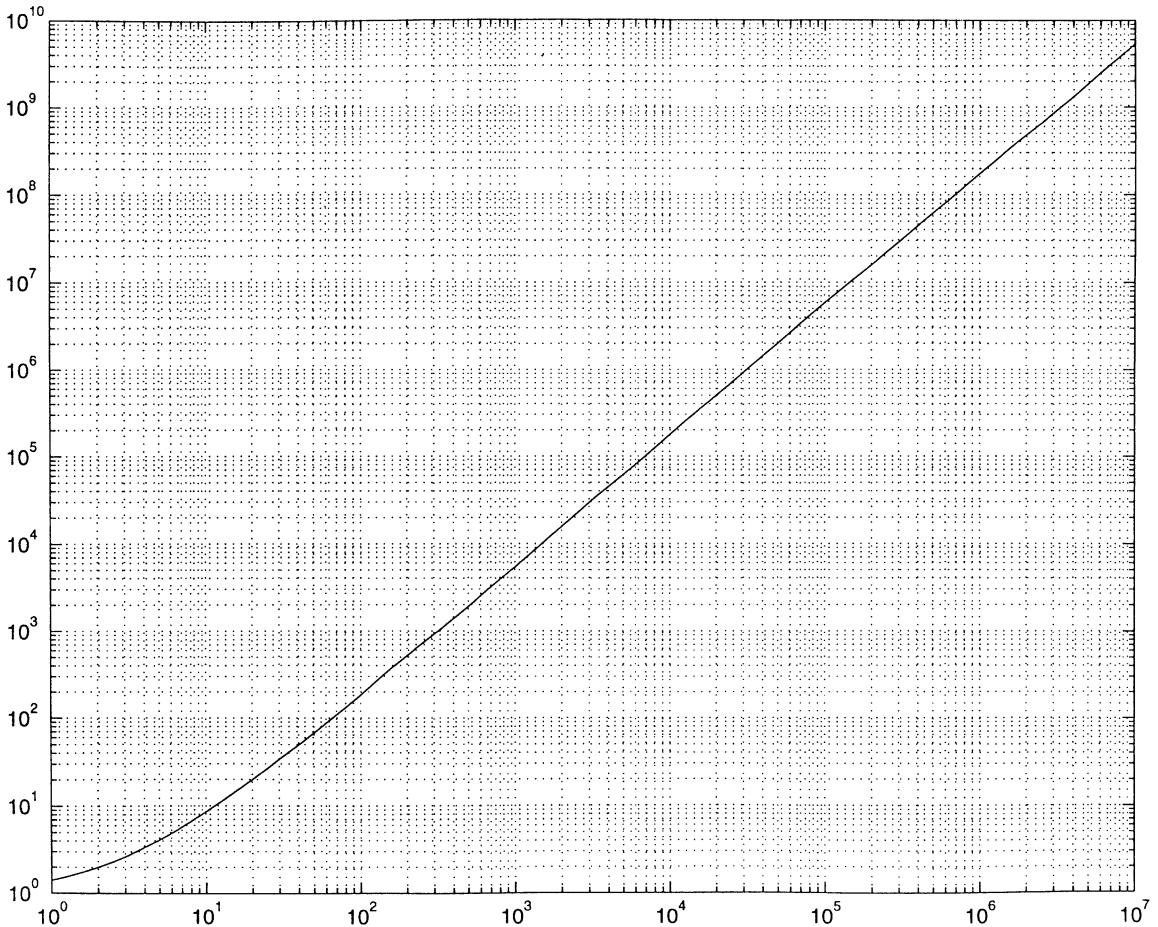
Fig. 37. Plot of the root-mean-square tracer pair separation $\sigma_{\Delta X}^2(t)$ versus time (from [86]). Hurst exponent $H = \frac{1}{3}$, initial separation $\ell_0 = 10^{-14}$, averaged over 1024 realizations.

graph of the logarithmic derivative of $\sigma_{\Delta x}^2(t)$ versus time in Fig. 38 oscillates mildly with a mean value 3, providing an independent and much more stringent confirmation of Richardson's t^3 law.

Finally, in Fig. 39, we graph the variation of $A_\Delta(t) = \sigma_{\Delta x}^2(t)t^{-3}$, which is just the prefactor in the Richardson's t^3 law. Remarkably, as the reader can see by comparing Figs. 37 and 39, the prefactor settles down over more than 7.5 decades of pair separation to the constant value 0.031 ± 0.004.

We recall that one of the main computational devices in the Monte Carlo algorithm used above is the approximation of an isotropic incompressible Gaussian random velocity field by a superposition of a large ($M_{\mathrm{dir}} = 32$) number of independent simple shear layers oriented in various directions with equiangular spacing. If instead only a small number of independent shear layer directions are utilized, then the simulated random field is anisotropic but with a similar energy spectrum as in the isotropic case. Pair dispersion simulations using only $M_{\mathrm{dir}} = 2$ or 4 directions were conducted in
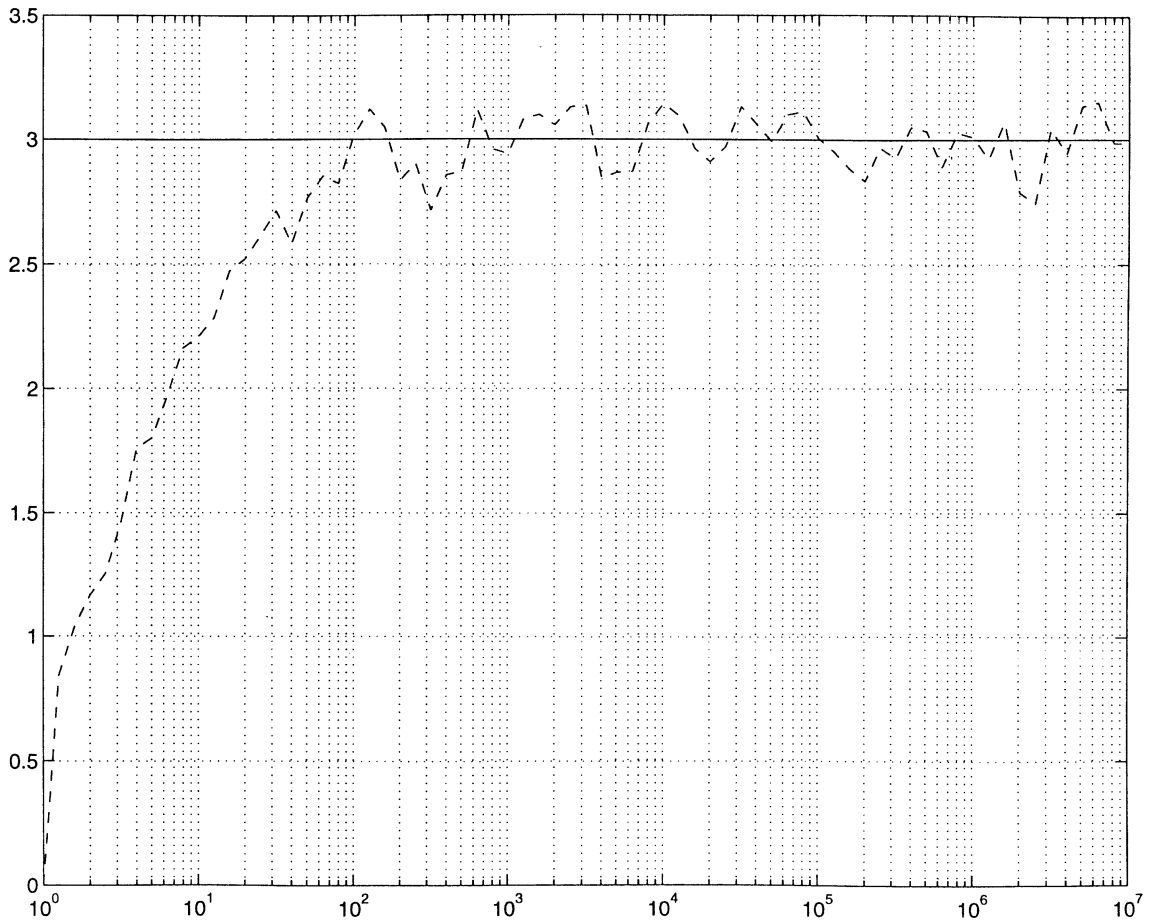
Fig. 38. Plot of the logarithmic derivative of root-mean-square tracer pair separation, $\gamma = \mathrm{d}\ln\sigma_{\Delta x}^2(t)/\mathrm{d}\ln t$ versus time (from [86]). Solid line indicates $\gamma = 3$ predicted by Richardson's t^3 law. Hurst exponent $H = \frac{1}{3}$, initial separation $\ell_0 = 10^{-14}$, averaged over 1024 realizations.
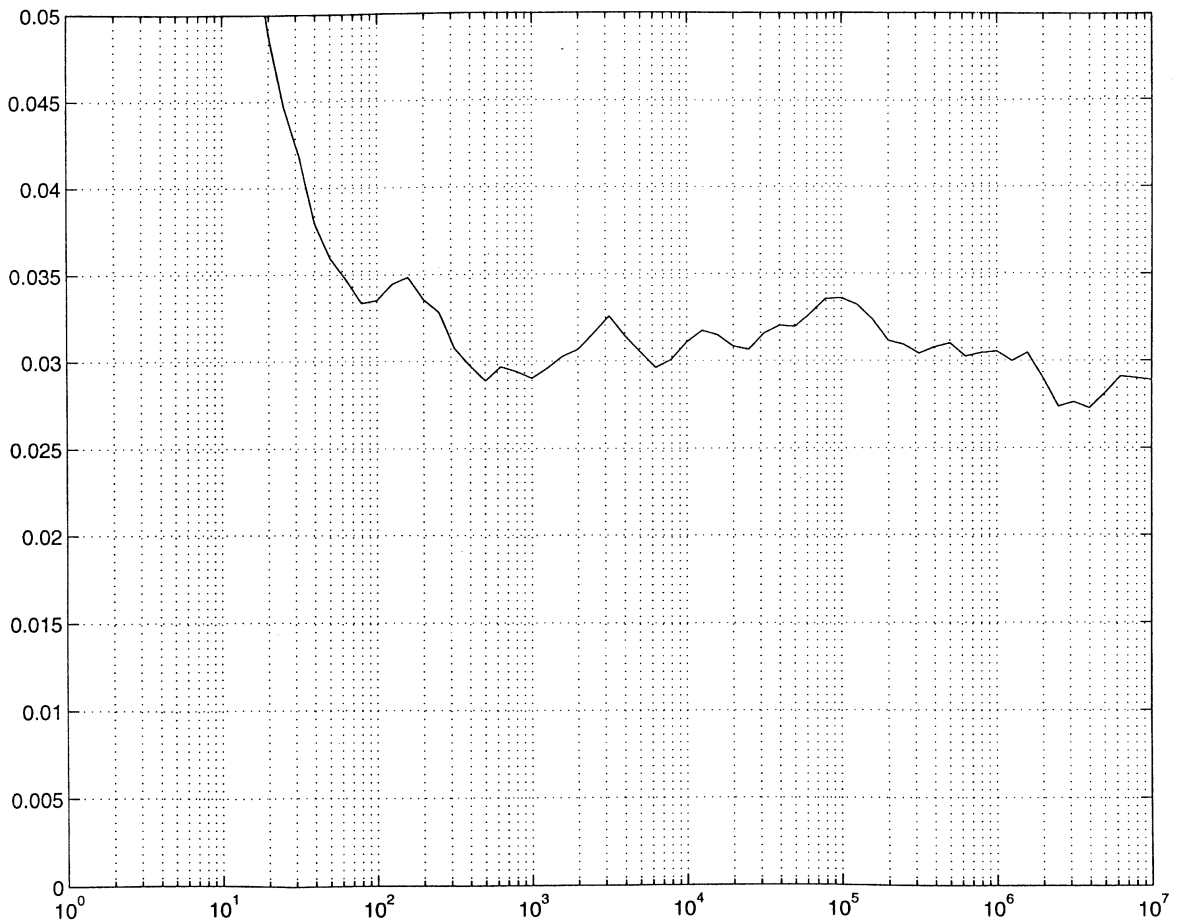
Fig. 39. Plot of the scaling prefactor in the root-mean-square tracer pair separation, $A_\Delta(t) \equiv \sigma^2_{\Delta x}(t) t^{-3}$ versus time (from [86]). Hurst exponent $H = \frac{1}{3}$, initial separation $\ell_0 = 10^{-14}$, averaged over 1024 realizations.

[83] to investigate the effects of anisotropy on Richardson's t^3 law. It was found that Richardson's t^3 law remains valid over many decades of separation. Moreover, the prefactor $A_\Delta(t)$ is approximately constant over the scaling regime and nearly universal. For both $M_{\mathrm{dir}} = 2$ and $M_{\mathrm{dir}} = 4$, with various angles between the constant sweep w and the directions of the shear flows comprising the velocity field, the best fit constant values for the scaling coefficient $A_\Delta(t)$ fell within the range of 0.029–0.032, which includes the isotropic value 0.031 computed above. These results give strong evidence that the Richardson constant C_R in (395) is universal for Gaussian random fields with a wide self-similar inertial range, whether they are isotropic or anisotropic. The adjustment time to achieve the scaling behavior can vary however with the degree of anisotropy.

Other statistics are measured in [86] which quantify the intermittency of the pair separation process. In particular, the separation distance $\Delta X(t)$ is found to have a broader-than-Gaussian distribution, and Richardson's t^3 law is *crudely* obeyed by the mean-square particle separation averaged over only two realizations.

6.5.4. Relation to other work concerning Richardson's t^3 law

In addition to providing a numerical demonstration of Richardson's t^3 law over many decades of scales, the results of the above Monte Carlo simulation pose some interesting challenges for various theories which seek to predict the statistics of pair separation in the inertial range. We shall separately discuss issues pertaining to the t^3 scaling of the mean-square particle separation and the computed value of the scaling preconstant.

6.5.4.1. Open problem: Theoretical explanations for Richardson's t^3 law for velocity field satisfying Taylor's hypothesis.
The mean-square pair separation $\sigma_{\Delta X}^2(t)$ has been demonstrated to obey Richardson's t^3 law in an extraordinarily clean way over eight decades of scales, and the underlying numerical algorithm has been extensively validated for simulating turbulent diffusion [84,85]. It is therefore most remarkable that no theory of which we are aware clearly predicts that Richardson's t^3 law should hold for the velocity field with the spatio-temporal dynamics used in the simulation!

Recall that the velocity field in the laboratory frame $v_{\text{LAB}}(x, t)$ is given by sweeping a frozen random velocity field $v(x, t)$, at a constant velocity w:

$$v_{\text{LAB}}(x, t) = v(x - wt) \ .$$

The frozen field $v(x)$ is Gaussian random, statistically isotropic, incompressible flow with a wide inertial range with the Kolmogorov value $H = \frac{1}{3}$ for the Hurst exponent. The tracers are advected by $v_{\text{LAB}}(x, t)$; see Eq. (397). A key difference between the simulated field $v_{\text{LAB}}(x, t)$ and the usual random velocity models assumed in turbulence theories is that the temporal decorrelation for $v_{\text{LAB}}(x, t)$ is explicitly set through Taylor's hypothesis by a constant sweep velocity w (which is naturally equated in magnitude with the large-scale velocity fluctuations in $v(x)$).

Physical scaling considerations [86] indicate that the sweep velocity w should be included along with $\bar{\varepsilon}$ and t in the list of a priori relevant parameters describing the inertial-range dynamics of pair separation in the simulation described above. Dimensional analysis is then insufficient to predict a unique inertial-range scaling behavior for $\sigma_{\Delta X}^2(t)$. Obukhov's inertial-range similarity arguments therefore do not even explain qualitatively Richardson's t^3 law for a velocity field with spatial statistics given by Kolmogorov theory and temporal statistics set by Taylor's hypothesis. We now briefly mention some other modern theories which suggest why Richardson's t^3 law should be observed in various contexts, and indicate why none of these, as they stand, provide a clear explanation for the scaling behavior observed in the Monte Carlo numerical simulations.

Some researchers [21,258,351] have pointed out that a cubic growth of the mean-square displacement could arise for reasons having nothing to do with inertial-range scaling. For example, Babiano and coworkers [21,351] show that a cubic growth of the mean-square distance between a pair of tracers will occur over ranges of scales in which the accelerations of the tracers are independent of one another and statistically stationary. These considerations may well describe reasons why Richardson's t^3 law is observed in experimental situations and numerical simulations (such as [108]) where Obukhov's similarity arguments do not apply or on scales extending outside the inertial range of the velocity field.

The $\sigma_{\Delta X}^2(t) \sim t^3$ scaling behavior in the Monte Carlo simulation reported in Section 6.5.3, however, cannot be explained so simply. This is demonstrated by other similar numerical simulations in [86] with different values of the Hurst exponent H describing the inertial-range scaling of the velocity field (396). It is found for $H = 0.2, 0.3$, and 0.4 that the mean-square particle separation

has power law scaling $\sigma^2_{\Delta X}(t) \sim t^\gamma$ over several decades, with $\gamma \approx 2/(1 - H)$ within the small error 0.03. Therefore, the scaling behavior of the pair dispersion in the Monte Carlo simulations under discussion is fundamentally related to the Hurst exponent H, and cannot be explained by the above class of theories which does not take the scaling properties of the inertial range into account.

It is moreover interesting to note that the dependence of the scaling exponent $\gamma = 2/(1 - H)$ is in accord with a variety of theories [178,192,351] which assume that the only relevant time scale describing the pair separation dynamics at a scale L in the inertial range is the *eddy turnover time*:

$$\tau_e(L) = \frac{L}{\Delta v_\|(L)} \approx (S^I_{v,\|})^{-1/2} L^{1-H} . \tag{400}$$

Here $\Delta v_\|(L) \approx \sqrt{S^I_{v,\|}} L^H$ is the mean-square longitudinal velocity difference observed between points separated by a distance L. As seen in Eq. (400), the eddy turnover time is simply a natural advective time scale at scale L. Consequently, any analytical or phenomenological theory for inertial-range pair dispersion (such as that described in [351]) which involves only length scales and the mean-square (longitudinal) velocity difference across such scales is implicitly assuming that the only relevant time scale is the eddy turnover time. For a flow satisfying Taylor's hypothesis, there is however another relevant time scale set by the time taken for the constant sweep to travel a distance L:

$$\tau_s(L) = L/|\boldsymbol{w}| .$$

When the sweep velocity is matched to the magnitude of the large-scale velocity fluctuations, as it is in the Monte Carlo simulations described above, then the sweeping time scale $\tau_s(L)$ is much shorter than the eddy turnover time $\tau_e(L)$ for all scales within the inertial range [86,319]. Therefore, the sweeping time scale has an a priori importance in the dynamics of tracers in a flow satisfying Taylor's hypothesis. Formally, it appears that $\tau_s(L)$ should be setting the Lagrangian correlation time, which as we have discussed in Section 3, plays a crucial role in determining the statistical dynamics of a tracer.

It is far from clear why pair separation in a flow satisfying Taylor's hypothesis should obey the scaling laws predicted by theories which ignore the presence of any large-scale sweeping mechanism. Indeed, there is unambiguous mathematical evidence [14,208] that the nature of the spatio-temporal energy spectrum can have a substantial influence on pair dispersion. Moreover, if the Lagrangian History Direction Interaction Approximation (LHDIA) used by Kraichnan [178] or the Eddy-Damped Quasi-Normal Markovian Approximation (EDQNM) used by Larchevêque and Lesieur [192] are *crudely* modified to account for the sweeping by replacing the appearance of the eddy turnover time $\tau_e(L)$ by the sweeping time scale $\tau_s(L)$, they will predict pair dispersion behavior very different from Richardson's t^3 law for $H = \frac{1}{3}$ and its generalization $\sigma^2_{\Delta X}(t) \sim t^{2/(1-H)}$ for general H. It would be most interesting to see whether and how these or other [200] turbulence closure theories could properly take sweeping effects into account in a more sophisticated way, and to obtain a clear understanding for why Richardson's t^3 (or more general $t^{2/(1-H)}$) law should still be observed within the inertial-range of a velocity field with temporal decorrelations set by Taylor's hypothesis. Some subtle consequences of sweeping have been explicitly and rigorously demonstrated for random shear flow models in [14,141], and were discussed in Section 3. The importance of sweeping effects is not limited to flows satisfying Taylor's hypothesis; tracer pairs in any turbulent flow are subjected to (nonconstant) sweeping by the large scales of the flow [319,320].

6.5.4.2. Theoretical overprediction of Richardson constant. Since the value of the Richardson constant C_R in his t^3 law (395) has been the object of extensive experimental [248,261,315], theoretical [124,178,192,200,241,299,322], and numerical [109,291] investigation in various contexts, we relate the results reported in Section 6.5.3 to those developed elsewhere. By comparing Eq. (399) with the prefactor $S_{v,\|}^I = 1$ to the theoretical Kolmogorov relation for the longitudinal velocity fluctuation:

$$\langle((\boldsymbol{v}(\boldsymbol{x}+\boldsymbol{r})-\boldsymbol{v}(\boldsymbol{x}))\cdot(\boldsymbol{r}/|\boldsymbol{r}|))^2\rangle = C_\|^I \bar{\varepsilon}^{2/3}|\boldsymbol{r}|^{2H},$$

with experimentally measured dimensionless constant $C_\|^I \approx 2.0$ (in three dimensions), we can associate an effective value of $\bar{\varepsilon} = (C_\|^I)^{-3/2} \approx 2.8$ to the simulation. The Monte Carlo simulations presented here therefore predict a Richardson constant of

$$C_R = 0.09 \pm 0.01$$

in the scaling law (395) for pair dispersion in a two-dimensional, incompressible, Gaussian, random, isotropic velocity field which possesses an isotropic Kolmogorov spectrum and satisfies Taylor's hypothesis.

This value agrees reasonably well with the one obtained by Tatarski [315], $C_R = 0.06$ in his experiments. Ozmidov [261] has argued from his experimental data that the appropriate range for C_R is $O(10^{-2})$. Sabelfeld [291] used the Randomization Method (Section 6.2.3) to study pair dispersion over one decade of scales in a three-dimensional, statistically isotropic synthetic turbulent flow satisfying Taylor's hypothesis, and obtained the value $C_R = 0.25 \pm 0.03$. Fung et al., in an interesting paper [109], did not study pair dispersion in a flow satisfying Taylor's hypothesis, but instead built synthetic three-dimensional turbulent velocity fields with Kolmogorov spatio-temporal statistics as in Section 3.4.3. Inertial-range scaling (396) was satisfied for less than one decade (in contrast to the 12 decades in the methods [84–86] utilized above); nevertheless, the Richardson's t^3 law was observed for 1.5 decades of pair separation with a Richardson constant $C_R = 0.1$. All of the empirical work just mentioned points to a small value of the Richardson constant, C_R, and the direct simulations spanning many decades of pair separation reported in [86] and Section 6.5.3 confirm a small value $C_R = 0.09 \pm 0.01$ for pair dispersion in a flow which has a wide inertial scaling range and satisfies the assumptions of Taylor's hypothesis.

On the other hand, turbulence closure theories produce values of C_R that are a full order of magnitude larger. With LHDIA, Kraichnan [178] predicted $C_R = 2.42$; with another Lagrangian-history closure, Lundgren [200] predicted $C_R = 3.06$; an EDQNM procedure [192] leads to $C_R = 3.50$; a stochastic, Markovian two-particle model [322] has $C_R = 1.33$; some quasi-Gaussian approximations predicted $C_R = 0.534$ [241] and $C_R = 2.49$ [57]; and some Langevin equation models [124,299] produced $C_R = 0.667$. What are the reasons for the wide discrepancies between these closure theories and the results mentioned in the previous paragraph regarding the value of C_R?

One source may be the way in which the closure theories treat the temporal dynamics of the tracers [86]. Kraichnan [178] found that under a certain rapid decorrelation in time limit within his LHDIA calculation, the pair separation would continue to obey Richardson's t^3 law but with a scaling constant 50 times larger. Another possibility for the depression of Richardson's constant below theoretically predicted values is the flow topology. The theories may not be taking into account the slowing of the relative diffusion of a tracer pair as it passes through regions in which vorticity dominates strain [109].

6.5.4.3. General remarks on the role of Monte Carlo simulations. We have seen in the above discussion an excellent instance of the valuable interaction between mathematics, reliable numerical simulations, and physical theories. Mathematical considerations suggested the basis of an efficient and accurate Monte Carlo algorithm for simulating turbulent diffusion in flows with a wide inertial range, and exactly solvable mathematical model problems and other considerations were used to validate and scrutinize the method (Section 6.3). This numerical algorithm was then utilized to explore turbulent diffusion in more realistic flows which are still described in a mathematically straightforward fashion (inertial-range scaling, Gaussian statistics, statistical isotropy), but for which exact solutions are no longer available. The results from these Monte Carlo simulations (Section 6.5.3) then pose new test problems for approximate physical theories for turbulent diffusion. One advantage of numerical simulations with synthetic velocity fields over laboratory experiments in this regard is the fact that the turbulent environment is specified in a mathematically transparent fashion, so the challenge for physical theories can be posed with a suitable degree of complexity. For example, the predictions of turbulent diffusion theories can be first examined for accuracy without taking into account intermittency and other nonideal features of a turbulent velocity field. Furthermore, as we discussed in Sections 4 and 5 above, Gaussian velocity fields can often induce similar non-Gaussian statistics in a passive scalar field at long times as more complex non-Gaussian velocity fields. For Richardson's t^3 law, such expected behavior has been confirmed recently [42].

7. Approximate closure theories and exactly solvable models

We have demonstrated throughout this report how simple mathematical models can illustrate various subtle physical mechanisms involved in turbulent diffusion. In Section 6, we also discussed how simple models manifesting a complex variety of behavior can be used to assess the virtues and shortcomings of numerical simulation methods, and how they can lead to and validate the design of more powerful and efficient algorithms. In this concluding section, we mention how the simple mathematical models can be used in a similar spirit to test the robustness of various approximate theoretical closure theories for turbulent diffusion. We will be intentionally brief because the reader may find extensive discussions of these applications in the original work of Avellaneda and the first author [13,17] and the recent review paper of Smith and Woodruff [300].

We discussed at the beginning of Section 3 the inherent difficulty of deriving effective large-scale equations for the mean passive scalar density due to the active fluctuations of the velocity field over a wide inertial range of scales. The rigorous homogenization theory described in Section 2 cannot be applied in general because there is usually no strong scale separation between the length scales of the passive scalar and velocity field. Various schemes for deriving approximate large-scale equations for the mean passive scalar density in the absence of scale separation have been proposed proceeding from a diverse collection of frameworks and formal assumptions [48,49,57,175,177,182, 227,285,286,321,327,328,344].

However, the equations produced by different theories are generally distinct, and it is usually difficult to determine whether the formal hypotheses are satisfied on which the different theories are founded. Tests of the theoretical predictions against laboratory experiments and direct numerical simulations are therefore crucial [133]. Experimental assessments however face certain limitations

concerning both the extent to which the input parameters can be faithfully matched between the theory and the laboratory setup, and the extent to which accurate and comprehensive data can be collected in high Reynolds number flows. Direct numerical simulations, on the other hand, are constrained by hardware limitations to moderate Reynolds numbers [59,154], particularly if nontrivial macroscale variations are present. Simplified mathematical models therefore provide an important complementary means of examining the accuracy and content of approximate closure theories. We have seen how exact characterization of the passive scalar statistics may be achieved in a variety of nontrivial mathematical models. These often allow precise characterization of turbulent diffusion in important asymptotic limits as well as at finite parameter values and over finite time intervals.

We particularly mention in this regard the Simple Shear Models described in Section 3 for which exact equations describing the high Reynolds number behavior of the mean passive scalar density have been derived using a rigorous renormalization procedure [10]. It is particularly instructive to compare these exact equations with the predictions of approximate closure theories to gain some insight into their strengths and shortcomings. Such a study was carried out by Avellaneda and the first author [13] for closures based on the renormalization group theory (RNG) [300,344] and renormalized perturbation theory (in particular, Kraichnan's Direct Interaction Approximation [173–175,177,197,285] and the first-order smoothing (quasi-normal) approximation [48,49]). Each of the approximate closure theories recovers the correct large-scale equations for a subset of the phase diagram of scaling exponents (ε, z) (see Section 3.4.3), but predicts incorrect equations in other substantial regions [13].

In particular, the RNG theory is exact for those Simple Shear Models in which the correlation time of the velocity field is much shorter than the dynamical time scale of the passive scalar field, but fails otherwise [13,17,300]. The RNG theory always predicts a local effective diffusion equation with some enhanced eddy diffusivity, but the rigorous results of the Simple Shear Model indicate that this is inappropriate in a wide variety of situations [10]. The RNG theory also predicts incorrect space–time rescalings for certain regimes. The renormalized perturbation theories, by contrast, predict the correct scaling exponents (after an elaborate analysis) for all phase regimes in the Simple Shear Model, but sometimes mistakenly suggest nonlocal evolution equations when the exact equations are in fact local [13]. (Other examples of this latter phenomenon in simple stochastic problems are presented in [328]). Both the RPT and RNG theories predict correct large-scale equations in one phase region abutting the Kolmogorov values $((\varepsilon, z) = (8/3, 2/3))$, but introduce discrepancies from the exact renormalized equation at this point and in the other neighboring regime. Note that the Eulerian and Lagrangian versions [177] of the renormalized perturbation theories are equivalent for the Simple Shear Model without a sweep as discussed in [13] because the Eulerian and Lagrangian velocity correlations coincide. We see in this way how simple mathematical models can yield both quantitative and qualitative insight into the strengths and shortcomings of approximate closure strategies.

Recently, van den Eijnden and the current authors have investigated how various closure theories, including a new "modified direction interaction approximation" [328,329], fare under the introduction of a temporally fluctuating cross sweep to a shear flow (Section 3). This is the simplest model problem with complex behavior where the Eulerian and Lagrangian correlations are unequal. These results will be reported in a forthcoming paper [330]. Our hope, in the long run, is to learn the strengths and weaknesses of various existing closure theories by applying them to the

simplified mathematical models described in this report, and thereby be instructed in the formulation of new and improved closure approximations.

Acknowledgements

References

[1] R.J. Adler, The Geometry of Random Fields, Sections 8.3, Wiley Series in Probability and Mathematical Statistics, Wiley, Chichester, 1981, pp. 198–203.

[2] L.Ts. Adzhemyan, N.V. Antonov, A.N. Vasil'ev, Renormalization group, Operator product expansion, and anomalous scaling in a model of advected passive scalar, chao-dyn/9801033, 1998.

[3] B.K. Alpert, Ph.D. Thesis, Department of Computer Science, Yale University, 1990.

[4] B.K. Alpert, Construction of simple multiscale bases for fast matrix operations, in: Ruskai et al. (Eds.), Wavelets and their Applications, Jones and Bartlett Publishers, Boston, MA, 1992, pp. 211–226.

[5] R.A. Antonia, E.J. Hopfinger, Y. Gagne, F. Anselmet, Temperature structure functions in turbulent shear flows, Phys. Rev. A 30 (5) (1984) 2704–2707.

[6] Neil W. Ashcroft, N.D. Mermin, Solid State Physics, Ch. 10, W.B. Saunders Company, Philadelphia, 1976, pp. 176–190.

[7] P. Auscher, G. Weiss, M.V. Wickerhauser, Local sine and cosine bases of Coifman and Meyer and the construction of smooth wavelets, in: C.K. Chui (Ed.), Wavelets: a Tutorial in Theory and Applications, Wavelet Analysis and its Applications, vol. 2, Academic Press, New York, 1992, pp. 237–256.

[8] M. Avellaneda, Jr., E. Frank, C. Apelian, Trapping, percolation, and anomalous diffusion of particles in a two-dimensional random field, J. Statist. Phys. 72 (5–6) (1993) 1227–1304.

[9] M. Avellaneda, A.J. Majda, Stieltjes integral representation and effective diffusivity bounds for turbulent transport, Phys. Rev. Lett. 62 (7) (1989) 753–755.

[10] M. Avellaneda, A.J. Majda, Mathematical models with exact renormalization for turbulent transport, Comm. Pure Appl. Math. 131 (1990) 381–429.

[11] M. Avellaneda, A.J. Majda, Homogenization and renormalization of multiple-scattering expansions for Green functions in turbulent transport, in: Composite Media and Homogenization Theory (Trieste, 1990), of Programme Nonlinear Differential Equations Applications, vol. 5, Birkhäuser, Boston, MA, 1991, pp. 13–35.

[12] M. Avellaneda, A.J. Majda, An integral representation and bounds on the effective diffusivity in passive advection by laminar and turbulent flows, Comm. Math. Phys. 138 (1991) 339–391.

[13] M. Avellaneda, A.J. Majda, Approximate and exact renormalization theories for a model for turbulent transport, Phys. Fluids A 4 (1) (1992) 41–56.

[14] M. Avellaneda, A.J. Majda, Mathematical models with exact renormalization for turbulent transport, II: fractal interfaces, non-Gaussian statistics and the sweeping effect, Comm. Pure. Appl. Math. 146 (1992) 139–204.

[15] M. Avellaneda, A.J. Majda, Renormalization theory for eddy diffusivity in turbulent transport, Phys. Rev. Lett. 68 (20) (1992) 3028–3031.

[16] M. Avellaneda, A.J. Majda, Superdiffusion in nearly stratified flows, J. Statist. Phys. 69 (3/4) (1992) 689–729.

[17] M. Avellaneda, A.J. Majda, Application of an approximate R-N-G theory, to a model for turbulent transport, with exact renormalization, in: Turbulence in Fluid Flows, IMA Vol. Math. Appl., vol. 55, Springer, Berlin, 1993, pp. 1–31.

[18] M. Avellaneda, A.J. Majda, Simple examples with features of renormalization for turbulent transport, Phil. Trans. R. Soc. Lond. A 346 (1994) 205–233.

[19] M. Avellaneda, S. Torquato, I.C. Kim, Diffusion and geometric effects in passive advection by random arrays of vortices, Phys. Fluids A 3 (8) (1991) 1880–1891.

[20] M. Avellaneda, M. Vergassola, Stieltjes integral representation of effective diffusivities in time-dependent flows, Phys. Rev. E 52 (3) (1995) 3249–3251.

[21] A. Babiano, C. Basdevant, P. Le Roy, R. Sadourny, Relative dispersion in two-dimensional turbulence, J. Fluid Mech. 214 (1990) 535–557.

[22] A. Babiano, C. Basdevant, R. Sadourny, Structure functions and dispersion laws in two-dimensional turbulence, J. Atmospheric Sci. 42 (9) (1985) 941–949.

[23] E. Balkovksy, V. Lebedev, Instanton for the Kraichnan passive scalar problem, chao-dyn/9803018, 12 March, 1998.

[24] G.I. Barenblatt, Dimensional Analysis, Gordon and Breach, New York, 1987.

[25] G.I. Barenblatt, Scaling, self-similarity, and intermediate asymptotics, Cambridge Texts in Applied Mathematics, vol. 14, Cambridge University Press, Cambridge, UK, 1996.

[26] G.I. Barenblatt, A.J. Chorin, Scaling laws and zero viscosity limits for wall-bounded shear flows and for local structure in developed turbulence, Commun. Pure Appl. Math. 50 (4) (1997) 381–398.

[27] G.K. Batchelor, Diffusion in a field of homogenous turbulence II. The relative motion of particles, Proc. Cambridge Phil. Soc. 48 (1952) 345–362.

[28] G.K. Batchelor, Small-scale variation of convected quantities like temperature in turbulent fluid. Part 1. General discussion and the case of small conductivity, J. Fluid. Mech. 5 (1959) 113–133.

[29] G.K. Batchelor, I.D. Howells, A.A. Townsend, Small-scale variation of convected quantities like temperature in a turbulent fluid. Part 2. The case of large conductivity, J. Fluid. Mech. 5 (1959) 134–139.

[30] C.M. Bender, S.A. Orszag, Advanced Mathematical Methods for Scientists and Engineers, International Series in Pure and Applied Mathematics, McGraw-Hill, New York, 1978.

[31] A.F. Bennett, A Lagrangian analysis of turbulent diffusion, Rev. Geophys. 25 (4) (1987) 799–822.

[32] A. Bensoussan, J.-L. Lions, G. Papanicolaou, Asymptotic Analysis for Periodic Structures, Studies in Mathematics and its Applications, vol. 5, North-Holland-Elsevier Science Publishers, Amsterdam, 1978.

[33] R. Benzi, L. Biferale, A. Wirth, Analytic calculation of anomalous scaling in random shell models for a passive scalar, Phys. Rev. Lett. 78 (26) (1997) 4926–4929.

[34] R. Benzi, S. Ciliberto, R. Tripiccione, C. Baudet, F. Massaioli, S. Succi, Extended self-similarity in turbulent flows, Phys. Rev. E 48 (1) (1993) R29–R32.

[35] D. Bernard, K. Gawędzki, A. Kupiainen, Anomalous scaling in the N-point functions of passive scalar, Phys. Rev. E 54 (3) (1996) 2564–2572.

[36] D. Bernard, K. Gawędzki, A. Kupiainen, Slow modes in passive advection, J. Statist. Phys. 90 (3-4) (1998) 519–569.

[37] G. Beylkin, R. Coifman, V. Rokhlin, Wavelets in numerical analysis, in: Ruskai et al. (Eds.), Wavelets and their Applications, Jones and Bartlett Publishers, Boston, MA, 1992, pp. 181–210.

[38] R.N. Bhattacharya, A central limit theorem for diffusions with periodic coefficients, Ann. Probab. 13(2) (1985) 385–396.

[39] R.N. Bhattacharya, V.K. Gupta, H.F. Walker, Asymptotics of solute dispersion in periodic porous media, SIAM J. Appl. Math. 49(1) (1989) 86–98.

[40] L. Biferale, A. Crisanti, M. Vergassola, A. Vulpiani, Eddy diffusivities in scalar transport, Phys. Fluids 7(11) (1995) 2725–2734.

[41] P. Billingsley, Probability and Measure, 3rd ed., Wiley, New York, 1995.

[42] G. Boffetta, A. Celani, A. Crisanti, A. Vulpiani, Relative dispersion in fully developed turbulence: from Eulerian to Lagrangian statistics in synthetic flows, preprint, 1998.

[43] R. Borghi, Turbulent combustion modelling, Prog. Energy Combust. Sci. 14 (1988) 245–292.

[44] A.N. Borodin, A limit theorem for solutions of differential equations with random right-hand side, Theory Probab. Appl. 22(3) (1977) 482–497.

[45] J.-P. Bouchaud, A. Comtet, A. Georges, P. Le Doussal, Anomalous diffusion in random media of any dimensionality, J. Physique 48 (1987) 1445–1450.

[46] J.-P. Bouchaud, A. Georges, J. Koplik, A. Provata, S. Redner, Superdiffusion in random velocity fields, Phys. Rev. Lett. 64(21) (1990) 2503–2506.

[47] J.-P. Bouchaud, A. Georges, Anomalous diffusion in disordered media: statistical mechanisms, models and physical applications, Phys. Rep. 195(4-5) (1990) 127–293.

[48] R.C. Bourret, An hypothesis concerning turbulent diffusion, Can. J. Phys. 38 (1960) 665–676.

[49] R.C. Bourret, Stochastically perturbed fields, with applications to wave propagation in random media, Nuovo Cimento (10) 26 (1962) 1–31.

[50] R.N. Bracewell, The Fourier Transform and its Applications, 2nd ed., McGraw-Hill, New York, 1986.

[51] J.C. Bronski, R.M. McLaughlin, Scalar intermittency and the ground state of periodic Schrödinger equations, Phys. Fluids 9(1) (1997) 181–190.

[52] R. Camassa, S. Wiggins, Transport of a passive tracer in time-dependent Rayleigh–Bénard convection, Phys. D 51(1-3) (1991) 472–481; Nonlinear science: the next decade, Los Alamos, NM, 1990.

[53] R.A. Carmona, J.P. Fouque, Diffusion-approximation for the advection-diffusion of a passive scalar by a space-time Gaussian velocity field, in: E. Bolthausen, M. Dozzi, F. Russo (Eds.), Seminar on Stochastic Analysis, Random Fields and Applications, Progress in Probability, vol. 36, Centro Stefano Franscini, Birkhäuser, Basel, 1995, pp. 37–49.

[54] R.A. Carmona, S.A. Grishin, S.A. Molchanov, Massively parallel simulations of motions in a Gaussian velocity field, Stochastic Modelling in Physical Oceanography, Progr. Prob., vol. 39, Birkhäuser, Boston, 1996, pp. 47–68.

[55] B. Castaing, G. Gunaratne, F. Heslot, L. Kadanoff, A. Libchaber, S. Thomae, X.-Z. Wu, S. Zaleski, G. Zanetti, Scaling of hard thermal turbulence in Rayleigh-Bénard convection, J. Fluid Mech. 204 (1989) 1–30.

[56] J. Chasnov, V.M. Canuto, R.S. Rogallo, Turbulence spectrum of a passive temperature field: results of a numerical simulation, Phys. Fluids 31(8) (1988) 2065–2067.

[57] V.R. Chechetkin, V.S. Lutovinov, A.A. Samokhin, On the diffusion of passive impurities in random flows, Physica A 175 (1991) 87–113.

[58] H. Chen, S. Chen, R.H. Kraichnan, Probability distribution of a stochastically advected scalar field, Phys. Rev. Lett. 63(24) (1989) 2657–2660.

[59] S. Chen, G.D. Doolen, R.H. Kraichnan, Z.-S. She, On statistical correlations between velocity increments and locally averaged dissipation in homogenous turbulence, Phys. Fluids A 5 (1993) 458–463.

[60] S. Chen, R.H. Kraichnan, Sweeping decorrelation in isotropic turbulence, Phys. Fluids A 1(12) (1989) 2019–2024.

[61] S. Chen, R.H. Kraichnan, Simulations of a randomly advected passive scalar field, Phys. Fluids (1998) in press.

[62] M. Chertkov, Instanton for random advection, Phys. Rev. E 55 (3) (1997) 2722–2735.

[63] M. Chertkov, G. Falkovich, Anomalous scaling exponents of a white-advected passive scalar, Phys. Rev. Lett. 76(15) (1996) 2706–2709.

[64] M. Chertkov, G. Falkovich, I. Kolokolov, V. Lebedev, Normal and anomalous scaling of the fourth-order correlation function of a randomly advected passive scalar, Phys. Rev. E 52(5) (1995) 4924–4941.

[65] M. Chertkov, G. Falkovich, I. Kolokolov, V. Lebedev, Statistics of a passive scalar advected by a large-scale two-dimensional velocity field: analytic solution, Phys. Rev. E 51(6) (1995) 5609–5627.

[66] M. Chertkov, A. Gamba, I. Kolokolov, Exact field-theoretical description of passive scalar convection in an N-dimensional long-range velocity field, Phys. Lett. A 192 (1994) 435–443.

[67] S. Childress, Alpha-effect in flux ropes and sheets, Phys. Earth Planet. Int. 20 (1979) 172–180.

[68] S. Childress, A.M. Soward, Scalar transport and alpha-effect for a family of cat's-eye flows, J. Fluid Mech. 205 (1989) 99–133.

[69] E.S.C. Ching, V.S. L'vov, E. Podivilov, I. Procaccia, Conditional statistics in scalar turbulence: theory versus experiment, Phys. Rev. E 54 (6) (1996) 6364–6371.

[70] E.S.C. Ching, V.S. L'vov, I. Procaccia, Fusion rules and conditional statistics in turbulent advection, Phys. Rev. E 54(5) (1996) R4520–R4523.

[71] E.S.C. Ching, Y. Tu, Passive scalar fluctuations with and without a mean gradient: a numerical study, Phys. Rev. E 49(2) (1994) 1278–1282.

[72] A.J. Chorin, Vorticity and turbulence, Applied Mathematical Sciences, vol. 103, Springer, New York, 1994.

[73] J.P. Clay, Turbulent mixing of temperature in water, air, and mercury, Ph.D. Thesis, University of California at San Diego, 1973.

[74] P. Constantin, I. Procaccia, The geometry of turbulent advection: Sharp estimates for the dimensions of level sets, Nonlinearity 7 (1994) 1045–1054.

[75] P. Constantin, I. Procaccia, K.R. Sreenivasan, Fractal geometry of isoscalar surfaces in turbulence: theory and experiments, Phys. Rev. Lett. 67 (13) (1991) 1739–1742.

[76] S. Corrsin, On the spectrum of isotropic temperature fluctuations in isotropic turbulence, J. Appl. Phys. 22 (1951) 469.

[77] A. Crisanti, M. Falcioni, G. Paladin, A. Vulpiani, Anisotropic diffusion in fluids with steady periodic velocity fields, J. Phys. A 23(14) (1990) 3307–3315.

[78] G.T. Csanady, Turbulent Diffusion in the Environment, Geophysics and Astrophysics Monographs, vol. 3, D. Reidel, Dordrecht, 1973.

[79] G. Dagan, Theory of solute transport by groundwater, in Annual Review of Fluid Mechanics, vol. 19, Annual Reviews, Palo Alto, CA, 1987, pp. 183–215.

[80] I. Daubechies, Ten Lectures on Wavelets, CBMS-NSF Regional Conf. Series in Applied Mathematics, vol. 61, Society for Industrial and Applied Mathematics (SIAM), Philadelphia, PA, 1992.

[81] D.R. Dowling, P.E. Dimotakis, Similarity of the concentration field of gas-phase turbulent jets, J. Fluid Mech. 218 (1990) 109–141.

[82] F.W. Elliott Jr, D.J. Horntrop, A.J. Majda, A Fourier-wavelet Monte Carlo method for fractal random fields, J. Comput. Phys. 132(2) (1997) 384–408.

[83] F.W. Elliott Jr, D.J. Horntrop, A.J. Majda, Monte Carlo methods for turbulent tracers with long range and fractal random velocity fields, Chaos 7(1) (1997) 39–48.

[84] F.W. Elliott Jr, A.J. Majda, A wavelet Monte Carlo method for turbulent diffusion with many spatial scales, J. Comput. Phys. 113(1) (1994) 82–111.

[85] F.W. Elliott Jr, A.J. Majda, A new algorithm with plane waves and wavelets for random velocity fields with many spatial scales, J. Comput. Phys. 117 (1995) 146–162.

[86] F.W. Elliott Jr, A.J. Majda, Pair dispersion over an inertial range spanning many decades, Phys. Fluids 8 (4) (1996) 1052–1060.

[87] F.W. Elliott Jr, A.J. Majda, D.J. Horntrop, R.M. McLaughlin, Hierarchical Monte Carlo methods for fractal random fields, J. Statist. Phys. 81 (1995) 717.

[88] P.F. Embid, A.J. Majda, P.E. Souganidis, Effective geometric front dynamics for premixed turbulent combustion with separated velocity scales, Comb. Sci. Technol. 103 (1994) 85–115.

[89] P.F. Embid, A.J. Majda, P.E. Souganidis, Comparison of turbulent flame speeds from complete averaging and the G-equation, Phys. Fluids 7(8) (1995) 2052–2060.

[90] P.F. Embid, A.J. Majda, P.E. Souganidis, Examples and counterexamples for Huygens Principle in premixed combustion, Comb. Sci. Technol. 120(1-6) (1996) 273–303.

[91] V. Eswaran, S.B. Pope, Direct numerical simulations of the turbulent mixing of a passive scalar, Phys. Fluids 31(3) (1988) 506–520.

[92] G. Eyink, J. Xin, Dissipation-independence of the inertial-convective range in a passive scalar model, Phys. Rev. Lett. 77(13) (1996) 2674–2677.

[93] G. Eyink, J. Xin, Existence and uniqueness of L^2-solutions at zero-diffusivity in the Kraichnan model of a passive scalar, chao-dyn/9605008, 15 May 1996.

[94] A.L. Fairhall, B. Galanti, V.S. L'vov, I. Procaccia, Direct numerical simulations of the Kraichnan Model: scaling exponents and fusion rules, Phys. Rev. Lett. 79(21) (1997).

[95] A.L. Fairhall, O. Gat, V. L'vov, I. Procaccia, Anomalous scaling in a model of passive scalar advection: exact results, Phys. Rev. E 53(4A) (1996) 3518–3535.

[96] G. Falkovich, I. Kolokolov, V. Lebedev, A. Migdal, Instantons and intermittency, Phys. Rev. E 54(5) (1996) 4896–4907.

[97] A. Fannjiang, G. Papanicolaou, Convection enhanced diffusion for periodic flows, SIAM J. Appl. Math. 54(2) (1994) 333–408.

[98] A. Fannjiang, G. Papanicolaou, Diffusion in turbulence, Probab. Theory Related Fields 105 (3) (1996) 279–334.

[99] A. Fannjiang, G. Papanicolaou, Convection-enhanced diffusion for random flows, J. Statist. Phys. 88(5-6) (1997) 1033–1076.

[100] J. Feder, in: Fractals, Chs. 9–14, Physics of Solids and Liquids, Plenum Press, New York, 1988, pp. 163–243.

[101] C. Fefferman, private communication.

[102] W. Feller, An Introduction to Probability Theory and its Applications, 3rd ed., vol. 1, Wiley, New York, 1968.

[103] W. Feller, An Introduction to Probability Theory and its Applications, 2nd ed., vol. 2, Section II.2, Wiley, New York, 1971, pp. 47, 48.

[105] G.B. Folland, Introduction to Partial Differential Equations, 2nd ed., Princeton University Press, Princeton, 1995.

[106] F.N. Frenkiel, P.S. Klebanoff, Two-dimensional probability distribution in a turbulent field, Phys. Fluids 8 (1965) 2291–2293.

[107] A. Friedman, Stochastic Differential Equations and Applications, vol. 1, Academic Press, New York, 1975.

[108] U. Frisch, A. Mazzino, M. Vergassola, Intermittency in passive scalar advection, Phys. Rev. Lett. 80(25) (1998) 5532–5535.

[109] J.C.H. Fung, J.C.R. Hunt, N.A. Malik, R.J. Perkins, Kinematic simulation of homogenous turbulence by unsteady random Fourier modes, J. Fluid Mech. 236 (1992) 281–318.

[111] F. Gao, Mapping closure and non-Gaussianity of the scalar probability density functions in isotropic turbulence, Phys. Fluids A 3(10) (1991) 2438–2444.

[112] T.C. Gard, Introduction to Stochastic Differential Equations, Pure and Applied Mathematics, vol. 114, Marcel Dekker, New York, 1988.

[113] A.E. Gargett, Evolution of scalar spectra with the decay of turbulence in a stratified fluid, J. Fluid Mech. 159 (1985) 379–407.

[114] O. Gat, V.S. L'vov, E. Podivilov, I. Procaccia, Nonperturbative zero modes in the Kraichnan model for turbulent advection, Phys. Rev. E 55(4) (1997) R3836–R3839.

[115] O. Gat, R. Zeitak, Multiscaling in passive scalar advection as stochastic shape dynamics, Phys. Rev. E 57(5) (1998) 5511–5519.

[116] K. Gawędzki, A. Kupiainen, Anomalous scaling of the passive scalar, Phys. Rev. Lett. 75(21) (1995) 3834–3837.

[117] K. Gawędzki, A. Kupiainen, Universality in turbulence: an exactly solvable model, in: Low-dimensional Models in Statistical Physics and Quantum Field Theory (Schladming, 1995), Lecture Notes in Physics, vol. 469, Springer, Berlin, 1996, pp. 71–105.

[118] I.M. Gel'fand, N.Ya. Vilenkin, Generalized Functions, Applications of Harmonic Analysis, Ch. 4, Academic Press, New York, 1964.

[119] L.W. Gelhar, A.L. Gutjahr, R.L. Naff, Stochastic analysis of macrodispersion in a stratified aquifer, Water Resour. Res. 15 (6) (1979) 1387–1397.

[120] C.H. Gibson, Fine structure of scalar fields mixed by turbulence. I, Zero-gradient points and minimal gradient surfaces, Phys. Fluids 11(11) (1968) 2305–2315.

[121] C.H. Gibson, Fine structure of scalar fields mixed by turbulence. II, Spectral Theory, Phys. Fluids 11(11) (1968) 2316–2327.

[122] C.H. Gibson, W.T. Ashurst, A.R. Kerstein, Mixing of strongly diffusive passive scalars like temperature by turbulence, J. Fluid Mech. 194 (1988) 261–293.

[123] C.H. Gibson, W.H. Schwarz, The universal equilibrium spectra of turbulent velocity and scalar fields, J. Fluid Mech. 16 (1963) 357–384.

[124] F.A. Gifford, Horizontal diffusion in the atmosphere: a Lagrangian-dynamical theory, Atmos. Environ. 16 (1982) 505–512.

[125] K. Golden, S. Goldstein, J.L. Lebowitz, Classical transport in modulated structures, Phys. Rev. Lett. 55 (24) (1985) 2629–2632.

[126] N. Goldenfeld, Lectures on Phase Transitions and the Renormalization Group, Frontiers in Physics, vol. 85, Addison-Wesley, Reading, MA, USA, 1992.

[127] J.P. Gollub, J. Clarke, M. Gharib, B. Lane, O.N. Mesquita, Fluctuations and transport in a stirred fluid with a mean gradient, Phys. Rev. Lett. 67(25) (1991) 3507–3510.

[128] F.C. Gouldin, Interpretation of jet mixing using fractals, AIAA J. 26 (1988) 1405–1407.

[129] H.L. Grant, B.A. Hughes, W.M. Vogel, A. Moilliet, The spectrum of temperature fluctuations in turbulent flow, J. Fluid Mech. 34 (1968) 423–442.

[130] V.K. Gupta, R.N. Bhattacharya, Solute dispersion in multidimensional periodic saturated porous media, Water Resour. Res. 22(2) (1986) 156–164.

[131] O. Güven, F.J. Molz, Deterministic and stochastic analyses of dispersion in an unbounded stratified porous medium, Water Resour. Res. 22(11) (1986) 1565–1574.

[132] H.G.E. Hentschel, I. Procaccia, Relative diffusion in turbulent media: the fractal dimension of clouds, Phys. Rev. A 29(3) (1983) 1461–1470.

[133] J.R. Herring, R.M. Kerr, Comparison of direct numerical simulations with predictions of two-point closures for isotropic turbulence convecting a passive scalar, J. Fluid Mech. 118 (1982) 205–219.

[134] R. Hersh, Random evolutions: a survey of results and problems, Rocky Mountain J. Math. 4 (3) (1974) 443–477.

[135] F. Heslot, B. Castaing, A. Libchaber, Transition to turbulence in helium gas, Phys. Rev. A 36 (1987) 5870–5873.

[136] R.J. Hill, Models of the scalar spectrum for turbulent advection, J. Fluid Mech. 88(3) (1978) 541–562.

[137] R.J. Hill, Solution of Howell's model of the scalar spectrum and comparison with experiment, J. Fluid Mech. 96(4) (1980) 705–722.

[138] M. Holzer, A. Pumir, Simple models of non-Gaussian statistics for a turbulently advected passive scalar, Phys. Rev. E 47(1) (1993) 202–219.

[139] M. Holzer, E.D. Siggia, Turbulent mixing of a passive scalar, Phys. Fluids 6(5) (1994) 1820–1837.

[140] D.J. Horntrop, Monte Carlo simulation for turbulent transport, Ph.D. Thesis, Princeton University, 1995. Program in Applied and Computational Mathematics.

[141] D.J. Horntrop, A.J. Majda, Subtle statistical behavior in simple models for random advection-diffusion, J. Math. Sci. Univ. Tokyo 1 (1994) 1–48.

[142] D.J. Horntrop, A.J. Majda, An overview of Monte Carlo simulation techniques for the generation of random fields, Proc. 9th Aha Huliko Hawaiian Winter Workshop, 1997, to appear.

[143] I.A. Ibragimov, Yu.V. Linnik, Independent and Stationary Sequences of Random Variables, Ch. 17, Wolters-Noordhoff Publishing, Groningen, The Netherlands, 1971.

[144] M.B. Isichenko, Ya.L. Kalda, E.B. Tatarinova, O.V. Tel'kovskaya, V.V. Yan'kov, Diffusion in a medium with vortex flow, Sov. Phys. JETP 69(3) (1989) 517–524.

[145] Jayesh, C. Tong, Z. Warhaft, On temperature spectra in grid turbulence, Phys. Fluids 6(1) (1994) 306–312.

[146] Jayesh, Z. Warhaft, Probability distribution of a passive scalar in grid-generated turbulence, Phys. Rev. Lett. 67(25) (1991) 3503–3506.

[147] Jayesh, Z. Warhaft, Probability distribution, conditional dissipation, and transport of passive temperature fluctuations in grid-generated turbulence, Phys. Fluids A 4(10) (1992) 2292–2307.

[148] V.V. Jikov, S.M. Kozlov, O.A. Oleinik, Homogenization of Differential Operators and Integral Functionals, Springer, Berlin, 1994.

[149] V.V. Jikov, S.M. Kozlov, O.A. Oleinik, Homogenization of Differential Operators and Integral Functionals, Ch. 2, Springer, Berlin, 1994, pp. 55–85.

[150] F. John, Partial Differential Equations, Applied Mathematical Sciences, 4th ed., Ch. 1, Springer, Berlin, 1982, 1–32.

[151] S. Karlin, H.M. Taylor, A Second Course in Stochastic Processes, section 16.1, Academic Press, Boston, 1981.

[152] A.P. Kazantsev, Enhancement of a magnetic field by a conducting fluid, Sov. Phys. JETP 26 (1968) 1031.

[153] R.M. Kerr, Higher-order derivative correlations and the alignment of small-scale structures in isotropic numerical turbulence, J. Fluid Mech. 153 (1985) 31–58.

[154] R.M. Kerr, Velocity, scalar and transfer spectra in numerical turbulence, J. Fluid Mech. 211 (1990) 309–322.

[155] R.M. Kerr, Rayleigh number scaling in numerical convection, J. Fluid Mech. 310 (1996) 139–179.

[156] A.R. Kerstein, Linear-eddy modelling of turbulent transport. Part 6. Microstructure of diffusive scalar mixing fields, J. Fluid Mech. 231 (1991) 361–394.

[157] A.R. Kerstein, P.A. McMurtry, Mean-field theories of random advection, Phys. Rev. E 49(1) (1994) 474–482.

[158] J. Kevorkian, J.D. Cole, Perturbation Methods in Applied Mathematics, Applied Mathematical Sciences, vol. 34, Ch. 4, Springer, Berlin, 1981, pp. 330–480.

[159] R.Z. Khas'minskii, A limit theorem for the solutions of differential equations with random right-hand sides, Theory Probab. Appl. 11(3) (1966) 390–406.

[160] R.Z. Khas'minskii, On stochastic processes defined by differential equations with a small parameter, Theory Probab. Appl. 11(2) (1966) 211–228.

[161] C.-B. Kim, J.A. Krommes, Improved rigorous upper bounds for transport due to passive advection described by simple models of bounded systems, J. Statist. Phys. 53(5-6) (1988) 1103–1137.

[162] Y. Kimura, R.H. Kraichnan, Statistics of an advected passive scalar, Phys. Fluids A 5 (9) (1993) 2264–2277.

[163] P.E. Kloeden, E. Platen, Numerical Solution of Stochastic Differential Equations, Applications of Mathematics: Stochastic Modelling and Applied Probability, vol. 23, Springer, Berlin, 1992.

[164] V.I. Klyatskin, W.A. Woyczynski, D. Gurarie, Short-time correlation approximations for diffusing tracers in random velocity fields: a functional approach, Stochastic Modelling in Physical Oceanography, Progr. Probab., vol. 39, Birkhäuser, Boston, 1996, pp. 221–269.

[165] E. Knobloch, W.J. Merryfield, Enhancement of diffusive transport in oscillatory flows, Astrophys. J. 401(1) (Part 1) (1992) 196–205.

[166] D.L. Koch, J.F. Brady, A non-local description of advection-diffusion with application to dispersion in porous media, J. Fluid Mech. 180 (1987) 387–403.

[167] D.L. Koch, J.F. Brady, Anomalous diffusion due to long-range velocity fluctuations in the absence of a mean flow, Phys. Fluids A 1(1) (1989) 47–51.

[168] D.L. Koch, R.G. Cox, H. Brenner, J.F. Brady, The effect of order on dispersion in porous media, J. Fluid Mech. 200 (1989) 173–188.

[169] A.N. Kolmogorov, The local structure of turbulence in incompressible viscous fluid for very large Reynolds numbers, Dokl. Akad. Nauk SSSR 30 (1941) 301–305.

[170] A.N. Kolmogorov, A refinement of previous hypotheses concerning the local structure of turbulence in a viscous incompressible fluid at high Reynolds number, J. Fluid Mech. 13 (1962) 82–85.

[171] S. Komori, T. Kanzaki, Y. Murakami, H. Ueda, Simultaneous measurements of instantaneous concentrations of two species being mixed in a turbulent flow by using a combined laser-induced fluorescence and laser-scattering technique, Phys. Fluids A 1(2) (1989) 349–352.

[172] T.W. Körner, Fourier Analysis, appendix C, Cambridge University Press, Cambridge, U.K., 1988, pp. 565–574.

[173] R.H. Kraichnan, Irreversible statistical mechanics of incompressible hydromagnetic turbulence, Phys. Rev. 109 (1958) 1407–1422.

[174] R.H. Kraichnan, The structure of isotropic turbulence, J. Fluid Mech. 5 (1959) 497–543.

[175] R.H. Kraichnan, Dynamics of nonlinear stochastic systems, J. Math. Phys. 2 (1961) 124–148.

[176] R.H. Kraichnan, Kolmogorov's hypotheses and Eulerian turbulence theory, Phys. Fluids 7(11) (1964) 1723–1734.

[177] R.H. Kraichnan, Lagrangian-history closure approximation for turbulence, Phys. Fluids 8(4) (1965) 575–598.

[178] R.H. Kraichnan, Dispersion of particle pairs in homogenous turbulence, Phys. Fluids 9 (1966) 1728–1752.

[179] R.H. Kraichnan, Small-scale structure of a scalar field convected by turbulence, Phys. Fluids 11(5) (1968) 945–953.

[180] R.H. Kraichnan, Diffusion by a random velocity field, Phys. Fluids 13(1) (1970) 22–31.

[181] R.H. Kraichnan, Turbulent diffusion: evaluation of primitive and renormalized perturbation series by Páde approximants and by expansion of Stieltjes transforms into contributions from continuous orthogonal functions. in: G.A. Baker, L. Gammel (Eds.), The Padé Approximant in Theoretical Physics, Academic Press, New York, 1970, pp. 129–170.

[182] R.H. Kraichnan, Eddy viscosity and diffusivity: exact formulas and approximations, Complex Systems 1 (1987) 805–820.

[183] R.H. Kraichnan, Anomalous scaling of a randomly advected passive scalar, Phys. Rev. Lett. 72 (7) (1994) 1016–1019.

[184] R.H. Kraichnan, V. Yakhot, S. Chen, Scaling relations for a randomly advected passive scalar field, Phys. Rev. Lett. 75(2) (1995) 240–243.

[185] P.R. Kramer, Passive scalar scaling regimes in a rapidly decorrelating turbulent flow, Ph.D. Thesis, Princeton University, November 1997.

[186] P.R. Kramer, Two different rapid decorrelation in time limits for turbulent diffusion, J. Statist. Phys. (1998) To be submitted.

[187] J.A. Krommes, R.A. Smith, Rigorous upper bounds for transport due to passive advection by inhomogeneous turbulence, Ann. Phys. 177(2) (1987) 246–329.

[188] R. Kubo, Stochastic Liouville equations, J. Math. Phys. 4(2) (1963) 174–183.

[189] H. Kunita, Stochastic Flows and Stochastic Differential Equations, Cambridge Studies in Advanced Mathematics, vol. 24, Cambridge University Press, Cambridge, UK, 1990.

[190] O.A. Kurbanmuradov, K.K. Sabelfeld, Statistical modelling of turbulent motion of particles in random velocity fields, Sov. J. Numer. Anal. Math. Modelling 4(1) (1989) 53–68.

[191] B.R. Lane, O.N. Mesquita, S.R. Meyers, J.P. Gollub, Probability distributions and thermal transport in a turbulent grid flow, Phys. Fluids A 5(9) (1993) 2255–2263.

[192] M. Larchevêque, M. Lesieur, The application of eddy-damped Markovian closures to the problem of dispersion of particle pairs, J. Mécanique 20 (1981) 113–134.

[193] J.C. LaRue, P.A. Libby, Thermal mixing layer downstream of half-heated turbulence grid, Phys. Fluids 24(4) (1981) 597–603.

[194] P. Le Doussal, Diffusion in layered random flows, polymers, electrons in random potentials, and spin depolarization in random fields, J. Statist. Phys. 69(5/6) (1992) 917–954.

[195] N.N. Lebedev, Special Functions and their Applications, Ch. 1, Dover, New York, 1972, pp. 1–15.

[196] M. Lesieur, Turbulence in Fluids, 2nd revised ed., vol. 1, in: Fluid Mechanics and its Applications, Kluwer, Dordrecht, 1990.

[197] D.C. Leslie, Developments in the Theory of Turbulence, Chs. 8–10, 12, Oxford Science Publications. The Clarendon Press Oxford University Press, New York, 1983, pp. 156–226, 267–284.

[198] T.C. Lipscombe, A.L. Frenkel, D. ter Haar, On the convection of a passive scalar by a turbulent Gaussian velocity field, J. Statist. Phys. 63(1-2) (1991) 305–313.

[199] S. Lovejoy, Area-perimeter relation for rain and cloud areas, Science 216(9) (1982) 185–187.

[200] R. Lundgren, Turbulent pairs dispersion and scalar diffusion, J. Fluid Mech. 111 (1981) 25–57.

[201] V. L'vov, E. Podivilov, I. Procaccia, Scaling behavior in turbulence is doubly anomalous, Phys. Rev. Lett. 76(21) (1996) 3963–3966.

[202] V. L'vov, I. Procaccia, Fusion rules in turbulent systems with flux equilibria, Phys. Rev. Lett. 76(16) (1996) 2898–2901.

[203] B.-K. Ma, Z. Warhaft, Some aspects of the thermal mixing layer in grid turbulence, Phys. Fluids 29(10) (1986) 3114–3120.

[204] S.-K. Ma, Modern Theory of Critical Phenomena, Frontiers in Physics, vol. 46, Addison-Wesley, Reading, MA, USA, 1976.

[205] A.J. Majda, Lectures on turbulent diffusion, Lecture Notes at Princeton University, 1990.

[206] A.J. Majda, Explicit inertial range renormalization theory in a model for turbulent diffusion, J. Statist. Phys. 73 (1993) 515–542.

[207] A.J. Majda, The random uniform shear layer: an explicit example of turbulent diffusion with broad tail probability distributions, Phys. Fluids A 5(8) (1993) 1963–1970.

[208] A.J. Majda, Random shearing direction models for isotropic turbulent diffusion, J. Statist. Phys. 25(5/6) (1994) 1153–1165.

[209] A.J. Majda, Lectures on turbulent diffusion, Lecture Notes at Courant Institute of Mathematical Sciences, 1996.

[210] A.J. Majda, R.M. McLaughlin, The effect of mean flows on enhanced diffusivity in transport by incompressible periodic velocity fields, Stud. Appl. Math. 89(3) (1993) 245–279.

[211] A.J. Majda, P.E. Souganidis, Large-scale front dynamics for turbulent reaction-diffusion equations with separated velocity scales, Nonlinearity 7(1) (1994) 1–30.

[212] A.J. Majda, P.E. Souganidis, Bounds on enhanced turbulent flame speeds for combustion with fractal velocity fields, J. Statist. Phys. 83(5-6) (1996) 933–954.

[213] A.J. Majda, P.E. Souganidis, Flame fronts in a turbulent combustion model with fractal velocity fields, C.P.A.M. Fritz John Vol. (1998) To appear.
[214] B.B. Mandelbrot, On the geometry of homogenous turbulence, with stress on the fractal dimension of the iso-surfaces of scalars, J. Fluid Mech. 72 (1975) 401–416.
[215] B.B. Mandelbrot, The Fractal Geometry of Nature, W.H. Freeman, San Francisco, New York, updated and augmented edition, 1983.
[216] B.B. Mandelbrot, Self-affine fractals and fractal dimension, Phys. Scripta 32 (1985) 257–260.
[217] B.B. Mandelbrot, Self-affine fractal sets, I: the basic fractal dimensions, in: L. Pietronero, E. Tosatti (Eds.), Fractals in Physics, ICTP, North Holland-Elsevier Science Publishers, Amsterdam, New York, 1986, pp. 3–15.
[218] B.B. Mandelbrot, Self-affine fractal sets, III: Hausdorff dimension anomalies and their implications, in: L. Pietronero, E. Tosatti (Eds.), Fractals in Physics, ICTP, North Holland-Elsevier Science Publishers, Amsterdam, New York, 1986, pp. 21–28.
[219] B.B. Mandelbrot, J.W. Van Ness, Fractional Brownian motions, fractional noises and applications, SIAM Rev. 10(4) (1968) 422–437.
[220] B.B. Mandelbrot, J.R. Wallis, Computer experiments with fractional Gaussian noises. Part 1, Averages and variances, Water Resour. Res. 5(1) (1969) 228–241.
[221] B.B. Mandelbrot, J.R. Wallis, Computer experiments with fractional Gaussian noises. Part 2, Rescaled ranges and spectra, Water Resour. Res. 5(1) (1969) 242–259.
[222] B.B. Mandelbrot, J.R. Wallis, Computer experiments with fractional Gaussian noises. Part 3, Mathematical appendix, Water Resour. Res. 5 (1) (1969) 260–267.
[223] G. Matheron, G. de Marsily, Is transport in porous media always diffusive? A counterexample, Water Resour. Res. 16(5) (1980) 901–917.
[224] R. Mauri, Dispersion, convection, and reaction in porous media, Phys. Fluids A 3 (5, part 1) (1991) 743–756.
[225] R.M. Mazo, C. Van den Broeck, The asymptotic dispersion of particles in N-layer systems: periodic boundary conditions, J. Chem. Phys. 86(1) (1987) 454–459.
[226] P. McCarty, W. Horsthemke, Effective diffusion coefficient for steady two-dimensional convective flow, Phys. Rev. A 37(6) (1988) 2112–2117.
[227] W.D. McComb, The Physics of Fluid Turbulence, Oxford Engineering Science Series, vol. 25, Clarendon Press, New York, 1991.
[228] A. McCoy, Ph.D. Thesis, Department of Mathematics, University of California at Berkeley, 1975.
[229] D.W. McLaughlin, G.C. Papanicolaou, O.R. Pironneau, Convection of microstructure and related problems, SIAM J. Appl. Math. 45(5) (1985) 780–797.
[230] R.M. McLaughlin, Turbulent transport, Ph.D. Thesis, Princeton University, November 1994, Program in Applied and Computational Mathematics.
[231] R.M. McLaughlin, Numerical averaging and fast homogenization, J. Statist. Phys. 90(3-4) (1998) 597–626.
[232] R.M. McLaughlin, M.G. Forest, An anelastic, scale-separated model for mixing, with application to atmospheric transport phenomena, Phys. Fluids (1998) Submitted.
[233] R.M. McLaughlin, A.J. Majda, An explicit example with non-Gaussian probability distribution for nontrivial scalar mean and fluctuation, Phys. Fluids 8(2) (1996) 536.
[234] P.A. McMurtry, T.C. Gansauge, A.R. Kerstein, S.K. Krueger, Linear eddy simulations of mixing in a homogenous turbulent flow, Phys. Fluids A 5(4) (1993) 1023–1034.
[235] C. Meneveau, K.R. Sreenivasan, Interface dimension in intermittent turbulence, Phys. Rev. A 41(4) (1990) 2246–2248.
[236] P. Mestayer, Local isotropy and anisotropy in a high-Reynolds-number turbulent boundary layer, J. Fluid Mech. 125 (1982) 475–503.
[237] O. Métais, M. Lesieur, Large eddy simulations of isotropic and stably-stratified turbulence, in: H.H. Fernholz, H.E. Fiedler (Eds.), Advances in Turbulence 2, Springer, Berlin, 1989, pp. 371–376.
[238] O. Métais, M. Lesieur, Spectral large-eddy simulation of isotropic and stably stratified turbulence, J. Fluid Mech. 239 (1992) 157–194.
[239] I. Mezić, J.F. Brady, S. Wiggins, Maximal effective diffusivity for time-periodic incompressible fluid flows, SIAM J. Appl. Math. 56 (1) (1996) 40–56.

[240] G.A. Mikhailov, Optimization of Weighted Monte Carlo Methods, Ch. 6, Springer Series in Computational Physics, Springer, Berlin, 1992, pp. 152–156, 161–164.

[241] T. Mikkelsen, S.E. Larsen, H.L. Pécseli, Diffusion of Gaussian Puffs, Q. J. Roy Meteorol. Soc. 113 (1987) 81–105.

[242] P.L. Miller, P.E. Dimotakis, Measurements of scalar power spectra in high Schmidt number turbulent jets, J. Fluid Mech. 308 (1996) 129–146.

[243] H.K. Moffatt, Transport effects associated with turbulence with particular attention to the influence of helicity, Rep. Prog. Phys. 46 (1983) 621–664.

[244] S.A. Molchanov, Ideas in the theory of random media, Acta Applicandae Math. 22 (1991) 139–282.

[245] S.A. Molchanov, L.I. Piterbarg, Averaging in turbulent diffusion problems, Probability Theory and Random Processes, Kijev, Naukova Dumka, 1987, pp. 35–47 (in Russian).

[246] S.A. Molchanov, A.A. Ruzmaikin, D.D. Sokoloff, Dynamo equations in a random short-term correlated velocity field, Magnitnaja Gidrodinamika 4 (1983) 67–73 (in Russian).

[247] A.S. Monin, A.M. Yaglom, Statistical Fluid Mechanics: Mechanics of Turbulence, vol. 1, MIT Press, Cambridge, MA, 1975.

[248] A.S. Monin, A.M. Yaglom, Statistical Fluid Mechanics: Mechanics of Turbulence, vol. 2, MIT Press, Cambridge, MA, 1975.

[249] F. Morgan, Geometric Measure Theory: A Beginner's Guide, Section 2.3, Academic Press, New York, 1988, pp. 8–10.

[250] A.H. Nayfeh, Introduction to Perturbation Techniques, Section 3.4, Wiley Classics Library, Wiley, New York, 1981, p. 86.

[251] J.O. Nye, R.S. Brodkey, The scalar spectrum in the viscous-convective subrange, J. Fluid Mech. 29 (1967) 151–163.

[252] A.M. Obukhov, Spectral energy distribution in a turbulent flow, Dokl. Akad. Nauk SSSR 32 (1) (1941) 22–24.

[253] A.M. Obukhov, Spectral energy distribution in a turbulent flow, Izv. Akad. Nauk. SSSR Ser. Geogr. Geophys. 5(4-5) (1941) 453–466.

[254] A.M. Obukhov, The structure of the temperature field in a turbulent flow, Izv. Akad. Nauk. SSSR Ser. Geogr. Geophys. 13 (1949) 58.

[255] A.M. Obukhov, Some specific features of atmospheric turbulence, J. Fluid Mech. 13 (1962) 77–81.

[256] K. Oelschläger, Homogenization of a diffusion process in a divergence-free random field, Ann. Probab. 16(3) (1988) 1084–1126.

[257] B. Øksendal, Stochastic Differential Equations, 5th ed., Universitext, Springer, Berlin, 1998. An introduction with applications.

[258] A. Okubo, Oceanic diffusion diagrams, Deep-Sea Res. 18 (1971) 789–802.

[259] S. Orey, Gaussian sample functions and the Hausdorff dimension of level crossings, Z. Wahrscheinlichkeitstheorie Verw. Geb. 15 (1970) 249–256.

[260] M.V. Osipenko, O.P. Pogutse, N.V. Chudin, Plasma diffusion in an array of vortices, Sov. J. Plasma Phys. 13(8) (1987) 550–554.

[261] R. Ozmidov, On the rate of dissipation of turbulent energy in sea currents and in the dimensionless constant in the '4/3 power law', Izv. Akad. Nauk. SSSR Ser. Geotiz (1960) 821–823.

[262] G.C. Papanicolaou, W. Kohler, Asymptotic theory of mixing stochastic ordinary differential equations, Commun. Pure Appl. Math. 27 (1974) 641–668.

[263] G.C. Papanicolaou, O.R. Pironeau, The asymptotic behavior of motions in random flows, in: L. Arnold, R. Lefever (Eds.), Stochastic Nonlinear Systems in Physics, Chemistry and Biology, Springer Series in Synergetics, vol. 8, Springer, Berlin, 1981, pp. 36–41.

[264] G.C. Papanicolaou, S.R.S. Varadhan, Boundary value problems with rapidly oscillating random coefficients, in: J. Fritz, J.L. Lebowitz, D. Szasz (Eds.), Random Fields: Rigorous Results in Statistical Mechanics and Quantum Field Theory, Colloquia Mathematica Societatis János Bolyai, vol. 2, North Holland-Elsevier Science Publishers, Amsterdam, New York, Oxford, 1979, pp. 835–873.

[265] F. Pasquill, F.B. Smith, Atmospheric Diffusion, 3rd ed., Ellis Horwood Series in Environmental Science, Ellis Horwood, Chichester, 1983.

[267] A.M. Polyakov, Turbulence without pressure, Phys. Rev. E 52(6) (1995) 6183–6188.

[268] S.B. Pope, The probability approach to the modelling of turbulent reacting flows, Combust. Flame 27 (1976) 299–312.

[269] S.B. Pope, Lagrangian PDF methods for turbulent flows, Annual Review of Fluid Mechanics, vol. 26, Annual Reviews, Palo Alto, CA, 1994, pp. 23–63.

[270] S.C. Port, C.J. Stone, Random measures and their application to motion in an incompressible fluid, J. Appl. Probab. 13 (1976) 498–506.

[271] R.R. Prasad, K.R. Sreenivasan, The measurement and interpretation of fractal dimensions of the scalar interface in turbulent flows, Phys. Fluids A 2(5) (1990) 792–807.

[272] R.R. Prasad, K.R. Sreenivasan, Quantitative three-dimensional imaging and the structure of passive scalar fields in fully turbulent flows, J. Fluid Mech. 216 (1990) 1–34.

[273] A.A. Praskovsky, E.B. Gledzer, M.Yu. Karyakin, Ye. Zhou, The sweeping decorrelation hypothesis and energy-inertial scale interaction in high Reynolds number flows, J. Fluid Mech. 248 (1993) 493–511.

[274] W.H. Press, S.A. Teukolsky, W.T. Vetterling, B.P. Flannery, Numerical Recipes in FORTRAN, 2nd ed., Ch. 7, Cambridge University Press, Cambridge, 1992, pp. 266–319.

[275] A. Pumir, Anomalous scaling behaviour of a passive scalar in the presence of a mean gradient, Europhys. Lett. 34(1) (1996) 25–29.

[276] A. Pumir, Determination of the three-point correlation function of a passive scalar in the presence of a mean gradient, Europhys. Lett. 37(8) (1997) 529–534.

[277] A. Pumir, B. Shraiman, E.D. Siggia, Exponential tails and random advection, Phys. Rev. Lett. 66(23) (1991) 2984–2987.

[278] A. Pumir, B.I. Shraiman, E.D. Siggia, Perturbation theory for the δ-correlated model of passive scalar advection near the Batchelor limit, J. Phys. Rev. E 55(2) (1997) R1263–R1266.

[279] S. Redner, Superdiffusive transport due to random velocity fields, Physica D 38 (1989) 287–290.

[280] S. Redner, Superdiffusion in random velocity fields, Physica A 168 (1990) 551–560.

[281] M. Reed, B. Simon, Methods of Modern Mathematical Physics. I, 2nd ed., Ch. 6, Academic Press [Harcourt Brace Jovanovich Publishers], New York, Functional Analysis, 1980, pp. 182–220.

[282] S.G. Resnick, Dynamical problems in non-linear advective partial differential equations, Ph.D. Thesis, University of Chicago, August 1995.

[283] L.F. Richardson, Some measurements of atmospheric turbulence, Phil. Trans. Roy. Soc. Lond. A 221 (1920) 1–28.

[284] L.F. Richardson, Atmospheric diffusion shown on a distance-neighbor graph, Proc. Roy. Soc. Lond. A 110 (1926) 709–737.

[285] P.H. Roberts, Analytical theory of turbulent diffusion, J. Fluid. Mech. 11 (1962) 257–283.

[286] H.A. Rose, Eddy diffusivity, eddy noise, and subgrid-scale modelling, J. Fluid. Mech. 81 (4) (1977) 719–734.

[287] M.N. Rosenbluth, H.L. Berk, I. Doxas, W. Horton, Effective diffusion in laminar convective flows, Phys. Fluids 30 (9) (1987) 2636–2647.

[288] H.L. Royden, Real Analysis, 3rd ed., MacMillan, New York, 1988.

[290] J.H. Rust, A. Sesonske, Turbulent temperature fluctuations in mercury and ethylene glycol in pipe flow, Int. J. Heat Mass Transfer 9 (1966) 215–227.

[291] K.K. Sabelfeld, Monte Carlo Methods in Boundary Value Problems, Ch. 1, 5, Springer Series in Computational Physics, Springer, Berlin, 1991, pp. 31–47, 228–238.

[292] A.I. Saichev, W.A. Woyczynski, Probability distributions of passive tracers in randomly moving media, in: S.A. Molchanov (Ed.), Stochastic Models in Geosystems, IMA Volumes in Mathematics and its Applications, Springer, Berlin, 1996.

[293] M. Sano, X.Z. Wu, A. Libchaber, Turbulence in helium-gas free convection, Phys. Rev. A 40 (11) (1989) 6421–6430.

[294] B.I. Shraiman, Diffusive transport in a Rayleigh–Bénard convection cell, Phys. Rev A 36(1) (1987) 261–267.

[295] B.I. Shraiman, E.D. Siggia, Lagrangian path integrals and fluctuations in random flow, Phys. Rev. E 49(4) (1994) 2912–2927.

[296] B. Simon, Functional Integration and Quantum Physics Section 4, Academic Press, New York, 1979, p. 38.

[297] Ya.G. Sinai, Introduction to Ergodic Theory, Princeton University Press, Princeton, 1976.

[298] Ya.G. Sinai, V. Yakhot, Limiting probability distributions of a passive scalar in a random velocity field, Phys. Rev. Lett. 63(18) (1989) 1962–1964.

[299] F.B. Smith, Conditional particle motions in a homogenous turbulent field, Atmos. Environ. 2 (1968) 491–508.

[300] L.M. Smith, S.L. Woodruff, Renormalization-group analysis of turbulence, in: Annual Review of Fluid Mechanics, Annu. Rev. Fluid Mech., vol. 30, Annual Reviews, Palo Alto, CA, 1998, pp. 275–310.

[301] T.H. Solomon, J.P. Gollub, Chaotic particle transport in time-dependent Rayleigh–Bénard convection, Phys. Rev. A 38 (12) (1988) 6280–6286.

[302] T.H. Solomon, J.P. Gollub, Passive transport in steady Rayleigh–Bénard convection, Phys. Fluids 31(6) (1988) 1372–1379.

[303] A.M. Soward, Fast dynamo action in a steady flow, J. Fluid Mech. 180 (1987) 267–295.

[304] A.M. Soward, S. Childress, Large magnetic Reynolds number dynamo action in a spatially periodic flow with mean motion, Philos. Trans. Roy. Soc. Lond. A 331 (1990) 649–733.

[305] K.R. Sreenivasan, Fractals and multifractals in fluid turbulence, in: Annual Review of Fluid Mechanics, vol. 23, Annual Reviews, Palo Alto, CA, 1991, pp. 539–600.

[306] K.R. Sreenivasan, On local isotropy of passive scalars in turbulent shear flows, Proc. Roy. Soc. Lond. A 434 (1991) 165–182.

[307] K.R. Sreenivasan, On the Universality of the Kolmogorov constant, Phys. Fluids 7(11) (1995) 2778–2784.

[308] K.R. Sreenivasan, The passive scalar spectrum and the Obukhov-Corrsin constant, Phys. Fluids 8(1) (1996) 189–196.

[309] K.R. Sreenivasan, R.A. Antonia, The phenomenology of small-scale turbulence, in: Annual Review of Fluid Mechanics, vol. 29, Annu. Rev. Fluid Mech., Annual Reviews, Palo Alto, CA, 1997, 435–472.

[310] K.R. Sreenivasan, R. Ramshankar, C. Meneveau, Mixing, entrainment and fractal dimension of surfaces in turbulent flows, Proc. Roy. Soc. Lond. A 421 (1989) 79–108.

[311] K.R. Sreenivasan, S. Tavoularis, R. Henry, S. Corrsin, Temperature fluctuations and scales in grid-generated turbulence, J. Fluid Mech. 100 (1980) 597–621.

[312] E.M. Stein, Harmonic Analysis – Real-Variable Methods, Orthogonality, and Oscillatory Integrals, of Princeton Mathematical Series, vol. 43, Section 8.1.3, Princeton University Press, Princeton, 1993, p. 334.

[313] R.L. Stratonovich, Topics in the Theory of Random Noise. vol. I: General Theory of Random Processes. Nonlinear Transformations of Signals and Noise, Sections 4.7–9, Gordon and Breach Science Publishers, New York, 1963, pp. 83–103. Revised English edition. Translated from the Russian by Richard A. Silverman.

[314] E.B. Tatarinova, P.A. Kalugin, A.V. Sokol, What is the propagation rate of the passive component in turbulent flows limited by?, Europhys. Lett. 14(8) (1991) 773–777.

[315] V. Tatarski, Radiophysical methods of investigating atmospheric turbulence, Izv. Vyssh. Ucheb. Zaved. 3 Radiofizika 4 (1960) 551–583.

[316] S. Tavoularis, S. Corrsin, Experiments in nearly homogenous turbulent shear flow with a uniform mean temperature gradient. Part 1, J. Fluid Mech. 104 (1981) 311–347.

[317] G.I. Taylor, Diffusion by continuous movements, Proc. Lond. Math. Soc. Ser. 2 (20) (1921) 196–212.

[318] G.I. Taylor, Dispersion of soluble matter in solvent flowing slowly through a tube, Proc. Roy. Soc. Lond. A 219 (1953) 186–203.

[319] H. Tennekes, Eulerian and Lagrangian time microscales in isotropic turbulence, J. Fluid Mech. 67(3) (1975) 561–567.

[320] H. Tennekes, J.L. Lumley, A First Course in Turbulence, MIT Press, Cambridge, MA, 1972.

[321] D.J. Thomson, Criteria for the selection of stochastic models of particle trajectories in turbulent flows, J. Fluid Mech. 180 (1987) 529–556.

[322] D.J. Thomson, A stochastic model for the motion of particle pairs in isotropic high-Reynolds-number turbulence, and its application to the problem of concentration variance, J. Fluid Mech. 216 (1990) 113–153.

[323] E.C. Titchmarsh, Eigenfunction Expansions Associated with Second-Order Differential Equations Part 1, Ch. V, Clarendon Press, Oxford, 1962, pp. 107–128.

[324] A.A. Townsend, The measurement of double and triple correlation derivatives in isotropic turbulence, Proc. Cambridge Phil. Soc. 43 (1947) 560.

[325] D.J. Tritton, Physical Fluid Dynamics, 2nd ed., Ch. 14.4, Clarendon, Press, Oxford, 1988, pp. 168–171.

[326] C.W. van Atta, W.Y. Chen, Correlation measurements in grid turbulence using digital harmonic analysis, J. Fluid Mech. 34 (1968) 497–515.

[327] H. van Dop, F.T.M. Nieuwstadt, J.C.R. Hunt, Random walk models for particle displacements in inhomogenous unsteady turbulent flows, Phys. Fluids 28(6) (1985) 1639–1653.

[328] E. Vanden Eijnden, Contribution to the statistical theory of turbulence: application to anomalous transport in plasmas, Ph.D. Thesis, Université Libre de Bruxelles, July 1997, Faculté des Sciences, Physique Statistique.

[329] E. Vanden Eijnden, An approximation for linear random differential equations, Phys. Rev. E 58 (1998) R5229–5232.

[330] E. Vanden Eijnden, A.J. Majda, P.R. Kramer, Testing approximate closures for turbulent diffusion on some model flows, In preparation, J. Statist. Phys. (1998) to be submitted.

[331] S.R.S. Varadhan, Large Deviations and Applications, CBMS-NSF Regional Conference Series in Applied Mathematics, vol. 46, SIAM Publ., Philadelphia, 1984.

[332] J.C. Vassilicos, On the geometry of lines in two-dimensional turbulence, in: Fernholz, Fiedler (Eds.), Advances in Turbulence 2, Springer, Berlin, 1989, pp. 404–411.

[333] M. Vergassola, Anomalous scaling for passively advected magnetic fields, Phys. Rev. E 53(4) (1996) R3021–R3024.

[334] M. Vergassola, A. Mazzino, Structures and intermittency in a passive scalar model, Phys. Rev. Lett. 79 (10) (1997) 1849–1852.

[335] J.A. Viecelli, E.H. Canfield Jr., Functional representation of power-law random fields and time series, J. Comput. Phys. 95 (1991) 29–39.

[336] R.F. Voss, Random fractal forgeries, in: R.A. Earnshaw (Ed.), Fundamental Algorithms for Computer Graphics, NATO ASI Series F: Computer and System Sciences, vol 17, NATO Science Affairs Divison, Springer, Berlin, 1985, pp. 805–835.

[337] J.C. Wheeler, R.G. Gordon, Bounds for averages using moment constraints, in: G.A. Baker, Gammel (Ed.), The Padé Approximant in Theoretical Physics, Academic Press, New York, 1970, pp. 99–128.

[338] B.S. Williams, D. Marteau, J.P. Gollub, Mixing of a passive scalar in magnetically forced two-dimensional turbulence, Phys. Fluids (1996), Submitted.

[339] F.A. Williams, Combustion Theory: The Fundamental Theory of Chemically Reacting Flow Systems, Chs. 3, 7, Addison-Wesley Series in Engineering Science, Addison-Wesley, Reading, MA, USA, 1965.

[340] A. Wirth, L. Biferale, Anomalous scaling in random shell models for passive scalars, Phys. Rev. E 54 (5) (1996) 4982–4989.

[341] A.M. Yaglom, Correlation Theory of Stationary and Related Random Functions. Vol. I: Basic Results, Springer, Berlin, 1987.

[342] A.M. Yaglom, Correlation Theory of Stationary and Related Random Functions. Vol. II: Supplementary Notes and References, Springer, Berlin, 1987.

[343] V. Yakhot, Passive scalar advected by a rapidly changing random velocity field: probability density of scalar differences, Phys. Rev. E 55(1) (1997) 329–336.

[344] V. Yakhot, S.A. Orszag, Renormalization group analysis of turbulence. I. Basic theory, J. Sci. Comput. 1(1) (1986) 3–51.

[345] V. Yakhot, S.A. Orszag, Z.-S. She, Space–time correlations in turbulence: kinematic versus dynamical effects, Phys. Fluids A 1(2) (1989) 184–186.

[346] W. Young, A. Pumir, Y. Pomeau, Anomalous diffusion of tracer in convection rolls, Phys. Fluids A 1(3) (1989) 462–469.

[347] W.R. Young, P.B. Rhines, C.J.R. Garrett, Shear-flow dispersion, internal waves and horizontal mixing in the ocean, J. Phys. Oceanogr. 12 (1982) 515–527.

[348] Ya.B. Zel'dovich, Exact solution of the problem of diffusion in a periodic velocity field, and turbulent diffusion, Sov. Phys. Dokl. 27(10) (1982) 797–799.

[349] C.L. Zirbel, E. Çinlar, Mass transport by Brownian flows, in: S.A. Molchanov (Ed.), Stochastic Models in Geosystems, IMA Volumes in Mathematics and its Applications, Springer, Berlin, 1996.

[350] C.L. Zirbel, Stochastic flows: dispersion of a mass distribution and Lagrangian observations of a random field, Ph.D. Thesis, Princeton University, 1993, Program in Applied and Computational Mathematics.

[351] N. Zouari, A. Babiano, Derivation of the relative dispersion law in the inverse energy cascade of two-dimensional turbulence, Physica D 76 (1994) 318–328.

[352] G. Zumofen, A. Blumen, J. Klafter, M.F. Shlesinger, Lévy walks for turbulence: a numerical study, J. Statist. Phys. 54(5/6) (1989) 1519–1528.

[353] G. Zumofen, J. Klafter, A. Blumen, Enhanced diffusion in random velocity fields, Phys. Rev. A 42(8) (1990) 4601–4608.

[354] G. Zumofen, J. Klafter, A. Blumen, Trapping aspects in enhanced diffusion, J. Statist. Phys. 65(5/6) (1991) 991–1013.